Metal Complexes of

4′-Substituted-2,2′:6′,2″-Terpyridines in

Supramolecular Chemistry

Inauguraldissertation

Zur

Erlangung der Würde eines Doktors der Philosophie

vorgelegt der

Philosophisch-Naturwissenschaftlichen Fakultät

der Universität Basel

Von

Hoi Shan CHOW

aus Hong Kong, China

Basel, 2005

Genehmigt von der Philosophisch-Naturwissenschaftlichen Fakultät der auf Antrag von:

Prof. Dr. E. C. Constable   Prof. Dr. A. Pfaltz

Basel, den 25 Januar 2005

                              Prof. Dr. H.-J. Wirz

                              Dekan

To

My Dear Parents

&

Wing Yin

Summary

This thesis presents 4′-substituted-2,2′:6′,2″-terpyridine ligands and their complexes within the perspective for supramolecular chemistry.

Chapter 1 gives a brief introduction to supramolecular chemistry, metallosupramolecular chemistry, 2,2′:6′,2″-terpyridine complexes and dynamic combinatorial libraries.

Chapter 2 discusses the synthesis and characterisation of ligands L^1-L^9 containing one 2,2′:6′,2″-terpyridine metal-binding domain. These ligands contain different substituents at the 4′-position of the 2,2′:6′,2″-terpyridine which differ from one another in the length of the chains, in the linkages of the chains or in the terminal domains.

Chapter 3 describes the synthesis and characterisation of the mononuclear iron(II) and ruthenium(II) complexes formed with L^1-L^9.

Chapter 4 describes the synthesis and characterisation of the mononuclear cobalt(II) complexes formed with L^1-L^9. A newly established method for the NMR spectroscopic assignment of Co(II) complexes, and some preliminary studies of combinatorial libraries by mixing two Co(II) complexes, are also discussed.

Chapter 5 discusses the synthesis and characterisation of ligands L^{10}-L^{17}, which contain two 2,2′:6′,2″-terpyridine metal-binding domains. These two 2,2′:6′,2″-terpyridine metal-binding domains are linked by different naphthalene bis(ethyleneoxy) spacers at their 4′-positions.

Chapter 6 discusses the synthesis and characterisation of dinuclear ruthenium(II) complexes formed by ligands L^{11}-L^{14}, L^{16}-L^{17}.

Chapter 7 describes the synthesis and characterisation of [n+n] ruthenium(II) and iron(II) metallomacrocycles which formed by cyclisation reactions involving ligands L^{11}-L^{17}.

Acknowledgements

Contents

Abbreviations

1. General

Ant	Anthryl
A sol	CH$_3$CN: saturated aqueous KNO$_3$: H$_2$O in 14:2:1 ratio
Bipy	2,2′-Bipyridine
Bbipy-(GalNHAc)	*N*-Acetyl galactropyranose functionalised with 2,2′-bipyridine
6-Br-terpy	6-Bromo-2,2′:6′,2″-terpyridine
CD	Circular dichromism
Cl-terpy	4′-Chloro-2,2′:6′,2″-terpyridine
DMF	*N*,*N*-Dimethylformamide
DMSO	Dimethylsulfoxide
DNA	Deoxyribonucleic acid
EtO-terpy	4′-Ethoxy-2,2′:6′,2″-terpyridine
Fc-terpy	4′-Ferrocenyl-2,2′:6′,2″-terpyridine
HO-terpy	4′-Hydroxy-2,2′:6′,2″-terpyridine
HPLC	High performance liquid chromatography
Nap	Naphthyl
NEM	*N*-Ethylmorpholine
OAc	Acetate
OMs	Methylsulfonyl
Phen	1,10-Phenanthroline
Poterpy	4′-(2-Propyn-1-oxy)-2,2′:6′,2″-terpyridine
Qterpy	2,2′:6′,2″:6″,2‴-Quaterpyridine
R$_f$	Retention factor
TDDFT	Time-dependent density functional theory
TEM	Transmission electron microscopy
Terpy	2,2′:6′,2″-Terpyridine
THF	Tetrahydrofuran
TLC	Thin layer chromatography
Ts	*p*-Toluenesulfonyl
X	Different substituents attached to the ligands (e.g. ***bipy***, ***phen***, ***terpy***)

2. Experimental methods

Nuclear Magnetic Resonance (NMR) Spectroscopy

^{1}H NMR	Proton nuclear magnetic resonance
^{13}C NMR	Carbon nuclear magnetic resonance
COSY	Correlated spectroscopy
NOESY	Nuclear Overhauser effect spectroscopy
HMQC	Heteronuclear multiple quantum correlation
HMBC	Heteronuclear multiple bond correlation
EXSY	Chemical exchange difference spectroscopy
ROESY	Rotating frame nuclear Overhauser effect spectroscopy
T_1	Relaxation time in seconds
δ	Chemical shift in ppm
J	Coupling constant in Hz
s	Singlet
d	Doublet
t	Triplet
dd	Doublet of doublets
ddd	Doublet of doublets of doublets
dt	Doublet of triplets
td	Triplet of doublets
m	Multiplet
br	Broad

Mass Spectrometry (MS)

EI	Electron impact
ES	Electrospray ionisation
FAB	Fast-atom bombardment
M	Parent ion
m/z	Mass to charge ratio

Ultra-violet Visible (UV/VIS) Spectroscopy

LC	Ligand centred
MLCT	Metal-to-ligand charge transfer
λ_{max}	Wavelength at which maximum absorption occurs in nm
ε_{max}	Extinction coefficient in $M^{-1}cm^{-1}$

Infrared (IR) Spectroscopy

w	Weak
m	Medium
s	Strong
br	Broad

Cyclic voltammetry

$^{t}Bu_4N$	Tetrabutylammonium
Fc	Ferrocene
Fc^+	Ferrocinium ion

Elemental analysis

Calc.	Calculated

General experimental

NMR spectroscopy

^{1}H NMR spectra were recorded on Bruker AM 250 MHz, AV 400 MHz, Bruker DRX-500 MHz and Bruker Avance 600 MHz spectrometers. ^{13}C NMR spectra were recorded at 125 MHz on Bruker DRX-500 MHz spectrometer and 100 MHz on AV 400 MHz spectrometer.

Mass spectrometry

Fast-atom bombardment (FAB) and electron impact (EI) mass spectra were recorded on Kratos MS-50, Kratos MS-890, VG 70-250 or Kratos MS 902 spectrometers. For FAB spectra, 3-nitrobenzyl alcohol was used as supporting matrix. Electrospray ionisation (ES) mass spectra were recorded on Micromass LCT or LCQ spectrometers.

Ultra-violet visible spectroscopy

Ultra-violet visible (UV/VIS) spectra were recorded on a Shimadzu UV-3101PC UV/VIS/NIR spectrophotometer and a Varian 5000 UV-VIS-NIR spectrophotometer.

Infrared Spectroscopy

Infrared spectra were recorded on a Shimadza FTIR-8300 fourier transform infrared spectrophotometer and a Shimadza FTIR-8400S fourier transform infrared spectrophotometer.

Cyclic voltammetry

Electrochemical measurements were performed with an Eco Chemie Autolab PGSTAT 20 system using glassy carbon working and platinum auxiliary electrodes with silver as reference using purified acetonitrile as solvent and 0.1M [^{t}Bu$_4$N][PF$_6$] as supporting electrolyte; ferrocene was added at the end of each experiment as an internal reference.

Compound labelling scheme

General labelling scheme of ligands L^1-L^9 describes in Chapter 2.

4′-(2-Hydroxyethoxy)-2,2′:6′,2″-terpyridine (L^1)
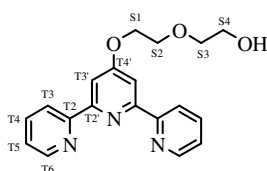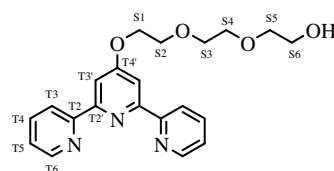
4′-[2-(2-Hydroxyethoxy)ethoxy]-2,2′:6′,2″-terpyridine (L^2)

4′-{2-[2-(2-Hydroxyethoxy)ethoxy]ethoxy}-2,2′:6′,2″-terpyridine (L^3)
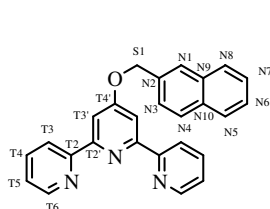
4′-(Naphthalen-2-ylmethoxy)-2,2′:6′,2″-terpyridine (L^4)
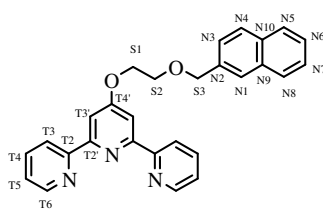
4′-[2-(Naphthalen-2-ylmethoxy)ethoxy]-2,2′:6′,2″-terpyridine (L^5)
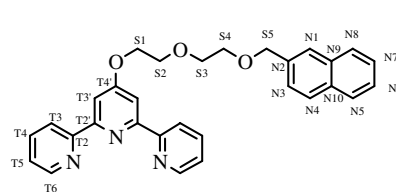
4′-{2-[2-(Naphthalen-2-ylmethoxy)ethoxy]ethoxy}-2,2′:6′,2″-terpyridine (L^6)
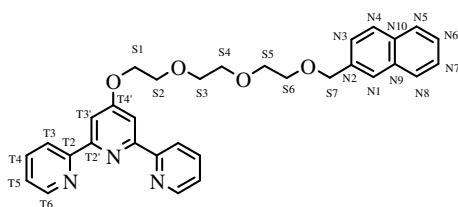
4′-(2-{2-[2-(Naphthalen-2-ylmethoxy)ethoxy]ethoxy}ethoxy)-2,2′:6′,2″-terpyridine (L^7)
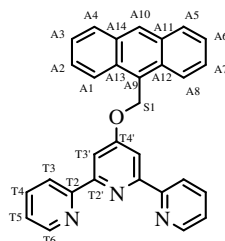
4′-(Anthracen-9-ylmethoxy)-2,2′:6′,2″-terpyridine (L^8)
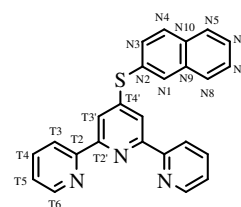
4′-(Naphthalen-2-ylsulfanyl)-2,2′:6′,2″-terpyridine (L^9)

The atom numbering scheme of ligands L^1-L^9 are also used in the mononuclear Fe(II), Ru(II) and Co(II) complexes in Chapter 3 and Chapter 4.

General labelling scheme of ligands L^{10}-L^{17} describes in Chapter 5.
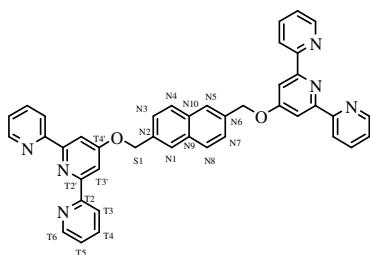
2,6-Bis(2,2′:6′,2″-terpyridin-4′-yloxymethyl)naphthalene (L^{10})
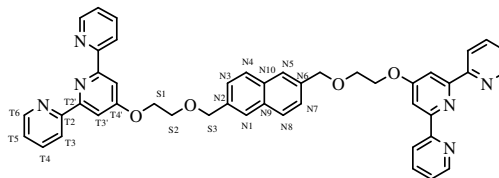
2,6-[Bis(2,2′:6′,2″-terpyridin-4′-yl)-1,4-dioxapentyl]naphthalene (L^{11})
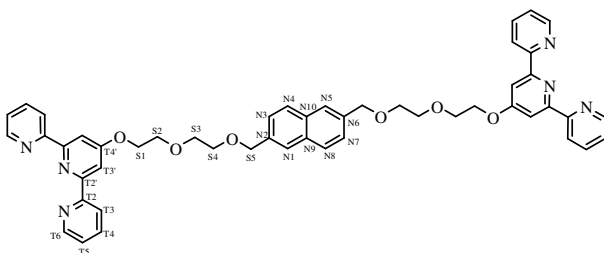
2,6-[Bis(2,2′:6′,2″-terpyridin-4′-yl)-1,4,7-trioxaoctyl]naphthalene (L^{12})
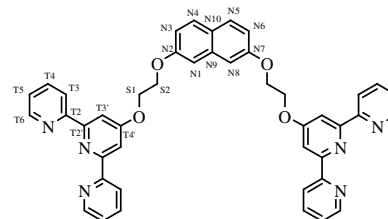
2,7-[Bis(2,2′:6′,2″-terpyridin-4′-yl)-1,4-dioxabutyl]naphthalene (L^{13})
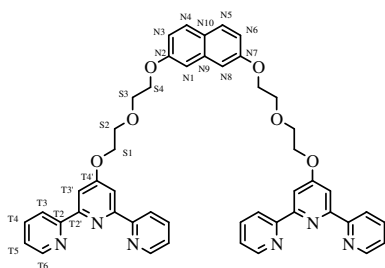
2,7-[Bis(2,2′:6′,2″-terpyridin-4′-yl)-1,4,7-trioxaheptyl]naphthalene (L^{14})
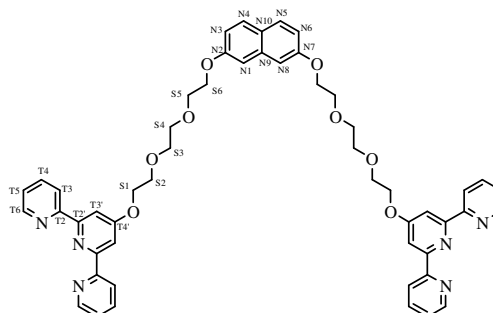
2,7-[Bis(2,2′:6′,2″-terpyridin-4′-yl)-1,4,7,10-tetraoxadecayl]naphthalene (L^{15})
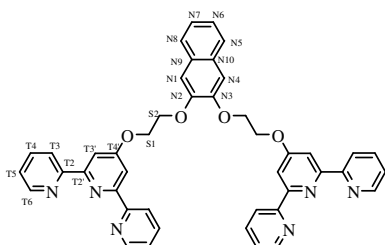
2,3-[Bis(2,2′:6′,2″-terpyridin-4′-yl)-1,4-dioxabutyl]naphthalene (L^{16})
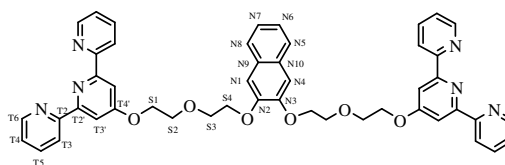
2,3-[Bis(2,2′:6′,2″-terpyridin-4′-yl)-1,4,7-trioxaheptyl]naphthalene (L^{17})

The atom numbering scheme of ligands L^{10}-L^{17} are also used in the dinuclear Fe(II) and Ru(II) complexes in Chapter 7.

Chapter 1

Introduction

In this chapter, a brief introduction to four areas related to this thesis is presented. The four areas are supramolecular chemisty, metallosupramolecular chemistry, 2,2′:6′,2″-terpyridine complexes and dynamic combinatorial libraries.

1.1   Supramolecular chemistry

Supramolecular chemistry has become an active research area over the past 25 years.[1-6] Lehn and Vögtle have defined supramolecular chemisty:

Lehn- *"Supramolecular chemistry is the chemistry of the intermolecular bond, covering the structures and functions of the entities formed by the association of two or more chemical species."*[1]

Vögtle- *"In contrast to molecular chemistry, which is predominantly based upon the covalent bonding of atoms, supramolecular chemistry is based upon intermolecular interactions, i.e. on the association of two or more building blocks, which are held together by intermolecular bonds."*[2]

Supramolecules normally contain more than one component held together by intermolecular non-covalent interactions, for example, hydrogen bonding, electrostatic interactions, hydrophobic or hydrophilic associations, π-stacking, metal coordination interactions and host-guest interactions.[7]

There are two important mechanisms for the construction of a supramolecule.

➢ Molecular recognition[1,6]

This involves selection and binding of substrates by a given receptor molecule similar to the "lock and key" concept devised by Emil Fischer.[8] The binding site can distinguish the shape, size, bonding, and electronic properties of the substrate.[9]

> Self-assembly[2,5]

This is a spontaneous assembly process of molecules into structured, stable, non-covalently joined aggregates by simply mixing two or more small species.

In nature, deoxyribonucleic acid (DNA)[10] forms a double helix from two complementary oligonucleotides and this is an example of a self-assembly process (**Figure 1**). Similar synthetic system can also be made. Lehn's group have reported oligobipyridine-based double helices $[Cu_3(\mathbf{1})_2]^{3+}$, which are held by metal-directed self-assembly interactions (**Figure 2**).[11,12]
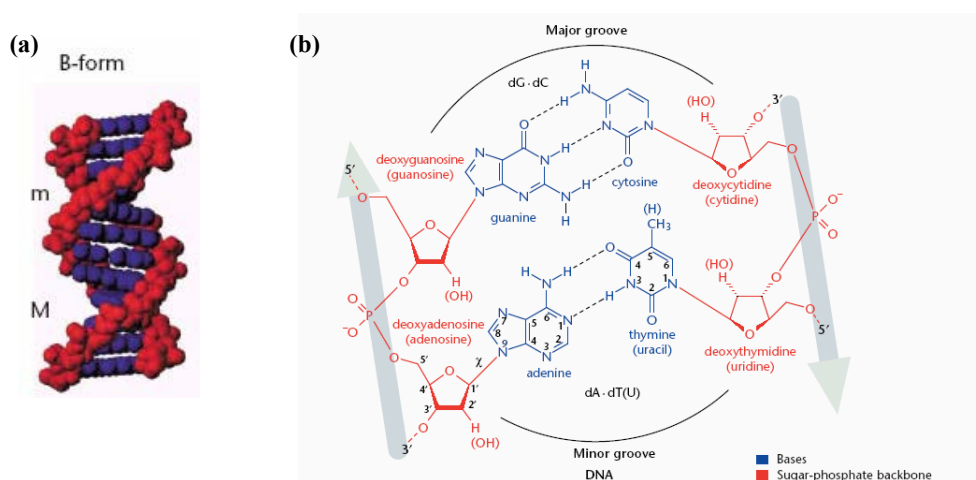
Figure 1. Diagram showing (a) three-dimensional space filling diagram of the B-form of DNA and (b) the structures of the DNA base pairs.[13]
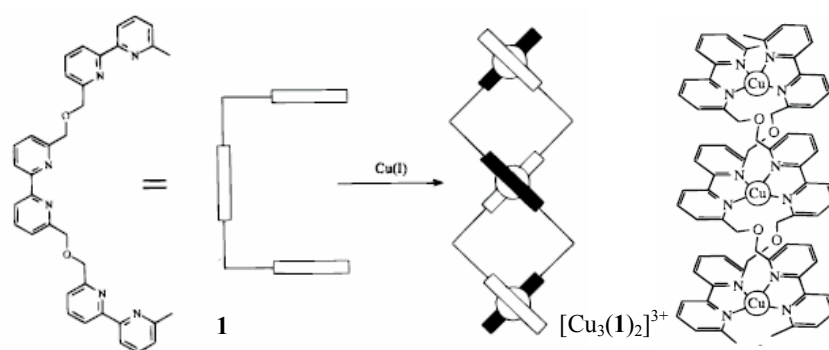
Figure 2. Diagram showing double helices which are held by metal-directed self-assembly interactions between three copper(I) metal ions and two tris(2,2′-bipyridine) ligands (**1**).

Finally, supramolecular chemistry not only offers us opportunities to gain a better understanding of biological systems such as binding of a substrate to a receptor

protein, enzymatic reactions, translation or transcription of genetic code and of complicated structures found in biological systems, but also has potential applications such as chemically, electrochemically and photochemically induced artificial molecular machines and devices[5-6,14-17], molecular wires[5,18] and sensors[19].

1.2   Metallosupramolecular chemistry

Metallosupramolecular chemistry has become a main research area in supramolecular chemistry. Constable has defined metallosupramolecular chemistry as follows:

"Metallosupramolecular chemistry is concerned with the use of metal ions to control the assembly of appropriate molecular components containing metal-binding domains."[20]

The principle of the formation of metallosupramolecules depends mainly on (1) the number and orientation of the coordination sites of ligands [molecular components containing metal-binding domains] and (2) the coordination number and geometry of the metal ions. A variety of metallosupramolecular architectures[21,22], including rods[23-27], helices[28-41], knots[42], catenates[42-45], rotaxanes[46-48], boxes[49-62], grids[63-71], racks[72], ladders[73], cylinders[74], cages[75-82], and dendrimers[83-86], has been formed spontaneous by self-assembly labile metal ions with multidentate ligands. In the following discussion, examples of a few metal-directed self-assembly systems are presented.

The supramolecular architectures obtained from copper ions and bidentate ligands (e.g. 2,2′-bipyridine and 1,10-phenanthroline), and/or tridentate ligands (e.g. 2,2′:6′,2″-terpyridine ligand) are good examples which demonstrate the importance of metal ion geometry and of number of the coordination sites of ligand. The Cu(I) ion has a d^{10} electron configuration. It prefers a coordination number of 4 and a tetrahedral geometry. It can achieve this with two bidentate 2,2′-bipyridine or 1,10-phenanthroline ligands. The Cu(II) ion has a d^9 electron configuration. It prefers a coordination number of 5 (or 6) and favours a square pyramidal geometry with one tridentate 2,2′:6′,2″-terpyridine and one bidentate 2,2′-bipyridine or 1,10-

phenanthroline ligands (or favours an octahedral geometry with two tridentate 2,2′:6′,2″-terpyridine or three bidentate 2,2′-bipyridine or 1,10-phenanthroline ligands).

Lehn recently reported ligands (**2-3**) that contain two different coordinated subunits.[87] Two self-assembled architectures resulted from using the same ligand but with different specific coordination algorithms. Ligand **2** contains four 2,2′-bipyridine units and one pyridazine unit. Two possible supramolecular architectures (A and B) could be formed by reacting ligand **2** with tetrahedral metal ions (**Figure 3a**). When ligand **2** reacted with Cu(I) ions, an almost quantitative yield of supramolecular architecture B was obtained (**Figure 3b**).
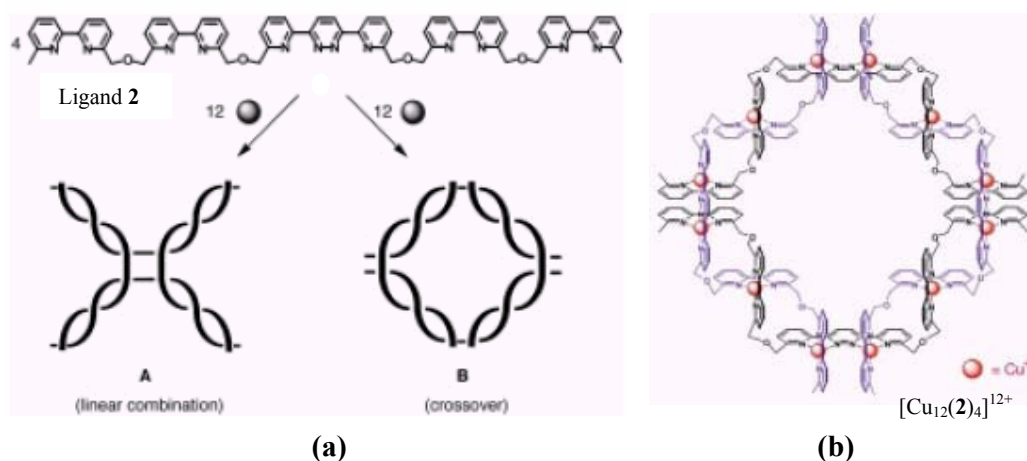
Figure 3. (a) Two possible self-assembled architectures (A and B) when ligand **2** reacted with tetrahedral metal ions and (b) the structure of the circular complex $[Cu_{12}(2)_4]^{12+}$ when ligand **2** reacted with Cu(I) ions.[87]

There are reports on the reaction of 4,6-bis(2′,2″-bipyrid-6′-yl)-2-methylpyrimidine (**3a**) with octahedral ions, such as Co(II), Ni(II), Cu(II), Zn(II). These result in a square [2x2] grid-type complex (**Figure 4**).[66,68] On the other hand, ligand **3b**, which contains two 2,2′-bipyridine units bridged by oxomethylene, reacted with tetrahedral coordination ions, such as Cu(I) and Ag(I), and gave a double-helical complex (**Figure 4**).[11,12,88]
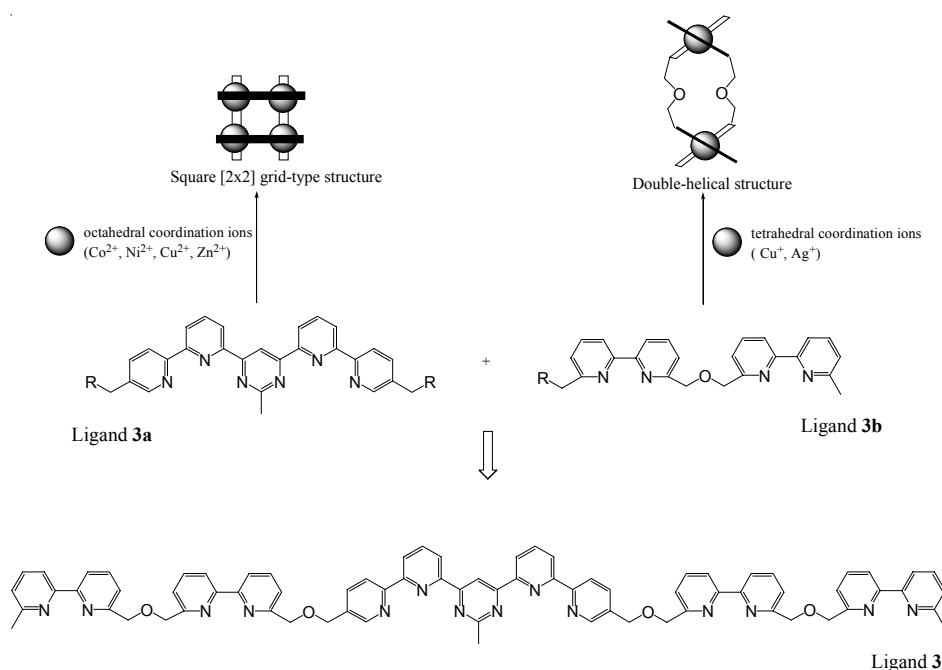
Figure 4. Diagram representing ligand **3**, which contains **3a** and **3b** units, and the structure of the complexes formed from **3a** and **3b**.[66,68,22,12,88,87]

Ligand **3** contains two subunits, two 2,2′-bipyridine units bridged by an oxomethylene unit (**3b**) and one 4,6-bis(2′,2″-bipyrid-6′-yl)-2-methylpyrimidine unit (**3a**) (**Figure 4**).[87] This ligand possesses both bidentate and teidentate binding sites which can bind to hexacoordinate, tetracoordinate and/or pentacoordinate ions. Therefore, ligand **3** will be expected to generate two possible supramolecular architectures (C and D) (**Figure 5**). When one equivalent of an octahedral ion [Fe(II), Co(II), Ni(II), Cu(II) ions] and two equivalents of a tetrahedral ion [Cu(I) ion] react with one equivalent of ligand **3**, architecture C , which combined a [2x2] grid-like structure in the centre and four double-helical structure at the corner, resulted. On the other hand, reacting two equivalents of a pentacoordinate ion [Cu(II) ion] and one equivalent of a tetrahedral ion [Cu(I) ion] with one equivalent of ligand **3** leaded to architecture D.[87]

In these two examples, the self-assembled architectures A, C and B, D could be obtained by self-assembly of different ligands with different metal ion coordination algorithms.
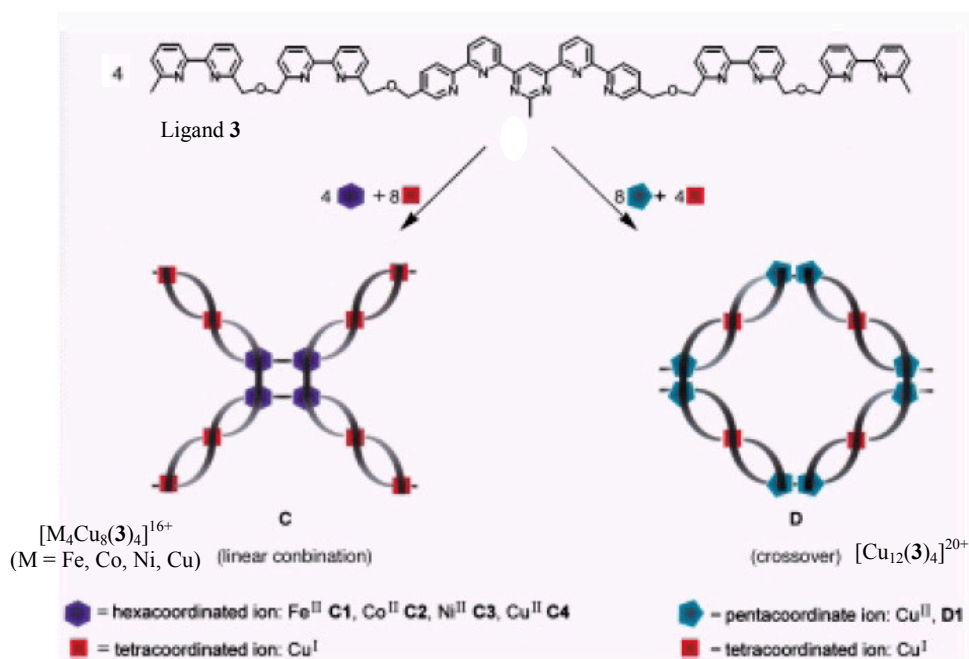
Figure 5. The diagrammatic representation of supramolecular architectures C and D when ligand **3** reacted with different metal ion with different coordination geometries.[87]
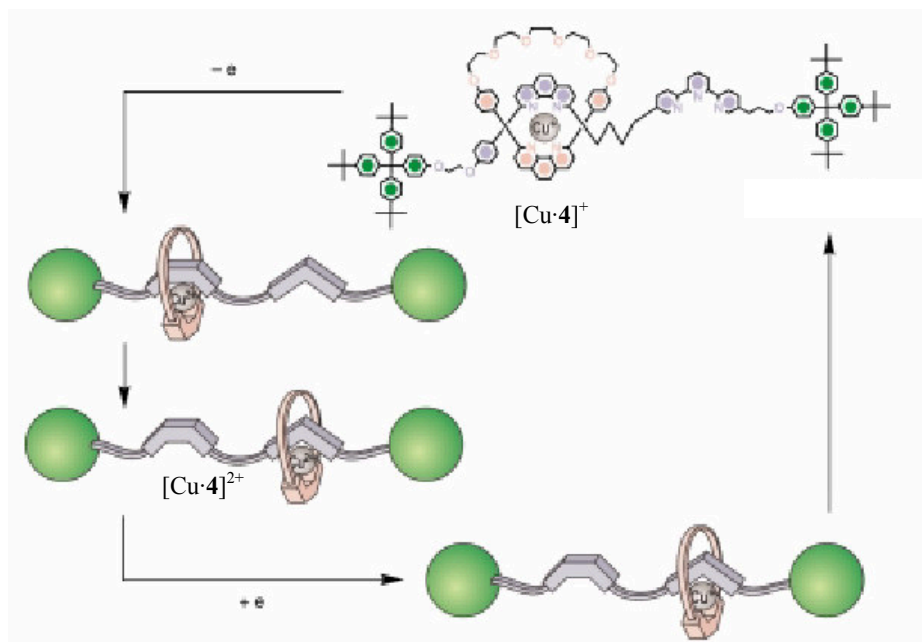
Figure 6. The diagrammatic representation of the molecular motion processes of the rotaxanes ([Cu·**4**]$^{+/2+}$) by oxidising and reducing the metal centre.[15]

Sauvage has reported a rotaxane [Cu·**4**]$^{+/2+}$ incorporating two different ligand domains (a 1,10-phenanthroline and a 2,2′:6′,2″-terpyridine) in the thread and a bidentate 1,10-phenanthroline unit in the ring.[47,48] The system can be switched from a four-coordinate Cu(I) to a five-coordinate Cu(II) and vice versa by oxidising or reducing the metal (**Figure 6**). There are other similar systems, a [2]catenate [Cu·**5**]$^+$ incorporating a terpyridine unit in one of its two macrocyclic components with a 1,10-phenanthroline unit in both and a [2]catenate [Cu·**6**]$^+$ incorporating two identical macrocyclic components with a 2,2′:6′,2″-terypridine unit and a 1,10-phenanthroline unit, have been reported by Sauvage (**Figure 7**).[89-91]

[Cu·**5**]$^+$ [Cu·**6**]$^+$
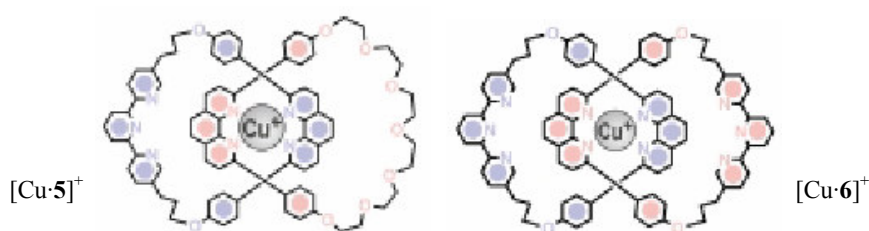
Figure 7. Diagram showing [2]catenate [Cu·**5**]$^+$ and [2]catenate [Cu·**6**]$^+$.[15]

From the above examples, we understand the importance of designing ligands with correct number and orientation of the coordination sites (molecular components containing metal-binding domains) and of choosing metal ions with the correct coordination number and geometry. More examples of different 2D and 3D metal-directed self-assembly molecular boxes are discussed below.

7^{4+} **8**$^{4+}$
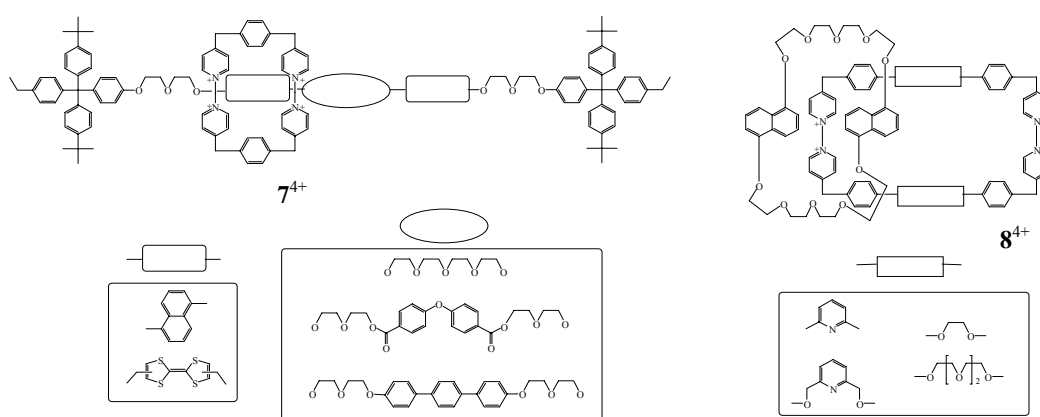
Figure 8. Diagram showing rotaxanes (**7**$^{4+}$) and catenands (**8**$^{4+}$) that were synthesised by the group of Stoddart.[92,93]

The supramolecular rotaxanes (7^{4+}) and catenands (8^{4+}), which contain 1,1′-bipyridinium as the building unit, were synthesised by Stoddart's group (**Figure 8**).[92,93] These rotaxanes and catenands were held by π-donor and π-acceptor interactions. Similar to these box like self-assembly molecules (7^{4+}) and (8^{4+}), Fujita and Steel reported numbers of metal-directed self-assembly molecular boxes, where the corner of the ring of the catenands are replaced by square planar Pt(II) and Pd(II) metal units (**Figure 9**).[49-52,94]
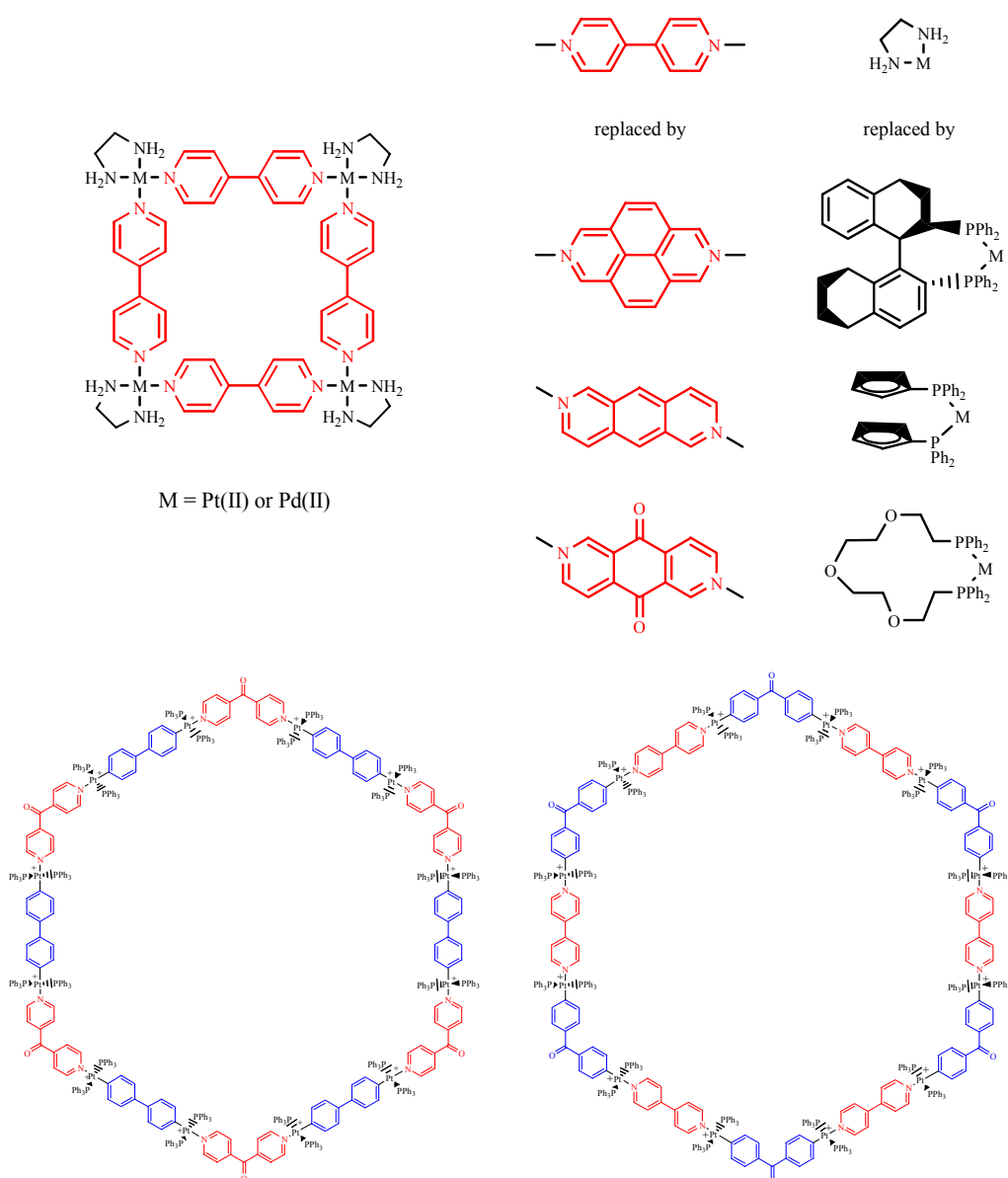
Figure 9. A variety of metal-directed self-assembly Pt(II) and Pd(II) molecular boxes.[49-52,94]
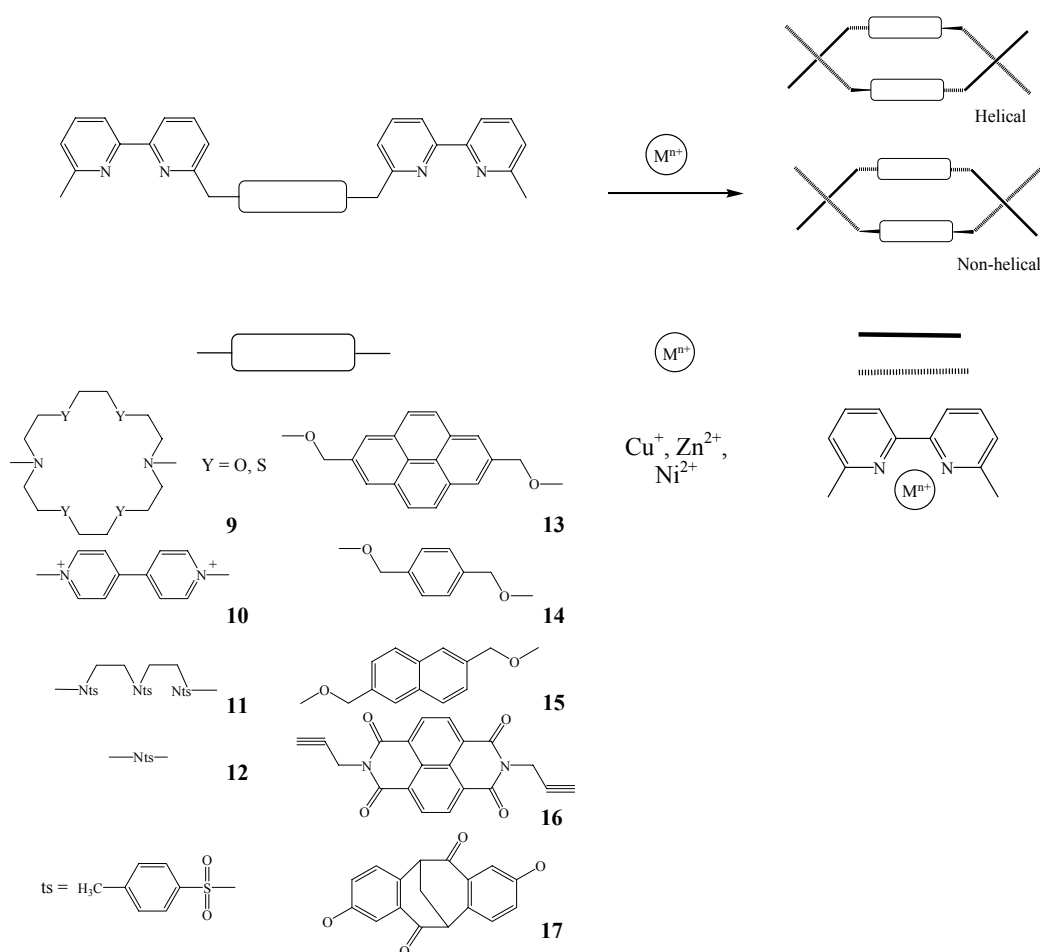
Figure 10. [2+2] Macrocycles formed by two metal ions and two ligands with 2,2′-bipyridine units which are linked by different spacer groups (**9-17**).[53-58]

The groups of Beer[53] and Harding[54-58] synthesised ligands (**9-17**) that contain two 2,2′-bipyridine units which are linked by different spacer groups (**Figure 10**). By mixing the ligand with metal ions, both [2+2] helical and [2+2] box (non-helical) were readily formed. When ligand **13** reacted with Zn(II) ions, a [2+2] non-helical species [Zn(**13**)]$_2$[CF$_3$SO$_3$]$_4$ was formed.[55] This was assigned by NMR spectroscopy and has been confirmed by X-ray crystallography. Each of the Zn(II) ions is bound to four nitrogen atoms from two 2,2′-bipyridine units and two oxygen atoms from the ether links in a distorted octahedral geometry. When ligand **15** reacted with Ni(II) ions, a [2+2] non-helical species [Ni(**15**)$_2$][PF$_6$]$_4$ was formed.[56] X-ray crystallography confirmed the structure of this species is similar to [Zn(**13**)]$_2$[CF$_3$SO$_3$]$_4$. When ligand **16** reacted with Zn(II) ions, a [2+2] helical species [Zn(**16**)]$_2$[CF$_3$SO$_3$]$_4$ was formed and this has been confirmed by X-ray crystallography.[57] Each of the Zn(II) ions is

bound to four nitrogen atoms from two 2,2′-bipyridine units and one oxygen atom from water molecule in a distorted trigonal bipyramidal geometry. The crystal structure of the helical $[Zn(\mathbf{16})]_2[CF_3SO_3]_4 \cdot 2H_2O$ contained either *p*- or *o*-dimethoxybenzene bound in the cavity in between the two spacer groups.

1.3   2,2′:6′,2″-Terpyridine complexes

2,2′:6′,2″-Terpyridine (*terpy*) is a molecule with three pyridine rings connected together through the α positions of the nitrogen. Its synthesis was first reported by Morgan in 1932.[95,96] 2,2′:6′,2″-Terpyridine readily reacts with M^{n+} octahedral metal ions to give $[M(terpy)_2]^{n+}$ complexes.[97] Making octahedral complexes formed by 2,2′:6′,2″-terpyridine with different substituted groups at the 4′-position avoids the formation of isomers that formed by bidentate 2,2′-bipyridine (*bipy*) and octahedral metal ions (**Figure 11**).[98-100] However, the photophysical properties of $[Ru(terpy)_2]^{2+}$ are not as promising as those of $[Ru(bipy)_3]^{2+}$ at room temperature.[98,99] Therefore, there are many attempts to introduce a wide variety of functional groups at the 4′-position of 2,2′:6′,2″-terpyridine to modify the photophysical properties of the complexes.

Δ-[M(*bipy*)$_3$]$^{n+}$ Λ-[M(*bipy*)$_3$]$^{n+}$ *mer*-[M(*X-bipy*)$_3$]$^{n+}$ *fac*-[M(*X-bipy*)$_3$]$^{n+}$

[M(*terpy*)$_2$]$^{n+}$ [M(*X-terpy*)$_2$]$^{n+}$
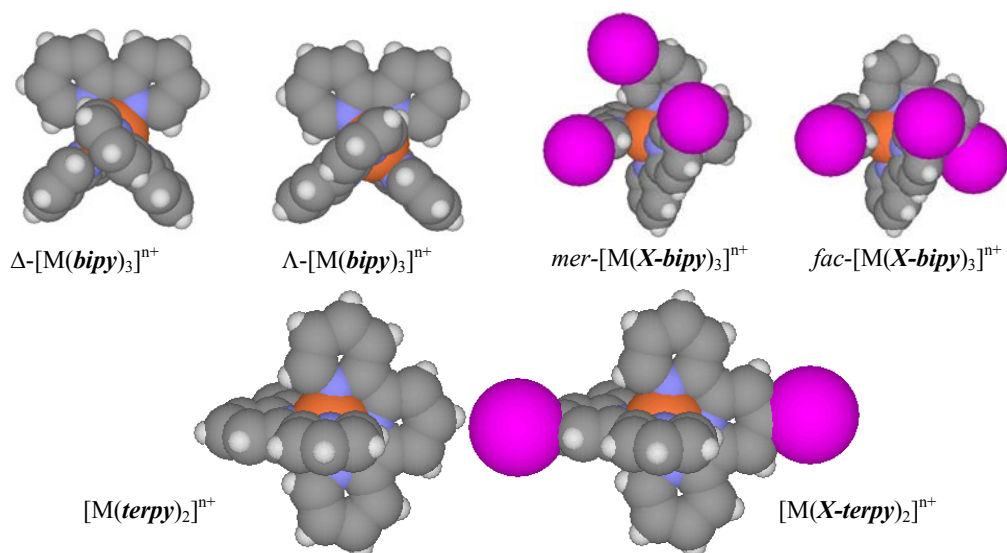
Figure 11. Structures representing some complexes of 2,2′-bipyridine and 2,2′:6′,2″-terpyridine with an octahedral metal centre (*X* = substituted groups).

$$X =$$
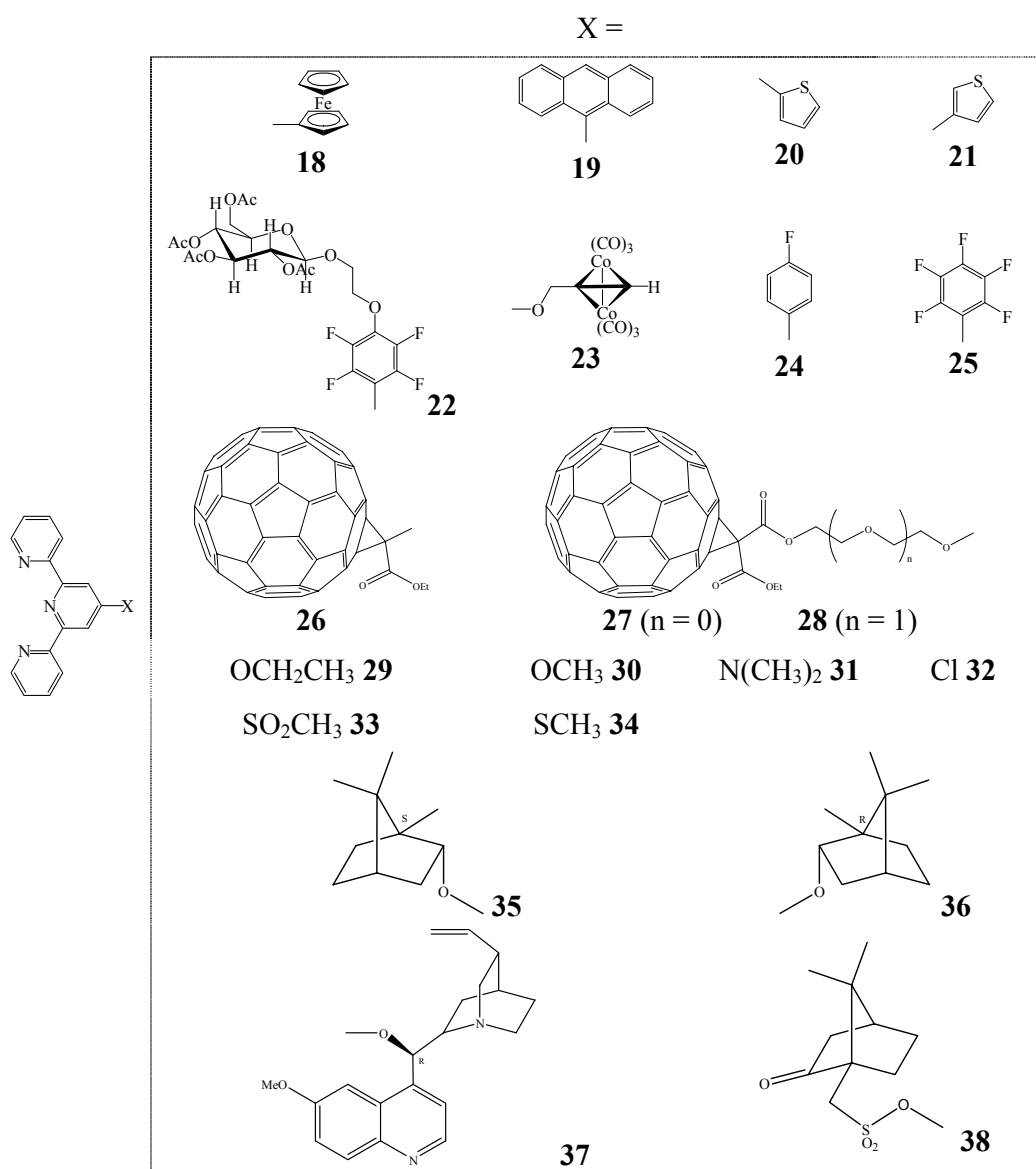
Figure 12. Diagram showing 2,2′:6′,2″-terpyridines with a variety of different functional groups (**18-38**) at the 4′-position.[101-113]

Constable and Housecroft have reported a variety of 2,2′:6′,2″-terpyridine ligands containing different functional groups at the 4′-position. These include ferrocene **18**[101], anthracene **19**[102], thienyl groups **20-21**[103,104], sugar functionalised group **22**[105], cobalt carbonyl cluster functionalised group **23**[106,107], 4-fluorophenyl **24**[108], pentafluorphynyl **25**[105], and C_{60} functionalised groups **26-28**[109,110]. The inclusion of these substituents alters the redox and photophysical properties of the complexes (**Figure 12**). There is a report that the different electron-withdrawing and -donating

groups (**29-34**) alter the photophysical properties of the ruthenium complexes.[111,112] Chiral substituents (**35-38**) have also been introduced at the 4′-position of 2,2′:6′,2″-terpyridine (**Figure 12**) in the group of Constable and Housecroft to investigate the possibility of forming an diasteromeric or enantiomeric excesses of products when mixing the *R* and *S* enantiomers with metal ion.[113]

X =
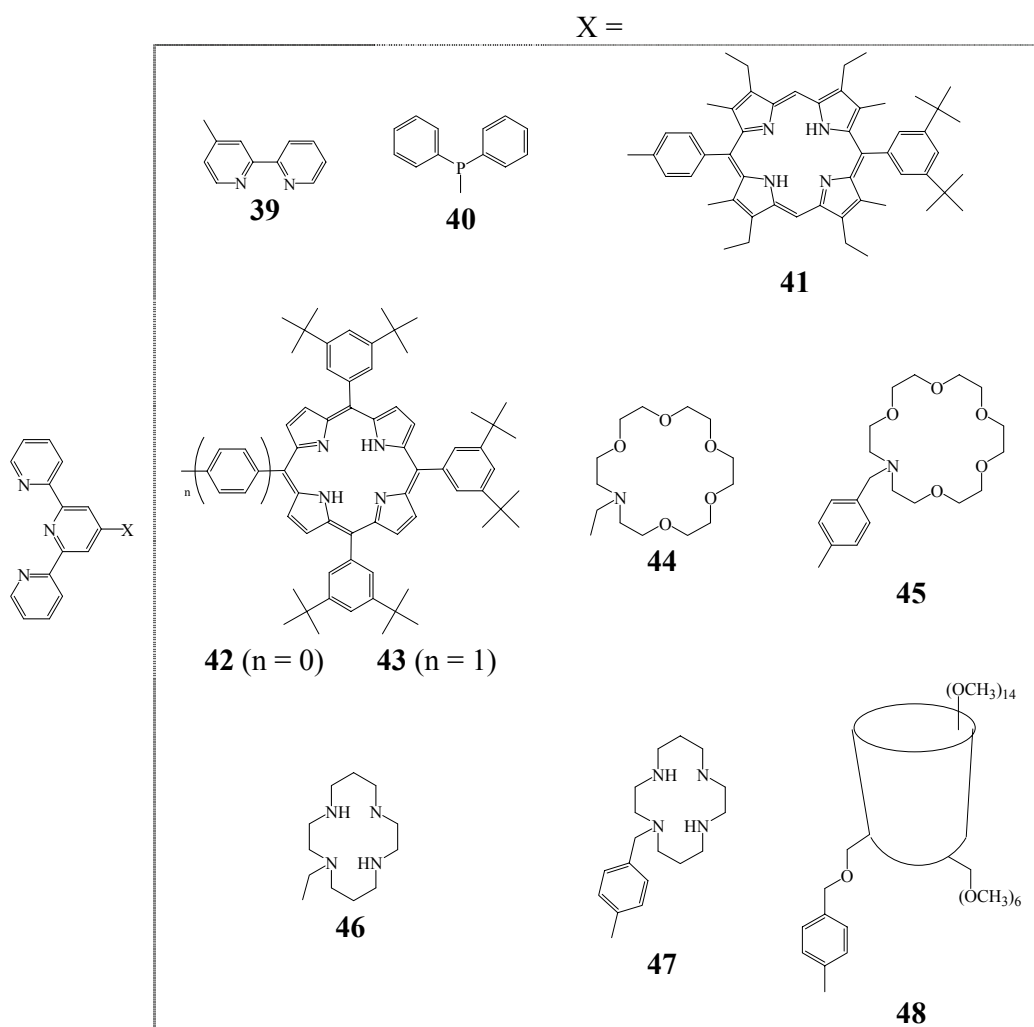
Figure 13. Diagram showing 2,2′:6′,2″-terpyridines with a variety of different functional groups (**39-48**) at the 4′-position.[114-125]

By introducing other binding functional groups, for example 2,2′-bipyridine **39**[114], diphenylphosphino **40**[115,116], porphyrins **41-43**[117-120], macrocycles **44-47**[121,122], and β-cyclodextin **48**[123-125] functional groups, it has been possible to bind a variety of metals or guest molecules (**Figure 13**). Constable and Housecroft's group synthesised ligand **39** with 2,2′-bipyridine directly attached at the 4′-position of 2,2′:6′,2″-terpyridine.

The two different binding domains of ligand **39** can bind to two different metal ions.[114] The 2,2′-bipyridine domain can bind to a Ru(II) metal centre while the 2,2′:6′,2″-terpyridine can bind to Co(II), Fe(II) or Os(II) metal centre.[114] Another ligand **40** contains the diphenylphosphino group at the 4′-position of 2,2′:6′,2″-terpyridine. The phosphorus atom of this diphenylphosphino group acts as a soft metal donor and can bind to soft metal centres, for example Pd(II) and Pt(II).[115,116]

Sauvage[117-120] has reported a few porphyrin-linked 2,2′:6′,2″-terpyridines **41-43** and investigated the photophysical properties of the complexes. The introduction of aza-crown macrocycles **44-47** at the 4′-position of 2,2′:6′,2″-terpyridine not only allows the binding of an appropriate guest but can sequentially trigger a change in the luminescence of the ruthenium complexes.[121,122] Ward *et al.*[121] have reported the synthesis of 4′-substituted and 4′-phenyl-substituted 2,2′:6′,2″-terpyridine with an aza-18-crown-6 group (**44-45**). Martínez-Máñez *et al.*[122] have described the preparation of 4′-substituted and 4′-phenyl-substituted 2,2′:6′,2″-terpyridine with 1,4,8,11-tetraazacyclotetradecane (**46-47**). Pikramenou *et al.*[123-125] have synthesised a 4′-phenyl-substituted 2,2′:6′,2″-terpyridine with β-cyclodextrin **48**. The β-cyclodextrin cavity can bind to a biphenyl group attached at the 4′-position of a 2,2′:6′,2″-terpyridine Os(II) complex. This results in electron transfer from the Ru(II) complex, which contains the β-cyclodextrin unit, through the β-cyclodextrin unit to the Os(II) complex, which contain the biphenyl group.

Ligands with two 2,2′:6′,2″-terpyridine metal-binding domains linked by a spacer can form rod-like complexes or cyclise to form macrocycles depending the rigidity of the spacer. Normally, the spacer has two main roles: (1) to control the supramolecular structure, especially the intercomponent distances and angles, and (2) to control the electronic communication between components through bond energy or electron transfer. Ligands **49-56** (**Figure 14**), which contain rigid spacer groups, were synthesised to investigate the photophysical properties of their dinuclear complexes.[24,126-131]

Ziessel *et al.*[61] have been reported the reaction of ligands **57**, **58** with Fe(II). A deep-blue insoluble compound, very likely a linear polymer, was formed when ligand **57**

reacted with Fe(II). When ligand **58** reacts with Fe(II), a soluble deep-violet solution was obtained. Using electrospray ionisation (ES) mass spectrometric and NMR spectroscopic analysis, it was found that there were two cationic polynuclear iron complexes (a [3+3] and [4+4] metallomacrocycles) present in the solution.
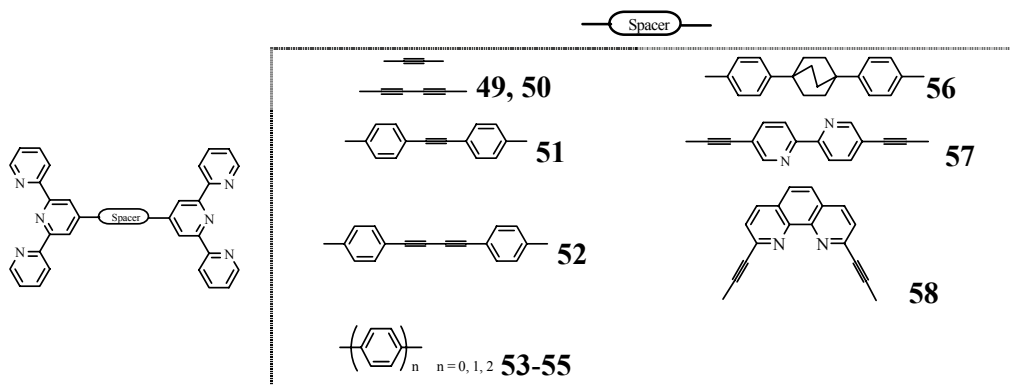
Figure 14. Diagram showing ligands (**49-58**) which contain two 2,2′:6′,2″-terpyridine metal domains with a spacer group linked at the 4′-position.[24,126-131,61]

A few metal-directed assembly systems (**59-63**) which involve ligands containing 2,2′:6′,2″-terpyridine metal-binding domains have been reported by Constable and Housecroft's group (**Figure 15**). A dinuclear octacationic box-like structure **59** is assembled by the reaction of a dicationic bis(2,2′:6′,2″-terpyridine) ligand with iron(II).[59] A [1+1] cyclometallopeptide **60** was obtained after purification by HPLC of the reaction product of a bis(2,2′:6′,2″-terpyridine) peptide-functionalised ligand and iron(II).[132] Similarly, a reaction of a heterotritopic ligand which contains one bis(5,5′-phenyl)-2,2′-bipyridine and two terpyridine metal-binding domains linked by a flexible $(OCH_2)_3O$ spacer, with iron(II) resulted in a [1+1] metallomacrocycle **61**.[133] A single crystal structure of **61** was also obtained. A ligand with a short spacer $(OCH_2)_3O$ linked between the two terpyridine domains reacts with iron(II) to give a [3+3] **62** and a [4+4] **63** metallomacrocycle. These were analysed by NMR spectroscopy and ES-MS.[60]
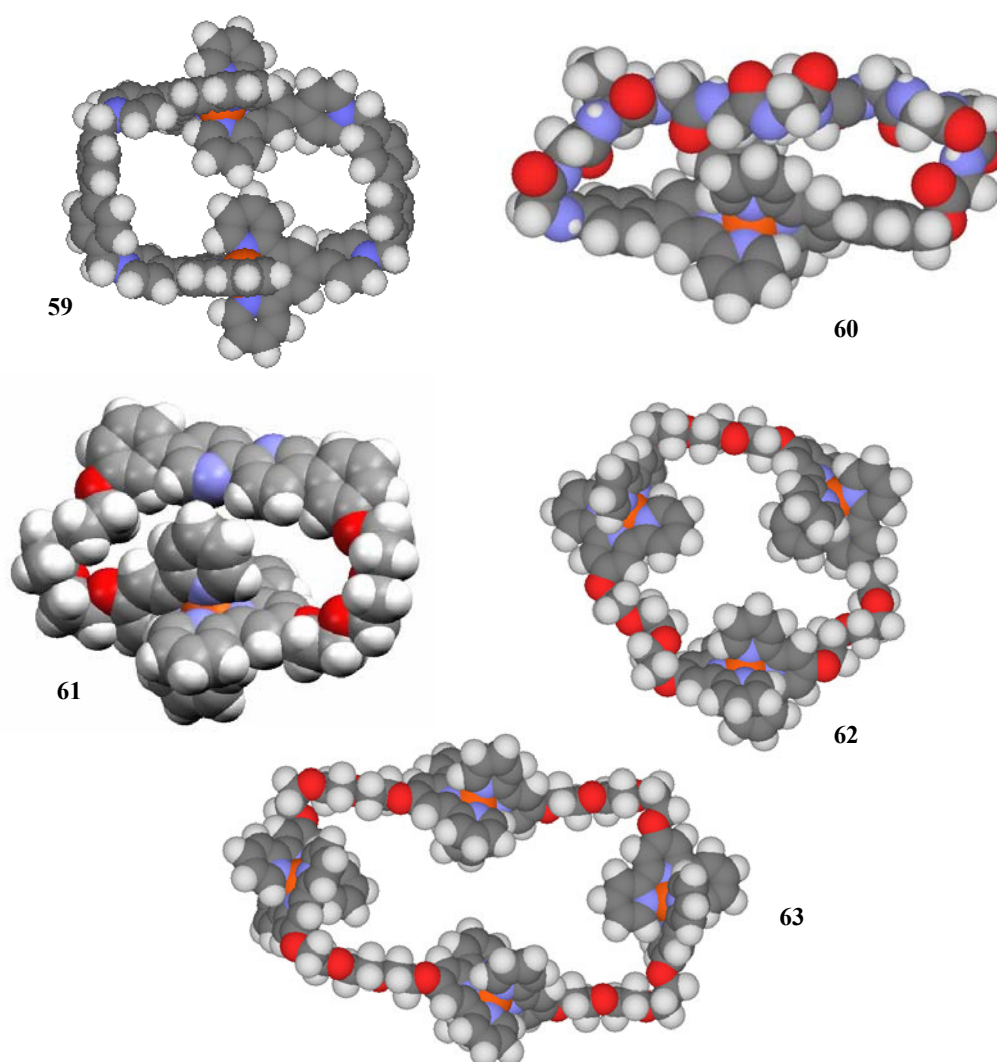
Figure 15. Diagram showing metal-directed assembly systems (**59-63**).[59,132,133,60]

Moore has reported the single crystal structures of [1+1] metallomacrocycles **64-65** formed from the reaction of 1,3-bis(2,2′:6′,2″-terpyridiyl-5-ylmethylsulfanyl)propane [which contains two 2,2′:6′,2″-terpyridine metal-binding domains that linked by a $CH_2S(CH_2)_3SCH_2$ spacer at the 5-position] or 1,4-bis(2,2′:6′,2″-terpyridiyl-5-ylmethylsulfanyl)butane [which contains two 2,2′:6′,2″-terpyridine metal-binding domains that linked by a $CH_2S(CH_2)_4SCH_2$ spacer at the 5-position] with Ni(II) respectively (**Figure 16**).[134] Sauvage has reported a single crystal structure of a double-stranded dinuclear iron(II) helix **66** which resulted from the reaction of Fe(II) with a bis(2,2′:6′,2″-terpyridine) ligand containing 2,2′:6′,2″-terpyridine metal-binding domains linked by a CH_2CH_2 group at the 5-positions (**Figure 16**).[135]

Newkome has described the self-assembly of hexagonal macrocyclic complexes **67-68**, where the ligands contain two 2,2′:6′,2″-terpyridine metal-binding domains. The hexanuclear iron(II) metallomacrocycle **68** was also studied with TEM (transmission electron microscopy) (**Figure 16**).[62]
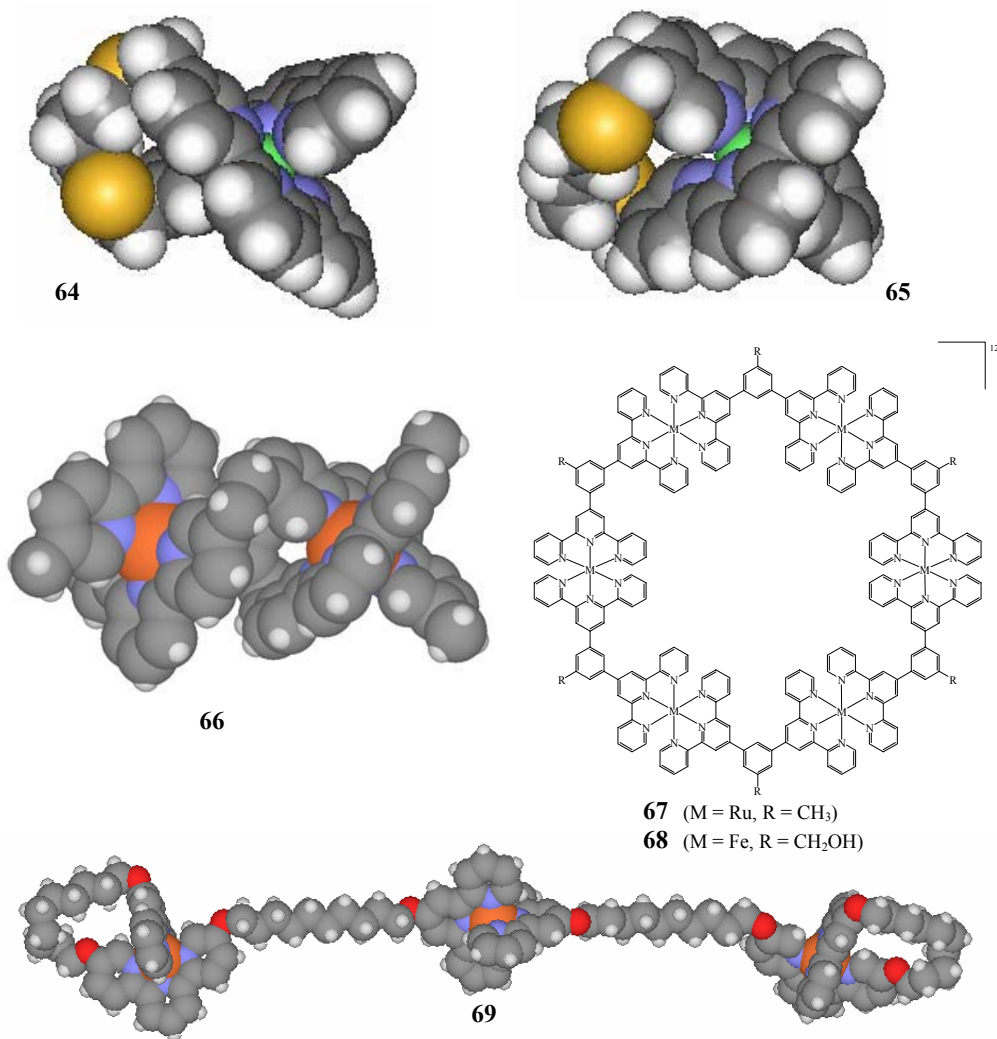
Figure 16. Diagram showing metal directed assembly systems (**64-69**).[134,135,62,136]

A doubly looped (bow tie) structure **69** formed when 3 equivalents of iron(II) reacted with two equivalents of a ligand which contains three 2,2′:6′,2″-terpyridine metal-binding domains linked by flexible $O(CH_2)_{10}O$ groups at the 4′-position and 5-position of the terpyridine domains (**Figure 16**).[136]
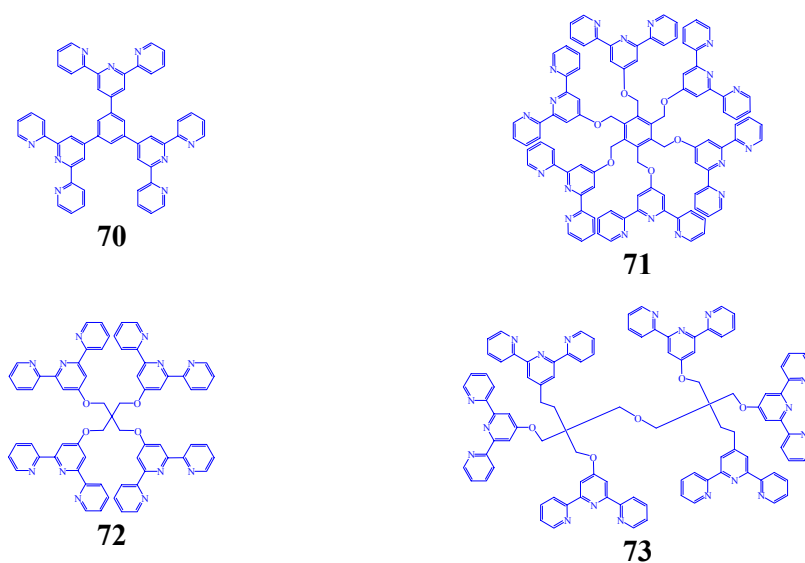
Figure 17. Diagram showing ligands **70-73** which contain multiple 2,2′:6′,2″-terpyridine metal-binding domains.[83]
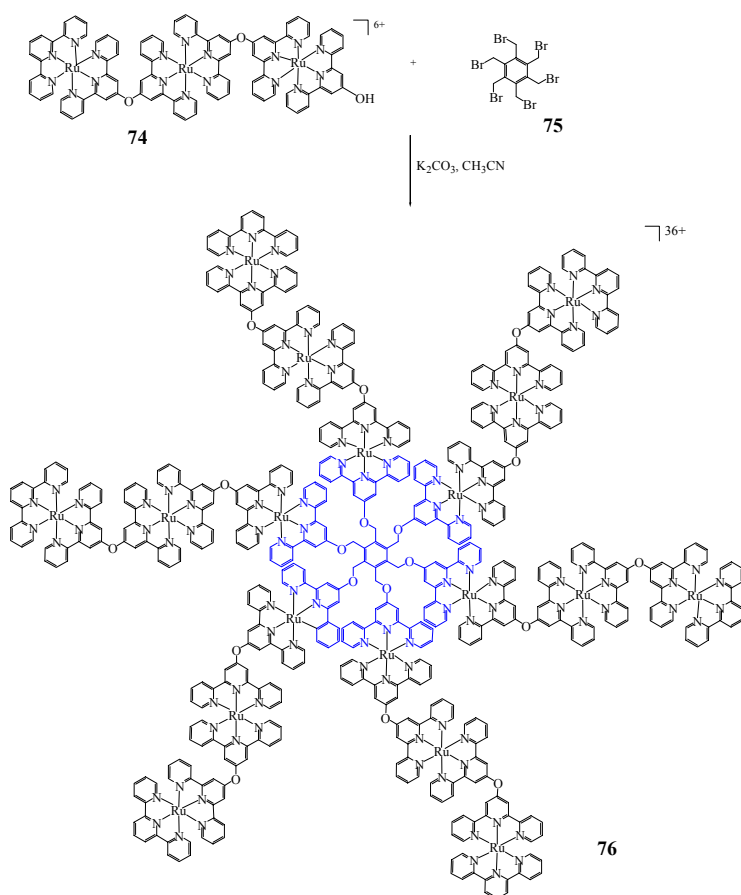
Figure 18. Reaction scheme for the synthesis of the octadecaruthenium complex **76**.[84]

Ligands **70-73** contain multiple 2,2′:6′,2″-terpyridine metal-binding domains and have been used as the dendritic core for building metallodendrimers (**Figure 17**).[83] The triruthenium complex **74** reacted with hexakis(bromomethyl)benzene **75** to give the desired octadecanuclear complex **76** (**Figure 18**). This contains the dendritic core **71**.[84] By using pentaerythritol functionalised with 2,2′:6′,2″-terpyridine to give cores **72**, reaction with the Ru(III) complex **77**, a first generation tetranuclear complex **78** was formed (**Figure 19**). The pentaerythritol functional groups in **78** allow the growth of second generations and resulted in complex **79** (**Figure 19**).[137]
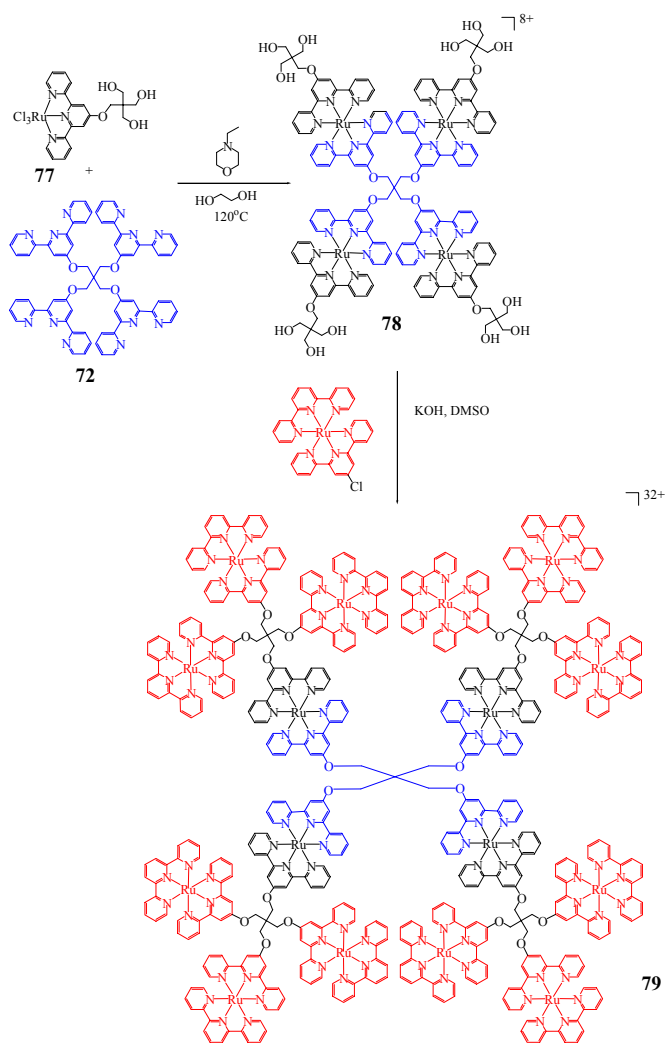
Figure 19. Reaction scheme for the synthesis of metallodendrimers **78** and **79**.[137]

The ligands described above, which contain one or more terpyridine metal-binding domains, illustrate the possibility of building a wide range of supramolecular

architectures. These oligopyridines have proved to be popular choices in self-assembly coordination chemistry.

1.4 Dynamic combinatorial libraries

Combinatorial chemistry has been used to produce a member of different molecules with different combination of several species in the area of pharmaceutical chemistry. The dynamic combinatorial library is based on the concept of combinatorial chemistry.[138-143] Lehn has stated the meaning of a dynamic combinatorial library as follows:

"Dynamic combinatorial libraries are designed as mixtures of components that can reversibly interconvert in a dynamic equilibrium that is driven by molecular recognition of a specific molecular target toward that assembly or a subset of components that form the library constituent best bound to the target."[143]

A dynamic combinatorial library is based on the two main principles of supramolecular chemistry: molecular recognition in interactions of the entities, and self-assembly in generation of the library components. In the library, all members exist in equilibrium. By introducing a template, the desired product may be stabilised. This results from a thermodynamic redistribution within the equilibrium mixture since the collection of molecules can reversibly form the initial building blocks. According to the Le Chatalier's principle, this will not only amplify the concentration of the "best fit" product but also reduce the concentration of the poorer binding product (**Figure 20**).[139]
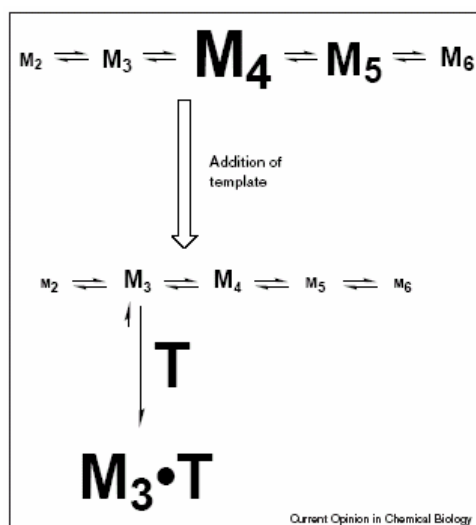
Figure 20. Schematic representation of the interconversion of a series of library members (M) by equilibrium processes and the subsequent product distribution change exerted by a template (T). The size of the letters (M and T) represented the concentration of library components.[139]
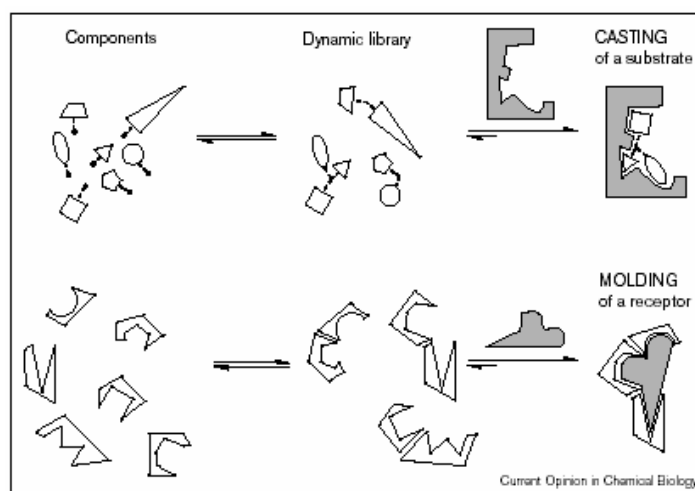
Figure 21. Diagrammatic representation of casting and molding in dynamic combinatorial libraries.[139]

Huc and Lehn have introduced two templating fashions, casting and molding, in dynamic combinatorial libraries (**Figure 21**).[142]

➢ Casting process:

▪ Receptor-induced self-assembly of the complementary substrate from a collection of components serving as building blocks.

- Selection of the optimal substrate from a virtual substrate library.

  e.g. In the presence of B$_4$ lectin, the desired product Λ-*mer*[Fe(***bipy-(GalNHAc)***$_3$]
  was amplified from a library of four stereomers of Λ-*mer*, Δ-*mer*, Δ-*fac* and
  Λ-*fac* iron(II) complexes [(***bipy-(GalNHAc)***) = *N*-acetyl galactropyranose
  functionalised with 2,2′-bipyridine].[139,144]

➢ Molding process:

- Substrate-induced self-assembly of the complementary receptor from a
  collection of structural components.

- Selection of the optimal receptor from a virtual receptor library.

  e.g. The hexanuclear circular helicate, {[Fe$_5$(**80**)$_5$][Cl]}$^{9+}$, was formed
  predominately in the presence of chloride ions (**Figure 22**).[145]
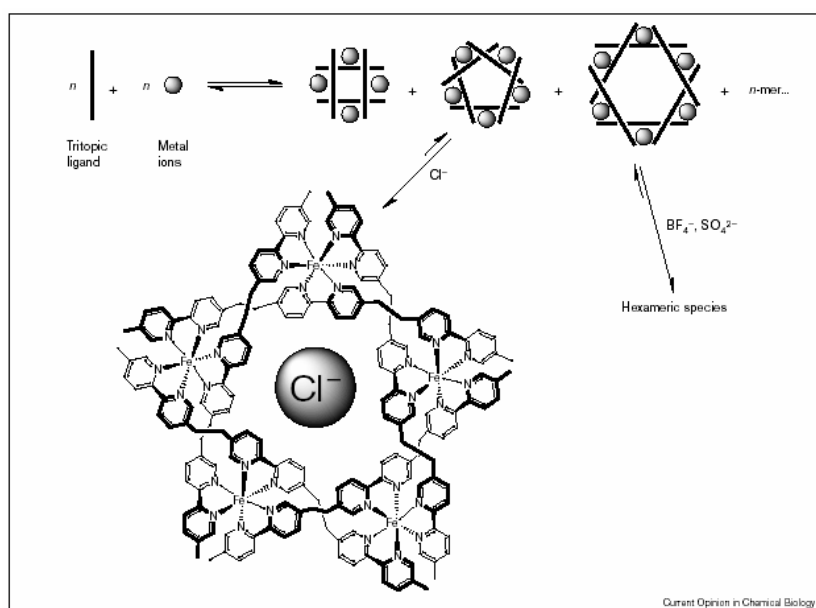
Figure 22. Dynamic combinatorial libraries of circular helicates generated from a
tritopic 2,2′-bipyridine ligand (**80**) and octahedral iron(II) ions.[139]

The above example shows the specific features of the dynamic combinatorial
libraries. They are reversible, recognition-directed and self-assembled in the presence
of the template or target. The dynamic combinatorial libraries offer the following
advantages.[138]

➢ There is no need to synthesise each substance individually since a range of substances is assembled from the libraries.

➢ Product distribution is controlled by the thermodynamic factors and template effects.

➢ There is no need to explicitly identify the library members because only the most strongly bound guest or host will result.

Therefore, many efforts have been made by scientists to seek the correct template that amplifies the desired product.

1.5   Aims

Ligands *L¹-L⁹* and *L¹⁰-L¹⁷* (see the compound labelling scheme in page x & xi), which contain one and two 2,2′:6′,2″-terpyridine metal-binding domains respectively, are synthesised and discussed in Chapter 2 and Chapter 5. Mononuclear Fe(II), Ru(II) and Co(II) complexes formed by ligands *L¹-L⁹* are fully presented in Chapter 3 and Chapter 4. A newly established method for the NMR spectroscopic assignment of Co(II) complexes, and some preliminary studies of combinatorial libraries by mixing two Co(II) complexes, are described in Chapter 4. The ligands *L¹¹-L¹⁴*, *L¹⁶-L¹⁷* containing two 2,2′:6′,2″-terpyridine metal-binding domains that linked by a naphthalene bis(ethyleneoxy) spacer, can formed linear diruthenium(II) complexes with [Ru(*L*)Cl₃] (*L = **terpy*** or *L⁴*) and the complexes are discussed in Chapter 6. Ligands *L¹¹-L¹⁷* can also cyclise to form [*n*+*n*] Fe(II) and Ru(II) metallomacrocycles and these metallomacrocycles are synthesised and presented in Chapter 7.

1.6   References

1.   J.-M. Lehn, *Supramolecular Chemistry. Concepts and perspectives*, VCH, Weinheim, 1995.

2.   F. Vögtle, *Supramolecular Chemistry. An Introduction*, Wiley, Chichester, 1993.

3.   J.-M. Lehn, *Proc. Natl. Acad. Sci. USA*, 2002, **99**, 4763.

4.   J.-M. Lehn, *Science*, 1993, **260**, 1762.

5.   J.-M. Lehn, *Angew. Chem. Int. Ed.*, 1990, **29**, 1304.

6.   J.-M. Lehn, *Angew. Chem. Int. Ed.*, 1988, **27**, 89.

7.   D. Philips, and J. F. Stoddart, *Angew. Chem. Int. Ed.,* 1996, **35**, 1154.

8.   E. Fischer, *Ber. Dtsch. Chem. Ges.*, 1894, **27**, 3985.

9.   J. S. Lindsay, *New J. Chem.*, 1991, **15**, 153.

10.   A. L. Lehninger, *Biochemistry: Molecular Basis of Cell Structure and Function*, Worth, New York, 1970.

11.   J.-M. Lehn, A. Rigault, J. Siegel, J. Harrowfield, B. Chevrier, and D. Moras, *Proc. Natl. Acad. Sci. USA*, 1987, **84**, 2565.

12.   W. Zarges, J. Hall, J.-M. Lehn, and C. Bolm, *Helv. Chim. Acta*, 1991, **74**, 1843.

13.   Picture taken from http://www.ehgonline.net/dnastructure.pdf.

14.   V. Balzani, *Photochem. Photobiol. Sci.*, 2003, **2**, 459.

15.   V. Balzani, A. Credi, F. M. Raymo, and J. F. Stoddart, *Angew. Chem. Int. Ed.*, 2000, **39**, 3348.

16.   P. R. Ashton, R. Ballardini, V. Balzani, A. Credi, K. R. Dress, E. Ishow, C. J. Kleverlaan, O. Kocian, J. A. Preece, N. Spencer, J. F. Stoddart, M. Venturi, and S. Wenger, *Chem. Eur. J.*, 2000, **6**, 3558.

17.   M. C. Jimenez-Molero, C. Dietrich-Buchecker, and J.-P. Sauvage, *Chem. Commun.*, 2003, 1613.

18.   F. Barigelletti, and L. Flamigni, *Chem. Soc. Rev.*, 2000, **29**, 1.

19.   J. P. Sauvage, *Prespectives in Supramolecular Chemistry, Vol 5, Transtion Metals in Supramolecular Chemistry*, Wiley, Chichester, 1999.

20.   E. C. Constable, *Pure and Appl. Chem.*, 1996, **68**, 253.

21.   G. F. Swiegers, and T. J. Malefetse, *Chem. Rev.*, 2000, **100**, 3483.

22.   C. Kaes, A. Katz, and M. W. Hosseini, *Chem. Rev.*, 2000, **100**, 3553.

23.   V. Grosshenny, and R. Ziessel, *J. Organomet. Chem.*, 1993, **453**, C19.

24.   F. Barigelletti, L. Flamigni, V. Balzani, J.-P. Collin, J.-P. Sauvage, A. Sour, E. C. Constable, and A. M. W. Cargill Thompson, *J. Am. Chem. Soc.*, 1994, **116**, 7692.

25.   E. C. Constable, and A. M. W. Cargill Thompson, *J. Chem. Soc., Dalton Trans.*, 1995, 1615.

26.   M. Hissler, A. El-ghayoury, A. Harriman, and R. Ziessel, *Angew. Chem. Int. Ed.*, 1998, **37**, 1717.

27.   S. Encinas, L. Flamigni, F. Barigelletti, E. C. Constable, C. E. Housecroft, E. R. Schofield, E. Figgemeier, D. Fenske, M. Neuburger, J. G. Vos, and M. Zehnder, *Chem. Eur. J.*, 2002, **8**, 137.

28.   E. C. Constable, *Tetrahedron*, 1992, **48**, 10013.

29.   C. Piguet, G. Bernardinelli, and G. Hopfgarten, *Chem. Rev.*, 1997, **97**, 2005.

30.   M. Albrecht, *Chem. Rev.*, 2001, **101**, 3457.

31.   E. C. Constable, M. D. Ward, and D. A. Tocher, *J. Am. Chem. Soc.,* 1990, **112**, 1256.

32.   M.-T. Youinou, R. Ziessel, and J.-M. Lehn, *Inorg. Chem.*, 1991, **30**, 2144.

33.   E. C. Constable, and J. V. Walker, *J. Chem. Soc., Chem. Commun.*, 1992, 884.

34.   B. Hasenknopf, and J.-M. Lehn, *Helv. Chim. Acta*, 1996, **79**, 1643.

35.   G. Baum, E. C. Constable, D. Fenske, and T. Kulke, *Chem. Commun.*, 1997, 2043.

36.   O. Mamula, A. von Zelewsky, and G. Bernardinelli, *Angew. Chem. Int. Ed.*, 1998, **37**, 290.

37.   G. Baum, E. C. Constable, D. Fenske, C. E. Housecroft, and T. Kulke, *Chem. Eur. J.*, 1999, **5**, 1862.

38.   G. Baum, E. C. Constable, D. Fenske, C. E. Housecroft, T. Kulke, M. Neuburger, and M. Zehnder, *J. Chem. Soc., Dalton Trans.*, 2000, 945.

39.   R. L. Paul, S. M. Couchman, J. C. Jeffery, J. A. McCleverty, Z. R. Reeves, and M. D. Ward, *J. Chem. Soc., Dalton Trans.*, 2000, 845.

40.   A. Lützen, M. Hapke, J. Griep-Raming, D. Haase, and W. Saak, *Angew. Chem. Int. Ed.*, 2002, **41**, 2086.

41.   E. C. Constable, I. A. Hougen, C. E. Housecroft, M. Neuburger, S. Schaffner, and L. A. Whall, *Inorg. Chem. Commun.*, 2004, **7**, 1128.

42.   J.-P. Sauvage, *Acc. Chem. Res.*, 1990, **23**, 319.

43.   C. Dietrich-Buchecker, and J.-P. Sauvage, *Tetrahedron*, 1990, **46**, 503.

44.   B. Mohr, M. Weck, J.-P. Sauvage, and R. H. Grubbs, *Angew. Chem. Int. Ed.*, 1997, **36**, 1308.

45. C. Dietrich-Buchecker, and J.-P. Sauvage, *Chem. Commun.*, 1999, 615.

46. F. Diederich, C. Dietrich-Buchecker, J.-F. Nierengarten, and J.-P. Sauvage, *J. Chem. Soc., Chem. Commun.*, 1995, 781.

47. P. Gaviña, and J.-P. Sauvage, *Tetrahedron Lett.*, 1997, **38**, 3521.

48. N. Armaroli, V. Balzani, J.-P. Collin, P. Gaviña, J.-P. Sauvage, and B. Ventura, *J. Am. Chem. Soc.*, 1999, **121**, 4397.

49. P. J. Stang, and B. Olenyuk, *Acc. Chem. Res.*, 1997, **30**, 502.

50. C. J. Jones, *Chem. Soc. Rev.*, 1998, **27**, 289.

51. P. J. Stang, *Chem. Eur. J.*, 1998, **4**, 19.

52. P. J. Stang, and B. Olenyuk, *Angew. Chem. Int. Ed.*, 1996, **35**, 732.

53. P. D. Beer, J. W. Wheeler, and C. P. Moore, *J. Chem. Soc., Dalton Trans.*, 1992, 2667.

54. A. Bilyk, and M. M. Harding, *J. Chem. Soc., Dalton Trans.*, 1994, 77.

55. A. Bilyk, M. M. Harding, P. Turner, and T. W. Hambley, *J. Chem. Soc., Dalton Trans.*, 1994, 2783.

56. A. Bilyk, M. M. Harding, P. Turner, and T. W. Hambley, *J. Chem. Soc., Dalton Trans.*, 1995, 2549.

57. M. A. Houghton, A. Bilyk, M. M. Harding, P. Turner, and T. W. Hambley, *J. Chem. Soc., Dalton Trans.*, 1997, 2725.

58. P. I. Anderberg, J. J. Turner, K. J. Evans, L. M. Hutchins, and M. M. Harding, *Dalton Trans.*, 2004, 1708.

59. E. C. Constable, and E. Schofield, *Chem. Commun.*, 1998, 403.

60. E. C. Constable, C. E. Housecroft, and C. B. Smith, *Inorg. Chem. Commun.*, 2003, **6**, 1011.

61. F. M. Romero, R. Ziessel, A. Dupont-Gervais, and A. V. Dorsselaer, *Chem. Commun.*, 1996, 551.

62. G. R. Newkome, T. J. Cho, C. N. Moorefield, R. Cush, P. S. Russo, L. A. Godínez, M. J. Saunders, and P. Mohapatra, *Chem. Eur. J.*, 2002, **8**, 2946.

63. M. Ruben, J. Rojo, F. J. Romero-Salguero, L. H. Uppadine, and J.-M. Lehn, *Angew. Chem. Int. Ed.*, 2004, **43**, 3644.

64. J. R. Nitschke, and J.-M. Lehn, *Proc. Natl. Acad. Sci. USA*, 2003, **100**, 11970.

65. P. N. W. Baxter, J.-M. Lehn, B. O. Kneisel, and D. Fenske, *Chem. Commun.*, 1997, 2231.

66. E. Breuning, M. Ruben, J.-M. Lehn, F. Renz, Y. Garcia, V. Ksenofontov, P. Gütlich, E. Wegelius, and K. Rissanen, *Angew. Chem. Int. Ed.*, 2000, **39**, 2504.

67. M. Ruben, E. Breuning, J.-P. Gisselbrecht, and J.-M. Lehn, *Angew. Chem. Int. Ed.*, 2000, **39**, 4139.

68. E. Breuning, U. Ziener, J.-M. Lehn, E. Wegelius, and K. Rissanen, *Eur. J. Inorg. Chem.*, 2001, 1515.

69. J. P. Plante, P. D. Jones, D. R. Powell, and T. E. Glass, *Chem. Commun.*, 2003, 336.

70. R. Ziessel, L. Charbonnière, M. Cesario, T. Prangé, and H. Nierengarten, *Angew. Chem. Int. Ed.*, 2002, **41**, 975.

71. T. Bark, A. von Zelewsky, D. Rappoport, M. Neuburger, S. Schaffner, J. Lacour, and J. Jodry, *Chem. Eur. J.*, 2004, **10**, 4839**.**

72. P. N. W. Baxter, H. Sleiman, J.-M. Lehn, and K. Rissanen, *Angew. Chem. Int. Ed.*, 1997, **36**, 1294.

73. P. N. W. Baxter, G. S. Hanan, and J.-M. Lehn, *Chem. Commun.*, 1996, 2019.

74. P. N. W. Baxter, J.-M. Lehn, B. O. Kneisel, G. Baum, and D. Fenske, *Chem. Eur. J.*, 1999, **5**, 113.

75. W.-Y. Sun, M. Yoshizawa, T. Kusukawa, and M. Fujita, *Curr. Opin. Chem. Bio.*, 2002, **6**, 757.

76. M. Aoyagi, S. Tashiro, M. Tominaga, K. Biradha, and M. Fujita, *Chem. Commun.*, 2002, 2036.

77. M. Yoshizawa, M. Nagao, K. Umemoto, K. Biradha, M. Fujita, S. Sakamoto, and K. Yamaguchi, *Chem. Commun.*, 2003, 1808.

78. M. D. Ward, J. A. McCleverty, and J. C. Jeffery, *Coord. Chem. Rev.*, 2001, **222**, 251.

79. P. L. Jones, K. J. Byrom, J. C. Jeffery, J. A. McCleverty, and M. D. Ward, *Chem. Commun.*, 1997, 1361.

80. Z. R. Bell, J. C. Jeffery, J. A. McCleverty, and M. D. Ward, *Angew. Chem. Int. Ed.*, 2002, **41**, 2515.

81. R. L. Paul, Z. R. Bell, J. C. Jeffery, J. A. McCleverty, and M. D. Ward, *Proc. Natl. Acad. Sci. USA*, 2002, **99**, 4883.

82. C. M. Hartshorn, and P. J. Steel, *Chem. Commun.*, 1997, 541.

83. E. C. Constable, *Chem. Commun.*, 1997, 1073.

84. E. C. Constable, and P. Harverson, *Inorg. Chim. Acta*, 1996, **252**, 9.

85. E. C. Constable, C. E. Housecroft, and I. Poleschak, *Inorg. Chem. Commun.*, 1999, **2**, 565.

86. E. C. Constable, C. E. Housecroft, M. Neuburger, I. Poleschak, and M. Zehnder, *Polyhedron*, 2003, **22**, 93.

87. D. P. Funeriu, J.-M. Lehn, K. M. Fromm, and D. Fenske, *Chem. Eur. J.*, 2002, **6**, 2103.

88. R. Krämer, J.-M. Lehn, and A. Marquis-Rigault, *Proc. Natl. Acad. Sci. USA*, 1993, **90**, 5394.

89. A. Livoreil, C. Dietrich-Buchecker, and J.-P. Sauvage, *J. Am. Chem. Soc.*, 1994, **116**, 9399.

90. A. Livoreil, J.-P. Sauvage, N. Armaroli, V. Balzani, L. Flamigni, and B. Ventura, *J. Am. Chem. Soc.*, 1997, **119**, 12114.

91. D. J. Cárdenas, A. Livoreil, and J.-P. Sauvage, *J. Am. Chem. Soc.*, 1996, **118**, 11980.

92. S. Kang, S. A. Vignon, H.-R. Tseng, and J. F. Stoddart, *Chem. Eur. J.*, 2004, **10**, 2555.

93. B. Cabezon, J. Cao, F. M. Raymo, J. F. Stoddart, A. J. P. White, and D. J. Williams, *Chem. Eur. J.*, 2000, **6**, 2262.

94. M. Fujita, J. Yazaki, and K. Ogura, *J. Am. Chem. Soc.*, 1990, **112**, 5645.

95. G. T. Morgan, and F. H Burstall, *J. Chem. Soc.*, 1932, 20.

96. G. T. Morgan, and F. H Burstall, *J. Chem. Soc.*, 1937, 1649.

97. E. C. Constable, *Adv. Inorg. Chem. Radiochem.*, 1987, **30**, 69.

98. V. Balzani, and A. Juris, *Coord. Chem. Rev.*, 2001, **211**, 97.

99. V. Balzani, A. Juris, M. Venturi, S. Campagna, and S. Serroni, *Chem. Rev.*, 1996, **96**, 759.

100. J.-P. Sauvage, J.-P. Collin, J.-C. Chambron, S. Guillerez, C. Coudret, V. Balzani, F. Barigelletti, L. De Cola, and L. Flamigni, *Chem. Rev.*, 1994, **94**, 993.

101. E. C. Constable, A. J. Edwards, R. Martínez-Máñez, P. R. Raithby, and A. M. W. Cargill Thompson, *J. Chem. Soc., Dalton Trans.*, 1994, 645.

102. G. Albano, V. Balzani, E. C. Constable, M. Maestri, and D. R. Smith, *Inorg. Chim. Acta*, 1998, **277**, 225.

103. E. C. Constable, R. Handel, C. E. Housecroft, M. Neuburger, E. R. Schofield, and M. Zehnder, *Polyhedron*, 2004, **23**, 135.

104. E. Figgemeier, V. Aranyos, E. C. Constable, R. W. Handel, C. E. Housecroft, C. Risinger, A. Hagfeldt, and E. Mukhtar, *Inorg. Chem. Commun.*, 2004, **7**, 117.

105. E. C. Constable, B. Kariuki, and A. Mahmood, *Polyhedron*, 2003, **22**, 687.

106. E. C. Constable, C. P. Hart, and C. E. Housecroft, *Appl. Organomet. Chem.*, 2003, **17**, 383.

107. E. C. Constable, C. E. Housecroft, L. A. Johnston, D. Armspach, M. Neuburger, and M. Zehnder, *Polyhedron*, 2001, **20**, 483.

108. E. C. Constable, M. Neuburger, D. R. Smith, and M. Zehnder, *Inorg. Chim. Acta*, 1998, **275-276**, 359.

109. D. Armspach, E. C. Constable, F. Diederich, C. E. Housecroft, and J.-F. Nierengarten, *Chem. Eur. J.*, 1998, **4**, 723.

110. D. Armspach, E. C. Constable, F. Diederich, C. E. Housecroft, and J.-F. Nierengarten, *Chem. Commun.*, 1996, 2009.

111. M. Maestri, N. Armaroli, V. Balzani, E. C. Constable, and A. M. W. Cargill Thompson, *Inorg. Chem.*, 1995, **34**, 2759.

112. E. C. Constable, and A. M. W. Cargill Thompson, *Polyhedron*, 1992, **11**, 2707.

113. E. C. Constable, T. Kulke, M. Neuburger, and M. Zehnder, *New J. Chem.*, 1997, **21**, 1091.

114. E. C. Constable, E. Figgemeier, C. E. Housecroft, J. Olsson, and Y. C. Zimmermann, *Dalton Trans.*, 2004, 1918.

115. E. C. Constable, C. E. Housecroft, M. Neuburger, A. G. Schneider, B. Springler, and M. Zehnder, *Inorg. Chim. Acta*, 2000, **300-302**, 49.

116. E. C. Constable, C. E. Housecroft, M. Neuburger, A. G. Schneider, and M. Zehnder, *J. Chem. Soc., Dalton Trans.*, 1997, 2427.

117. L. Flamigni, F. Barigelletti, N. Armaroli, J.-P. Collin, I. M. Dixon, J.-P. Sauvage, and J. A. G. Williams, *Coord. Chem. Rev.*, 1999, **190-192**, 671.

118. J.-P. Collin, A. Harriman, V. Heitz, F. Odobel, and J.-P. Sauvage, *Coord. Chem. Rev.*, 1996, **148**, 63.

119. A. Harriman, F. Odobel, and J.-P. Sauvage, *J. Am. Chem. Soc.*, 1995, **117**, 9461.

120. J.-P. Collin, V. Heitz, and J.-P. Sauvage, *Tetrahedron Lett.*, 1991, **32**, 5977.

121. B. Whittle, S. R. Batten, J. C. Jeffery, L. H. Rees, and M. D. Ward, *J. Chem. Soc., Dalton Trans.*, 1996, 4249.

122. M. E. Padilla-Tosta, J. M. Lloris, R. Martónez-Máñez, A. Benito, J. Soto, T. Pardo, M. A. Miranda, and M. D. Marcos, *Eur. J. Inorg. Chem.*, 2000, 741.

123. J. M. Haider, M. Chavarot, S. Weidner, I. Sadler, R. M. Williams, L. De Cola, and Z. Pikramenou, *Inorg. Chem.*, 2001, **40**, 3912.

124. J. M. Haider, and Z. Pikramenou, *Eur. J. Inorg. Chem.*, 2001, 189.

125. S. Weidner, and Z. Pikramenou, *Chem. Commun.*, 1998, 1473.

126. A. Harriman, and R. Ziessel, *Chem. Commun.*, 1996, 1707.

127. V. Grosshenny, A. Harriman, J.-P. Gisselbrecht, and R. Ziessel, *J. Am. Chem. Soc.*, 1996, **118**, 10315.

128. V. Grosshenny, A. Harriman, and R. Ziessel, *Angew. Chem. Int. Ed.*, 1995, **34**, 1100.

129. A. C. Benniston, V. Grosshenny, A. Harriman, and R. Ziessel, *Angew. Chem. Int. Ed.*, 1994, **33**, 1884.

130. F. Barigelletti, L. Flamigni, V. Balzani, J.-P. Collin, J.-P. Sauvage, A. Sour, E. C. Constable, and A. M. W. Cargill Thompson, *J. Chem. Soc., Chem. Commun.*, 1993, 942.

131. F. Barigelletti, L. Flamigni, J.-P. Collin, and J.-P. Sauvage, *Chem. Commun.*, 1997, 333.

132. E. C. Constable, C. E. Housecroft, and S. Mundwiler, *Dalton Trans.*, 2003, 2112.

133. C. B. Smith, E. C. Constable, C. E. Housecroft, and B. M. Kariuki, *Chem. Commun.*, 2002, 2068.

134. G. U. Priimov, P. Moore, P. K. Maritim, P. K. Butalanyi, and N. W. Alcock, *J. Chem. Soc., Dalton Trans.*, 2000, 445.

135. G. Rapenne, B. T. Patterson, J.-P. Sauvage, and F. R. Keene, *Chem. Commun.*, 1999, 1853.

136. E. C. Constable, and D. Phillips, *Chem. Commun.*, 1997, 827.

137. E. C. Constable, C. E. Housecroft, M. Cattalini, and D. Phillips, *New J. Chem.*, 1998, **22**, 193.

138. S. J. Rowan, S. J. Cantrill, G. R. L. Cousins, J. K. M. Sanders, and J. F. Stoddart, *Angew. Chem. Int. Ed.*, 2002, **41**, 898.

139. G. R. L. Cousins, S.-A. Poulsen, and J. K. M. Sanders, *Curr. Opin. Chem. Biol.*, 2000, **4**, 270.

140. J.-M. Lehn, and A. V. Eliseev, *Science*, 2001, **291**, 2331.

141. J.-M. Lehn, *Chem. Eur. J.*, 1999, **5**, 2455.

142. I. Huc, and J.-M. Lehn, *Proc. Natl. Acad. Sci. USA*, 1997, **94**, 2106.

143. V. Goral, M. I. Nelen, A. V. Eliseev, and J.-M. Lehn, *Proc. Natl. Acad. Sci. USA*, 2001, **98**, 1347.

144. S. Sakai, Y. Shigemasa, and T. Sasaki, *Tetrahedron Lett.*, 1997, **38**, 8145.

145. B. Hasenknopf, J.-M. Lehn, N. Boumediene, A. Dupont-Gervais, A. V. Dorsselaer, B. Kneisel, and D. Fenske, *J. Am. Chem. Soc.*, 1997, **119**, 10956.

Chapter 2

Synthesis of 4′-Substituted-2,2′:6′,2″-Terpyridine Ligands

2,2′:6′,2″-Terpyridine is a molecule with three pyridine rings connected together through the α positions of the nitrogen. The synthesis was first reported by Morgan in 1932.[1,2] It was obtained from the oxidative coupling of pyridine using $FeCl_3$ at elevated temperature and pressure in a steel autoclave.

Besides the coupling methodology mentioned above, certain general strategies were used to synthesise the 2,2′:6′,2″-terpyridine and its derivatives. The Hantzsch synthesis is one of the oldest methods used to synthesise pyridine rings.[3] This reaction involves reaction of a β-ketoester or other activated methylene compound with an aldehyde in the presence of ammonia (**Scheme 1**).
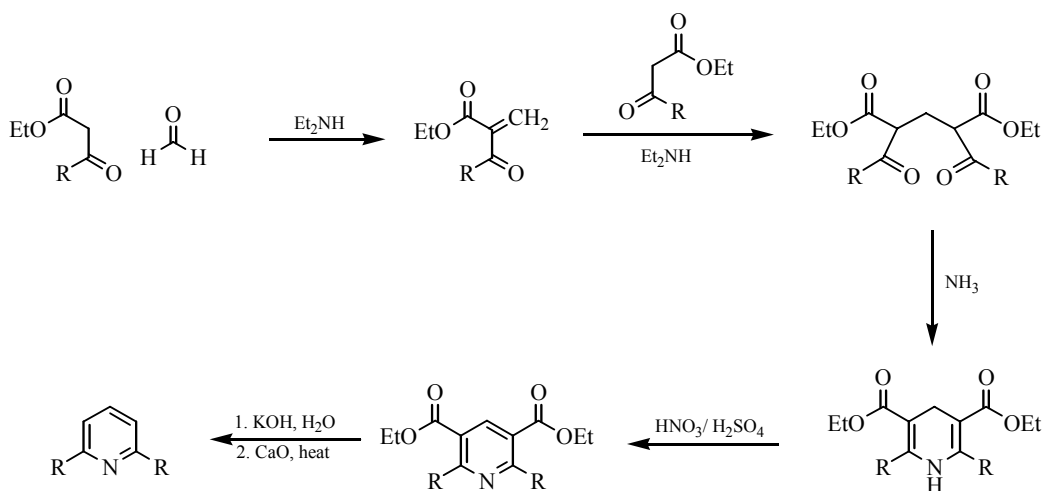
Scheme 1. The Hantzsch pyridine synthesis.

The Kröhnke synthesis is another method for the synthesis of pyridine rings.[4] This reaction involves a ring closure of a 1,5-diketone intermediate by ammonium acetate. The 1,5-diketone intermediate was obtained by Michael addition[5] of an unsaturated ketone with a pyridinium salt (**Scheme 2**). In comparison with the Hantzsch reaction, there is no formal oxidative dehydrogenation reaction, with the required oxidation of the dihydropyridine intermediate being achieved by the loss of pyridinium.
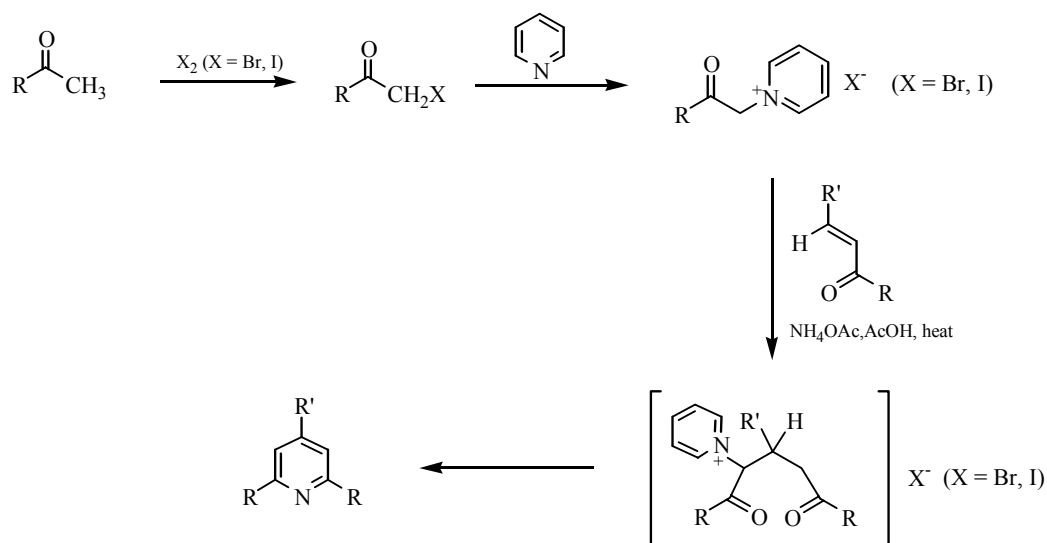
Scheme 2. The Kröhnke pyridine synthesis.

Potts and co-workers reported another method which involved methyl ketone enolates as a reaction intermediate. These are generated with potassium *tert*-butoxide and further react with α-oxoketene dithioacetals to form 4′-methylthio-2,2′:6′,2″-terpyridine. The α-oxoketene dithioacetals are prepared from 2-acetylpyridine by reaction with CS_2 and CH_3I. Ring closure with ammonium acetate of the enedione intermediate results in 4′-methylthio-2,2′:6′,2″-terpyridine (**Scheme 3**).[6-9]
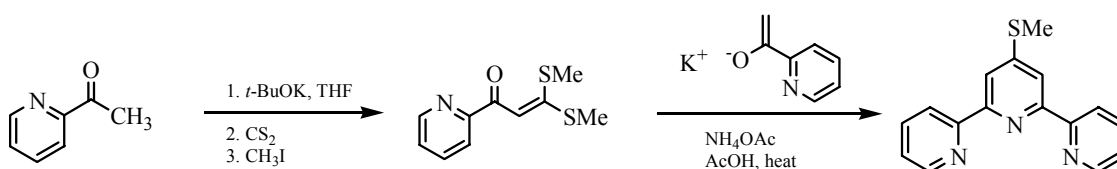
Scheme 3. The Potts' terpyridine synthesis.

By introducing other functional groups onto the 4′-position of the 2,2′:6′,2″-terpyridines described above, other 4′-substituted-2,2′:6′,2″-terpyridines can be synthesised.[10-14]

In this chapter, the syntheses of several 4′-substituted-2,2′:6′,2″-terpyridine ligands (***L¹-L⁹***) are discussed. Most of these 4′-substituted-2,2′:6′,2″-terpyridine ligands

contain polyethyleneoxy chains and differ from one another in the length of the chains, in the terminal domains or in the linkages.
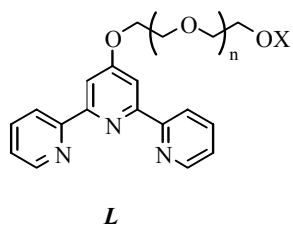
L	n	X
L^1	0	H
L^2	1	H
L^3	2	H
L^5	0	CH_2-2-naphthyl
L^6	1	CH_2-2-naphthyl
L^7	2	CH_2-2-naphthyl
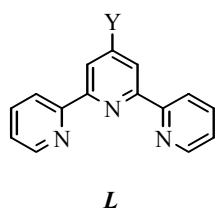
L	Y
L^4	O-CH_2-2-naphthyl
L^8	O-CH_2-9-anthryl
L^9	S-2-naphthyl

2.1   Synthesis

Different substituents can be introduced at the 4′-position of preformed 2,2′:6′,2″-terpyridine ligands by nucleophilic substitution as shown in **Scheme 4**. Starting with 4′-hydroxy-2,2′:6′,2″-terpyridine (**HO-terpy**), an oxygen nucleophile is generated by deprotonating the hydroxyl group, which subsequently reacts with electrophiles to form the desired substituents.[15-17] Alternatively, one can start with 4′-chloro-2,2′:6′,2″-terpyridine (**Cl-terpy**) as an electrophile to react with nucleophilic reagents such as X-SH, X-OH, X-NH_2.[14,18-30]

The syntheses of different 4′-substituted-2,2′:6′,2″-terpyridine ligands are described below. The ligands **L^4-L^9** were designed with a tridentate binding site for complexation with metal ions and with terminal domains (i.e. 2-naphthyl or 9-anthryl

domains). These have potential for π-π stacking interactions either between like molecules or with appropriate substrates.[31-35] The 2,2′:6′,2″-terpyridine and naphthyl or anthryl domains were connected by different linking groups, which were also important for controlling potential intermolecular interactions.
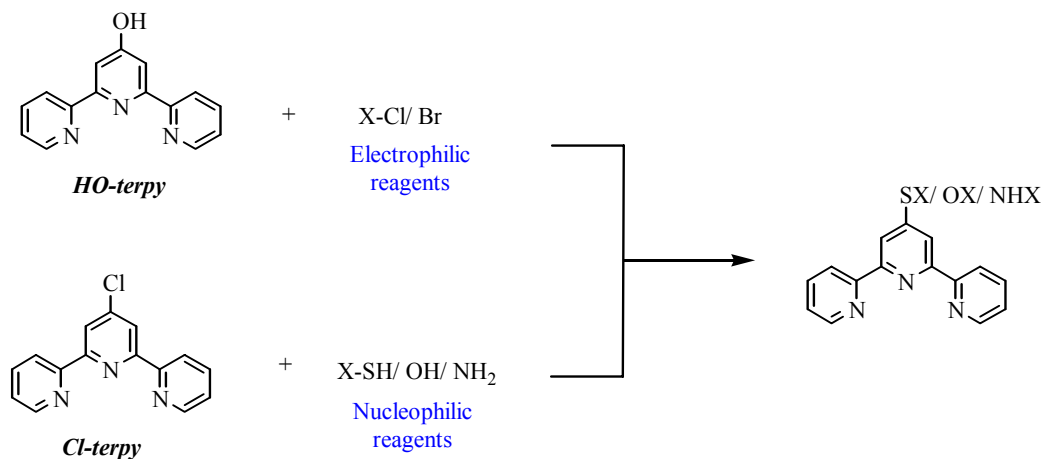
Scheme 4. Nucleophilic substitution reactions to prepare 4′-substituted-2,2′:6′,2″-terpyridines.

The syntheses of 4′-(2-hydroxyethoxy)-2,2′:6′,2″-terpyridine (**L^1**), 4′-[2-(2-hydroxyethoxy)ethoxy]-2,2′:6′,2″-terpyridine (**L^2**) and 4′-{2-[2-(2-hydroxyethoxy)ethoxy]ethoxy}-2,2′:6′,2″-terpyridine (**L^3**) are depicted in **Scheme 5**.[15,16]
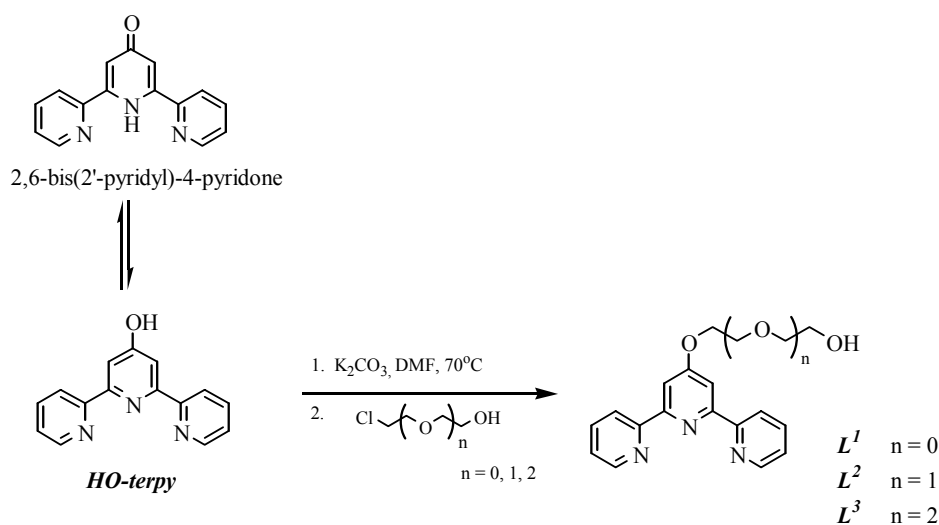
Scheme 5. Syntheses of **L^1**, **L^2** and **L^3**.

L^1, L^2 and L^3 were prepared from 4′-hydroxy-2,2′:6′,2″-terpyridine (**HO-terpy**), which is a tautomer of 2,6-bis(2′-pyridyl)-4-pyridone[36,37], $ClCH_2(CH_2OCH_2)_nCH_2OH$ in which n = 0, 1, 2 and K_2CO_3 in DMF at 70°C for 2 days. These reactions gave the desired products in 45-56% yield after work up.

Treatment of **HO-terpy**, K_2CO_3 and 2-bromomethylnaphthalene in DMF at 70°C for 3 days followed by recrystallisation from methanol gave the 4′-(naphthalen-2-ylmethoxy)-2,2′:6′,2″-terpyridine (L^4) as white fine needles in 48% yield (**Scheme 6**).[38-40]
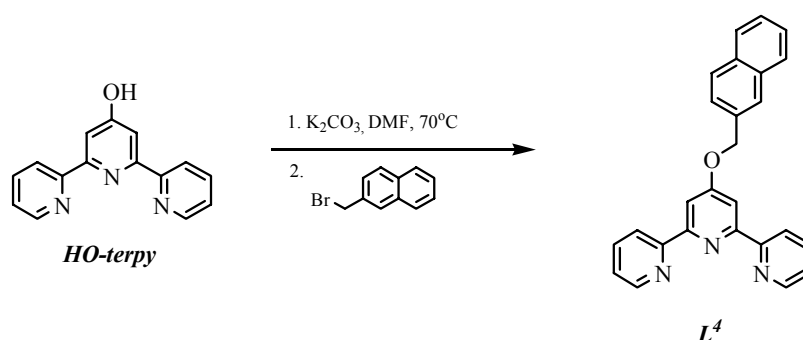
Scheme 6. Synthesis of L^4.

4′-[2-(Naphthalen-2-ylmethoxy)ethoxy]-2,2′:6′,2″-terpyridine (L^5), 4′-{2-[2-(naphthalene-2-ylmethoxy)ethoxy]ethoxy}-2,2′:6′,2″-terpyridine (L^6) and 4′-(2-{2-[2-(naphthalen-2-ylmethoxy)ethoxy]ethoxy}ethoxy)-2,2′:6′,2″-terpyridine (L^7) were prepared from L^1, L^2 and L^3 respectively in 68%, 53% and 15% yields. Treatment of L^1, L^2 and L^3, NaH and 2-bromomethylnaphthalene in THF at 80°C for 2-3 days, followed by work up using alumina column chromatography with CH_2Cl_2/ 1% CH_3OH as eluent resulted in L^5 as a white powder, and L^6 and L^7 as pale yellow oily liquids (**Scheme 7**).[41]
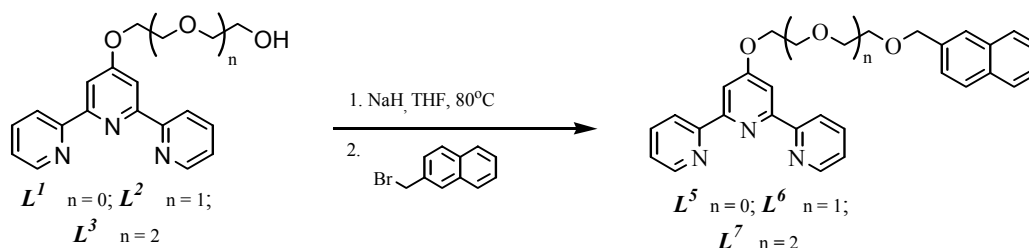
Scheme 7. Syntheses of L^5-L^7.

4′-(Anthracen-9-ylmethoxy)-2,2′:6′,2″-terpyridine (***L^8***) was prepared by a similar method for synthesising ***L^4*** (**Scheme 8**). Treatment of ***HO-terpy***, K_2CO_3 and 9-bromomethylanthracene in DMF at 70°C for 1 week in the dark followed by column chromatography (alumina, CH_2Cl_2/ hexane 3:1 and then CH_2Cl_2/ hexane 2:1) gave ***L^8*** as a yellow powder in 15% yield.[42-44] The product is stored in the dark as it tends to decompose in sunlight.
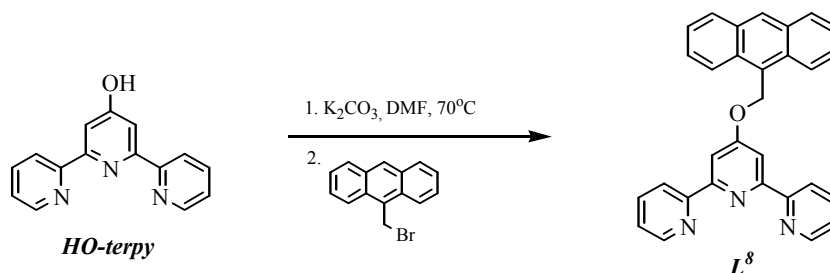
Scheme 8. Synthesis of ***L^8***.

Heating 4′-chloro-2,2′:6′,2″-terpyridine (***Cl-terpy***) and naphthalene-2-thiol at 200°C for 2 days, followed by column chromatography (alumina, CH_2Cl_2/ hexane 2:1), gave the white product 4′-(naphthalen-2-ylsulfanyl)-2,2′:6′,2″-terpyridine (***L^9***) in 67% yield (**Scheme 9**).[45]
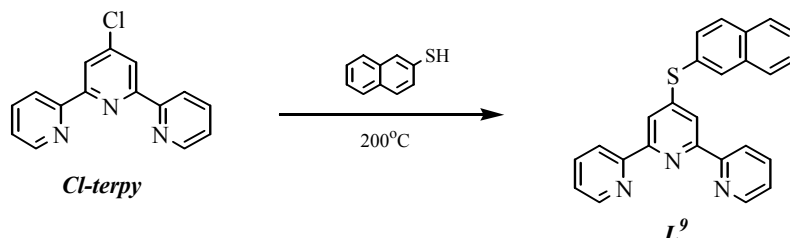
Scheme 9. Synthesis of ***L^9***.

2.2 ^{1}H NMR spectroscopic characterisation

All the ligands were characterised by ^{1}H NMR spectroscopy in $CDCl_3$ solution. The spectroscopic signatures of the ligands compare well with those of other terpy systems, and the terpyridine proton signals are similar in all ligands with the exception of $H^{T3′}$ (the atom labelling scheme is given in **Table 2** and **Table 3**) which

is subject to the influence of the 4′-substituents attached to the terpyridine domain (**Table 1**).[17,46-48]

The ^{1}H NMR spectra of CDCl₃ solutions of the ligands **L¹**, **L²** and **L³** have the usual features of other terpyridine based ligands.[17,46-48] The terpyridine proton signals are essentially the same as those in 4′-(2-propyn-1-oxy)-2,2′:6′,2″-terpyridine (**poterpy**).[17] There are five signals in the aromatic region and the ethyleneoxy spacer signals are found between δ 3.6-4.5 (**Table 2**).

L³ has the longest spacer group of the three ligands **L¹**, **L²**, **L³**. There are five signals in the aromatic region excluding the signal for CHCl₃ (**Figure 1**). The assignment of the spacer protons was made by COSY and NOESY techniques and confirmed by HMQC and HMBC spectroscopy. The triplet in the ^{1}H NMR spectrum at δ 4.42, which exhibits an NOE signal to $H^{T3'}$ at δ 8.05, is assigned to H^{S1} (**Figure 2a**). The signal for H^{S1} gives a COSY cross peak to the signal for H^{S2} at δ 3.94 (**Figure 3**). The signal for H^{S2} exhibits an NOE signal to the signal at δ 3.77 and this signal is assigned to H^{S3} (**Figure 2b**). The signal for H^{S3} gives a COSY cross peak to the signal for H^{S4} at δ 3.69 (**Figure 3**). The signal for H^{S4} exhibits an NOE signal to the signal at δ 3.62, which is assigned to H^{S5} (**Figure 2b**). Finally, the signal for H^{S5} gives a COSY cross peak to the signal at δ 3.73, and this signal is assigned to H^{S6} (**Figure 3**).
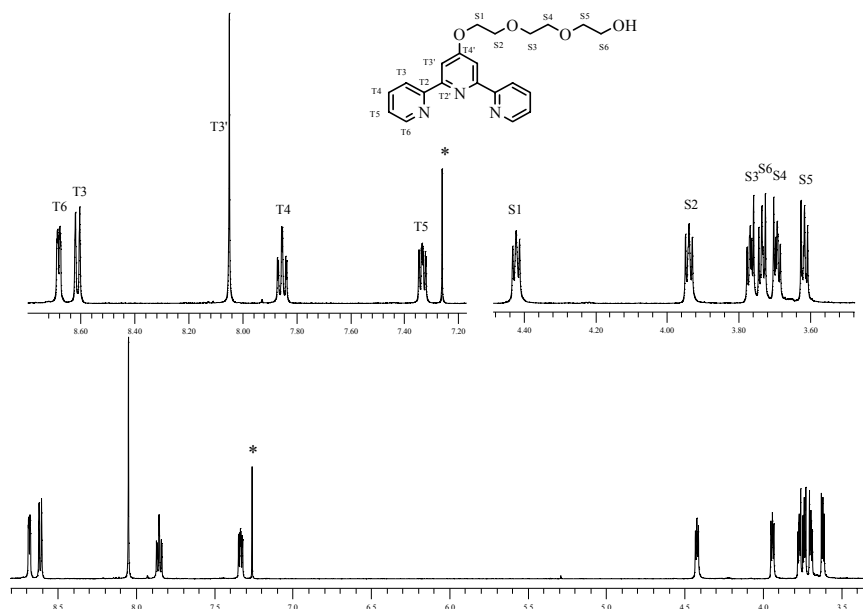
Figure 1. ^{1}H NMR (500 MHz) spectrum of **L³** in CDCl₃ solution at room temperature. (the signal marked * is the signal for CHCl₃)

Figure 2. NOESY spectrum (500 MHz) of L^3 in CDCl$_3$ solution at room temperature. (the signal marked * is the signal for CHCl$_3$)
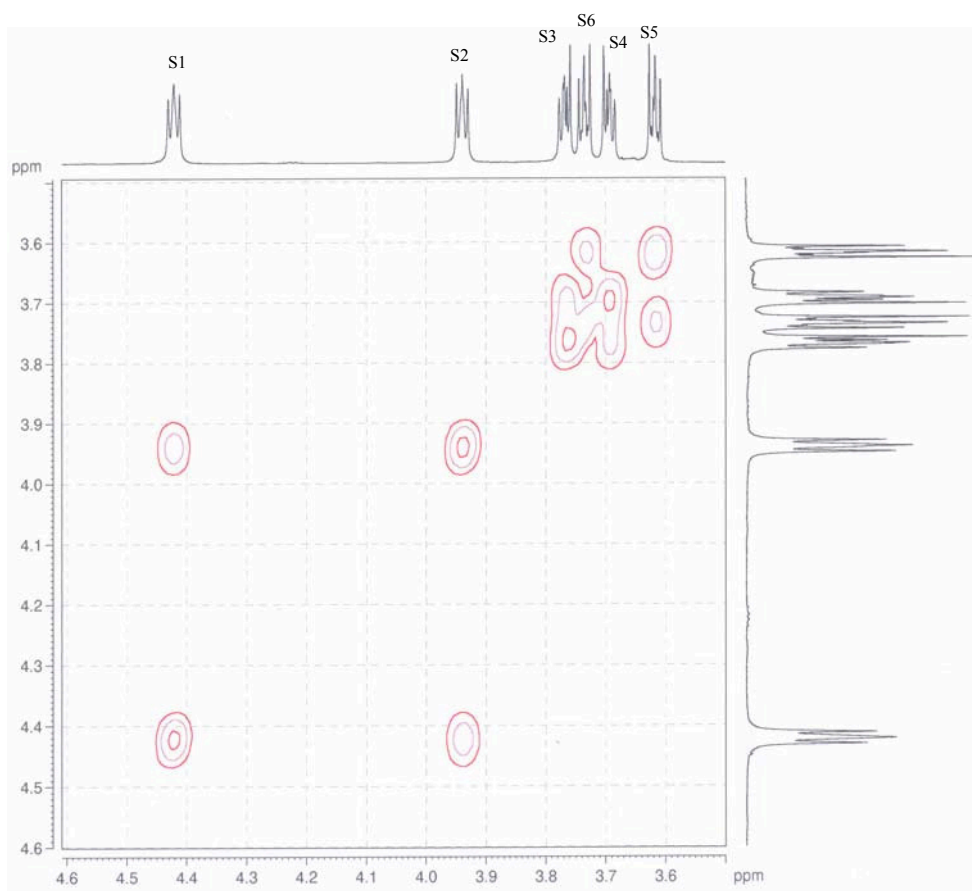
Figure 3. COSY spectrum (500 MHz) of L^3 in CDCl$_3$ solution at room temperature.

L	Proton resonance (δ)				
	H^{T5}	H^{T4}	$H^{T3'}$	H^{T3}	H^{T6}
terpy[47,48]	7.42 (ddd)	7.95 (td)	8.54 (d)	8.66 (d)	8.69 (dd)
poterpy[*,17]	7.30 (ddd)	7.81 (td)	8.06 (s)	8.58 (d)	8.66 (dd)
L^1	7.34 (ddd) J 1.3, 4.8, 7.3 Hz	7.85 (td) J 1.7, 7.7 Hz	8.05 (s)	8.62 (d) J 7.6 Hz	8.69 (d) J 5.3 Hz
L^2	7.35 (ddd) J 1.0, 5.1, 7.6 Hz	7.87 (td) J 1.7, 7.7 Hz	8.13 (s)	8.62 (d) J 7.6 Hz	8.69 (d) J 4.0 Hz
L^3	7.33 (ddd) J 1.1, 4.8, 7.5 Hz	7.85 (td) J 1.8, 7.7 Hz	8.05 (s)	8.61 (d) J 8.0 Hz	8.68 (ddd) J 0.8, 1.7, 4.8 Hz
L^4	7.34 (ddd) J 1.2, 4.8, 7.5 Hz	7.86 (m)	8.17 (s)	8.63 (dt) J 1.0, 8.0 Hz	8.70 (ddd) J 0.9, 1.8, 4.8 Hz
L^5	7.32 (ddd) J 1.0, 4.8, 7.5 Hz	7.82 (m)	8.09 (s)	8.62 (dt) J 1.0, 8.0 Hz	8.69 (ddd) J 0.9, 1.8, 4.8 Hz
L^6	7.32 (ddd) J 1.2, 4.8, 7.5 Hz	7.82 (m)	8.08 (s)	8.62 (dt) J 1.0, 8.0 Hz	8.69 (ddd) J 0.9, 1.8, 4.8 Hz
L^7	7.34 (ddd) J 0.9, 4.9, 7.3 Hz	7.86 (td) J 1.6, 7.7 Hz	8.07 (s)	8.62 (d) J 8.0 Hz	8.69 (dd) J 0.7, 4.7 Hz
L^8	7.35 (ddd) J 1.2, 4.7, 7.5 Hz	7.88 (td) J 1.8, 7.8 Hz	8.29 (s)	8.66 (dt) J 1.1, 8.0 Hz	8.69 (ddd) J 0.9, 1.8, 4.7 Hz
L^9	7.34 (ddd) J 1.1, 4.9, 7.4 Hz	7.88 (m)	8.27 (s)	8.59 (d) J 8.0 Hz	8.65 (dd) J 0.7, 4.8 Hz

Table 1. Terpyridine proton signals of L^1-L^9 in CDCl$_3$ solution at room temperature. (The ^{1}H NMR spectra for L^1 and L^2 were measured at 400 MHz and all the others were measured at 500 MHz; [*]**poterpy** = 4'-(2-propyn-1-oxy)-2,2':6',2''-terpyridine).
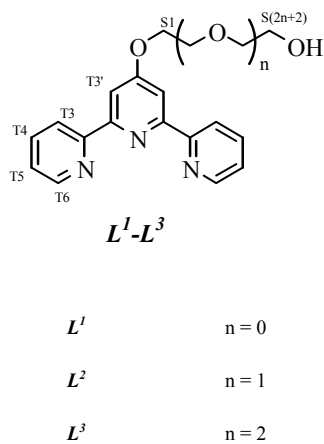
L	Proton resonance (δ)					
	H^{S1}	H^{S2}	H^{S3}	H^{S4}	H^{S5}	H^{S6}
L^1	4.37 (t) J 4.5 Hz	4.04 (m)				
L^2	4.45 (m)	3.93 (m)	3.77 (m)	3.68 (m)		
L^3	4.42 (t) J 4.7 Hz	3.94 (t) J 4.7 Hz	3.77 (m)	3.69 (m)	3.62 (m)	3.73 (m)

L^1-L^3

L^1 n = 0

L^2 n = 1

L^3 n = 2

Table 2. ^{1}H NMR spectroscopic data of CDCl$_3$ solutions of L^1 and L^2 (400 MHz) and L^3 (500 MHz) at room temperature (see **Table 1** for the terpyridine signals).

L^5 n = 0
L^6 n = 1
L^7 n = 2

L^4 L^5-L^7

L	Proton resonance (δ)						
	H^{S1}	H^{S2}	H^{S3}	H^{S4}	H^{S5}	H^{S6}	H^{S7}
L^4	5.50 (s)						
L^5	4.45 (t, J 4.7 Hz)	3.94 (t, J 4.7 Hz)	4.82 (s)				
L^6	4.42 (t, J 4.7 Hz)	3.95 (t, J 4.7 Hz)	3.81 (m)	3.71 (m)	4.74 (s)		
L^7	4.41 (t, J 4.7 Hz)	3.94 (t, J 4.7 Hz)	3.78 (m)	3.71 (m)		3.68 (m)	4.72 (s)

L	Proton resonance (δ)				
	$H^{N6, N7}$	H^{N3}	$H^{N5, N8}$	H^{N4}	H^{N1}
L^4	7.50 (m)	7.59 (dd, J 1.7, 8.4 Hz)	7.86 (m)	7.89 (d, J 8.6 Hz)	7.97 (s)
L^5	7.46 (m)	7.51 (dd, J 1.7, 8.4 Hz)	7.82 (m)		
L^6	7.44 (m)	7.49 (dd, J 1.6, 8.4 Hz)	7.82 (m)		7.79 (s)
L^7	7.44 (m)	7.46 (dd, J 1.7, 8.4 Hz)	7.80 (m)		7.77 (s)

Table 3. ^{1}H NMR spectroscopic data (500 MHz) of CDCl$_3$ solutions of L^4, L^5, L^6, L^7 at room temperature (see **Table 1** for the terpyridine signals).

There are thirteen signals excluding the signal for CHCl$_3$ in the ^{1}H NMR spectrum of a CDCl$_3$ solution of the ligand L^4 (**Figure 4**). Five terpyridine signals were found as expected by comparison with L^3; the rest of the signals belonging to the naphthyl rings and the methylene group were further identified by NOESY and COSY techniques. The singlet at δ 5.50, which exhibits an NOE signal to the signal for H$^{T3'}$ at δ 8.17, is assigned to H^{S1} (**Figure 5a**). The signal for H^{S1} also exhibits NOE signals to H^{N1} and H^{N3} at δ 7.97 and δ 7.59 respectively (**Figure 5a**). The signal for H^{N1} exhibits an NOE signal to the signal at δ 7.86 and this signal is assigned to H^{N8} (**Figure 5b**). H^{N8} gives COSY cross peak to the signal for H^{N7} at δ 7.50 (**Figure 6**). From the COSY spectrum (**Figure 6**), the signal for H^{N3} gives a cross peak at δ 7.89, is assigned to H^{N4}. Finally, the last two signals at δ 7.86 and δ 7.50 are assigned to H^{N5} and H^{N6} respectively according to the fact from the NOESY spectrum that H^{N4} at δ 7.89 does not exhibit an NOE signal to the signal at δ 7.50, which is now assigned to H^{N6} (**Figure 5b**). The assignment is also confirmed by HMQC and HMBC.
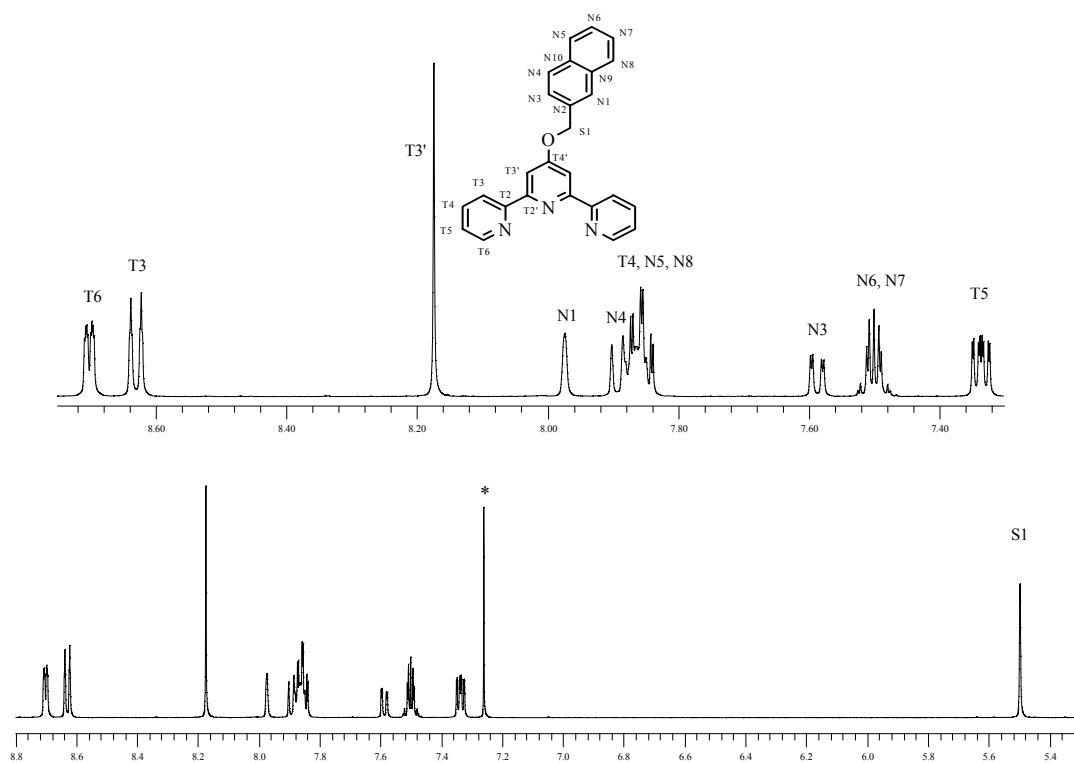
Figure 4. ^{1}H NMR (500 MHz) spectrum of L^4 in CDCl$_3$ solution at room temperature. (the signal marked * is the signal for CHCl$_3$)
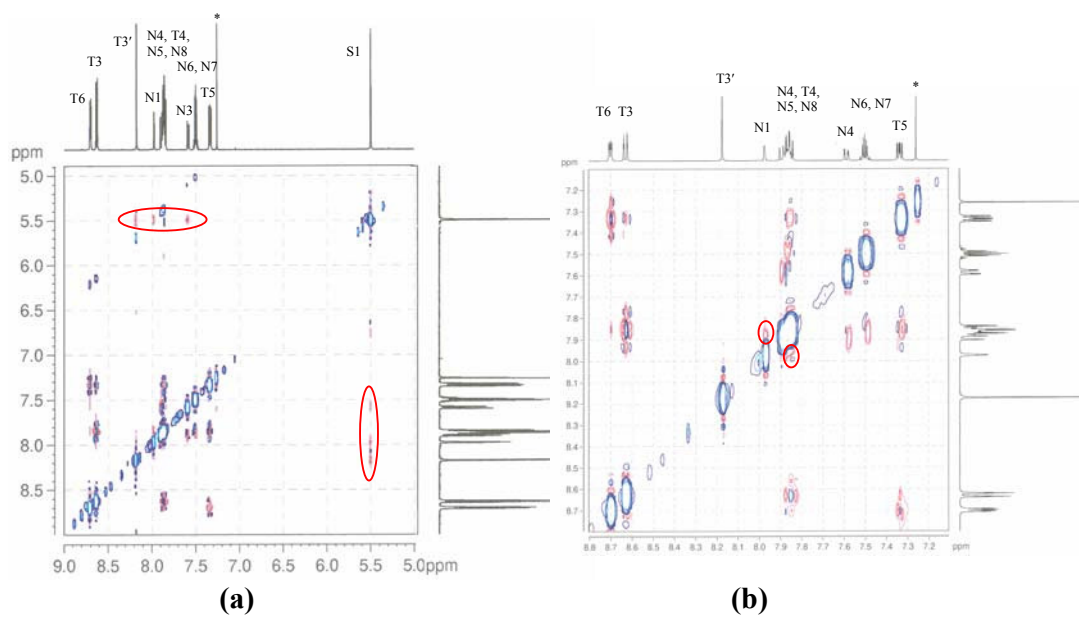
Figure 5. NOESY spectrum (500 MHz) of L^4 in CDCl$_3$ solution at room temperature. (the signal marked * is the signal for CHCl$_3$)
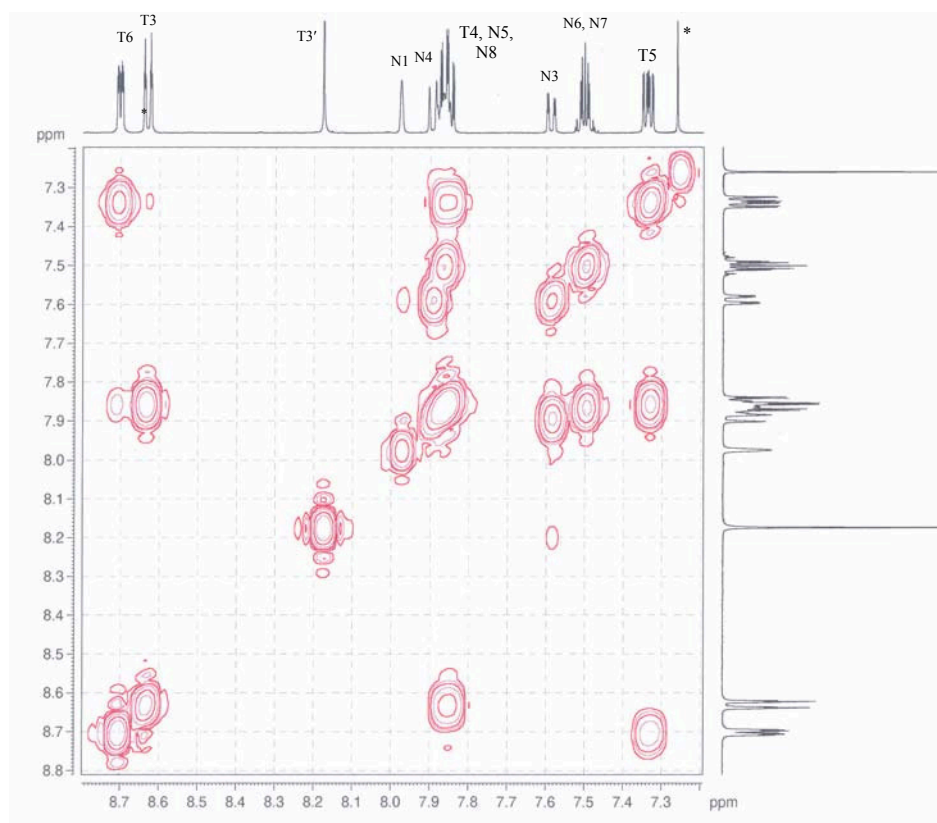
Figure 6. COSY spectrum (500 MHz) of L^4 in CDCl$_3$ solution at room temperature. (the signal marked * is the signal for CHCl$_3$)

The ^{1}H NMR spectra of $\boldsymbol{L^5}$, $\boldsymbol{L^6}$ and $\boldsymbol{L^7}$ are also assigned by using COSY and NOESY. The $H^{N6,\,N7}$ signal of all the 2-naphthyl attached ligands appeared as a multiplet rather than a simple triplet and the multiplicity of the signal could be simulated using the Mestrec programme. All the naphthalene protons are shifted to slightly higher field as the ethyleneoxy spacer gets longer (**Table 3**).

The ^{1}H NMR spectrum of $\boldsymbol{L^8}$ in CDCl$_3$ solution exhibits ten signals from the terpyridine and the anthryl domains. The five terpyridine signals are assigned as before. The singlet signal at δ 6.26 is assigned to H^{S1}. The signal for H^{S1} gives an NOE signal to a singlet at δ 8.29 and a doublet at δ 8.31, which is assigned to $H^{T3'}$ and $H^{A1,\,A8}$ respectively (**Figure 7**). From the COSY spectrum, the signal for $H^{A1,\,A8}$ gives a cross peak to a signal at δ 7.55 and this is assigned to $H^{A2,\,A7}$ (**Figure 8**). The singlet at δ 8.57, which has half the relative integral of the signal for H^{S1}, is assigned to H^{A10}. The signal for H^{A10} gives an NOE signal to a signal at δ 8.07, and this signal is assigned to $H^{A4,\,A5}$ (**Figure 7**). From the COSY spectrum, the signal for $H^{A4,\,A5}$ gives a cross peak to a signal at δ 7.51 which is assigned to $H^{A3,\,A6}$ (**Figure 8**).
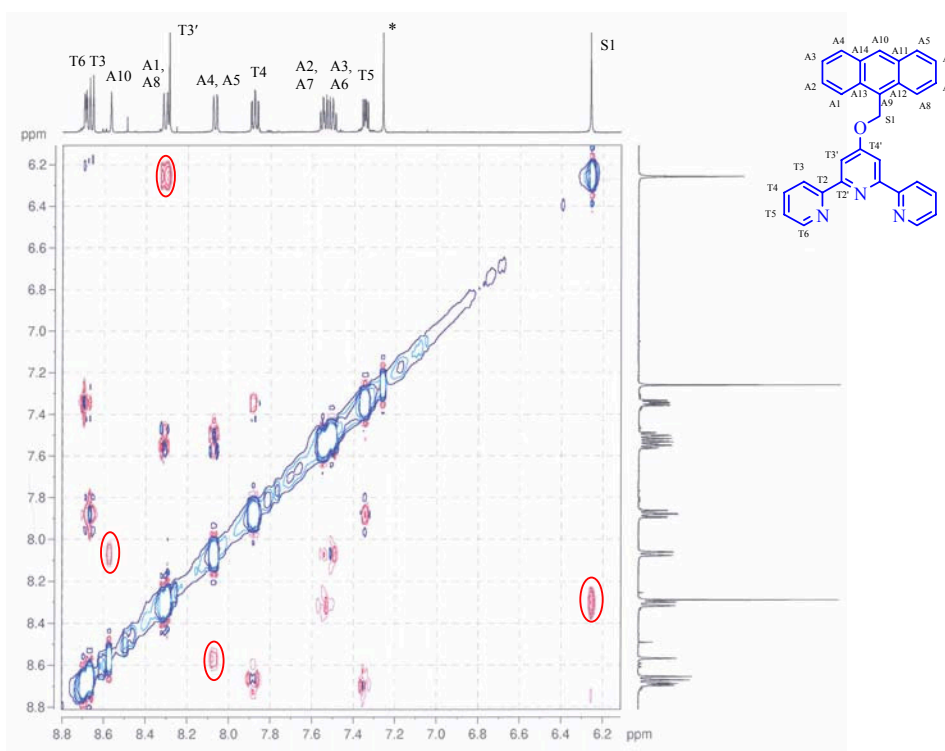
Figure 7. NOESY spectrum (500 MHz) of $\boldsymbol{L^8}$ in CDCl$_3$ solution at room temperature. (the signal marked * is the signal for CHCl$_3$)
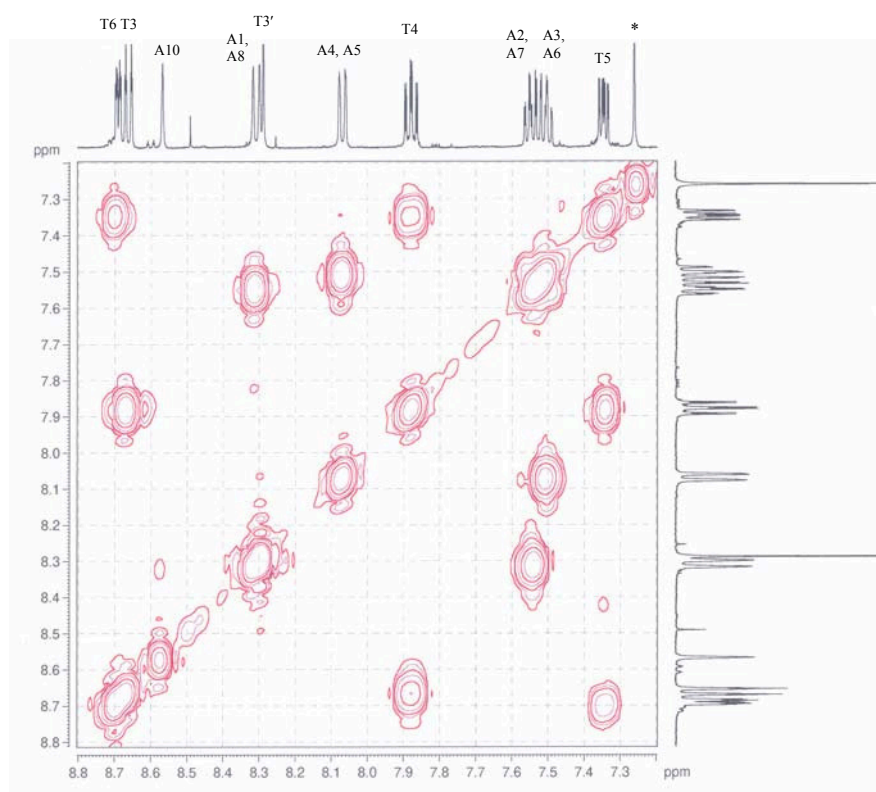
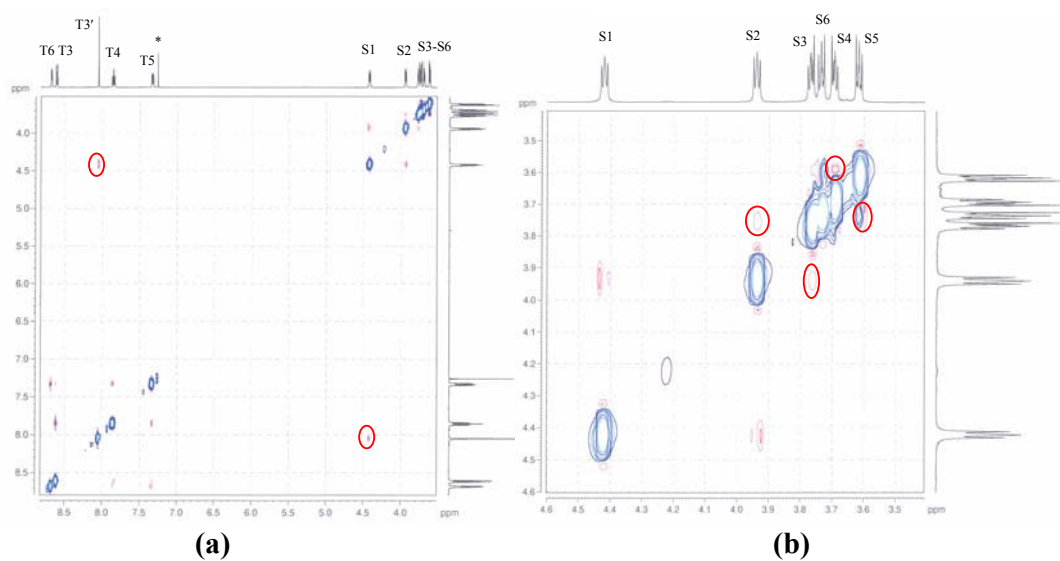**Figure 8.** COSY spectrum (500 MHz) of L^8 in CDCl$_3$ solution at room temperature. (the signal marked * is the signal for CHCl$_3$)
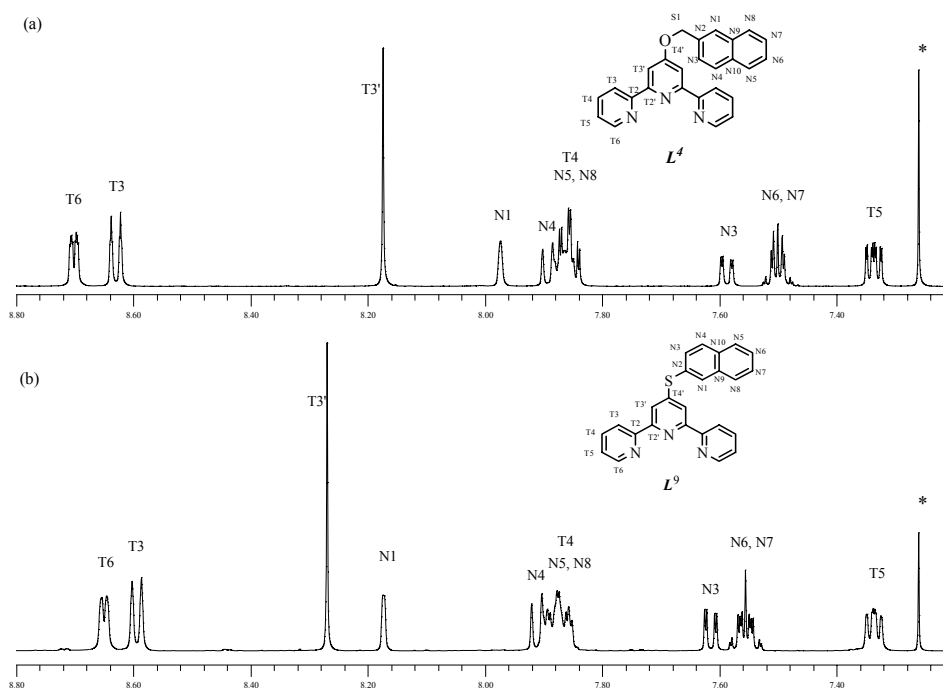

Figure 9. ^{1}H NMR spectra (500 MHz) of (a) L^4 and (b) L^9 in CDCl$_3$ solution at room temperature. (the signal marked * is the signal for CHCl$_3$)

The ^{1}H NMR spectrum of a CDCl$_3$ solution of ligand L^9 is very similar to the spectrum of L^4 (**Figure 9**) and was fully assigned using COSY and NOESY methods.

It is worth noting that H$^{T3'}$ of L^4 is shifted to higher field than those of L^8 and L^9 because the inductive and anisotropic π-cloud effects associated with the adjacent substituents are weaker.

2.3 ^{13}C NMR spectroscopic characterisation

Table 4(a) shows the terpyridine carbon signals of L^3-L^9 in CDCl$_3$ solution. The assignments were done by using HMQC and HMBC techniques. There are no significant changes in these signals as the length of the spacer between the terpyridine and the substituents is lengthened. However, there are 12 ppm, -2 ppm, -15 ppm changes of C$^{T3'}$, C$^{T2'}$, C$^{T4'}$ (the atom labelling scheme is given in **Table 4(a)**) respectively when the OCH$_2$ linkage between the terpyridine domain and the substituent in L^4 is changed to the S linkage in L^9. All the signals of the naphthyl and anthryl rings lie between the C^{T5} and C^{T4} signals. The naphthyl carbons also show no significant shifts as the length of the spacer is varied. However, there is -8 to +8 ppm shift in the signals for C^{N1-N4} when the OCH$_2$ linkage is changed to the S linkage (**Figure 10** and **Table 4(b)**).

L³

L⁴

L⁵-L⁷ (n = 0, 1 2)

L⁸

L⁹
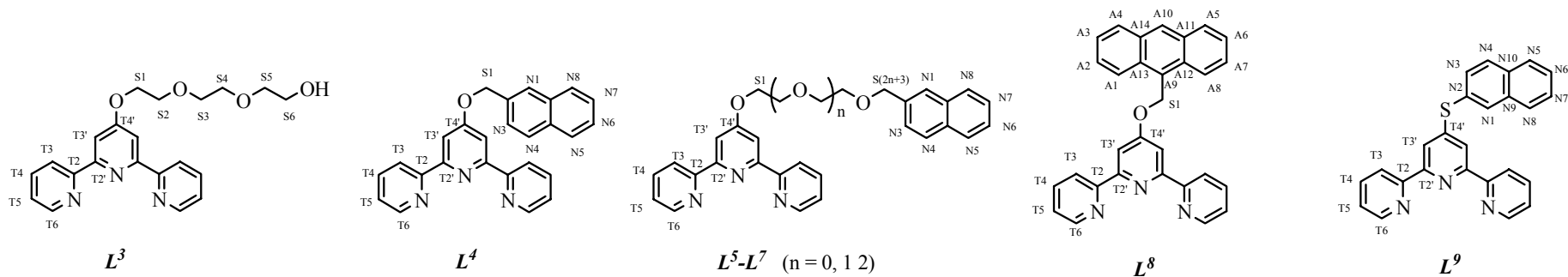
L	Carbon resonance (δ)							
	$C^{T3'}$	C^{T3}	C^{T5}	C^{T4}	C^{T6}	C^{T2}	$C^{T2'}$	$C^{T4'}$
L³	107.6	121.5	123.9	137.0	148.9	155.8	156.9	167.1
L⁴	107.7	121.4	123.9	136.8	149.1	156.1	157.3	167.0
L⁵	107.5	121.4	123.8	136.8	149.0	156.1	157.1	167.1
L⁶	107.6	121.4	123.9	136.9	149.0	155.9	157.0	167.1
L⁷	107.8	121.6	124.0	137.2	148.7	155.6	156.6	167.2
L⁸	107.8	121.6	124.0	137.0	149.2	156.3	157.6	167.5
L⁹	119.1	121.8	124.1	137.6	148.6	155.1	154.8	152.2

Table 4(a). Terpyridine ^{13}C NMR signals of **L³-L⁹** in CDCl₃ solution at room temperature. (The ^{13}C NMR spectra for all the **L** were measured at 125 MHz)

47

L	Carbon resonance (δ)								
	C^{N3}	$C^{N6, N7}$	C^{N1}	C^{N5}	C^{N8}	C^{N4}	C^{N10}	C^{N9}	C^{N2}
L⁴	125.2	126.2, 126.3	126.4	127.8	128.0	128.5	133.1	133.3	133.6
L⁵	126.1	125.7, 125.9	126.5	127.7, 127.9, 128.3			133.0	133.3	135.5
L⁶	125.80, 125.84, 126.0		126.5	127.7, 127.9, 128.2			133.0	133.2	135.8
L⁷	125.78, 125.83, 126.03		126.5	127.8, 127.9, 128.1			133.0	133.3	135.8
L⁹	130.8	126.8, 127.2	134.4	127.9, 128.0		129.7	133.3	134.0	127.5
	$C^{A1, A8}$	$C^{A3, A6}$	C^{A9}	$C^{A2, A7}$	$C^{A4, A5}$	C^{A10}	$C^{A12, A13}$	$C^{A11, A14}$	
L⁸	124.1	125.3	126.1	126.9	129.3	129.5	131.3	131.6	

Table 4(b). ¹³C NMR spectroscopic data for **L³**-**L⁹** in CDCl₃ solution at room temperature. (The ¹³C spectra for **L** were measured at 125 MHz).
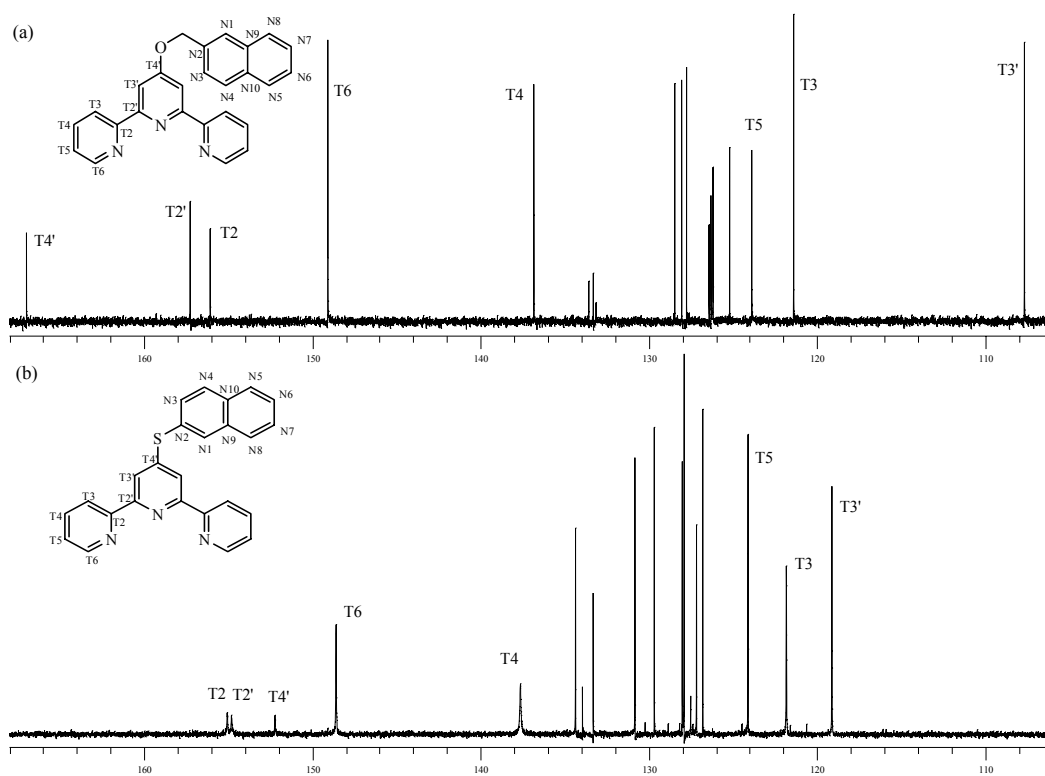
Figure 10. ^{13}C NMR spectra (125 MHz) of (a) L^4 and (b) L^9 in CDCl$_3$ solution at room temperature.

2.4 Mass spectrometric characterisation

Electrospray ionisation (ES) and electron impact (EI) mass spectrometry were also used to characterise the ligands. Since ES-MS is a relatively soft ionisation method, no fragmentation occurs. The value recorded for each signal is the mass to charge ratio (*m/z*). Normally, [M+Na]$^+$ and [M+H]$^+$ peaks are found as the major peaks. However, EI-MS is a harsher method and fragmentation is observed. Therefore, not only is the parent peak [M+H]$^+$ usually found, but also other fragmentation peaks are detected (see **Section 2.7**).

2.5   Crystal structures of L^2 and $[HL^9]^+Cl^-·H_2O$

(a) Crystal structure of L^2

A single crystal of L^2 which was obtained by recrystallisation from ethanol was suitable for X-ray crystallographic analysis (**Figure 11**). Crystallographic data are given in **Appendix I** and selected bond lengths and angles are given in **Table 5**. The crystal structure of L^2, like other free 2,2′:6′,2″-terpyridine ligands[13,17,49], exists in a *trans-trans* conformation which minimises the repulsive N-N lone pair interactions that are present in the *cis-cis* conformation. The interannular C-C bonds, C8-C7, 1.485(4) Å and C13-C14, 1.491(3) Å, and the other N-C, C-C bond lengths are within the reported range of 4′-[3-(1,2-dicarbadecaboranyl)propoxy]-2,2′:6′,2″-terpyridine.[17] The three pyridine rings are not exactly coplanar and the torsion angles C12-C8-C7-N2 and C15-C14-C13-N2 are 7.88° and 6.20° respectively. These small deviations from planarity are typical for the free ligands.[13]
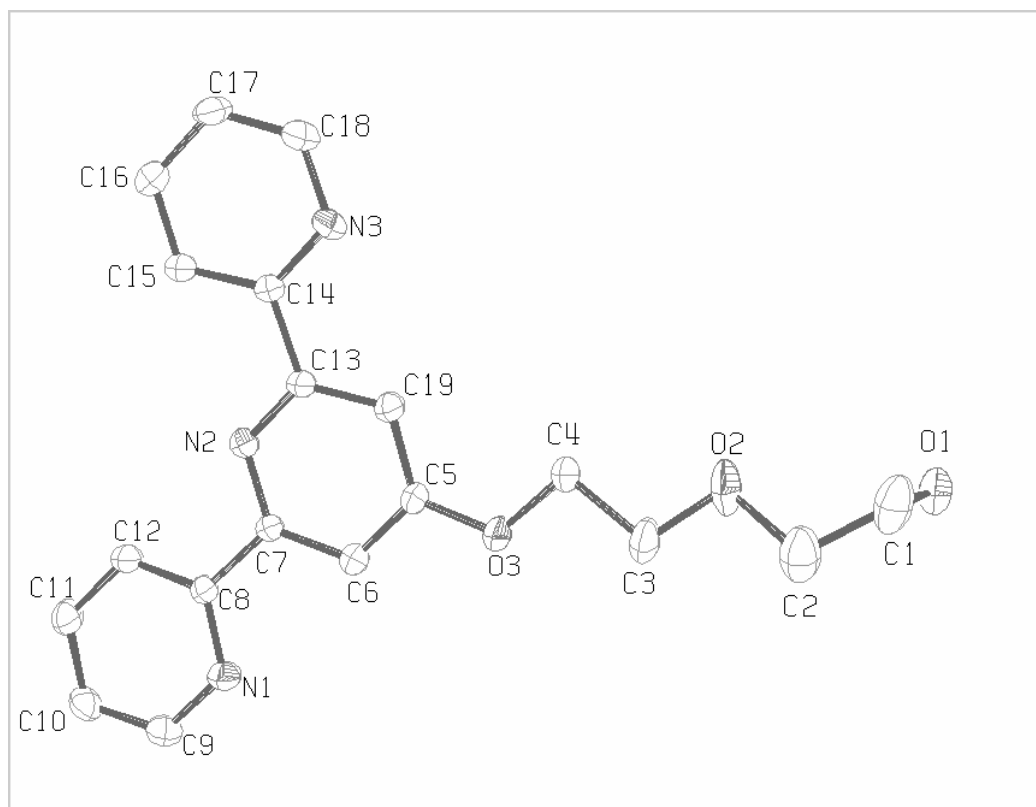
Figure 11. An ORTEP representation (50% probability ellipsoids) of L^2. Hydrogen atoms are omitted for clarity.

C7-C8	1.485(4)	C6-C7	1.396(4)	O3-C5	1.360(3)
C13-C14	1.491(3)	N2-C13	1.341(3)	O3-C4	1.424(4)
N1-C8	1.346(3)	C13-C19	1.400(4)	C3-C4	1.514(4)
C8-C12	1.390(4)	N3-C14	1.337(4)	O2-C3	1.406(4)
N1-C9	1.343(4)	C14-C15	1.391(4)	O2-C2	1.470(5)
N2-C7	1.342(3)	N3-C18	1.352(4)	C1-C2	1.452(6)
				O1-C1	1.417(4)
C8-N1-C9	117.5(3)	N2-C13-C19	123.6(2)	O3-C5-C19	124.4(3)
N1-C8-C12	122.0(3)	N2-C13-C14	116.3(2)	O3-C5-C6	115.4(2)
N1-C8-C7	116.8(2)	C14-C13-C19	120.1(2)	C4-O3-C5	118.8(2)
C7-C8-C12	121.1(2)	N3-C14-C13	117.7(2)	O3-C4-C3	103.9(3)
C6-C7-C8	120.3(2)	C13-C14-C15	120.2(2)	O2-C3-C4	109.0(3)
N2-C7-C8	116.6(2)	N3-C14-C15	122.0(2)	C2-O2-C3	107.5(3)
N2-C7-C6	123.0(2)	C14-N3-C18	117.9(3)	O2-C2-C1	110.1(3)
C7-N2-C13	118.0(2)	C6-C5-C19	120.1(3)	O1-C1-C2	110.9(3)
C12-C8-C7-N2	7.88		C19-C5-O3-C4	1.33	
C15-C14-C13-N2	6.20				

Table 5. Selected bond lengths (Å) and angles (°) of L^2.

For the ethyleneoxy chain, the angle C5-O3-C4 is 118.8(2)°, which is comparable with the corresponding angle in 4′-ethoxy-5,5″-dimethyl-2,2′:6′,2″-terpyridine[50] and 4′-[3-(1,2-dicarbadecaboranyl)propoxy]-2,2′:6′,2″-terpyridine[17]. The bond length O3-C5 is 1.360(3) Å which, within experimental error, is the same as that in 4′-ethoxy-5,5″-dimethyl-2,2′:6′,2″-terpyridine (1.357(3) Å)[50] and 4′-[3-(1,2-dicarbadecaboranyl)propoxy]-2,2′:6′,2″-terpyridine (1.361(1) Å)[17]. Also, the bond length O3-C4 is 1.424(4) Å, which is within the range reported in 4′-ethoxy-5,5″-dimethyl-2,2′:6′,2″-terpyridine (1.425(3) Å)[50] and 4′-[3-(1,2-dicarbadecaboranyl)propoxy]-2,2′:6′,2″-terpyridine (1.428(1) Å)[17]. The bond length O3-C5 is shorter than O3-C4 which suggests a degree of π-conjugation of the oxygen O3 atom with the aromatic ring. The C and O atoms of the chain (except O1) are nearly coplanar with the central pyridine ring with a small torsion angle (C19-C5-O3-C4) 1.33°. Interestingly, there is a hydrogen bonding interaction between O1-H1 of one molecule to N3 atom of another molecule (**Figure 12**). Since the hydrogen positions in the crystal structure were calculated instead of measured, the hydrogen-bonded interactions were investigated by measuring the distance between the atom connected to the hydrogen, which is the oxygen atom O1, and the nitrogen atom N3. The O1···N3 distance is 2.871 Å, which is within a range for a hydrogen bond.[51]
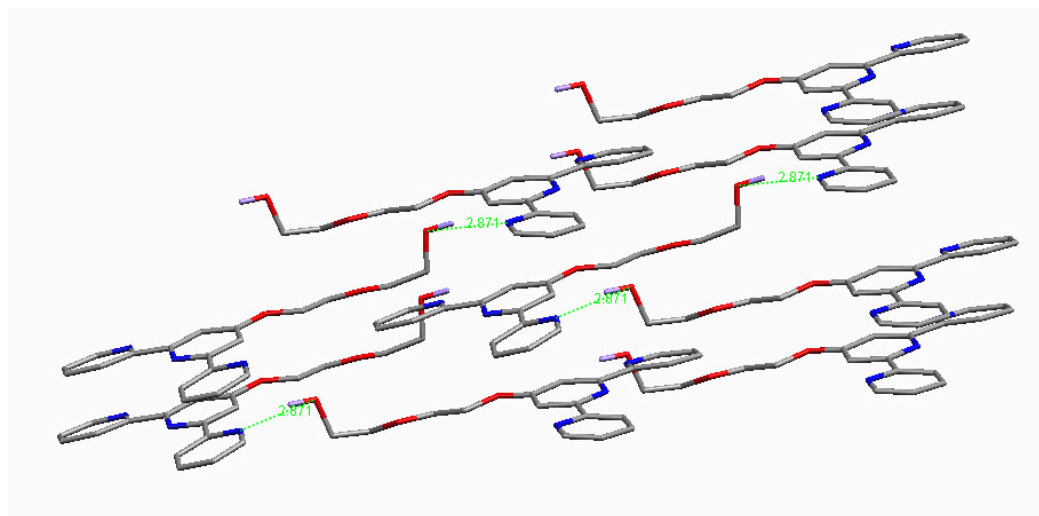
Figure 12. Packing diagram of L^2 in the crystal lattice (the dotted lines are the hydrogen bonding interactions).

(b) Crystal structure of [HL^9]$^+$Cl$^-$·H$_2$O

A single crystal of [HL^9]$^+$Cl$^-$·H$_2$O which was suitable for X-ray crystallographic analysis was obtained by the slow diffusion of diethyl ether into a chloroform solution of L^9. The crystallographic data are given in **Appendix I** and the selected bond lengths and angles are given in **Table 6**. In contrast to the *trans-trans* conformation in L^2, the three pyridine rings in [HL^9]$^+$Cl$^-$·H$_2$O exists in a *cis-trans* conformation because one of its pyridine rings is protonated (**Figure 13**). This has been previously described in the solid-state structure of 2,2′:6′,2″-terpyridinium trifluoromethanesulfonate.[52] One water molecule of crystallisation is present in the crystal structure. The oxygen atom of the water molecule acts as a hydrogen bond acceptor to the hydrogen atom H3 and H221. The distances between O1 and N1, O1 and C22 are 2.735 Å and 3.416 Å respectively, which are comparable with the hydrogen bonds with water molecules as acceptors reported by Steiner *et al.*[51] These H-bonding interactions stabilise the *cis-trans* conformation in the crystal structure. Interestingly, if the pyridine rings are diprotonated, the three pyridine rings exist in a *trans-trans* conformation. This is reported in 2,2′:6′,2″-terpyridinium bis(tetraphenylborate) monohydrate[53] and bis(2,2′:6′,2″-terpyridinium) hexakis(nitrato-O,O′)-lanthanum nitrate acetonitrile solvate[54].
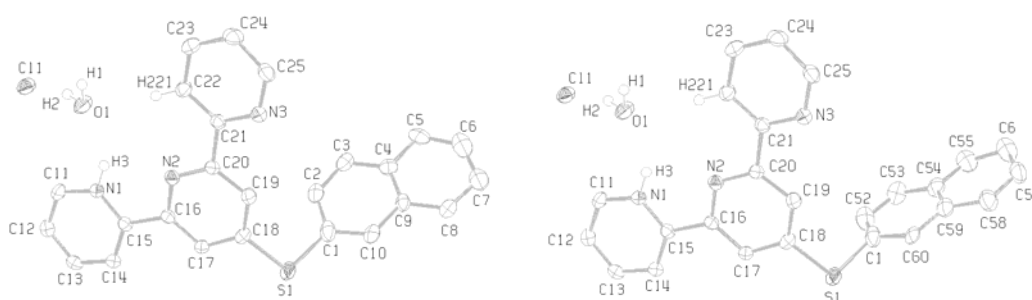
Figure 13. An ORTEP representation (50% probability ellipsoids) of [H*L*⁹]⁺Cl⁻·H₂O. Hydrogen atoms (expect H1, H2 and H221) are omitted for clarity. The structure is disordered; the two structures show the two orientations of the naphthyl group that lead to the disorder.

C15-C16	1.478(4)	C16-C17	1.394(3)	S1-C18	1.763(3)
C20-C21	1.481(4)	N2-C20	1.334(3)	S1-C1	1.778(3)
N1-C15	1.348(3)	C19-C20	1.392(3)		
C14-C15	1.376(4)	N3-C21	1.335(3)		
N1-C11	1.340(3)	C21-C22	1.390(3)		
N2-C16	1.341(3)	N3-C25	1.323(3)		
C11-N1-C15	123.2(2)	N2-C20-C19	122.8(2)	S1-C18-C19	120.5(2)
N1-C15-C14	118.4(2)	N2-C20-C21	117.9(2)	S1-C18-C17	119.6(2)
N1-C15-C16	116.4(2)	C19 -C20-C21	119.3(2)	C1-S1-C18	100.0(1)
C14-C15-C16	125.1(2)	N3-C21-C20	116.0(2)		
C15-C16-C17	120.8(2)	C20-C21-C22	121.0(2)		
N2-C16-C15	115.0(2)	N3-C21-C22	123.1(2)		
N2-C16-C17	124.1(2)	C21-N3-C25	118.0(2)		
C16-N2-C20	117.4(2)	C17-C18-C19	119.8(2)		
O1···Cl1	3.132	O1···N1	2.735	O1···C22	3.416
O1-H2-Cl1	165.53	O1-H3-N1	143.11	O1-H221-C22	172.81
O1···Cl1	3.141				
O1-H1-Cl1	160.78				
N1-C15-C16-N2	6.65		C19-C18-S1-C1		-41.49
C22-C21-C20-N2	-7.99				

Table 6. Selected bond lengths (Å) and angles (°) of [H*L*⁹]⁺Cl⁻·H₂O.

The interannular C-C bonds in [HL^9]$^+$, C15-C16, 1.478(4) Å and C20-C21, 1.481(4) Å, are within the range reported in terpyridine ligands[13] and 4′-[2-(1,3-dioxlan-2-yl)ethylsulfanyl]-2,2′:6′,2″-terpyridine[55]. This is also in the case of 2,2′:6′,2″-terpyridinium trifluoromethanesulfonate[52], 2,2′:6′,2″-terpyridinium bis(tetraphenylborate) monohydrate[53] and bis(2,2′:6′,2″-terpyridinium) hexakis(nitrato-O,O′)-lanthanum nitrate acetonitrile solvate[54]. All the other N-C, C-C bond lengths are within the typical range for free 2,2′:6′,2″-terpyridine ligands.[13] Again, the three pyridine rings are not in the same plane and the torsion angles N1-C15-C16-N2 and C22-C21-C20-N2 are 6.65° and -7.99° respectively.[13] There are some differences between the bond angles in the protonated pyridine ring and the non-protonated pyridine rings. The angle C11-N1-C15 is 123.2(2)°, which is, 5.8(2)° and 5.2(2)° bigger than the angles C16-N2-C20 and C21-N3-C25 respectively. The angle N1-C15-C14 is decreased by 5.7(2)°, 4.4(2)° and 4.7(2)° compared to N2-C16-C17, N2-C20-C19 and N3-C21-C22 respectively. This is also observed in the solid-state structure of 2,2′:6′,2″-terpyridinium trifluoromethanesulfonate.[52]

The angle between C18-S1-C1 is 100.0(1)°, which is slightly smaller than the corresponding angle in 4′-[2-(1,3-dioxlan-2-yl)ethylsulfanyl]-2,2′:6′,2″-terpyridine[55] and 4-methyl-4′-ethylthio-2,2′:6′,2″:6″,2‴-quaterpyridine[56,57]. The bond lengths S1-C18 and S1-C1 are 1.763(3) Å and 1.778(3) Å respectively. The bond length S1-C18 is typical for a Csp^2-S distance.[55] The torsion angle between the central pyridine and the S-naphthyl domain (C19-C18-S1-C1) is -41.49°. The naphthyl domain is disordered and two orientations of the group that result in the disorder are shown in **Figure 13**.

The chloride ion in the structure is hydrogen-bonded to H2 of the water molecule. The distance of O1 and Cl1 is 3.132 Å and the angle of O1-H2-Cl1 is 165.53, which is typical for O-H⋯Cl distance.[51] Also, there is another hydrogen-bonding interactions between the chloride ion and H1 of the water molecule. The distance of O1 and Cl1 is 3.141 Å and the angle of O1-H1-Cl1 is 160.78, which is typical for O-H⋯Cl distance.[51] It is worth noting that there are no π-π stacking interactions between the terpyridine and naphthyl domains. The chloride ions and water molecules form channels and these can be seen in the packing diagram in **Figure 14**.
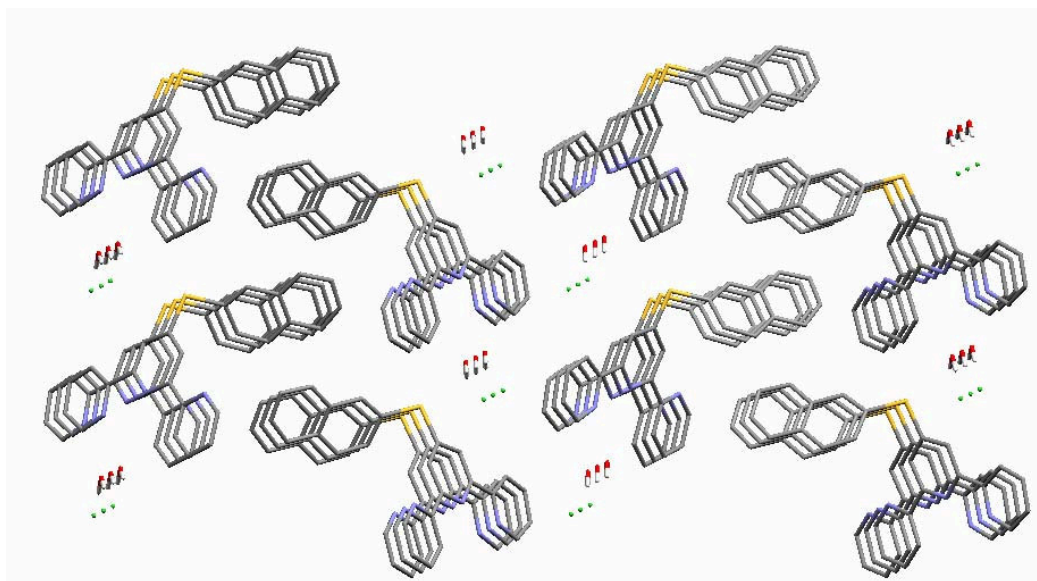
Figure 14. A view of the lattice of [H*L⁹*]⁺Cl⁻·H₂O showing the water molecules and chloride ions in channels; the disorder in the naphthyl group is not shown.

2.6   Conclusion

In this chapter, ligands *L¹*-*L⁹*, which contain polyethyleneoxy chains and differ from one another in the length of the chains, in the terminal domains or in the linkages, have been synthesised and characterised with ^{1}H and ^{13}C NMR spectroscopy, mass spectrometry (ES and EI), IR spectroscopy and elemental analysis. The solid-state structure of ligand *L²* and protonated *L⁹* ([H*L⁹*]⁺Cl⁻·H₂O) were determined by X-ray crystallography.

2.7 Experimental

❖ 4′-(2-Hydroxyethoxy)-2,2′:6′,2″-terpyridine (***L¹***)

❖ 4′-[2-(2-Hydroxyethoxy)ethoxy]-2,2′:6′,2″-terpyridine (***L²***)

❖ 4′-{2-[2-(2-Hydroxyethoxy)ethoxy]ethoxy}-2,2′:6′,2″-terpyridine (***L³***)

❖ 4′-(Naphthalen-2-ylmethoxy)-2,2′:6′,2″-terpyridine (***L⁴***)

❖ 4′-[2-(Naphthalen-2-ylmethoxy)ethoxy]-2,2′:6′,2″-terpyridine (***L⁵***)

❖ 4′-{2-[2-(Naphthalen-2-ylmethoxy)ethoxy]ethoxy}-2,2′:6′,2″-terpyridine (***L⁶***)

❖ 4′-(2-{2-[2-(Naphthalen-2-ylmethoxy)ethoxy]ethoxy}ethoxy)-2,2′:6′,2″-terpyridine (***L⁷***)

❖ 4′-(Anthracen-9-ylmethoxy)-2,2′:6′,2″-terpyridine (***L⁸***)

❖ 4′-(Naphthalen-2-ylsulfanyl)-2,2′:6′,2″-terpyridine (***L⁹***)

4′-Hydroxy-2,2′:6′,2″-terpyridine (***HO-terpy***)[36], 4′-chloro-2,2′:6′,2″-terpyridine (***Cl-terpy***)[36] and 9-bromomethylanthracene[58] were prepared as previously reported in the literature.

❖ 4′-(2-Hydroxyethoxy)-2,2′:6′,2″-terpyridine (***L¹***)
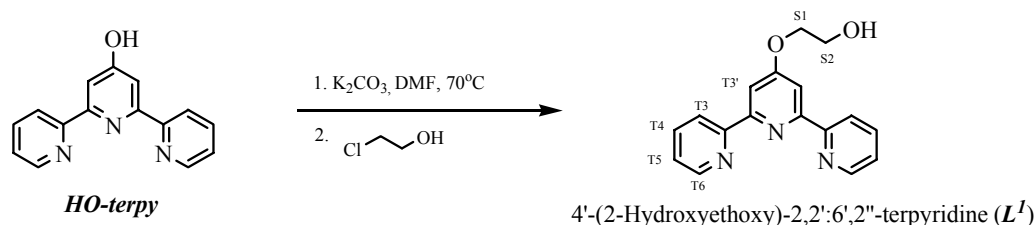
Molecular formula: $C_{17}H_{15}N_3O_2$
Molecular weight: 293.32

4′-Hydroxy-2,2′:6′,2″-terpyridine (1.50 g, 6.02 mmol) and K_2CO_3 (2.50 g, 18.1 mmol) were added to anhydrous DMF (50 mL). The reaction mixture was stirred at 70°C for 1 hour. 2-Chloroethanol (0.485 g, 6.02 mmol) was added dropwise to the suspension and the mixture was stirred at 70°C for a further day. The reaction mixture was kept stirring at 70°C throughout the reaction. Another 1 equivalent of 2-chloroethanol (0.485 g, 6.02 mmol) was added dropwise to the reaction mixture. After 1 day, the solvent was removed under reduced pressure. The crude product was dissolved in CH_2Cl_2 (70 mL) and was

washed with water. The organic phase was collected, dried (MgSO$_4$) and evaporated to dryness. The product L^1 was collected as a white powder (1.0 g, 3.4 mmol, 56%) after column chromatography (Al$_2$O$_3$, CH$_2$Cl$_2$ then CH$_2$Cl$_2$/ 5% CH$_3$OH).

The ligand has been made previously by a different route[15,16]; the sample was checked by spectroscopic analysis and the data below agree with those in the literature.

^{1}H NMR (400 MHz, CDCl$_3$): δ$_H$ 4.04 (m, 2H, H^{S2}), 4.37 (t, *J* 4.5 Hz, 2H, H^{S1}), 7.34 (ddd, *J* 1.3, 4.8, 7.3 Hz, 2H, H^{T5}), 7.85 (td, *J* 1.7, 7.7 Hz, 2H, H^{T4}), 8.05 (s, 2H, H$^{T3'}$), 8.62 (d, *J* 7.6 Hz, 2H, H^{T3}), 8.69 (d, *J* 5.3 Hz, 2H, H^{T6}).

MS (ES): *m/z* = 316.1 [M+Na]$^+$, 294.1 [M+H]$^+$.

IR(solid, cm^{-1}): 3742w, 3202br, 2955w, 2869w, 2361w, 1867w, 1744w, 1682w, 1558s, 1450m, 1404s, 1366s, 1327m, 1258m, 1204s, 1057s, 1026s, 918m, 864m, 787s, 741s.

Melting point: 150.2-151.5°C (lit. m.p. 150-151°C).

❖ 4′-[2-(2-Hydroxyethoxy)ethoxy]-2,2′:6′,2″-terpyridine (*L^2*)

4'-[2-(2-Hydroxyethoxy)ethoxy]-2,2':6',2"-terpyridine (*L^2*)
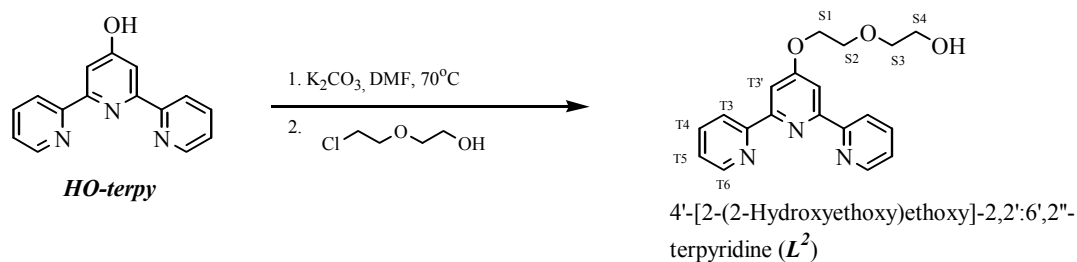
Molecular formula: C$_{19}$H$_{19}$N$_3$O$_3$

Molecular weight: 337.37

4′-Hydroxy-2,2′:6′,2″-terpyridine (1.50 g, 6.02 mmol) and K$_2$CO$_3$ (2.50 g, 18.1 mmol) were added to anhydrous DMF (30 mL). The reaction mixture was stirred at 70°C for 30 mins. 2-(2-Chloroethoxy)ethanol (0.750 g, 6.02 mmol) was added dropwise to the suspension and the mixture was stirred at 70°C for a further day. The reaction mixture was kept stirring at 70°C throughout the reaction. More 2-(2-chloroethoxy)ethanol (0.750 g, 6.02 mmol) was added to the reaction mixture and the mixture was stirred for 1 day. The solvent was removed under reduced pressure. Water (35 mL) was added to the residue and aqueous NaOH (2M) was added to adjust the pH to 12. The solution was washed with CHCl$_3$ (40 mL) twice. The organic layer was dried (MgSO$_4$), filtered and evaporated to dryness. The product L^2 was collected as a white powder (0.921 g, 2.73 mmol, 45.3%) after column chromatography (Al$_2$O$_3$, CH$_2$Cl$_2$, then CH$_2$Cl$_2$/ 10% CH$_3$OH).

The ligand has been made previously by a different route[15,16]; the sample was checked by spectroscopic analysis and the data below agree with those in the literature.

^{1}H NMR (400 MHz, CDCl$_3$): δ_H 3.68 (m, 2H, H^{S4}), 3.77 (m, 2H, H^{S3}), 3.93 (m, 2H, H^{S2}), 4.45 (m, 2H, H^{S1}), 7.35 (ddd, *J* 1.0, 5.1, 7.6 Hz, 2H, H^{T5}), 7.87 (td, *J* 1.7, 7.7 Hz, 2H, H^{T4}), 8.13 (s, 2H, H$^{T3'}$), 8.62 (d, *J* 7.6 Hz, 2H, H^{T3}), 8.69 (d, *J* 4.0 Hz, 2H, H^{T6}).

MS (ES): *m/z* = 360 [M+Na]$^+$.

IR (solid, cm^{-1}): 3788w, 3252br, 2943m, 2885m, 1724w, 1659w, 1582s, 1562s, 1470m, 1443s, 1404s, 1366m, 1323s, 1254m, 1204s, 1119s, 1038s, 988m, 895m, 860m, 787s, 745s.

Melting point: 109.3-111.5ºC (lit. m.p. 113-114ºC).

❖ 4′-{2-[2-(2-Hydroxyethoxy)ethoxy]ethoxy}-2,2′:6′,2″-terpyridine (*L^3*)
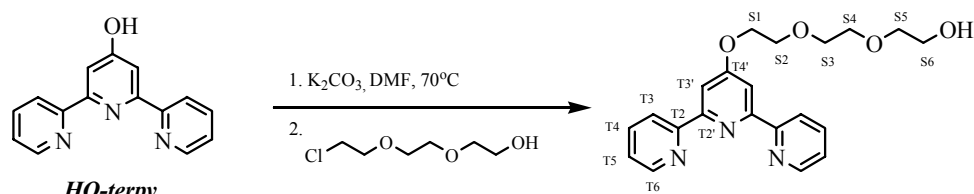
4'-{2-[2-(2-Hydroxyethoxy)ethoxy]ethoxy}-2,2':6',2"-terpyridine (*L^3*)

Molecular formula: C$_{21}$H$_{23}$N$_3$O$_4$
Molecular weight: 381.43

4′-Hydroxy-2,2′:6′,2″-terpyridine (0.50 g, 2.0 mmol) and K$_2$CO$_3$ (0.83 g, 6.0 mmol) were added to anhydrous DMF (20 mL). The reaction mixture was stirred at 70ºC for 1 hour. 2-[2-(2-Chloroethoxy)ethoxy]ethanol (0.34 g, 2.0 mmol) was added dropwise to the suspension and the mixture was stirred at 70ºC for 1 day. The reaction mixture was kept stirring at 70ºC throughout the reaction. Another 1 equivalent of 2-[2-(2-chloroethoxy)ethoxy]ethanol (0.34 g, 2.0 mmol) was added dropwise to the suspension and the mixture was stirred for another day. The solvent was removed under reduced pressure. Water (15 mL) was added to the yellow oily liquid and aqueous NaOH (2M) was added to adjust the pH to 12 or above. The yellow solution was extracted with CHCl$_3$ (20 mL) twice. The organic phase was dried (MgSO$_4$), filtered and evaporated to dryness. All the excess 2-[2-(2-chloroethoxy)ethoxy]ethanol was removed under high vacuum. Then, the product *L^3* was collected as a pale yellow liquid (0.37 g, 0.97 mmol, 49%) after column chromatography (Al$_2$O$_3$, CH$_2$Cl$_2$ then CH$_2$Cl$_2$/ 10% CH$_3$OH).

^{1}H NMR (500 MHz, CDCl$_3$): δ_H 3.62 (m, 2H, H^{S5}), 3.69 (m, 2H, H^{S4}), 3.73 (m, 2H, H^{S6}), 3.77 (m, 2H, H^{S3}), 3.94 (t, J 4.7 Hz, 2H, H^{S2}), 4.42 (t, J 4.7 Hz, 2H, H^{S1}), 7.33 (ddd, J 1.1, 4.8, 7.5 Hz, 2H, H^{T5}), 7.85 (td, J 1.8, 7.7 Hz, 2H, H^{T4}), 8.05 (s, 2H, H$^{T3'}$), 8.61 (d, J 8.0 Hz, 2H, H^{T3}), 8.68 (ddd, J 0.8, 1.7, 4.8 Hz, 2H, H^{T6}).

^{13}C NMR (125 MHz, CDCl$_3$): δ_C 61.8 (C^{S6}), 67.9 (C^{S1}), 69.5 (C^{S2}), 70.5 (C^{S4}), 71.1 (C^{S3}), 72.5 (C^{S5}), 107.6 (C$^{T3'}$), 121.5 (C^{T3}), 123.9 (C^{T5}), 137.0 (C^{T4}), 148.9 (C^{T6}), 155.8 (C^{T2}), 156.9 (C$^{T2'}$), 167.1 (C$^{T4'}$).

MS (ES): m/z = 404.2 [M+Na]$^+$.

IR (solid, cm^{-1}): 3757w, 3418br, 3055w, 2878m, 2885m, 1735m, 1566s, 1450m, 1412m, 1350m, 1250m, 1203m, 1057m, 995w, 964w, 872w, 795m, 740w, 702w.

Elemental Analysis: Found: C, 64.80; H, 6.12; N, 10.97. Calc. for C$_{21}$H$_{23}$N$_3$O$_4$·⅓H$_2$O: C, 65.10; H, 6.17; N, 10.85%.

❖ 4′-(Naphthalen-2-ylmethoxy)-2,2′:6′,2″-terpyridine (***L***^{4})

4'-(Naphthalene-2-ylmethoxy)-2,2':6',2"-terpyridine (***L***^{4})
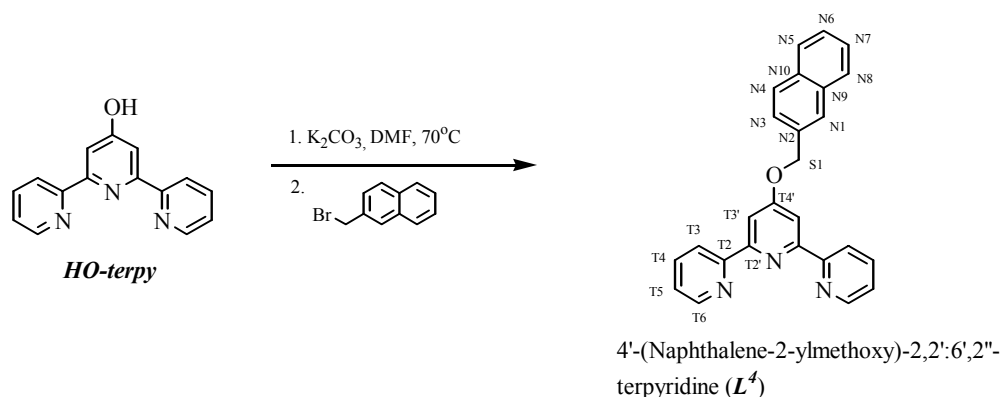
Molecular formula: C$_{26}$H$_{19}$N$_3$O
Molecular weight: 389.45

4′-Hydroxy-2,2′:6′,2″-terpyridine (1.21 g, 4.85 mmol) was stirred with dry K$_2$CO$_3$ (2.01 g, 14.5 mmol) in 50 mL DMF for 1 hour at 70°C under nitrogen and 2-bromomethylnaphthalene (1.33 g, 6.02 mmol) was added to the reaction mixture. The reaction mixture was kept stirring at 70°C throughout the reaction. The reaction mixture was stirred for 1 day and then more 2-bromomethylnaphthalene (0.40 g, 1.8 mmol) was added. After 2 days, the reaction mixture was then filtered and the solvent was removed. The crude product was extracted with CH$_2$Cl$_2$ and water. The white powder was

recrystallised from methanol to give 4′-(naphthalene-2-ylmethoxy)-2,2′:6′,2″-terpyridine as white fine needles (0.91 g, 2.34 mmol, 48.2%).

^{1}H NMR (500 MHz, CDCl$_3$) δ_H 5.50 (s, 2H, H^{S1}), 7.34 (ddd, *J* 1.2, 4.8, 7.5 Hz, 2H, H^{T5}), 7.50 (m, 2H, H^{N6} and H^{N7}), 7.59 (dd, *J* 1.7, 8.4 Hz, 2H, H^{N3}), 7.86 (m, 4H, H^{T4}, H^{N5} and H^{N8}), 7.89 (d, *J* 8.6 Hz, 1H, H^{N4}), 7.97 (s, 1H, H^{N1}), 8.17 (s, 2H, H$^{T3'}$), 8.63 (dt, *J* 1.0, 8.0 Hz, 2H, H^{T3}), 8.70 (ddd, *J* 0.9, 1.8, 4.8 Hz, 2H, H^{T6}).

^{13}C NMR (125 MHz, CDCl$_3$): δ_C 70.0 (C^{S1}), 107.7 (C$^{T3'}$), 121.4 (C^{T3}), 123.9 (C^{T5}), 125.2 (C^{N3}), 126.2 (C$^{N6/N7}$), 126.3 (C$^{N7/N6}$), 126.4 (C^{N1}), 127.8 (C^{N5}), 128.0 (C^{N8}), 128.5 (C^{N4}), 133.1 (C^{N10}), 133.3 (C^{N9}), 133.6 (C^{N2}), 136.8 (C^{T4}), 149.1 (C^{T6}), 156.1 (C^{T2}), 157.3 (C$^{T2'}$), 167.0 (C$^{T4'}$).

MS (EI): *m/z* = 389.2 [M]$^+$ (39.8%), 234.1 [M-OCH$_2$Nap]$^+$ (18.1%), 141.1 [M-***Oterpy***]$^+$ (100%).

IR (solid, cm^{-1}): 3101w, 3055w, 3016w, 2870w, 2546w, 1790w, 1735w, 1558s, 1443m, 1404m, 1342s, 1258m, 1188s, 1126w, 1095w, 1003s, 926w, 903w, 864m, 825m, 787s, 741m.

Elemental Analysis: Found: C, 79.43; H, 4.88; N, 10.58. Calc. for C$_{26}$H$_{19}$N$_3$O·¼CH$_3$OH: C, 79.25; H, 5.03; N, 10.57%.

Melting point: 186.8-188.4ºC.

❖ 4′-[2-(Naphthalen-2-ylmethoxy)ethoxy]-2,2′:6′,2″-terpyridine (***L^5***)

4'-(2-Hydroxyethoxy)-2,2':6',2"-terpyridine (***L^1***)

4'-[2-(Naphthalen-2-ylmethoxy)ethoxy]-2,2:6',2"-terpyridine (***L^5***)
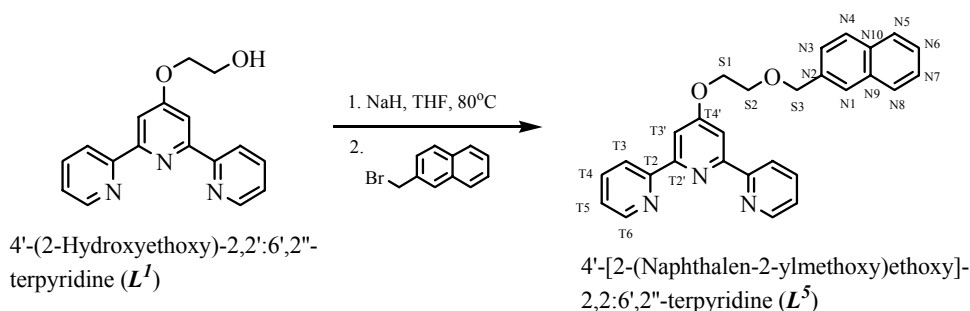
Molecular formula: C$_{28}$H$_{23}$N$_3$O$_2$

Molecular weight: 433.50

4′-(2-Hydroxyethoxy)-2,2′:6′,2″-terpyridine (0.20 g, 0.68 mmol) and NaH (60% suspended in oil) (48 mg, 1.2 mmol) were added to 40 mL dry THF and the mixture stirred at 80ºC for 1 hour. The reaction mixture was kept stirring at 80ºC throughout the

reaction. Then, 2-bromomethylnaphthalene (0.18 g, 0.82 mmol) in 5 mL of dry THF was added slowly to the mixture. The reaction mixture was stirred at 80°C for 2 days. Methanol (10 mL) and water (10 mL) were added slowly to quench the reaction. The solvent was removed under reduced pressure. The yellow residue was washed with hexane and dissolved in water. The solution was then extracted with $CHCl_3$ twice. The organic layer was dried ($MgSO_4$) and concentrated. Column chromatography (Al_2O_3, CH_2Cl_2/ 1% CH_3OH) yielded 0.20 g (0.46 mmol, 68%) of white solid $\boldsymbol{L^5}$.

^{1}H NMR (500 MHz, $CDCl_3$) δ_H 3.94 (t, *J* 4.7 Hz, 2H, H^{S2}), 4.45 (t, *J* 4.7 Hz, 2H, H^{S1}), 4.82 (s, 2H, H^{S3}), 7.32 (ddd, *J* 1.0, 4.8, 7.5 Hz, 2H, H^{T5}), 7.46 (m, 2H, H^{N6} and H^{N7}), 7.51 (dd, *J* 1.7, 8.4 Hz, 1H, H^{N3}), 7.82 (m, 6H, H^{N1}, H^{N4}, H^{N5}, H^{N8} and H^{T4}), 8.09 (s, 2H, $H^{T3'}$), 8.62 (dt, *J* 1.0, 8.0 Hz, 2H, H^{T3}), 8.69 (ddd, *J* 0.9, 1.8, 4.8 Hz, 2H, H^{T6}).

^{13}C NMR (125 MHz, $CDCl_3$): δ_C 67.8 (C^{S1}), 68.3 (C^{S2}), 73.5 (C^{S3}), 107.5 ($C^{T3'}$), 121.4 (C^{T3}), 123.8 (C^{T5}), 125.7 ($C^{N6/\,N7}$), 125.9 ($C^{N7/\,N6}$), 126.1 (C^{N3}), 126.5 (C^{N1}), 127.7 ($C^{N4/\,N5/\,N8}$), 127.9 ($C^{N4/\,N5/\,N8}$), 128.3 ($C^{N4/\,N5/\,N8}$), 133.0 (C^{N10}), 133.3 (C^{N9}), 135.5 (C^{N2}), 136.8 (C^{T4}), 149.1 (C^{T6}), 156.1 (C^{T2}), 157.1 ($C^{T2'}$), 167.1 ($C^{T4'}$).

MS (ES): *m/z* = 456.1 [M+Na]$^+$, 434.2 [M+H]$^+$.

IR (solid, cm^{-1}): 3086w, 3063w, 2970w, 2847w, 1713w, 1558s, 1466m, 1404m, 1342s, 1281m, 1250m, 1196s, 1103s, 1056s, 987s, 957s, 894m, 864s, 825m, 787s, 741s.

Elemental Analysis: Found: C, 77.45; H, 5.37; N, 9.69. Calc. for $C_{28}H_{23}N_3O_2$: C, 77.58; H, 5.35; N, 9.69%.

Melting point: 97.8-99.1ºC.

❖ 4′-{2-[2-(Naphthalen-2-ylmethoxy)ethoxy]ethoxy}-2,2′:6′,2″-terpyridine (*L⁶*)

4'-[2-(2-Hydroxyethoxy)ethoxy]-
2,2':6',2"-terpyridine (*L²*)

4'-{2-[2-(Naphthalen-2-ylmethoxy)ethoxy]
ethoxy}-2,2':6',2"-terpyridine (*L⁶*)
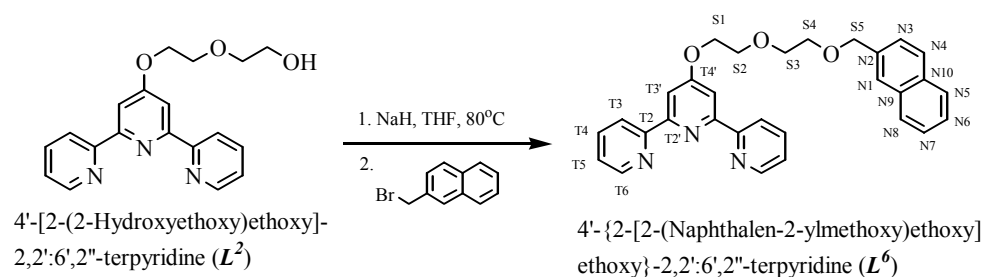
Molecular formula: $C_{30}H_{27}N_3O_3$

Molecular weight: 477.55

4′-[2-(2-Hydroxyethoxy)ethoxy]-2,2′:6′,2″-terpyridine (0.20 g, 0.59 mmol) and NaH (60% suspended in oil) (71.2 mg, 1.78 mmol) were added to 20 mL dry THF and the mixture stirred at 80°C for 1 hour. The reaction mixture was kept stirring at 80°C throughout the reaction. Then, 2-bromomethylnaphthalene (0.2 g, 0.9 mmol) in 5 mL of dry THF was added slowly to the mixture. The reaction mixture was stirred at 80°C for 1 day. A further one-third equivalent of 2-bromomethylnaphthalene (0.07 g, 0.3 mmol) was added and stirred for a further day. Methanol (10 mL) and water (10 mL) were added slowly to quench the reaction. The solvent was removed under reduced pressure. The yellow residue was washed with hexane and dissolved in water. The solution was then extracted with $CHCl_3$ twice. The organic layer was dried ($MgSO_4$) and concentrated. Column chromatography (Al_2O_3, CH_2Cl_2/ 1% CH_3OH) yielded 0.15 g (0.31 mmol, 53%) of colourless oily liquid **L^6**.

^1H NMR (500 MHz, $CDCl_3$): δ_H 3.71 (m, 2H, H^{S4}), 3.81 (m, 2H, H^{S3}), 3.95 (t, J 4.7 Hz, 2H, H^{S2}), 4.42 (t, J 4.7 Hz, 2H, H^{S1}), 4.74 (s, 2H, H^{S5}), 7.32 (ddd, J 1.2, 4.8, 7.5 Hz, 2H, H^{T5}), 7.44 (m, 2H, H^{N6} and H^{N7}), 7.49 (dd, J 1.6, 8.4 Hz, 1H, H^{N3}), 7.79 (s, 1H, H^{N1}), 7.82 (m, 5H, H^{T4}, H^{N4}, H^{N5} and H^{N8}), 8.08 (s, 2H, $H^{T3'}$), 8.62 (dt, J 1.0, 8.0 Hz, 2H, H^{T3}), 8.69 (ddd, J 0.9, 1.8, 4.8 Hz, 2H, H^{T6}).

^{13}C NMR (125 MHz, $CDCl_3$): δ_C 67.9 (C^{S1}), 69.5 ($C^{S2/ S4}$), 69.6 ($C^{S4/ S2}$), 71.1 (C^{S3}), 73.4 (C^{S5}), 107.6 ($C^{T3'}$), 121.4 (C^{T3}), 123.9 (C^{T5}), 125.80 ($C^{N6/ N7/ N3}$), 125.84 ($C^{N7/ N6/ N3}$), 126.0 ($C^{N7/ N6/ N3}$), 126.5 (C^{N1}), 127.7 ($C^{N4/ N5/ N8}$), 127.9 ($C^{N4/ N5/ N8}$), 128.2 ($C^{N4/ N5/ N8}$), 133.0 (C^{N10}), 133.2 (C^{N9}), 135.8 (C^{N2}), 136.9 (C^{T4}), 149.0 (C^{T6}), 155.9 (C^{T2}), 157.0 ($C^{T2'}$), 167.1 ($C^{T4'}$).

MS (ES): m/z = 500 [M+Na]$^+$, 478 [M+H]$^+$.

IR (solid, cm^{-1}): 3055w, 2870br, 1566s, 1450m, 1404m, 1350m, 1250w, 1204m, 1126m, 1095m, 1049w, 995w, 964w, 864w, 795m, 748m.

Elemental Analysis: Found: C, 74.88; H, 5.91; N, 8.85. Calc. for $C_{30}H_{27}N_3O_3 \cdot \frac{1}{4}CH_3OH$: C, 74.83; H, 5.81; N, 8.65%.

❖ 4′-(2-{2-[2-(Naphthalen-2-ylmethoxy)ethoxy]ethoxy}ethoxy)-2,2′:6′,2″-terpyridine (**L**^{7})

4'-{2-[2-(2-Hydroxyethoxy)ethoxy]
ethoxy}-2,2':6',2"-terpyridine (**L**^{3})

4'-(2-{2-[2-(Naphthalen-2-ylmethoxy)ethoxy]
ethoxy}ethoxy)-2,2':6',2"-terpyridine (**L**^{7})
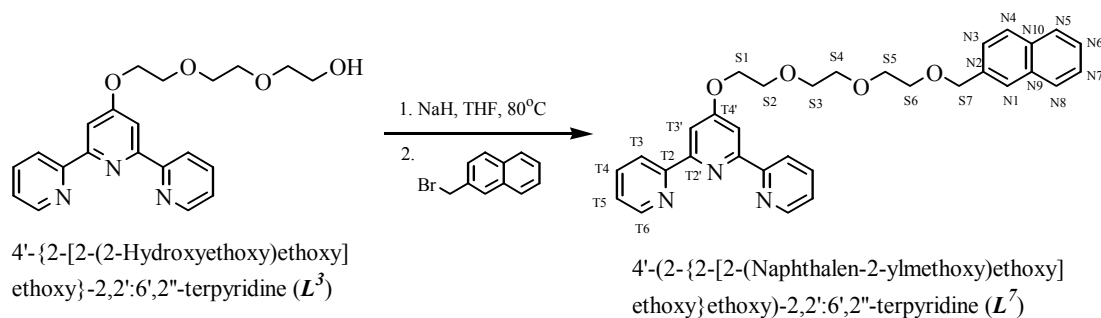
Molecular formula: $C_{32}H_{31}N_3O_4$

Molecular weight: 521.61

4′-{2-[2-(2-Hydroxyethoxy)ethoxy]ethoxy}-2,2′:6′,2″-terpyridine (0.15 g, 0.39 mmol) and NaH (60% suspended in oil) (19 mg, 0.47 mmol) were added to 20 mL dry THF and the mixture was stirred at 80°C for 1 hour. The reaction mixture was kept stirring at 80°C throughout the reaction. Then, 2-bromomethylnaphthalene (261 mg, 1.18 mmol) was added slowly to the mixture. The reaction mixture was stirred at 80°C for 3 days. Methanol (10 mL) and water (10 mL) were added slowly to quench the reaction. The solvent was removed under reduced pressure. The yellow residue was washed with hexane and water. The solution was then extracted with CHCl$_3$ twice. The organic layer was dried (MgSO$_4$) and concentrated. The crude product was purified by column chromatography (Al$_2$O$_3$, CH$_2$Cl$_2$/ 1% CH$_3$OH) to yield 0.031 g (0.060 mmol, 15%) of yellow oily liquid **L**^{7}.

^{1}H NMR (500 MHz, CDCl$_3$) δ_H 3.68 (m, 2H, H^{S6}), 3.71 (m, 4H, H^{S4} and H^{S5}), 3.78 (m, 2H, H^{S3}), 3.94 (t, J 4.7 Hz, 2H, H^{S2}), 4.41 (t, J 4.7 Hz, 2H, H^{S1}), 4.72 (s, 2H, H^{S7}), 7.34 (ddd, J 0.9, 4.9, 7.3 Hz, 2H, H^{T5}), 7.44 (m, 2H, H^{N6} and H^{N7}), 7.46 (dd, J 1.7, 8.4 Hz, 1H, H^{N3}), 7.77 (s, 1H, H^{N1}), 7.80 (m, 3H, H^{N4}, H^{N5} and H^{N8}), 7.86 (td, J 1.6, 7.7 Hz, 2H, H^{T4}), 8.07 (s, 2H, H$^{T3'}$), 8.62 (d, J 8.0 Hz, 2H, H^{T3}), 8.69 (dd, J 0.7, 4.7 Hz, 2H, H^{T6}).

^{13}C NMR (125 MHz, CDCl$_3$): δ_C 68.0 (C^{S1}), 69.46 (C^{S2}), 69.48 (C^{S6}), 70.75 (C^{S4}), 70.77 (C^{S5}), 71.0 (C^{S3}), 73.3 (C^{S7}), 107.8 (C$^{T3'}$), 121.6 (C^{T3}), 124.0 (C^{T5}), 125.78 (C$^{N6/ N7/ N3}$), 125.83 (C$^{N7/ N6/ N3}$), 126.03 (C$^{N7/ N6/ N3}$), 126.5 (C^{N1}), 127.8 (C$^{N4/ N5/ N8}$), 127.9 (C$^{N4/ N5/ N8}$), 128.1 (C$^{N4/ N5/ N8}$), 133.0 (C^{N10}), 133.3 (C^{N9}), 135.8 (C^{N2}), 137.2 (C^{T4}), 148.7 (C^{T6}), 155.6 (C^{T2}), 156.6 (C$^{T2'}$), 167.2 (C$^{T4'}$).

MS (ES): *m/z* = 544.4 [M+Na]$^+$, 522.5 [M+H]$^+$.

IR (solid, cm^{-1}): 3055w, 2870br, 1713m, 1566s, 1466m, 1404m, 1350m, 1281m, 1204m, 1126m, 1095m, 1049w, 995w, 964w, 872m, 795m, 741w.

Elemental Analysis: Found: C, 72.15; H, 5.94; N, 8.23. Calc. for $C_{32}H_{31}N_3O_4 \cdot \frac{1}{2}H_2O$: C, 72.43; H, 6.08; N, 7.92%.

❖ 4′-(Anthracen-9-ylmethoxy)-2,2′:6′,2″-terpyridine (***L^8***)

4'-(Anthracen-9-ylmethoxy)-
2,2':6',2"-terpyridine (***L^8***)
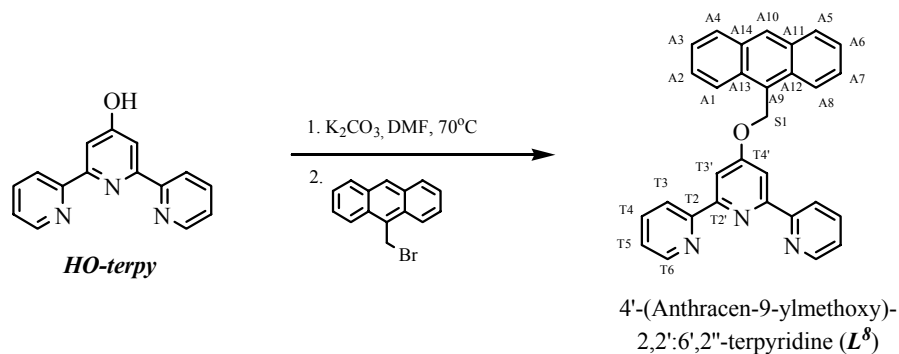
Molecular formula: $C_{30}H_{21}N_3O$
Molecular weight: 439.51

4′-Hydroxy-2,2′:6′,2″-terpyridine (0.50 g, 2.0 mmol) was stirred with dry K_2CO_3 (0.83 g, 6.0 mmol) in 60 mL DMF for 1 hour at 70°C under nitrogen and 9-bromomethylanthracene (0.54 mg, 2.0 mmol) was added to the reaction mixture. The reaction was kept at 70°C under nitrogen in the dark for 1 week. The solvent was then removed in *vacuo* and the yellow crude product was extracted with CH_2Cl_2 and water. The organic layer was collected, dried (MgSO$_4$) and concentrated. ***L^8*** was obtained as a yellow product (0.13 g, 0.30 mmol, 15%) after column chromatography (Al$_2$O$_3$, CH_2Cl_2/ hexane 3:1 and then CH_2Cl_2/ hexane 2:1).

^{1}H NMR (500 MHz, CDCl$_3$) δ_H 6.26 (s, 2H, H^{S1}), 7.35 (ddd, *J* 1.2, 4.7, 7.5 Hz, 2H, H^{T5}), 7.51 (m, 2H, H$^{A3, A6}$), 7.55 (m, 2H, H$^{A2, A7}$), 7.88 (td, *J* 1.8, 7.8 Hz, 2H, H^{T4}), 8.07 (d, *J* 8.6 Hz, 2H, H$^{A4, A5}$), 8.29 (s, 2H, H$^{T3'}$), 8.31 (d, *J* 8.6 Hz, 2H, H$^{A1, A8}$), 8.57 (s, 2H, H^{A10}), 8.66 (dt, *J* 1.1, 8.0 Hz, 2H, H^{T3}), 8.69 (ddd, *J* 0.9, 1.8, 4.7 Hz, 2H, H^{T6}).

^{13}C NMR (125 MHz, CDCl$_3$): δ_C 63.2 (C^{S1}), 107.8 (C$^{T3'}$), 121.6 (C^{T3}), 124.0 (C^{T5}), 124.1 (C$^{A1, A8}$), 125.3 (C$^{A3, A6}$), 126.1 (C^{A9}), 126.9 (C$^{A2, A7}$), 129.3 (C$^{A4, A5}$), 129.5 (C^{A10}), 131.3 (C$^{A12, A13}$), 131.6 (C$^{A11, A14}$), 137.0 (C^{T4}), 149.2 (C^{T6}), 156.3 (C^{T2}), 157.6 (C$^{T2'}$), 167.5 (C$^{T4'}$).

MS (EI): m/z = 439.2 [M]$^+$ (12.42%), 249 [M-Ant-CH$_2$]$^+$ (12.11%), 191.1 [M-***Oterpy***]$^+$ (100%).

IR (solid, cm^{-1}): 3055br, 1666w, 1558s, 1443m, 1404m, 1342m, 1250w, 1188s, 1088w, 1057w, 995s, 926w, 872m, 787s, 725s.

Elemental Analysis: Found: C, 80.24; H, 4.89; N, 9.28. Calc. for C$_{30}$H$_{21}$N$_3$O·½H$_2$O: C, 80.26; H, 4.91; N, 9.36%.

Melting point: 248.6-250.2ºC.

❖ 4′-(Naphthalen-2-ylsulfanyl)-2,2′:6′,2″-terpyridine (***L^9***)

4'-(Naphthalen-2-ylsulfanyl)-
2,2';6',2"-terpyridine (***L^9***)
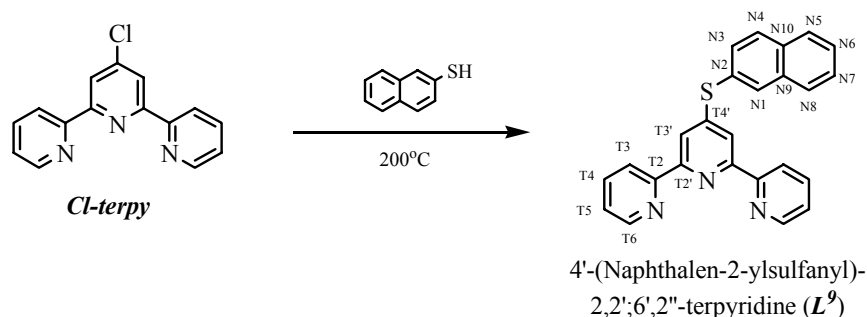
Molecular formula: C$_{25}$H$_{17}$N$_3$S
Molecular weight: 391.49

4′-Chloro-2,2′:6′,2″-terpyridine (1.16 g, 4.33 mmol) and naphthalene-2-thiol (0.694 g, 4.33 mmol) were heated at 200ºC for 2 days. The black crude product was extracted with CH$_2$Cl$_2$ and water. The organic layer was collected, dried (MgSO$_4$) and concentrated. ***L^9*** was obtained as a white product (1.13 g, 2.89 mmol, 66.7%) after column chromatography (Al$_2$O$_3$, DCM/ hexane 2:1).

^{1}H NMR (500 MHz, CDCl$_3$) δ_H 7.34 (ddd, J 1.1, 4.9, 7.4 Hz, 2H, H^{T5}), 7.56 (m, 2H, H^{N6} and H^{N7}), 7.61 (dd, J 1.8, 8.5 Hz, 1H, H^{N3}), 7.88 (m, 4H, H^{T4}, H^{N5} and H^{N8}), 7.91 (d, J 8.7 Hz, 1H, H^{N4}), 8.17 (d, J 1.4 Hz, 1H, H^{N1}), 8.27 (s, 2H, H$^{T3'}$), 8.59 (d, J 8.0 Hz, 2H, H^{T3}), 8.65 (dd, J 0.7, 4.8 Hz, 2H, H^{T6}).

^{13}C NMR (125 MHz, CDCl$_3$): δ_C 119.1 (C$^{T3'}$), 121.8 (C^{T3}), 124.1 (C^{T5}), 126.8 (C$^{N6/ N7}$), 127.2 (C$^{N7/ N6}$), 127.5 (C^{N2}), 127.9 (C$^{N5/ N8}$), 128.0 (C$^{N5/ N8}$), 129.7 (C^{N4}), 130.8 (C^{N3}), 133.3 (C^{N10}), 134.0 (C^{N9}), 134.4 (C^{N1}), 137.6 (C^{T4}), 148.6 (C^{T6}), 152.2 (C$^{T4'}$), 154.8 (C$^{T2'}$), 155.1(C^{T2}).

MS (EI): m/z = 390.1 [M]$^+$ (100%), 195.6 [NapSH+Cl+H]$^+$ (11%).

IR (solid, cm^{-1}): 3055w, 3009w, 1975w, 1690w, 1620w, 1151s, 1466m, 1427w, 1389m, 1327w, 1265w, 1196w, 1119w, 1072w, 1034w, 987m, 941w, 879w, 848.6m, 810m, 779m, 733s.

Elemental Analysis: Found: C, 75.85; H, 4.52; N, 10.79. Calc. for $C_{25}H_{17}N_3S \cdot \frac{1}{4}H_2O$: C, 75.83; H, 4.45; N, 10.61%.

Melting point: 137.9-138.9ºC.

2.8   References

1.   G. T. Morgan, and F. H Burstall, *J. Chem. Soc.*, 1932, 20.

2.   G. T. Morgan, and F. H Burstall, *J. Chem. Soc.*, 1937, 1649.

3.   T. L. Gilchrist, *Heterocyclic Chemistry 2nd ed.*, Longman, Harlow, 1992.

4.   F. Kröhnke, *Synthesis*, 1976, 1.

5.   T. W. G. Solomons, and C. B. Fryhle, *Organic Chemistry 7th ed.*, Wiley, New York, 1998.

6.   K. T. Potts, M. J. Cipullo, P. Ralli, and G. Theodoridis, *J. Am. Chem. Soc.*, 1981, **103**, 3585.

7.   K. T. Potts, M. J. Cipullo, P. Ralli, and G. Theodoridis, *J. Org. Chem.*, 1982, **47**, 3027.

8.   K. T. Potts, P. Ralli, G. Theodoridis, and P. Winslow, *Org. Synth.*, 1985, **26**, 189.

9.   K. T. Potts, D. A. Usifer, A. Guadalupe, and H. D. Abruna, *J. Am. Chem. Soc.*, 1987, **109**, 3961.

10.   M. Heller, and U. S. Schubert, *Eur. J. Org. Chem.*, 2003, 947.

11   A. M. W. Cargill Thompson, *Coord. Chem. Rev.*, 1997, **160**, 1.

12.   K. T. Potts, and D. Konwar, *J. Org. Chem.*, 1991, **56**, 4815.

13.   E. C. Constable, A. M. W. Cargill Thompson, D. A. Tocher, and M. A. M. Daniels, *New J. Chem.*, 1992, **16**, 855.

14.   G. R. Newkome, F. Cardullo, E. C. Constable, C. N. Moorefield, and A. M. W. Cargill Thompson, *J. Chem. Soc., Chem. Commun.*, 1993, 925.

15.   D. Armspach, E. C. Constable, F. Diederich, C. E. Housecroft, and J.-F. Nierengarten, *Chem. Commun.*, 1996, 2009.

16.   D. Armspach, E. C. Constable, F. Diederich, C. E. Housecroft, and J.-F. Nierengarten, *Chem. Eur. J.*, 1998, **4**, 723.

17.   D. Armspach, E. C. Constable, C. E. Housecroft, M. Neuburger, and M. Zehnder, *J. Organomet. Chem.*, 1998, **550**, 193.

18.   P. R. Andres, R. Lunkwitz, G. R. Pabst, K. Böhn, D. Wouters, S. Schmatloch, and U. S. Schubert, *Eur. J. Org. Chem.*, 2003, 3769.

19.   L. Zapata, K. Bathany, J.-M. Schmitter, and S. Moreau, *Eur. J. Org. Chem.*, 2003, 1022.

20.   C. Kim, and H. Kim, *J. Organomet. Chem.*, 2003, **673**, 77.

21.   B. G. G. Lohmeijer, and U. S. Schubert, *Angew. Chem. Int. Ed.*, 2002, **41**, 3825.

22. Y. Molard, and H. Parrot-Lopez, *Tetrahedron Lett.*, 2002, **43**, 6355.

23. O. Inhoff, J. M. Richards, J. W. Brîet, G. Lowe, and R. L. Krauth-Siegel, *J. Med. Chem.*, 2002, **45**, 4524.

24. U. S. Schubert, C. Eschbaumer, O. Hien, and P. R. Andres, *Tetrahedron Lett.*, 2001, **42**, 4705.

25. T. Mutai, J.-D. Cheon, S. Arita, and K. Araki, *J. Chem. Soc., Perkin Trans. 2*, 2001, 1045.

26. G. R. Newkome, E. He, L. A. Godínez, and G. R. Gregory, *J. Am. Chem. Soc.*, 2000, **122**, 9993.

27. G. R. Newkome, E. He, L. A. Godínez, and G. R. Baker, *Chem. Commun.*, 1999, 27.

28. G. Lowe, A. S. Droz, T. Vilaivan, G. W. Weaver, L. Tweedale, J. M. Pratt, P. Rock, V. Yardley, and S. L. Croft, *J. Med. Chem.*, 1999, **42**, 999.

29. G. Lowe, A.-S. Droz, J. J. Park, and G. W. Weaver, *Bioorg. Chem.*, 1999, **27**, 477.

30. V. Marvaud, and D. Astruc, *Chem. Commun.*, 1997, 773.

31. E. C. Constable, C. E. Housecroft, M. Neuburger, and A. G. Schneider, *Inorg. Chem. Commun.*, 2003, **6**, 912.

32. E. C. Constable, C. E. Housecroft, M. Neuburger, A. G. Schneider, and M. Zehnder, *J. Chem. Soc., Dalton Trans.*, 1997, 2427.

33. H. Krass, E. A. Plummer, J. M. Haider, P. R. Barker, N. W. Alcock, Z. Pikramenou, M. J. Hannon, and D. G. Kurth, *Angew. Chem. Int. Ed.*, 2001, **40**, 3862.

34. N. W. Alcock, P. R. Barker, J. M. Haider, M. J. Hannon, C. L. Painting, Z. Pikramenou, E. A. Plummer, K. Rissanen, and P. Saarenketo, *J. Chem. Soc., Dalton Trans.*, 2000, 1447.

35. M.-C. Tse, K.-K. Cheung, M. C.-W. Chan, and C.-M. Che, *Chem. Commun.*, 1998, 2295.

36. E. C. Constable, and M. D. Ward, *J. Chem. Soc., Dalton Trans.*, 1990, 1405.

37. E. Murguly, T. B. Norsten, and N. Branda, *J. Chem. Soc., Perkin Trans. 2*, 1999, 2789.

38. J.- X. Wang, M. Zhang, Z. Xing, and Y. Hu, *Synth. Commun.*, 1996, **26**, 301.

39. T. G. C. Bird, P. Bruneau, G. C. Crawley, M. P. Edwards, S. J. Foster, J.-M. Girodeau, J. F. Kingston, and R. M. McMillan, *J. Med. Chem.*, 1991, **34**, 2176.

40. E. A. Coats, K. J. Shah, S. R. Milstein, C. S. Genther, D. M. Nene, J. Rosener, J. Schmidt, M. Pleiss, and E. Wagner, *J. Med. Chem.*, 1982, **25**, 57.

41. J.-S. Yang, C.-S. Lin, and C.-Y. Hwang, *Org. Lett.*, 2001, **3**, 889.

42. J. Rigaudy, A. M. Seuleiman, and N. K. Cuong, *Tetrahedron*, 1982, **38**, 3143.

43. Y. Tamura, G. Yamamoto, and M. Oki, *Chem. Lett.*, 1986, 1619.

44. Y. Tamura, G. Yamamoto, and M. Oki, *Bull. Chem. Soc. Jpn.*, 1987, **60**, 1781.

45. Y. Tao, Ph. D. Thesis, University of Birmingham, 2004.

46. E. C. Constable, C. E. Housecroft, L. A. Johnston, D. Armspach, M. Neuburger, and M. Zehnder, *Polyhedron*, 2001, **20**, 483.

47. E. C. Constable, M. Neuburger, D. R. Smith, and M. Zehnder, *Inorg. Chim. Acta*, 1998, **275-276**, 359.

48. E. C. Constable, and A. M. W. Cargill Thompson, *J. Chem. Soc., Dalton Trans.,* 1992, 2947.

49. E. C. Constable, J. Lewis, M. C. Liptrot, and P. R. Raithby, *Inorg. Chim. Acta*, 1990, **178**, 47.

50. R.-A. Fallahpour, M. Neuburger, and M. Zehnder, *Polyhedron*, 1999, **18**, 2445.

51. T. Steiner, *Angew. Chem. Int. Ed.*, 2002, **41**, 48.

52. A. Hergold-Brundic, Z. Popovic, and D. Matkovic-Calogovic, *Acta Crystallogr., Sect. C*, 1996, **52**, 3154.

53. K. N. Robertson, P. K. Bakshi, S. D. Lantos, T. S. Cameron, and O. Knop, *Can. J. Chem.*, 1998, **76**, 583.

54. M. G. B. Drew, P. B. Iveson, M. J. Hudson, J. O. Liljenzin, L. Spjuth, P.-Y. Cordier, Å. Enarsson, C. Hill, and C. Madic, *J. Chem. Soc., Dalton Trans.*, 2000, 821.

55. U. Sampath, W. C. Putnam, T. A. Osiek, S. Touami, J. Xie, D. Cohen, A. Cagnolini, P. Droege, D. Klug, C. L. Barnes, A. Modak, J. K. Bashkin, and S. S. Jurisson, *J. Chem. Soc., Dalton Trans.*, 1999, 2049.

56. E. C, Constable, F. R. Heirtzler, M. Neuburger, and M. Zehnder, *Supramol. Chem.*, 1995, **5**, 197.

57. E. C, Constable, F. R. Heirtzler, M. Neuburger, and M. Zehnder, *J. Am. Chem. Soc.*, 1997, **119**, 5606.

58. J. H. Clements, and S. E. Webber, *J. Phys. Chem. B*, 1999, **103**, 9366.

Chapter 3

Synthesis of Homoleptic Mononuclear Iron(II) and Ruthenium(II) Complexes of 4′-Substituted-2,2′:6′,2″-Terpyridine Ligands

Over the past 30 years, the photochemical and photophysical properties of Ru(II) complexes of 2,2′-bipyridine (**bipy**) and its derivatives have been widely investigated.[1-16] Complexes of 2,2′-bipyridine derivatives are of particular interest because of their redox properties, luminescence intensities and excited state lifetimes.[1,2,17] Although the Ru(II) complexes of 2,2′:6′,2″-terpyridine derivatives exhibit lower luminescence intensities and shorter excited state lifetimes at room temperature than those of 2,2′-bipyridine and its derivatives, complexes of 2,2′:6′,2″-terpyridine derivatives are still of great interest. This is because of their synthetic and structural advantages (see **Section 1.3**).[2,17,18] Therefore, many efforts have been made to design luminescent supramolecular systems that can undergo photoinduced energy-transfer or electron-transfer process.[6,12,19-37]

$$[M(\textit{X-terpy})_2]^{2+}$$

M = Fe or Ru
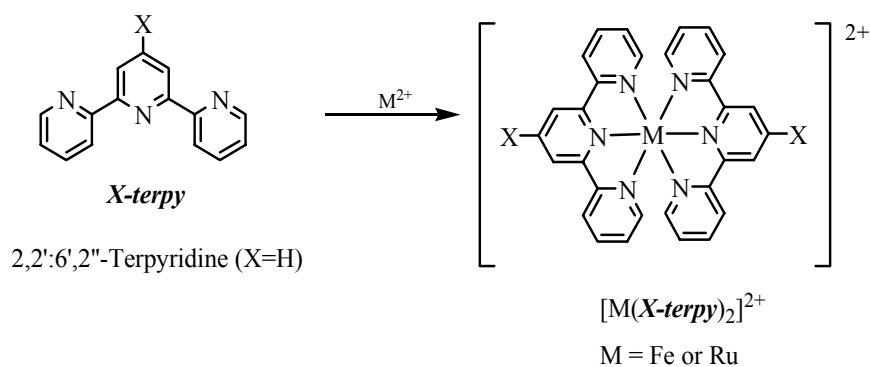
Scheme 1. Complexation reaction between a metal centre and 2,2′:6′,2″-terpyridine and its derivatives.

2,2′:6′,2″-Terpyridine derivatives (**X-terpy**) can form metal complexes with a variety of transition metal ions. The spatial properties of a complex are determined by (1) the coordination number and coordination geometry of the metal ion and (2) the number, type and distribution of the coordination sites of the ligand.[38,39] Therefore, when the 2,2′:6′,2″-terpyridine and its derivatives (**X-terpy**) [which act as tridentate ligands]

react with metal ions such as Fe(II) or Ru(II), achiral octahedral complexes (strictly D_{2d} symmetry) are usually formed (**Scheme 1**).[40] Fe(II) and Ru(II) are d^6 ions and in the low-spin state, they are kinetically inert [Ru(II) > Fe(II)]; this is a great advantage for synthesis as the complexes are relatively stable.

The coordination behaviour of the mononuclear Fe(II) and Ru(II) complexes of 4′-substituted-2,2′:6′,2″-terpyridine ligands described in Chapter 2 will be fully explored in this chapter (**Scheme 2**).

[M(**L**^{4})$_2$][PF$_6$]$_2$
M = Fe or Ru

[M(**L**)$_2$][PF$_6$]$_2$ (**L** = **L**^{5}-**L**^{7})
M = Fe or Ru
n = 0, **L** = **L**^{5}
n = 1, **L** = **L**^{6}
n = 2, **L** = **L**^{7}

[M(**L**^{8})$_2$][PF$_6$]$_2$
M = Fe or Ru

[M(**L**^{9})$_2$][PF$_6$]$_2$
M = Fe or Ru
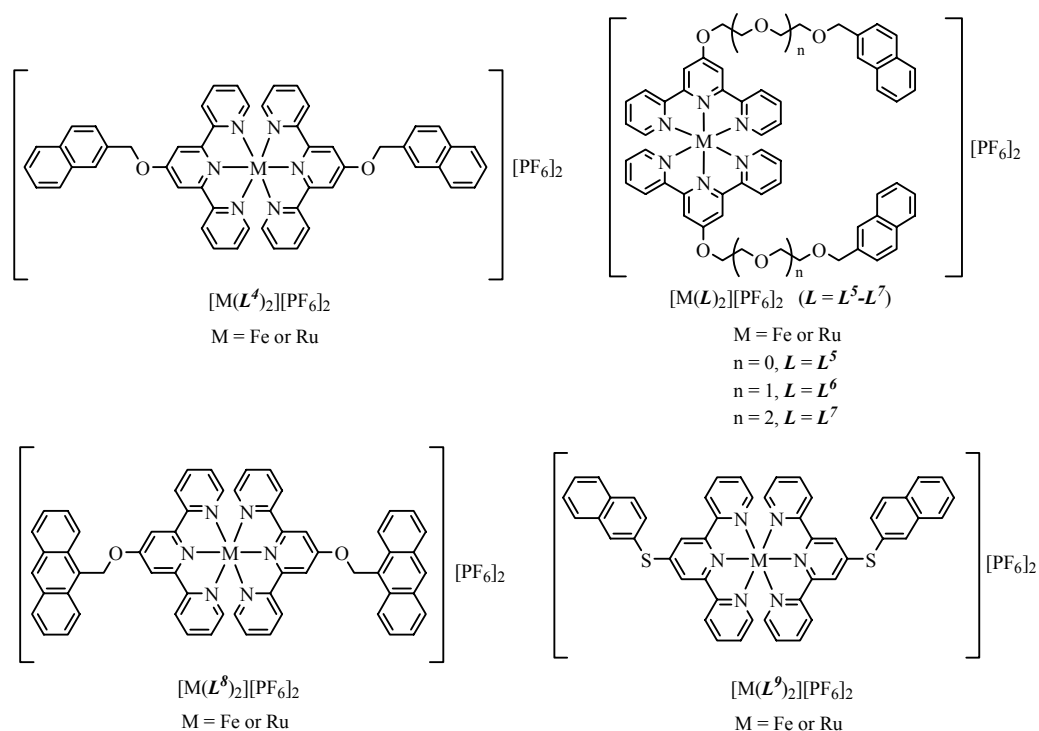
Scheme 2. Fe(II) and Ru(II) complexes of 4′-substituted-2,2′:6′,2″-terpyridine ligands studies in this chapter.

3.1   Synthesis

(a) Syntheses of homoleptic iron(II) complexes

Homoleptic Fe(II) complexes are readily prepared by reacting 2 equivalents of ligand (**L**) and 1 equivalent of FeCl$_2$·4H$_2$O in methanol for 1 hour. The solution turned purple immediately. A purple precipitate appeared when excess aqueous NH$_4$PF$_6$ was

added. The purple precipitate was filtered and collected.[23,41] The yield of [Fe(**L**)$_2$][PF$_6$]$_2$ (where **L** = **L^4**-**L^9**) complexes ranged from 74-98% (**Scheme 3**).
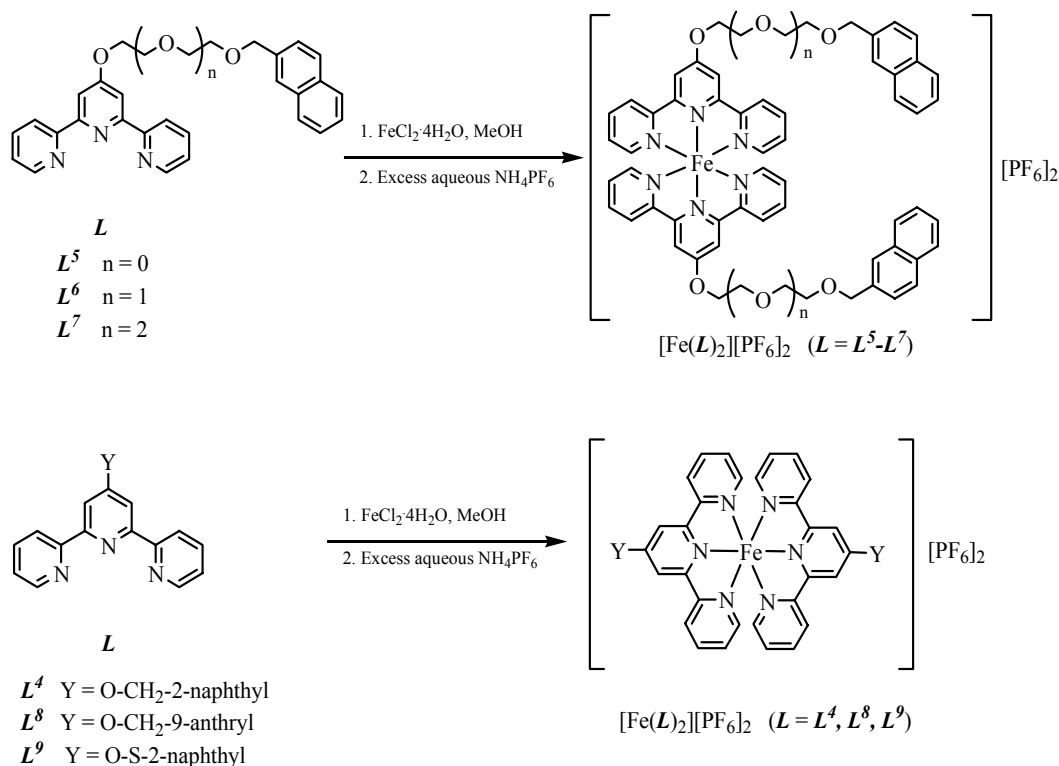
Scheme 3. The general syntheses of [Fe(**L**)$_2$][PF$_6$]$_2$ (where **L** = **L^4**-**L^9**).

(b) Syntheses of homoleptic ruthenium(II) complexes

There are three methods of synthesising homoleptic Ru(II) complexes shown in **Scheme 2**. The first method involves refluxing 2 equivalents of ligand (**L**) and 1 equivalent of RuCl$_3$·3H$_2$O in ethylene glycol and the reducing agent *N*-ethylmorpholine (NEM) for 3 hour.[23,31,42] The solution turns red and a red precipitate appears when excess aqueous NH$_4$PF$_6$ is added. The red precipitate [Ru(**L**)$_2$][PF$_6$]$_2$ is filtered and collected. The second method involves heating 2 equivalents of ligand (**L**) and 1 equivalent of RuCl$_3$·3H$_2$O in ethylene glycol and NEM in a microwave oven (600 W) for 2 minutes.[36,43] Then, the same work up procedure as described in the first method is applied to obtain the [Ru(**L**)$_2$][PF$_6$]$_2$ complexes.
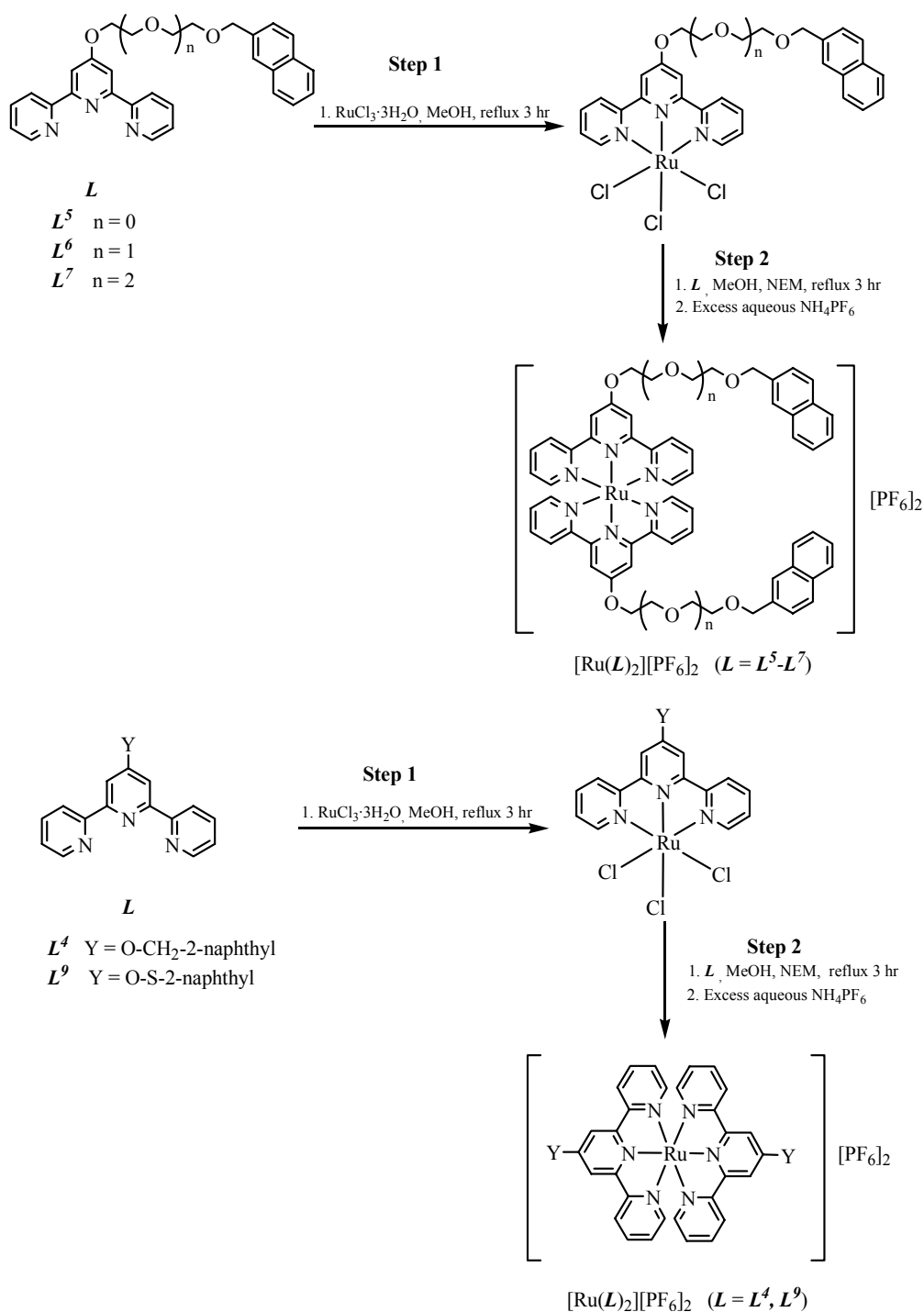
Scheme 4. The general syntheses of [Ru(***L***)₂][PF₆]₂ (where ***L*** = ***L⁴-L⁷***, ***L⁹***).

The third method is most widely used to synthesise the homoleptic Ru(II) complexes and it was used to synthesise all the [Ru(***L***)₂][PF₆]₂ complexes in this chapter except for [Ru(***L⁸***)₂][PF₆]₂. The homoleptic Ru(II) complexes are synthesised in a stepwise manner.[24,26,29] Firstly, 1 equivalent of ligand (***L***) and 1 equivalent of RuCl₃·3H₂O were

refluxed in methanol for 3 hours. Then, the dark brown insoluble [Ru*L*Cl$_3$] was collected and washed well with water. Secondly, 1 equivalent of [Ru*L*Cl$_3$] and 1 equivalent of ligand (*L*) were refluxed in methanol and few drops of the reducing agent *N*-ethylmorpholine (NEM) for another 3 hours. By adding excess aqueous NH$_4$PF$_6$, a red precipitate of the product appeared. Then, the red precipitate [Ru(*L*)$_2$][PF$_6$]$_2$ was filtered, collected and washed well with water. The overall yield of [Ru(*L*)$_2$][PF$_6$]$_2$ (where *L* = *L^4*-*L^7*, *L^9*) ranged from 35-69% (**Scheme 4**).

An attempt to synthesise [Ru(*L^8*)$_2$][PF$_6$]$_2$ using the above three methods failed. Therefore, another procedure was used (**Scheme 5**).[42] [Ru(***HO-Terpy***)$_2$][PF$_6$]$_2$, which is synthesised in two steps by the previously described procedure, and dry K$_2$CO$_3$ were stirred in dry acetonitrile at 70°C for 2 hours. The reaction mixture was kept at 70°C throughout the reaction. Then, 9-bromomethylanthracene was added to the reaction mixture and the mixture was stirred for 1 day. Excess aqueous NH$_4$PF$_6$ was added to the solution. The dark brown precipitate was filtered and collected. The crude product was purified by column chromatography (silica, A sol). The yield of [Ru(*L^8*)$_2$][PF$_6$]$_2$ is 71%.
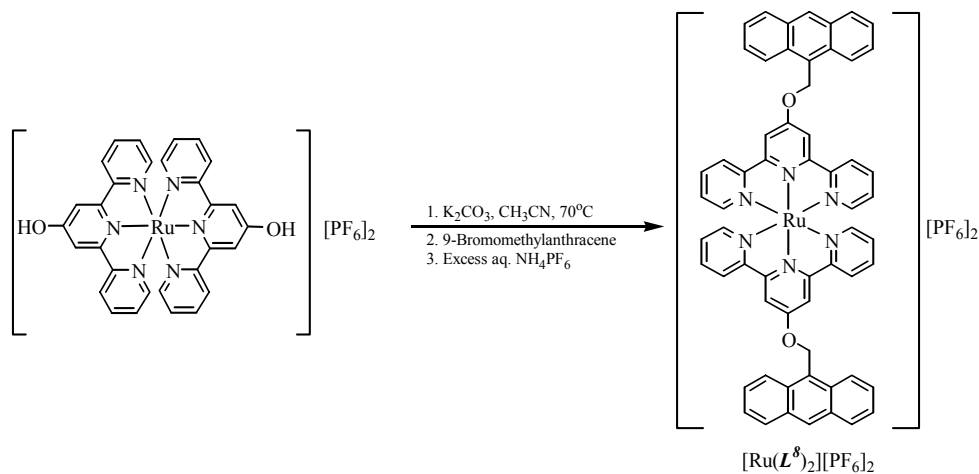
Scheme 5. The synthesis of [Ru(*L^8*)$_2$][PF$_6$]$_2$.

3.2 ^{1}H NMR spectroscopic characterisation

All the complexes were characterised by ^{1}H NMR spectroscopy in CD$_3$CN solution. The ^{1}H NMR spectra of the complexes were similar to those of other related

bis(terpyridine) systems. The terpyridine proton signals are similar in all complexes with the exception of the signals H^{T6} and $H^{T3'}$ which are subject to the influence of the metal centre and of the 4′-substituents attached to the terpyridine domain (**Table 1**).[41,42]

	Proton resonance (δ)				
	H^{T5}	H^{T6}	H^{T4}	H^{T3}	$H^{T3'}$
[Fe(***poterpy***)₂][PF₆]₂[*,41]	7.08 (td) J 1.2, 6.0 Hz	7.14 (d) J 4.2 Hz	7.87 (td) J 1.8, 7.4 Hz	8.43 (d) J 8.1 Hz	8.50 (s)
[Fe(***L⁴***)₂][PF₆]₂	7.08 (ddd) J 1.3, 5.6, 7.5 Hz	7.17 (ddd) J 0.7, 1.4, 5.6 Hz	7.87 (td) J 1.5, 7.8 Hz	8.44 (ddd) J 0.8, 1.2, 8.0 Hz	8.60 (s)
[Fe(***L⁵***)₂][PF₆]₂	6.99 (m)	7.09 (dd) J 0.6, 5.6 Hz	7.79 (m)	8.36 (d) J 8.0 Hz	8.49 (s)
[Fe(***L⁶***)₂][PF₆]₂	7.00 (t) J 7.1 Hz	7.11 (d) J 5.6 Hz	7.81 (m)	8.37 (d) J 8.1 Hz	8.46 (s)
[Fe(***L⁷***)₂][PF₆]₂	7.00 (t) J 6.3 Hz	7.11 (d) J 5.1 Hz	7.81 (m)	8.36 (d) J 8.1 Hz	8.44 (s)
[Fe(***L⁸***)₂][PF₆]₂	7.15 (ddd), J 1.3, 5.6, 7.5 Hz	7.27 (ddd) J 0.7, 1.4, 5.6Hz	7.90 (td) J 1.4, 7.8 Hz	8.45 (dt) J 1.0, 8.0 Hz	8.73 (s)
[Fe(***L⁹***)₂][PF₆]₂	7.06 (ddd) J 1.3, 5.6, 7.6 Hz	7.14 (ddd) J 0.7, 1.4, 5.6 Hz	7.77 (td) J 1.5, 7.8 Hz	8.20 (m)	8.56 (s)
J	J_{34} 8.0 Hz; J_{45} 7.5 Hz; J_{46} 1.4 Hz; J_{53} 1.3 Hz; J_{56} 5.6 Hz; J_{63} 0.7 Hz				
[Ru(***poterpy***)₂][PF₆]₂[*,42]	7.16 (td) J 1.3, 7.0 Hz	7.38 (dd) J 1.1, 5.0 Hz	7.90 (td) J 1.4, 8.0 Hz	8.47 (d) J 8.0 Hz	8.35 (s)
[Ru(***L⁴***)₂][PF₆]₂	7.16 (ddd) J 1.4, 5.7, 7.5 Hz	7.39 (ddd) J 0.6, 1.4, 5.6 Hz	7.90 (td) J 1.5, 7.9 Hz	8.47 (dt) J 0.9, 8.1 Hz	8.45 (s)
[Ru(***L⁵***)₂][PF₆]₂	7.08 (ddd) J 1.4, 5.7, 7.5 Hz	7.33 (ddd) J 0.6, 1.4, 5.6 Hz	7.83 (m)	8.39 (dt) J 0.8, 8.1 Hz	8.33 (s)
[Ru(***L⁶***)₂][PF₆]₂	7.08 (ddd) J 1.6, 5.7, 7.5 Hz	7.34 (d) J 5.1 Hz	7.82 (m)	8.40 (d) J 8.1 Hz	8.31 (s)
[Ru(***L⁷***)₂][PF₆]₂	7.08 (t) J 6.6 Hz	7.34 (d) J 5.1 Hz	7.82 (m)	8.39 (d) J 8.1 Hz	8.29 (s)
[Ru(***L⁸***)₂][PF₆]₂	7.22 (ddd) J 1.3, 5.6, 7.5 Hz	7.47 (ddd) J 0.7, 1.5, 5.6Hz	7.93 (ddd) J 1.5, 7.6, 8.1 Hz	8.47 (ddd) J 0.8, 1.3, 8.1 Hz	8.56 (s)
[Ru(***L⁹***)₂][PF₆]₂	7.14 (ddd) J 1.3, 5.6, 7.6 Hz	7.38 (ddd) J 0.7, 1.5, 5.6 Hz	7.81 (ddd) J 1.5, 7.7, 8.1 Hz	8.22 (ddd) J 0.8, 1.3, 8.2 Hz	8.43 (s)
J	J_{34} 8.1 Hz; J_{45} 7.6 Hz; J_{46} 1.5 Hz; J_{53} 1.3 Hz; J_{56} 5.6 Hz; J_{63} 0.7 Hz				

Table 1. ^{1}H NMR spectroscopic data (500 MHz) for the 5 terpyridine proton signals of the 12 complexes in CD₃CN solution at room temperature (except [M(***L⁶***)₂][PF₆]₂ and [M(***L⁷***)₂][PF₆]₂ were measured at 400 MHz, where M = Fe or Ru). (* ***poterpy*** = 4′-(2-propynyl-1-oxy)-2,2′:6′,2″-terpyridine)

	Proton resonance (δ)					
	$H^{N6, N7}$	H^{N3}	H^{N5}	H^{N8}	H^{N4}	H^{N1}
$[Fe(L^4)_2][PF_6]_2$	7.63 (m)	7.83 (dd) J 1.8, 8.4 Hz	8.01 (m)	8.05 (m)	8.10 (d) J 8.4 Hz	8.24 (s)
$[Fe(L^5)_2][PF_6]_2$	7.45 (m)	7.60 (dd) J 1.6, 8.4 Hz	7.79 (m)	7.85 (d) J 8.1 Hz	7.87 (d) J 8.5 Hz	7.94 (s)
$[Fe(L^6)_2][PF_6]_2$	7.44 (m)	7.51 (d) J 8.6 Hz	7.81 (m)			
$[Fe(L^7)_2][PF_6]_2$	7.43 (m)	7.48 (d) J 8.6 Hz	7.81 (m)			
$[Fe(L^9)_2][PF_6]_2$	7.71 (m)	7.94 (dd) J 1.8, 8.6 Hz	8.09 (m)		8.20 (m)	8.53 (d) J 1.5 Hz
$[Ru(L^4)_2][PF_6]_2$	7.62 (m)	7.79 (dd) J 1.8, 8.4 Hz	8.00 (m)	8.03 (m)	8.08 (d) J 8.5 Hz	8.20 (s)
$[Ru(L^5)_2][PF_6]_2$	7.45 (m)	7.59 (dd) J 1.7, 8.4 Hz	7.83 (m)		7.88 (d) J 8.5 Hz	7.92 (s)
$[Ru(L^6)_2][PF_6]_2$	7.44 (m)	7.50 (dd) J 1.3, 8.3 Hz	7.82 (m)			
$[Ru(L^7)_2][PF_6]_2$	7.43 (m)	7.47 (dd) J 1.5, 8.6 Hz	7.82 (m)			
$[Ru(L^9)_2][PF_6]_2$	7.66 (m)	7.85 (dd) J 1.9, 8.6 Hz	8.07 (m)		8.16 (d) J 8.6 Hz	8.46 (d) J 1.6 Hz

	Proton resonance (δ)					
	H^{S1} (s)	$H^{A3, A6}$ (ddd)	$H^{A2, A7}$ (ddd)	$H^{A4, A5}$ (dt)	$H^{A1, A8}$ (dd)	H^{A10} (s)
$[Fe(L^8)_2][PF_6]_2$	6.70	7.67 J 0.9, 6.5, 8.5 Hz	7.77 J 1.3, 6.5, 9.0 Hz	8.26 J 0.6, 8.5 Hz	8.63 J 0.9, 9.0 Hz	8.83
$[Ru(L^8)_2][PF_6]_2$	6.63	7.67 J 0.9, 6.5, 8.4 Hz	7.75 J 1.3, 6.5, 8.9 Hz	8.24 J 0.6, 8.5 Hz	8.59 J 0.9, 9.0 Hz	8.80

Table 2. ^{1}H NMR spectroscopic data (500 MHz) for the naphthyl or the anthryl proton signals of the 12 complexes in CD$_3$CN solution at room temperature (except $[M(L^6)_2][PF_6]_2$ and $[M(L^7)_2][PF_6]_2$ were measured at 400 MHz, where M = Fe or Ru).

The ^{1}H NMR spectrum of $[Fe(L^4)_2][PF_6]_2$ in CD$_3$CN solution is shown in **Figure 1**. Five terpyridine proton signals were found as expected by comparison to a similar Fe(II) system;[41] the rest of the proton signals belonging to the naphthyl rings and the methylene group were further identified by NOESY and COSY techniques. The singlet at δ 5.87, which exhibits an NOE signal (**Figure 2a**) to $H^{T3'}$ singlet at δ 8.60, is assigned to H^{S1}. The signal for H^{S1} also exhibits NOE signals to a singlet H^{N1} and a doublet of doublets H^{N3} at δ 8.24 and δ 7.83 respectively (**Figure 2a**). The signal for H^{N1} exhibits an NOE signal to a signal at δ 8.05, which is assigned to H^{N8} (**Figure 2b**). The signal for H^{N8} gives a COSY cross peak to H^{N7} at δ 7.63 (**Figure 3**). Also,

the signal for H^{N3} gives a COSY cross peak to a doublet at δ 8.10, and is therefore assigned to H^{N4}. The signal for H^{N4} exhibits an NOE signal to a signal at δ 8.01, which is assigned to H^{N5} (**Figure 2b**). The signal for H^{N5} gives a COSY cross peak to the signal assigned to H^{N6} at δ 7.63 (**Figure 3**).
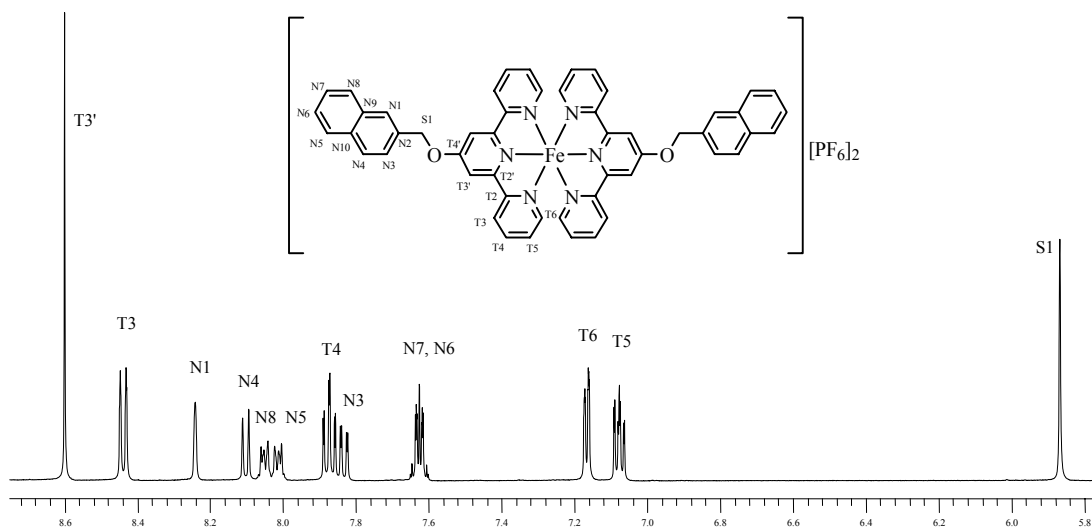
Figure 1. ^{1}H NMR (500 MHz) spectrum of [Fe($\textbf{\textit{L}}^4$)$_2$][PF$_6$]$_2$ in CD$_3$CN solution at room temperature.

(a)   (b)
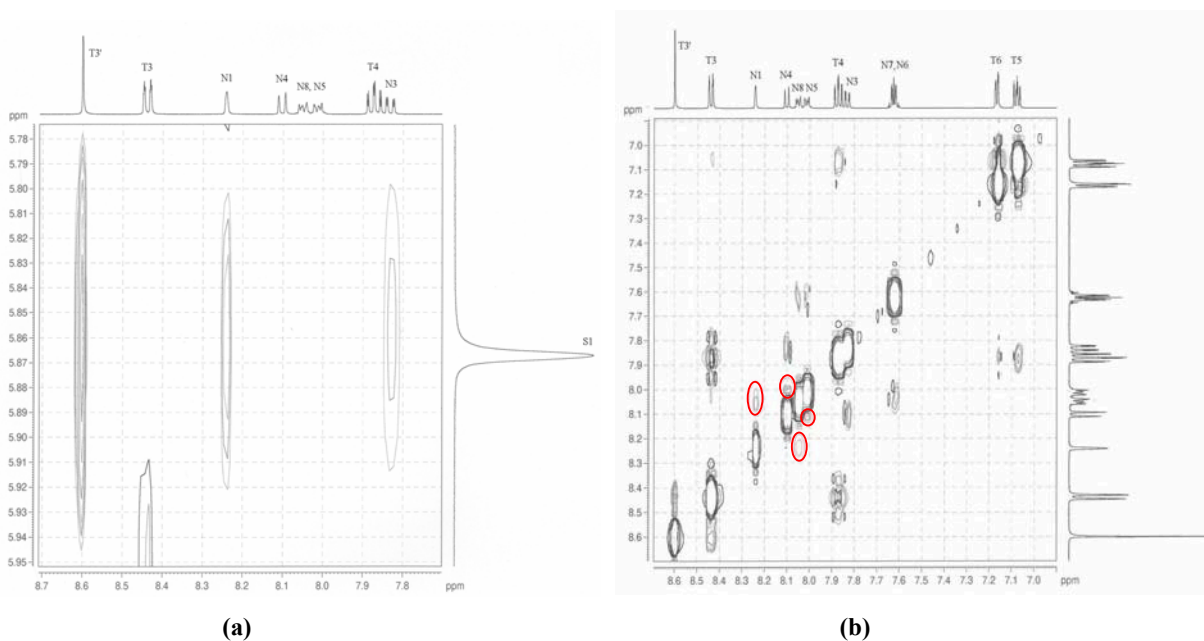
Figure 2. NOESY spectra (500 MHz) of [Fe($\textbf{\textit{L}}^4$)$_2$][PF$_6$]$_2$ in CD$_3$CN solution at room temperature.

Figure 3. COSY spectrum (500 MHz) of [Fe(L^4)$_2$][PF$_6$]$_2$ in CD$_3$CN solution at room temperature.

(a)	**(b)**

Figure 4. COSY spectrum (500 MHz) of [Fe(L^5)$_2$][PF$_6$]$_2$ in CD$_3$CN solution at room temperature.

The five terpyridine signals and the naphthyl signals of [Fe(L^5)$_2$][PF$_6$]$_2$ are assigned as in [Fe(L^4)$_2$][PF$_6$]$_2$ and these are confirmed by a COSY spectrum (**Figure 4a**). The rest of the ethyleneoxy chain signals are assigned by using a COSY spectrum (**Figure 4b**).

The signal for H^{S1} is expected to be at a higher chemical shift than H^{S2}. Therefore, the triplet at δ 4.83 is assigned as H^{S1} and the one at δ 4.18 is assigned as H^{S2}.

The ^{1}H NMR spectra of [Fe(*L⁶*)₂][PF₆]₂ and [Fe(*L⁷*)₂][PF₆]₂ in CD₃CN solution are assigned according to the spectrum for [Fe(*L⁵*)₂][PF₆]₂. There is not much difference in the chemical shifts of the terpyridine signals or of the naphthyl signals as the length of the ethyleneoxy chain varies. However, the proton signals in the spectrum of [Fe(*L⁴*)₂][PF₆]₂, which has the shortest distance between the terpyridine and naphthyl domain, shifted to lower field (**Table 1** and **Table 2**).

The ^{1}H NMR spectrum of [Fe(*L⁸*)₂][PF₆]₂ in CD₃CN solution exhibits ten signals from the terpyridine and the anthryl domains (**Figure 5**). The 5 terpyridine signals are assigned as before. The singlet signal at δ 6.70 is assigned to H^{S1}. The signal for H^{S1} gives NOE signals to a singlet at δ 8.73 and a doublet of doublets at δ 8.63, which are assigned to $H^{T3'}$ and $H^{A1,\ A8}$ respectively (**Figure 6**). From the COSY spectrum (**Figure 7**), $H^{A1,\ A8}$ gives a COSY cross peak to a signal at δ 7.77, which is then assigned to $H^{A2,\ A7}$. The singlet at δ 8.83, which has half of the relative integral of the signal for H^{S1}, is assigned to H^{A10}. H^{A10} gives an NOE signal to a triplet of doublets at δ 8.26; the signal is assigned to $H^{A4,\ A5}$ (**Figure 6**). From the COSY spectrum (**Figure 7**), $H^{A4,\ A5}$ gives a COSY cross peak to a signal at δ 7.67, which is assigned to $H^{A3,\ A6}$.
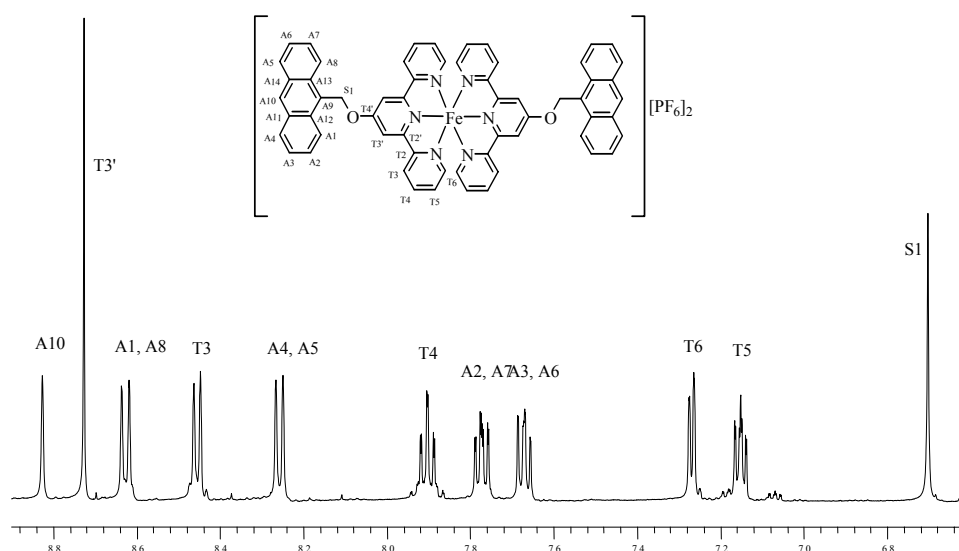
Figure 5. ^{1}H NMR (500 MHz) spectrum of [Fe(*L⁸*)₂][PF₆]₂ in CD₃CN solution at room temperature.
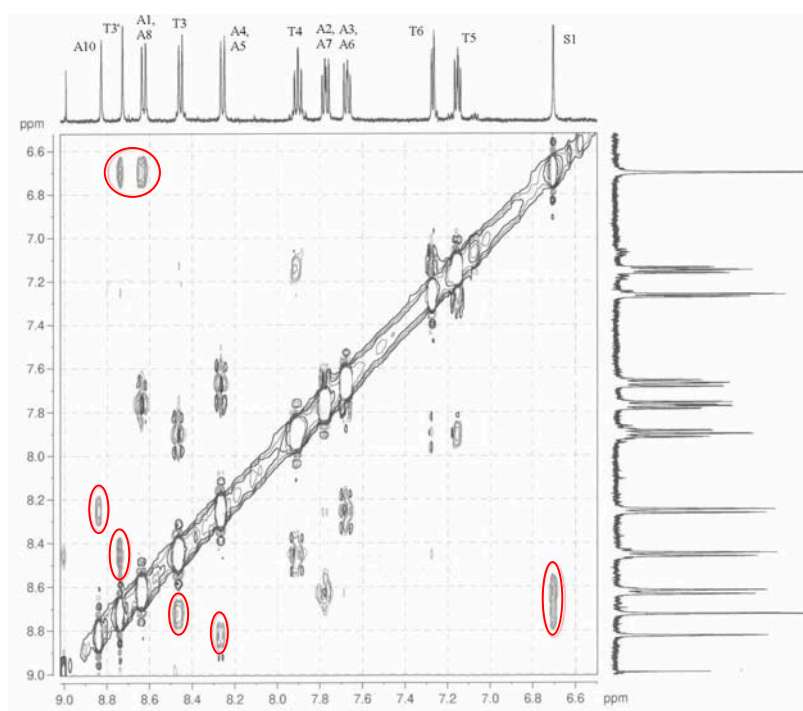
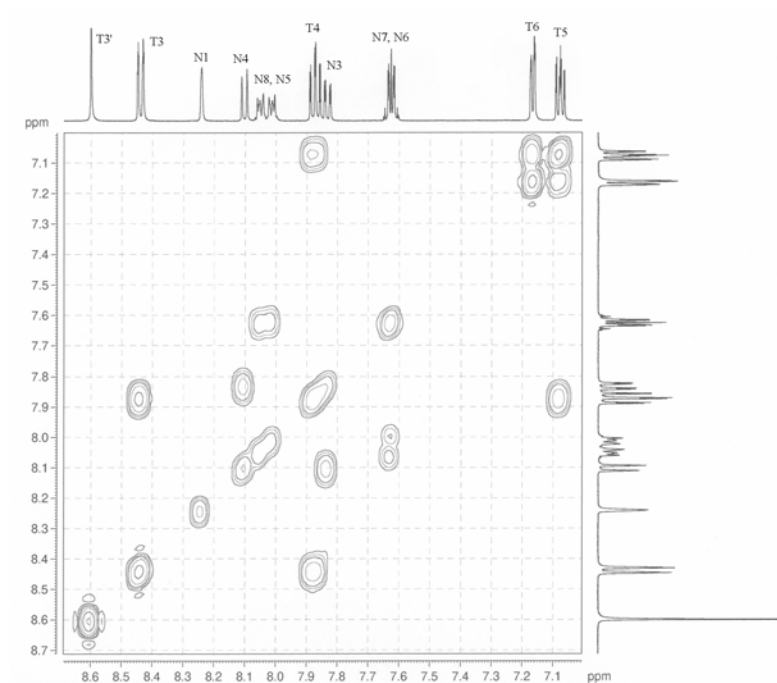**Figure 6.** NOESY spectrum (500 MHz) of [Fe(L^8)$_2$][PF$_6$]$_2$ in CD$_3$CN solution at room temperature.

Figure 7. COSY spectrum (500 MHz) of [Fe(L^8)$_2$][PF$_6$]$_2$ in CD$_3$CN solution at room temperature.

The ^{1}H NMR spectrum of [Fe(L^9)$_2$][PF$_6$]$_2$ in CD$_3$CN solution is shown in **Figure 8b**. By comparing the spectrum to that of [Fe(L^4)$_2$][PF$_6$]$_2$, there are very different chemical shifts for the naphthyl ring when the linkage was changed from OCH$_2$ to S between the terpyridine and naphthyl domain (**Figure 8**). Five terpyridine signals were assigned as previously described. The rest of the signals belonging to the naphthyl ring were further identified by NOESY and COSY techniques. The doublet with a coupling constant of 1.5 Hz at δ 8.53 is assigned to H^{N1}. The signal for H^{N1} exhibits NOE signals to signals at δ 8.09 and δ 7.94, which are assigned to H^{N8} and H^{N3} respectively (**Figure 9**). Then, the signal for H^{N8} gives a COSY cross peak to the signal at δ 7.71, and is therefore assigned to H^{N7}. Also, the signal for H^{N3} gives a COSY cross peak to a signal at δ 8.20, and is then assigned to H^{N4} (**Figure 10**). The signal for H^{N4} exhibits an NOE signal to a signal at δ 8.09, which is assigned to H^{N5} (**Figure 9**). H^{N5} gives a COSY cross peak to H^{N6} signal at δ 7.71 (**Figure 10**).

Within the series of [Fe(L)$_2$][PF$_6$]$_2$ complexes (L = L^4-L^7), the terpyridine signals in the ^{1}H NMR spectra vary, especially the H$^{T3'}$ signal, as the end domain is varied. It is worth noting that there are no significant differences when the length of the ethyleneoxy linkage is varied in the case of [Fe(L)$_2$][PF$_6$]$_2$ (L = L^5-L^7).
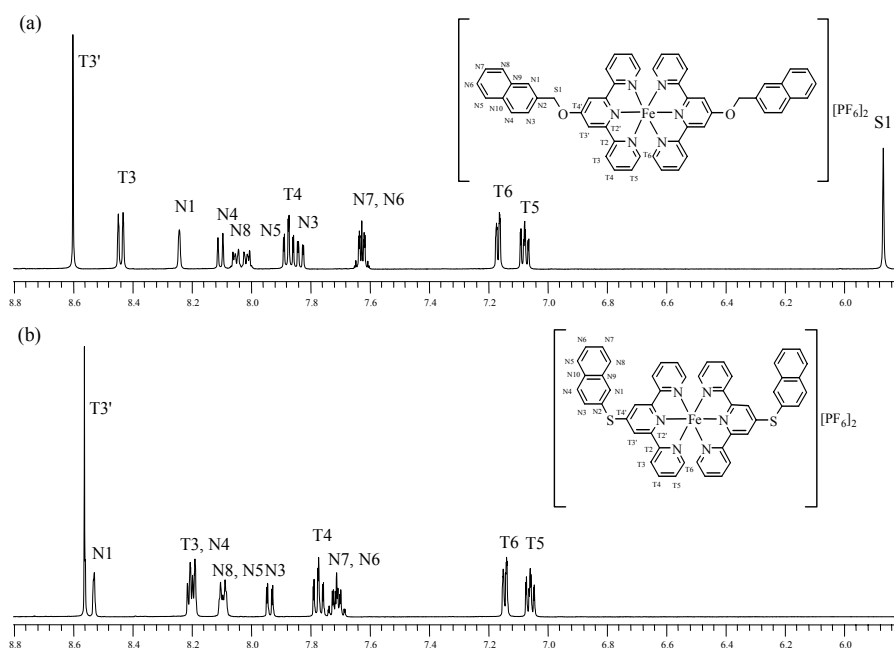
Figure 8. ^{1}H NMR (500 MHz) spectra of (a) [Fe(L^4)$_2$][PF$_6$]$_2$ and (b) [Fe(L^9)$_2$][PF$_6$]$_2$ in CD$_3$CN solution at room temperature.
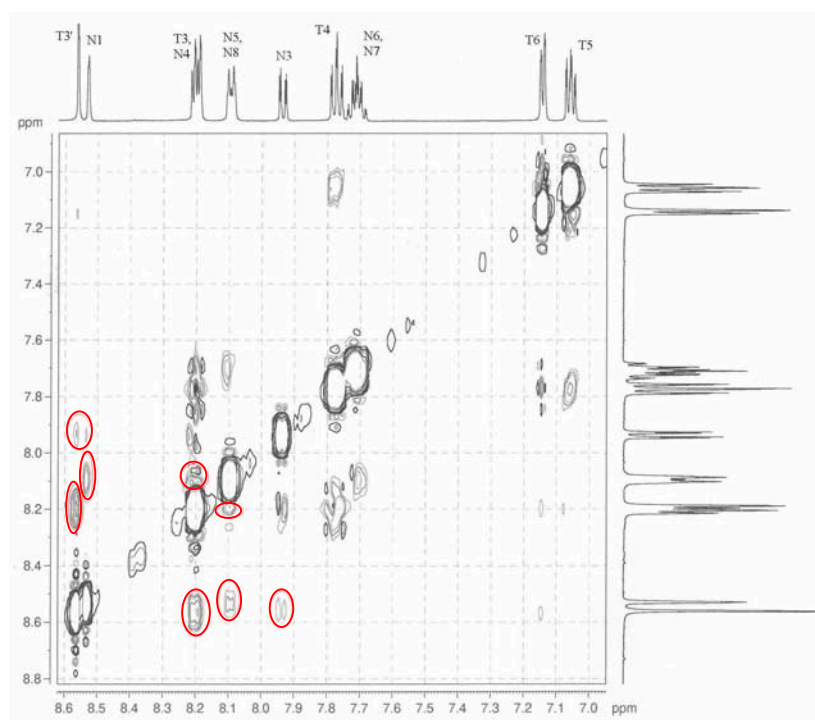
Figure 9. NOESY spectrum (500 MHz) of [Fe(L^9)$_2$][PF$_6$]$_2$ in CD$_3$CN solution at room temperature.
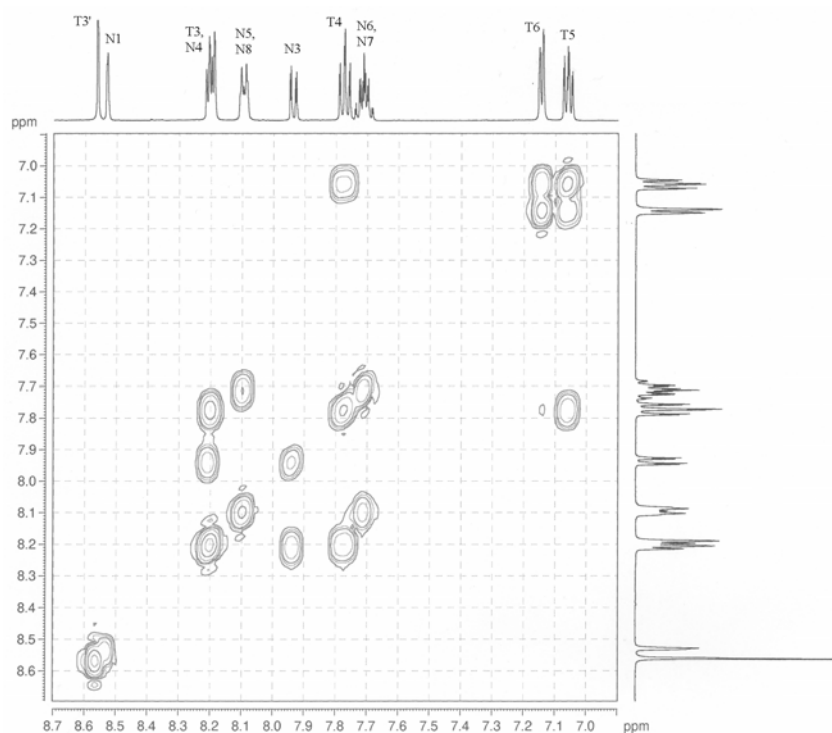
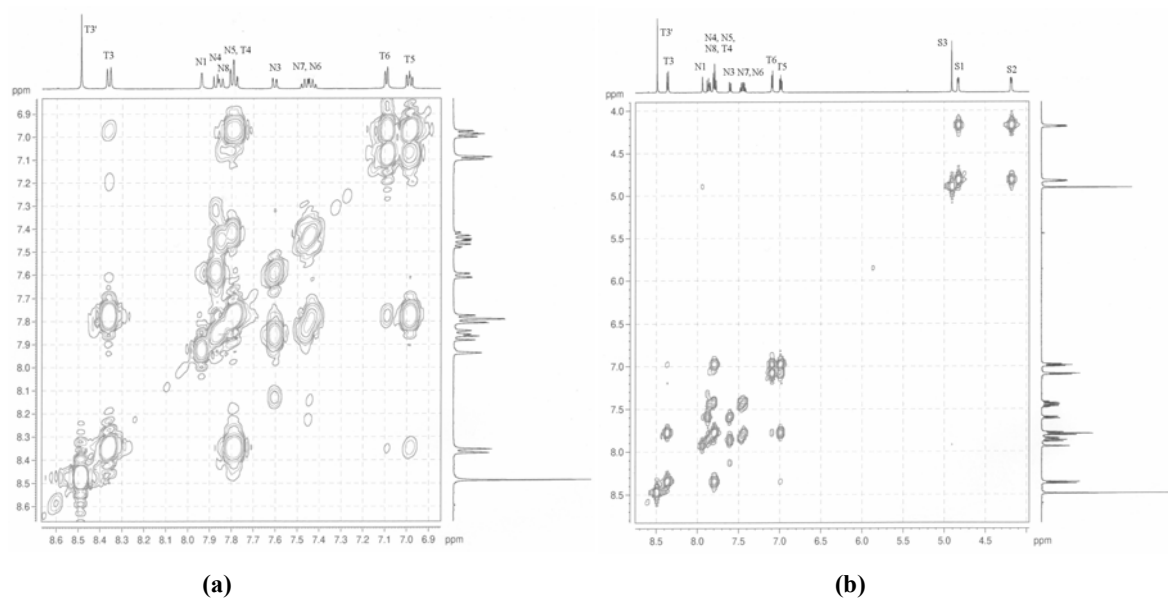**Figure 10.** COSY spectrum (500 MHz) of [Fe(L^9)$_2$][PF$_6$]$_2$ in CD$_3$CN solution at room temperature.

The ^{1}H NMR spectrum of [Ru(L^4)$_2$][PF$_6$]$_2$ in CD$_3$CN solution is shown in **Figure 11**. The five terpyridine signals were found as expected by comparison to a similar Ru(II) system;[42] the rest of the signals belonging to the naphthyl ring and methylene protons were further assigned by NOESY and COSY experiments. The singlet at δ 5.79, which exhibits an NOE signal to the signal for H$^{T3'}$ at δ 8.45, is assigned to H^{S1} (**Figure 12a**). The signal for H^{S1} also exhibits NOE signals to signals for H^{N1} and H^{N3} at δ 8.20 and δ 7.79 respectively (**Figure 12a**). The signal for H^{N1} exhibits an NOE signal to a signal at δ 8.03, which is assigned to H^{N8} (**Figure 12b**). The signal for H^{N8} gives a COSY cross peak to the signal for H^{N7} at δ 7.62 (**Figure 13**). In the COSY spectrum (**Figure 13**), the signal for H^{N3} gives a COSY cross peak to the signal at δ 8.08, and this is therefore assigned to H^{N4}. The signal for H^{N4} exhibits an NOE signal to the signal at δ 8.00, which is assigned to H^{N5} (**Figure 12b**). The signal for H^{N5} gives a COSY cross peak to the signal for H^{N6} at δ 7.62 (**Figure 13**).
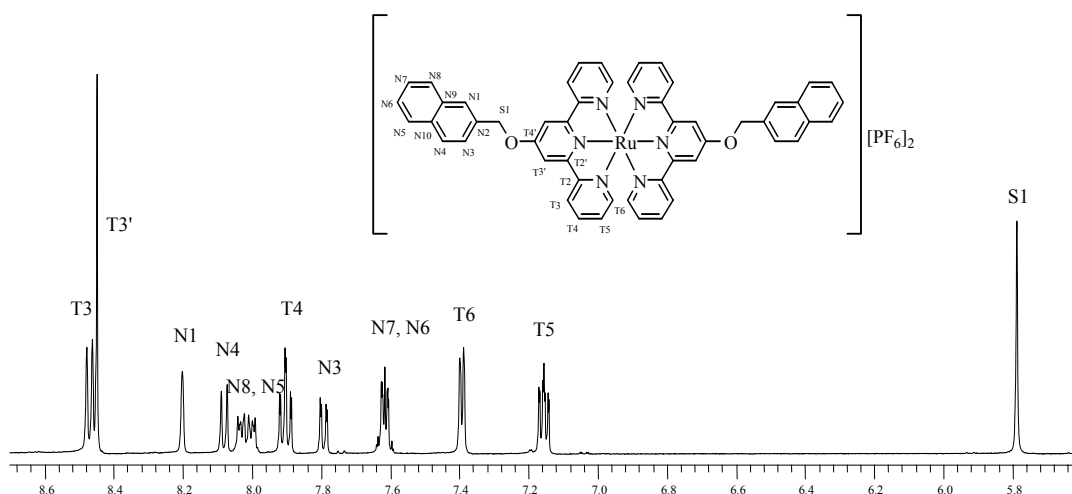
Figure 11. ^{1}H NMR (500 MHz) spectrum of [Ru(L^4)$_2$][PF$_6$]$_2$ in CD$_3$CN solution at room temperature.

(a)   (b)
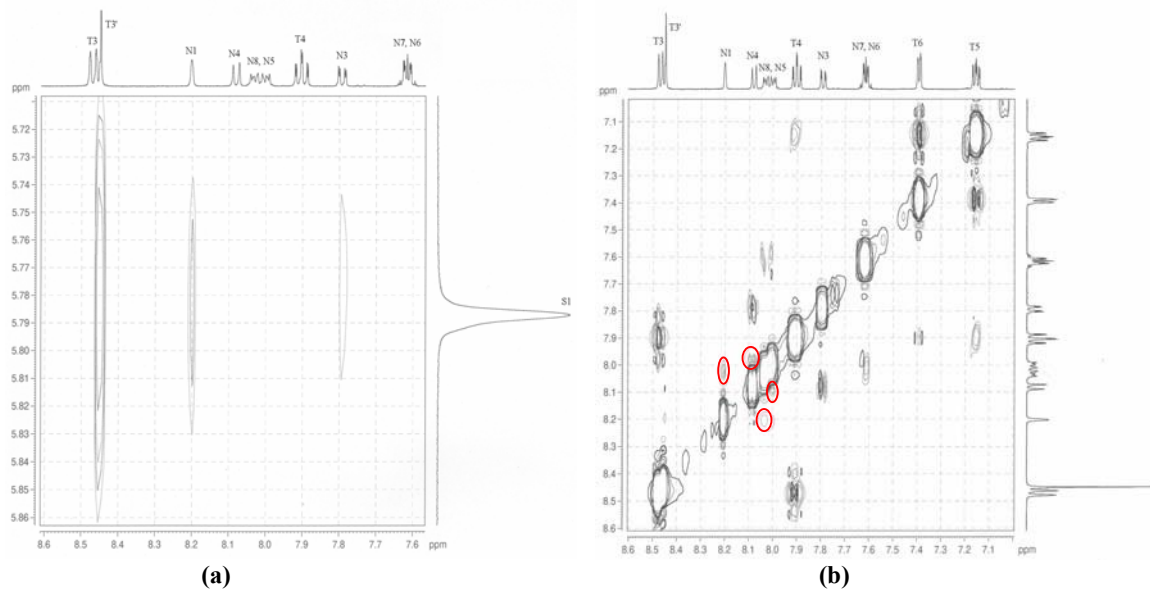
Figure 12. NOESY spectra (500 MHz) of $[Ru(L^4)_2][PF_6]_2$ in CD_3CN solution at room temperature.

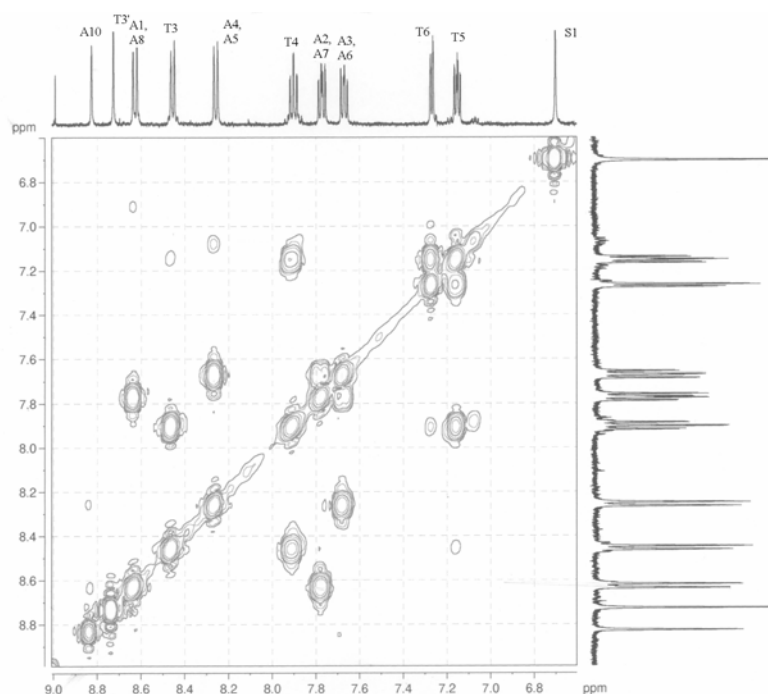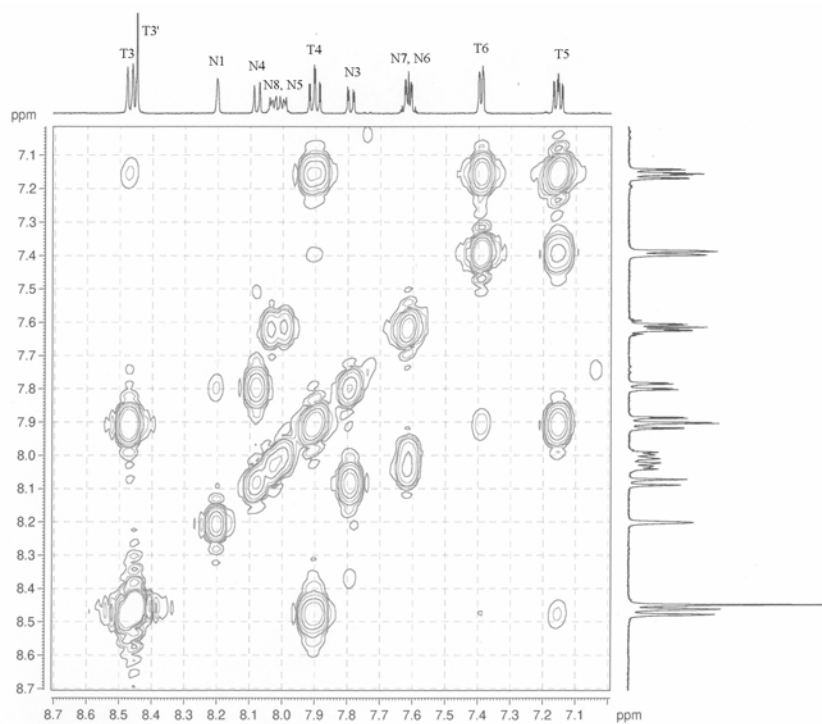**Figure 13**. COSY spectrum (500 MHz) of $[Ru(L^4)_2][PF_6]_2$ in CD_3CN solution at room temperature.

The ^1H NMR spectrum of $[Ru(L^5)_2][PF_6]_2$ in CD_3CN solution is shown in **Figure 14**. The five terpyridine signals and the naphthyl signals have been assigned in the same

way as for $[Ru(\textbf{\textit{L}}^{4})_{2}][PF_{6}]_{2}$ and the assignments were confirmed by COSY and NOESY.
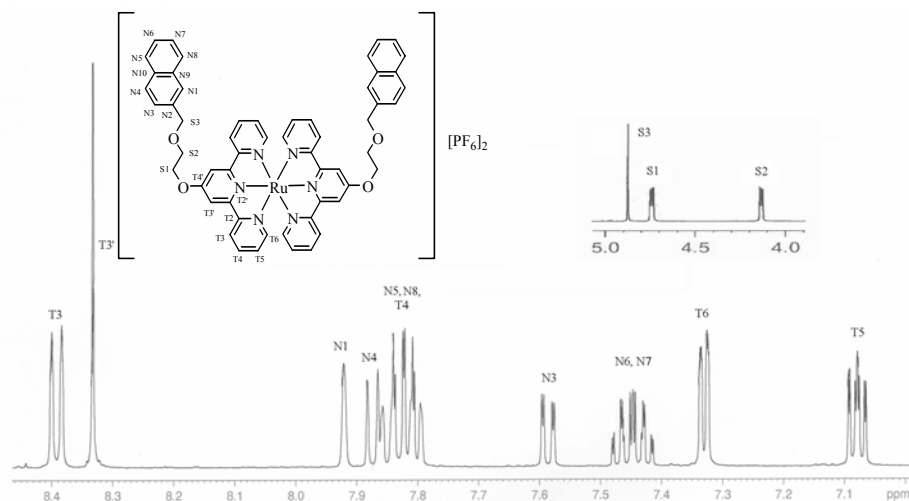
Figure 14. ^{1}H NMR (500 MHz) spectrum of $[Ru(\textbf{\textit{L}}^{5})_{2}][PF_{6}]_{2}$ in CD$_{3}$CN solution at room temperature.

The ^{1}H NMR spectra of $[Ru(\textbf{\textit{L}}^{6})_{2}][PF_{6}]_{2}$ and $[Ru(\textbf{\textit{L}}^{7})_{2}][PF_{6}]_{2}$ in CD$_{3}$CN solution were assigned by a comparison of the spectra to that of $[Ru(\textbf{\textit{L}}^{5})_{2}][PF_{6}]_{2}$. There are no significant differences between the chemical shifts of the terpyridine signals and naphthyl signals in this series of compounds even though the length of the ethyleneoxy chain varies (**Table 1** and **Table 2**).

The ^{1}H NMR spectrum of $[Ru(\textbf{\textit{L}}^{8})_{2}][PF_{6}]_{2}$ in CD$_{3}$CN solution exhibits ten signals from the terpyridine and the anthryl domains (**Figure 15**). The five terpyridine signals were assigned as previously described. The singlet at δ 6.63 is assigned to H^{S1}. The signal for H^{S1} gives NOE signals to a singlet at δ 8.56 and a doublet of doublets at δ 8.59 (**Figure 16**). These signals are therefore assigned to H$^{T3'}$ and H$^{A1, A8}$ respectively. In the COSY spectrum (**Figure 17**), H$^{A1, A8}$ gives a cross peak to the signal at δ 7.75, and this signal is assigned to H$^{A2, A7}$. The singlet at δ 8.80, which has half of the relative integral of the signal for H^{S1}, is assigned to H^{A10}. The signal for H^{A10} gives an NOE signal to a signal at δ 8.24, which is assigned to H$^{A4, A5}$ (**Figure 16**). In the COSY spectrum (**Figure 17**), H$^{A4, A5}$ gives a cross peak to a signal at δ 7.67, and this signal is assigned to H$^{A3, A6}$. Interestingly, there are no significant differences in the anthryl signals when the metal centre changes from Fe(II) to Ru(II) (**Table 2**).
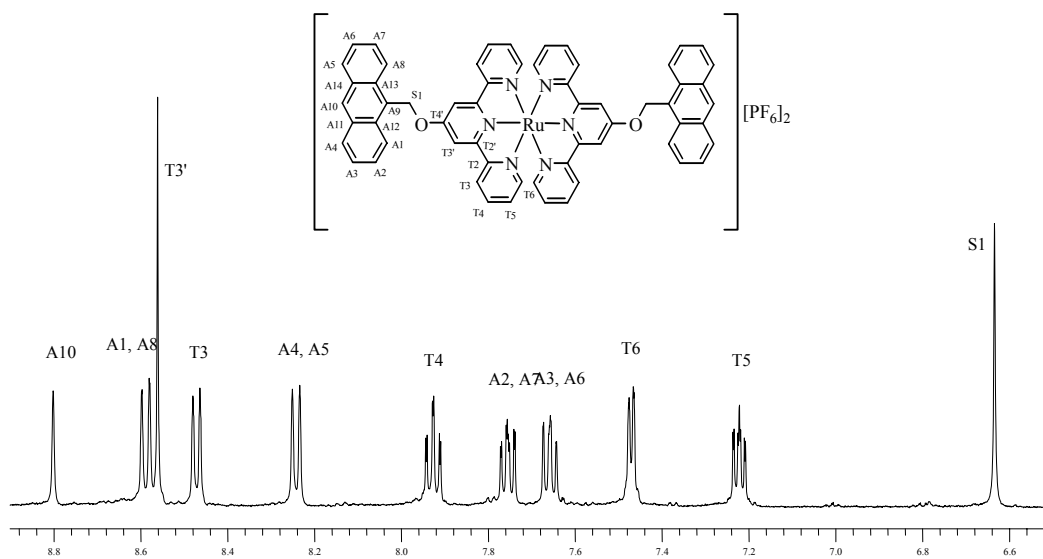
Figure 15. ^{1}H NMR spectrum (500 MHz) of [Ru($\textbf{\textit{L}}^{\textbf{\textit{8}}}$)$_2$][PF$_6$]$_2$ in CD$_3$CN solution at room temperature.
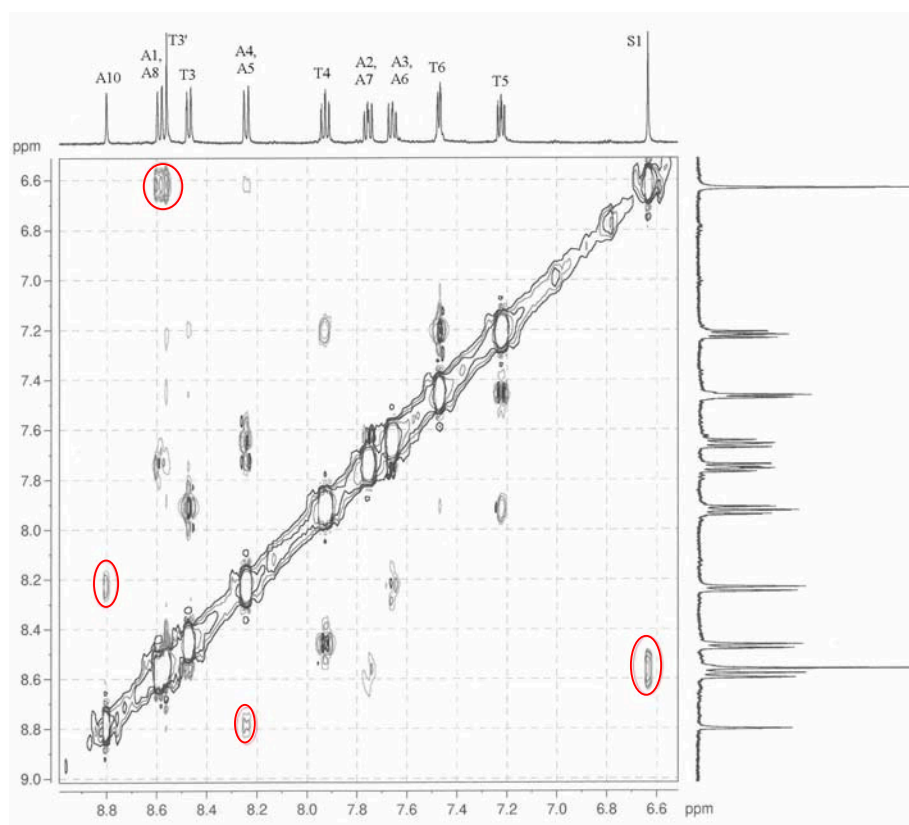
Figure 16. NOESY spectrum (500 MHz) of [Ru($\textbf{\textit{L}}^{\textbf{\textit{8}}}$)$_2$][PF$_6$]$_2$ in CD$_3$CN solution at room temperature.
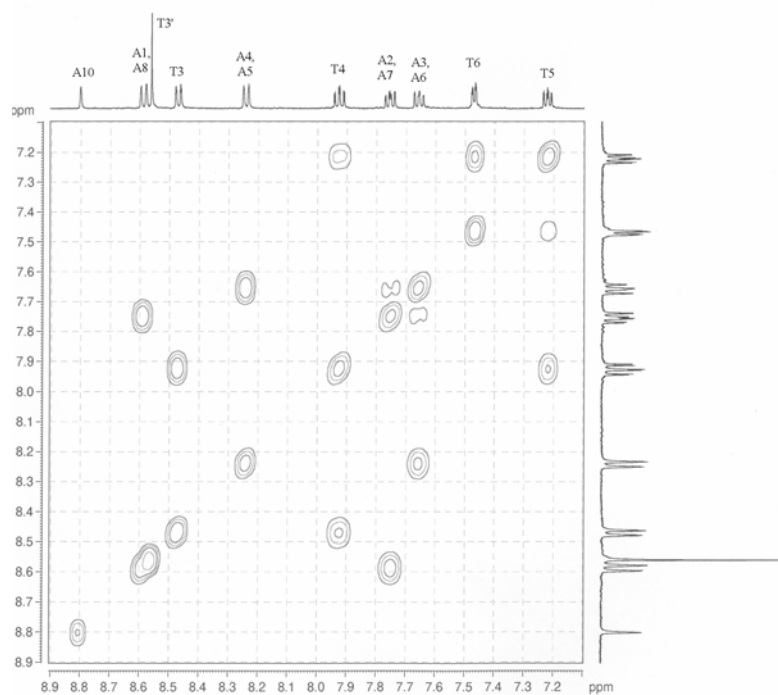
Figure 17. COSY spectrum (500 MHz) of [Ru(L^8)$_2$][PF$_6$]$_2$ in CD$_3$CN solution at room temperature.
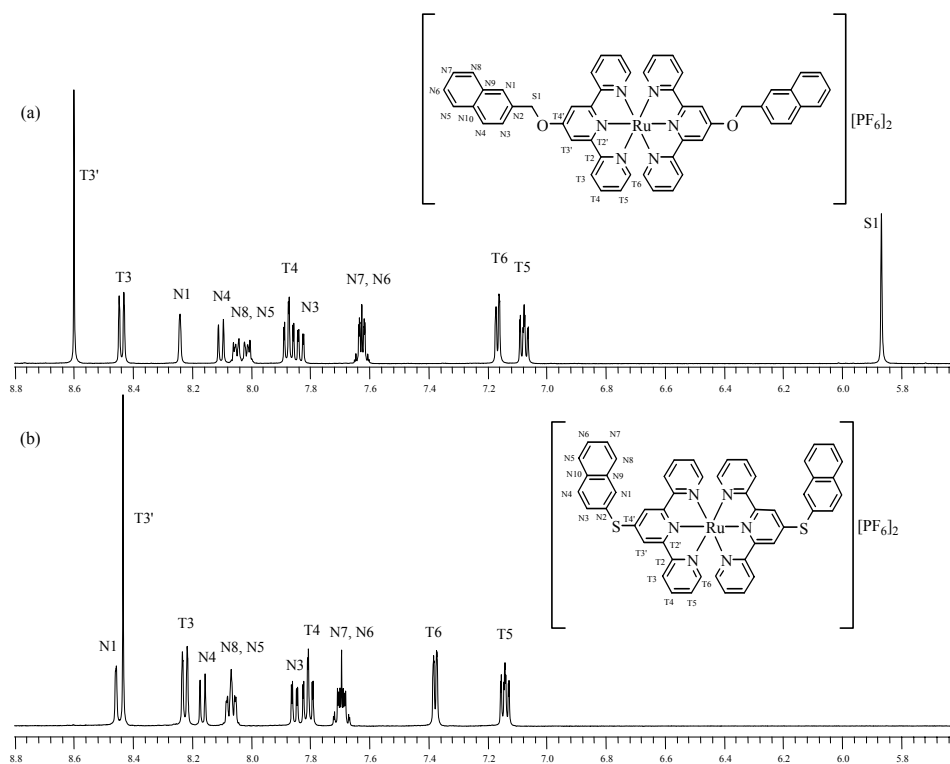
Figure 18. ^{1}H NMR spectra (500 MHz) of (a) [Ru(L^4)$_2$][PF$_6$]$_2$ and (b) [Ru(L^9)$_2$][PF$_6$]$_2$ in CD$_3$CN solution at room temperature.

The ^{1}H NMR spectrum of [Ru($\textbf{\textit{L}}^9$)$_2$][PF$_6$]$_2$ in CD$_3$CN solution is shown in **Figure 18b**. Comparing this with the spectrum for [Ru($\textbf{\textit{L}}^4$)$_2$][PF$_6$]$_2$ shows that there is a significant change in the chemical shifts for the naphthyl ring protons when the linkage between the terpyridine and naphthyl domain is changed from OCH$_2$ to S (**Figure 18**). The five terpyridine signals were assigned as previously described. The signals belonging to the naphthyl rings were further identified by NOESY and COSY experiments.

In conclusion, with the exception of the signal for H$^{T3'}$, there are only slight differences in the terpyridine signals when the terminal domain is altered within a series of complexes for a given metal centre. It is also worth noting that there are no significant differences when the length of the ethyleneoxy linkage varies in the case of [Ru($\textbf{\textit{L}}$)$_2$][PF$_6$]$_2$ ($\textbf{\textit{L}} = \textbf{\textit{L}}^5\textbf{-}\textbf{\textit{L}}^7$). In addition, varying the metal centre from Fe(II) to Ru(II) does not lead to major differences in the signals for the substituents in the ^{1}H NMR spectra of [M($\textbf{\textit{L}}$)$_2$][PF$_6$]$_2$ (where M = Fe or Ru and $\textbf{\textit{L}} = \textbf{\textit{L}}^4\textbf{-}\textbf{\textit{L}}^9$) (**Table 2**).

3.3 Mass spectrometric characterisation

Electrospray ionisation mass spectrometry (ES-MS) was used to characterise the new complexes. The mass spectrum shows peaks for ions with particular mass to charge ratios (m/z). Each signal has a unique combination of the isotopes of the elements in the complexes. The difference between each of the signals of the isotope pattern is the reciprocal of the charge on the fragment from which the signal originates; e.g. if $z = 2$, the separation between peaks in an envelope will be 0.5 mass units. Normally, ES-MS is a relatively soft ionisation method and, $[M-PF_6]^+$ and $[M-2PF_6]^{2+}$ peaks are found as the major peaks for mononuclear Fe(II) and Ru(II) complexes. However, if the voltage used to ionise the samples is relatively high, some other fragments are observed in the spectra (**Table 3**).

	m/z			
	$[M-PF_6]^+$	$[M-PF_6-PF_5]^+$	$[M-2PF_6]^{2+}$	Others
$[Fe(L^4)_2][PF_6]_2$	979.0	853.1		1147.0, 693.4, 552.3, 464.1
$[Fe(L^5)_2][PF_6]_2$	1067.1	940.9	461.5	737.4, 552.3, 508.3
$[Fe(L^6)_2][PF_6]_2$	1154.9		505.2	781.2
$[Fe(L^7)_2][PF_6]_2$	1243.0		549.2	825.3
$[Fe(L^8)_2][PF_6]_2$	1079.0	953.0		743.2, 552.3, 191.4
$[Fe(L^9)_2][PF_6]_2$			419.6	466.4
$[Ru(L^4)_2][PF_6]_2$	1025.1	899.1		739.1, 598.1
$[Ru(L^5)_2][PF_6]_2$	1113.2		484.1	783.3
$[Ru(L^6)_2][PF_6]_2$	1201.1		528.1	827.2
$[Ru(L^7)_2][PF_6]_2$	1289.1		572.1	
$[Ru(L^8)_2][PF_6]_2$	1125.1			1189.1, 1157.0, 821.1, 598.1, 191.1
$[Ru(L^9)_2][PF_6]_2$	1029.0		442.1	

Table 3. The ES-MS data of the twelve complexes.

In the ES-MS spectrum of $[Fe(L^6)_2][PF_6]_2$, which is shown in **Figure 19**, a peak at m/z 505.2 assigned to $[M-2PF_6]^{2+}$ was the major signal. The other 2 minor signals at m/z

1154.9 and 781.2 correspond to $[M\text{-}PF_6]^+$ and $[M\text{-}2PF_6\text{-}O(CH_2CH_2O)_2CH_2Nap]^+$ respectively.
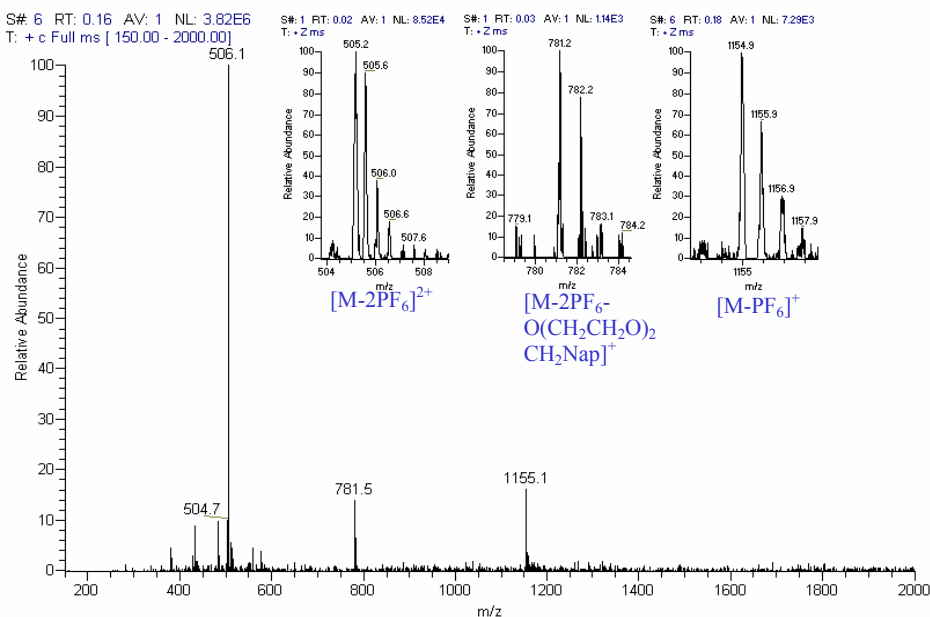
Figure 19. The ES-MS spectrum of $[Fe(\boldsymbol{L^6})_2][PF_6]_2$.

In **Figure 20**, the ES-MS spectrum of $[Ru(\boldsymbol{L^9})_2][PF_6]_2$ is shown. Two major signals were recorded at *m/z* 1029.0 and 442.1 which correspond to $[M\text{-}PF_6]^+$ and $[M\text{-}2PF_6]^{2+}$ respectively. The isotope patterns match those of the simulated spectra.
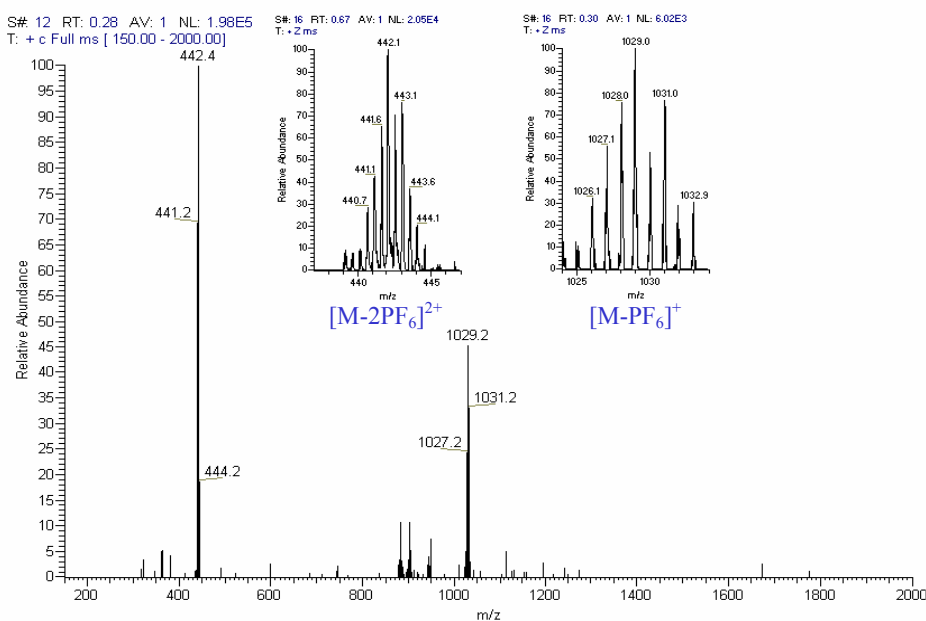
Figure 20. The ES-MS spectrum of $[Ru(\boldsymbol{L^9})_2][PF_6]_2$.

3.4 Absorption spectroscopic characterisation

The electronic spectra of the homoleptic Fe(II) and Ru(II) complexes were recorded in HPLC grade acetonitrile solution. The absorption spectra of these complexes are similar to the sum of the spectra of $[M(terpy)_2]^{2+}$, where M is Fe(II) or Ru(II), and those of the substituents. The absorption data for these twelve homoleptic complexes are summarised in **Table 4**.

	λ_{max}, nm ($\varepsilon/ 10^3$, $M^{-1}cm^{-1}$)	
	LC	MLCT
$[Fe(terpy)_2][PF_6]_2$	270 (39.9), 278 (35.2), 317 (52.2)	549 (11.6)
$[Fe(L^4)_2][PF_6]_2$	223 (195), 245 (60.7), 273 (71.0), 315 (33.5)	556 (10.5)
$[Fe(L^5)_2][PF_6]_2$	224 (241), 244 (59.7), 272(68.1), 315 (38.8)	556 (11.7)
$[Fe(L^6)_2][PF_6]_2$	224 (289), 241 (74.7), 274 (74.0), 315 (31.8)	554 (8.41)
$[Fe(L^7)_2][PF_6]_2$	224 (236), 241 (65.6), 272 (70.1), 315 (43.1)	557 (12.8)
$[Fe(L^8)_2][PF_6]_2$	254 (333), 272 (75.9), 316 (48.2), 349 (20.8), 366 (28.0), 386 (23.8)	557 (15.9)
$[Fe(L^9)_2][PF_6]_2$	221 (151), 283 (84.3), 314 (54.9)	566 (23.1)
$[Ru(terpy)_2][PF_6]_2$	268 (66.9), 305 (111.1)	473 (25.4)
$[Ru(L^4)_2][PF_6]_2$	223(241), 242 (77.5), 269 (90.7), 304 (73.5)	485 (21.2)
$[Ru(L^5)_2][PF_6]_2$	227 (236), 245 (60.8), 270 (68.1), 307 (67.4)	488 (19.0)
$[Ru(L^6)_2][PF_6]_2$	224 (31.4), 241 (8.08), 267 (8.86), 304 (9.16)	486 (1.71)
$[Ru(L^7)_2][PF_6]_2$	224 (213), 241 (61.6), 267 (62.1), 304 (63.5)	485 (16.9)
$[Ru(L^8)_2][PF_6]_2$	251 (261), 267 (55.3), 302 (49.9), 346 (16.4), 363 (18.9), 384 (16.5)	483 (16.0)
$[Ru(L^9)_2][PF_6]_2$	222 (129), 280 (76.0), 301 (66.6)	490 (26.3)

Table 4. Electronic spectroscopic data for the complexes in acetonitrile solution.

The very intense bands in the UV region are assigned to the ligand-centred $\pi^* \leftarrow \pi$ transitions. The Fe(II) complexes and Ru(II) complexes exhibit a low energy metal-to-ligand charge transfer (MLCT) transition with λ_{max} between 554 to 566 nm and with λ_{max} between 483 to 490 nm respectively. The MLCT transitions occur when an electron is transferred from the metal-centred d orbital to an unfilled ligand-centred π^*

orbital. The data in **Table 4** indicate that substitution in the 4′-position of the terpyridine ligand causes a dramatic red shift compared to the 2,2′:6′,2″-terpyridine ligand. Balzani and Constable *et al.*[44] have reported that there is a red shift of the MLCT band of Ru(II) complexes irrespective of whether the substituent at the 4′-position of the terpyridine ligand is electron-donating or electron-accepting. This indicates that, in spite of the electron-donating or electron-withdrawing nature of the substituents at the 4′-position, the energy of the absorption maximum decreases.

A red shift of the MLCT band is observed when the linkage between the terpyridine ligand and the substituent is changed from OCH_2 to S. It seems that there is no influence on the absorption data when the length of the linkage chain is changed, nor when the nature of the terminal domain is altered.

3.5   Electrochemical studies

The new complexes are redox active and were studied by cyclic voltammetry in acetonitrile solution. The redox potential data (vs. Fc/Fc^+) are presented in **Table 5**. Except for $[Fe(L^8)_2][PF_6]_2$, $[Fe(L^9)_2][PF_6]_2$, $[Ru(L^8)_2][PF_6]_2$ and $[Ru(L^9)_2][PF_6]_2$, the processes of these complexes are reversible and they exhibit a M(II)/M(III) process and two reversible ligand-centred reductions.

The observed Ru(II)/Ru(III) redox potentials for $[Ru(L)_2][PF_6]_2$ (where $L = L^4-L^8$) are the same as the corresponding potential for $[Ru(EtO\text{-}terpy)_2][PF_6]_2$ (+0.74 V), where ***EtO-terpy*** = 4′-ethoxy-2,2′:6′,2″-terpyridine.[44-46] This indicates that the electronic character of the substituents in the 4′-position of the terpyridine ligand is not influenced by the length of the chain or the end terminal domain. There are two and one non-reversible ligand-centred oxidation processes observed in $[Ru(L^8)_2][PF_6]_2$ and $[Ru(L^9)_2][PF_6]_2$. The Ru(II)/Ru(III) redox potential for $[Ru(L^9)_2][PF_6]_2$ are more positive than others. This indicates that the S-2-naphthyl substituent has less electron-donating power than all the other OCH_2 substituents.

The electronic character of substituents in the 4′-position of the terpyridine ligands can be quantified by the use of a Hammett σ^+ parameter. The Hammett σ^+ parameter can be defined by using the formula $E_{ox}(Ru) = 0.245\sigma^+ + 0.944$.[45,47,48] The σ^+ parameters for all the OCH_2 linkage substituents are -0.87 ($E_{ox}(Ru) = 0.73$ V) and -0.83 ($E_{ox}(Ru) = 0.74$ V). By substituting the σ^+ value obtained from the formula of $E_{ox}(Ru)$ into the following formula, $E_{ox}(Fe) = 0.212\sigma^+ + 0.755$, the $E_{ox}(Fe)$ value for iron complexes with OCH_2 linked 4′-substituent terpyridine can be calculated. The calculated $E_{ox}(Fe)$ values, which are +0.57 V and +0.58 V, correspond well to the observed potential (+0.59 V). The σ^+ parameter for the S-2-naphthyl substituent is -0.42 which obtained from the formula of $E_{ox}(Ru)$ and the calculated $E_{ox}(Fe)$ potential (+0.67 V) is comparable to the observed value (+0.68 V).

	E_{red} (V) 2nd reduction	E_{red} (V) 1st reduction	E_{ox} (V) Ru(II/III)	E_{ox} (V)	E_{ox} (V)
[Fe(**terpy**)$_2$][PF$_6$]$_2$	-1.85	-1.65	0.77		
[Fe(**L^4**)$_2$][PF$_6$]$_2$	-1.86	-1.72	0.59		
[Fe(**L^5**)$_2$][PF$_6$]$_2$	-1.90	-1.74	0.59		
[Fe(**L^6**)$_2$][PF$_6$]$_2$	-1.87	-1.73	0.59		
[Fe(**L^7**)$_2$][PF$_6$]$_2$	-1.90	-1.73	0.59		
[Fe(**L^8**)$_2$][PF$_6$]$_2$	-1.65*	-1.62*	0.59	0.73*	0.95*
[Fe(**L^9**)$_2$][PF$_6$]$_2$	-1.69	-1.58	0.68	0.84*	
[Ru(**terpy**)$_2$][PF$_6$]$_2$	-1.92	-1.67	0.92		
[Ru(**L^4**)$_2$][PF$_6$]$_2$	-1.89	-1.71	0.74		
[Ru(**L^5**)$_2$][PF$_6$]$_2$	-1.91	-1.73	0.74		
[Ru(**L^6**)$_2$][PF$_6$]$_2$	-1.92	-1.72	0.73		
[Ru(**L^7**)$_2$][PF$_6$]$_2$	-1.91	-1.72	0.74		
[Ru(**L^8**)$_2$][PF$_6$]$_2$	-1.64		0.73		0.97*
[Ru(**L^9**)$_2$][PF$_6$]$_2$		-1.58	0.84		

Table 5. Cyclic voltammetry data for the complexes in acetonitrile solution, with 0.1M [^{t}Bu$_4$N][PF$_6$] as supporting electrolyte and Fc/Fc$^+$ as reference. Redox potentials marked * are non-reversible ligand-centred oxidation processes.

In conclusion, these complexes show an M(II)/(III) process at lower potential than those for [M(**terpy**)$_2$]$^{2+}$. This indicates that these substituents in the 4′-position of the

terpyridine ligand (L^4-L^9) have higher electron donating properties than a proton in the 4′-position of 2,2′:6′,2″-terpyridine.

3.6 Crystal structures of [M(L^4)₂][PF₆]₂·CH₃CN and [M(L^5)₂][PF₆]₂ (where M = Fe and Ru)

(a) Crystal structure of [Fe(L^4)₂][PF₆]₂·CH₃CN
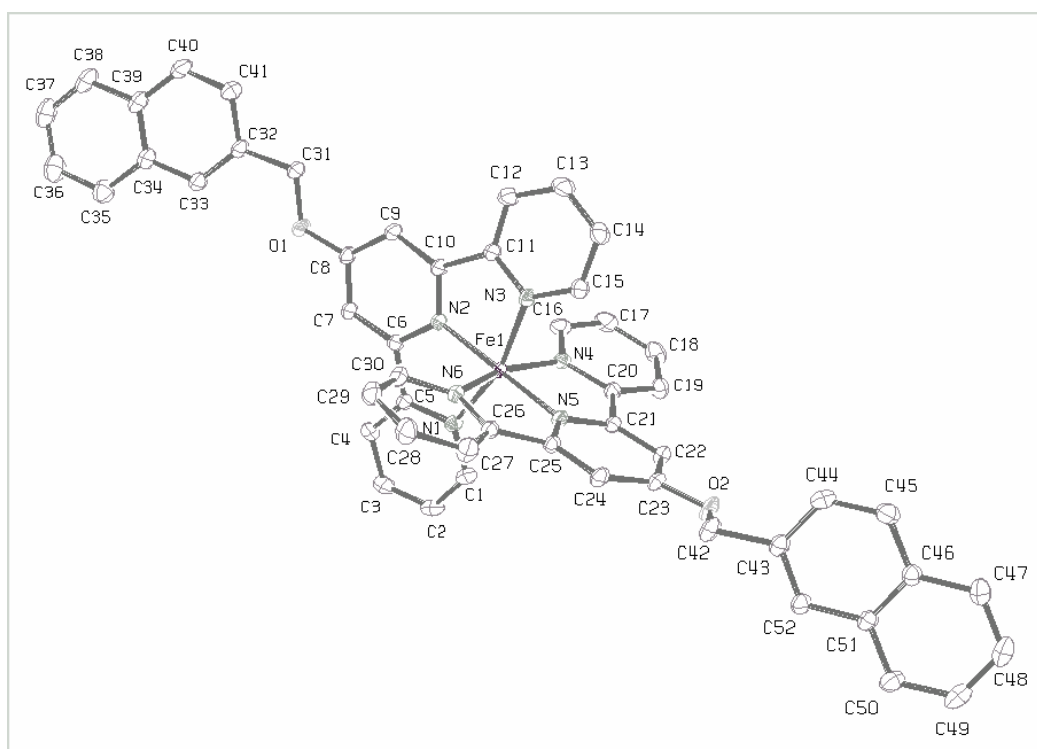
Figure 21. An ORTEP representation (50% probability ellipsoids) of the [Fe(L^4)₂]²⁺ cation in [Fe(L^4)₂][PF₆]₂·CH₃CN. Hydrogen atoms are omitted for clarity.

Crystals of [Fe(L^4)₂][PF₆]₂·CH₃CN were obtained by slow diffusion of diethyl ether vapour into an acetonitrile solution of [Fe(L^4)₂][PF₆]₂. The crystals were of X-ray quality and the molecular structure of [Fe(L^4)₂][PF₆]₂·CH₃CN was determined. The structure of the [Fe(L^4)₂]²⁺ cation is presented in **Figure 21**. Crystallographic data are given in **Appendix II** and selected bond lengths and angles are given in **Table 6**. As expected, the tridentate ligands exhibit the *cisoid* conformation about the interannular C-C bonds, which is necessary for the adoption of the chelating mode. The

coordination sphere of the Fe(II) centre is similar to those in other complexes containing tridentate 2,2′:6′,2″-terpyridine ligands. The three pyridine rings in each ligand are close to being coplanar and the torsion angles N1-C5-C6-N2, N2-C10-C11-N3, N4-C20-C21-N5 and N5-C25-C26-N6 are 2.59°, -5.48°, 1.73° and -0.58°. The angle between the planes containing atoms N1, N2, N3 and N4, N5, N6 is 88.9°.[49-52]

Fe1-N1	1.983(1)	N1-C1	1.337(2)	C5-C6	1.466(2)
Fe1-N2	1.887(1)	N1-C5	1.364(2)	C10-C11	1.470(2)
Fe1-N3	1.972(1)	N2-C6	1.346(2)	C20-C21	1.469(2)
Fe1-N4	1.971(1)	N2-C10	1.340(2)	C25-C26	1.466(2)
Fe1-N5	1.882(1)	N3-C11	1.361(2)		
Fe1-N6	1.981(1)	N3-C15	1.341(2)		
		N4-C16	1.344(2)	C8-O1	1.340(2)
		N4-C20	1.361(2)	C31-O1	1.429(2)
		N5-C21	1.349(2)	C23-O2	1.347(2)
		N5-C25	1.344(2)	C42-O2	1.454(2)
		N6-C26	1.361(2)		
		N6-C30	1.343(2)		
N1-Fe1-N2	80.54(5)	N4-Fe1-N5	80.83(5)	C7-C8-O1	115.3(1)
N1-Fe1-N3	160.99(4)	N4-Fe1-N6	161.21(4)	C9-C8-O1	124.4(1)
N2-Fe1-N3	80.61(5)	N5-Fe1-N6	80.55(5)	C8-O1-C31	117.6(1)
N1-Fe1-N4	92.99(5)	N3-Fe1-N6	92.10(5)	C22-C23-O2	115.4(1)
N2-Fe1-N4	100.92(5)	N1-Fe1-N5	100.54(5)	C24-C23-O2	124.6(1)
N3-Fe1-N4	88.14(5)	N1-Fe1-N6	92.85(5)	C23-O2-C42	116.7(1)
N3-Fe1-N5	98.38(5)	N2-Fe1-N6	97.65(5)		
		N2-Fe1-N5	177.92(5)		

Table 6. Selected bond lengths (Å) and angles (°) of the $[Fe(\boldsymbol{L^4})_2]^{2+}$ cation in $[Fe(\boldsymbol{L^4})_2][PF_6]_2 \cdot CH_3CN$.

All the bond lengths of the interannular C-C bonds and N-C bonds are comparable to the corresponding bond lengths of other Fe(II) complexes containing tridentate 2,2′:6′,2″-terpyridine ligands.[49,50,52] The Fe-N contacts to the central ring of the 4′-(naphthalen-2-ylmethoxy)-2,2′:6′,2″-terpyridine ligand (Fe1-N2 and Fe1-N5) are shorter than those to the terminal rings (Fe1-N1, Fe1-N3, Fe1-N4 and Fe1-N6), which are within the reported range of Fe(II) complexes with 2,2′:6′,2″-terpyridine ligands.[49-52] The methyleneoxy chain is nearly coplanar with the central pyridine ring. The torsion angles C9-C8-O1-C31 and C24-C23-O2-C42 are -2.09° and -8.06°. The bond lengths O1-C8 and O2-C23 are 1.340(2) Å and 1.347(2) Å respectively which are similar to the corresponding distances in bis[4′-(2-propynyl-1-oxy)-2,2′:6′,2″-

terpyridine]-ruthenium   bis(hexafluorophosphate)   acetone   solvate ([Ru(***poterpy***)$_2$][PF$_6$]$_2$·(CH$_3$)$_2$CO)[42]. The bond angles C7-C8-O1, C9-C8-O1, C22-C23-O2 and C24-C23-O2 are within the range reported in the [Ru(***poterpy***)$_2$]$^{2+}$ cation in the solid-state structure of [Ru(***poterpy***)$_2$][PF$_6$]$_2$·(CH$_3$)$_2$CO. Also the bond angles C8-O1-C31 and C23-O2-C42 are 117.6(1)° and 116.7(1)° respectively which, within experimental error, are comparable to the corresponding angles in ([Ru(***poterpy***)$_2$]$^{2+}$ cation (117.5(3)° and 118.1(3)°).[42]
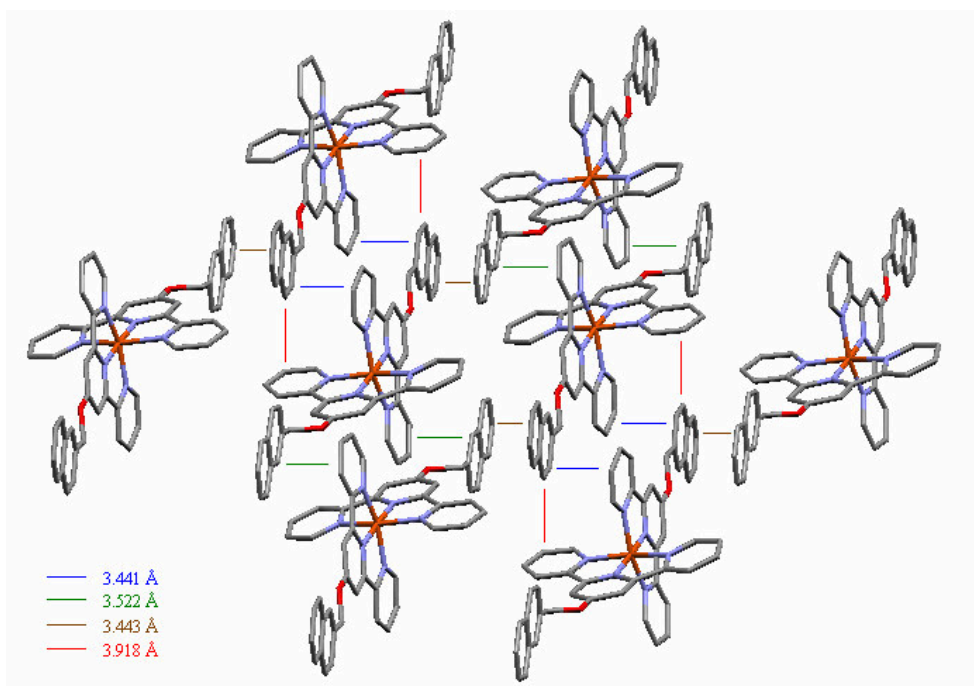
Figure 22. Packing of the [Fe(***L⁴***)$_2$]$^{2+}$ cations that shows the face-to-face naphthyl-pyridrine (blue line and green line), naphthyl-naphthyl (brown line) and face-to-edge (red line) interactions between the naphthyl rings and the pyridine rings. Hydrogen atoms are omitted for clarity.

The dihedral angles of the planes of 2,2′:6′,2″-terpyridine and the naphthyl ring i.e. the planes containing N4, N5, N6 and C43, C46, C49, and N1, N2, N3 and C32, C36, C39 are 79.2° and 13.8° respectively. The two dihedral angles are very different. This is because of the intermolecular interactions between the naphthyl rings and pyridine rings between the molecules. The distance from the centroid of the pyridine N3 ring to the C40 atom of the naphthyl ring is 3.441 Å. The closest separation (C14 to C40) is 3.433 Å. The other pair is from the naphthyl to the pyridine N1 ring. The distance

from the centroid of the pyridine N1 ring to the C51 atom of the naphthyl ring is 3.522 Å. The closest distance (C3 to C51) is 3.525 Å. In addition, there are naphthyl-naphthyl π-π stacking interactions in the lattice. The distance from the centroid of one naphthyl ring (C32-C34, C39-C41) to the C52 atom of the other naphthyl ring is 3.443 Å. The shortest distance between two atoms of two rings (C32 to C52) is 3.481 Å. Also, there are face-to-edge interactions between the naphthyl rings and the pyridine rings. The closest separation between CH⋯π, that is from the centroid of pyridine N6 ring to C40 atom of naphthyl ring, is 3.918 Å. The intermolecular interactions can be seen in the packing diagram presented in **Figure 22**.

*(b) Crystal structure of [Ru(**L**^{4})$_2$][PF$_6$]$_2$·CH$_3$CN*
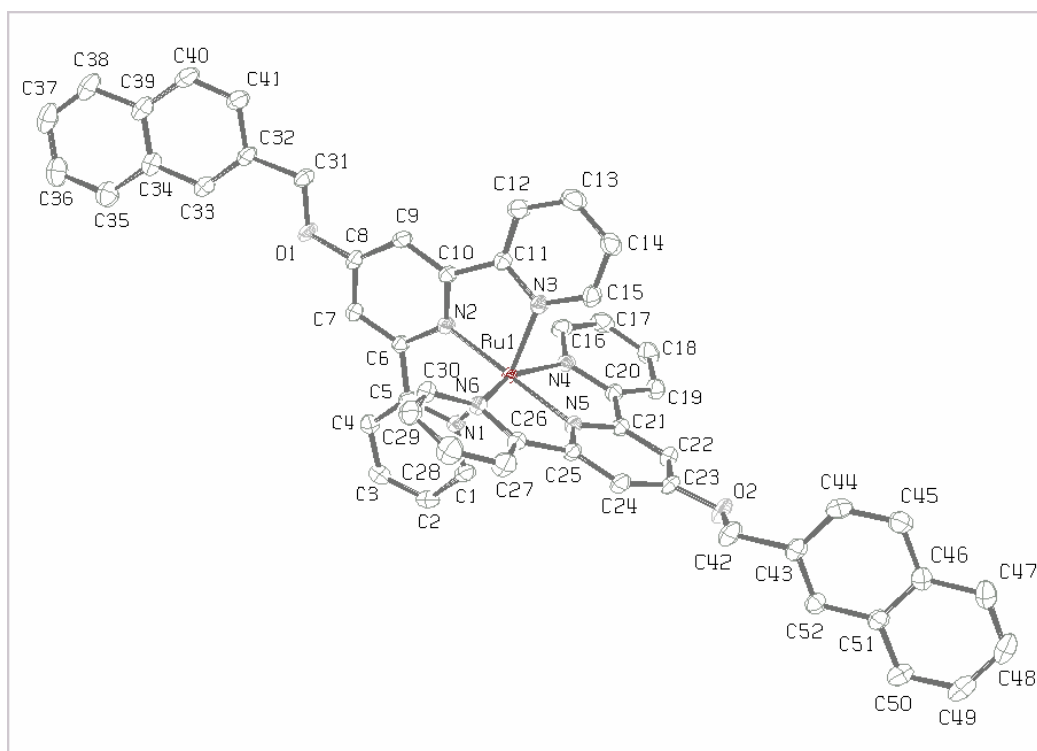
Figure 23. An ORTEP representation (50% probability ellipsoids) of the [Ru(**L**^{4})$_2$]$^{2+}$ cation in [Ru(**L**^{4})$_2$][PF$_6$]$_2$·CH$_3$CN. Hydrogen atoms are omitted for clarity.

X-ray quality crystals of [Ru(**L**^{4})$_2$][PF$_6$]$_2$·CH$_3$CN were also obtained by slow diffusion of diethyl ether vapour into an acetonitrile solution of [Ru(**L**^{4})$_2$][PF$_6$]$_2$. The structure of the [Ru(**L**^{4})$_2$]$^{2+}$ cation is presented in **Figure 23** and the crystallographic data are given in **Appendix II**. The structure is very similar to that of [Fe(**L**^{4})$_2$][PF$_6$]$_2$·CH$_3$CN

described above. The tridentate ligands exhibit the *cisoid* conformation about the interannular C-C bonds to adopt the chelating mode.[40,42,45] The three pyridine rings in each ligand are close to being coplanar and the torsion angles N1-C5-C6-N2, N2-C10-C11-N3, N4-C20-C21-N5 and N5-C25-C26-N6 are 4.13˚, -5.72˚, 2.67˚ and -1.02˚. The angle between the planes containing atoms N1, N2, N3 and N4, N5, N6 is 88.8˚.[42,45]

Ru1-N1	2.080(2)	N1-C1	1.342(3)	C5-C6	1.469(3)
Ru1-N2	1.981(2)	N1-C5	1.372(2)	C10-C11	1.471(3)
Ru1-N3	2.058(2)	N2-C6	1.349(2)	C20-C21	1.468(3)
Ru1-N4	2.064(2)	N2-C10	1.344(2)	C25-C26	1.471(3)
Ru1-N5	1.973(2)	N3-C11	1.370(2)		
Ru1-N6	2.066(2)	N3-C15	1.343(3)	C8-O1	1.342(2)
		N4-C16	1.340(3)	C31-O1	1.428(2)
		N4-C20	1.367(2)	C23-O2	1.349(2)
		N5-C21	1.354(2)	C42-O2	1.454(2)
		N5-C25	1.339(2)		
		N6-C26	1.366(2)		
		N6-C30	1.345(3)		
N1-Ru1-N2	78.73(6)	N4-Ru1-N5	79.23(7)	C7-C8-O1	115.0(2)
N1-Ru1-N3	157.34(6)	N4-Ru1-N6	157.66(6)	C9-C8-O1	124.3(2)
N2-Ru1-N3	78.72(7)	N5-Ru1-N6	78.63(7)	C8-O1-C31	117.7(2)
N1-Ru1-N4	94.27(6)	N3-Ru1-N6	92.32(7)	C22-C23-O2	115.1(2)
N2-Ru1-N4	102.55(7)	N1-Ru1-N5	103.09(6)	C24-C23-O2	124.6(2)
N3-Ru1-N4	88.47(6)	N1-Ru1-N6	93.54(6)	C23-O2-C42	116.7(2)
N3-Ru1-N5	99.53(7)	N2-Ru1-N6	99.50(7)		
		N2-Ru1-N5	177.42(7)		

Table 7. Selected bond lengths (Å) and angles (˚) of the $[Ru(L^4)_2]^{2+}$ cation in $[Ru(L^4)_2][PF_6]_2 \cdot CH_3CN$.

Selected bond lengths and angles are given in **Table 7**. All the bond lengths of the interannular C-C bonds and N-C bonds are comparable to the corresponding bond lengths of other Ru(II) complexes containing tridentate 2,2′:6′,2″-terpyridine ligands.[42,45] The Ru-N contacts to the central ring of the 4′-(naphthalen-2-ylmethoxy)-2,2′:6′,2″-terpyridine ligand (Ru1-N2 and Ru-N5) are shorter than those to the terminal rings (Ru1-N1, Ru1-N3, Ru1-N4 and Ru1-N6), which are within the reported range for Ru(II) complexes with 2,2′:6′,2″-terpyridine ligands.[42,45] The methyleneoxy chain is nearly coplanar with the central pyridine ring. The torsion angles C9-C8-O1-C31 and C24-C23-O2-C42 are -2.44˚ and -8.23˚. The bond lengths O1-C8 and O2-

C23 are 1.342(2) Å and 1.349(2) Å respectively which, within experimental error, are the similar to the corresponding bond lengths in the [Ru(***poterpy***)$_2$]$^{2+}$ cation of [Ru(***poterpy***)$_2$][PF$_6$]$_2$·(CH$_3$)$_2$CO.[42] The bond angles C7-C8-O1, C9-C8-O1, C22-C23-O2 and C24-C23-O2 are within the range reported in the solid-state structure of [Ru(***poterpy***)$_2$][PF$_6$]$_2$·(CH$_3$)$_2$CO. Also the bond angles C8-O1-C31 and C23-O2-C42 are 117.7(2)° and 116.7(2)° respectively, which is comparable to the corresponding angles in the [Ru(***poterpy***)$_2$]$^{2+}$ cation (117.5(3)° and 118.1(3)°).[42]
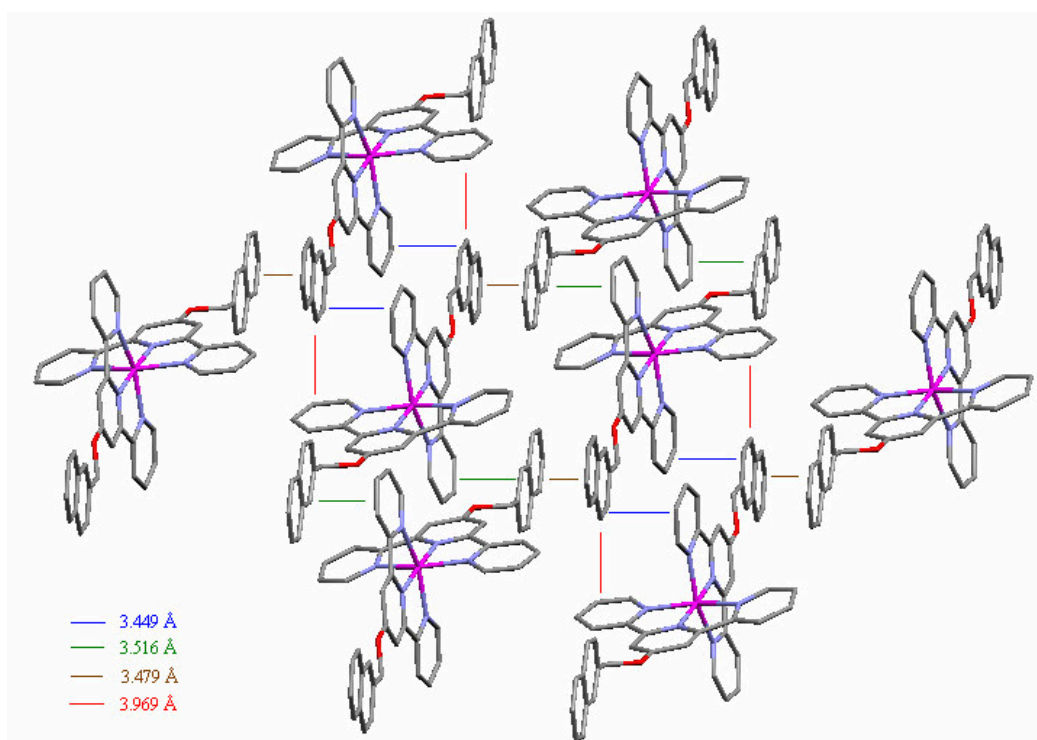
Figure 24. Packing of the [Ru(***L***^{4})$_2$]$^{2+}$ cations that shows the face-to-face naphthyl-pyridine (blue line and green line), naphthyl-naphthyl (brown line) and face-to-edge (red line) interactions between the naphthyl rings and the pyridine rings. Hydrogen atoms are omitted for clarity.

The dihedral angles of the planes of 2,2′:6′,2″-terpyridine and the naphthyl ring i.e. the planes containing N4, N5, N6 and C43, C46, C49, and N1, N2, N3 and C32, C36, C39 are 79.8° and 13.4° respectively. The two dihedral angles are very different. Just as in the Fe(II)-containing structure described above, this is due to a consequence of intermolecular interactions between the pyridine and naphthyl rings between molecules. The separation from the centroid of the pyridine N3 ring to the C40 atom of the naphthyl ring is 3.449 Å and the closest separation (C14 to C40) is 3.409 Å.

The other pair is from the naphthyl to the pyridine N1 ring. The distance from the centroid of the pyridine N1 ring to the C51 atom of the naphthyl ring is 3.516 Å. The closest distance (C3 to C51) is 3.539 Å. In addition, there are naphthyl-naphthyl π-π stacking interactions in the lattice. The distance from the centroid of one naphthyl ring (C32-C34, C39-C40) to the C52 atom in the other naphthyl ring is 3.479 Å. The shortest distance between two atoms of two rings (C32 to C52) is 3.479 Å. Again, there are face-to-edge interactions between the naphthyl rings and the pyridine rings. The closest separation of CH$\cdots\pi$ interactions, that is from the centroid of the plane C26, C28, C30 to C40, is 3.969 Å. These intermolecular interactions are shown in **Figure 24**.

(c) Crystal structure of [Fe($\mathbf{L^5}$)$_2$][PF$_6$]$_2$

The purple crystals of this iron complex, which were suitable for X-ray crystallographic analysis, were obtained by slow diffusion of diethyl ether vapour into acetonitrile solution of [Fe($\mathbf{L^5}$)$_2$][PF$_6$]$_2$. The lattice contains two non-equivalent, but very similar, [Fe($\mathbf{L^5}$)$_2$]$^{2+}$ cations (**Figure 25**). Crystallographic data are given in **Appendix II**.

The expected six-coordinate structure is confirmed. As described before, the tridentate ligands exhibit the *cisoid* conformation about the interannular C-C bonds in order to chelating to the metal. The three pyridine rings in each ligand are close to being coplanar and the torsion angles N1-C5-C6-N2, N2-C10-C11-N3, N4-C20-C21-N5 and N5-C25-C26-N6 in molecule A and the corresponding angles in molecule B are within 4° of each other. The angle between the planes containing atoms N1, N2, N3 and N4, N5, N6 is 88.0° for molecule A and that between the corresponding planes in molecule B is 88.9°.[49-52]
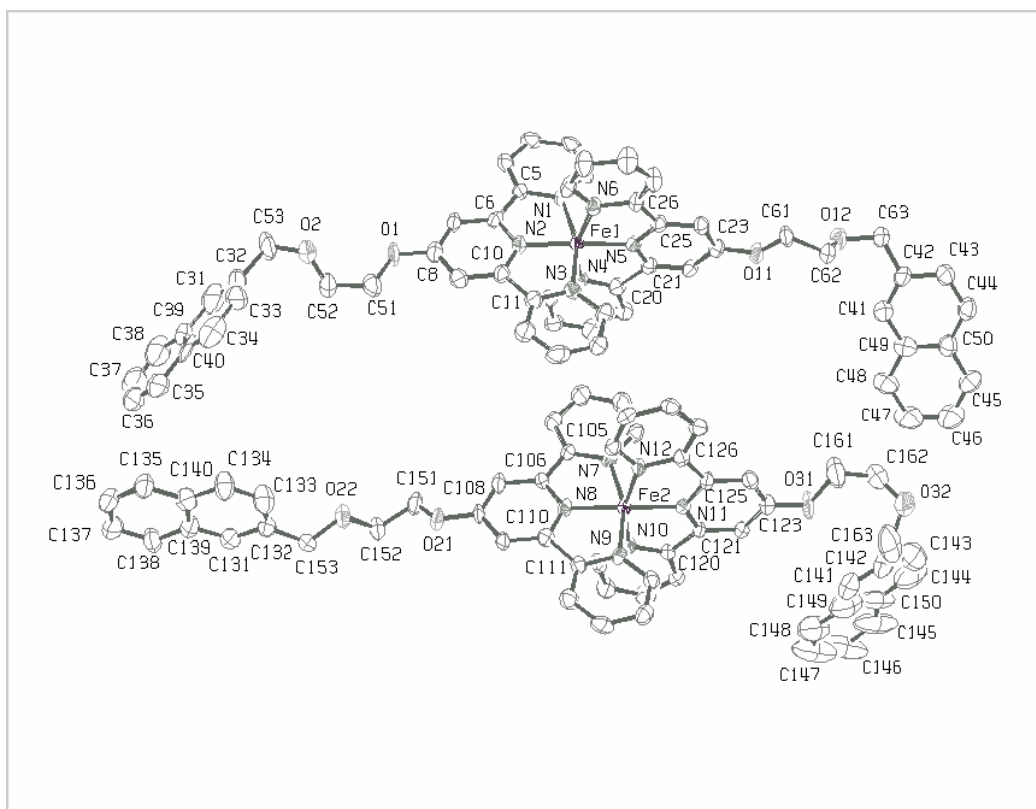
Figure 25. The crystal structure of the two independent $[Fe(\boldsymbol{L^5})_2]^{2+}$ cations in $[Fe(\boldsymbol{L^5})_2][PF_6]_2$ by an ORTEP representation (50% probability ellipsoids). The upper one is molecule A and the bottom one is molecule B. Hydrogen atoms are omitted for clarity. Carbon atoms are numbered sequentially around each ring.

Selected bond lengths and angles of the two independent molecules (A and B) are given in **Table 8**. All the bond lengths of the interannular C-C bonds and N-C bonds which, within experimental error, are comparable to the corresponding bond lengths of other Fe(II) complexes containing tridentate 2,2′:6′,2″-terpyridine ligands.[49,50,52] The Fe-N contacts to the central ring of the 4′-[2-(naphthalen-2-ylmethoxy)ethoxy]-2,2′:6′,2″-terpyridine ligand (Fe1-N2 and Fe-N5) are shorter than those to the terminal rings (Fe1-N1, Fe1-N3, Fe1-N4 and Fe1-N6), which are within the reported range of Fe(II) complexes with 2,2′:6′,2″-terpyridine ligands.[49-52]

Molecule A		Molecule B	
Fe1-N1	1.972(6)	Fe2-N7	1.976(5)
Fe1-N2	1.887(5)	Fe2-N8	1.884(5)
Fe1-N3	1.989(5)	Fe2-N9	1.979(5)
Fe1-N4	1.967(6)	Fe2-N10	1.986(6)
Fe1-N5	1.878(5)	Fe2-N11	1.889(5)
Fe1-N6	1.975(6)	Fe2-N12	1.959(6)
O1-C8	1.345(8)	O21-C108	1.325(7)
O1-C51	1.41(1)	O21-C151	1.442(9)
O11-C23	1.341(8)	O31-C123	1.344(8)
O11-C61	1.438(8)	O31-C161	1.48(1)
N1-Fe1-N2	81.3(2)	N7-Fe2-N8	81.1(2)
N1-Fe1-N3	161.4(2)	N7-Fe2-N9	161.6(2)
N2-Fe1-N3	80.2(2)	N8-Fe2-N9	80.5(2)
N1-Fe1-N4	89.9(2)	N7-Fe2-N10	92.8(2)
N2-Fe1-N4	97.9(2)	N8-Fe2-N10	99.0(2)
N3-Fe1-N4	92.9(2)	N9-Fe2-N10	91.2(2)
N3-Fe1-N5	98.5(2)	N7-Fe2-N11	99.1(2)
N4-Fe1-N5	80.3(2)	N10-Fe2-N11	80.4(2)
N4-Fe1-N6	161.1(2)	N10-Fe2-N12	161.8(2)
N5-Fe1-N6	80.8(2)	N11-Fe2-N12	81.4(2)
N3-Fe1-N6	89.1(2)	N9-Fe2-N12	92.4(2)
N1-Fe1-N5	100.1(2)	N7-Fe2-N11	99.1(2)
N1-Fe1-N6	94.1(2)	N7-Fe2-N12	89.5(2)
N2-Fe1-N6	101.0(2)	N8-Fe2-N12	99.2(2)
N2-Fe1-N5	177.7(2)	N8-Fe2-N11	179.4(2)
O1-C8-C7	116.6(7)	O21-C108-C107	124.1(6)
O1-C8-C9	122.7(7)	O21-C108-C109	115.8(6)
C8-O1-C51	119.6(6)	C108-O21-C151	116.5(5)
O11-C23-C22	115.8(6)	O31-C123-C122	114.9(6)
O11-C23-C24	124.0(6)	O31-C123-C124	124.8(6)
C23-O11-C61	118.4(5)	C123-O31-C161	117.9(6)

Table 8. Selected bond lengths (Å) and angles (°) of the two independent $[Fe(\boldsymbol{L^5})_2]^{2+}$ cations in $[Fe(\boldsymbol{L^5})_2][PF_6]_2$.

The ethyleneoxy chains in a given molecule are very different from each other and adopt different conformations. The bond lengths between the O atoms to the directly connected C atoms of central pyridine rings are range from 1.325(7)-1.345(8) Å which, within experimental error, are the same as that in the $[Ru(\boldsymbol{poterpy})_2]^{2+}$ cation in the solid-state structure of $[Ru(\boldsymbol{poterpy})_2][PF_6]_2 \cdot (CH_3)_2CO$[42]. The bond angles C7-C8-O1, C9-C8-O1, C22-C23-O11 and C24-C23-O11 in molecule A and C107-C108-

O21, C109-C108-C21, C122-C123-O31 and C124-C123-O31 in molecule B are within the range reported in the solid-state structure of [Ru(*poterpy*)$_2$][PF$_6$]$_2$·(CH$_3$)$_2$CO.[42] Also the bond angles C8-O1-C51 and C23-O11-C61 in molecule A are 119.6(6)° and 118.4(5)° and C108-O21-C151 and C123-O31-C161 in molecule B are 116.5(5)° and 117.9(6)°, which is comparable to the corresponding angles in [Ru(*poterpy*)$_2$]$^{2+}$ cation (117.5(3)° and 118.1(3)°). Along the ethyleneoxy chain, the C-C and C-O bond lengths are different in the two molecules (**Table 7**). The C-C and C-O bond lengths are range from 1.46(1)-1.63(2) Å and 1.33(1)-1.48(1) Å respectively.

There are 2 pairs of face-to-face π-π stacking interactions between the pyridine rings in the unit cell. One pair is between the pyridine N3 and N7 ring and the other one is between the pyridine N1 and N10 ring. The distance between the centroid of the pyridine N7 ring and C14 atom of the pyridine N3 ring is 3.537 Å, and the distance between the centroid of the pyridine N10 ring and C3 atom of the pyridine N1 ring is 3.578 Å. The packing diagram is shown in **Figure 26**.
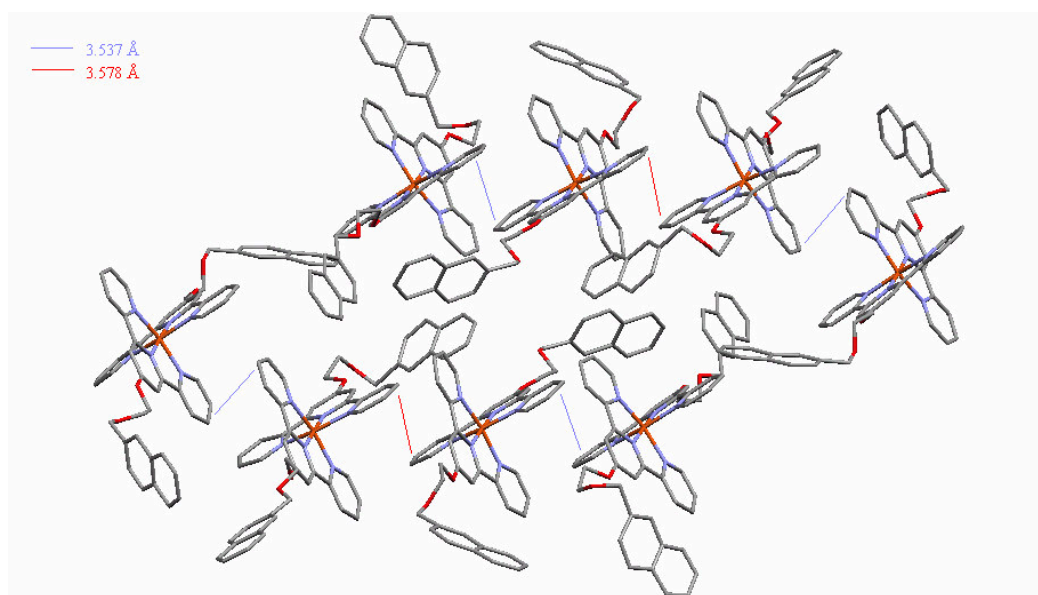
Figure 26. Packing of the [Fe(L^5)$_2$]$^{2+}$ cations that shows the face-to-face π-π stacking interactions between the pyridine rings. Blue line is from pyridine ring N3 to N7; red line is from pyridine ring N1 to N10. Hydrogen atoms are omitted for clarity.

(d) Crystal structure of [Ru(L^5)$_2$][PF$_6$]$_2$

By slow diffusion of diethyl ether vapour into an acetonitrile solution of [Ru(L^5)$_2$][PF$_6$]$_2$, red crystals of this ruthenium complex were obtained. The lattice contains two non-equivalent, but very similar, [Ru(L^5)$_2$]$^{2+}$ cations A and B (**Figure 27**). Crystallographic data are given in **Appendix II**. As in the three crystal structures described above, the tridentate ligands exhibit the *cis-cis* conformation about the interannular C-C bonds.[40,42,45] The three pyridine rings in each ligand are close to being coplanar and the torsion angles N1-C5-C6-N2, N2-C10-C11-N3, N4-C20-C21-N5 and N5-C25-C26-N6 in molecule A are -1.79˚, 1.95˚, -0.20˚, -1.86˚ and those corresponding to molecule B are -3.21˚, 2.88˚, 0.89˚, -0.01˚. The angle between the planes containing atoms N1, N2, N3 and N4, N5, N6 is 88.3˚ for molecule A and that between the corresponding planes in molecule B is 88.6˚.[42,45]
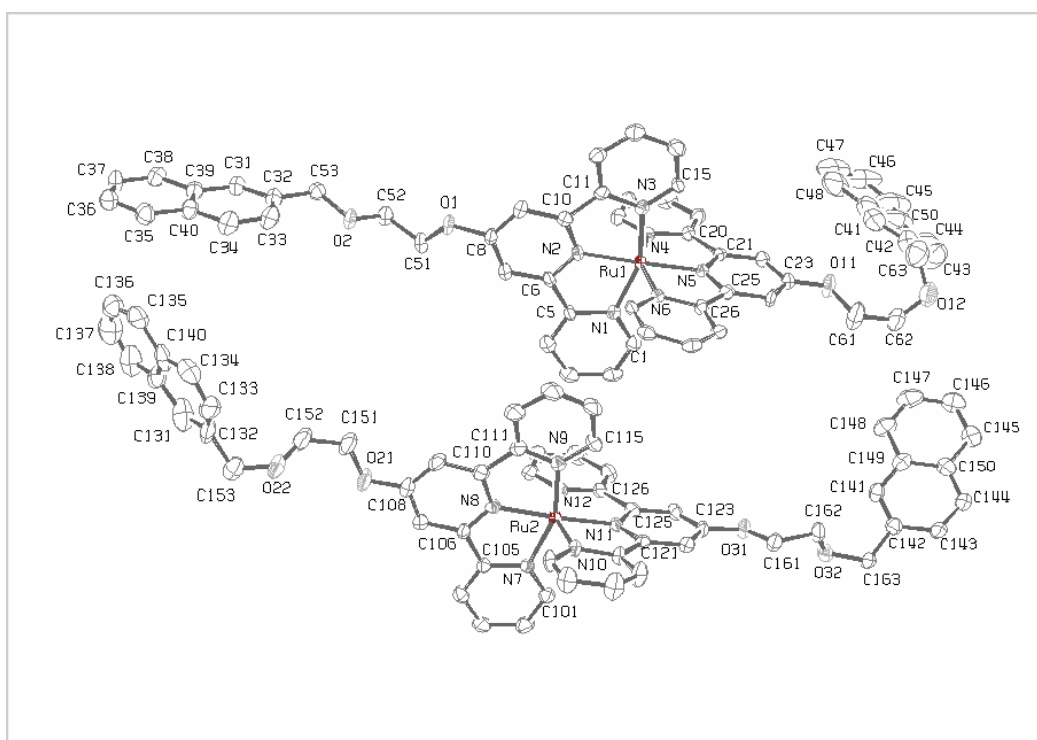
Figure 27. The crystal structure of the two independent [Ru(L^5)$_2$]$^{2+}$ cations in [Ru(L^5)$_2$][PF$_6$]$_2$ by an ORTEP representation (50% probability ellipsoids). The upper one is molecule A and the bottom one is molecule B. Hydrogen atoms are omitted for clarity. Carbon atoms are numbered sequentially around each ring.

Molecule A		Molecule B	
Ru1-N1	2.065(3)	Ru2-N7	2.065(3)
Ru1-N2	1.981(2)	Ru2-N8	1.978(2)
Ru1-N3	2.069(3)	Ru2-N9	2.059(3)
Ru1-N4	2.070(3)	Ru2-N12	2.051(3)
Ru1-N5	1.976(2)	Ru2-N11	1.971(2)
Ru1-N6	2.057(3)	Ru2-N10	2.062(3)
O1-C8	1.357(3)	O21-C108	1.348(4)
O1-C51	1.447(4)	O21-C151	1.427(5)
O11-C23	1.340(4)	O31-C123	1.349(4)
O11-C61	1.464(5)	O31-C161	1.433(4)
N1-Ru1-N2	78.9(1)	N7-Ru2-N8	78.8(1)
N1-Ru1-N3	157.83(9)	N7-Ru2-N9	157.9(1)
N2-Ru1-N3	78.9(1)	N8-Ru2-N9	79.1(1)
N1-Ru1-N4	93.7(1)	N7-Ru2-N12	91.1(1)
N2-Ru1-N4	100.5(1)	N8-Ru2-N12	98.4(1)
N3-Ru1-N4	91.0(1)	N9-Ru2-N12	92.6(1)
N3-Ru1-N5	100.3(1)	N9-Ru2-N11	98.8(1)
N4-Ru1-N5	79.0(1)	N11-Ru2-N12	79.1(1)
N4-Ru1-N6	157.8(1)	N10-Ru2-N12	157.8(1)
N5-Ru1-N6	78.8(1)	N10-Ru2-N11	78.7(1)
N3-Ru1-N6	93.8(1)	N9-Ru2-N10	90.3(1)
N1-Ru1-N5	101.9(1)	N7-Ru2-N11	103.2(1)
N1-Ru1-N6	89.9(1)	N7-Ru2-N10	94.5(1)
N2-Ru1-N6	101.7(1)	N8-Ru2-N10	103.8(1)
N2-Ru1-N5	179.1(1)	N8-Ru2-N11	176.7(1)
O1-C8-C7	123.4(3)	O21-C108-C107	116.0(3)
O1-C8-C9	115.5(3)	O21-C108-C109	123.5(3)
C8-O1-C51	116.2(3)	C108-O21-C151	118.9(3)
O11-C23-C22	114.8(3)	O31-C123-C124	115.1(3)
O11-C23-C24	124.7(3)	O31-C123-C122	124.4(3)
C23-O11-C61	118.3(3)	C123-O31-C161	116.6(3)

Table 9. Selected bond lengths (Å) and angles (°) of the two independent $[Ru(\boldsymbol{L^5})_2]^{2+}$ cations in $[Ru(\boldsymbol{L^5})_2][PF_6]_2$.

Selected bond lengths and angles of the two independent molecules (A and B) are given in **Table 9**. All the bond lengths of the interannular C-C bonds and N-C bonds are, within experimental error, comparable to the corresponding bond lengths of other Ru(II) complexes containing tridentate 2,2′:6′,2″-terpyridine ligands.[42,45] The Ru-N distances show the typical trend for 2,2′:6′,2″-terpyridine containing complexes with bonds to the central terpyridine ring (1.971(2)-1.981(2) Å) being significantly shorter

than those to the terminal rings (2.051(3)-2.070(3) Å). All bond lengths and angles within the [Ru(*terpy*)$_2$] moiety are normal.[42,45]

The ethyleneoxy chains are very different from each other. They adopt different conformations, like those in the case of [Fe(*L^5*)$_2$][PF$_6$]$_2$. The bond lengths of the O atoms to the directly connected C atoms of central pyridine rings are range from 1.340(4)-1.357(3) Å which, within experimental error, are the same as that in the [Ru(*poterpy*)$_2$][PF$_6$]$_2$·(CH$_3$)$_2$CO.[42] The bond angles C7-C8-O1, C9-C8-O1, C22-C23-O11 and C24-C23-O11 in molecule A and C107-C108-O21, C109-C108-C21, C124-C123-O31 and C122-C123-O31 in molecule B are within the range reported in the solid-state structure of [Ru(*poterpy*)$_2$][PF$_6$]$_2$·(CH$_3$)$_2$CO.[42] Also the bond angles C8-O1-C51 and C23-O11-C61 in molecule A are 116.2(3)° and 118.3(3)° and C108-O21-C151 and C123-O31-C161 in molecule B are 118.9(3)° and 116.6(3)°, which is comparable to the corresponding angles in [Ru(*poterpy*)$_2$]$^{2+}$ cation (117.5(3)° and 118.1(3)°).[42] Along the ethyleneoxy chain, the C-C and C-O bond lengths are different in the two molecules (**Table 8**).
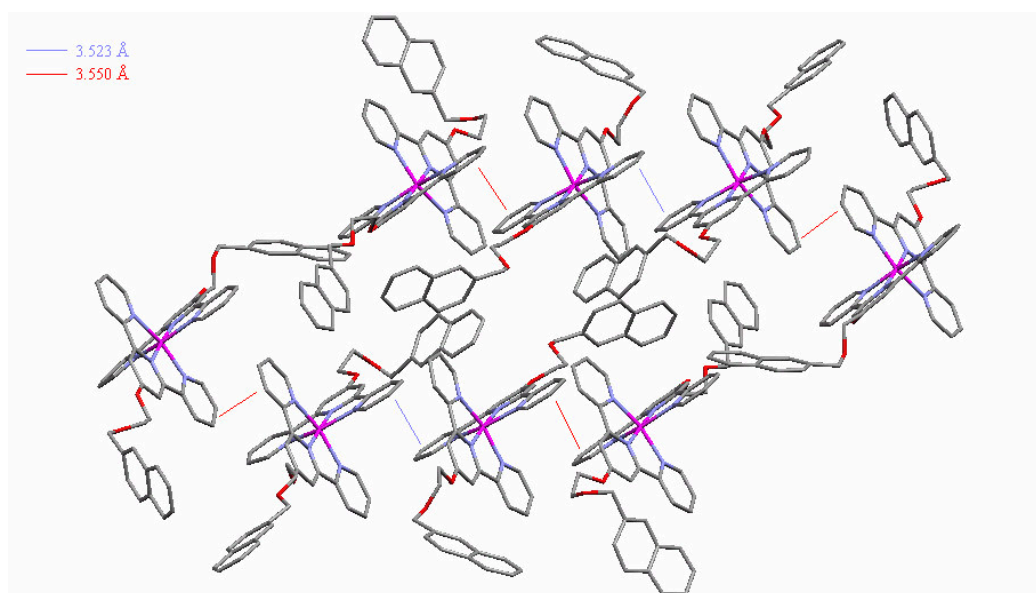
Figure 28. Packing of the [Ru(*L^5*)$_2$]$^{2+}$ cations that shows the face-to-face π-π stacking interactions between the pyridine rings. Blue line is from pyridine ring N4 to N7; red line is from pyridine ring N1 to N9. Hydrogen atoms are omitted for clarity.

There are 2 pairs of face-to-face π-π stacking interactions between the pyridine rings in the unit cell. One pair is between pyridine ring N1 and N9 and the other one is between pyridine ring N4 and N7. The closest separation between the centroid of the pyridine N1 ring and C114 atom of the pyridine N9 ring is 3.550 Å. The other pair of π-π stacking interactions are between the pyridine N4 ring and N7 ring. The closest distance between the centroid of pyridine N4 ring and C103 atom of N7 ring is 3.523 Å. The packing diagram is shown in **Figure 28**.

3.7   Conclusion

The mononuclear Fe(II) and Ru(II) complexes of different 4′-substituted-2,2′:6′,2″-terpyridine ligands L^4-L^9, which contain polyethyleneoxy chains and differ from one another in the length of the chains, in the terminal domains or in the linkages, have been synthesised. The complexes have been characterised with ^{1}H NMR spectroscopy, mass spectrometry (ES), UV/VIS spectroscopy, cyclic voltammetry and elemental analysis. The solid-state structures of $[M(L^4)_2][PF_6]_2$ and $[M(L^5)_2][PF_6]_2$ (where M = Fe and Ru) were determined by X-ray crystallography.

3.8 Experimental

- ❖ [Fe(L^4)$_2$][PF$_6$]$_2$
- ❖ [Fe(L^5)$_2$][PF$_6$]$_2$
- ❖ [Fe(L^6)$_2$][PF$_6$]$_2$
- ❖ [Fe(L^7)$_2$][PF$_6$]$_2$
- ❖ [Fe(L^8)$_2$][PF$_6$]$_2$
- ❖ [Fe(L^9)$_2$][PF$_6$]$_2$

- ❖ [Ru(L^4)$_2$][PF$_6$]$_2$
- ❖ [Ru(L^5)$_2$][PF$_6$]$_2$
- ❖ [Ru(L^6)$_2$][PF$_6$]$_2$
- ❖ [Ru(L^7)$_2$][PF$_6$]$_2$
- ❖ [Ru(L^8)$_2$][PF$_6$]$_2$
- ❖ [Ru(L^9)$_2$][PF$_6$]$_2$

where L^4 4′-(Naphthalen-2-ylmethoxy)-2,2′:6′,2″-terpyridine

   L^5 4′-[2-(Naphthalen-2-ylmethoxy)ethoxy]-2,2′:6′,2″-terpyridine

   L^6 4′-{2-[2-(Naphthalen-2-ylmethoxy)ethoxy]ethoxy}-2,2′:6′,2″-terpyridine

   L^7 4′-(2-{2-[2-(Naphthalen-2-ylmethoxy)ethoxy]ethoxy}ethoxy)-2,2′:6′,2″-terpyridine

   L^8 4′-(Anthracen-9-ylmethoxy)-2,2′:6′,2″-terpyridine

   L^9 4′-(Naphthalen-2-ylsulfanyl)-2,2′:6′,2″-terpyridine

[Ru(**HO-terpy**)$_2$][PF$_6$]$_2$[45] and 9-bromomethylanthracene[53] were prepared as previously reported in the literature. L^4, L^5, L^6, L^7, L^8 and L^9 were prepared as in Chapter 2.

(a) General method for synthesising iron(II) complexes
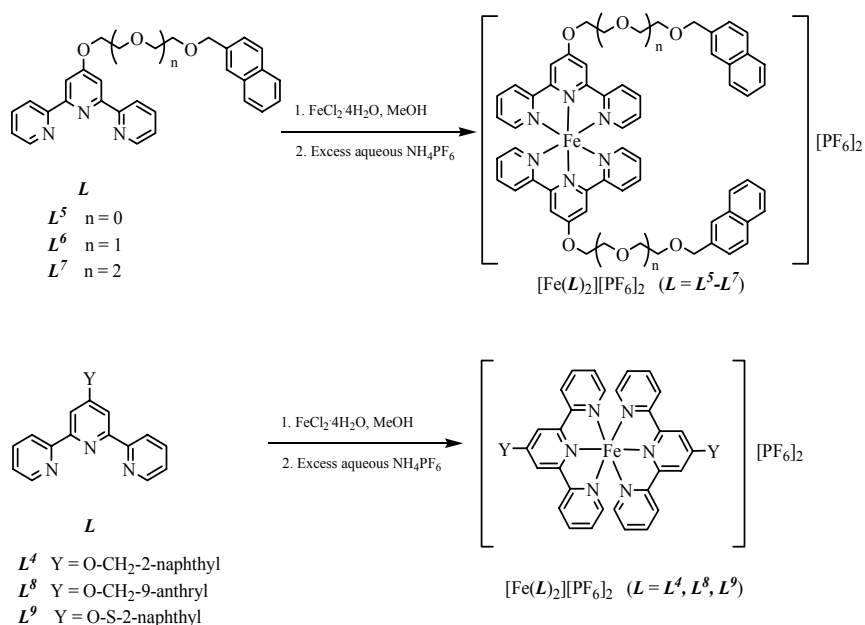
FeCl$_2$·4H$_2$O (1 equivalent) and **L** (2 equivalents) were added into 5 mL CH$_3$OH. The purple solution was stirred at room temperature for about 1 hour. Excess aqueous NH$_4$PF$_6$ was added

to the solution. The purple precipitate was filtered, washed with water and collected without purification to give a purple powder.[23,41]

❖ [Fe(L^4)$_2$][PF$_6$]$_2$

Molecular formula: $C_{52}H_{38}N_6O_2FeP_2F_{12}$

Molecular weight: 1124.67
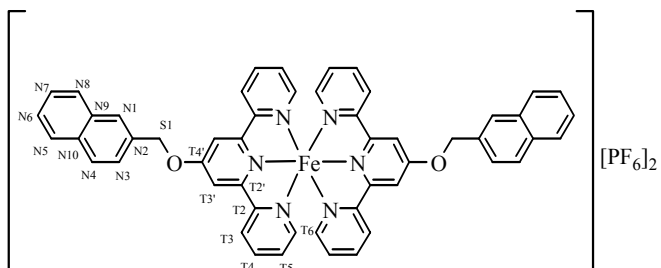
L^4 (40 mg, 0.10 mmol) and FeCl$_2$·4H$_2$O (10 mg, 0.050 mmol) were used. A purple powder (54.8 mg, 97.4%) was obtained.

^{1}H NMR (500 MHz, CD$_3$CN): δ_H 5.87 (s, 4H, H^{S1}), 7.08 (ddd, J 1.3, 5.6, 7.5 Hz, 4H, H^{T5}), 7.17 (ddd, J 0.7, 1.4, 5.6 Hz, 4H, H^{T6}), 7.63 (m, 4H, H^{N7} and H^{N6}), 7.83 (dd, J 1.8, 8.4 Hz, 2H, H^{N3}), 7.87 (td, J 1.5, 7.8 Hz, 4H, H^{T4}), 8.01 (m, 2H, H^{N5}), 8.05 (m, 2H, H^{N8}), 8.10 (d, J 8.4 Hz, 2H, H^{N4}), 8.24 (s, 2H, H^{N1}), 8.44 (ddd, J 0.8, 1.2, 8.0 Hz, 4H, H^{T3}), 8.60 (s, 4H, H$^{T3'}$).

MS (ES): m/z = 1147.0 [M+Na]$^+$, 979.0 [M-PF$_6$]$^+$, 853.1 [M-PF$_6$-PF$_5$]$^+$, 693.4 [M-2PF$_6$-CH$_2$Nap]$^+$, 552.3 [M-2PF$_6$-2CH$_2$Nap]$^+$, 464.1 [L^4+ Fe+ F]$^+$.

UV/VIS (CH$_3$CN): λ_{max}/ nm (ε_{max}, M^{-1}cm^{-1}) 223 (195 x 10^3), 245 (60.7 x 10^3), 273 (71.0 x 10^3), 315 (33.5 x 10^3), 556 (10.5 x 10^3).

Cyclic voltammetry data (CH$_3$CN, 0.1 M [^{t}Bu$_4$N]PF$_6$, Fc/Fc$^+$): +0.59 V, -1.72 V, -1.86 V.

Found: C, 55.19; H, 3.48; N, 8.07. Calc. for $C_{52}H_{38}N_6O_2P_2F_{12}Fe$·½CH$_3$CN: C, 55.58; H, 3.48; N, 7.95%.

❖ [Fe(L^5)$_2$][PF$_6$]$_2$

Molecular formula: $C_{56}H_{46}N_6O_4FeP_2F_{12}$

Molecular weight: 1212.78
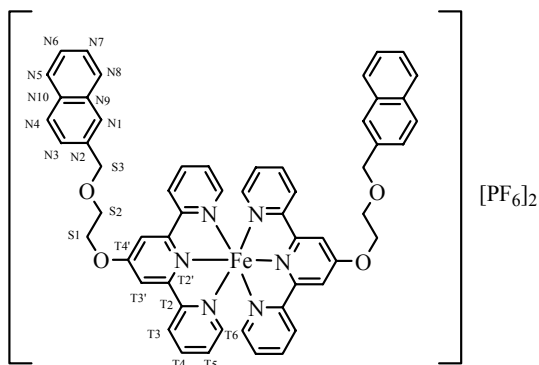
L^5 (17 mg, 0.040 mmol) and FeCl$_2$·4H$_2$O (4.0 mg, 0.020 mmol) were used. A purple powder (24.8 mg, 98.0%) was obtained.

^{1}H NMR (500 MHz, CD$_3$CN): δ_H 4.18 (m, 4H, H^{S2}), 4.83 (m, 4H, H^{S1}), 4.91 (s, 4H, H^{S3}), 6.99 (m, 4H, H^{T5}), 7.09 (dd, *J* 0.6, 5.6 Hz, 4H, H^{T6}), 7.45 (m, 4H, H^{N7} and H^{N6}), 7.60 (dd, *J* 1.6, 8.4 Hz, 2H, H^{N3}), 7.79 (m, 6H, H^{T4} and H^{N5}), 7.85 (d, *J* 8.1 Hz, 2H, H^{N8}), 7.87 (d, *J* 8.5 Hz, 2H, H^{N4}), 7.94 (s, 2H, H^{N1}), 8.36 (d, *J* 8.0 Hz, 4H, H^{T3}), 8.49 (s, 4H, H$^{T3'}$).

^{13}C NMR (125 MHz, CD$_3$CN): δ_C 69.6 (C^{S2}), 71.0 (C^{S1}), 74.0 (C^{S3}), 112.5 (C$^{T3'}$), 124.5 (C^{T3}), 126.9 (C^{N3}), 127.0 (C$^{N6/N7/N1}$), 127.25 (C$^{N6/N7/N1}$), 127.27 (C$^{N6/N7/N1}$), 128.1 (C^{T5}), 128.6 (C$^{N5/N8}$), 128.7 (C$^{N8/N5}$), 129.1 (C^{N4}), 133.9 (C^{N10}), 134.2 (C^{N9}), 137.1 (C^{N2}), 139.4 (C^{T4}), 154.2 (C^{T6}), 159.0 (C^{T2}), 161.7 (C$^{T2'}$), 168.9 (C$^{T4'}$).

MS (ES): *m/z* = 1067.1 [M-PF$_6$]$^+$, 940.9 [M-PF$_6$-PF$_5$]$^+$, 737.4 [M-2PF$_6$-CH$_2$CH$_2$OCH$_2$Nap]$^+$, 552.3 [M-2PF$_6$-2CH$_2$CH$_2$OCH$_2$Nap]$^+$, 508.3 [L^5+Fe+F]$^+$, 461.5 [M-2PF$_6$]$^{2+}$.

UV/VIS (CH$_3$CN): λ_{max}/ nm (ε_{max}, M^{-1}cm^{-1}) 224 (241 x 10^3), 244 (59.7 x 10^3), 272 (68.1 x 10^3), 315 (38.8 x 10^3), 556 (11.7 x 10^3).

Cyclic voltammetry data (CH$_3$CN, 0.1 M [^{t}Bu$_4$N]PF$_6$, Fc/Fc$^+$): +0.59 V, -1.74 V, -1.90 V.

Found: C, 54.91; H, 4.04; N, 6.64. Calc. for C$_{56}$H$_{46}$N$_6$O$_4$P$_2$F$_{12}$Fe·½H$_2$O: C, 55.05; H, 3.88; N, 6.88%.

❖ [Fe(L^6)$_2$][PF$_6$]$_2$

Molecular formula: C$_{60}$H$_{54}$N$_6$O$_6$FeP$_2$F$_{12}$

Molecular weight: 1300.78
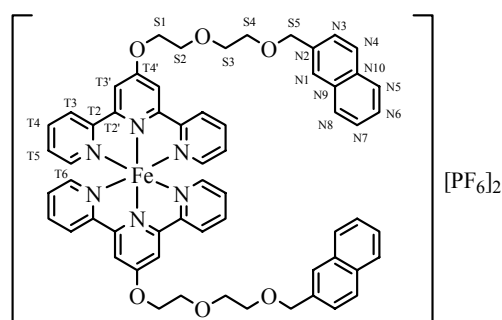
L^6 (59.5 mg, 0.125 mmol) and FeCl$_2$·4H$_2$O (12.4 mg, 0.0625 mmol) were used. A purple powder (69.4 mg, 85.7%) was obtained.

^{1}H NMR (400 MHz, CD$_3$CN): δ_H 3.79 (m, 4H, H^{S4}), 3.88 (m, 4H, H^{S3}), 4.12 (m, 4H, H^{S2}), 4.75 (s, 4H, H^{S5}), 4.76 (m, 4H, H^{S1}), 7.00 (t, *J* 7.1 Hz, 4H, H^{T5}), 7.11 (d, *J* 5.6 Hz, 4H, H^{T6}), 7.44 (m, 4H, H^{N6} and H^{N7}), 7.51 (d, *J* 8.6 Hz, 2H, H^{N3}), 7.81 (m, 12H, H^{N5}, H^{N8}, H^{T4}, H^{N4} and H^{N1}), 8.37 (d, *J* 8.1 Hz, 4H, H^{T3}), 8.46 (s, 4H, H$^{T3'}$).

MS (ES): m/z = 1154.9 [M-PF$_6$]$^+$, 781.2 [M-2PF$_6$-O(CH$_2$CH$_2$O)$_2$CH$_2$Nap]$^+$, 505.2 [M-2PF$_6$]$^{2+}$.

UV/VIS (CH$_3$CN): λ_{max}/ nm (ε_{max}, M^{-1}cm^{-1}) 224 (289 x 10^3), 241 (74.7 x 10^3), 274 (74.0 x 10^3), 315 (31.8 x 10^3), 554 (8.41 x 10^3).

Cyclic voltammetry data (CH$_3$CN, 0.1 M [^{t}Bu$_4$N]PF$_6$, Fc/Fc$^+$): +0.59 V, -1.73 V, -1.87 V.

Found: C, 55.21; H, 4.21; N, 6.41. Calc. for C$_{60}$H$_{54}$N$_6$O$_6$P$_2$F$_{12}$Fe: C, 55.39; H, 4.18; N, 6.46%.

❖ [Fe($\boldsymbol{L^7}$)$_2$][PF$_6$]$_2$

Molecular formula: C$_{64}$H$_{62}$N$_6$O$_8$FeP$_2$F$_{12}$

Molecular weight: 1388.99
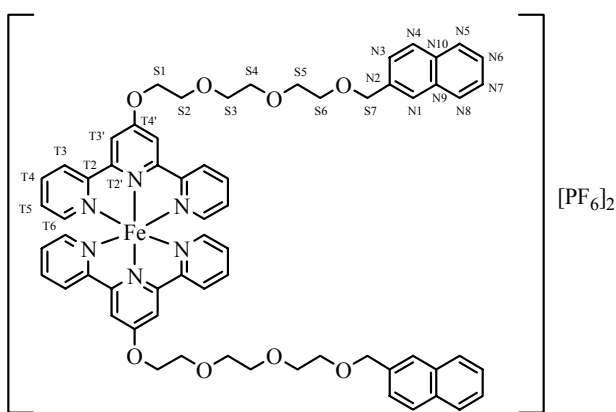
$\boldsymbol{L^7}$ (40 mg, 0.077 mmol) and FeCl$_2$·4H$_2$O (7.65 mg, 0.0385 mmol) were used. The purple powder (42.6 mg, 79.7%) was obtained.

^{1}H NMR (400 MHz, CD$_3$CN): δ_H 3.72 (m, 12H, H^{S4}, H^{S5} and H^{S6}), 3.82 (t, J 4.2 Hz, 4H, H^{S3}), 4.11 (t, J 4.0 Hz, 4H H^{S2}), 4.69 (s, 4H, H^{S7}), 4.74 (t, J 4.0 Hz, 4H, H^{S1}), 7.00 (t, J 6.3 Hz, 4H, H^{T5}), 7.11 (d, J 5.1 Hz, 4H, H^{T6}), 7.43 (m, 4H, H^{N6} and H^{N7}), 7.48 (d, J 8.6 Hz, 2H, H^{N3}), 7.81 (m, 12H, H^{N5}, H^{N8}, H^{T4}, H^{N4} and H^{N1}), 8.36 (d, J 8.1 Hz, 4H, H^{T3}), 8.44 (s, 4H, H$^{T3'}$).

MS (ES): m/z = 1243.0 [M-PF$_6$]$^+$, 825.3 [M-2PF$_6$-(CH$_2$CH$_2$O)$_3$CH$_2$Nap]$^+$, 549.2 [M-2PF$_6$]$^{2+}$.

UV/VIS (CH$_3$CN): λ_{max}/ nm (ε_{max}, M^{-1}cm^{-1}) 224 (236 x 10^3), 241 (65.6 x 10^3), 272 (70.1 x 10^3), 315 (43.1 x 10^3), 557 (12.8 x 10^3).

Cyclic voltammetry data (CH$_3$CN, 0.1 M [^{t}Bu$_4$N]PF$_6$, Fc/Fc$^+$): +0.59 V, -1.73 V, -1.90 V.

Found: C, 54.53; H, 4.47; N, 6.02. Calc. for C$_{64}$H$_{62}$N$_6$O$_8$P$_2$F$_{12}$Fe·H$_2$O: C, 54.63; H, 4.59; N, 5.97%.

❖ [Fe(**L⁸**)₂][PF₆]₂

Molecular formula: C₆₀H₄₂N₆O₂FeP₂F₁₂

Molecular weight: 1224.79
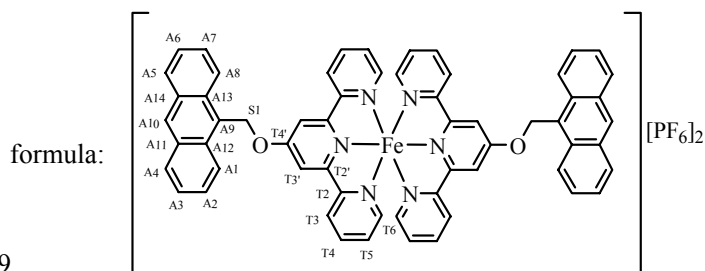
L⁸ (35 mg, 0.080 mmol) and FeCl₂·4H₂O (7.9 mg, 0.040 mmol) were used. A purple powder (36.3 mg, 74.0%) was obtained.

^{1}H NMR (500 MHz, CD₃CN): δ$_H$ 6.70 (s, 4H, H^{S1}), 7.15 (ddd, *J* 1.3, 5.6, 7.5 Hz, 4H, H^{T5}), 7.27 (ddd, *J* 0.7, 1.4, 5.6 Hz, 4H, H^{T6}), 7.67 (ddd, *J* 0.9, 6.5, 8.5 Hz, 4H, H$^{A3, A6}$), 7.77 (ddd, *J* 1.3, 6.5, 9.0 Hz, 4H, H$^{A2, A7}$), 7.90 (td, *J* 1.4, 7.8 Hz, 4H, H^{T4}), 8.26 (dt, *J* 0.6, 8.5 Hz, 4H, H$^{A4, A5}$), 8.45 (dt, *J* 1.0, 8.0 Hz, 4H, H^{T3}), 8.63 (dd, *J* 0.9, 9.0 Hz, 4H, H$^{A1, A8}$), 8.73 (s, 4H, H$^{T3'}$), 8.83 (s, 2H, H^{A10}).

MS (ES): *m/z* = 1079.0 [M-PF₆]⁺, 953.0 [M-PF₆-PF₅]⁺, 743.2 [M-2PF₆-CH₂Ant]⁺, 552.3 [M-2PF₆-2CH₂Ant]⁺, 191.4 [CH₂Ant]⁺.

UV/VIS (CH₃CN): λ$_{max}$/ nm (ε$_{max}$, M⁻¹cm⁻¹) 254 (333 x 10³), 272 (75.9 x 10³), 316 (48.2 x 10³), 349 (20.8 x 10³), 366 (28.0 x 10³), 386 (23.8 x 10³), 557 (15.9 x 10³).

Cyclic voltammetry data (CH₃CN, 0.1 M [^{t}Bu₄N]PF₆, Fc/Fc⁺): +0.95 V, +0.73 V, +0.59 V, -1.62 V, -1.65 V.

Found: C, 57.79; H, 3.73; N, 6.72. Calc. for C₆₀H₄₂N₆O₂P₂F₁₂Fe·H₂O: C, 57.98; H, 3.57; N, 6.76%.

❖ [Fe(**L⁹**)₂][PF₆]₂

Molecular formula: C₅₀H₃₄N₆S₂FeP₂F₁₂

Molecular weight: 1128.75
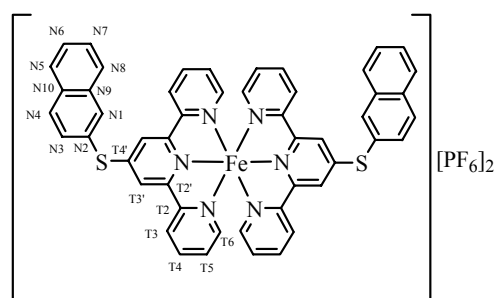
L⁹ (40 mg, 0.10 mmol) and FeCl₂·4H₂O (9.9 mg, 0.050 mmol) were used. A purple powder (51.2 mg, 90.8%) was obtained.

^{1}H NMR (500 MHz, CD$_3$CN): δ_H 7.06 (ddd, J 1.3, 5.6, 7.6 Hz, 4H, H^{T5}), 7.14 (ddd, J 0.7, 1.4, 5.6 Hz, 4H, H^{T6}), 7.71 (m, 4H, H^{N6} and H^{N7}), 7.77 (td, J 1.5, 7.8 Hz, 4H, H^{T4}), 7.94 (dd, J 1.8, 8.6 Hz, 2H, H^{N3}), 8.09 (m, 4H, H^{N5} and H^{N8}), 8.20 (m, 6H, H^{T3} and H^{N4}), 8.53 (d, J 1.5 Hz, 2H, H^{N1}), 8.56 (s, 4H, H$^{T3'}$).

MS (ES): m/z = 466.4 [$\boldsymbol{L^9}$+Fe+F]$^+$, 419.6 [M-2PF$_6$]$^{2+}$.

UV/VIS (CH$_3$CN): λ_{max}/ nm (ε_{max}, M^{-1}cm^{-1}) 221 (151 x 10^3), 283 (84.3 x 10^3), 314 (54.9 x 10^3), 566 (23.1 x 10^3).

Cyclic voltammetry data (CH$_3$CN, 0.1 M [^{t}Bu$_4$N]PF$_6$, Fc/Fc$^+$): +0.84 V, +0.68 V, -1.58 V, -1.69 V.

Found: C, 53.21; H, 3.16; N, 7.21. Calc. for C$_{50}$H$_{34}$N$_6$S$_2$P$_2$F$_{12}$Fe: C, 53.20; H, 3.04; N, 7.45%.

(b) General method for synthesising ruthenium(II) complexes

Step 1

1. RuCl$_3$·3H$_2$O, MeOH, reflux 3 hr

L

L^5 n = 0
L^6 n = 1
L^7 n = 2

Step 2

1. *L*, MeOH, reflux 3 hr, NEM
2. Excess aqueous NH$_4$PF$_6$

[PF$_6$]$_2$

[Ru(*L*)$_2$][PF$_6$]$_2$ (*L* = *L^5*-*L^7*)

Step 1

1. RuCl$_3$·3H$_2$O, MeOH, reflux 3 hr

L

L^4 Y = O-CH$_2$-2-naphthyl
L^9 Y = O-S-2-naphthyl

Step 2

1. *L*, MeOH, reflux 3 hr, NEM
2. Excess aqueous NH$_4$PF$_6$

[PF$_6$]$_2$

[Ru(*L*)$_2$][PF$_6$]$_2$ (*L* = *L^4*, *L^9*)
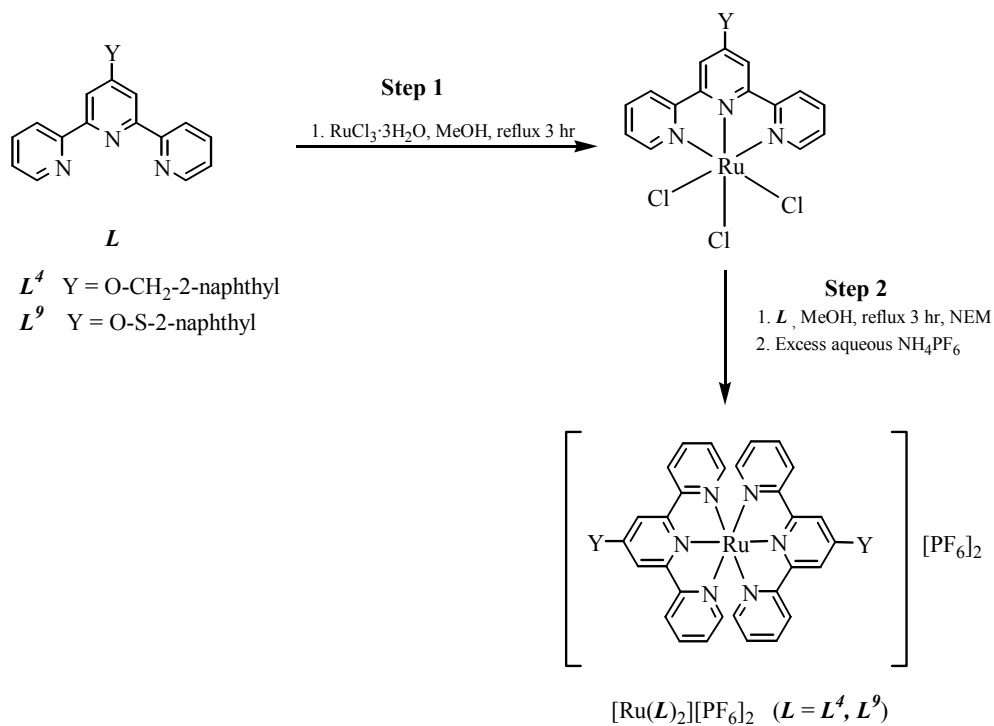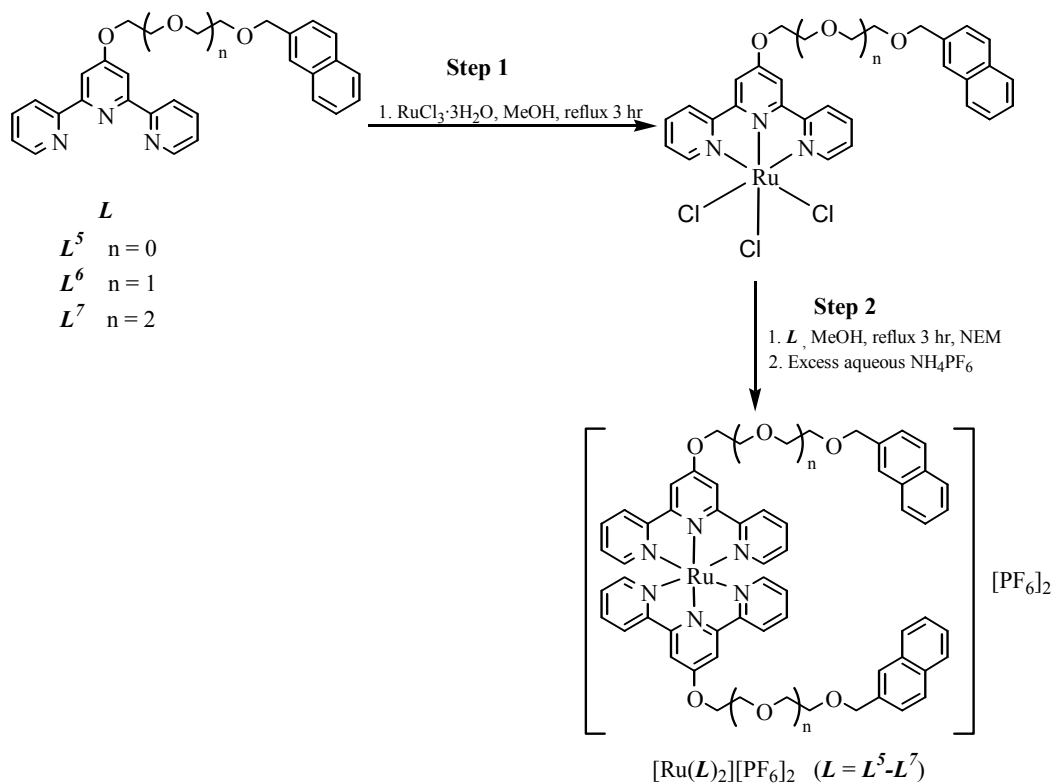
Step 1

RuCl$_3$·3H$_2$O (1 equivalent) and **L** (1 equivalent) were added to 10 mL CH$_3$OH. The solution was heated to reflux for 3 hours. Then, the brownish yellow precipitate which had formed was filtered off and air dried to give [Ru**L**Cl$_3$]. The product was used without any purification.

Step 2

The complex [Ru**L**Cl$_3$] (1 equivalent) and **L** (1 equivalent) were suspended in CH$_3$OH (10 mL). *N*-Ethylmorpholine (NEM) (2 drops) was added and the mixture was heated to reflux for 3 hours. Then, the resulting dark solution was allowed to cool, and excess aqueous NH$_4$PF$_6$ was added to the solution. The dark red precipitate was filtered and washed with water. The dark red precipitate was collected without purification to give a red powder.[24,26,29]

❖ [Ru(**L^4**)$_2$][PF$_6$]$_2$

Molecular formula: C$_{52}$H$_{38}$N$_6$O$_2$RuP$_2$F$_{12}$

Molecular weight: 1169.90
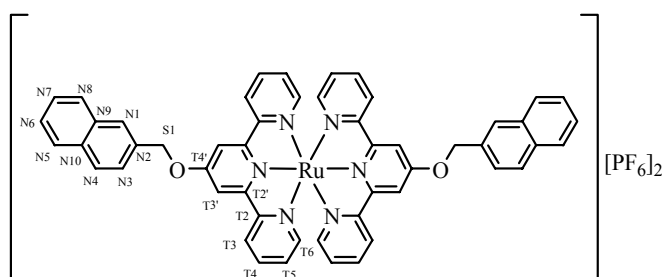
RuCl$_3$·3H$_2$O (17 mg, 0.064 mmol) and **L^4** (25 mg, 0.064 mmol) were used for step 1 and 30.3 mg of [Ru**L^4**Cl$_3$] was obtained. Then, another 1 equivalent of **L^4** (20 mg, 0.051 mmol) was used for the second step. A reddish brown powder (41.2 mg, 55.0%) was obtained.

^{1}H NMR (500 MHz, CD$_3$CN): δ_H 5.79 (s, 4H, H^{S1}), 7.16 (ddd, *J* 1.4, 5.7, 7.5 Hz, 4H, H^{T5}), 7.39 (ddd, *J* 0.6, 1.4, 5.6 Hz, 4H, H^{T6}), 7.62 (m, 4H, H^{N7} and H^{N6}), 7.79 (dd, *J* 1.8, 8.4 Hz, 2H, H^{N3}), 7.90 (td, *J* 1.5, 7.9 Hz, 4H, H^{T4}), 8.00 (m, 2H, H^{N5}), 8.03 (m, 2H, H^{N8}), 8.08 (d, *J* 8.5 Hz, 2H, H^{N4}), 8.20 (s, 2H, H^{N1}), 8.45 (s, 4H, H$^{T3'}$), 8.47 (dt, *J* 0.9, 8.1 Hz, 4H, H^{T3}).

MS (ES): *m/z* = 1025.1 [M-PF$_6$]$^+$, 899.1 [M-PF$_6$-PF$_5$]$^+$, 739.1 [M-2PF$_6$-CH$_2$Nap]$^+$, 598.1 [M-2PF$_6$-2CH$_2$Nap]$^+$.

UV/VIS (CH$_3$CN): λ_{max}/ nm (ε_{max}, M^{-1}cm^{-1}) 223 (241 x 10^3), 242 (77.5 x 10^3), 269 (90.7 x 10^3), 304 (73.5 x 10^3), 485 (21.2 x 10^3).

Cyclic voltammetry data (CH$_3$CN, 0.1 M [^{t}Bu$_4$N]PF$_6$, Fc/Fc$^+$): +0.74 V, -1.71 V, -1.89 V.

Found: C, 52.91; H, 3.35; N, 7.09. Calc. for $C_{52}H_{38}N_6O_2P_2F_{12}Ru\cdot\frac{1}{2}H_2O$: C, 52.97; H, 3.33; N, 7.13%.

❖ $[Ru(L^5)_2][PF_6]_2$

Molecular formula: $C_{56}H_{46}N_6O_4RuP_2F_{12}$

Molecular weight: 1258.00
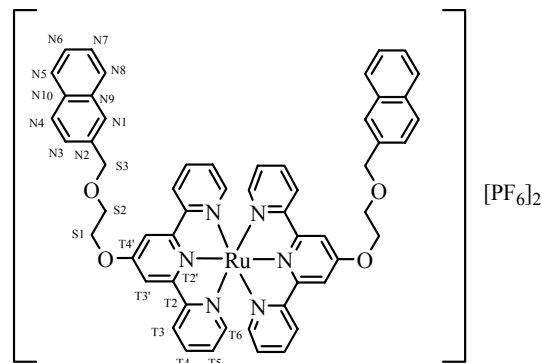
RuCl$_3$·3H$_2$O (21 mg, 0.080 mmol) and L^5 (35 mg, 0.080 mmol) were used for step 1 and 26.4 mg of $[RuL^5Cl_3]$ was obtained. Then, another 1 equivalent of L^5 (16 mg, 0.037 mmol) was used for the second step. A reddish brown powder (35.5 mg, 35.3%) was obtained.

^{1}H NMR (500 MHz, CD$_3$CN): δ_H 4.14 (m, 4H, H^{S2}), 4.75 (m, 4H, H^{S1}), 4.88 (s, 4H, H^{S3}), 7.08 (ddd, J 1.4, 5.7, 7.5 Hz, 4H, H^{T5}), 7.33 (ddd, J 0.6, 1.4, 5.6 Hz, 4H, H^{T6}), 7.45 (m, 4H, H^{N7} and H^{N6}), 7.59 (dd, J 1.7, 8.4 Hz, 2H, H^{N3}), 7.83 (m, 8H, H^{N8}, H^{T4} and H^{N5}), 7.88 (d, J 8.5 Hz, 2H, H^{N4}), 7.92 (s, 2H, H^{N1}), 8.33 (s, 4H, H$^{T3'}$), 8.39 (dt, J 0.8, 8.1 Hz, 4H, H^{T3}).

^{13}C NMR (125 MHz, CD$_3$CN): δ_C 69.6 (C^{S2}), 70.7 (C^{S1}), 74.0 (C^{S3}), 112.1 (C$^{T3'}$), 125.2 (C^{T3}), 126.9 (C^{N3}), 127.0 (C$^{N6/\ N7}$), 127.2 (C^{N1} and C$^{N6/\ N7}$), 128.3 (C^{T5}), 128.6 (C$^{N5/\ N8}$), 128.7 (C$^{N8/\ N5}$), 129.1 (C^{N4}), 133.9 (C^{N10}), 134.2 (C^{N9}), 137.1 (C^{N2}), 138.6 (C^{T4}), 153.4 (C^{T6}), 157.3 (C^{T2}), 159.2 (C$^{T2'}$), 166.9 (C$^{T4'}$).

MS (ES): m/z = 1113.2 [M-PF$_6$]$^+$, 783.3 [M-2PF$_6$-CH$_2$CH$_2$OCH$_2$Nap]$^+$, 484.1 [M-2PF$_6$]$^{2+}$.

UV/VIS (CH$_3$CN): λ_{max}/ nm (ε_{max}, M^{-1}cm^{-1}) 227 (236 x 10^3), 245 (60.8 x 10^3), 270 (68.1 x 10^3), 307 (67.4 x 10^3), 488 (19.0 x 10^3).

Cyclic voltammetry data (CH$_3$CN, 0.1 M [^{t}Bu$_4$N]PF$_6$, Fc/Fc$^+$): +0.74 V, -1.73 V, -1.91 V.

Found: C, 53.09; H, 3.79; N, 6.49. Calc. for $C_{56}H_{46}N_6O_4P_2F_{12}Ru\cdot\frac{1}{2}H_2O$: C, 53.08; H, 3.74; N, 6.63%.

❖ [Ru(***L***⁶)₂][PF₆]₂

Molecular formula: $C_{60}H_{54}N_6O_6RuP_2F_{12}$

Molecular weight: 1346.11
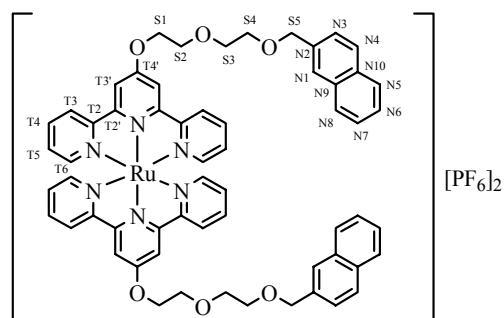
RuCl₃·3H₂O (37 mg, 0.14 mmol) and ***L***⁶ (68 mg, 0.14 mmol) were used for step 1 and 88.0 mg of [Ru***L***⁶Cl₃] was obtained. Then, another 1 equivalent of ***L***⁶ (62 mg, 0.13 mmol) was used for the second step. A reddish brown powder (77.3 mg, 41.0%) was obtained after recrystallisation with ethanol.

¹H NMR (400 MHz, CD₃CN): δ_H 3.77 (m, 4H, H^{S4}), 3.85 (m, 4H, H^{S3}), 4.07 (t, *J* 4.3 Hz, 4H, H^{S2}), 4.68 (t, *J* 4.3 Hz, 4H, H^{S1}), 4.73 (s, 4H, H^{S5}), 7.08 (ddd, *J* 1.6, 5.7, 7.5 Hz, 4H, H^{T5}), 7.34 (d, *J* 5.1 Hz, 4H, H^{T6}), 7.44 (m, 4H, H^{N6} and H^{N7}), 7.50 (dd, *J* 1.3, 8.3 Hz, 2H, H^{N3}), 7.82 (m, 12H, H^{N8}, H^{T4}, H^{N5}, H^{N4} and H^{N1}), 8.31 (s, 4H, H$^{T3'}$), 8.40 (d, *J* 8.1 Hz, 4H, H^{T3}).

MS (ES): *m/z* = 1201.1 [M-PF₆]⁺, 827.2 [M-2PF₆-(CH₂CH₂O)₂CH₂Nap]⁺, 528.1 [M-2PF₆]²⁺.

UV/VIS (CH₃CN): λ_{max}/ nm (ε_{max}, M⁻¹cm⁻¹) 224 (31.4 x 10³), 241 (8.08 x 10³), 267 (8.86 x 10³), 304 (9.16 x 10³), 486 (1.71 x 10³).

Cyclic voltammetry data (CH₃CN, 0.1 M [ᵗBu₄N]PF₆, Fc/Fc⁺): +0.73 V, -1.72 V, -1.92 V.

Found: C, 53.07; H, 3.85; N, 6.25. Calc. for $C_{60}H_{54}N_6O_6P_2F_{12}Ru·½H_2O$: C, 53.17; H, 4.09; N, 6.20%.

❖ [Ru(***L***⁷)₂][PF₆]₂

Molecular formula: $C_{64}H_{62}N_6O_8RuP_2F_{12}$

Molecular weight: 1434.21
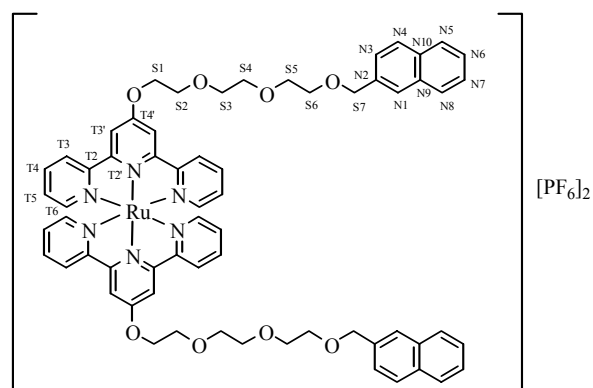
RuCl$_3\cdot$3H$_2$O (14 mg, 0.052 mmol) and *L⁷* (27 mg, 0.052 mmol) were used for step 1 and 21.3 mg of [Ru*L⁷*Cl$_3$] was obtained. Then, another 1 equivalent of *L⁷* (15 mg, 0.029 mmol) was used for the second step. A reddish brown powder (39.8 mg, 53.5%) was obtained.

^{1}H NMR (400 MHz, CD$_3$CN): δ_H 3.70 (m, 12H, H^{S4}, H^{S5} and H^{S6}) 3.79 (m, 4H, H^{S3}), 4.06 (t, *J* 4.3 Hz, 4H, H^{S2}), 4.66 (t, *J* 4.3 Hz, 4H, H^{S1}), 4.68 (s, 4H, H^{S7}), 7.08 (t, *J* 6.6 Hz, 4H, H^{T5}), 7.34 (d, *J* 5.1 Hz, 4H, H^{T6}), 7.43 (m, 4H, H^{N7} and H^{N6}), 7.47 (dd, *J* 1.5, 8.6 Hz, 2H, H^{N3}), 7.82 (m, 12H, H^{N8}, H^{T4}, H^{N5}, H^{N4} and H^{N1}), 8.29 (s, 4H, H$^{T3'}$), 8.39 (d, *J* 8.1 Hz, 4H, H^{T3}).

MS (ES): *m/z* = 1289.1 [M-PF$_6$]$^+$, 572.1 [M-2PF$_6$]$^{2+}$.

UV/VIS (CH$_3$CN): λ_{max}/ nm (ε_{max}, M^{-1}cm^{-1}) 224 (213 x 10^3), 241 (61.6 x 10^3), 267 (62.1 x 10^3), 304 (63.5 x 10^3), 485 (16.9 x 10^3).

Cyclic voltammetry data (CH$_3$CN, 0.1 M [^{t}Bu$_4$N]PF$_6$, Fc/Fc$^+$): +0.74 V, -1.72 V, -1.91 V.

Found: C, 52.65; H, 4.44; N, 5.91. Calc. for C$_{64}$H$_{62}$N$_6$O$_8$P$_2$F$_{12}$Ru$\cdot$H$_2$O: C, 52.93; H, 4.44; N, 5.79%.

❖ [Ru(*L⁹*)$_2$][PF$_6$]$_2$

Molecular formula: C$_{50}$H$_{34}$N$_6$S$_2$RuP$_2$F$_{12}$

Molecular weight: 1173.97
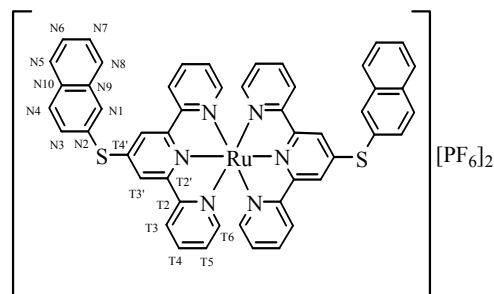
RuCl$_3\cdot$3H$_2$O (20 mg, 0.077 mmol) and *L⁹* (30 mg, 0.077 mmol) were used for step 1 and 39.6 mg of [Ru*L⁹*Cl$_3$] was obtained. Then, another 1 equivalent of *L⁹* (26 mg, 0.066 mmol) was used for the second step. A reddish brown powder (62.5 mg, 69.1%) was obtained after recrystallisation with ethanol.

^{1}H NMR (500 MHz, CD$_3$CN): δ_H 7.14 (ddd, *J* 1.3, 5.6, 7.6 Hz, 4H, H^{T5}), 7.38 (ddd, *J* 0.7, 1.5, 5.6 Hz, 4H, H^{T6}), 7.66 (m, 4H, H^{N6} and H^{N7}), 7.81 (ddd, *J* 1.5, 7.7, 8.1 Hz, 4H, H^{T4}), 7.85 (dd, *J* 1.9, 8.6 Hz, 2H, H^{N3}), 8.07 (m, 4H, H^{N5} and H^{N8}), 8.16 (d, *J* 8.6 Hz, 2H, H^{N4}), 8.22 (ddd, *J* 0.8, 1.3, 8.2 Hz, 4H, H^{T3}), 8.43 (s, 4H, H$^{T3'}$), 8.46 (d, *J* 1.6 Hz, 2H, H^{N1}).

MS (ES): *m/z* = 1029.0 [M-PF$_6$]$^+$, 442.1 [M-2PF$_6$]$^{2+}$.

UV/VIS (CH_3CN): λ_{max}/ nm (ε_{max}, $M^{-1}cm^{-1}$) 222 (129 x 10^3), 280 (76.0 x 10^3), 301 (66.6 x 10^3), 490 (26.3 x 10^3).

Cyclic voltammetry data (CH_3CN, 0.1 M [$^tBu_4N$]PF_6, Fc/Fc$^+$): +0.84 V, -1.58 V.

Found: C, 51.10; H, 2.97; N, 7.08. Calc. for $C_{50}H_{34}N_6S_2P_2F_{12}Ru$: C, 51.15; H, 2.92; N, 7.16%.

❖ [Ru($\boldsymbol{L^8}$)$_2$][PF_6]$_2$

Molecular formula: $C_{60}H_{42}N_6O_2RuP_2F_{12}$

Molecular weight: 1270.01
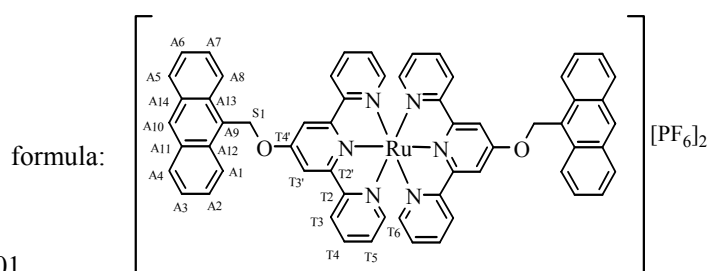
Since the attempt to use the above method to synthesise [Ru($\boldsymbol{L^8}$)$_2$][PF_6]$_2$ was not successful, the following method is used to synthesise [Ru($\boldsymbol{L^8}$)$_2$][PF_6]$_2$.[42]

[Ru($\boldsymbol{L^8}$)$_2$][PF_6]$_2$
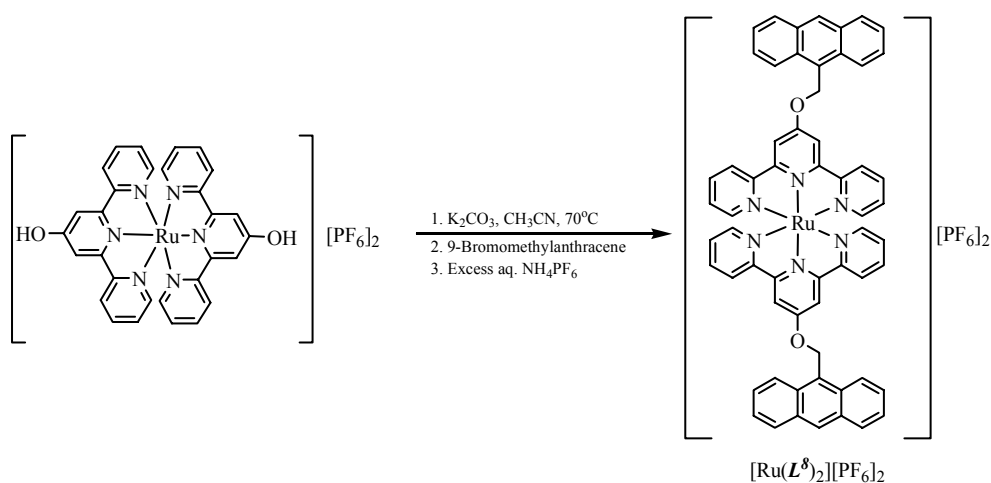
[Ru(***HO-Terpy***)$_2$][PF_6]$_2$ (89 mg, 0.10 mmol), which was synthesised in two steps as in the literature[45], and dry K_2CO_3 (0.426 g, 3.08 mmol) were stirred in dry CH_3CN (20 mL) at 70°C for 2 hours. The reaction mixture was kept at 70°C throughout the reaction. Then, 9-bromomethylanthracene (66 mg, 0.30 mmol) was added to the reaction mixture. The reaction mixture was kept at 70°C for 1 day. Excess methanolic NH_4PF_6 was added to the solution. The dark brown precipitate was filtered and collected. The crude product was

purified by column chromatography (SiO$_2$, CH$_3$CN: saturated aqueous KNO$_3$: H$_2$O 14:2:1). A red product (90.6 mg, 71.3%) was obtained.

^{1}H NMR (500 MHz, CD$_3$CN): δ_H 6.63 (s, 4H, H^{S1}), 7.22 (ddd, *J* 1.3, 5.6, 7.5 Hz, 4H, H^{T5}), 7.47 (ddd, *J* 0.7, 1.5, 5.6 Hz, 4H, H^{T6}), 7.67 (ddd, *J* 0.9, 6.5, 8.4 Hz, 4H, H$^{A3, A6}$), 7.75 (ddd, *J* 1.3, 6.5, 8.9 Hz, 4H, H$^{A2, A7}$), 7.93 (ddd, *J* 1.5, 7.6, 8.1 Hz, 4H, H^{T4}), 8.24 (dt, *J* 0.6, 8.5 Hz, 4H, H$^{A4, A5}$), 8.47 (ddd, *J* 0.8, 1.3, 8.1 Hz, 4H, H^{T3}), 8.56 (s, 4H, H$^{T3'}$), 8.59 (dd, *J* 0.9, 9.0 Hz, 4H, H$^{A1, A8}$), 8.80 (s, 2H, H^{A10}).

MS (ES): *m/z* =1189.1 [M-PF$_6$+2CH$_3$OH]$^+$, 1157.0 [M-PF$_6$+CH$_3$OH]$^+$, 1125.1 [M-PF$_6$]$^+$, 821.1 [M-PF$_6$-PF$_5$-Ant]$^+$, 598.1 [M-2PF$_6$-2CH$_2$Ant]$^+$, 191.1 [CH$_2$Ant]$^+$.

UV/VIS (CH$_3$CN): λ_{max}/ nm (ε_{max}, M^{-1}cm^{-1}) 251 (261 x 10^3), 267 (55.3 x 10^3), 302 (49.9 x 10^3), 346 (16.4 x 10^3), 363 (18.9 x 10^3), 384 (16.5 x 10^3), 483 (16.0 x 10^3).

Cyclic voltammetry data (CH$_3$CN, 0.1 M [^{t}Bu$_4$N]PF$_6$, Fc/Fc$^+$): +0.97V, +0.73, -1.64 V.

Found: C, 58.04; H, 3.74; N, 6.28. Calc. for C$_{60}$H$_{42}$N$_6$O$_2$Ru·(PF$_6$)$_{1.6}$·(SiF$_6$)$_{0.2}$: C, 58.09; H, 3.41; N, 6.78%.

3.9   References

1.   A. Juris, V. Balzani, F. Barigelletti, S. Campagna, P. Belser, and A. von Zelewsky, *Coord. Chem. Rev.*, 1988, **84**, 85.

2.   V. Balzani, and A. Juris, *Coord. Chem. Rev.*, 2001, **211**, 97.

3.   M. Plevoets, F. Vögtle, L. De Cola, and V. Balzani, *New J. Chem.*, 1999, **23**, 63.

4.   A. De Nicola, Y. Liu, K. S. Schanze, and R. Ziessel, *Chem. Commun.*, 2003, 288.

5.   P. R. Ashton, V. Balzani, O. Kocian, L. Prodi, N. Spencer, and J. F. Stoddart, *J. Am. Chem. Soc.*, 1998, **120**, 11190.

6.   P. R. Ashton, R. Ballardini, V. Balzani, E. C. Constable, A. Credi, O. Kocian, S. J. Langford, J. A. Preece, L. Prodi, E. R. Schofield, N. Spencer, J. F. Stoddart, and S. Wenger, *Chem. Eur. J.*, 1998, **4**, 2413.

7.   P. R. Ashton, R. Ballardini, V. Balzani, A. Credi, K. R. Dress, E. Ishow, C. J. Kleverlaan, O. Kocian, J. A. Preece, N. Spencer, J. F. Stoddart, M. Venturi, and S. Wenger, *Chem. Eur. J.*, 2000, **6**, 3558.

8.   R. Ballardini, V. Balzani, M. Clemente-León, A. Credi, M. T. Gandolfi, E. Ishow, J. Perkins, J. F. Stoddart, H.-R. Tseng, and S. Wenger, *J. Am. Chem. Soc.*, 2002, **124**, 12786.

9.   M. Venturi, F. Marchioni, V. Balzani, D. M. Opris, O. Henze, and A. D. Schlüter, *Eur. J. Org. Chem.*, 2003, 4227.

10.   A. González-Cabello, P. Vázquez, T. Torres, and D. M. Guldi, *J. Org. Chem.*, 2003, **68**, 8635.

11.   H. Wolpher, M. Borgström, L. Hammarström, J. Bergquist, V. Sundström, S. Styring, L. Sun, and B. Åkermark, *Inorg. Chem. Commun.*, 2003, **6**, 989.

12.   O. Johansson, M. Borgström, R. Lomoth, M. Palmblad, J. Bergquist, L. Hammarström, L. Sun, and B. Åkermark, *Inorg. Chem.*, 2003, **42**, 2908.

13.   V. Aranyos, A. Hagfeldt, H. Grennberg, and E. Figgemeier, *Polyhedron*, 2004, **23**, 589.

14.   J. A. Moss, J. C. Yang, J. M. Stipkala, X. Wen, C. A. Bignozzi, G. J. Meyer, and T. J. Meyer, *Inorg. Chem.*, 2004, **43**, 1784.

15.   H. Wolpher, O. Johansson, M. Abrahamsson, M. Kritikos, L. Sun, and B. Åkermark, *Inorg. Chem. Commun.*, 2004, **7**, 337.

16.   R. T. F. Jukes, V. Adamo, F. Hartl, P. Belser, and L. De Cola, *Inorg. Chem.*, 2004, **43**, 2779.

17.   V. Balzani, A. Juris, M. Venturi, S. Campagna, and S. Serroni, *Chem. Rev.*, 1996, **96**, 759.

18. J.-P. Sauvage, J.-P. Collin, J.-C. Chambron, S. Guillerez, C. Coudret, V. Balzani, F. Barigelletti, L. De Cola, and L. Flamigni, *Chem. Rev.*, 1994, **94**, 993.

19. J.-P. Collin, A. Harriman, V. Heitz, F. Odobel, and J.-P. Sauvage, *Coord. Chem. Rev.*, 1996, **148**, 63.

20. J.-P. Collin, P. Gaviña, V. Heitz, and J-P. Sauvage, *Eur. J. Inorg. Chem.*, 1998, 1.

21. L. Flamigni, F. Barigelletti, N. Armaroli, J.-P. Collin, I. M. Dixon, J.-P. Sauvage, and J. A. G. Williams, *Coord. Chem. Rev.*, 1999, **190-192**, 671.

22. J.-P. Collin, S. Guillerez, J.-P. Sauvage, F. Barigelletti, L. De Cola, L. Flamigni, and V. Balzani, *Inorg. Chem.*, 1991, **30**, 4230.

23. E. C. Constable, A. J. Edwards, R. Martínez-Máñez, P. R. Raithby, and A. M. W. Cargill Thompson, *J. Chem. Soc., Dalton Trans.*, 1994, 645.

24. E. C. Constable, and A. M. W. Cargill Thompson, *J. Chem. Soc., Dalton Trans.*, 1994, 1409.

25. B. Whittle, S. R. Batten, J. C. Jeffery, L. H. Rees, and M. D. Ward, *J. Chem. Soc., Dalton Trans.*, 1996, 4249.

26. G. Albano, V. Balzani, E. C. Constable, M. Maestri, and D. R. Smith, *Inorg. Chim. Acta*, 1998, **277**, 225.

27. D. Armspach, E. C. Constable, F. Diederich, C. E. Housecroft, and J.-F. Nierengarten, *Chem. Eur. J.*, 1998, **4**, 723.

28. A. Harriman, M. Hissler, A. Khatyr, and R. Ziessel, *Chem. Commun.*, 1999, 735.

29. N. W. Alcock, P. R. Barker, J. M. Haider, M. J. Hannon, C. L. Painting, Z. Pikramenou, E. A. Plummer, K. Rissanen, and P. Saarenketo, *J. Chem. Soc., Dalton Trans.*, 2000, 1447.

30. E. C. Constable, R. W. Handel, C. E. Housecroft, A. F. Morales, L. Flamigni, and F. Barigelletti, *Dalton Trans.*, 2003, 1220.

31. U. Siemeling, J. V. der Brüggen, U. Vorfeld, B. Neumann, A. Stammler, H.-G. Stammler, A. Brockhinke, R. Plessow, P. Zanello, F. Laschi, F. F. de Biani, M. Fontani, S. Steenken, M. Stapper, and G. Gurzadyan, *Chem. Eur. J.*, 2003, **9**, 2819.

32. V. W.-W. Yam, K. M.-C. Wong, and N. Zhu, *Angew. Chem. Int. Ed.*, 2003, **42**, 1400.

33. R. Passalacqua, F. Loiseau, S. Campagna, Y.-Q. Fang, and G. S. Hanan, *Angew. Chem. Int. Ed.*, 2003, **42**, 1608.

34. J. M. Haider, R. M. Williams, L. De Cola, and Z. Pikramenou, *Angew. Chem. Int. Ed.*, 2003, **42**, 1830.

35. A. C. Benniston, A. Harriman, D. J. Lawrie, and S. A. Rostron, *Tetrahedron Lett.*, 2004, **45**, 2503.

36. E. C. Constable, R. W. Handel, C. E. Housecroft, M. Neuburger, E. R. Schofield, and M. Zehnder, *Polyhedron*, 2004, **23**, 135.

37. E. Figgemeier, V. Aranyos, E. C. Constable, R. W. Handel, C. E. Housecroft, C. Risinger, A. Hagfeldt, and E. Mukhtar, *Inorg. Chem. Commun.*, 2004, **7**, 117.

38. E. C. Constable, *Metals and Ligands Reactivity*, VCH, Weinheim, 1995.

39. G. F. Swiegers, and T. J. Malefetse, *Chem. Rev.*, 2000, **100**, 3483.

40. E. C. Constable, *Adv. Inorg. Chem. Radiochem.*, 1987, **30**, 69.

41. E. C. Constable, C. P. Hart, and C. E. Housecroft, *Appl. Organomet. Chem.*, 2003, **17**, 383.

42. E. C. Constable, C. E. Housecroft, L. A. Johnston, D. Armspach, M. Neuburger, and M. Zehnder, *Polyhedron*, 2001, **20**, 483.

43. S. Encinas, L. Flamigni, F. Barigelletti, E. C. Constable, C. E. Housecroft, E. R. Schofield, E. Figgemeier, D. Fenske, M. Neuburger, J. G. Vos, and M. Zehnder, *Chem. Eur. J.*, 2002, **8**, 137.

44. M. Maestri, N. Armaroli, V. Balzani, E. C. Constable, and A. M. W. Cargill Thompson, *Inorg. Chem.*, 1995, **34**, 2759.

45. E. C. Constable, A. M. W. Cargill Thompson, D. A. Tocher, and M. A. M. Daniels, *New J. Chem.*, 1992, **16**, 855.

46. E. C. Constable, A. M. W. Cargill Thompson, N. Armaroli, V. Balzani, and M. Maestri, *Polyhedron*, 1992, **11**, 2707.

47. E. C. Constable, P. Harverson, D. R. Smith, and L. Whall, *Polyhedron*, 1997, **16**, 3615.

48. E. C. Constable, M. Neuburger, D. R. Smith, and M. Zehnder, *Inorg. Chim. Acta*, 1998, **275-276**, 359.

49. A. T. Baker, and H. A. Goodwin, *Aust. J. Chem.*, 1985, **38**, 207.

50. P. Lainé, A. Gourdon, and J.-P. Launay, *Inorg. Chem.*, 1995, **34**, 5156.

51. E. C. Constable, J. E. Davies, D. Phillips, and P. R. Raithby, *Polyhedron*, 1998, **17**, 3989.

52. E. C. Constable, C. E. Housecroft, M. Neuburger, D. Phillips, P. R. Raithby, E. Schofield, E. Sparr, D. A. Tocher, M. Zehnder, and Y. Zimmermann, *J. Chem. Soc., Dalton Trans.*, 2000, 2219.

53. J. H. Clements, and S. E. Webber, *J. Phys. Chem. B*, 1999, **103**, 9366.

Chapter 4

Synthesis of Homoleptic Mononuclear Cobalt(II) Complexes of 4′-Substituted-2,2′:6′,2″-Terpyridine Ligands

As discussed in the previous chapter, when 2,2′:6′,2″-terpyridine and its derivatives react with Co(II) ions, achiral octahedral complexes (strictly D_{2d} symmetry) are formed.[1-5] In contrast to kinetically inert low spin d^6 transition metal ions, Co(II) [which is a labile metal centre] allows equilibrium to be reached rapidly.[6,7]

Studies of mononuclear Co(II) complexes of 4′-substituted-2,2′:6′,2″-terpyridine ligands described in Chapter 2 will be fully presented in this chapter (**Scheme 1**).

$[Co(L)_2][PF_6]_2$ $(L = L^1-L^3)$ L^1 n = 0
L^2 n = 1
L^3 n = 2

$[Co(L)_2][PF_6]_2$ $(L = L^5-L^7)$ L^5 n = 0
L^6 n = 1
L^7 n = 2

L^4 Y = OCH$_2$-2-naphthyl
L^8 Y = OCH$_2$-9-anthryl
L^9 Y = S-2-naphthyl
$[Co(L)_2][PF_6]_2$ $(L = L^4, L^8, L^9, terpy)$ $terpy$ Y = H
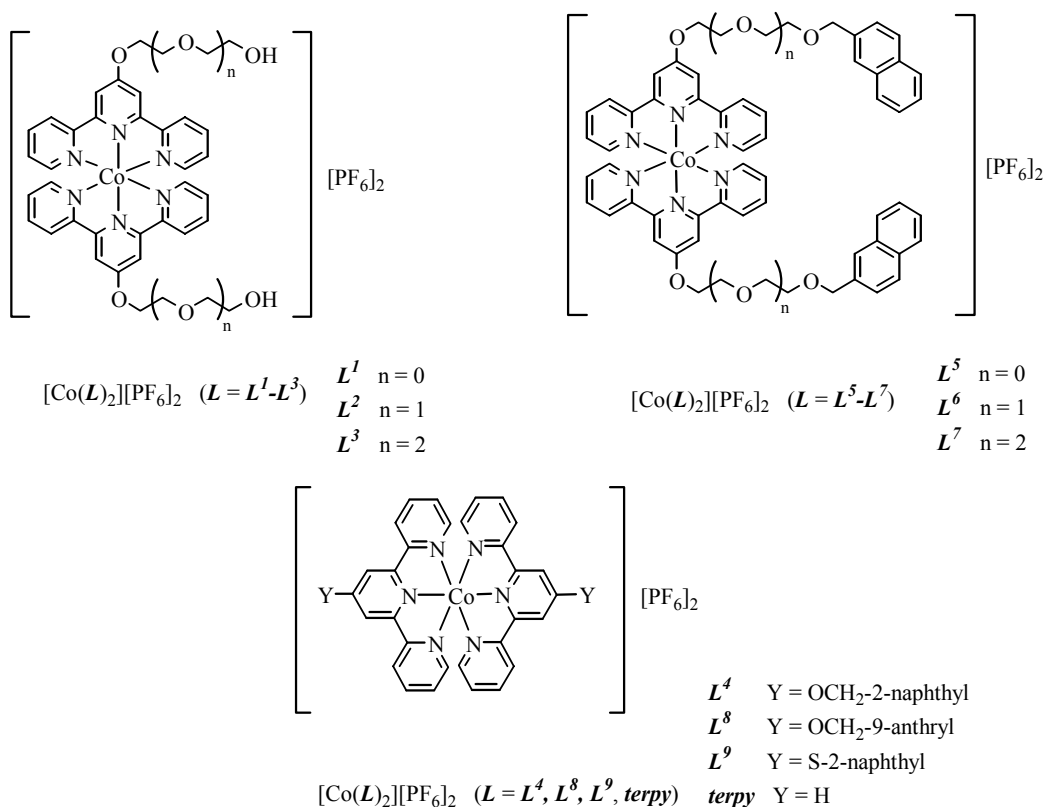
Scheme 1. Co(II) complexes of 4′-substituted-2,2′:6′,2″-terpyridine ligands studied in this chapter.

As mentioned before, Co(II) complexes are very labile[8-14] (e.g. exchange rate of $[Co(H_2O)_6]^{3+}$ and $[Co(H_2O)_6]^{2+}$ is $\approx 0.75\ M^{-1}s^{-1}$)[11,12] and this makes it an ideal metal centre for the self-assembly of molecular architectures. The exchange processes of 5,5″-disubstituted-2,2′:6′,2″-terpyridine ligands[15] and 4′-substituted-2,2′:6′,2″-terpyridine ligands[6] have been studied by the groups of Lehn and Constable. In this chapter, some preliminary studies of the combinatorial library which is formed when two or more $[Co(L)_2]^{2+}$ complexes are mixed, are discussed.

4.1 Synthesis
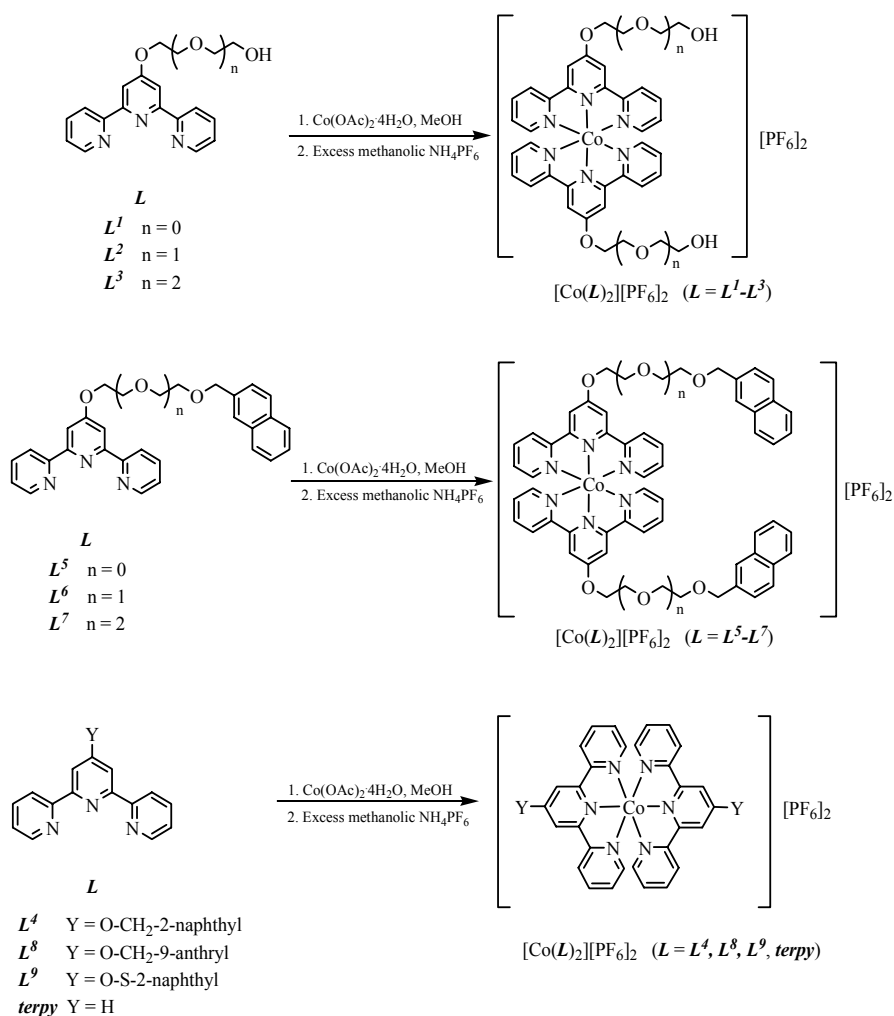
Scheme 2. The general syntheses of $[Co(L)_2][PF_6]_2$ (where **L = L¹-L⁹, terpy**).

The homoleptic Co(II) complexes were easily prepared by reacting 2 equivalents of ligand (*L*) with 1 equivalent of Co(OAc)$_2$·4H$_2$O in methanol for 0.5 hour. The solution turned brown immediately. A brown precipitate appeared when excess methanolic NH$_4$PF$_6$ was added. The brown precipitate was filtered and collected.[4-7,15-20] The yield of [Co(*L*)$_2$][PF$_6$]$_2$ (where *L* = *L^1*-*L^9*, *terpy*) complexes ranged from 47-87% (**Scheme 2**).

4.2 ^{1}H NMR spectroscopic characterisation

Cobalt(II) is a d^7 transition metal ion which provides some practical handles.[21] Octahedral Co(II) complexes possess either one (low-spin) or three (high-spin) unpaired electron(s) (**Figure 1**).
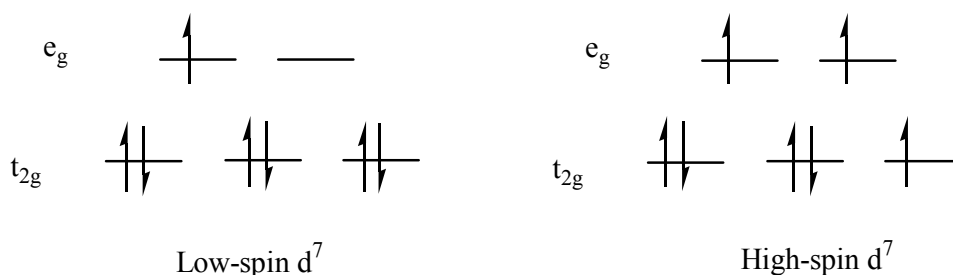
Figure 1. The two possibilities for the arrangement of electrons for an octahedral Co(II) metal ion.

This has two effects on the ^{1}H NMR spectra of Co(II) complexes, namely, paramagnetically shifted signals and broadened signals.[6,7] The shifting is caused by a significant difference between the local magnetic field at the protons and the applied field, in which the difference is due to the association of magnetic field and the unpaired electrons. The broadened signals result from an efficient relaxation mechanism, which arises from coupling between the electronic and magnetic spin. Low-spin cobalt(II) bis(terpyridine) complexes exhibit resonances down to around δ 110 [22,23] while high-spin cobalt(II) bis(terpyridine) complexes can exhibit even lower field resonances in the δ 200-250 region[24]. Constable and coworkers synthesised high-

spin [Co(**6-Br-terpy**)$_2$][PF$_6$]$_2$ and in CD$_3$CN solution, this gave ^{1}H NMR signals with the lowest field signal at δ 250.[24]

For Co(II) complexes, the ^{1}H NMR signals are broad and coupling patterns cannot be used to aid assignments. In the past, we assumed the ^{1}H nuclei in closest proximity to the Co(II) centre should be affected the most and show the greatest paramagnetic shifting. Recently, we established a method for assigning the broadened terpyridine proton signals. We found that the chemical exchange between Co(II) and Co(III) species could be used to assign the terpyridine proton signals. The assignment of the protons of the Co(II) complexes are made by a range of NMR techniques including COSY and chemical exchange difference spectroscopy (EXSY) experiments.

A mixture of [Co(**terpy**)$_2$]$^{3+}$ and [Co(**terpy**)$_2$]$^{2+}$ is a classical self-exchange system and the rate of electron transfer is ≈ 50 M^{-1}s^{-1} at room temperature.[12,13] The exchange rates are within the medium to slow range of chemical exchange on the NMR time scale. Therefore, the electron transfer reaction interconverts Co(II) and Co(III) complexes and can be detected by NMR spectroscopy as an apparent chemical exchange of Co(II) and Co(III) cations.

The ^{1}H NMR spectrum of a roughly 5:1 mixture of [Co(**L^7**)$_2$][PF$_6$]$_2$ and [Co(**L^7**)$_2$][PF$_6$]$_3$ complexes in CD$_3$CN solution exhibits two subspectra (**Figure 2**). The chemical exchange between the Co(II) and Co(III) complexes is slow on the NMR time scale and therefore the terpyridine proton signals can now be assigned by EXSY experiments. Irradiating the proton signals of the low spin Co(II) d^7 species at δ 112, 75, 71, 35 and 15 gives exchange peaks to the signals in the "normal" range (δ 3.5-9). The latter are the corresponding proton signals for the Co(III) low-spin d^6 species. For example, irradiating the Co(II) proton signal at δ 112 gives an exchange peak to a doublet signal at δ 7.3, which is the H^{T6} signal (see **Figure 2** for the atom labelling scheme) of the Co(III) species (**Figure 4**). Therefore, the signal at δ 112 is the H^{T6} signal of Co(II) species. Similarly, the signals at δ 75, 71, 35 and 15 are assigned to H$^{T3'}$, H^{T3}, H^{T5} and H^{S1} of the Co(II) species (**Figure 4**). The signal for Co(II) H^{T5} at δ 35 gives a cross peak to a signal at δ 6.4, which is assigned to Co(II) H^{T4} (**Figure 3**). All the terpyridine proton signals are now assigned. The rest of the signals were assigned by using the COSY and NOESY techniques.
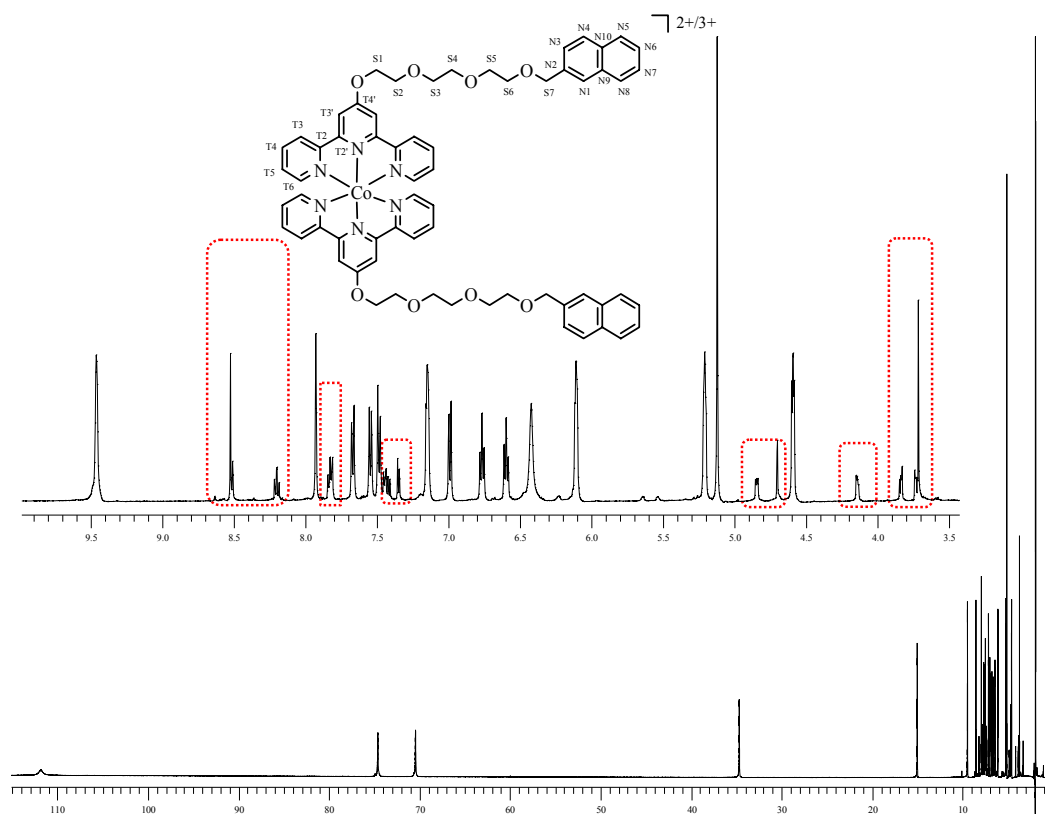
Figure 2. ^{1}H NMR (500 MHz) spectrum of a 5:1 mixture of $[Co(L^7)_2][PF_6]_2$ and $[Co(L^7)_2][PF_6]_3$ in CD$_3$CN solution at room temperature. In the inset spectrum (δ 3.5-10), the signals in the dash-lined boxes are the subspectrum of the $[Co(L^7)_2][PF_6]_3$ species.
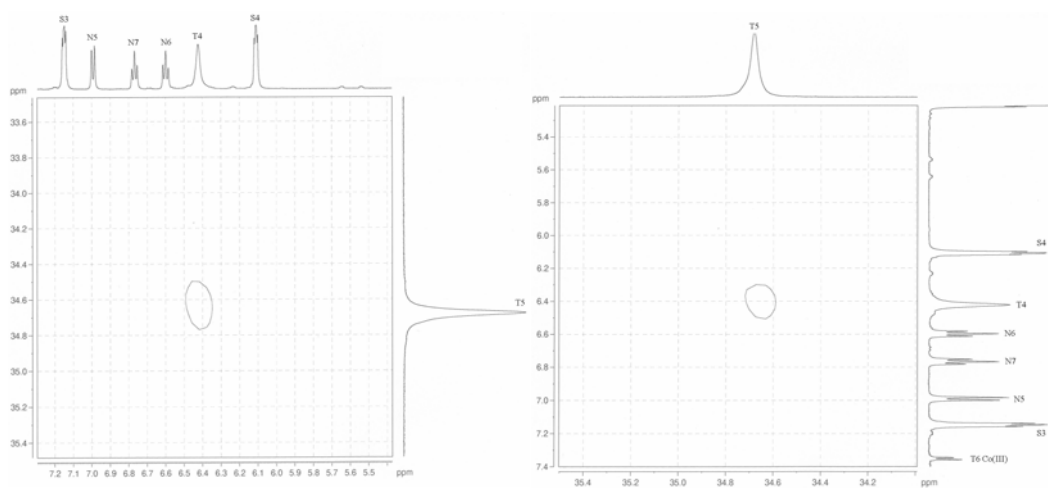
Figure 3. COSY spectrum (500 MHz) of a mixture of $[Co(L^7)_2][PF_6]_2$ and $[Co(L^7)_2][PF_6]_3$ in CD$_3$CN solution at room temperature.
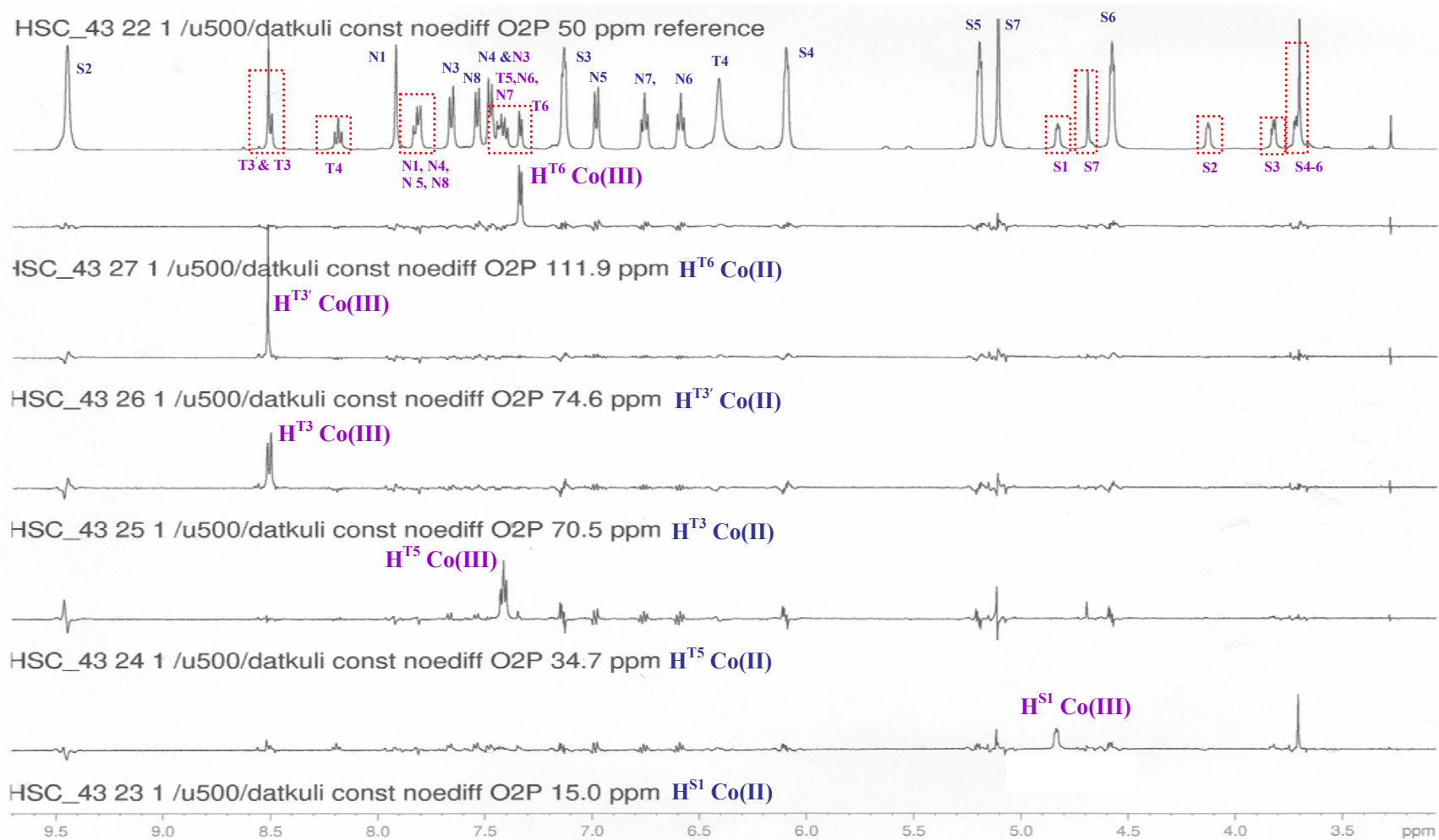
Figure 4. The spectra of the exchange peaks between the mixture of $[Co(L^7)_2][PF_6]_2$ and $[Co(L^7)_2][PF_6]_3$ species were measured at 500 MHz. The signals with dash-lined boxes are the Co(III) species; all the rest are the signals of Co(II) species.

	Proton resonance (δ)					
	H^{T6} (br)	$H^{T3'}$ (s)	H^{T3} (s)	H^{T5} (s)	H^{T4} (s)	$H^{T4'}$ (s)
[Co(***terpy***)$_2$][PF$_6$]$_2$ (without Co(III) species, measured at 250 MHz)	99.2	48.1	57.1	34.5	8.94	21.9
[Co(***terpy***)$_2$][PF$_6$]$_2$ (with 20% Co(III) species, measured at 500 MHz)	97.5	45.9	56.0	34.1	9.12	22.0
[Co(***L^1***)$_2$][PF$_6$]$_2$	112.1	75.2	70.7	34.7	6.42	
[Co(***L^2***)$_2$][PF$_6$]$_2$	111.8	74.6	70.5	34.7	6.47	
[Co(***L^3***)$_2$][PF$_6$]$_2$	111.9	74.6	70.5	34.7	6.46	
[Co(***L^4***)$_2$][PF$_6$]$_2$	113.6	76.3	71.5	35.1	6.35	
[Co(***L^5***)$_2$][PF$_6$]$_2$	111.4	74.6	70.2	34.6	6.38	
[Co(***L^6***)$_2$][PF$_6$]$_2$	111.2	74.5	70.1	34.5	6.35	
[Co(***L^7***)$_2$][PF$_6$]$_2$	111.8	74.6	70.4	34.7	6.42	
[Co(***L^8***)$_2$][PF$_6$]$_2$	110.9	73.8	69.7	34.7	6.56	
[Co(***L^9***)$_2$][PF$_6$]$_2$	102.8	55.9	61.6	34.1	8.08	

	H^{S1}	H^{S2}	H^{S3}	H^{S4}	H^{S5}	H^{S6}	OH
[Co(***L^1***)$_2$][PF$_6$]$_2$	14.98 (s)	9.49 (s)					8.00 (t) J 5.9 Hz
[Co(***L^2***)$_2$][PF$_6$]$_2$	14.90 (s)	9.43 (s)	7.09 (t) J 5.0 Hz	6.12 (t) J 5.0 Hz			5.17 (t) J 5.0 Hz
[Co(***L^3***)$_2$][PF$_6$]$_2$	14.89 (s)	9.38 (s)	7.07 (s)	6.04 (s)	5.06 (t) J 5.0 Hz	4.60 (s)	3.97 (s)

	H^{S1}	H^{S2}	H^{S3}	H^{S4}	H^{S5}	H^{S6}	H^{S7}
[Co(***L^4***)$_2$][PF$_6$]$_2$	16.25 (s)						
[Co(***L^5***)$_2$][PF$_6$]$_2$	14.90 (s)	9.54 (s)	8.14 (s)				
[Co(***L^6***)$_2$][PF$_6$]$_2$	14.90 (s)	9.44 (s)	7.16 (m)	6.10 (m)			
[Co(***L^7***)$_2$][PF$_6$]$_2$	15.01 (s)	9.46 (s)	7.15 (t) J 4.6 Hz	6.11 (t) J 4.4 Hz	5.21 (t) J 4.5 Hz	4.59 (t) J 4.5 Hz	5.12 (s)
[Co(***L^8***)$_2$][PF$_6$]$_2$	16.77 (s)						

Table 1. ^{1}H NMR spectroscopic data for terpyridine proton and the linkage CH$_2$ proton signals of [Co(***L***)$_2$][PF$_6$]$_2$ (***L*** = ***L^1***-***L^9***, ***terpy***) in CD$_3$CN solution at room temperature. The ^{1}H NMR spectra for [Co(***L***)$_2$][PF$_6$]$_2$ (***L*** = ***L^1***-***L^3***) were measured at 250 MHz, for [Co(***L***)$_2$][PF$_6$]$_2$ (***L*** = ***L^5***, ***L^6***) were measured at 400 MHz and all the others were measured at 500 MHz.

	Proton resonance (δ)						
	H^{N1} (s)	H^{N3} (d)	H^{N4} (d)	H^{N5} (d)	H^{N6} (t)	H^{N7} (t)	H^{N8} (d)
$[Co(L^4)_2][PF_6]_2$	13.48	13.10 J 7.4 Hz	10.55 J 7.4 Hz	9.39 J 8.4 Hz	8.55 J 7.7 Hz	8.67 J 6.9 Hz	10.18 J 7.3 Hz
$[Co(L^5)_2][PF_6]_2$	10.16	9.99 J 7.9 Hz	8.10 J 7.9 Hz	7.44 J 8.7 Hz	6.99 J 7.5 Hz	6.72 J 7.5 Hz	7.28 J 7.9 Hz
$[Co(L^6)_2][PF_6]_2$	8.58	8.38 J 7.9 Hz	7.53 J 7.9 Hz	7.16 (m)	6.86 (t) J 7.5 Hz	6.77 (t) J 7.1 Hz	7.66 J 7.9 Hz
$Co(L^7)_2][PF_6]_2$	7.93	7.67 J 7.7 Hz	7.48 J 8.2 Hz	6.99 J 8.1 Hz	6.60 J 7.4 Hz	6.77 J 7.3 Hz	7.55 J 8.0 Hz
$Co(L^9)_2][PF_6]_2$	12.37	12.67 J 8.3 Hz	10.15 J 8.3 Hz	9.13 J 8.4 Hz	8.36 J 7.8 Hz	8.47 J 7.7 Hz	9.63 J 8.4 Hz

	$H^{A1, A8}$ (d)		H^{A10} (s)	$H^{A2, A7}$ (m)	$H^{A4, A5}$ (d)		$H^{A3, A6}$ (m)
$[Co(L^8)_2][PF_6]_2$	14.63 J 8.9 Hz		10.63	10.13	9.84 J 8.8 Hz		9.13

Table 2. ^{1}H NMR spectroscopic data for the naphthyl and anthryl proton signals of $[Co(L)_2][PF_6]_2$ ($L = L^4$-L^9) in CD$_3$CN solution at room temperature. The ^{1}H NMR spectra for $[Co(L)_2][PF_6]_2$ ($L = L^5$, L^6) were measured at 400 MHz and all the others were measured at 500 MHz.

It was found that all the $[Co(L)_2][PF_6]_2$ species in which the 4′-position of the 2,2′:6′,2″-terpyridine domain has an oxygen linker to another domain, have very similar chemical shifts for the signals in the range δ 35-115. Therefore, the terpyridine proton signals of the other $[Co(L)_2][PF_6]_2$ complexes (where $L = L^1$-L^6, L^8) described in this chapter are assigned according to $[Co(L^7)_2][PF_6]_2$. **Table 1** shows the chemical shifts of all the terpyridine protons of $[Co(L)_2][PF_6]_2$ in CD$_3$CN solution at room temperature. Now, the assignment of all the Co(II) complexes in which the 4′-substituted-2,2′:6′,2″-terpyridine ligands contain an oxygen linker is clear.

The assignment of the ethyleneoxy CH$_2$ linkage of $[Co(L)_2][PF_6]_2$ complexes (where $L = L^1$-L^3) was made by the use of a COSY spectrum (δ 0-16, 250 MHz) and the chemical shifts of the terpyridine domain protons are compatible with those of $[Co(L^7)_2][PF_6]_2$. The ^{1}H NMR spectrum of $[Co(L^3)_2][PF_6]_2$ in CD$_3$CN solution and the COSY spectrum (δ 0-16, 250 MHz) are shown in **Figure 5** and **Figure 6** respectively.

Figure 5. The full ^{1}H NMR (250 MHz) spectrum of [Co($\boldsymbol{L^3}$)$_2$][PF$_6$]$_2$ in CD$_3$CN solution at room temperature. (* is the signal for CH$_3$CN)

The 5 terpyridine signals are assigned as those in [Co($\boldsymbol{L^7}$)$_2$][PF$_6$]$_2$. The proton signals of the CH$_2$ linkages were assigned by COSY spectrum (δ 0-16, 250 MHz). A singlet at δ 3.97 which has half of the relative integral of the signal for H^{T4} at δ 6.46 is assigned to OH. The OH signal gives a COSY cross peak to a singlet at δ 4.60 and is assigned to H^{S6}. The signal for H^{S6} gives a cross peak to a signal at δ 5.06 and is assigned to H^{S5}. The other two pairs of cross peaks at δ 14.89, 9.38 and δ 7.07, 6.04 are assigned to H^{S1}, H^{S2} and H^{S3}, H^{S4} respectively as they are compatible with those proton chemical shifts of [Co($\boldsymbol{L^7}$)$_2$][PF$_6$]$_2$. Protons in the ethyleneoxy chains which are closest to the Co(II) metal centre give rise to ^{1}H NMR signals that are shifted to the lowest field (**Table 1**). An experiment was set up on a 500 MHz spectrometer to measure the T_1 relaxation time via an inversion recovery sequence.[25] The approximated T_1 values of the five terpyridine proton signals (H^{T6}, H$^{T3'}$, H^{T3}, H^{T5} and H^{T4}) are shorter than those of the ethyleneoxy linkage proton signals (**Table 3**). Constable *et al.*[7] had been reported the T_1 relaxation times of the six protons of

133

[Co(***terpy***)$_2$][PF$_6$]$_2$ in CD$_3$CN solution by the inversion recovery technique. The T_1 values of the terpyridine protons of [Co(***L^3***)$_2$][PF$_6$]$_2$ were found to vary from 1.5 ms to 75 ms, which compares well with those values of [Co(***terpy***)$_2$][PF$_6$]$_2$ (vary from 1.54 ms to 76.0 ms).[7]

	H^{T6} (br)	H$^{T3'}$ (s)	H^{T3} (s)	H^{T5} (s)	H^{T4} (s)		
T_1	1.5 ms	13.9 ms	18.8 ms	34.6 ms	75 ms		
	H^{S1}	H^{S2}	H^{S3}	H^{S4}	H^{S5}	H^{S6}	OH
T_1	92.4 ms	222.2 ms	432.9 ms	476.2 ms	533.9 ms	447.3 ms	1.6 s

Table 3. The relaxation times T_1 of the proton signals of [Co(***L^3***)$_2$][PF$_6$]$_2$ in CD$_3$CN solution at room temperature. The spectrum was measured at 500 MHz.
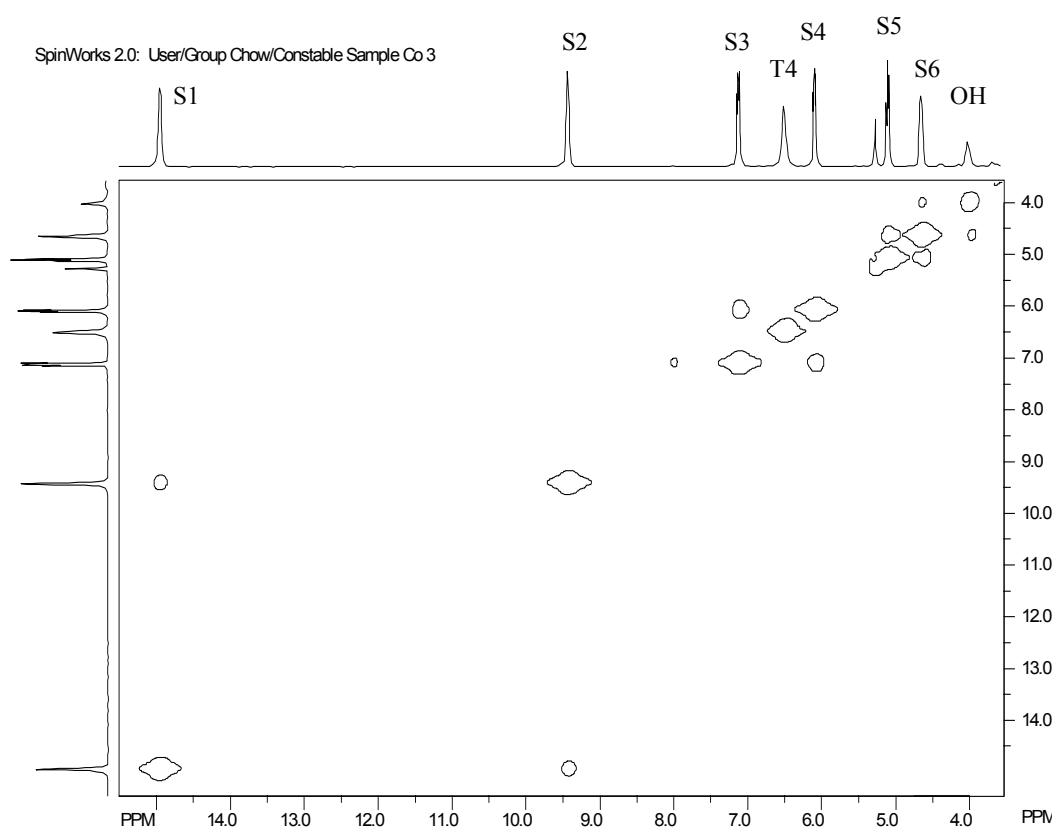
Figure 6. The COSY (δ 3.5-15.5, 250 MHz) spectrum of [Co(***L^3***)$_2$][PF$_6$]$_2$ in CD$_3$CN solution at room temperature.

The ^{1}H NMR spectrum of $[Co(\textbf{\textit{L}}^4)_2][PF_6]_2$ in CD$_3$CN solution exhibits thirteen signals from the terpyridine and the naphthyl domains (**Figure 7**). The 5 terpyridine signals are assigned as before. The COSY spectrum in **Figure 8** shows the cross peak between H^{T3} (δ 71.5), H^{T4} (δ 6.35) and H^{T5} (δ 35.1). The singlet signal at δ 16.25, which has the same relative integral of the signal for H^{T4} at δ 6.35, is assigned to H^{S1}. The singlet at δ 13.48, which has half of the relative integral of the signal for H^{S1}, is assigned to H^{N1}.

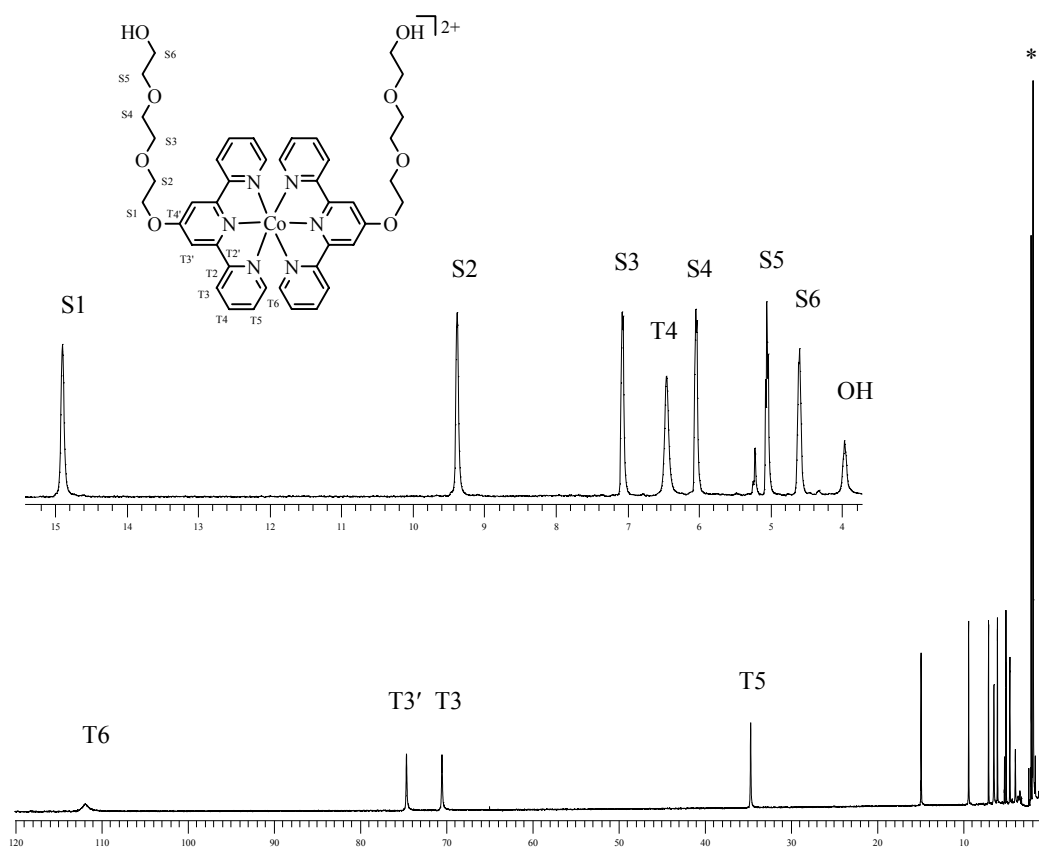**Figure 7.** ^{1}H NMR (500 MHz) spectrum of $[Co(\textbf{\textit{L}}^4)_2][PF_6]_2$ in CD$_3$CN solution at room temperature. (* is the signal for CH$_3$CN)
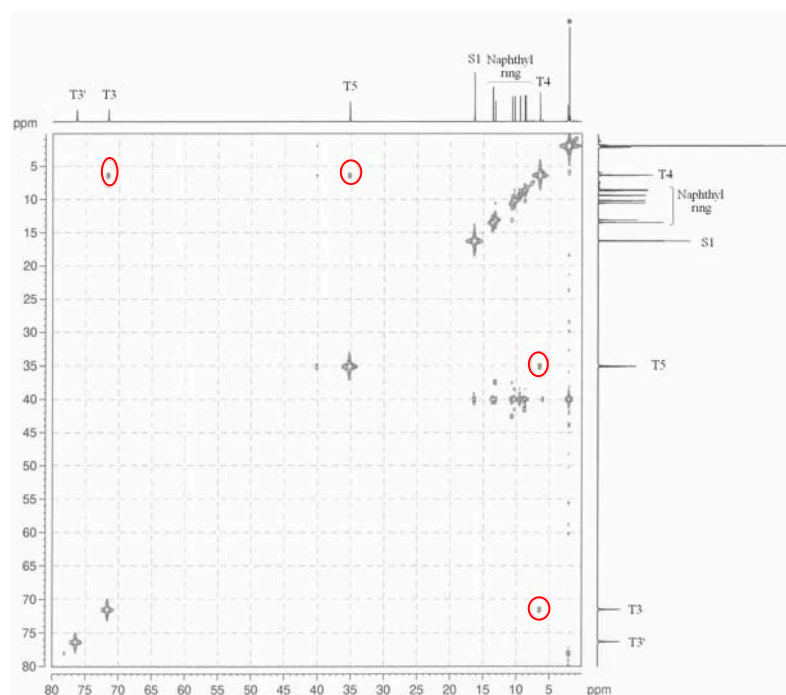
Figure 8. COSY spectrum (δ 0-80, 500 MHz) of [Co(***L***⁴)₂][PF₆]₂ in CD₃CN solution at room temperature. (* is the signal for CH₃CN)

By using NOE difference experiments, the rest of the naphthyl proton signals were assigned (**Figure 9**). Irradiating the H^{N1} singlet at δ 13.5 gives an exchange peak to a doublet at δ 10.2. This is therefore assigned to H^{N8} (**Figure 9e**). Then, irradiating the signal for H^{N8} gives exchange peaks to a singlet at δ 13.5 and a triplet at δ 8.7. These signals correspond to H^{N1} and H^{N7} respectively (**Figure 9c**). In the COSY spectrum (**Figure 10**), there is a cross peak from H^{N7} at δ 8.7 to a triplet at δ 8.6, which is assigned to H^{N6}. The signal for H^{N6} gives a cross peak to a doublet at δ 9.4 which is assigned to H^{N5}. Finally, irradiating the signal for H^{N5} at δ 9.4 gives exchange peaks to a doublet at δ 10.6 and a triplet at δ 8.6, which are assigned to H^{N4} and H^{N6} respectively (**Figure 9b**). The signal for H^{N4} gives a cross peak to H^{N3} at δ 13.1. With the help of COSY and NOE difference experiments, all the naphthyl proton signals were therefore assigned.
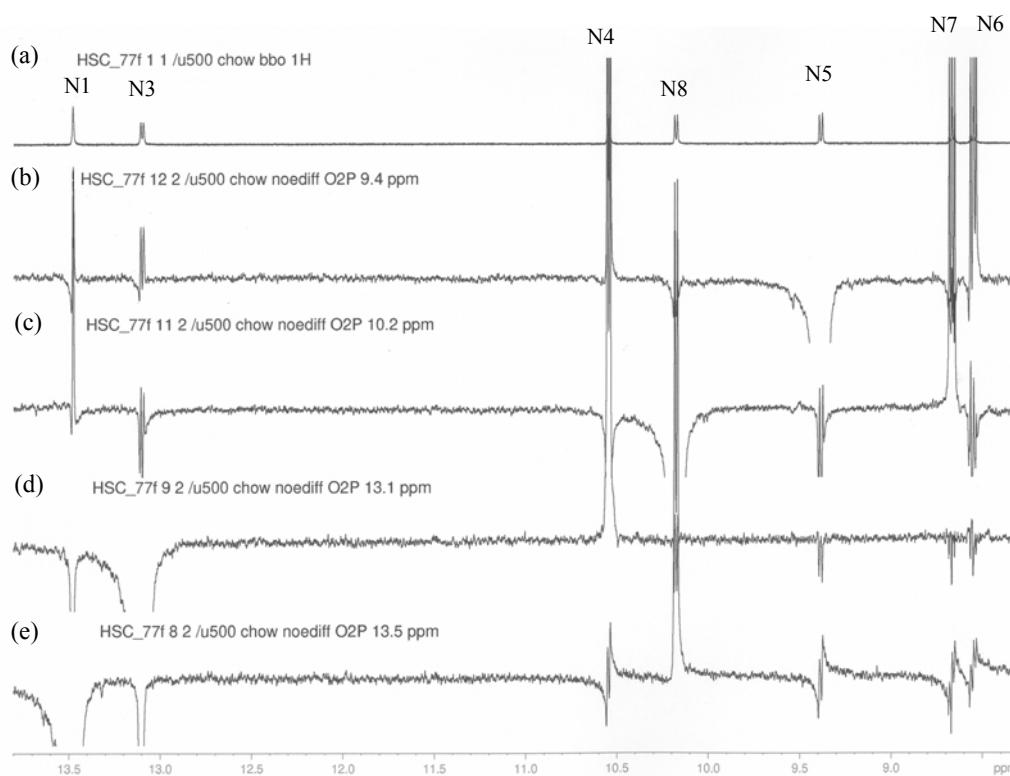
Figure 9. Spectra (500 MHz) showing the NOE difference experiments of [Co(L^4)$_2$][PF$_6$]$_2$ in CD$_3$CN solution at room temperature.
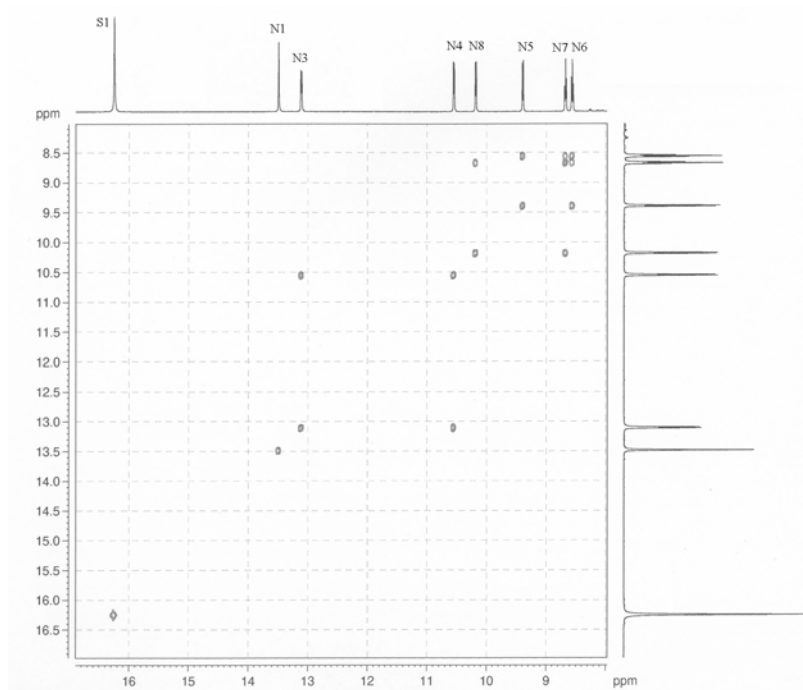
Figure 10. COSY spectrum (δ 6-17, 500 MHz) of [Co(L^4)$_2$][PF$_6$]$_2$ in CD$_3$CN solution at room temperature.

The proton signals of $[Co(L)_2][PF_6]_2$ (where $L = L^5$-L^6) were fully assigned with the help of COSY and NOE difference experiments. The chemical shifts for the ethyleneoxy chain CH_2 signals and the naphthyl signals are shown in **Table 1** and **Table 2**. The sequence of the chemical shifts for the CH_2 proton signals of the ethyleneoxy chain seem to be predictable but this is not true for the chemical shifts of the naphthyl ring signals. The proton signals of $[Co(L^8)_2][PF_6]_2$ were assigned by using COSY techniques. The proton signals of the terpyridine ring are comparable with those of $[Co(L^7)_2][PF_6]_2$ (**Table 1**).

The ^1H NMR spectrum of $[Co(L^9)_2][PF_6]_2$ in CD_3CN solution is shown in **Figure 11**. The five terpyridine signals are different from those of $[Co(L)_2][PF_6]_2$ (where $L = L^1$-L^8), except the signal at around δ 34. Assuming the signal at δ 34 is still H^{T5}. The COSY spectrum in **Figure 12** shows the cross peak between H^{T5} (δ 34.1) to H^{T4} (δ 8.08) and H^{T4} (δ 8.08) to H^{T3} (δ 61.6). The signals at δ 102.8 and δ 55.9 are H^{T6} and $H^{T3'}$ respectively.

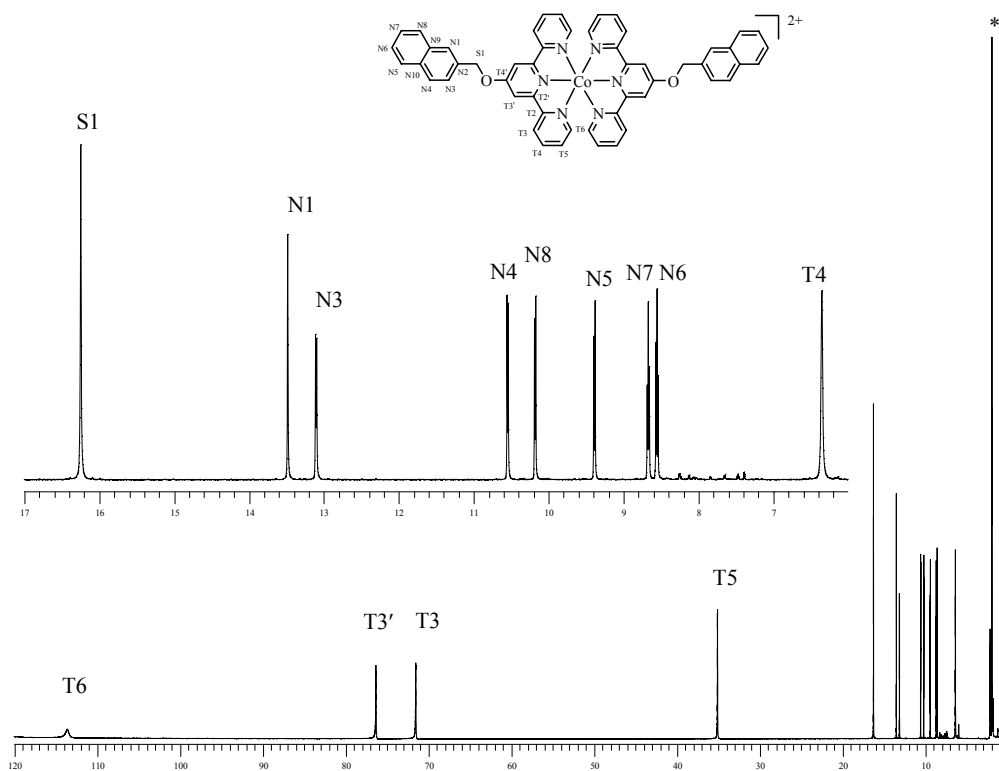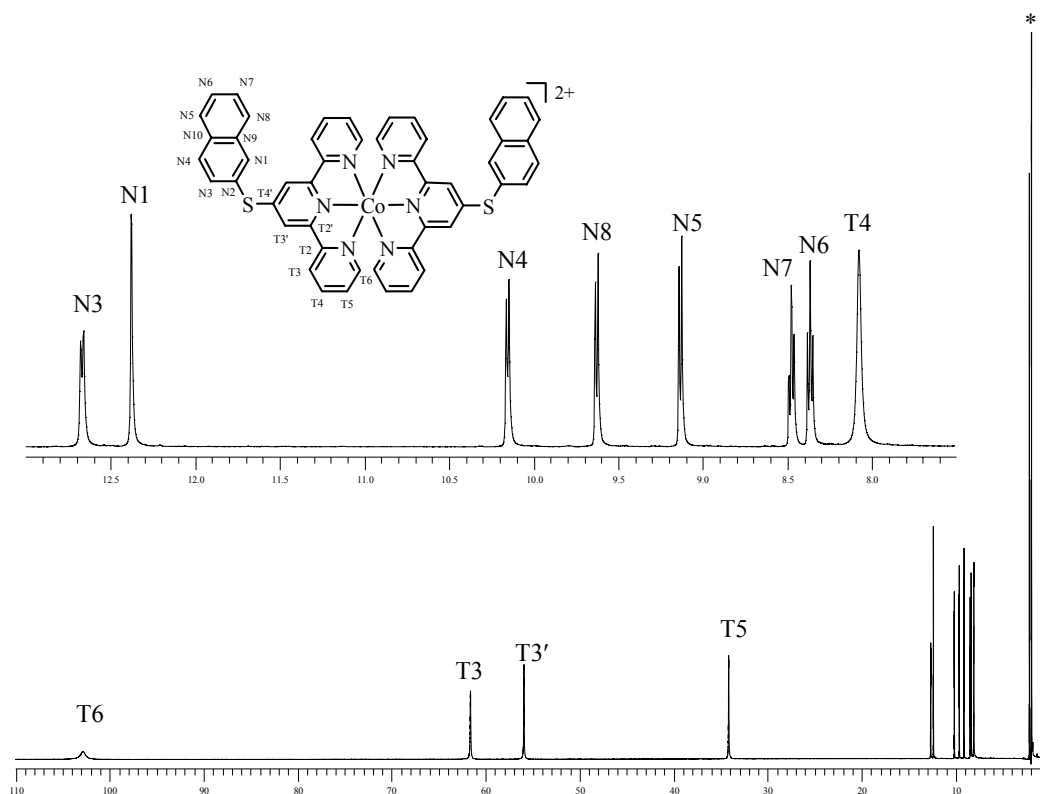**Figure 11.** ^1H NMR (500 MHz) spectrum of $[Co(L^9)_2][PF_6]_2$ in CD_3CN solution at room temperature. (* is the signal for CH_3CN)
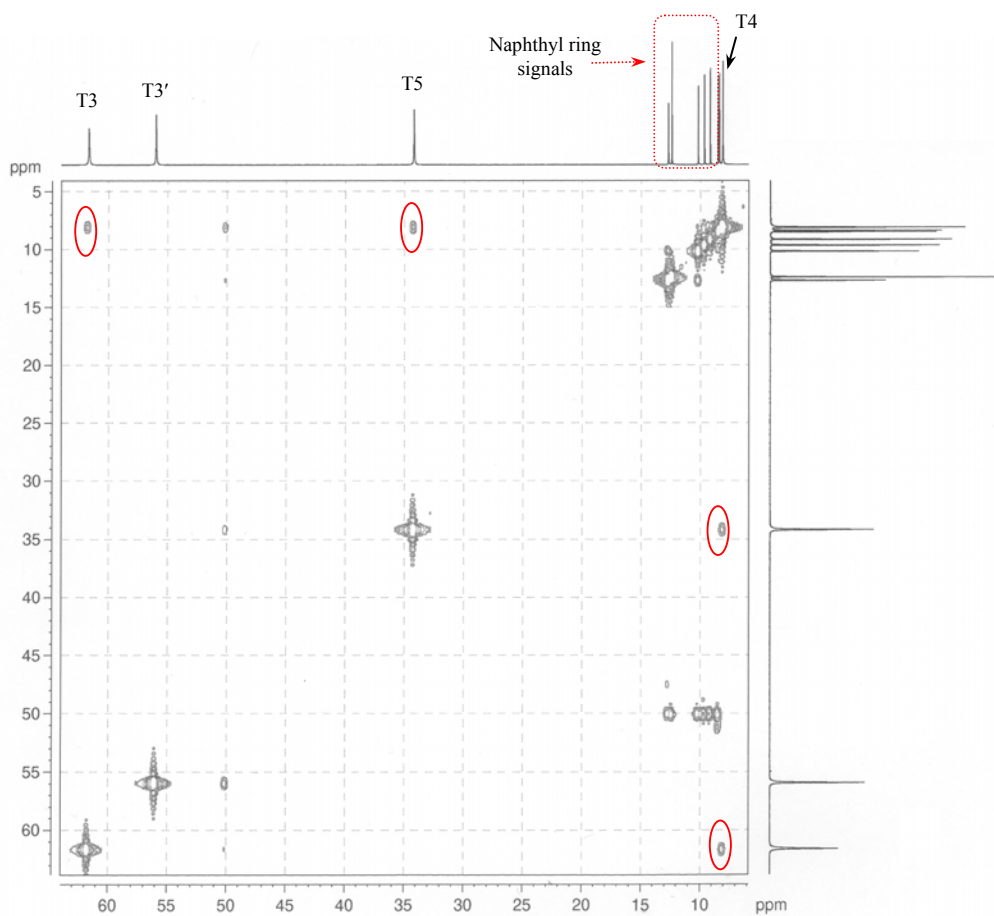
Figure 12. COSY spectrum (δ 5-65, 500 MHz) of $[Co(\boldsymbol{L^9})_2][PF_6]_2$ in CD$_3$CN solution at room temperature.

The singlet at δ 12.37, which has half of the relative integral of the signal for H^{T4}, is assigned to H^{N1}. The rest of the naphthyl proton signals were assigned by COSY and long-range COSY techniques. In the long-range COSY spectrum (**Figure 13**), there is a cross peak from the signal for H^{N1} at δ 12.37 to a doublet at δ 9.13, which is assigned to H^{N5}. The signal for H^{N5} gives a cross peak to a triplet at δ 8.36 which is assigned to H^{N6}. The signal for H^{N6} gives a cross peak to a triplet at δ 8.47 which is assigned to H^{N7}. Finally, H^{N7} gives a cross peak to a doublet at δ 9.63 which is assigned to H^{N8}. The signal for H^{N8} gives a cross peak to H^{N4} at δ 10.15. Then, the signal for H^{N4} gives a cross peak to a doublet at δ 12.67 which is assigned to H^{N3}.
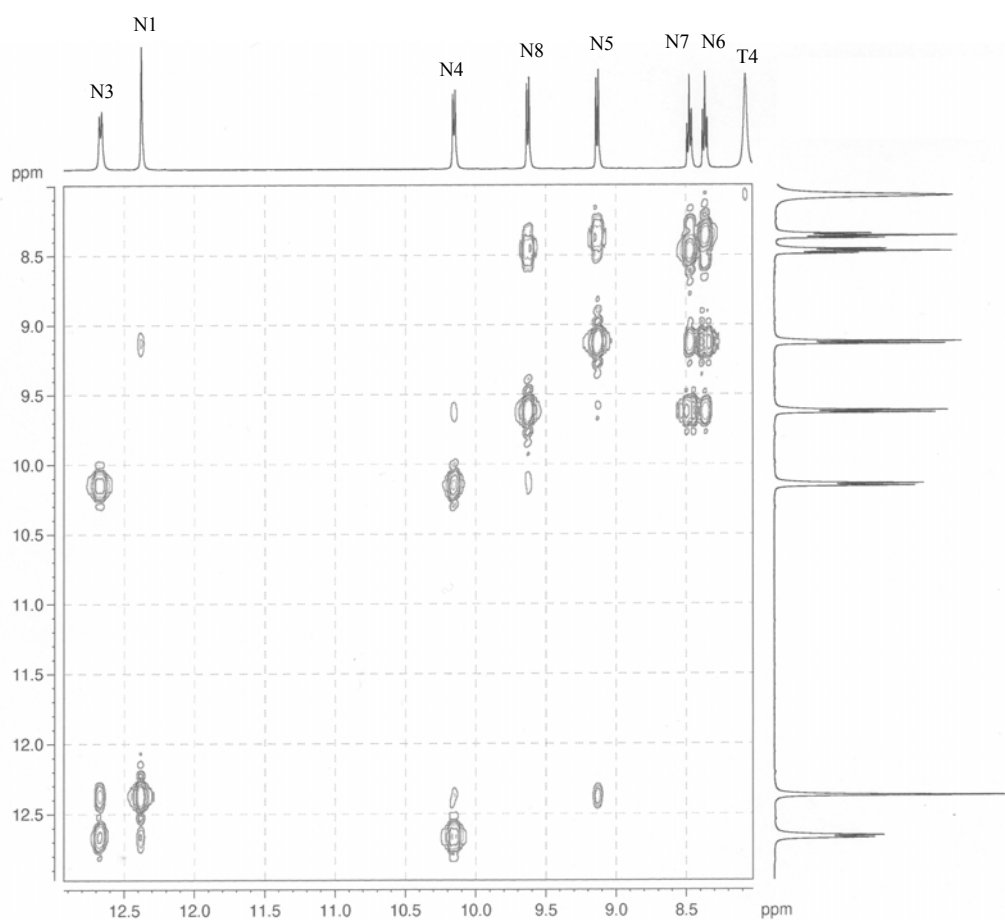
Figure 13. The long-range COSY spectrum (500 MHz) of [Co(L^9)$_2$][PF$_6$]$_2$ in CD$_3$CN solution at room temperature.

Constable *et al.*[7] have reported the ^{1}H NMR spectrum and the T_1 relaxation times of [Co(*terpy*)$_2$][PF$_6$]$_2$ in CD$_3$CN solution. Since the resonances were so broad that no coupling was observed in a wide range of techniques, it was not possible to give an unambiguous assignment of the spectrum at that time. Recently, by applying the EXSY difference experiments to a mixture of [Co(*terpy*)$_2$]$^{2+}$ and [Co(*terpy*)$_2$]$^{3+}$, the proton signals of [Co(*terpy*)$_2$]$^{2+}$ in CD$_3$CN solution were assigned. **Figure 14** shows the COSY spectrum in the chemical shift range for the [Co(*terpy*)$_2$]$^{3+}$. The six terpyridine protons of the [Co(*terpy*)$_2$]$^{3+}$ in D$_2$O solution have been fully assigned and reported in the literature.[26] The order of the terpyridine proton signals is the same in both D$_2$O and CD$_3$CN solution (H^{T6}, H^{T5}, H^{T4}, H^{T3}, H$^{T4' \& T3'}$, from higher to lower field). Since the terpyridine signals of the Co(III) species are known, the assignment of the terpyridine signals of Co(II) species can be done by applying the EXSY difference experiment to each terpyridine signals of the Co(II) species in the

paramagnetic range. Irradiating the Co(II) proton signal at δ 97.5 gives an exchange peak to a doublet at δ 7.24, which is the H^{T6} signal of Co(III) species. Therefore, the signal at δ 97.5 is assigned to the H^{T6} signal of Co(II) species. Similarly, the signals at δ 56.0, 45.9, 34.1, 22.0 and 9.12 are assigned to H^{T3}, $H^{T3'}$, H^{T5}, $H^{T4'}$ and H^{T4} of Co(II) species (**Figure 15**). The chemical shifts of the proton signals are shown in **Table 1**.
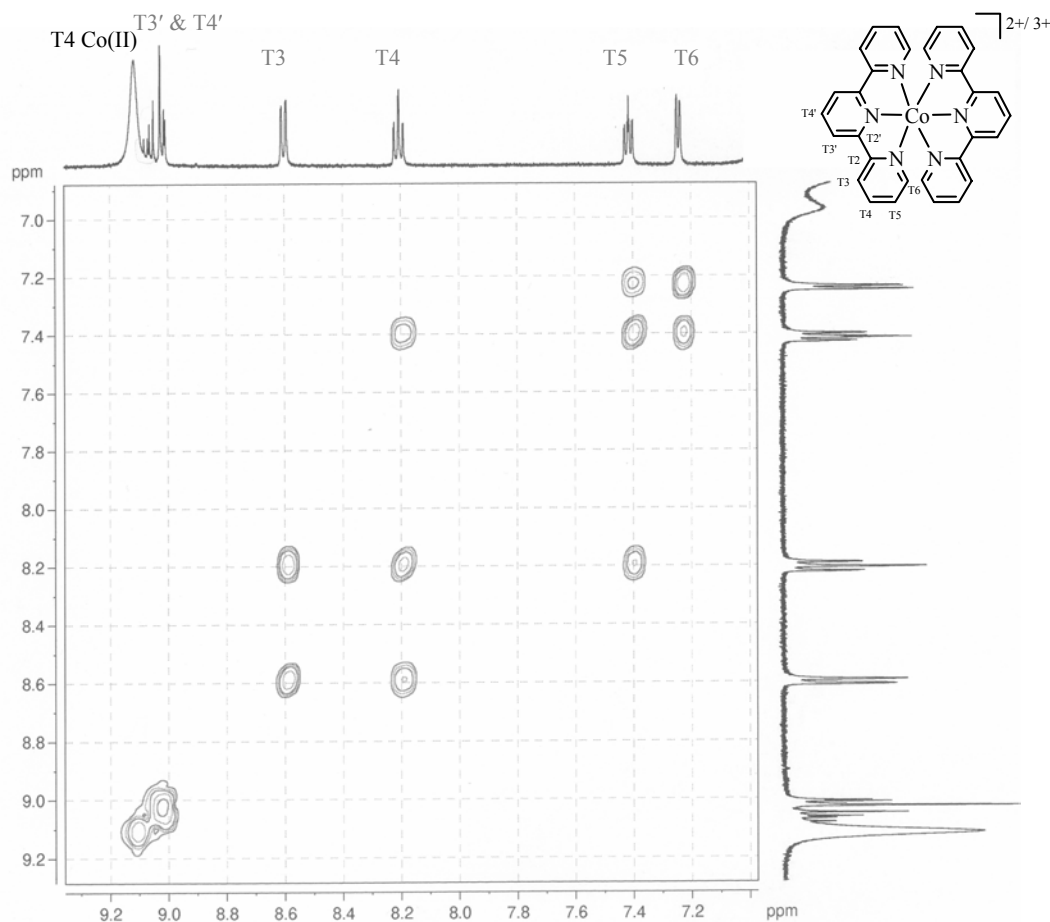
Figure 14. COSY spectrum (δ 7-9.5, 500 MHz) of mixture of [Co(***terpy***)$_2$][PF$_6$]$_2$ and [Co(***terpy***)$_2$][PF$_6$]$_3$ in CD$_3$CN solution at room temperature. Only the signal at δ 9.12 belongs to Co(II) species; all the rest belong to Co(III) species.
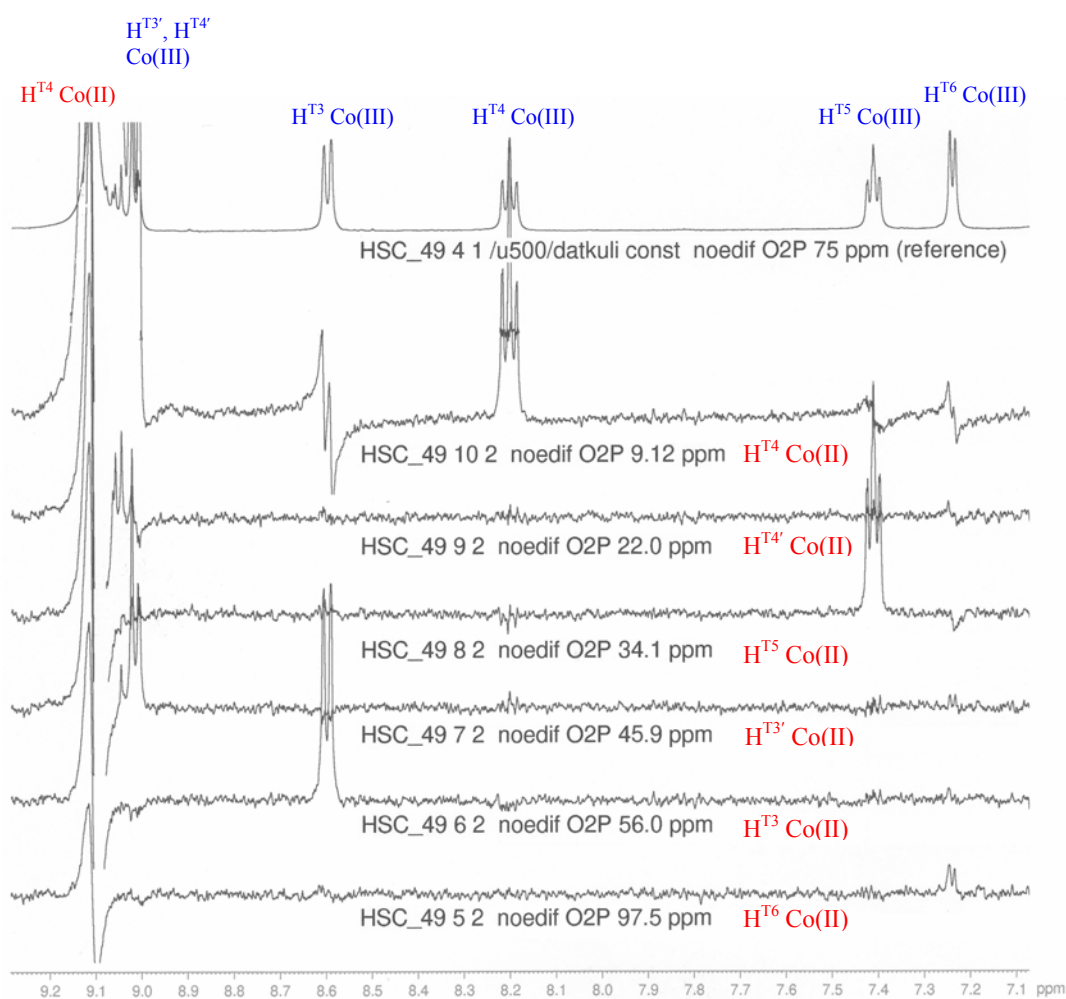
Figure 15. The exchange spectra (500 MHz) of [Co(***terpy***)$_2$][PF$_6$]$_2$ and [Co(***terpy***)$_2$][PF$_6$]$_3$ in CD$_3$CN solution.

The ^{1}H NMR spectra of [Co(***L***)$_2$][PF$_6$]$_2$ where ***L*** = ***L^1-L^9***, ***terpy*** were fully assigned. The terpyridine proton signals of [Co(***L***)$_2$][PF$_6$]$_2$ (where ***L*** = ***L^1-L^8***), in which the terpyridine domain is linked to the end domain with an oxygen bridge, are very similar. However, the one with the sulfur linked between the terpyridine and naphthyl domain is very different from the rest. The terpyridine proton signals are in the order H^{T6}, H$^{T3'}$, H^{T3}, H^{T5}, H^{T4} (from lower to higher field) in the case of [Co(***L***)$_2$][PF$_6$]$_2$ (where ***L*** = ***L^1-L^8***); the sequential order of [Co(***L^9***)$_2$][PF$_6$]$_2$ and also [Co(***terpy***)$_2$][PF$_6$]$_2$ is H^{T6}, H^{T3}, H$^{T3'}$, H^{T5}, H^{T4} (from lower to higher field). The H$^{T3'}$ signals are influenced by the substituent at the 4′-position of the 2,2′:6′,2″-terpyridine ligand.

4.3　^{13}C NMR spectroscopic characterisation of [Co(L^7)$_2$][PF$_6$]$_2$ and [Co(L^9)$_2$][PF$_6$]$_2$

In addition to the ^{1}H NMR spectra of the paramagnetic Co(II) complexes being paramagnetically shifted, we also observed that the ^{13}C NMR spectra of the Co(II) complexes were shifted and signals ranged from δ -150 to 500 compared to the Co(III) complexes in the "normal" range (δ 0-200). Except for the ^{13}C NMR signals of the Co(II) terpyridine protons (T5, T3, T3′, T4′, T6, T2′ and T2), all the rest of the signals are still in the "normal" range (δ 0-200). The ^{13}C NMR signals in the range δ 0-200 can be assigned by using HMQC and HMBC techniques. The assignment of ^{13}C NMR signals outside this range is not possible using routine experimental conditions for the HMQC and HMBC experiments. Therefore, selective proton decoupling experiments were applied to make the assignments.
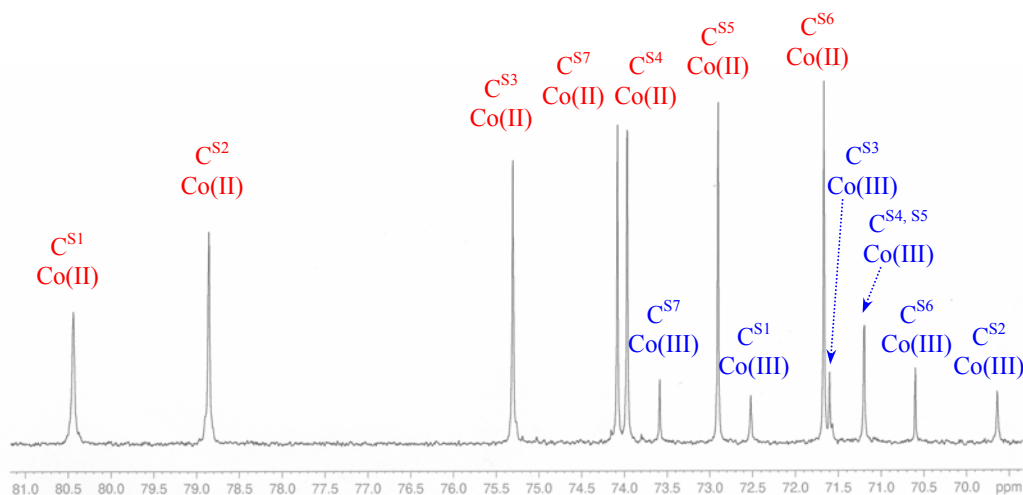
Figure 16. The ^{13}C NMR spectrum (125 MHz, δ 69-81) of the mixture of [Co(L^7)$_2$][PF$_6$]$_2$ and [Co(L^7)$_2$][PF$_6$]$_3$ in CD$_3$CN solution at room temperature.

The ^{13}C NMR spectrum of a [Co(L^7)$_2$][PF$_6$]$_2$ and [Co(L^7)$_2$][PF$_6$]$_3$ mixture (5:1) were measured in CD$_3$CN solution. A total of thirteen singlet signals in δ 69-81 region (**Figure 16**) was found for seven pairs of the symmetric CH$_2$ carbon of the ethyleneoxy chains in each of the Co(II) and Co(III) analogous and were assigned by the use of ^{1}H-^{13}C correlation HMQC and HMBC spectra. **Table 4** shows the chemical shifts of the ^{13}C NMR signals of the ethyleneoxy chains of Co(II) and Co(III) species.

The signals of the Co(II) species are shifted to lower field than those of the Co(III) species. When one compares analogous Co(II) and Co(III) complexes, there is 0.5-10 ppm difference between the signals for a particular proton (**Table 4**).

	^{13}C resonance (δ)						
	C^{S1}	C^{S2}	C^{S3}	C^{S4}	C^{S5}	C^{S6}	C^{S7}
$[Co(\boldsymbol{L^7})_2]^{2+}$	80.4	78.9	75.3	74.0	72.9	71.7	74.1
$[Co(\boldsymbol{L^7})_2]^{3+}$	72.5	69.6	71.6	71.2		70.6	73.6
difference	7.9	9.3	3.7	2.8	1.7	1.1	0.5

Table 4. ^{13}C NMR spectroscopic data for the ethyleneoxy chains signals of $[Co(\boldsymbol{L^7})_2][PF_6]_2$ and $[Co(\boldsymbol{L^7})_2][PF_6]_3$ in CD$_3$CN solution at room temperature. The spectra were measured at 125 MHz.
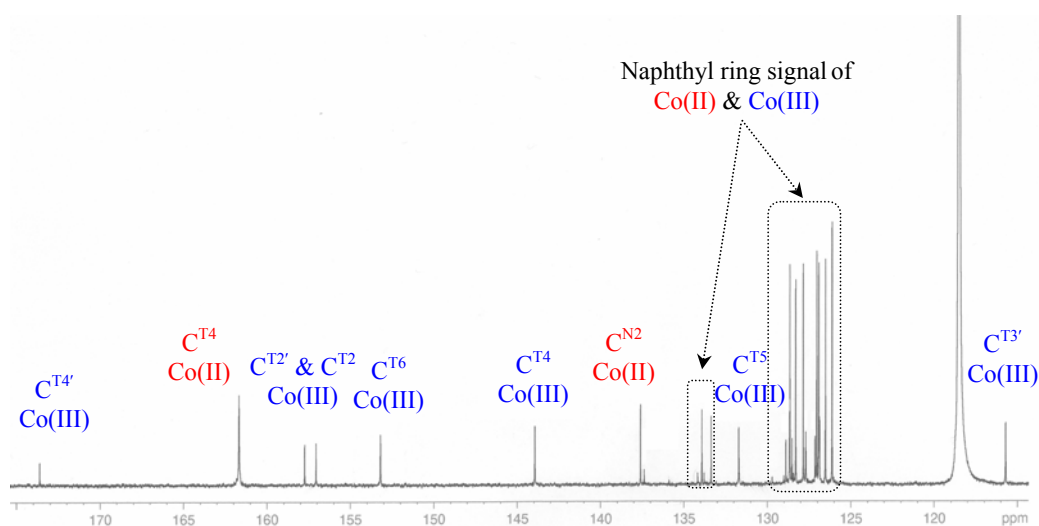
Figure 17. The ^{13}C NMR spectrum (125 MHz, δ 115-175) of the mixture of $[Co(\boldsymbol{L^7})_2][PF_6]_2$ and $[Co(\boldsymbol{L^7})_2][PF_6]_3$ in CD$_3$CN solution at room temperature.

The ^{13}C NMR spectrum in the normal aromatic region is shown in **Figure 17**. All the Co(II) and Co(III) naphthyl signals can be assigned by the use of HMQC and HMBC techniques. However, most of the proton signals of the Co(III) species are not well separated. It is not possible to fully assign the carbon signals of the Co(III) species. There is no significant difference (within 1 ppm) between the Co(II) and Co(III) naphthyl carbon signals. With the help of selective proton decoupling experiments, the terpyridine carbon signals of the Co(II) species were assigned. Irradiating the proton signal at δ 112 (i.e. H^{T6} of Co(II) species), the carbon signal at δ -74.6 is decoupled. Therefore, the carbon signal at δ -74.6 is C^{T6} of the Co(II) species (**Figure**

19). By using the same method, the carbon signals at δ 383.2, 353.6 and 499.4 are assigned to the $C^{T3'}$, C^{T3} and C^{T5} signals of the Co(II) species, respectively. The carbon signal at δ 161.7 is assigned to C^{T4} of Co(II) because there is a cross peak between the H^{T4} signal of Co(II) at δ 6.42 and the signal at δ 161.7 in the HMQC spectrum (**Figure 18**). There are three quaternary carbon signals at δ 304.8, -49.1 and -127.7 (**Figure 19**). By looking at the relative integrals, we found that the integral for the signal at δ 304.8 is roughly half of those for the two signals at δ -49.1 and δ -127.7. Therefore, the signal at δ 304.8 belongs to $C^{T4'}$ but the two signals at δ -49.1 and δ -127.7 can only be assigned to $C^{T2'}$ and C^{T2}, and not unambiguously to one or other of these carbon centres. **Table 5** shows the ^{13}C NMR signals of the terpyridine carbon of Co(II) and Co(III) species. The terpyridine carbon NMR signals of Co(III) species was assigned by using the HMBC and HMQC techniques.
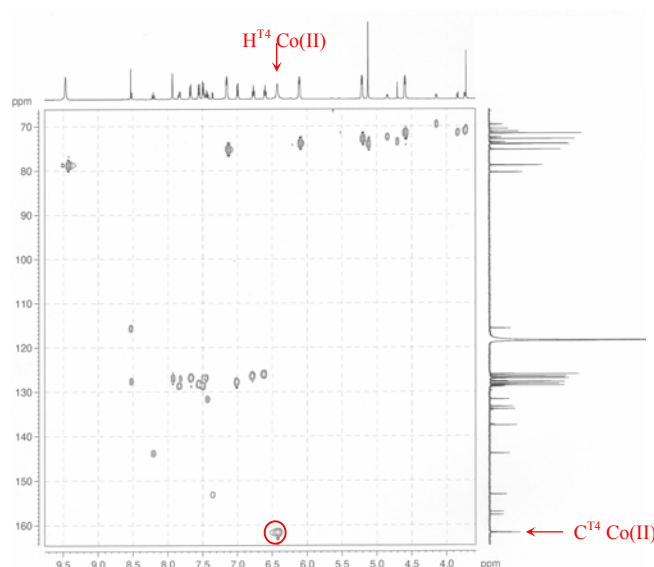
Figure 18. The HMQC spectrum of the mixture of $[Co(\boldsymbol{L^7})_2][PF_6]_2$ and $[Co(\boldsymbol{L^7})_2][PF_6]_3$ in CD$_3$CN solution at room temperature. The spectrum was measured at 125 MHz.

	^{13}C resonance (δ)							
	$C^{T2'}$	C^{T2}	C^{T6}	C^{T4}	$C^{T4'}$	C^{T3}	$C^{T3'}$	C^{T5}
$[Co(\boldsymbol{L^7})_2]^{2+}$	-49.1, -127.7		-74.6	161.7	304.8	353.6	383.2	499.4
$[Co(\boldsymbol{L^7})_2]^{3+}$	157.8	157.1	153.2	144.0	173.7	127.7	115.7	131.7

Table 5. ^{13}C NMR spectroscopic data for the terpyridine signals of $[Co(\boldsymbol{L^7})_2][PF_6]_2$ and $[Co(\boldsymbol{L^7})_2][PF_6]_3$ in CD$_3$CN solution at room temperature. The spectra were measured at 125 MHz.
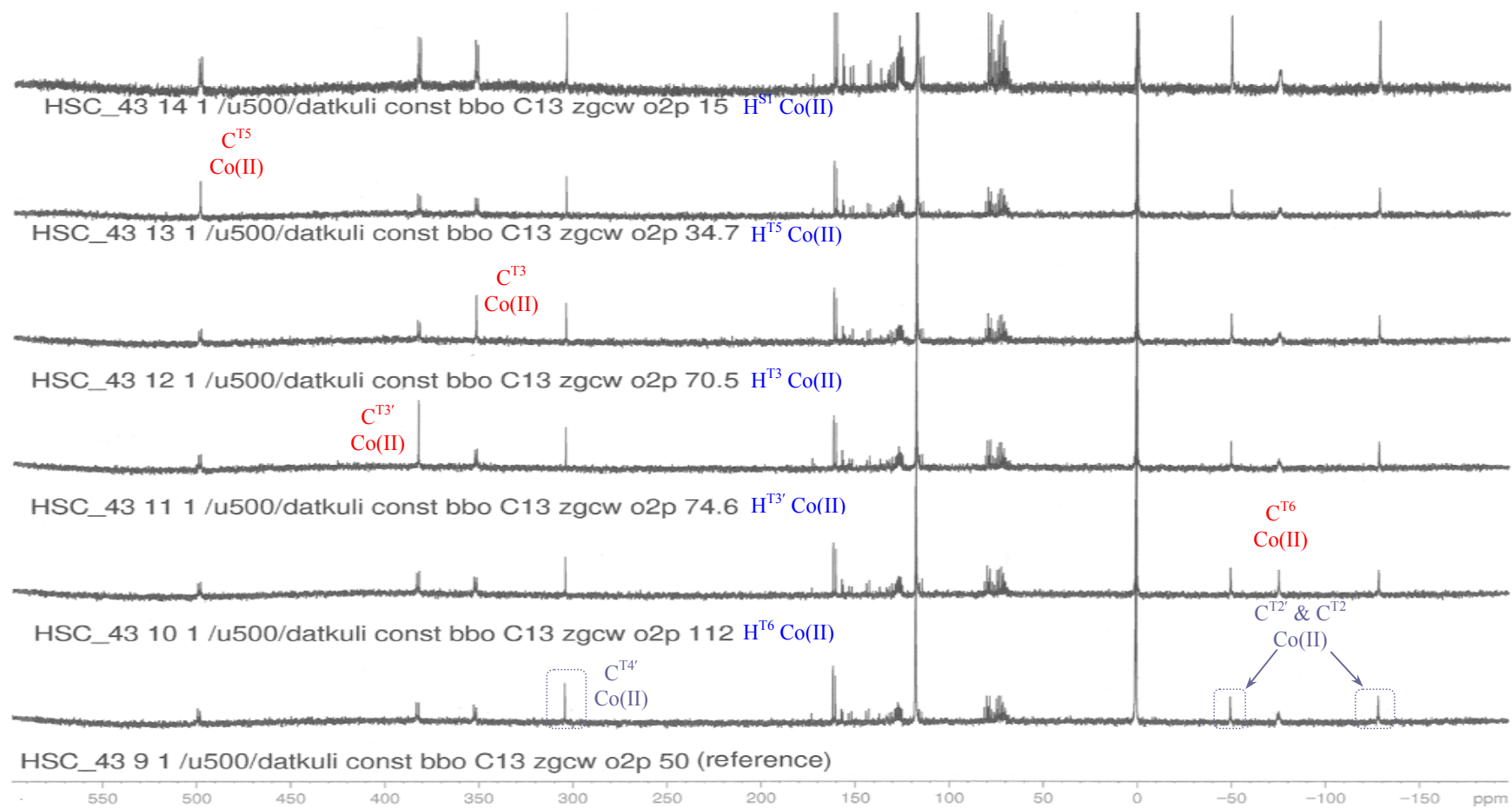
Figure 19. The ^{13}C selective proton decoupling spectra (125 MHz) of the mixture of [Co(L^7)$_2$][PF$_6$]$_2$ and [Co(L^7)$_2$][PF$_6$]$_3$ in CD$_3$CN solution at room temperature. (The carbon signals in the dash-lined box are the quaternary carbon signals)

The ^{13}C NMR spectrum of $[Co(\textbf{\textit{L}}^{9})_2][PF_6]_2$ was measured in CD_3CN solution. There are twenty signals in total, including the two signals of CD_3CN. In the range δ 120-160, there are eleven carbon signals. With the help of HMQC and HMBC experiments, these ^{13}C NMR signals at δ 120-160 were assigned to the carbon signals for naphthyl ring and the carbon signal for C^{T4} (**Figure 20**).
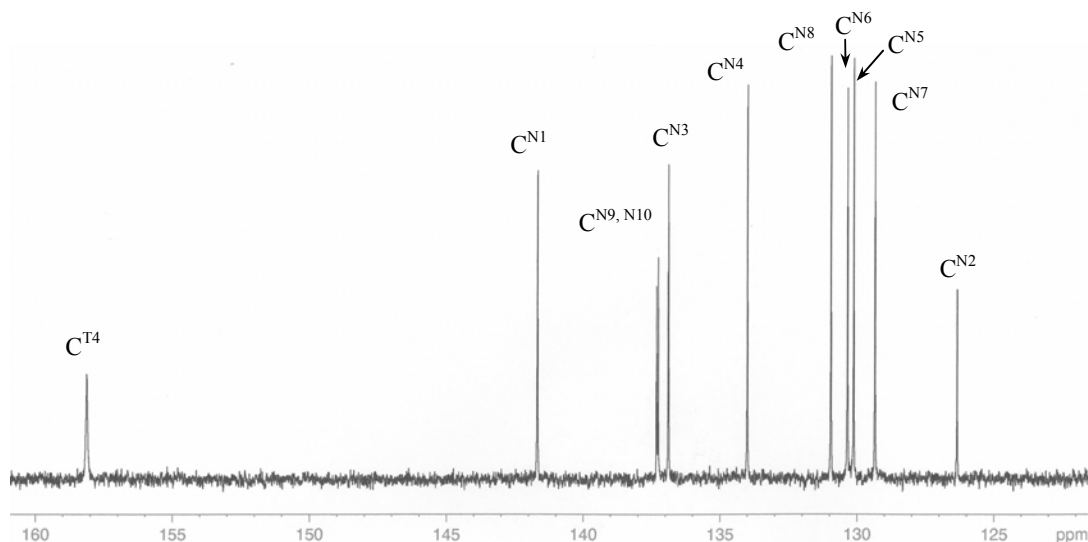
Figure 20. The ^{13}C NMR spectrum (125 MHz, δ 120-160) of $[Co(\textbf{\textit{L}}^{9})_2][PF_6]_2$ in CD_3CN solution at room temperature.

The rest of ^{13}C NMR signals were assigned by using selective proton decoupling experiments. Irradiating the proton at δ 102.8 (i.e. H^{T6} of Co(II) species), the carbon signal at δ -55.5 is decoupled. Therefore, the carbon signal at δ -55.5 is C^{T6} of the Co(II) species (**Figure 21**). By using the same method, the carbon signals at δ 336.5, 339.0 and 464.5 are assigned to $C^{T3'}$, C^{T3} and C^{T5} of the Co(II) species respectively. In the HMQC spectrum (**Figure 22**), there is a cross peak between the H^{T4} signal of Co(II) at δ 8.08 and the δ 158.2 of the ^{13}C NMR signal. Therefore, the signal at δ 158.2 is assigned to C^{T4}. There are three quaternary carbon signals at δ 247.0, -11.7 and -85.8. The relative integral for the signal at δ 247.0 is roughly half of those for the two signals at δ -11.7 and δ -85.5. Therefore, the signal at δ 247.0 is assigned to $C^{T4'}$. An HMBC experiment was done attempting to distinguish $C^{T2'}$ and C^{T2} since we know that H^{T4} is at δ 8.08. However, no cross peak was observed. Therefore, the two signals at δ -49.1 and δ -127.7 could not be unambiguously assigned.
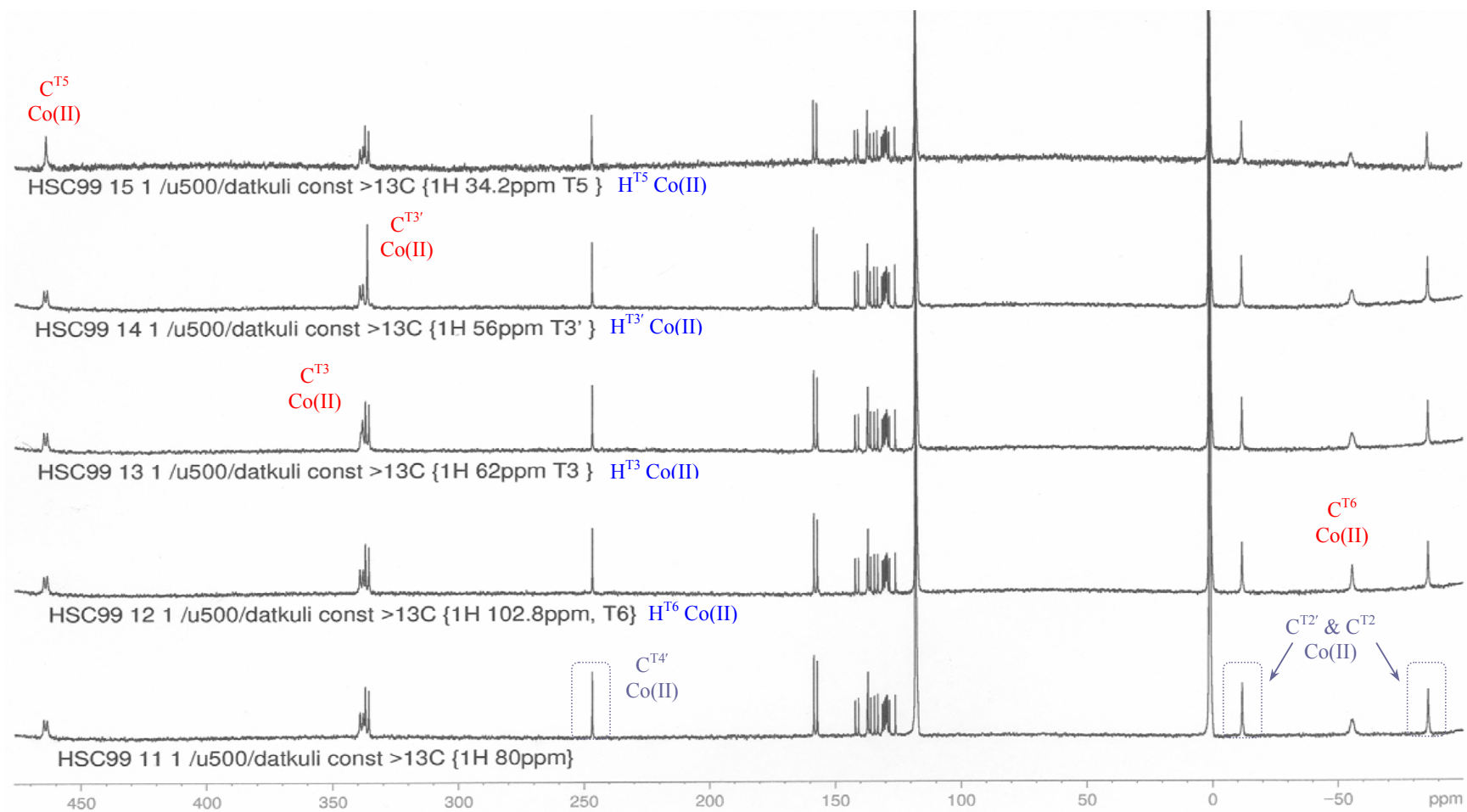
Figure 21. The ^{13}C selective proton decoupling spectra (125 MHz) of $[Co(L^9)_2]^2$ in CD_3CN solution at room temperature. (The carbon signals in the dash-lined box are the quaternary carbon signals)
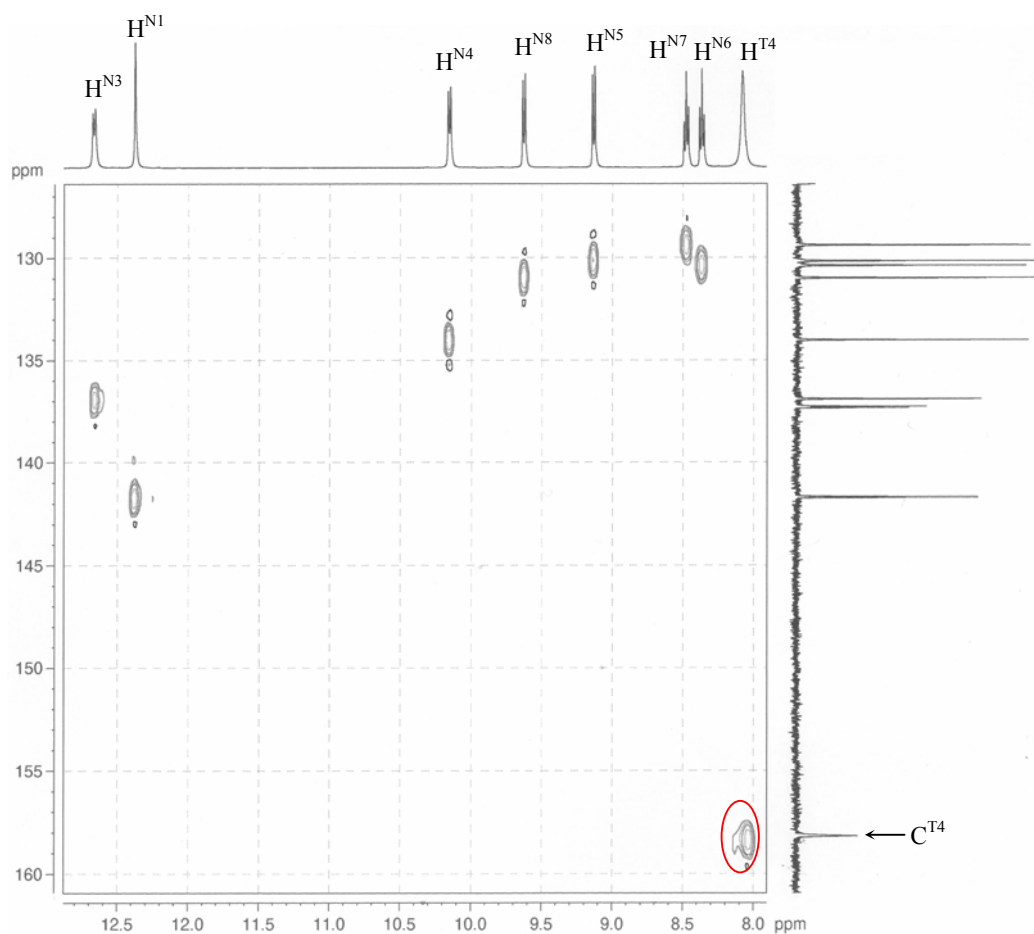
Figure 22. The HMQC spectrum (125 MHz) of $[Co(\mathbf{L^9})_2][PF_6]_2$ in CD$_3$CN solution at
room temperature.

The carbon NMR spectra of $[Co(\mathbf{L^7})_2][PF_6]_2$ and $[Co(\mathbf{L^9})_2][PF_6]_2$ were fully assigned except the signals for $C^{T2'}$ and C^{T2} could not be distinguished. It is worth nothing that there were significant differences in the ^{13}C chemical shifts for the terpyridine unit in $[Co(\mathbf{L^7})_2][PF_6]_2$ and $[Co(\mathbf{L^9})_2][PF_6]_2$ (**Table 6**). This includes the C^{T6} which is the furthest away form the 4′-substitution position of the terpyridine ligand.

	^{13}C resonance (δ)							
	$C^{T2'}$	C^{T2}	C^{T6}	C^{T4}	$C^{T4'}$	C^{T3}	$C^{T3'}$	C^{T5}
$[Co(\mathbf{L^7})_2]^{2+}$	-49.1, -127.7		-74.6	161.7	304.8	353.6	383.2	499.4
$[Co(\mathbf{L^9})_2]^{2+}$	-85.8, -11.7		-55.5	158.2	247.0	339.0	336.5	464.5

Table 6. ^{13}C NMR spectroscopic data for terpyridine signals of $[Co(\mathbf{L^7})_2][PF_6]_2$ and $[Co(\mathbf{L^9})_2][PF_6]_2$ in CD$_3$CN solution at room temperature. The spectra were measured at 125 MHz.

4.4   Mass spectrometric characterisation

Electrospray ionisation mass spectrometry (ES-MS) was used to characterise the complexes. The mass spectrum shows peaks for ions with particular mass to charge ratios (*m/z*). Each signal has a unique combination of the isotopes of the elements in the complexes. And the difference between each of the signals of the isotope pattern is the reciprocal of the charge on the fragment from which the signal originates. Normally, ES-MS is a relatively soft ionisation method. Therefore, $[M-PF_6]^+$ and $[M-2PF_6]^{2+}$ peaks are found as the major peaks for mononuclear Co(II) complexes. However, the voltage used to ionise the samples is rather high for these complexes, and some other fragments are observed in the spectra (**Table 7**).

|	*m/z*			
	$[M-PF_6]^+$	$[M-PF_6-PF_5]^+$	$[M-2PF_6]^{2+}$	Others
$[Co(L^1)_2][PF_6]_2$	790.3		322.6	644.2, 300.6, 278.6
$[Co(L^2)_2][PF_6]_2$	878.3		366.6	1062.2, 1046.3, 732.3, 644.2, 556.2, 322.6, 278.6
$[Co(L^3)_2][PF_6]_2$	965.9		410.6	1007.9, 431.6
$[Co(L^4)_2][PF_6]_2$	982.0	856.0		696.4, 555.5, 467.3
$[Co(L^5)_2][PF_6]_2$	1070.3		462.7	740.2, 493.3
$[Co(L^6)_2][PF_6]_2$	1158.3		506.6	784.2, 500.2
$[Co(L^7)_2][PF_6]_2$	1246.2		551.7	828.5, 599.4
$[Co(L^8)_2][PF_6]_2$	1083.2	956.2		876.1, 746.3, 555.5, 540.6, 517.1, 191.4
$[Co(L^9)_2][PF_6]_2$	985.9		421.2	
$[Co(terpy)_2][PF_6]_2$	669.9	544.0	262.9	

Table 7. The ES-MS data of the ten Co(II) complexes.

In contrast to Fe and Ru, Co has only one isotope. Therefore, the isotopic pattern is mainly because of the presence of $^{12}C/^{13}C$. In the ES-MS spectrum of $[Co(L^7)_2][PF_6]_2$ (**Figure 23**), *m/z* 599.4 was the major signal. This corresponds to $[L^7+Co+F]^+$. The other signals at *m/z* 1246.0, 828.4 and 551.2 correspond to $[M-PF_6]^+$, $[M-PF_6-(CH_2CH_2O)_2OCH_2Nap]^+$, $[M-2PF_6]^{2+}$ respectively. Traces of $[Co(L^7)_2][PF_6]_3$ were detected. $[M-PF_6]^+$ and $[M-3PF_6]^{3+}$ peaks are found less than 20% of relative abundance at *m/z* 1391 and 367.
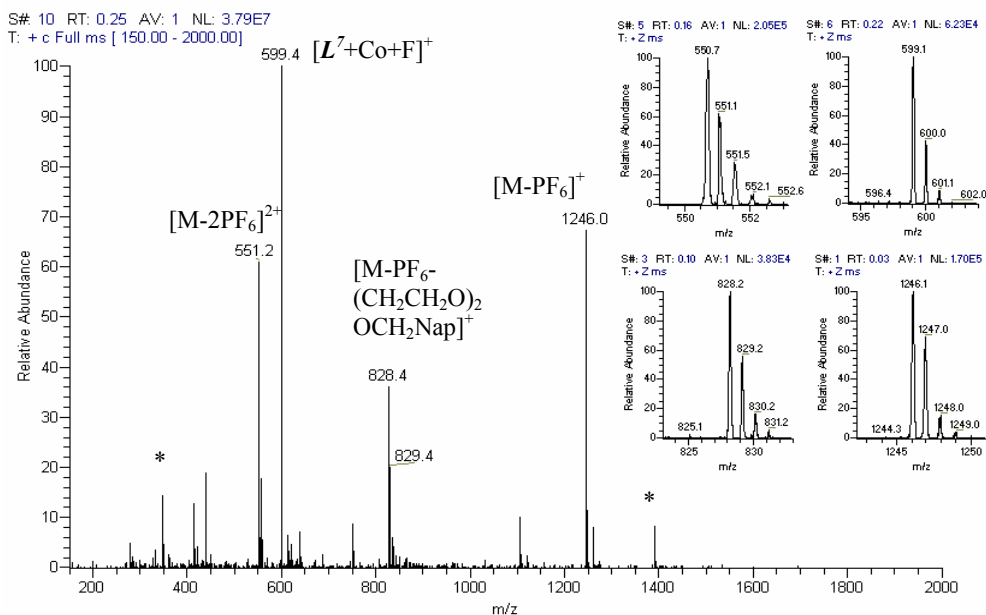
Figure 23. The ES-MS spectrum of [Co(L^7)$_2$][PF$_6$]$_2$ (the peaks marked * are belong to [Co(L^7)$_2$][PF$_6$]$_3$ complex).

In the ES-MS spectrum of [Co(L^9)$_2$][PF$_6$]$_2$ (**Figure 24**), a peak assigned to [M-2PF$_6$]$^{2+}$ at *m/z* 421.2 was the major signal. The other minor signal at *m/z* 985.9 corresponds to [M-PF$_6$]$^+$.
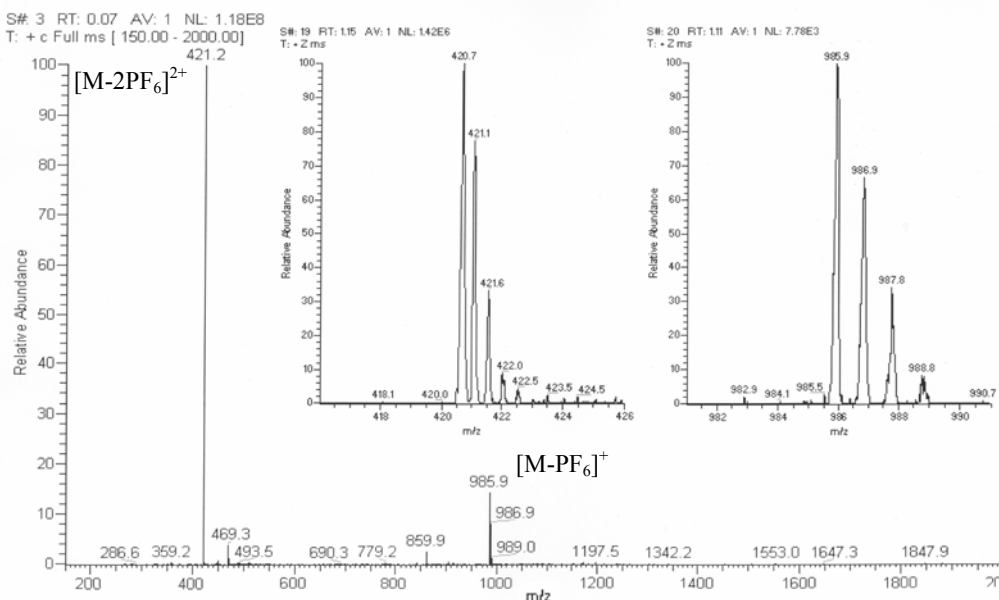
Figure 24. The ES-MS spectrum of [Co(L^9)$_2$][PF$_6$]$_2$.

4.5   Absorption spectroscopic characterisation

The electronic spectra of the homoleptic Co(II) complexes were recorded in HPLC grade acetonitrile solution. The absorption spectra of these complexes are similar to the sum of the spectra of $[Co(terpy)_2]^{2+}$ and the substituents. The absorption data for these ten homoleptic complexes are summarised in **Table 8**.

	λ_{max}, nm (ε / 10^3, $M^{-1}cm^{-1}$)		
	LC		
$[Co(L^1)_2][PF_6]_2$	242 (52.0), 270 (44.4), 303 (22.9)		
$[Co(L^2)_2][PF_6]_2$	244 (55.3), 270 (46.9), 302 (25.0)		
$[Co(L^3)_2][PF_6]_2$	242 (58.6), 270 (49.8), 301 (26.5)		
$[Co(L^4)_2][PF_6]_2$	223 (221), 249 (71.5), 273 (66.2), 311 (23.7)		
$[Co(L^5)_2][PF_6]_2$	222 (251), 244 (64.1), 270 (61.5), 303 (27.9)		
$[Co(L^6)_2][PF_6]_2$	222 (233), 241 (60.4), 270 (57.3), 303 (27.2)		
$[Co(L^7)_2][PF_6]_2$	224 (260), 241 (63.1), 272 (63.7), 305 (29.4)		
$[Co(L^8)_2][PF_6]_2$	254 (298), 281 (45.1), 315 (21.5), 348 (16.0), 366 (21.1), 386 (19.3)		
$[Co(L^9)_2][PF_6]_2$	221 (146), 283 (74.0), 310 (49.7)		
$[Co(terpy)_2][PF_6]_2$	280 (44.1), 314 (36.7)		

Table 8. Electronic spectroscopic data for the complexes in acetonitrile solution.

The very intense bands in the UV region are assigned to the ligand-centred $\pi^*\leftarrow\pi$ transitions. But the low energy metal-to-ligand charge transfer (MLCT) transition band is not intense enough to detect in dilute solution ($\sim10^{-6}$ M) for the UV/VIS measurement. The MLCT transitions of the Co(II) terpyridine type normally occur at 450-510 nm in a more concentrated sample ($\sim10^{-4}$ M).[27,28]

4.6 Crystal structures of [Co(L^4)$_2$][PF$_6$]$_2$ and [Co(L^8)$_2$][PF$_6$]$_2$·1¾CH$_3$CN

(a) Crystal structure of [Co(L^4)$_2$][PF$_6$]$_2$
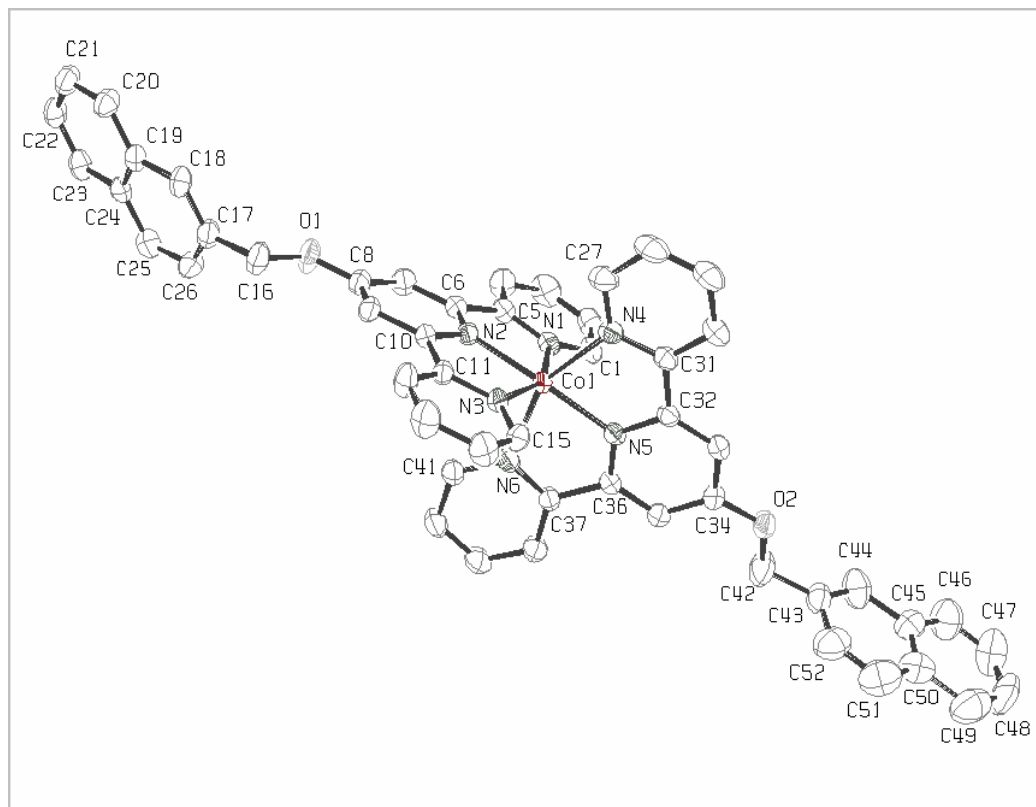
Figure 25. An ORTEP representation (50% probability ellipsoids) of the [Co(L^4)$_2$]$^{2+}$ cation in [Co(L^4)$_2$][PF$_6$]$_2$. Hydrogen atoms are omitted for clarity. Carbon atoms are numbered sequentially around each ring.

Crystals of [Co(L^4)$_2$][PF$_6$]$_2$ were obtained by slow diffusion of diethyl ether vapour into an acetonitrile solution of [Co(L^4)$_2$][PF$_6$]$_2$. The crystals were of X-ray quality and the molecular structure of [Co(L^4)$_2$][PF$_6$]$_2$ was determined. The structure of the [Co(L^4)$_2$]$^{2+}$ cation is presented in **Figure 25**. Crystallographic data are given in **Appendix III** and selected bond lengths and angles are given in **Table 9**. As expected, the tridentate ligands exhibit the *cisoid* conformation about the interannular C-C bonds, which is necessary for the adoption of the chelating mode. The coordination sphere of the Co(II) centre is similar to those in other complexes containing tridentate 2,2′:6′,2″-terpyridine ligands. The three pyridine rings in each

ligand are close to being coplanar and the torsion angles N1-C5-C6-N2, N2-C10-C11-N3, N4-C31-C32-N5 and N5-C36-C37-N6 are 6.76˚, -4.30˚, -5.82˚ and 3.03˚. The angle between the planes containing atoms N1, N2, N3 and N4, N5, N6 is 86.4˚.[29-33]

Co1-N1	2.161(3)	N1-C1	1.335(4)	C5-C6	1.481(5)
Co1-N2	2.005(3)	N1-C5	1.341(4)	C10-C11	1.477(4)
Co1-N3	2.126(3)	N2-C6	1.339(4)	C31-C32	1.477(4)
Co1-N4	2.126(3)	N2-C10	1.338(4)	C36-C37	1.481(4)
Co1-N5	2.010(3)	N3-C11	1.345(4)		
Co1-N6	2.110(3)	N3-C15	1.338(4)	C8-O1	1.345(4)
		N4-C27	1.335(4)	C16-O1	1.447(4)
		N4-C31	1.344(4)	C34-O2	1.342(4)
		N5-C32	1.345(4)	C42-O2	1.449(5)
		N5-C36	1.329(4)		
		N6-C37	1.350(4)		
		N6-C41	1.324(4)		
N1-Co1-N2	77.2(1)	N4-Co1-N5	76.5(1)	C7-C8-O1	115.0(3)
N1-Co1-N3	154.2(1)	N4-Co1-N6	152.3(1)	C9-C8-O1	124.6(3)
N2-Co1-N3	77.0(1)	N5-Co1-N6	76.8(1)	C8-O1-C16	118.3(3)
N1-Co1-N4	99.3(1)	N3-Co1-N6	91.4(1)	C33-C34-O2	116.2(3)
N2-Co1-N4	110.2(1)	N1-Co1-N5	95.3(1)	C35-C34-O2	124.6(3)
N3-Co1-N4	90.7(1)	N1-Co1-N6	90.6(1)	C34-O2-C42	118.3(3)
N3-Co1-N5	110.2(1)	N2-Co1-N6	97.2(1)		
		N2-Co1-N5	170.5(1)		

Table 9. Selected bond lengths (Å) and angles (˚) of the $[Co(L^4)_2]^{2+}$ cation in $[Co(L^4)_2][PF_6]_2$.

All the bond lengths of the interannular C-C bonds and N-C bonds are comparable to the corresponding bond lengths of other Co(II) complexes containing tridentate 2,2′:6′,2″-terpyridine ligands.[29-33] The Co-N contacts to the central ring of the 4′-(naphthalen-2-ylmethoxy)-2,2′:6′,2″-terpyridine ligand (Co1-N2 and Co1-N5) are shorter than those to the terminal rings (Co1-N1, Co1-N3, Co1-N4 and Co1-N6), which are within the reported range of Co(II) complexes with 2,2′:6′,2″-terpyridine ligands.[29-33] The methyleneoxy chains are nearly coplanar with the central pyridine rings. The torsion angles C9-C8-O1-C16 and C35-C34-O2-C42 are -3.96˚ and 12.38˚. The bond lengths O1-C8 and O2-C34 are 1.345(4) Å and 1.342(4) Å respectively which are similar to the corresponding distances in $[Ru(\textit{poterpy})_2][PF_6]_2 \cdot (CH_3)_2CO$.[34] The bond angles C7-C8-O1, C9-C8-O1, C33-C34-O2 and C35-C34-O2 are within the range reported in the $[Ru(\textit{poterpy})_2]^{2+}$ cation in the solid-state structure of

[Ru(***poterpy***)$_2$][PF$_6$]$_2$·(CH$_3$)$_2$CO. Also the bond angles C8-O1-C16 and C34-O2-C42 are both 118.3(3)° which, within experimental error, are comparable with the corresponding angles in ([Ru(***poterpy***)$_2$]$^{2+}$ cation (117.5(3)° and 118.1(3)°).[30]

The dihedral angles of the planes of 2,2′:6′,2″-terpyridine and the naphthyl ring i.e. the planes containing N4, N5, N6 and C43, C47, C50, and N1, N2, N3 and C17, C21, C24 are 85.0° and 63.4° respectively. There are two pairs of intermolecular interactions between the naphthyl rings and pyridine rings between the molecules. The distance between the centroid of the pyridine N4 ring and the C38 atom of the pyridine N6 ring is 3.847 Å. The closest separation (C29 to C38) is 3.796 Å. The other pair is from the pyridine N1 ring to the naphthyl C43 ring. The distance between the centroid of the pyridine N1 ring and the C44 atom of the naphthyl ring is 3.661 Å. The closest distance (C2 to C44) is 3.725 Å. The intermolecular interactions can be seen in the packing diagram presented in **Figure 26**.
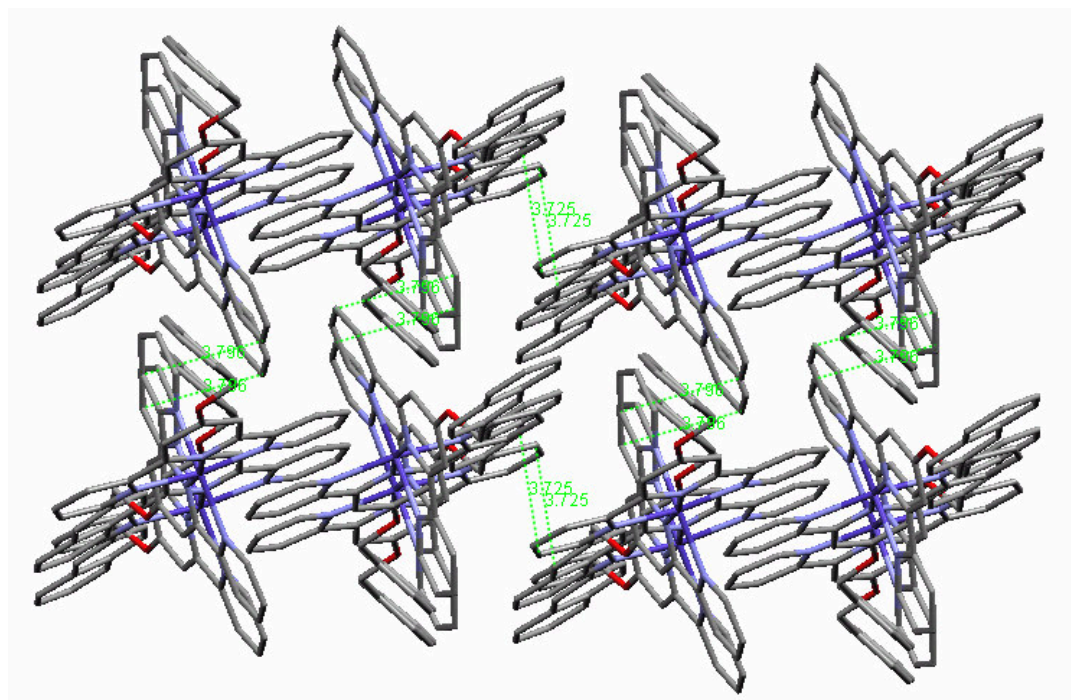
Figure 26. Packing of the [Co(***L***^{4})$_2$]$^{2+}$ cations that shows the face-to-face pyridine-pyridrine and pyridine-naphthyl interactions between the naphthyl rings and the pyridine rings. Hydrogen atoms are omitted for clarity.

(b) Crystal structure of [Co(L^8)$_2$][PF$_6$]$_2$·1¾CH$_3$CN

Crystals of [Co(L^8)$_2$][PF$_6$]$_2$·1¾CH$_3$CN were obtained by slow diffusion of diethyl ether vapour into an acetonitrile solution of [Co(L^8)$_2$][PF$_6$]$_2$. The brown crystals were of X-ray quality and the molecular structure of [Co(L^8)$_2$][PF$_6$]$_2$ was determined. The structure of the [Co(L^8)$_2$]$^{2+}$ cation is presented in **Figure 27**. Crystallographic data are given in **Appendix III**. The expected six-coordinate metal environment is shown. As described before, the tridentate ligands exhibit the *cisoid* conformation about the interannular C-C bonds in order to chelate to the metal. The coordination sphere of the Co(II) centre is similar to those in other complexes containing tridentate 2,2′:6′,2″-terpyridine ligands. The three pyridine rings in each ligand are close to being coplanar and the torsion angles N1-C5-C6-N2, N2-C10-C11-N3, N4-C35-C36-N5 and N5-C40-C41-N6 are 2.40˚, 1.17˚, -7.00˚ and 5.78˚. The angle between the planes containing atoms N1, N2, N3 and N4, N5, N6 is 87.8˚.[29-33]
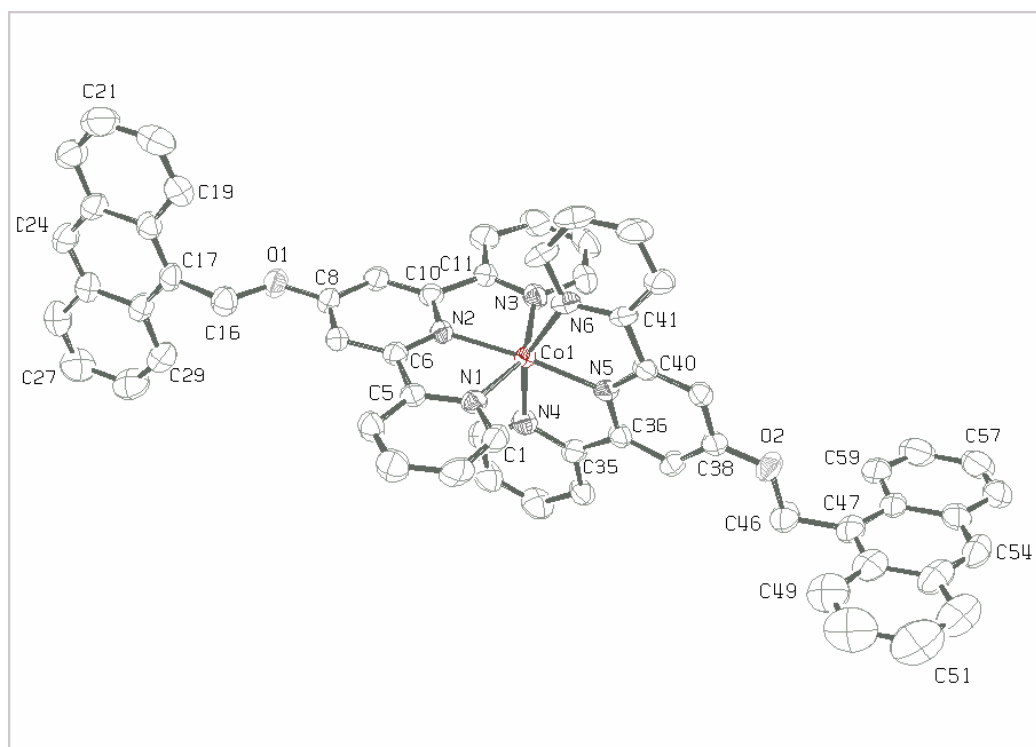
Figure 27. An ORTEP representation (50% probability ellipsoids) of the [Co(L^8)$_2$]$^{2+}$ cation in [Co(L^8)$_2$][PF$_6$]$_2$·1¾CH$_3$CN. Hydrogen atoms are omitted for clarity. Carbon atoms are numbered sequentially around each ring.

Selected bond lengths and angles of the $[Co(L^8)_2]^{2+}$ cation are given in **Table 10**. All the bond lengths of the interannular C-C bonds and N-C bonds which, within experimental error, are comparable to the corresponding bond lengths of other Co(II) complexes containing tridentate 2,2′:6′,2″-terpyridine ligands.[29-33] The Co-N distances show the typical trend for 2,2′:6′,2″-terpyridine containing complexes with bonds to the central terpyridine ring (1.995(4)-1.998(3) Å) being significantly shorter than those to the terminal rings (2.102(4)-2.132(4) Å). All bond lengths and angles within the [Co(***terpy***)$_2$] moiety are normal.[29-33]

Co1-N1	2.132(4)	N1-C1	1.325(6)	C5-C6	1.462(6)
Co1-N2	1.998(3)	N1-C5	1.355(5)	C10-C11	1.477(6)
Co1-N3	2.122(4)	N2-C6	1.334(6)	C35-C36	1.477(7)
Co1-N4	2.121(4)	N2-C10	1.352(6)	C40-C41	1.480(6)
Co1-N5	1.995(4)	N3-C11	1.341(6)		
Co1-N6	2.102(4)	N3-C15	1.335(6)	C8-O1	1.348(5)
		N4-C31	1.341(6)	C16-O1	1.424(6)
		N4-C35	1.351(6)	C38-O2	1.340(6)
		N5-C36	1.330(5)	C46-O2	1.446(6)
		N5-C40	1.344(6)		
		N6-C41	1.352(6)		
		N6-C45	1.337(6)		
N1-Co1-N2	76.9(1)	N4-Co1-N5	77.1(1)	C7-C8-O1	124.6(4)
N1-Co1-N3	153.2 (1)	N4-Co1-N6	154.2 (2)	C9-C8-O1	115.8(4)
N2-Co1-N3	77.1(2)	N5-Co1-N6	77.4(1)	C8-O1-C16	116.8(4)
N1-Co1-N4	94.4(2)	N3-Co1-N6	88.6(2)	C37-C38-O2	125.1(4)
N2-Co1-N4	97.6(2)	N1-Co1-N5	101.1(1)	C39-C38-O2	115.9(4)
N3-Co1-N4	94.9 (2)	N1-Co1-N6	93.8(1)	C38-O2-C46	118.5(4)
N3-Co1-N5	105.5(2)	N2-Co1-N6	108.0(2)		
		N2-Co1-N5	174.2(2)		

Table 10. Selected bond lengths (Å) and angles (°) of the $[Co(L^8)_2]^{2+}$ cation in $[Co(L^8)_2][PF_6]_2 \cdot 1\frac{3}{4}CH_3CN$.

The methyleneoxy chains are nearly coplanar with the central pyridine rings. The torsion angles C7-C8-O1-C16 and C37-C38-O2-C46 are 6.33° and -2.68°. The bond lengths O1-C8 and O2-C38 are 1.348(5) Å and 1.340(6) Å respectively which are similar to the corresponding distances in $[Ru(***poterpy***)_2][PF_6]_2 \cdot (CH_3)_2CO$[34]. The bond angles C7-C8-O1, C9-C8-O1, C37-C38-O2 and C39-C38-O2 are within the range reported in the $[Ru(***poterpy***)_2]^{2+}$ cation in the solid-state structure of $[Ru(***poterpy***)_2][PF_6]_2 \cdot (CH_3)_2CO$. Also the bond angles C8-O1-C16 and C38-O2-C46

are 116.8(4) and 118.5(4)° respectively which, within experimental error, are comparable with the corresponding angles in ([Ru(***poterpy***)$_2$]$^{2+}$ cation (117.5(3)° and 118.1(3)°).[34]
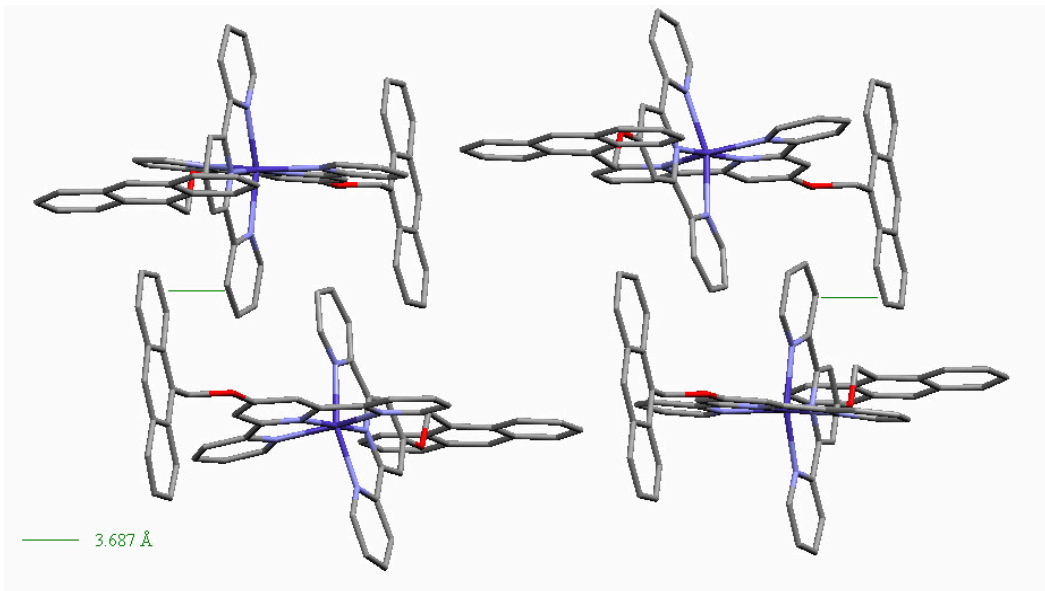
Figure 28. Packing of the [Co(L^8)$_2$]$^{2+}$ cations that shows anthryl-pyridine (green lines) interactions between the anthryl rings and the pyridine rings in the unit cell. Hydrogen atoms are omitted for clarity.

The dihedral angles of the planes of 2,2′:6′,2″-terpyridine and the anthryl ring (i.e. the planes containing N1, N2, N3 and C17, C21, C27, and N4, N5, N6 and C47, C51, C57) are 81.3° and 85.3° respectively. There are three pairs of intermolecular interactions between the anthryl rings and pyridine rings in the molecules. The distance from the centroid of the pyridine N4 ring to the C51 atom of the anthryl ring is 3.687 Å (**Figure 28**). The closest separation (C32 to C51) is 3.873 Å. Interestingly, 2 pairs of anthryl-anthryl π-π stacking interactions are found in the packing of the [Co(L^8)$_2$]$^{2+}$ cations (**Figure 29**). The plane-to-plane distances are around 3.7 Å between the 2 anthryl rings. The shortest distance between the C57 atom of one anthryl ring to C29 atom of the other one is 3.419 Å. The other pair which has a shortest distance between C23 atom of one anthryl ring to C20 atom of the other one is 3.549 Å.

↔ π-π stacking interactions
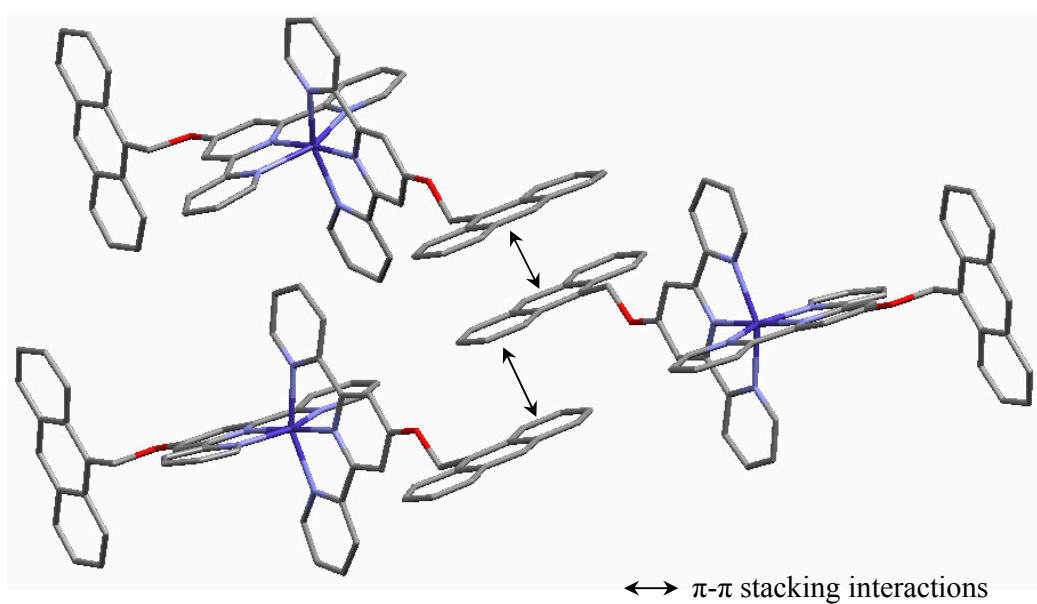
Figure 29. A diagram to show the anthryl-anthryl π-π stacking interactions between three anthryl rings of the $[Co(L^8)_2]^{2+}$ cations. Hydrogen atoms are omitted for clarity.

4.7 ^{1}H NMR spectroscopic exchange experiments of the Co(II) complexes

Equal molar amounts of homoleptic [Co(***A***)$_2$][PF$_6$]$_2$ and [Co(***B***)$_2$][PF$_6$]$_2$ were mixed in CD$_3$CN and the heteroleptic complex, [Co(***A***)(***B***)]$^{2+}$ resulted.[6,7,35] The exchange reactions were monitored by ^{1}H NMR spectroscopy. The proton resonances of Co(II) complexes (which contain paramagnetic d^7 ions) shift to low field and are well separated. This allows the intensity of each signal to be followed easily in the exchange process by using ^{1}H NMR spectroscopy (see **Section 4.2** for details). Several combinations of two homoleptic Co(II) complexes were chosen to study the exchange reactions. The results are summarised in **Table 11**.

Combination	[Co(***A***)$_2$][PF$_6$]$_2$	[Co(***B***)$_2$][PF$_6$]$_2$	Time for the equilibrium reached
(a)	[Co(***L^1***)$_2$][PF$_6$]$_2$	[Co(***L^2***)$_2$][PF$_6$]$_2$	Immediately after mixing
(b)	[Co(***L^4***)$_2$][PF$_6$]$_2$	[Co(***L^9***)$_2$][PF$_6$]$_2$	Immediately after mixing
(c)	[Co(***L^8***)$_2$][PF$_6$]$_2$	[Co(***L^9***)$_2$][PF$_6$]$_2$	Immediately after mixing
(d)	[Co(***L^4***)$_2$][PF$_6$]$_2$	[Co(***L^8***)$_2$][PF$_6$]$_2$	5 hr after mixing
(e)	[Co(***terpy***)$_2$][PF$_6$]$_2$	[Co(***L^8***)$_2$][PF$_6$]$_2$	45 mins after mixing
(f)	[Co(***Fc-terpy***)$_2$][PF$_6$]$_2$	[Co(***L^8***)$_2$][PF$_6$]$_2$	Immediately after mixing

Table 11.   The combination of homoleptic Co(II) complexes with different 4′-substituted-2,2′:6′,2″-terpyridine used for the studies of the exchange reactions.

In the equilibrium mixture of [Co(***L^1***)$_2$]$^{2+}$, [Co(***L^1***)(***L^2***)]$^{2+}$ and [Co(***L^2***)$_2$]$^{2+}$, there are four resonances: two belong to the homoleptic complexes and the remaining two belong to the heteroleptic complex. From the ^{1}H NMR spectrum (**Figure 30**), the number of resonances doubled and this indicated the formation of [Co(***L^1***)(***L^2***)]$^{2+}$ cation. The exchange reaction mixture equilibrates immediately after mixing. The rate of the exchange reaction between the two complexes is faster than the 5-substituted 2,2′:6′,2″-terpyridine previously studied by Constable *et al.*[7]. Since the resonances at δ 74 and δ 34 revealed the distribution of [Co(***L^1***)$_2$]$^{2+}$, [Co(***L^1***)(***L^2***)]$^{2+}$ and [Co(***L^2***)$_2$]$^{2+}$ was 1:2:1 ratio, it was concluded that the product distribution is statistical.
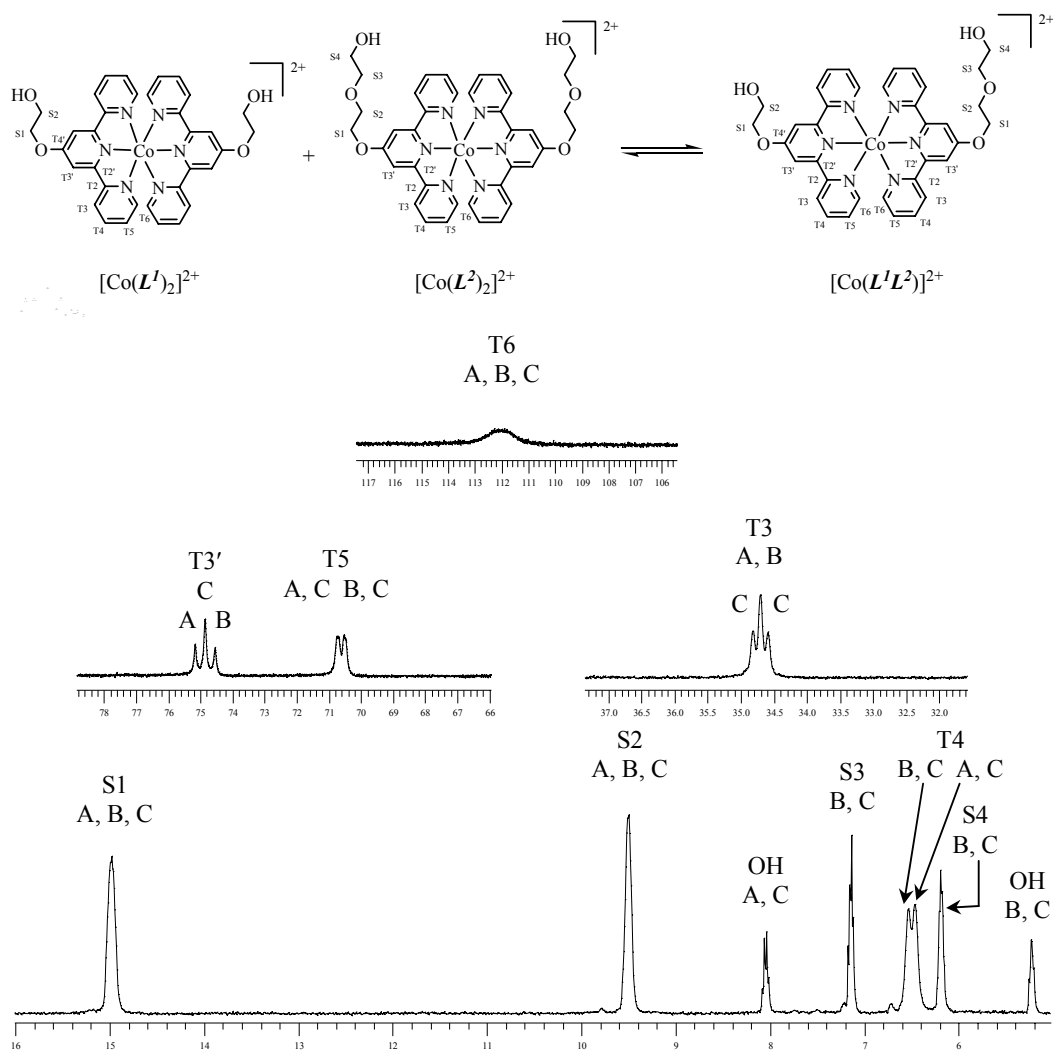
Figure 30. ^{1}H NMR spectroscopic data (250 MHz) for the mixture of $[Co(\boldsymbol{L^1})_2][PF_6]_2$ and $[Co(\boldsymbol{L^2})_2][PF_6]_2$ in CD$_3$CN solution at room temperature. (A = $[Co(\boldsymbol{L^1})_2]^{2+}$, B = $[Co(\boldsymbol{L^2})_2]^{2+}$, C = $[Co(\boldsymbol{L^1L^2})]^{2+}$)

For the exchange experiment of $[Co(\boldsymbol{L^4})_2][PF_6]_2$ and $[Co(\boldsymbol{L^8})_2][PF_6]_2$, the exchange reaction took around 5 hours to reach equilibrium after mixing the equal molar Co(II) complexes together (**Figure 31**). As mentioned before, four resonances are observed in a 1:1:1:1 ratio when the mixture reaches equilibrium. The spectra (δ 30-78) measured at different time intervals of the exchange experiment are shown in **Figure 32**.
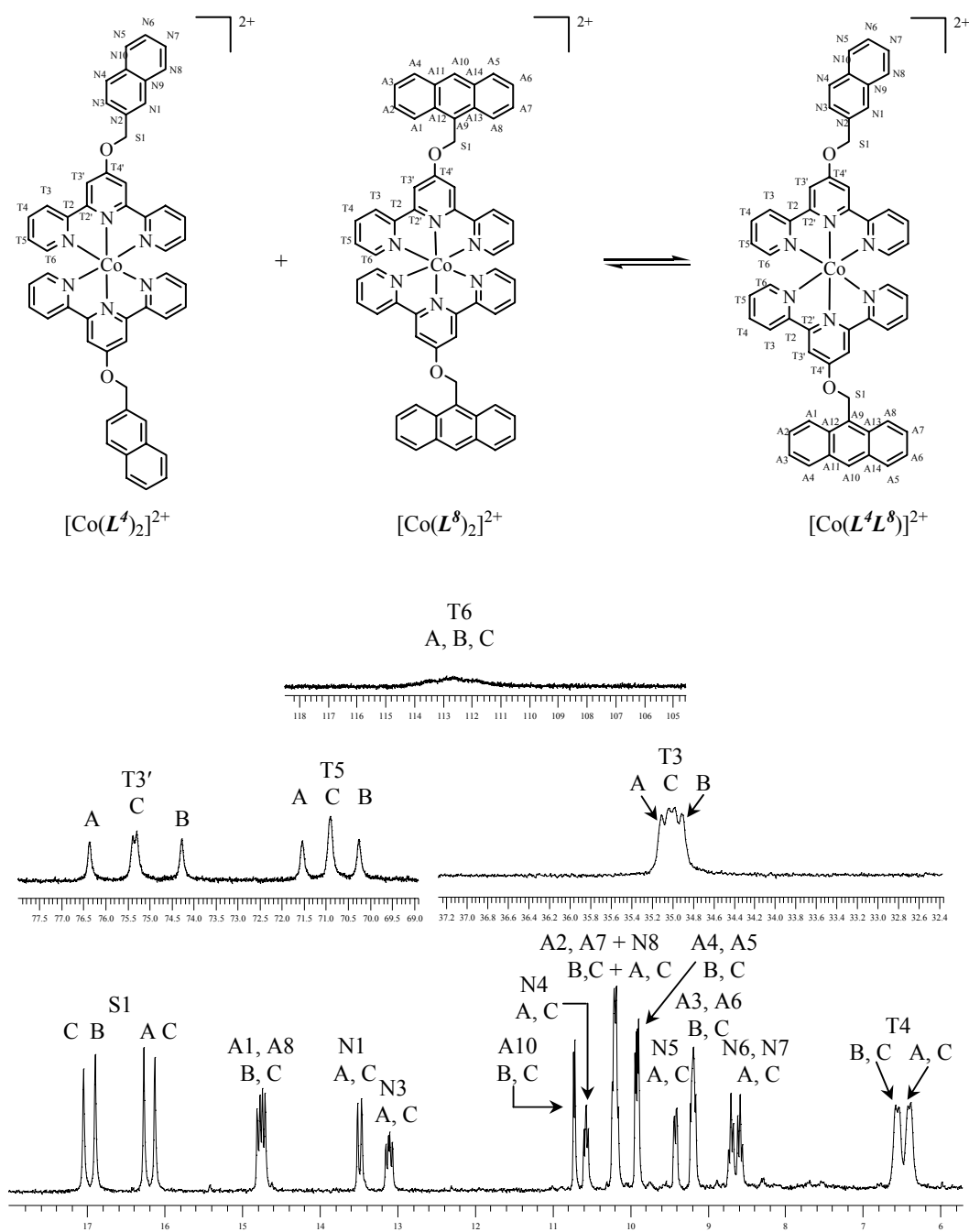
Figure 31. ^{1}H NMR spectroscopic data (250 MHz) for the mixture of $[Co(L^4)_2][PF_6]_2$ and $[Co(L^8)_2][PF_6]_2$ in CD_3CN solution at room temperature. (A = $[Co(L^4)_2]^{2+}$, B = $[Co(L^8)_2]^{2+}$, C = $[Co(L^4L^8)]^{2+}$)
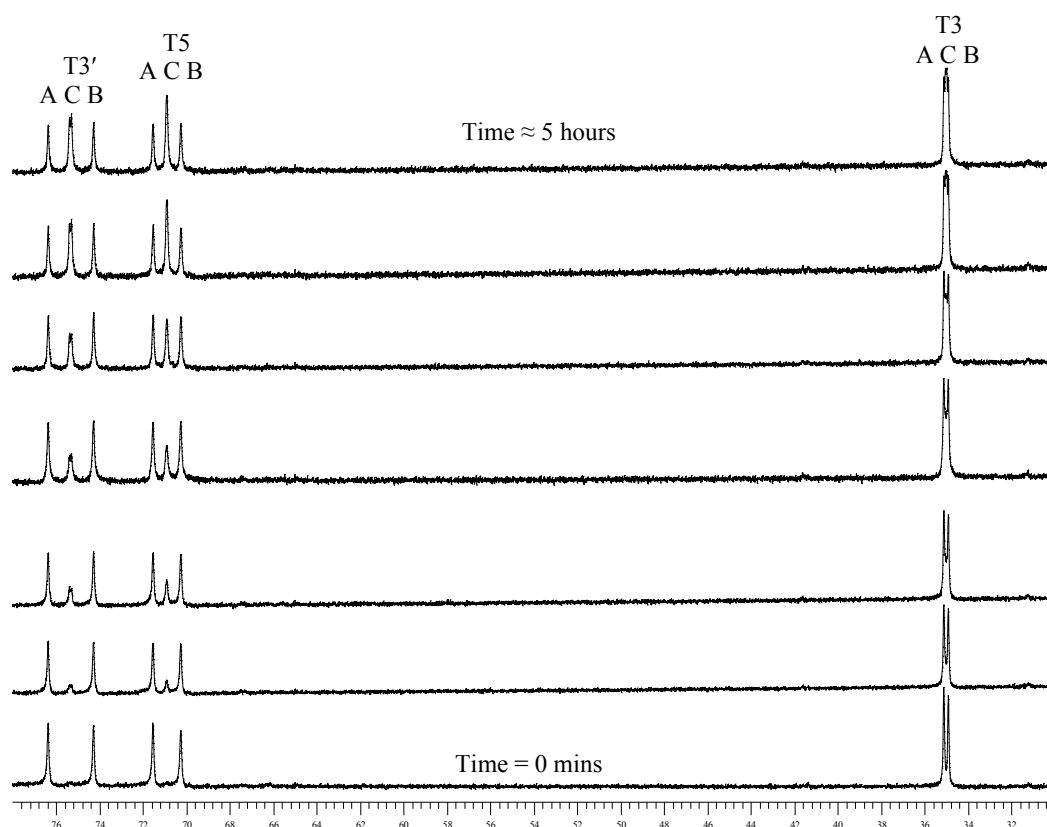
Figure 32. ^{1}H NMR spectra (δ 30-78, 250 MHz) for the mixture of $[Co(\boldsymbol{L^4})_2][PF_6]_2$
and $[Co(\boldsymbol{L^8})_2][PF_6]_2$ in CD$_3$CN solution at room temperature measured at
different time intervals. (A = $[Co(\boldsymbol{L^4})_2]^{2+}$, B = $[Co(\boldsymbol{L^8})_2]^{2+}$, C = $[Co(\boldsymbol{L^4L^8})]^{2+}$)

The equilibrium between two Co(II) complexes was attained very rapidly in most
cases. It is not possible to predict which combination will take the longest time to
reach equilibrium. The Constable group has investigated the electronic effects
associated with the 4′-substituted-2,2′:6′,2″-terpyridine; however, changes in the
nature of the 4′-substituent did not influence the position of equilibrium.[7]

Some preliminary ^{1}H NMR experiments were done, for example adding substrates
(C$_6$F$_6$, C$_{60}$, cyclodextrin) to $[Co(\boldsymbol{L})_2][PF_6]_2$ ($\boldsymbol{L} = \boldsymbol{L^5}$-$\boldsymbol{L^7}$) for exploring the possibility of
reequilibration of $[Co(\boldsymbol{A})_2][PF_6]_2$ and $[Co(\boldsymbol{B})_2][PF_6]_2$. However, there is solubility
problem between the substrate and the Co(II) complexes in mixture of solvent
(CD$_3$CN, CD$_3$OD, D$_2$O). There is no significant shifting for the signals of the Co(II)
complexes by adding the substrate to the NMR tube.

4.8 Conclusion

The mononuclear Co(II) complexes of different 4′-substituted-2,2′:6′,2″-terpyridine ligands L^1-L^9, which contain polyethyleneoxy chains and differ from one another in the length of the chains, in the terminal domains or in the linkages, have been synthesised. The complexes have been characterised with ^{1}H NMR spectroscopy, mass spectrometry (ES), UV/VIS spectroscopy and elemental analysis. A newly established method for the assignment of Co(II) complexes using the EXSY difference experiment were presented. This is based on the self exchange system between Co(II) and Co(III) species, which is slow enough on the NMR time scale. The solid-state structures of $[Co(L^4)_2][PF_6]_2$ and $[Co(L^8)_2][PF_6]_2$ were determined by X-ray crystallography. Finally, some preliminary studies of the combinatorial library were discussed.

4.9   Experimental

❖ $[Co(\textbf{\textit{L}}^1)_2][PF_6]_2$

❖ $[Co(\textbf{\textit{L}}^2)_2][PF_6]_2$

❖ $[Co(\textbf{\textit{L}}^3)_2][PF_6]_2$

❖ $[Co(\textbf{\textit{L}}^4)_2][PF_6]_2$

❖ $[Co(\textbf{\textit{L}}^5)_2][PF_6]_2$

❖ $[Co(\textbf{\textit{L}}^6)_2][PF_6]_2$

❖ $[Co(\textbf{\textit{L}}^7)_2][PF_6]_2$

❖ $[Co(\textbf{\textit{L}}^8)_2][PF_6]_2$

❖ $[Co(\textbf{\textit{L}}^9)_2][PF_6]_2$

❖ $[Co(\textbf{\textit{terpy}})_2][PF_6]_2$

where $\textbf{\textit{L}}^1$ 4′-(2-Hydroxyethoxy)-2,2′:6′,2″-terpyridine

$\textbf{\textit{L}}^2$ 4′-[2-(2-Hydroxyethoxy)ethoxy]-2,2′:6′,2″-terpyridine

$\textbf{\textit{L}}^3$ 4′-{2-[2-(2-Hydroxyethoxy)ethoxy]ethoxy}-2,2′:6′,2″-terpyridine

$\textbf{\textit{L}}^4$ 4′-(Naphthalen-2-ylmethoxy)-2,2′:6′,2″-terpyridine

$\textbf{\textit{L}}^5$ 4′-[2-(Naphthalen-2-ylmethoxy)ethoxy]-2,2′:6′,2″-terpyridine

$\textbf{\textit{L}}^6$ 4′-{2-[2-(Naphthalen-2-ylmethoxy)ethoxy]ethoxy}-2,2′:6′,2″-terpyridine

$\textbf{\textit{L}}^7$ 4′-(2-{2-[2-(Naphthalen-2-ylmethoxy)ethoxy]ethoxy}ethoxy)-2,2′:6′,2″-terpyridine

$\textbf{\textit{L}}^8$ 4′-(Anthracen-9-ylmethoxy)-2,2′:6′,2″-terpyridine

$\textbf{\textit{L}}^9$ 4′-(Naphthalen-2-ylsulfanyl)-2,2′:6′,2″-terpyridine

$\textbf{\textit{terpy}}$ 2,2′:6′,2″-terpyridine

$\textbf{\textit{L}}^1$, $\textbf{\textit{L}}^2$, $\textbf{\textit{L}}^3$, $\textbf{\textit{L}}^4$, $\textbf{\textit{L}}^5$, $\textbf{\textit{L}}^6$, $\textbf{\textit{L}}^7$, $\textbf{\textit{L}}^8$ and $\textbf{\textit{L}}^9$ were prepared as in Chapter 2. 4′-Ferrocenyl-2,2′:6′,2″-terpyridine (***Fc-terpy***) were prepared as in the literature.[36]

General method for synthesising cobalt(II) complexes

A solution of $Co(OAc)_2 \cdot 4H_2O$ (1 equivalent) in 10 mL CH_3OH was treated with the appropriate ligand $\textbf{\textit{L}}$ (2 equivalents) and the mixture stirred for 0.5 hour at room temperature during which period a brown colour developed. Excess methanolic NH_4PF_6 was added to the solution. The resultant brown precipitate was collected by filtration, washed with diethyl ether and dried.[4-7,16-20]
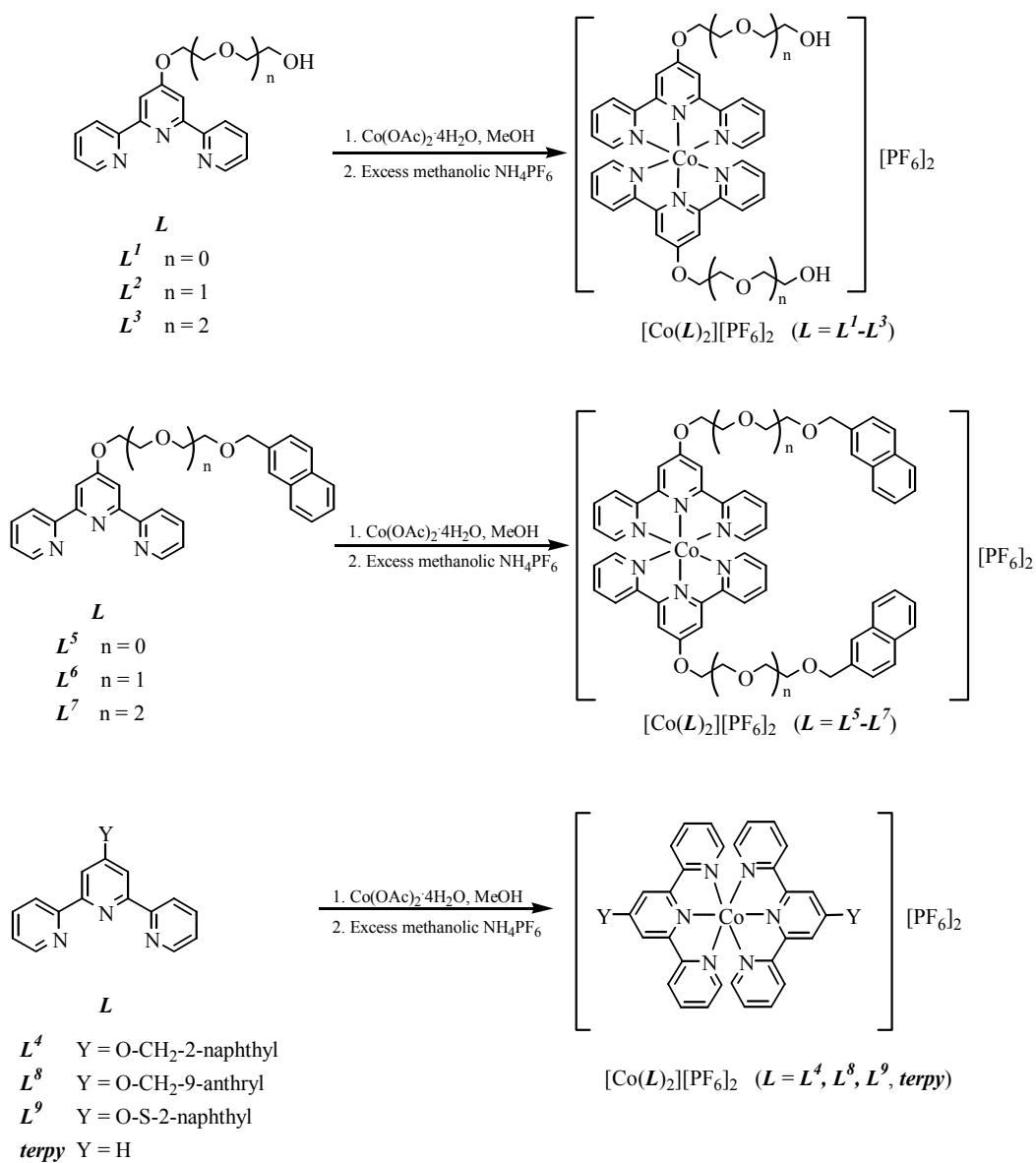
❖ [Co(**L**^{1})$_2$][PF$_6$]$_2$

Molecular formula: C$_{34}$H$_{30}$N$_6$O$_4$CoP$_2$F$_{12}$

Molecular weight: 935.50
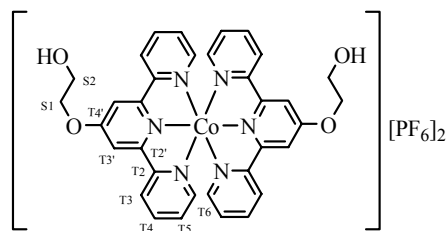
L^1 (50 mg, 0.17 mmol) and Co(OAc)$_2$·4H$_2$O (21 mg, 0.085 mmol) were used. A brown powder (38.6 mg, 48.6%) was obtained.

^{1}H NMR (250 MHz, CD$_3$CN): δ_H 6.42 (s , 4H, H^{T4}), 8.00 (t, *J* 5.9 Hz, 2H, OH), 9.49 (s, 4H, H^{S2}), 14.98 (s, 4H, H^{S1}), 34.7 (s, 4H, H^{T5}), 70.7 (s, 4H, H^{T3}), 75.2 (s, 4H, H$^{T3'}$), 112.1 (br, 4H, H^{T6}).

MS (ES): *m/z* = 790.3 [M-PF$_6$]$^+$, 644.2 [M-2PF$_6$-H]$^+$, 322.6 [M-2PF$_6$]$^{2+}$, 300.6 [M-2PF$_6$-CH$_2$CH$_2$O]$^{2+}$, 278.6 [M-2PF$_6$-2CH$_2$CH$_2$O]$^{2+}$.

UV/VIS (CH$_3$CN): λ_{max}/ nm (ε_{max}, M^{-1}cm^{-1}) 242 (52.0 x 10^3), 270 (44.4 x 10^3), 303 (22.9 x 10^3).

Found: C, 43.51; H, 3.33; N, 8.88. Calc. for C$_{34}$H$_{30}$N$_6$O$_4$P$_2$F$_{12}$Co: C, 43.65; H, 3.23; N, 8.98%.

❖ [Co(***L***^{2})$_2$][PF$_6$]$_2$

Molecular formula: C$_{38}$H$_{38}$N$_6$O$_6$CoP$_2$F$_{12}$

Molecular weight: 1023.61
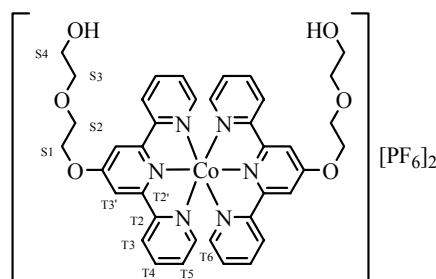
L^2 (50 mg, 0.15 mmol) and Co(OAc)$_2$·4H$_2$O (19 mg, 0.075 mmol) were used. A brown powder (44.2 mg, 57.6%) was obtained.

^{1}H NMR (250 MHz, CD$_3$CN): δ_H 5.17 (t, *J* 5.0 Hz, 2H, OH), 6.12 (t, *J* 5.0 Hz, 4H, H^{S4}), 6.47 (s, 4H, H^{T4}), 7.09 (t, *J* 5.0 Hz, 4H, H^{S3}), 9.43 (s, 4H, H^{S2}), 14.90 (s, 4H, H^{S1}), 34.7 (s, 4H, H^{T5}), 70.5 (s, 4H, H^{T3}), 74.6 (s, 4H, H$^{T3'}$), 111.8 (br, 4H, H^{T6}).

MS (ES): *m/z* = 1062.2 [M+K]$^+$, 1046.3 [M+Na]$^+$, 878.3 [M-PF$_6$]$^+$, 732.3 [M-2PF$_6$-H]$^+$, 644.2 [M-2PF$_6$-(CH$_2$CH$_2$O)$_2$H]$^+$, 556.2 [M-2PF$_6$-2(CH$_2$CH$_2$O)$_2$H]$^+$, 366.6 [M-2PF$_6$]$^{2+}$, 322.6 [M-2PF$_6$-(CH$_2$CH$_2$O)$_2$]$^{2+}$, 278.6 [M-2PF$_6$-2(CH$_2$CH$_2$O)$_2$]$^{2+}$.

UV/VIS (CH$_3$CN): λ_{max}/ nm (ε_{max}, M^{-1}cm^{-1}) 244 (55.3 x 10^3), 270 (46.9 x 10^3), 302 (25.0 x 10^3).

Found: C, 43.95; H, 3.86; N, 7.96. Calc. for C$_{38}$H$_{38}$N$_6$O$_6$P$_2$F$_{12}$Co·CH$_3$OH: C, 44.37; H, 4.01; N, 7.96%

❖ [Co(**L³**)₂][PF₆]₂

Molecular formula: $C_{42}H_{46}N_6O_8CoP_2F_{12}$

Molecular weight: 1111.71
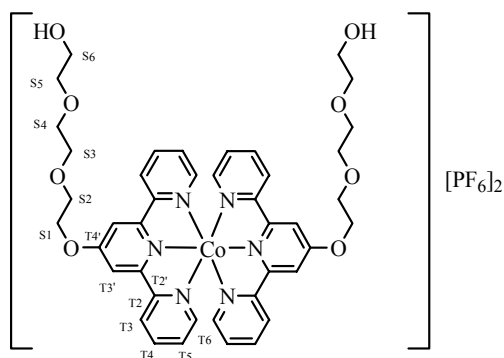
L³ (57 mg, 0.15 mmol) and Co(OAc)₂·4H₂O (19 mg, 0.075 mmol) were used. A brown powder (50.7 mg, 60.8%) was obtained.

¹H NMR (250 MHz, CD₃CN): δ_H 3.97 (s, 2H, OH), 4.60 (s, 4H, H^S6), 5.06 (t, *J* 5.0 Hz, 4H, H^S5), 6.04 (s, 4H, H^S4), 6.46 (s, 4H, H^T4), 7.07 (s, 4H, H^S3), 9.38 (s, 4H, H^S2), 14.89 (s, 4H, H^S1), 34.7 (s, 4H, H^T5), 70.5 (s, 4H, H^T3), 74.6 (s, 4H, H^T3′), 111.9 (br, 4H, H^T6).

MS (ES): *m/z* = 1007.9 [M-PF₆+CH₃CN]⁺, 965.9 [M-PF₆]⁺, 431.6 [M-2PF₆+CH₃CN]²⁺, 410.6 [M-2PF₆]²⁺.

UV/VIS (CH₃CN): λ_max/ nm (ε_max, M⁻¹cm⁻¹) 242 (58.6 x 10³), 270 (49.8 x 10³), 301 (26.5 x 10³).

Found: C, 45.11; H, 4.25; N, 7.42. Calc. for C₄₂H₄₆N₆O₈P₂F₁₂Co: C, 45.38; H, 4.17; N, 7.56%.

❖ [Co(**L⁴**)₂][PF₆]₂

Molecular formula:
$C_{52}H_{38}N_6O_2CoP_2F_{12}$

Molecular weight: 1127.76
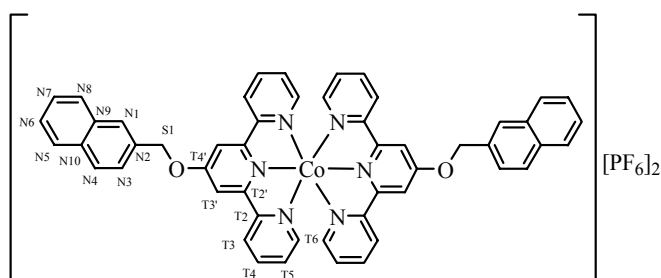
L⁴ (50 mg, 0.13 mmol) and Co(OAc)₂·4H₂O (16 mg, 0.065 mmol) were used. The brown powder (63.9 mg, 87.2%) was obtained.

¹H NMR (500 MHz, CD₃CN): δ_H 6.35 (s, 4H, H^T4), 8.55 (t, *J* 7.7 Hz, 2H, H^N6), 8.67 (t, *J* 6.9 Hz, 2H, H^N7), 9.39 (d, *J* 8.4 Hz, 2H, H^N5), 10.18 (d, *J* 7.3 Hz, 2H, H^N8), 10.55 (d, *J* 7.4 Hz, 2H, H^N4), 13.10 (d, *J* 7.4 Hz, 2H, H^N3), 13.48 (s, 2H, H^N1), 16.25 (s, 4H, H^S1), 35.1 (s, 4H, H^T5), 71.5 (s, 4H, H^T3), 76.3 (s, 4H, H^T3′), 113.6 (br, 4H, H^T6).

MS (ES): m/z = 982.0 [M-PF$_6$]$^+$, 856.0 [M-PF$_6$-PF$_5$]$^+$, 696.4 [M-2PF$_6$-CH$_2$Nap]$^+$, 555.5 [M-2PF$_6$-2CH$_2$Nap]$^+$, 467.3 [L^4+Co+F]$^+$.

UV/VIS (CH$_3$CN): λ_{max}/ nm (ε_{max}, M^{-1}cm^{-1}) 223 (221 x 10^3), 249 (71.5 x 10^3), 273 (66.2 x 10^3), 311 (23.7 x 10^3).

Found: C, 55.26; H, 3.52; N, 7.55. Calc. for C$_{52}$H$_{38}$N$_6$O$_2$P$_2$F$_{12}$Co: C, 55.38; H, 3.40; N, 7.45%.

❖ [Co(L^5)$_2$][PF$_6$]$_2$

Molecular formula:
C$_{56}$H$_{46}$N$_6$O$_4$CoP$_2$F$_{12}$

Molecular weight: 1215.86
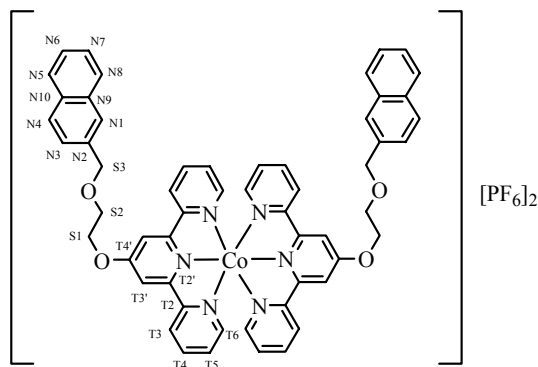
L^5 (50.0 mg, 0.12 mmol) and Co(OAc)$_2$·4H$_2$O (15 mg, 0.060 mmol) were used. A brown powder (42.9 mg, 58.8%) was obtained.

^{1}H NMR (400 MHz, CD$_3$CN): δ_H 6.38 (s, 4H, H^{T4}), 6.72 (t, J 7.5 Hz, 2H, H^{N7}), 6.99 (t, J 7.5 Hz, 2H, H^{N6}), 7.28 (d, J 7.9 Hz, 2H, H^{N8}), 7.44 (d, J 8.7 Hz, 2H, H^{N5}), 8.10 (d, J 7.9 Hz, 2H, H^{N4}), 8.14 (s, 4H, H^{S3}), 9.54 (s, 4H, H^{S2}), 9.99 (d, J 7.9 Hz, 2H, H^{N3}), 10.16 (s, 2H, H^{N1}), 14.90 (s, 4H, H^{S1}), 34.6 (s, 4H, H^{T5}), 70.2 (s, 4H, H^{T3}), 74.6 (s, 4H, H$^{T3'}$), 111.4 (br, 4H, H^{T6}).

MS (ES): m/z = 1070.3 [M-PF$_6$]$^+$, 740.2 [M-2PF$_6$-CH$_2$CH$_2$OCH$_2$Nap]$^+$, 493.3 [L^5+Co+H]$^+$, 462.7 [M-2PF$_6$]$^{2+}$.

UV/VIS (CH$_3$CN): λ_{max}/ nm (ε_{max}, M^{-1}cm^{-1}) 222 (251 x 10^3), 244 (64.1 x 10^3), 270 (61.5 x 10^3), 303 (27.9 x 10^3).

Found: C, 55.16; H, 3.71; N, 6.88. Calc. for C$_{56}$H$_{46}$N$_6$O$_4$P$_2$F$_{12}$Co: C, 55.32; H, 3.81; N, 6.91%.

❖ [Co(**L**^6^)₂][PF₆]₂

Molecular formula: $C_{60}H_{54}N_6O_6CoP_2F_{12}$

Molecular weight: 1303.97
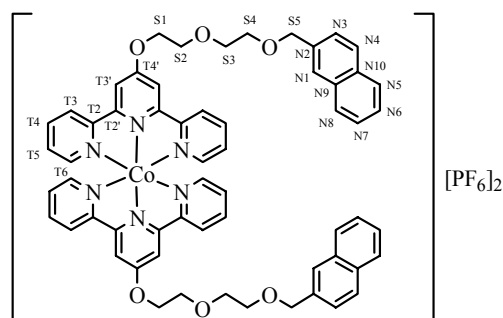
L^6^ (61 mg, 0.13 mmol) and Co(OAc)₂·4H₂O (16 mg, 0.065 mmol) were used. A brown powder (39.7 mg, 46.7%) was obtained.

¹H NMR (400 MHz, CD₃CN): δ_H 6.10 (m, 8H, H^{S5} and H^{S4}), 6.35 (s, 4H, H^{T4}), 6.77 (t, *J* 7.1 Hz, 2H, H^{N7}), 6.86 (t, *J* 7.5 Hz, 2H, H^{N6}), 7.16 (m, 6H, H^{N5} and H^{S3}), 7.53 (d, *J* 7.9 Hz, 2H, H^{N4}), 7.66 (d, *J* 7.9 Hz, 2H, H^{N8}), 8.38 (d, *J* 7.9 Hz, 2H, H^{N3}), 8.58 (s, 2H, H^{N1}), 9.44 (s, 4H, H^{S2}), 14.90 (s, 4H, H^{S1}), 34.5 (s, 4H, H^{T5}), 70.1 (s, 4H, H^{T3}), 74.5 (s, 4H, H^{T3'}), 111.2 (br, 4H, H^{T6}).

MS (ES): *m/z* = 1158.3 [M-PF₆]⁺, 784.2 [M-2PF₆-(CH₂CH₂O)₂CH₂Nap]⁺, 506.6 [M-2PF₆]²⁺, 500.2 [**L**^6^+Na]⁺.

UV/VIS (CH₃CN): λ_{max}/ nm (ε_{max}, M⁻¹cm⁻¹) 222 (233 x 10³), 241 (60.4 x 10³), 270 (57.3 x 10³), 303 (27.2 x 10³).

Found: C, 54.28; H, 4.25; N, 6.50. Calc. for $C_{60}H_{54}N_6O_6P_2F_{12}Co \cdot H_2O$: C, 54.51; H, 4.27; N, 6.36%.

❖ [Co(**L**^7^)₂][PF₆]₂

Molecular formula:
$C_{64}H_{62}N_6O_8CoP_2F_{12}$

Molecular weight: 1392.07
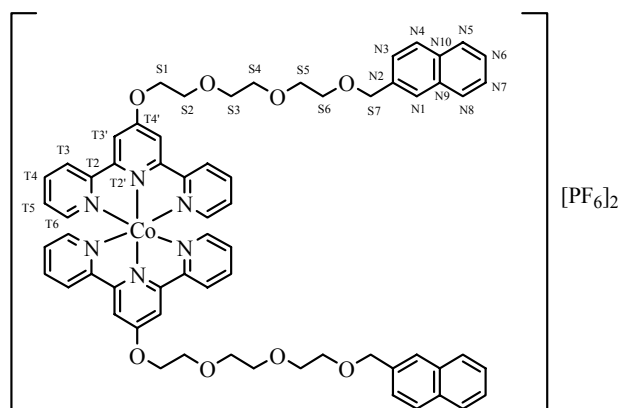
L^7^ (50 mg, 0.096 mmol) and Co(OAc)₂·4H₂O (12 mg, 0.048 mmol) were used. A brown powder (54.4 mg, 81.5%) was obtained.

^{1}H NMR (500 MHz, CD$_3$CN):

For Co(III) species: δ_H 3.73 (m, 2.1H, H^{S4}, H^{S5} and H^{S6}), 3.83 (m, 0.7H, H^{S3}), 4.14 (m, 0.7H, H^{S2}), 4.70 (s, 0.7H, H^{S7}), 4.85 (m, 0.7H, H^{S1}), 7.35 (dd, *J* 1.1, 6.1 Hz, 0.7H, H^{T6}), 7.43 (m, 1.4H, H^{T5}, H^{N6} and H^{N7}), 7.48 (m, 0.35H, H^{N3}), 7.83 (m, 1.4H, H^{N1}, H^{N4}, H^{N5} and H^{N8}), 8.20 (td, *J* 1.4, 8.8 Hz, 0.7H, H^{T4}), 8.51 (m, 1.4H, H^{T3} and H$^{T3'}$).

For Co(II) species: δ_H 4.59 (t, *J* 4.5 Hz, 4H, H^{S6}), 5.12 (s, 4H, H^{S7}), 5.21 (t, *J* 4.5 Hz, 4H, H^{S5}), 6.11 (t, *J* 4.4 Hz, 4H, H^{S4}), 6.42 (s, 4H, H^{T4}), 6.60 (t, *J* 7.4 Hz, 2H, H^{N6}), 6.77 (t, *J* 7.3 Hz, 2H, H^{N7}), 6.99 (d, *J* 8.1 Hz, 2H, H^{N5}), 7.15 (t, *J* 4.6 Hz, 4H, H^{S3}), 7.48 (d, *J* 8.2 Hz, 2H, H^{N4}), 7.55 (d, *J* 8.0 Hz, 2H, H^{N8}), 7.67 (d, *J* 7.7 Hz, 2H, H^{N3}), 7.93 (s, 2H, H^{N1}), 9.46 (s, 4H, H^{S2}), 15.01 (s, 4H, H^{S1}), 34.7 (s, 4H, H^{T5}), 70.4 (s, 4H, H^{T3}), 74.6 (s, 4H, H$^{T3'}$), 111.8 (br, 4H, H^{T6}).

^{13}C NMR (125 MHz, CD$_3$CN):

For Co(III) species: δ_C 69.6 (C^{S2}), 70.6 (C^{S6}), 71.2 (C^{S4} and C^{S5}), 71.6 (C^{S3}), 72.5 (C^{S1}), 73.6 (C^{S7}), 115.7 (C$^{T3'}$), 126.9 (C^N), 127.2 (C^N), 127.7 (C^{T3}), 128.6 (C^N), 128.7 (C^N), 128.9 (C^N), 131.7 (C^{T5}), 133.8 (C$^{N9/\,N10}$), 134.2 (C$^{N10/\,N9}$), 137.4 (C^{N2}), 144.0 (C^{T4}), 153.2 (C^{T6}), 157.1 (C^{T2}), 157.8 (C$^{T2'}$), 173.7 (C$^{T4'}$).

For Co(II) species: δ_C -127.7 (C$^{T2/\,T2'}$), -74.6 (C^{T6}), -49.1 (C$^{T2/\,T2'}$), 71.7 (C^{S6}), 72.9 (C^{S5}), 74.0 (C^{S4}), 74.1 (C^{S7}), 75.3 (C^{S3}), 78.9 (C^{S2}), 80.4 (C^{S1}), 126.2 (C^{N6}), 126.6 (C^{N7}), 127.0 (C^{N3}), 127.1 (C^{N1}), 127.9 (C^{N5}), 128.3 (C^{N8}), 128.7 (C^{N4}), 133.4 (C^{N10}), 134.0 (C^{N9}), 137.6 (C^{N2}), 161.7 (C^{T4}), 304.8 (C$^{T4'}$), 353.6 (C^{T3}), 383.2 (C$^{T3'}$), 499.4 (C^{T5}).

MS (ES): *m/z* = 1246.2 [M-PF$_6$]$^+$, 828.5 [M-2PF$_6$-(CH$_2$CH$_2$O)$_2$OCH$_2$Nap]$^+$, 599.4 [***L***^{7}+Co+F]$^+$, 551.7 [M-2PF$_6$]$^{2+}$.

UV/VIS (CH$_3$CN): λ_{max}/ nm (ε_{max}, M^{-1}cm^{-1}) 224 (260 x 10^3), 241 (63.1 x 10^3), 272 (63.7 x 10^3), 305 (29.4 x 10^3).

Found: C, 51.27; H, 4.17; N, 5.58. Calc. for ⅓C$_{64}$H$_{62}$N$_6$O$_8$P$_2$F$_{12}$Co and ⅔C$_{64}$H$_{62}$N$_6$O$_8$P$_3$F$_{18}$Co: C, 51.64; H, 4.20; N, 5.65%.

❖ [Co(***L***^{8})$_2$][PF$_6$]$_2$

Molecular formula:
C$_{60}$H$_{42}$N$_6$O$_2$CoP$_2$F$_{12}$

Molecular weight: 1227.88
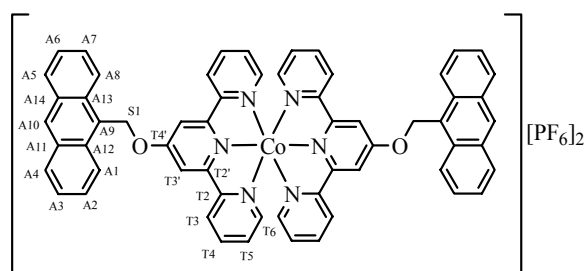
L^8 (50 mg, 0.11 mmol) and Co(OAc)$_2$·4H$_2$O (14 mg, 0.055 mmol) were used. A brown powder (44.5 mg, 65.8%) was obtained.

^{1}H NMR (500 MHz, CD$_3$CN): δ_H 6.56 (s, 4H, H^{T4}), 9.13 (m, 4H, H$^{A3, A6}$), 9.84 (d, J 8.8 Hz, 4H, H$^{A4, A5}$), 10.13 (m, 4H, H$^{A2, A7}$), 10.63 (s, 2H, H^{A10}), 14.63 (d, J 8.9 Hz, 4H, H$^{A1, A8}$), 16.77 (s, 4H, H^{S1}), 34.7 (s, 4H, H^{T5}), 69.7 (s, 4H, H^{T3}), 73.8 (s, 4H, H$^{T3'}$), 110.9 (br, 4H, H^{T6}).

MS (ES): m/z = 1083.2 [M-PF$_6$]$^+$, 956.2 [M-PF$_6$-PF$_5$]$^+$, 876.1 [M-PF$_6$-OCH$_2$Ant]$^+$, 746.3 [M-2PF$_6$-CH$_2$Ant]$^+$, 555.5 [M-2PF$_6$-2CH$_2$Ant]$^+$, 540.6 [M-2PF$_6$-OCH$_2$Ant-CH$_2$Ant]$^+$, 517.1 [L^8+Co+F]$^+$, 191.4 [CH$_2$Ant]$^+$.

UV/VIS (CH$_3$CN): λ_{max}/ nm (ε_{max}, M^{-1}cm^{-1}) 254 (298 x 10^3), 281 (45.1 x 10^3), 315 (21.5 x 10^3), 348 (16.0 x 10^3), 366 (21.1 x 10^3), 386 (19.3 x 10^3).

Found: C, 57.90; H, 3.53; N, 6.54. Calc. for C$_{60}$H$_{42}$N$_6$O$_2$P$_2$F$_{12}$Co·H$_2$O: C, 57.84; H, 3.56; N, 6.75%.

❖ [Co(L^9)$_2$][PF$_6$]$_2$

Molecular formula: C$_{50}$H$_{34}$N$_6$S$_2$CoP$_2$F$_{12}$

Molecular weight: 1131.84
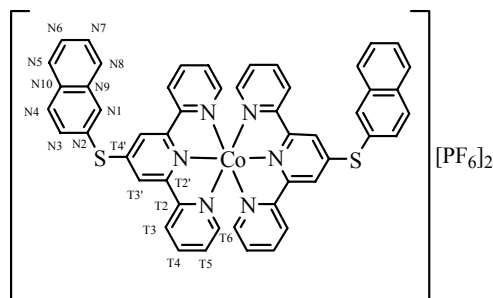
L^9 (54 mg, 0.14 mmol) and Co(OAc)$_2$·4H$_2$O (17 mg, 0.070 mmol) were used. A brown powder (44.5 mg, 56.1%) was obtained.

^{1}H NMR (500 MHz, CD$_3$CN): δ_H 8.08 (s, 4H, H^{T4}), 8.36 (t, J 7.8 Hz, 2H, H^{N6}), 8.47 (t, J 7.7 Hz, 2H, H^{N7}), 9.13 (d, J 8.4 Hz, 2H, H^{N5}), 9.63 (d, J 8.4 Hz, 2H, H^{N8}), 10.15 (d, J 8.3 Hz, 2H, H^{N4}), 12.37 (s, 2H, H^{N1}), 12.67 (d, J 8.3 Hz, 2H, H^{N3}), 34.1 (s, 4H, H^{T5}), 55.9 (s, 4H, H$^{T3'}$), 61.6 (s, 4H, H^{T3}), 102.8 (br, 4H, H^{T6}).

^{13}C NMR (125 MHz, CD$_3$CN): δ_C -85.8 (C$^{T2/T2'}$), -55.5 (C^{T6}), -11.7 (C$^{T2/T2'}$), 126.4 (C^{N2}), 129.4(C^{N7}), 130.2 (C^{N5}), 130.4 (C^{N6}), 131.0 (C^{N8}), 134.0 (C^{N4}), 136.9 (C^{N3}), 137.3 (C^{N9}), 137.3 (C^{N10}), 141.7 (C^{N1}), 158.2 (C^{T4}), 247.0 (C$^{T4'}$), 336.5 (C$^{T3'}$), 339.0 (C^{T3}), 464.5 (C^{T5}).

MS (ES): m/z = 985.9 [M-PF$_6$]$^+$, 421.2 [M-2PF$_6$]$^{2+}$.

UV/VIS (CH$_3$CN): λ_{max}/ nm (ε_{max}, M^{-1}cm^{-1}) 221 (146 x 10^3), 283 (74.0 x 10^3), 310 (49.7 x 10^3).

Found: C, 52.38; H, 3.24; N, 7.32. Calc. for C$_{50}$H$_{34}$N$_6$S$_2$P$_2$F$_{12}$Co·CH$_3$OH: C, 52.63; H, 3.29; N, 7.22%.

❖ [Co(***terpy***)$_2$][PF$_6$]$_2$

Molecular formula: C$_{30}$H$_{22}$N$_6$CoP$_2$F$_{12}$

Molecular weight: 815.40
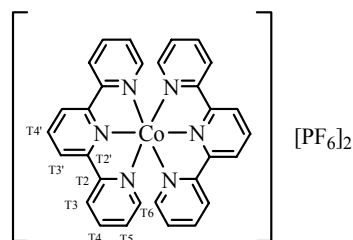
Terpy (20 mg, 0.086 mmol) and Co(OAc)$_2$·4H$_2$O (11 mg, 0.043 mmol) were used. A brown powder (30.1 mg, 85.8%) was obtained.

^{1}H NMR (250 MHz, CD$_3$CN): δ_H 8.94 (s, 4H, H^{T4}), 21.9 (s, 2H, H$^{T4'}$), 34.5 (s, 4H, H^{T5}), 48.1 (s, 4H, H$^{T3'}$), 57.1 (s, 4H, H^{T3}), 99.2 (br, 4H, H^{T6}).

MS (ES): m/z = 669.9 [M-PF$_6$]$^+$, 544.0 [M-PF$_6$-PF$_5$]$^+$, 262.9 [M-2PF$_6$]$^{2+}$.

UV/VIS (CH$_3$CN): λ_{max}/ nm (ε_{max}, M^{-1}cm^{-1}) 280 (44.1 x 10^3), 314 (36.7 x 10^3).

Found: C, 43.65; H, 2.64; N, 10.11. Calc. for C$_{30}$H$_{22}$N$_6$P$_2$F$_{12}$Co·H$_2$O: C, 43.23; H, 2.91; N, 10.09%.

Partially oxidise the [Co(***terpy***)$_2$][PF$_6$]$_2$ to a mixture of Co(II) and Co(III) species by adding one drop of Br$_2$ to the [Co(***terpy***)$_2$][PF$_6$]$_2$ in CH$_3$CN. Then, aqueous NH$_4$PF$_6$ was added to the solution. The resultant brown precipitate was collected by filtration, washed and dried.

^{1}H NMR (500 MHz, CD$_3$CN):

For Co(III) species: δ_H 7.24 (d, J 5.6 Hz, 4H, H^{T6}), 7.41 (t, J 6.4 Hz, 4H, H^{T5}), 8.21 (t, J 7.7 Hz, 4H, H^{T4}), 8.60 (d, J 7.8 Hz, 4H, H^{T3}), 9.03 (m, 6H, H$^{T4'}$ and H$^{T3'}$).

For Co(II) species: δ_H 9.12 (s, 4H, H^{T4}), 22.0 (s, 4H, H$^{T4'}$), 34.1 (s, 4H, H^{T5}), 45.9 (s, 4H, H$^{T3'}$), 56.0 (s, 4H, H^{T3}), 97.5 (br, 4H, H^{T6}).

General method for the exchange experiments of the cobalt(II) complexes

The solutions of the cobalt(II) complexes were prepared fresh, mixed and transferred immediately in an NMR tube. After an initial delay for shimming (about 5 mins), the spectra were recorded.

(a) $[Co(L^1)_2][PF_6]_2$ and $[Co(L^2)_2][PF_6]_2$

Each $[Co(L^1)_2][PF_6]_2$ (4.7 mg, 5×10^{-3} mmol) and $[Co(L^2)_2][PF_6]_2$ (5.1 mg, 5×10^{-3} mmol) were dissolved in 0.5 mL CD$_3$CN. 0.3 mL of each $[Co(L^1)_2][PF_6]_2$ and $[Co(L^2)_2][PF_6]_2$ were mixed together. The reaction mixture was monitored immediately by ^{1}H NMR spectroscopy until equilibrium was established.

(b) $[Co(L^4)_2][PF_6]_2$ and $[Co(L^9)_2][PF_6]_2$

Each $[Co(L^4)_2][PF_6]_2$ (5.6 mg, 5.0×10^{-3} mmol) and $[Co(L^9)_2][PF_6]_2$ (5.7 mg, 5.0×10^{-3} mmol) were dissolved in 0.5 mL CD$_3$CN. 0.3 mL of each $[Co(L^4)_2][PF_6]_2$ and $[Co(L^9)_2][PF_6]_2$ were mixed together. The reaction mixture was monitored immediately by ^{1}H NMR spectroscopy until equilibrium was established.

(c) $[Co(L^8)_2][PF_6]_2$ and $[Co(L^9)_2][PF_6]_2$

Each $[Co(L^8)_2][PF_6]_2$ (6.1 mg, 5.0×10^{-3} mmol) and $[Co(L^9)_2][PF_6]_2$ (5.7 mg, 5.0×10^{-3} mmol) were dissolved in 0.5 mL CD$_3$CN. 0.3 mL of each $[Co(L^8)_2][PF_6]_2$ and $[Co(L^9)_2][PF_6]_2$ were mixed together. The reaction mixture was monitored immediately by ^{1}H NMR spectroscopy until equilibrium was established.

(d) $[Co(L^4)_2][PF_6]_2$ and $[Co(L^8)_2][PF_6]_2$

Each $[Co(L^4)_2][PF_6]_2$ (5.6 mg, 5.0×10^{-3} mmol) and $[Co(L^8)_2][PF_6]_2$ (6.1 mg, 5.0×10^{-3} mmol) were dissolved in 0.5 mL CD$_3$CN. 0.3 mL of each $[Co(L^4)_2][PF_6]_2$ and $[Co(L^8)_2][PF_6]_2$ were mixed together. The reaction mixture was monitored immediately by ^{1}H NMR spectroscopy until equilibrium was established.

(e) [Co(*terpy*)$_2$][PF$_6$]$_2$ and [Co(L^8)$_2$][PF$_6$]$_2$

Each [Co(*terpy*)$_2$][PF$_6$]$_2$ (4.1 mg, 5.0x10^{-3} mmol) and [Co(L^8)$_2$][PF$_6$]$_2$ (6.1 mg, 5.0x10^{-3} mmol) were dissolved in 0.5 mL CD$_3$CN. 0.3 mL of each [Co(*terpy*)$_2$][PF$_6$]$_2$ and [Co(L^8)$_2$][PF$_6$]$_2$ were mixed together. The reaction mixture was monitored immediately by ^{1}H NMR spectroscopy until equilibrium was established.

(f) [Co(*Fc-terpy*)$_2$][PF$_6$]$_2$ and [Co(L^8)$_2$][PF$_6$]$_2$

Each [Co(*Fc-terpy*)$_2$][PF$_6$]$_2$ (4.1 mg, 5.0x10^{-3} mmol) and [Co(L^8)$_2$][PF$_6$]$_2$ (6.1 mg, 5.0x10^{-3} mmol) were dissolved in 0.5 mL CD$_3$CN. 0.3 mL of each [Co(*Fc-terpy*)$_2$][PF$_6$]$_2$ and [Co(L^8)$_2$][PF$_6$]$_2$ were mixed together. The reaction mixture was monitored immediately by ^{1}H NMR spectroscopy until equilibrium was established.

4.10   References

1.   E. C. Constable, *Adv. Inorg. Chem. Radiochem.*, 1987, **30**, 69.

2.   A. B. Gaspar, M. C. Muñoz, V. Niel, and J. A. Real, *Inorg. Chem.*, 2001, **40**, 9.

3.   B. Whittle, E. L. Horwood, L. H. Rees, S. R. Batten, J. C. Jeffery, and M. D. Ward, *Polyhedron*, 1998, **17**, 373.

4.   A. Jouaiti, V. Jullien, M. W. Hosseini, J.-M. Planeix, and A. De Cian, *Chem. Commun.*, 2001, 1114.

5.   N. W. Alcock, P. R. Barker, J. M. Haider, M. J. Hannon, C. L. Painting, Z. Pikramenou, E. A. Plummer, K. Rissanen, and P. Saarenketo, *J. Chem. Soc., Dalton Trans.*, 2000, 1447.

6.   E. C. Constable, C. E. Housecroft, T. Kulke, C. Lazzarini, E. R. Schofield, and Y. Zimmermann, *J. Chem. Soc., Dalton Trans.*, 2001, 2864.

7.   E. C. Constable, T. Kulke, M. Neuburger, and M. Zehnder, *New J. Chem.*, 1997, **21**, 1091.

8.   C. E. Housecroft, and A. G. Sharpe, *Inorganic Chemistry*, Pearson, Harlow, 2005, Chapter 25.

9.   M. Gerloch, and E. C. Constable, *Transition Metal Chemistry*, VCH, New York, 1994.

10.   B. R. Baker, F. Basolo, and H. M. Neumann, *J. Phys. Chem.*, 1959, **63**, 371.

11.   R. Farina, and R. G. Wilkins, *Inorg. Chem.*, 1968, **7**, 514.

12.   R. M. L. Warren, A. G. Lappin, B. Dev Mehta, and H. M. Neumann, *Inorg. Chem.*, 1990, **29**, 4185.

13.   J. K. Beattie, and H. Elsbernd, *Inorg. Chim. Acta*, 1995, **240**, 641.

14.   R. H. Holyer, C. D. Hubbard, S. F. A. Kettle, and R. G. Wilkins, *Inorg. Chem.*, 1965, **5**, 622.

15.   V. Goral, M. I. Lelen, A. V. Eliseev, and J.-M. Lehn, *Proc. Natl. Acad. Sci. USA*, 2001, **98**, 1347.

16.   E. C. Constable, C. P. Hart, and C. E. Housecroft, *Appl. Organomet. Chem.*, 2003, **17**, 383.

17.   E. C. Constable, C. E. Housecroft, M. Neuburger, and A. G. Schneider, *Inorg. Chem. Commun.*, 2003, **6**, 912.

18.   E. C. Constable, C. E. Housecroft, M. Neuburger, A. G. Schneider, and M. Zehnder, *J. Chem. Soc., Dalton Trans.*, 1997, 2427.

19.   E. C. Constable, M. Neuburger, D. R. Smith, and M. Zehnder, *Inorg. Chim. Acta*, 1998, **275-276**, 359.

20. E. C. Constable, P. Harverson, D. R. Smith, and L. Whall, *Polyhedron*, 1997, **16**, 3615.

21. J. D. Epperson, L.-J. Ming, B. D. Woosley, G. R. Baker, and G. R. Newkome, *Inorg. Chem*., 1999, **38**, 4498.

22. E. C. Constable, R. Handel, C. E. Housecroft, M. Neuburger, E. R. Schofield, and M. Zehnder, *Polyhedron*, 2004, **23**, 135.

23. B. G. G. Lohmeijer, and U. S. Schubert, *Macromol. Chem. Phys.*, 2003, **204**, 1072.

24. R. Chotalia, E. C. Constable, M. J. Hannon, and D. A. Tocher, *J. Chem. Soc., Dalton Trans.*, 1995, 3571.

25. A. E. Derome, *Modern NMR Techniques for Chemistry Research*, Pergamon, Oxford, 1987, Chapter 4.

26. H. Elsbernd, and J. K. Beattie, *J. Inorg. Nucl. Chem.*, 1972, **34**, 771.

27. R. Hogg, and R. G. Wilkins, *J. Chem. Soc.*, 1962, 341.

28. S. A. Sapp, C. M. Elliott, C. Contado, S. Caramori, and C. A. Bignozzi, *J. Am. Chem. Soc.*, 2002, **124**, 11215.

29. C. L. Raston, and A. H. White, *J. Chem. Soc., Dalton Trans.*, 1976, 7.

30. E. N. Maslen, C. L. Raston, and A. H. White, *J. Chem. Soc., Dalton Trans.*, 1974, 1803.

31. B. N. Figgis, E. S. Kucharski, and A. H. White, *Aust. J. Chem.*, 1983, **36**, 1527.

32. B. N. Figgis, E. S. Kucharski, and A. H. White, *Aust. J. Chem.*, 1983, **36**, 1537.

33. B. N. Figgis, E. S. Kucharski, and A. H. White, *Aust. J. Chem.*, 1983, **36**, 1563.

34. E. C. Constable, C. E. Housecroft, L. A. Johnston, D. Armspach, M. Neuburger, and M. Zehnder, *Polyhedron*, 2001, **20**, 483.

35. E. R. Schofield, Ph.D. thesis, University of Basel, 1998.

36. E. C. Constable, A. J. Edwards, R. Martínez-Máñez, P. R. Raithby, and A. M. W. Cargill Thompson, *J. Chem. Soc., Dalton Trans.*, 1994, 645.

Chapter 5

Synthesis of Homoditopic 4′-Substituted-2,2′:6′,2″-Terpyridine Ligands

In Chapter 2, we discussed a few methodologies for synthesising 4′-substituted-2,2′:6′,2″-terpyridine ligands. Homoditopic 4′-substituted-2,2′:6′,2″-terpyridine ligands can also be synthesised by using the same method. Most of the known rigid bis(terpyridine) ligands were synthesised by the Kröhnke method or a coupling method.[1,2] For example, 1,4-bis[4′-(2,2′:6′,2″-terpyridinyl)]benzene[1] and 2,5-bis[4′-(2,2′:6′,2″-terpyridinyl)]thiophene[3] were synthesised in two steps by the Kröhnke strategy (**Scheme 1**). 1,1′-Bis[4′-(2,2′:6′,2″-terpyridinyl)]ferrocene can also be prepared from ferrocene-1,1′-dicarboxaldehyde by the Kröhnke methodology.[4]

1,4-Bis[4'-(2,2':6',2"-terpyridinyl)]
benzene

2,5-Bis[4'-(2,2':6',2"-terpyridinyl)]
thiophene
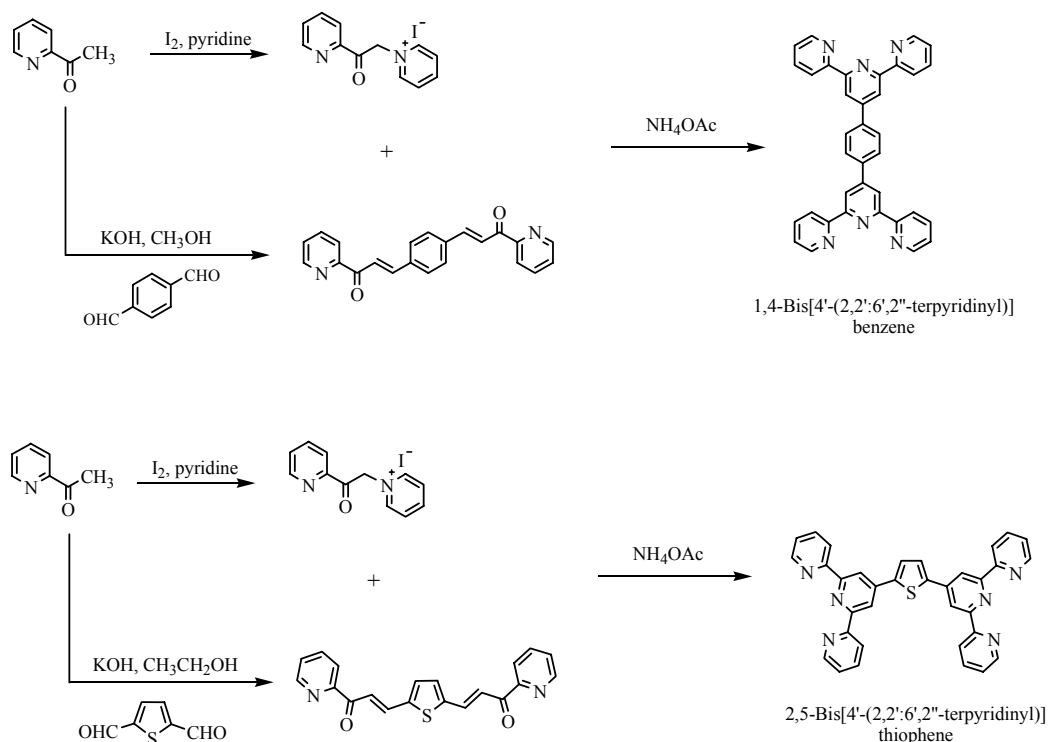
Scheme 1. The Kröhnke strategy for synthesising 1,4-bis[4′-(2,2′:6′,2″-terpyridinyl)]benzene and 2,5-bis[4′-(2,2′:6′,2″-terpyridinyl)]thiophene.

The coupling reaction can also be used to prepare "back-to-back" terpyridine ligands, for example, 4,4′-bis[4′-(2,2′:6′,2″-terpyridinyl)]biphenyl[5] and 6′,6″-bis(2-pyridyl)-2,2′:4′,4″:2″,2‴-quaterpyridine[6-8]. 4,4′-Bis[4′-(2,2′:6′,2″-terpyridinyl)]biphenyl can be prepared by coupling two equivalents of 4′-(4-chlorophenyl)-2,2′:6′,2″-terpyridine or 4′-(4-bromophenyl)-2,2′:6′,2″-terpyridine with nickel(0)[5], while 6′,6″-bis(2-pyridyl)-2,2′:4′,4″:2″,2‴-quaterpyridine can be synthesised by coupling two equivalents of 4′-chloro-2,2′:6′,2″-terpyridine with nickel(0)[6-8]. Ziessel and co-workers have prepared a range of 2,5-diethynyl-3,4-dibutylthiophene-bridged "back-to-back" terpyridine ligands.[9]
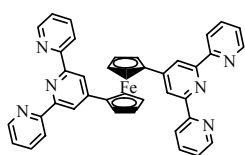
1,1'-Bis[4'-(2,2':6',2"-terpyridinyl)] ferrocene
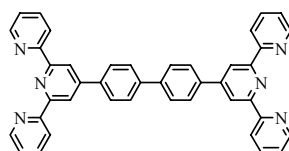
4,4'-Bis[4'-(2,2':6',2"-terpyridinyl)]biphenyl
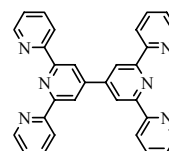
6',6"-Bis(2-pyridyl)-2,2':4',4":2",2"'-quaterpyridine
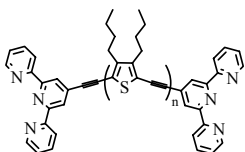
2,5-Diethynyl-3,4-dibutylthiophene-bridged 'back-to-back' terpyridine ligands
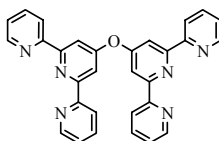
Bis[4'-(2,2':6',2"-terpyridinyl)]ether
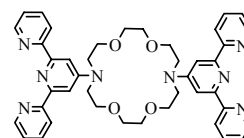
1,10-Bis[4'-(2,2':6',2"-terpyridinyl)]diaza-18-crown-6(1,4,10,13-tetraoxa-7,16-diazacyclooctadecane)
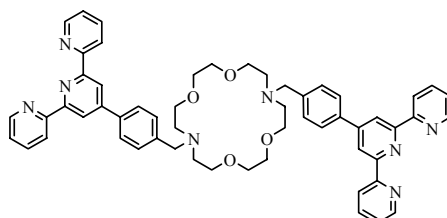
1,10-Bis[4'-(4-methylphenyl-2,2':6',2"-terpyridinyl)]diaza-18-crown-6(1,4,10,13-tetraoxa-7,16-diazacyclooctadecane)

4′-Hydroxy-2,2′:6′,2″-terpyridine (**HO-terpy**) can be coupled with 4′-chloro-2,2′:6′,2″-terpyridine (**Cl-terpy**) using potassium hydroxide in *N,N*-dimethylformamide at reflux to give the oxygen-bridged "back-to-back" ligand bis[4′-(2,2′:6′,2″-terpyridinyl)]ether.[10] Reaction of 1,10-diaza-18-crown-6(1,4,10,13-tetraoxa-7,16-diazacyclooctadecane) with two equivalents of 4′-bromo-2,2′:6′,2″-terpyridine or two equivalents of 4′-[(4-bromomethyl)phenyl]-2,2′:6′,2″-terpyridine afforded 1,10-bis[4′-(2,2′:6′,2″-terpyridinyl)]diaza-18-crown-6(1,4,10,13-tetraoxa-

7,16-diazacyclooctadecane) or 1,10-bis[4′-(4-methylphenyl-2,2′:6′,2″-terpyridinyl)]diaza-18-crown-6(1,4,10,13-tetraoxa-7,16-diazacyclooctadecane).[11]

In this chapter, the syntheses of several new homoditopic ligands based upon a naphthalene unit bearing two 4′-substituted-2,2′:6′,2″-terpyridine-terminated bis(ethyleneoxy) ligands (*L*[10]-*L*[17]) are discussed (**Scheme 2**). All of these homoditopic 4′-substituted-2,2′:6′,2″-terpyridine ligands contain polyethyleneoxy chains which link to two different positions of the naphthalene unit and differ from one another in the length of the chains.
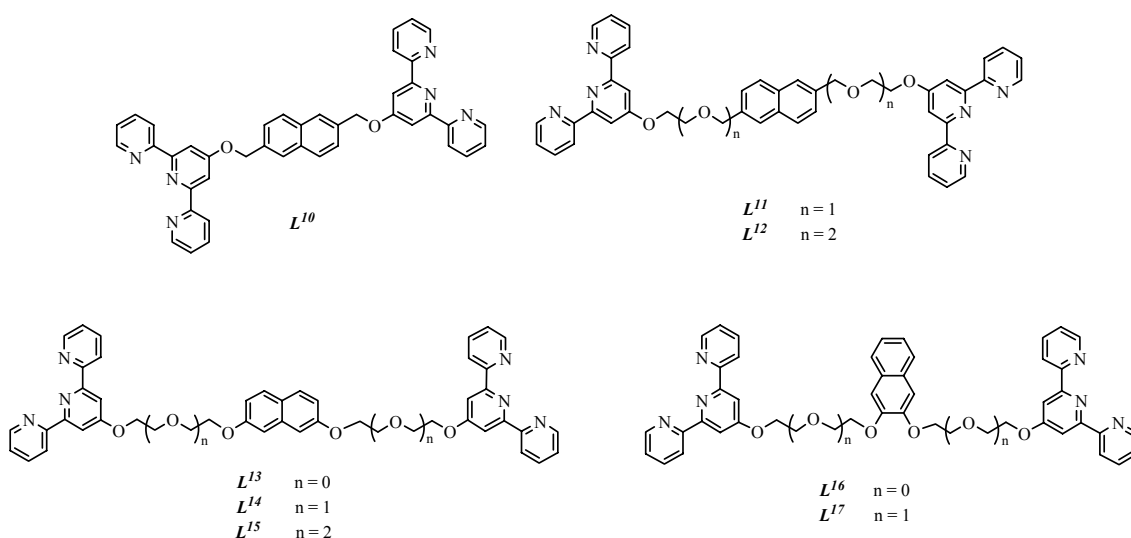
Scheme 2. Diagram showing the homoditopic ligands *L*[10]-*L*[17].

5.1 Synthesis

As discussed in Chapter 2, different substituents can be introduced at the 4′-position of 2,2′:6′,2″-terpyridine ligands by electrophiles reacting with 4′-hydroxy-2,2′:6′,2″-terpyridine (**HO-terpy**) or nucleophiles reacting with 4′-chloro-2,2′:6′,2″-terpyridine (**Cl-terpy**).[12-30]

The syntheses of different homoditopic 4′-substituted-2,2′:6′,2″-terpyridine ligands are described below. The ligands *L*[10]-*L*[17] were designed with two tridentate binding

sites for complexation with metal ions and with bridging naphthalene domain. The 2,2′:6′,2″-terpyridine and naphthyl domains in ligands L^{11}-L^{17} were connected by ethyleneoxy linkage groups of different lengths. This is also important for controlling the size of metallomacrocycles when they react with metal ions.

The reaction of 2,6-bis(hydroxymethyl)naphthalene, KOH and *Cl-terpy* in dry DMSO at 70°C for 3 days, followed by column chromatography (alumina, CH_2Cl_2: hexane 2:1, then CH_2Cl_2/ 1% CH_3OH) gave L^{10} as a yellow powder in 30% yield (**Scheme 3**).[29,30] The product tends to readily decompose.
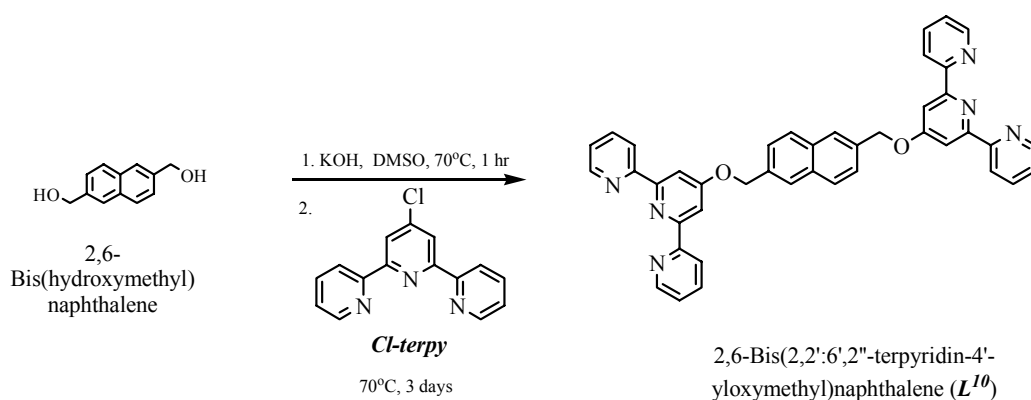
Scheme 3. Synthesis of L^{10}.

2,6-[Bis(2,2′:6′,2″-terpyridin-4′-yl)-1,4-dioxapentyl]naphthalene (L^{11}) and 2,6-[bis(2,2′:6′,2″-terpyridin-4′-yl)-1,4,7-trioxaoctyl]naphthalene (L^{12}) were prepared from L^1 and L^2 respectively in 57% and 15% yields. The reaction of L^1 or L^2 with NaH and 2,6-bis(bromomethyl)naphthalene in THF at 80°C for 2-4 days, followed by work up using column chromatography (alumina, CH_2Cl_2/ 1% CH_3OH) resulted in L^{11} as a white powder and L^{12} as yellow oily liquid (**Scheme 4**).[31]
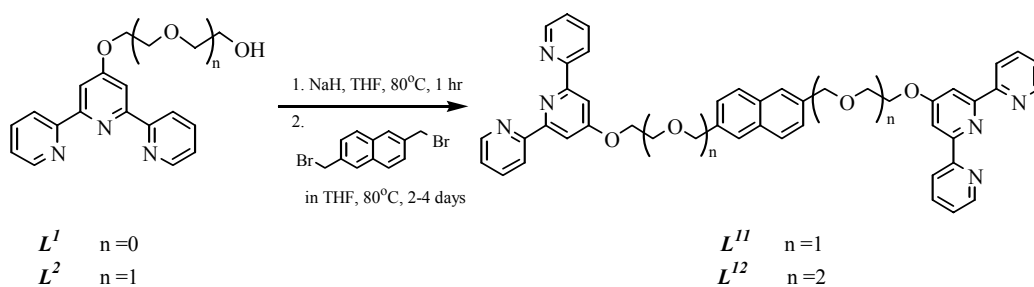
Scheme 4. Syntheses of L^{11} and L^{12}.

Heating **HO-terpy**, K_2CO_3 and 2,7-bis(2-methanesulfonatoethoxy)naphthalene in dry acetone at 70ºC for 4 days, followed by column chromatography (alumina, CH_2Cl_2/ 0.5% CH_3OH) resulted in the formation of L^{13} as a white powder in 58% yield (**Scheme 5**).
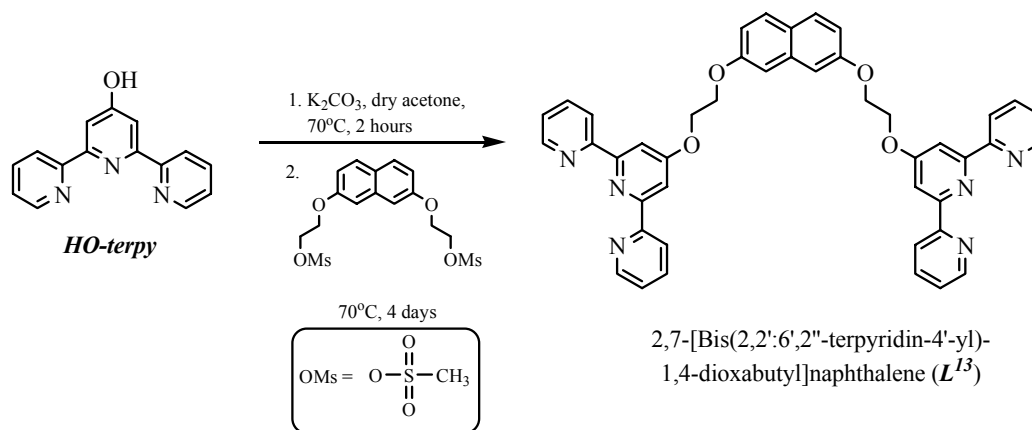
Scheme 5. Synthesis of L^{13}.

The synthesis of L^{14} is depicted in **Scheme 6**. L^{14} was prepared in 28% overall yield from 2,7-dihydroxynaphthalene in two steps; reaction of $ClCH_2CH_2OCH_2CH_2OH$ with 2,7-dihydroxynaphthalene and K_2CO_3 in DMF gave the diol-functionalised compound 2,7-di[2-(2-hydroxyethoxy)ethoxy]naphthalene which was converted to L^{14} by reaction with **Cl-terpy** and KOH in DMSO.[29,30]
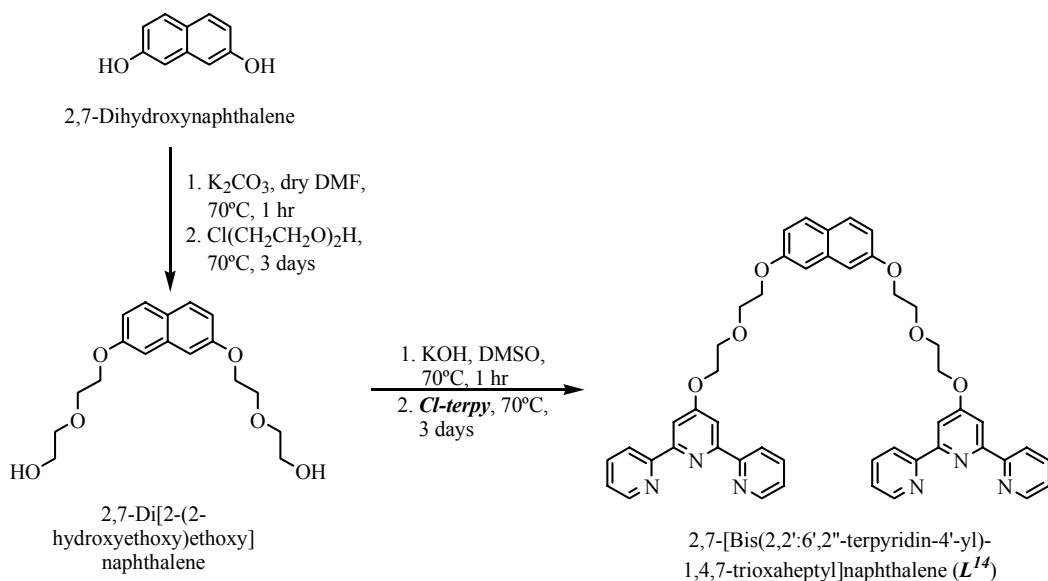
Scheme 6. Synthesis of L^{14}.

The synthesis of L^{15} is depicted in **Scheme 7**. L^{15} was prepared in 12% overall yield from 2,7-dihydroxynaphthalene in two steps; reaction of $ClCH_2(CH_2OCH_2)_2CH_2OH$ with 2,7-dihydroxynaphthalene in dry acetone gave the diol-functionalised compound 2,7-di{2-[2-(2-hydroxyethoxy)ethoxy]ethoxy}naphthalene which was converted to L^{15} by reaction with **Cl-terpy** and KOH in DMSO.[29,30]
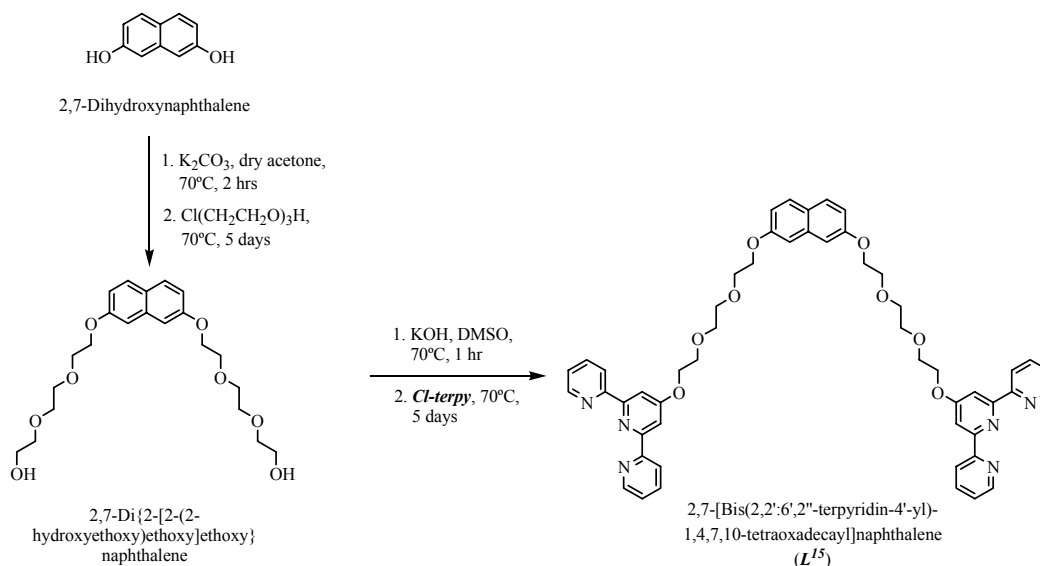
Scheme 7. Synthesis of L^{15}.
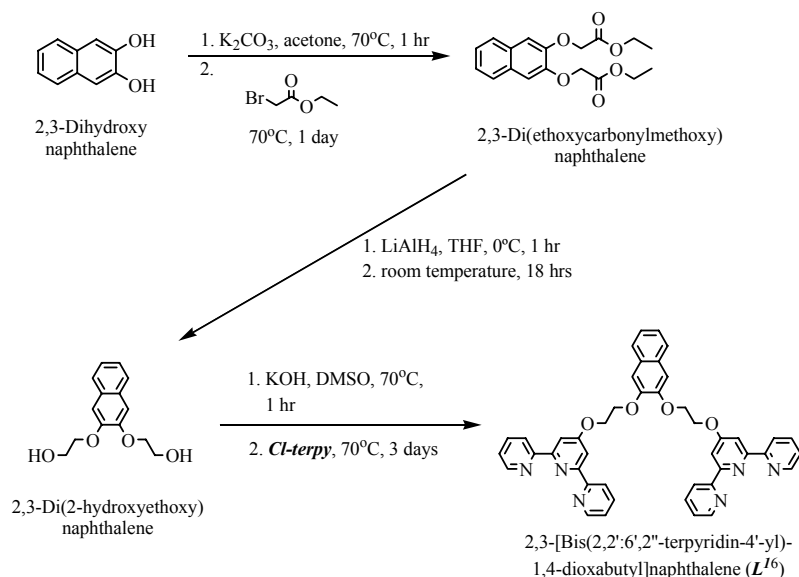
Scheme 8. Synthesis of L^{16}.

The synthesis of L^{16} is depicted in **Scheme 8**. L^{16} was prepared in 16% overall yield from 2,3-dihydroxynaphthalene in three steps; reaction of ethyl bromoacetate with

2,3-dihydroxynaphthalene and K_2CO_3 in acetone gave 2,3-di(ethoxycarbonylmethoxy)naphthalene. The diester was then reduced to the diol-functionalised compound 2,3-di(2-hydroxyethoxy)naphthalene which was converted to L^{16} by reaction with *Cl-terpy* and KOH in DMSO.[29,30]
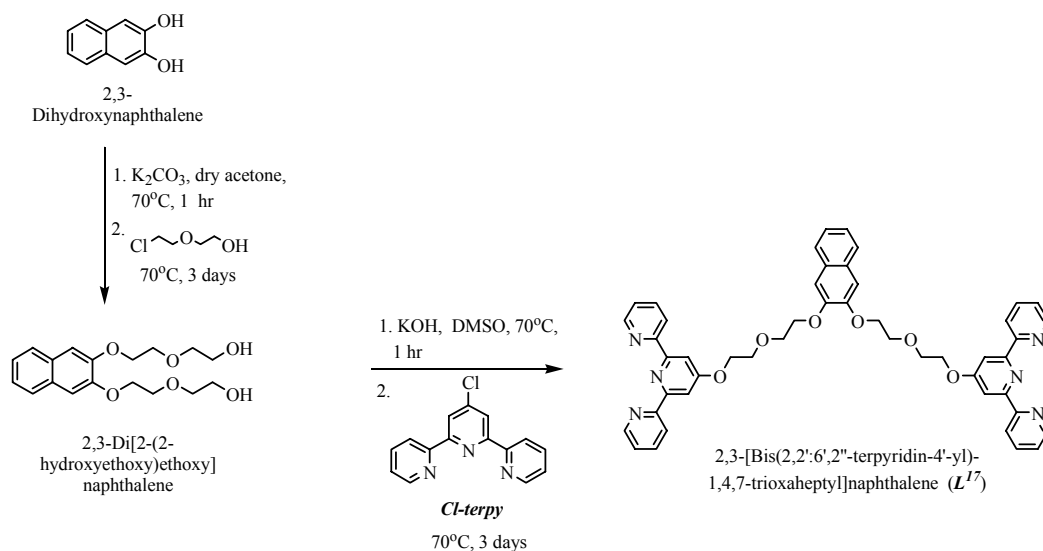
Scheme 9. Synthesis of L^{17}.

L^{17} was prepared by using the similar reaction scheme for synthesis of L^{14} (**Scheme 9**). L^{17} was prepared in 32% overall yield from 2,3-dihydroxynaphthalene in two steps; reaction of $ClCH_2CH_2OCH_2CH_2OH$ with 2,3-dihydroxynaphthalene and K_2CO_3 in acetone gave the diol-functionalised compound 2,3-di[2-(2-hydroxyethoxy)ethoxy]naphthalene which was converted to L^{17} by reaction with *Cl-terpy* and KOH in DMSO.[29,30]

5.2 ^{1}H NMR spectroscopic characterisation

All the ligands were characterised by ^{1}H NMR spectroscopy in CDCl$_3$ solution. The spectroscopic signatures of the ligands compare well with those of other terpy systems[29], and the terpyridine proton signals are very similar from one ligand to another (**Table 1**). **Table 2** shows the chemical shifts for the ethyleneoxy spacer and naphthalene ring proton signals.
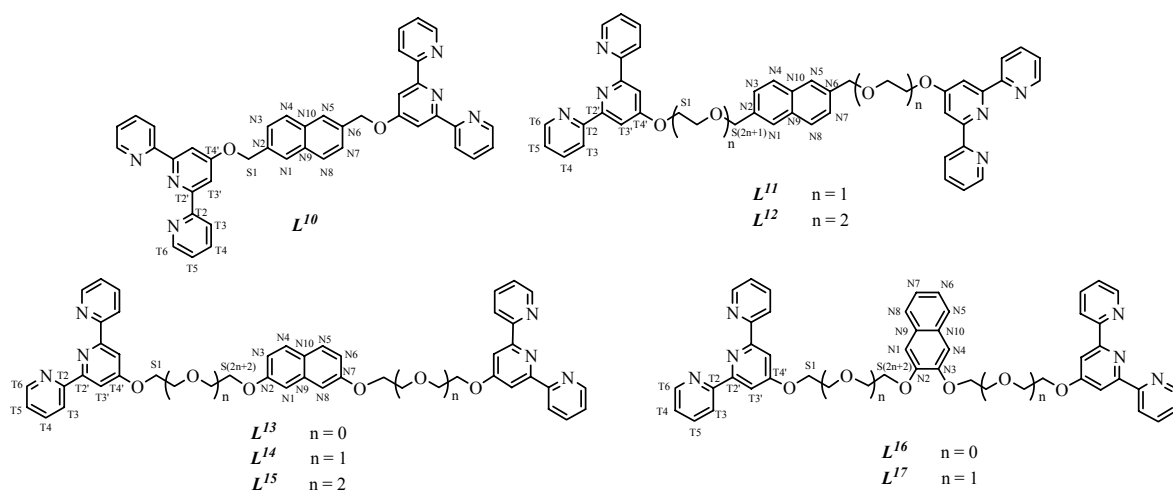
L	Proton resonance (δ)				
	H^{T5}	H^{T4}	H$^{T3'}$	H^{T3}	H^{T6}
L^{10}	7.35 (ddd) J 1.0, 4.8, 7.3 Hz	7.87 (td) J 1.7, 7.7 Hz	8.19 (s)	8.64 (d) J 8.1 Hz	8.72 (dd) J 1.0, 4.0 Hz
L^{11}	7.32 (ddd) J 1.1, 4.8, 7.4 Hz	7.84 (td) J 1.8, 7.7 Hz	8.07 (s)	8.61 (d) J 7.9 Hz	8.68 (m)
L^{12}	7.32 (dd) J 4.9, 6.5 Hz	7.84 (td) J 1.6, 7.7 Hz	8.05 (s)	8.60 (d) J 7.9 Hz	8.67 (d) J 4.1 Hz
L^{13}	7.33 (ddd) J 1.2, 4.8, 7.5 Hz	7.85 (td) J 1.8, 7.7 Hz	8.14 (s)	8.63 (dt) J 1.0, 8.0 Hz	8.69 (ddd) J 0.9, 1.8, 4.8 Hz
L^{14}	7.31 (ddd) J 1.2, 4.8, 7.5 Hz	7.84 (td) J 1.8, 7.7 Hz	8.05 (s)	8.60 (dt) J 1.0, 8.0 Hz	8.67 (ddd) J 0.9, 1.8, 4.8 Hz
L^{15}	7.31 (ddd) J 1.2, 4.8, 7.5 Hz	7.83 (td) J 1.8, 7.7 Hz	8.04 (s)	8.59 (dt) J 1.0, 7.9 Hz	8.66 (ddd) J 0.9, 1.8, 4.8 Hz
L^{16}	7.30 (dd) J 5.1, 7.0 Hz	7.83 (t) J 7.5 Hz	8.06 (s)	8.57 (d) J 8.0 Hz	8.64 (d) J 4.0 Hz
L^{17}	7.28 (m)	7.80 (td) J 1.8, 7.7 Hz	8.02 (s)	8.56 (dt) J 1.0, 8.0 Hz	8.64 (ddd) J 0.9, 1.8, 4.8 Hz

Table 1. ^{1}H NMR spectroscopic data for the terpyridine proton signals of *L^{10}*-*L^{17}* in CDCl$_3$ solution at room temperature. The ^{1}H NMR spectrum for *L^{10}* was measured at 400 MHz and all the others were measured at 500 MHz.

L	Proton resonance (δ)					
	H^S1	H^S2	H^S3	H^S4	H^S5	H^S6
L^10	5.51 (s)					
L^11	4.45 (t) J 4.7 Hz	3.95 (t) J 4.7 Hz	4.82 (s)			
L^12	4.41 (t) J 4.7 Hz	3.95 (t) J 4.7 Hz	3.80 (m)	3.70 (m)	4.72 (s)	
L^13	4.67 (m)	4.52 (m)				
L^14	4.44 (t) J 4.7 Hz	4.02 (m)		4.25 (t) J 4.8 Hz		
L^15	4.39 (t) J 4.7 Hz	3.93 (t) J 4.7 Hz	3.78 (m)		3.91 (t) J 4.8 Hz	4.19 (t) J 4.9 Hz
L^16	4.70 (t) J 4.6 Hz	4.56 (t) J 4.8 Hz				
L^17	4.39 (t) J 4.7 Hz	4.04 (m)		4.29 (t) J 4.9 Hz		

L	Proton resonance (δ)		
	H^N3, N7	H^N4, N8	H^N1, N5
L^10	7.62 (dd) J 1.3, 8.3 Hz	7.92 (d) J 8.1 Hz	7.99 (s)
L^11	7.49 (dd) J 1.3, 8.3 Hz	7.81 (m)	
L^12	7.44 (d) J 8.2 Hz	7.77 (d) J 8.4 Hz	7.74 (s)
	H^N3, N6	H^N1, N8	H^N4, N5
L^13	7.07 (dd) J 2.5, 8.9 Hz	7.15 (d) J 2.5 Hz	7.67 (d) J 9.0 Hz
L^14	7.02 (m)		7.60 (d) J 8.7 Hz
L^15	6.98 (m)		7.58 (d) J 9.6 Hz
	H^N1, N4	H^N6, N7	H^N5, N8
L^16	7.28 (s)	7.35 (m)	7.70 (m)
L^17	7.14 (s)	7.28 (m)	7.63 (m)

Table 2. ^{1}H NMR spectroscopic data for the ethyleneoxy spacer proton and naphthyl proton signals of *L*^10-*L*^17 in CDCl$_3$ solution at room temperature. The ^{1}H NMR spectrum for *L*^10 was measured at 400 MHz and all the others were measured at 500 MHz.
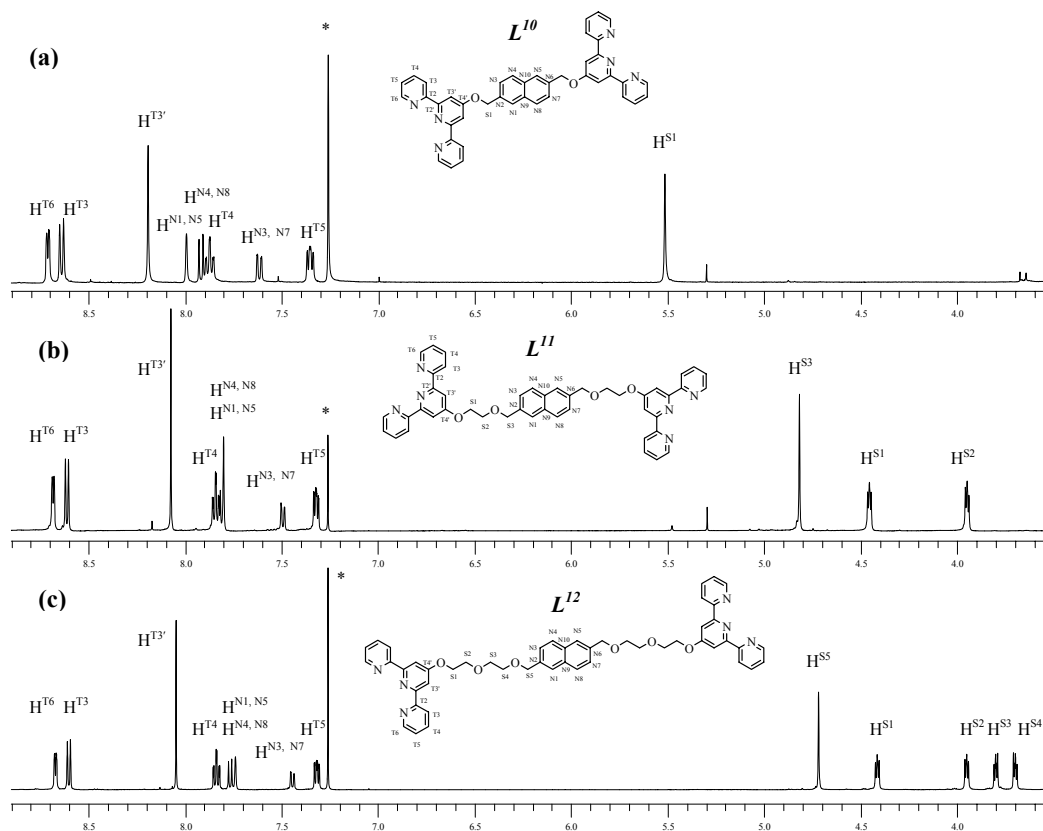
Figure 1. ¹H NMR spectra of (a) **L^{10}** (400 MHz), (b) **L^{11}** (500 MHz) and (c) **L^{12}** (500 MHz) in CDCl₃ solution at room temperature. The signal marked * is the signal for CHCl₃.

The ¹H NMR spectra of **L^{10}**, **L^{11}** and **L^{12}** in CDCl₃ solution have very similar features from one to the other (**Figure 1**). **L^{12}** has the longest ethyleneoxy spacer groups among **L^{10}**, **L^{11}**, **L^{12}**. There are eight signals for **L^{12}** in the aromatic region excluding the signal for CHCl₃ (**Figure 1c**). The five terpyridine proton signals were assigned according to the ligands **L^{1}-L^{8}** in Chapter 2. The assignment of the CH₂ protons was made by COSY and NOESY and confirmed by HMQC and HMBC. The triplet at δ 4.41, which exhibits an NOE signal to H$^{T3'}$ at δ 8.05, is assigned to H^{S1} (**Figure 2**). H^{S1} gives a COSY cross peak to H^{S2} at δ 3.95 (**Figure 3**). H^{S2} exhibits an NOE signal to the signal at δ 3.80 and this signal is assigned to H^{S3} (**Figure 2**). And then, H^{S3} gives a COSY cross peak to the signal for H^{S4} at δ 3.70 (**Figure 3**). H^{S4} exhibits an NOE signal to a singlet at δ 4.72, which is assigned to H^{S5} (**Figure 2**). Finally, H^{S5} exhibits NOE signals to a doublet and a singlet at δ 7.44 and 7.74, which are assigned to H$^{N3, N7}$ and H$^{N1, N5}$ respectively (**Figure 2**). H$^{N3, N7}$ at δ 7.44 gives a COSY cross peak to a doublet at δ 7.77, and this signal is assigned to H$^{N4, N8}$ (**Figure 3**).

Figure 2. NOESY spectrum (500 MHz) of L^{12} in CDCl$_3$ solution at room temperature. The signal marked * is the signal for CHCl$_3$.
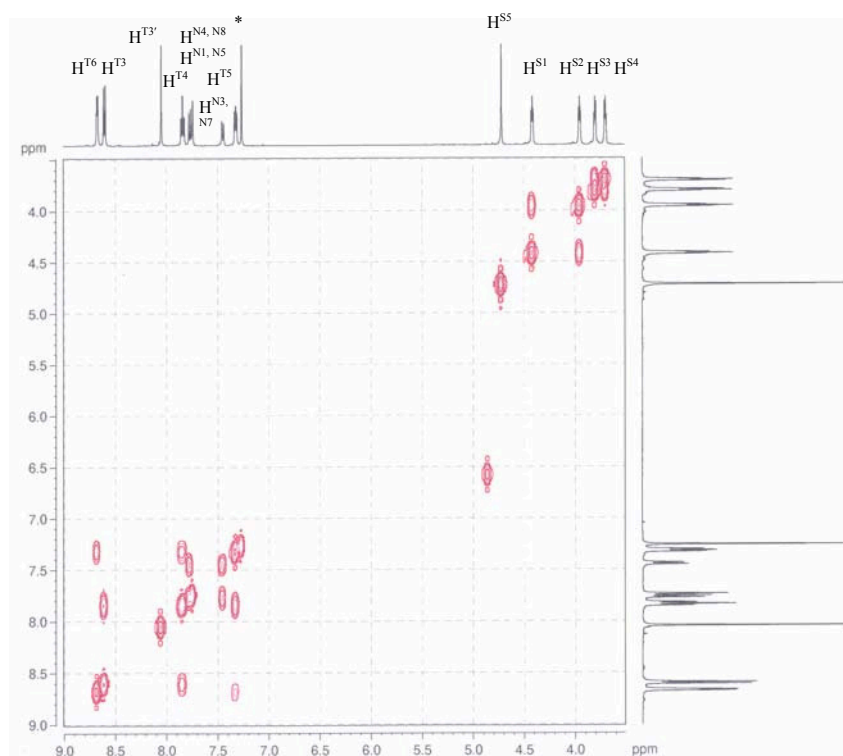
Figure 3. COSY spectrum (500 MHz) of L^{12} in CDCl$_3$ solution at room temperature. The signal marked * is the signal for CHCl$_3$.
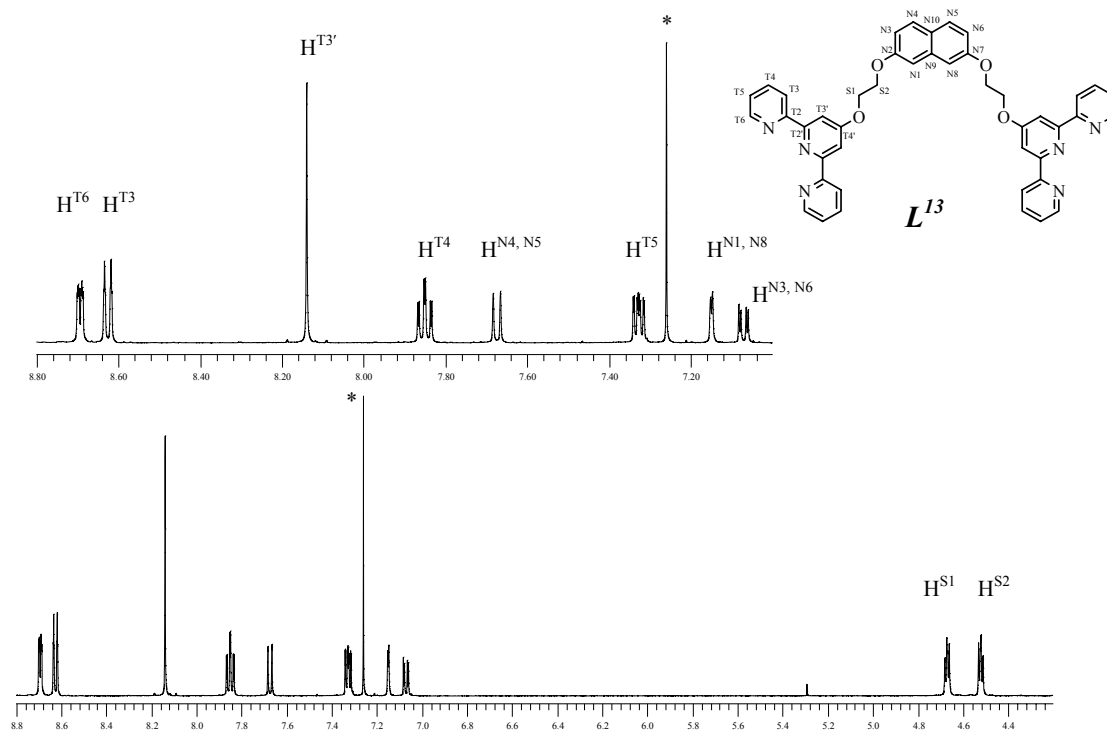
Figure 4. ^{1}H NMR spectrum (500 MHz) of L^{13} in CDCl$_3$ solution at room temperature. The signal marked * is the signal for CHCl$_3$.

There are ten signals in the ^{1}H NMR spectrum of a CDCl$_3$ solution of the ligand L^{13} excluding the signal for CHCl$_3$ (**Figure 4**). Five terpyridine signals were found as expected by comparison with L^{10}-L^{12}; the rest of the signals belong to the naphthyl ring and ethyleneoxy protons and were further identified by NOESY and COSY techniques. The triplet at δ 4.67, which exhibits an NOE signal to H$^{T3'}$ at δ 8.14, is assigned to H^{S1} (**Figure 5**). The signal for H^{S1} gives a COSY cross peak to a signal for H^{S2} at δ 4.52 (**Figure 6**). The signal for H^{S2} exhibits an NOE signal to a doublet with a coupling constant of 2.5 Hz at δ 7.15, which is assigned to H$^{N1, N8}$ (**Figure 5**). The doublet of doublets at δ 7.07, with coupling constants of 2.5 Hz and 8.9 Hz, is assigned to H$^{N3, N6}$. From the COSY spectrum (**Figure 6**), the signal for H$^{N3, N6}$ gives a cross peak to a signal at δ 7.67, and is assigned to H$^{N4, N5}$. The assignment was also confirmed by HMQC and HMBC.
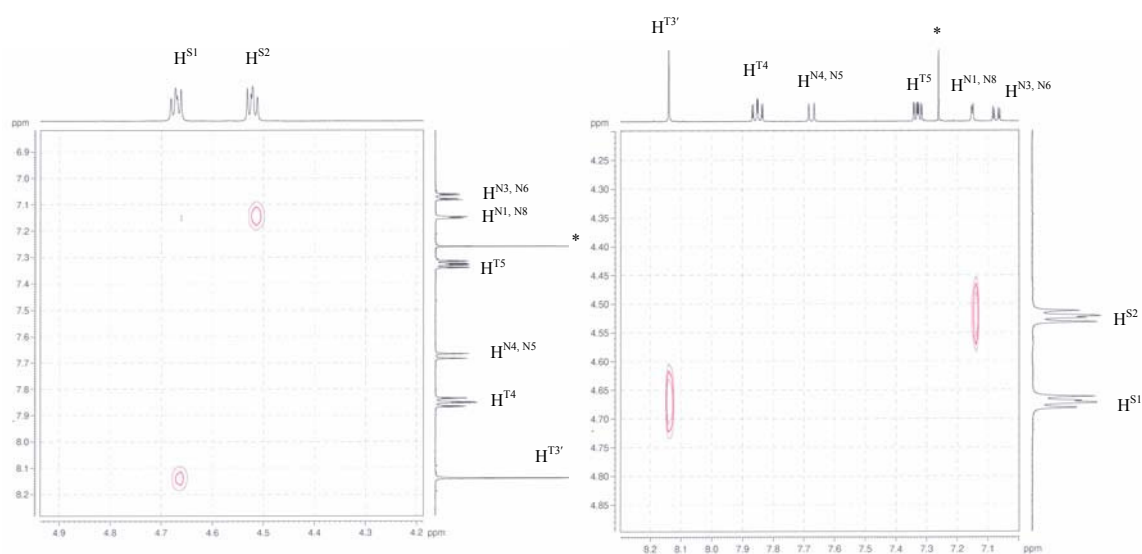
Figure 5. NOESY spectrum (500 MHz) of L^{13} in CDCl$_3$ solution at room temperature. The signal marked * is the signal for CHCl$_3$.

Figure 6. COSY spectrum (500 MHz) of L^{13} in CDCl$_3$ solution at room temperature. The signal marked * is the signal for CHCl$_3$.

191
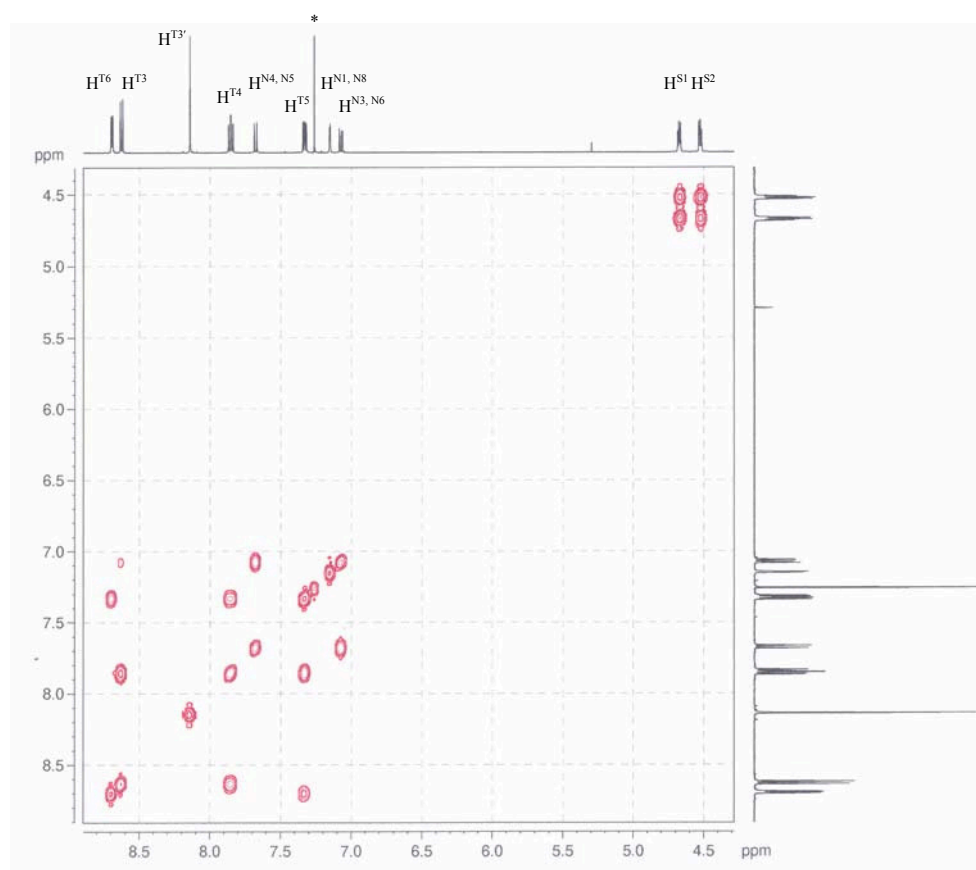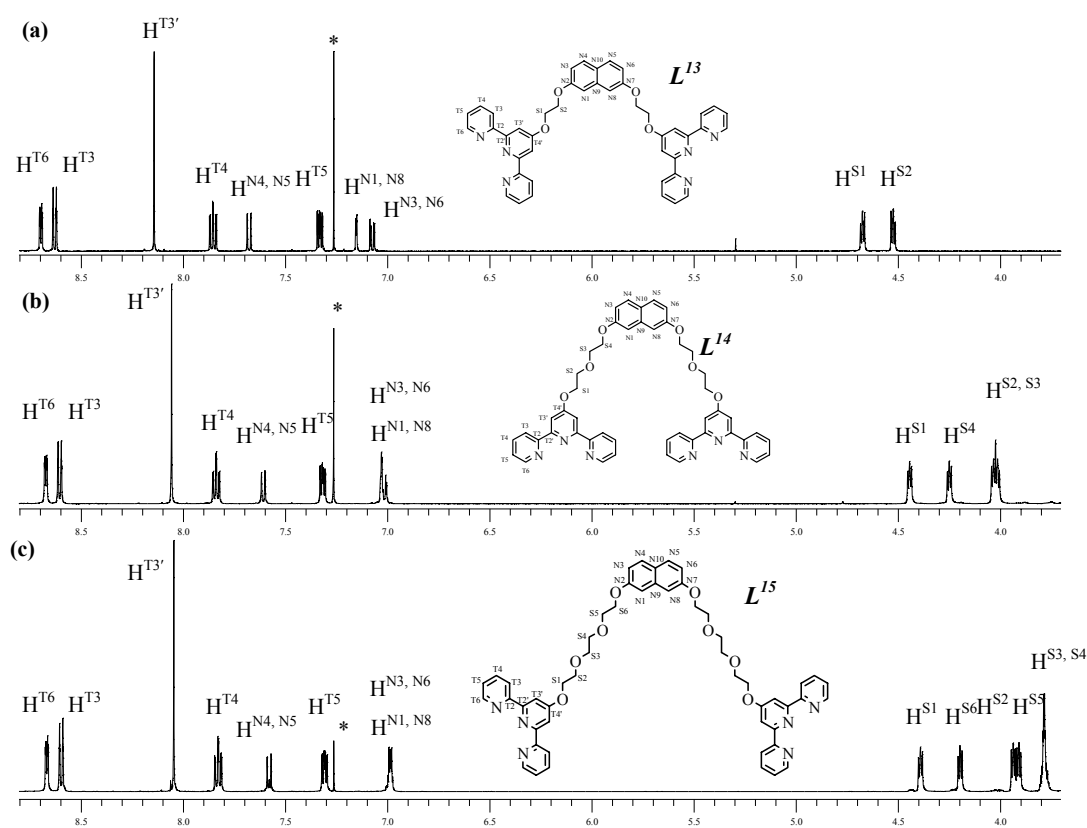
Figure 7. ¹H NMR spectra (500 MHz) of (a) L^{13}, (b) L^{14} and (c) L^{15} in CDCl₃ solution at room temperature. The signal marked * is the signal for CHCl₃.

The ¹H NMR spectra of CDCl₃ solutions of the ligand L^{14} and L^{15} are similar to the spectrum of L^{13} (**Figure 7**). The assignment was made by using NOESY and COSY and confirmed by HMQC and HMBC techniques. There are no significant differences of the terpyridine signals, except $H^{T3'}$. However, the naphthalene protons are shifted to slightly higher field as the ethyleneoxy spacer gets longer (**Table 2**).
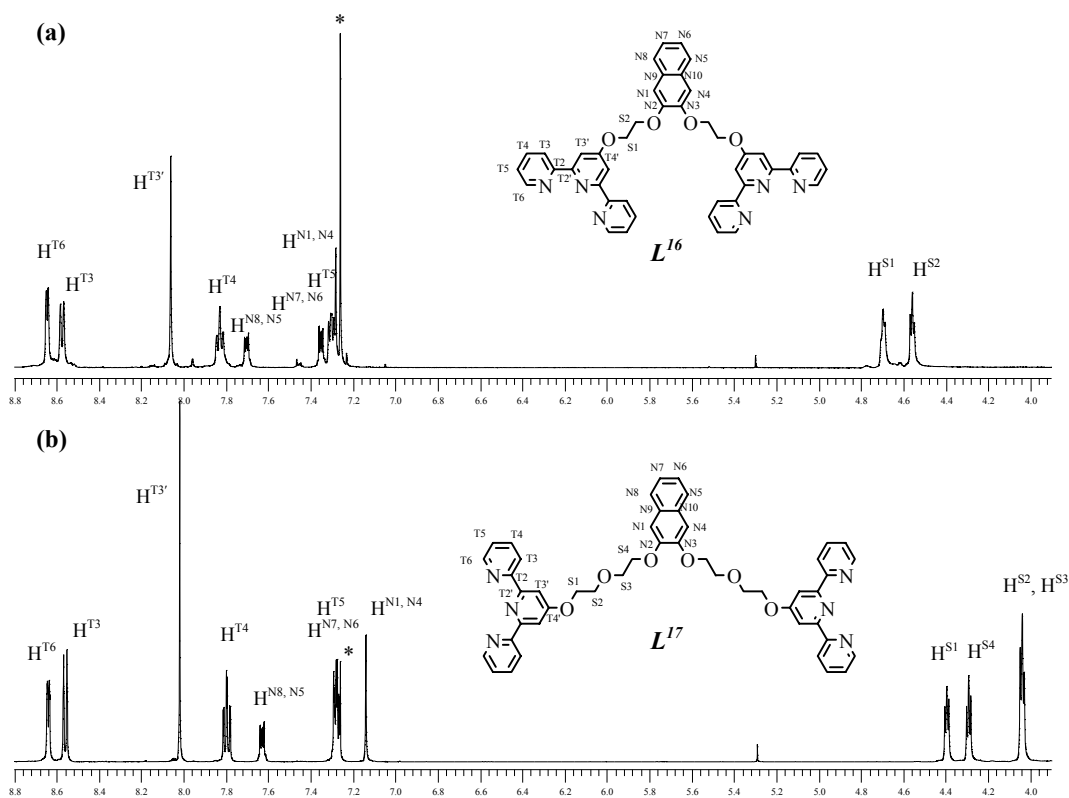
Figure 8. ^{1}H NMR spectra (500 MHz) of (a) L^{16} and (b) L^{17} in CDCl$_3$ solution at room temperature. The signal marked * is the signal for CHCl$_3$.

The ^{1}H NMR spectrum of L^{17} in CDCl$_3$ solution exhibits 12 signals excluding the signal for CHCl$_3$ (**Figure 8b**). The five terpyridine signals are assigned as before. The singlet for H$^{T3'}$ at δ 8.02 exhibits an NOE signal to a triplet at δ 4.39, which is assigned to H^{S1} (**Figure 9**). The signal for H^{S1} gives a cross peak to a signal at δ 4.04 and this is assigned to H^{S2} (**Figure 10**). The singlet at δ 7.14, which has half the relative integral of the signal for H^{S1}, is assigned to H$^{N1, N4}$. The signal for H$^{N1, N4}$ gives NOE signals to a triplet at δ 4.29 and a multiplet at δ 7.63, and so the signals are assigned to H^{S4} and H$^{N8, N5}$ respectively (**Figure 9**). The signal for H^{S4} gives a cross peak to a signal at δ 4.04 which is assigned to H^{S3} (**Figure 10**). Also, the signal for H$^{N8, N5}$ gives a cross peak to a multiplet at δ 7.28 which is assigned to H$^{N7, N6}$ (**Figure 10**). There are no significant differences between the ^{1}H NMR spectra of L^{17} and L^{16}, except the naphthalene and ethyleneoxy protons are shifted to higher field as the ethyleneoxy spacer gets longer (**Figure 8** and **Table 2**).
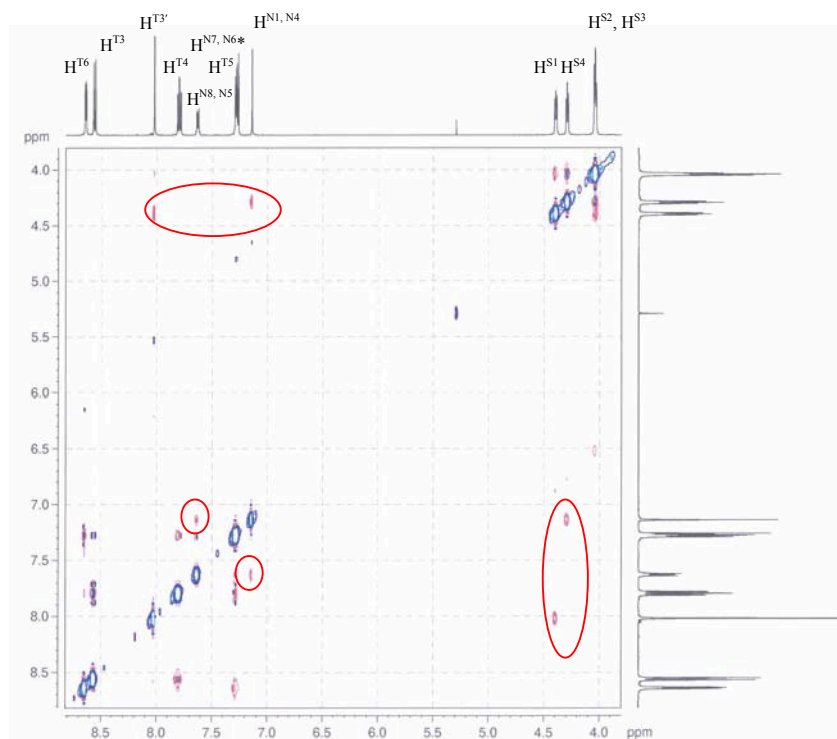
Figure 9. NOESY spectrum (500 MHz) of L^{17} in CDCl$_3$ solution at room temperature. The signal marked * is the signal for CHCl$_3$.

Figure 10. COSY spectrum (500 MHz) of L^{17} in CDCl$_3$ solution at room temperature. The signal marked * is the signal for CHCl$_3$.

194
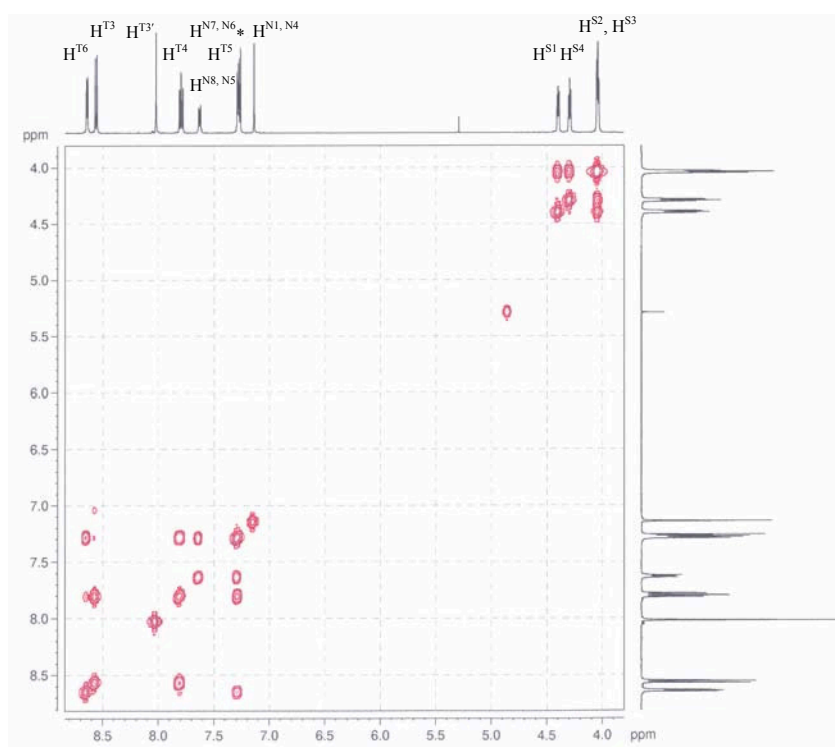
5.3 ^{13}C NMR spectroscopic characterisation

Table 3 shows the terpyridine, ethyleneoxy spacer and naphthalene ring ^{13}C signals of $\boldsymbol{L^{10}}$-$\boldsymbol{L^{17}}$ in CDCl$_3$ solution (see p.186 for the atom labelling scheme). The assignments were done by using HMQC and HMBC techniques. There are no significant changes in these signals as the length of the spacer between the terpyridine and the substituents is lengthened. All the terpyridine carbon signals of these ligands are comparable to each other.

L	$C^{T3'}$	C^{T3}	C^{T5}	C^{T4}	C^{T6}	C^{T2}	$C^{T2'}$	$C^{T4'}$
L^{10}	107.8	121.5	124.0	137.0	149.2	156.2	157.4	167.1
L^{11}	107.5	121.3	123.8	136.8	149.1	156.1	157.1	167.0
L^{12}	107.5	121.3	123.8	136.8	149.1	156.1	157.1	167.0
L^{13}	107.7	121.4	123.8	136.8	148.9	156.0	157.2	167.0
L^{14}	107.6	121.5	124.0	136.9	149.2	156.2	157.3	167.1
L^{15}	107.6	121.5	124.0	137.0	149.0	156.0	157.1	167.1
L^{16}	108.1	121.8	124.2	137.5	148.7	155.3	156.5	167.2
L^{17}	107.6	121.4	123.9	136.8	149.13	156.1	157.2	167.1

L	C^{S1}	C^{S2}	C^{S3}	C^{S4}	C^{S5}	$C^{N3, N7}$	$C^{N1, N5}$	$C^{N4, N8}$	$C^{N9, N10}$	$C^{N2, N6}$
L^{10}	70.1					125.8	126.4	128.7	133.1	134.1
L^{11}	67.8	68.3	73.5			126.0	126.3	128.3	132.9	135.5
L^{12}	67.8	69.5	71.1	69.5	73.4	126.0	126.3	128.2	132.8	135.7

L	C^{S1}	C^{S2}	C^{S3}	C^{S4}	C^{S5}	C^{S6}	$C^{N1, N8}$	$C^{N3, N6}$	C^{N10}	$C^{N4, N5}$	C^{N9}	$C^{N2, N7}$
L^{13}	66.7	66.4					106.8	116.5	124.9	129.3	135.8	157.2
L^{14}	68.0	69.8	70.2	67.6			106.4	116.6	124.6	129.2	135.9	157.4
L^{15}	67.9	69.6	71.2	71.0	69.9	67.4	106.3	116.5	124.5	129.1	135.8	157.4

L	C^{S1}	C^{S2}	C^{S3}	C^{S4}	$C^{N1, N4}$	$C^{N6, N7}$	$C^{N5, N8}$	$C^{N9, N10}$	$C^{N2, N3}$
L^{16}	67.0	67.6			110.1	124.7	126.6	129.7	149.1
L^{17}	68.0	69.9	70.0	68.7	108.7	124.3	126.5	129.5	149.10

Table 3. ^{13}C NMR spectroscopic data (125 MHz) for the terpyridine, ethyleneoxy spacer and naphthyl ring carbon signals of $\boldsymbol{L^{10}}$-$\boldsymbol{L^{17}}$ in CDCl$_3$ solution at room temperature.

5.4 Mass spectrometric characterisation

Fast-atom bombardment mass spectrometry (FAB-MS) was used to characterise the ligands. FAB-MS is relatively harsh methods and fragmentation is observed when these techniques are used. Therefore, not only is the parent peak [M+H]$^+$ typically observed, but also other fragmentation peaks are detected (see **Section 5.8**).

5.5 Crystal structures of L^{14} and 2,7-di(2-hydroxyethoxy)naphthalene

(a) Crystal structure of L^{14}

A single crystal of L^{14}, which was obtained by the slow diffusion of diethyl ether into a chloroform solution of L^{14}, was suitable for X-ray crystallographic analysis (**Figure 11**). Crystallographic data are given in **Appendix IV** and selected bond lengths and angles are given in **Table 4**. The crystal structure of L^{14}, like other free 2,2′:6′,2″-terpyridine ligands[14,32,33], exists in a *trans-trans* conformation which minimises the repulsive N-N lone pair interactions that are present in the *cis-cis* conformation. The interannular C-C bonds, C5-C6, 1.491(6) Å, C7-C8, 1.472(6) Å, C37-C36, 1.468(7) Å, and C43-C44, 1.487(7) Å, and the other N-C, C-C bond lengths are within the reported range of 4′-[3-(1,2-dicarbadecaboranyl)propoxy]-2,2′:6′,2″-terpyridine.[14] The three pyridine rings of each domain are not exactly coplanar and the torsion angles between C4-C5-C6-N2, C9-C8-C7-N2, C41-C37-C36-N5 and C45-C44-C43-N5 are -1.53°, -16.11°, -2.68° and 1.19° respectively. These small deviations from planarity are typical for the free ligands.[32]
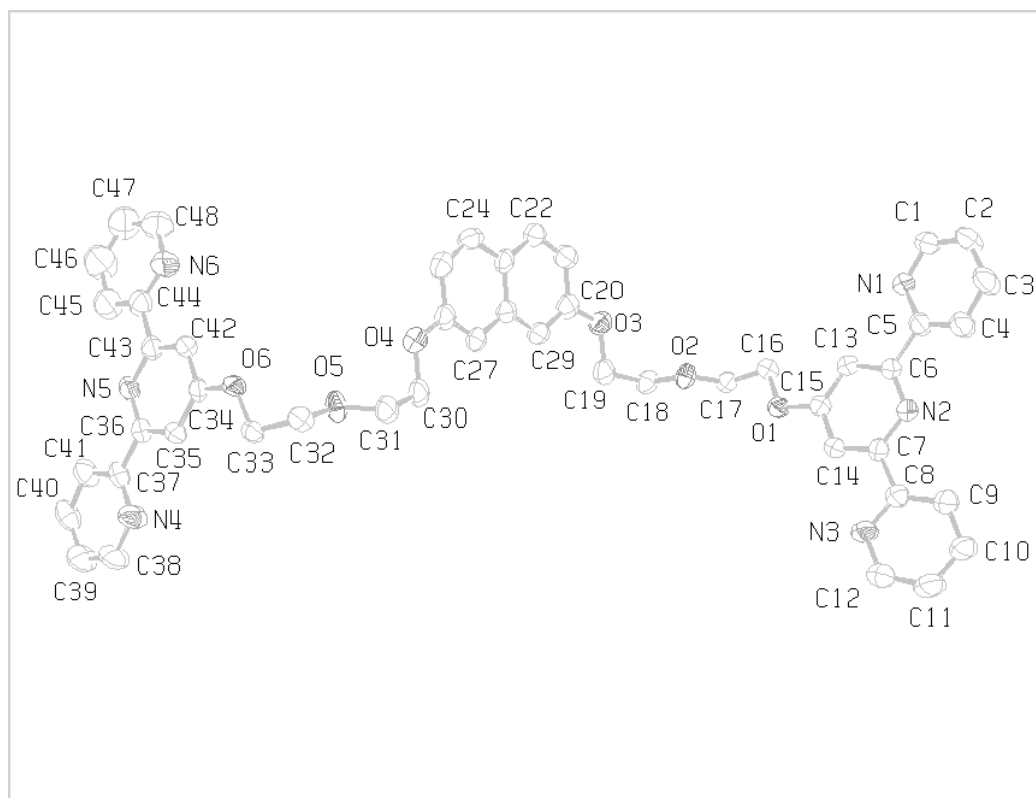
Figure 11. An ORTEP representation (50% probability ellipsoids) of **L^{14}**. Hydrogen atoms are omitted for clarity. Carbon atoms of the naphthyl group are numbered sequentially around the rings.

For the ethyleneoxy chain, the angles C15-O1-C16 and C34-O6-C33 are 117.8(3)° and 118.4(3)° respectively, which are comparable to the corresponding angle in 4′-ethoxy-5,5″-dimethyl-2,2′:6′,2″-terpyridine[34] and 4′-[3-(1,2-dicarbadecaboranyl)propoxy]-2,2′:6′,2″-terpyridine[14]. The bond lengths O1-C15 and O6-C34 are 1.363(5) Å and 1.355(5) Å respectively which, within experimental error, are the same as those in 4′-ethoxy-5,5″-dimethyl-2,2′:6′,2″-terpyridine (1.357(3) Å)[34] and 4′-[3-(1,2-dicarbadecaboranyl)propoxy]-2,2′:6′,2″-terpyridine (1.361(1) Å)[14]. Also, the bond lengths O1-C16, 1.425(5) Å and O6-C33, 1.436(5) Å are within the range reported in 4′-ethoxy-5,5″-dimethyl-2,2′:6′,2″-terpyridine (1.425(3) Å)[34] and 4′-[3-(1,2-dicarbadecaboranyl)propoxy]-2,2′:6′,2″-terpyridine (1.428(1) Å)[14]. The bond lengths of O1-C15 and O6-C34 are shorter than O1-C16 and O6-C33 and this suggests a degree of π-conjugation between the oxygen O1 and O6 atoms with the adjacent aromatic rings.

C5-C6	1.491(6)	C37-C36	1.468(7)	C15-O1	1.363(5)
C7-C8	1.472(6)	C43-C44	1.487(7)	O1-C16	1.425(5)
N1-C5	1.319(6)	N4-C37	1.325(7)	C19-O3	1.424(6)
C4-C5	1.389(7)	C37-C41	1.381(7)	O3-C20	1.359(6)
N1-C1	1.333(6)	N4-C38	1.339(7)	C26-O4	1.353(6)
N2-C6	1.335(6)	N5-C36	1.342(6)	O4-C30	1.425(6)
C6-C13	1.391(6)	C36-C35	1.389(6)	C33-O6	1.436(5)
N2-C7	1.351(6)	N5-C43	1.337(6)	O6-C34	1.355(5)
C7-C14	1.378(6)	C43-C42	1.376(7)		
N3-C8	1.330(6)	N6-C44	1.321(7)		
C8-C9	1.366(7)	C44-C45	1.370(8)		
N3-C12	1.337(7)	N6-C48	1.327(8)		
C5-N1-C1	117.6(4)	C37-N4-C38	117.3(5)	O1-C15-C13	124.1(4)
N1-C5-C4	122.3(5)	N4-C37-C41	121.9(5)	O1-C15-C14	115.9(4)
N1-C5-C6	116.6(4)	N4-C37-C36	116.5(4)	C16-O1-C15	117.8(3)
C4-C5-C6	121.1(4)	C41-C37-C36	121.7(5)	C19-O3-C20	118.4(4)
C13-C6-C5	119.4(4)	C35-C36-C37	120.2(4)	O3-C20-C21	114.9(5)
N2-C6-C5	116.7(4)	N5-C36-C37	117.1(4)	O3-C20-C29	124.7(5)
N2-C6-C13	123.6(4)	N5-C36-C35	122.6(4)	O6-C34-C35	125.1(4)
C6-N2-C7	117.1(4)	C36-N5-C43	118.0(4)	O6-C34-C42	115.3(4)
N2-C7-C14	122.5(4)	N5-C43-C42	122.7(4)	C33-O6-C34	118.4(3)
N2-C7-C8	116.7(4)	N5-C43-C44	117.2(4)	C30-O4-C26	117.8(4)
C8-C7-C14	120.7(4)	C44-C43-C42	120.1(5)	O4-C26-C25	113.9(4)
N3-C8-C7	116.0(4)	N6-C44-C43	115.3(5)	O4-C26-C27	125.2(5)
C7-C8-C9	121.4(5)	C43-C44-C45	121.5(5)		
N3-C8-C9	122.6(5)	N6-C44-C45	123.2(5)		
C8-N3-C12	117.1(5)	C44-N6-C48	117.1(6)		
C13-C15-C14	120.0(4)	C35-C34-C42	119.5(4)		
C4-C5-C6-N2	-1.53		C13-C15-O1-C16	14.62	
C9-C8-C7-N2	-16.11		C19-O3-C20-C29	2.79	
C41-C37-C36-N5	-2.68		C35-C34-O6-C33	4.59	
C45-C44-C43-N5	1.19		C30-O4-C26-C27	4.03	

Table 4. Selected bond lengths (Å) and angles (˚) of *L¹⁴*.

There are face-to-face π stacking interactions between the terpyridine domains. The plane-to-plane distance between the two terpyridine domains is around 3.6 Å. The closest distance between atom C4 of one pyridine ring and atom C37 of the other pyridine ring, and atom N2 of one pyridine ring and atom C42 of the other pyridine ring are 3.496 Å and 3.541 Å respectively (**Figure 12**).
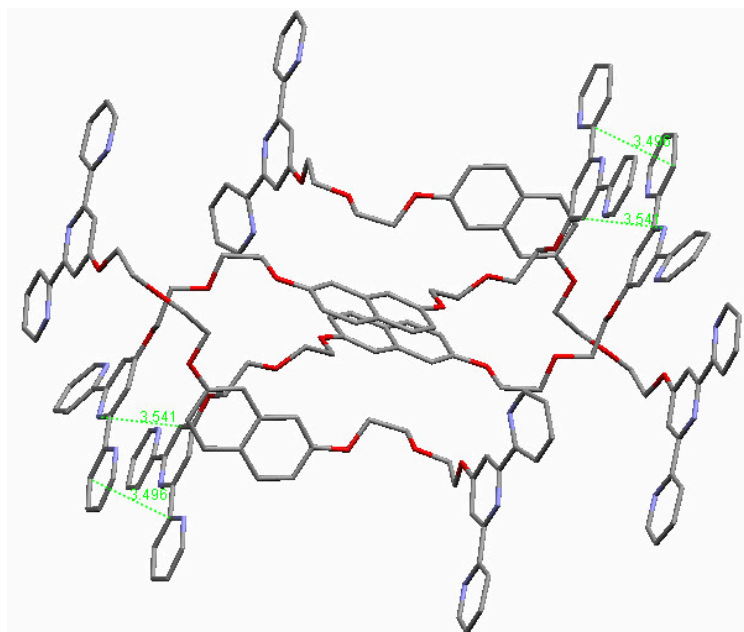
Figure 12. Packing diagram showing the π-π stacking interactions between the terpyridine domains in the unit cell (the dotted lines are the closest distance between two atoms involved in the π-π stacking interactions).

(b) Crystal structure of 2,7-di(2-hydroxyethoxy)naphthalene
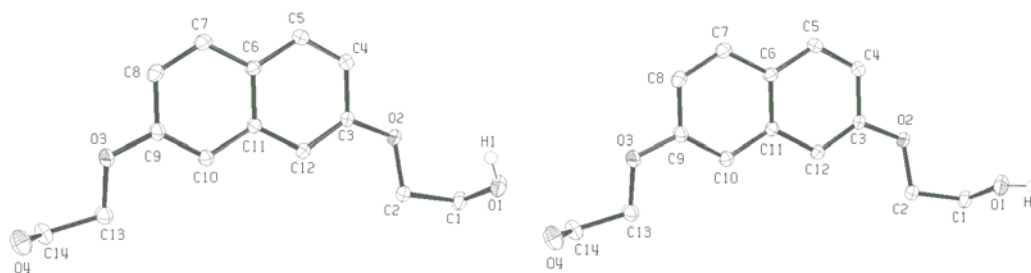
Figure 13. An ORTEP representation (50% probability ellipsoids) of 2,7-di(2-hydroxyethoxy)naphthalene. Hydrogen atoms (except H1 and H2) are omitted for clarity. The structure is disordered; with the H atom occupying two sites (H1 and H2) with 50% occupancy in each.

A single crystal of 2,7-di(2-hydroxyethoxy)naphthalene which was obtained by recrystallisation from methanol was suitable for X-ray crystallographic analysis

(**Figure 13**). Crystallographic data are given in **Appendix IV** and selected bond lengths and angles are given in **Table 5**.

O2-C3	1.362(1)	C3-C4	1.409(2)	C9-C10	1.374(2)
O2-C2	1.423(2)	C4-C5	1.362(2)	C10-C11	1.418(2)
O1-C1	1.422(2)	C5-C6	1.416(2)	C11-C12	1.419(2)
O3-C9	1.363(1)	C6-C7	1.411(2)	C12-C3	1.374(2)
O3-C13	1.423(2)	C7-C8	1.364(2)	C6-C11	1.416(2)
O4-C14	1.418(2)	C8-C9	1.408(2)		
O1-C1-C2	111.0(1)	C3-C4-C5	119.8(1)	C9-C10-C11	119.7(1)
C2-O2-C3	118.27(9)	C4-C5-C6	120.8(1)	C10-C11-C6	119.4(1)
O2-C3-C4	113.6(1)	C5-C6-C11	119.2(1)	C10-C11-C12	121.3(1)
O2-C3-C12	125.0(1)	C5-C6-C7	121.7(1)	C11-C12-C3	119.4(1)
O4-C14-C13	113.3(1)	C6-C7-C8	120.8(1)	C12-C3-C4	121.4(1)
C13-O3-C9	117.7(1)	C7-C8-C9	120.1(1)	C7-C6-C11	119.1(1)
O3-C9-C8	113.7(1)	C8-C9-C10	120.9(1)	C6-C11-C12	119.3(1)
O3-C9-C10	125.4(1)				
O1···O4	2.886	O4···O4	2.811	O1···O1	2.819
O1-H1-O4	172.26	O4-H4-O4	138.68	O1-H2-O1	167.03
C2-O2-C3-C12	-12.61		C13-O3-C9-C10	-5.49	

Table 5. Selected bond lengths (Å) and angles (°) of 2,7-di(2-hydroxyethoxy)naphthalene.

This is the precursor for the synthesis of L^{13}. One of the two OH groups in every molecule is disordered, with the H atom occupying two sites (H1 and H2) with 50% occupancy in each (**Figure 13**). **Figures 14a**, **14b** and **14c** show the intermolecular hydrogen bonding involving OH1 and OH2 respectively. There are hydrogen bonding intermolecular interactions between the O1-H1 and the O4 atoms, between the O4-H4 and O4 atoms, and between the O1-H2 and O1 atoms. Since the hydrogen positions in the crystal structure were calculated instead of measured, the hydrogen-bonded interactions were investigated by measuring the distance between the atom connected to the hydrogen, which is the oxygen atom, and the other oxygen atom. The O1-O4, O4-O4 and O1-O1 distance are 2.886 Å, 2.811 Å and 2.819 Å, which are within the usual range for a hydrogen bond.[35]
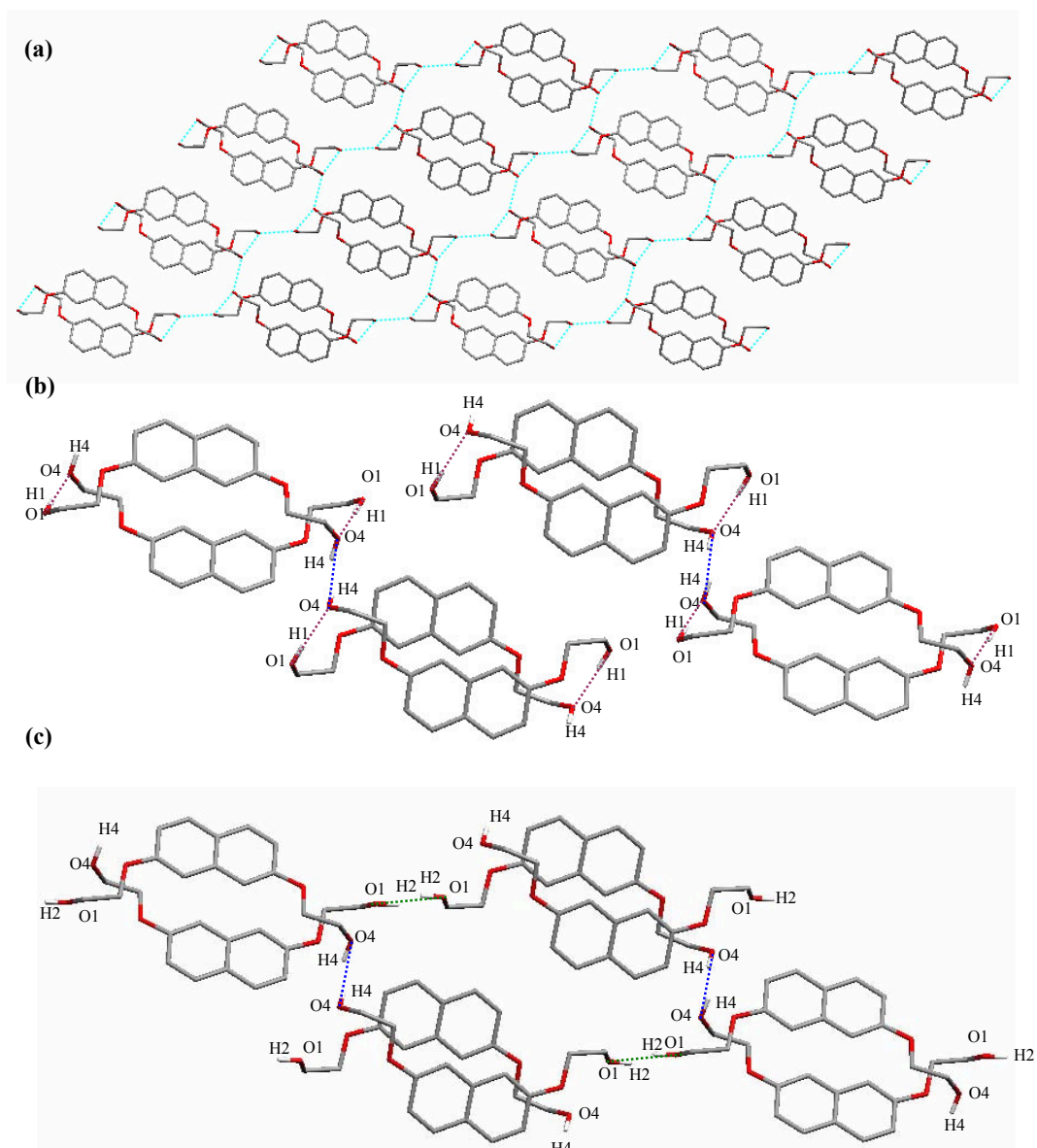
Figure 14. A view of the packing diagram of 2,7-di(2-hydroxyethoxy)naphthalene. The purple, blue and green lines indicate the hydrogen bonding intermolecular interactions between atom O1-H1 and atom O4, atom O4-H4 and atom O4, and atom O1-H1 and atom O1 respectively. Hydrogen atoms are omitted for clarity except atoms H1, H2 and H4.

5.6 The side product of the synthesis of L^{13}

From the ^{1}H NMR spectrum of the side product of the synthesis of L^{13} (**Figure 15b**), the ethyleneoxy proton signals at δ 4.2-4.7 and some of the naphthyl signals in the range δ 7.0-7.2 are no longer symmetrical compared to those of L^{13} (**Figure 15a**). Therefore, it seems that only one side of the ester-functional group of the 2,7-bis(2-methanesulfonatoethoxy)naphthalene was attached to the ***HO-terpy***. The terpyridine proton signals were compatible to L^{13} and were assigned as those of L^{13}.
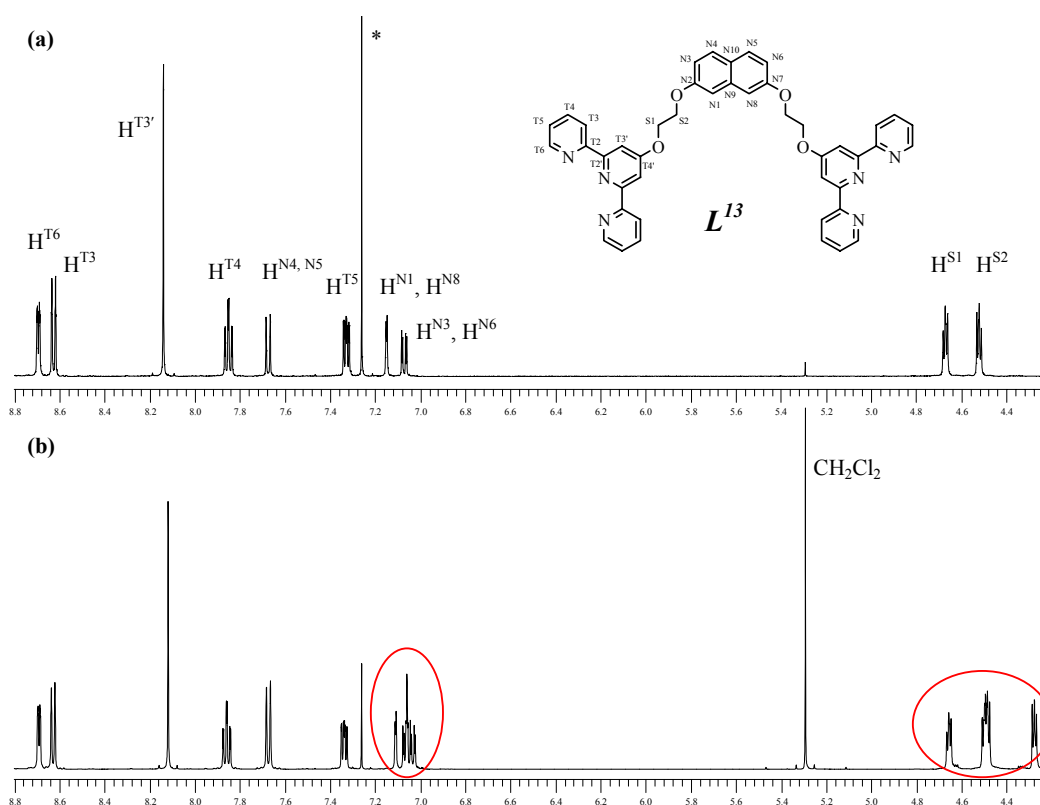
Figure 15. ^{1}H NMR spectra (500 MHz) of (a) L^{13} and (b) the side product of the synthesis of L^{13} in CDCl₃ solution at room temperature. The signal marked * is the signal for CHCl₃.

The ^{13}C NMR spectrum of this side product shows that the molecule is asymmetrical with respect to the central naphthalene unit. From the HMBC spectrum, there is an extra quaternary signal at δ 171, which coupled to the proton signals at δ 4.66 and δ 2.12 (**Figure 16**).The spectroscopic and FAB-MS data are consistent with the side product being 2-(2-acetoxyethoxy)-7-{2-(2,2′:6′,2″-terpyridin-4′-

yloxy)ethoxy}naphthalene. This implies that the side product arises from reaction of **HO-terpy** with the mono(methansulfonate)ester: 2-(2-acetoxyethoxy)-7-(2-methanesulfonyloxyethoxy)naphthalene (**Scheme 10**). This was probably formed by excess NH$_4$OAc remaining from the reaction of **HO-terpy** with the 2,7-bis(2-methanesulfonatoethoxy)naphthalene.
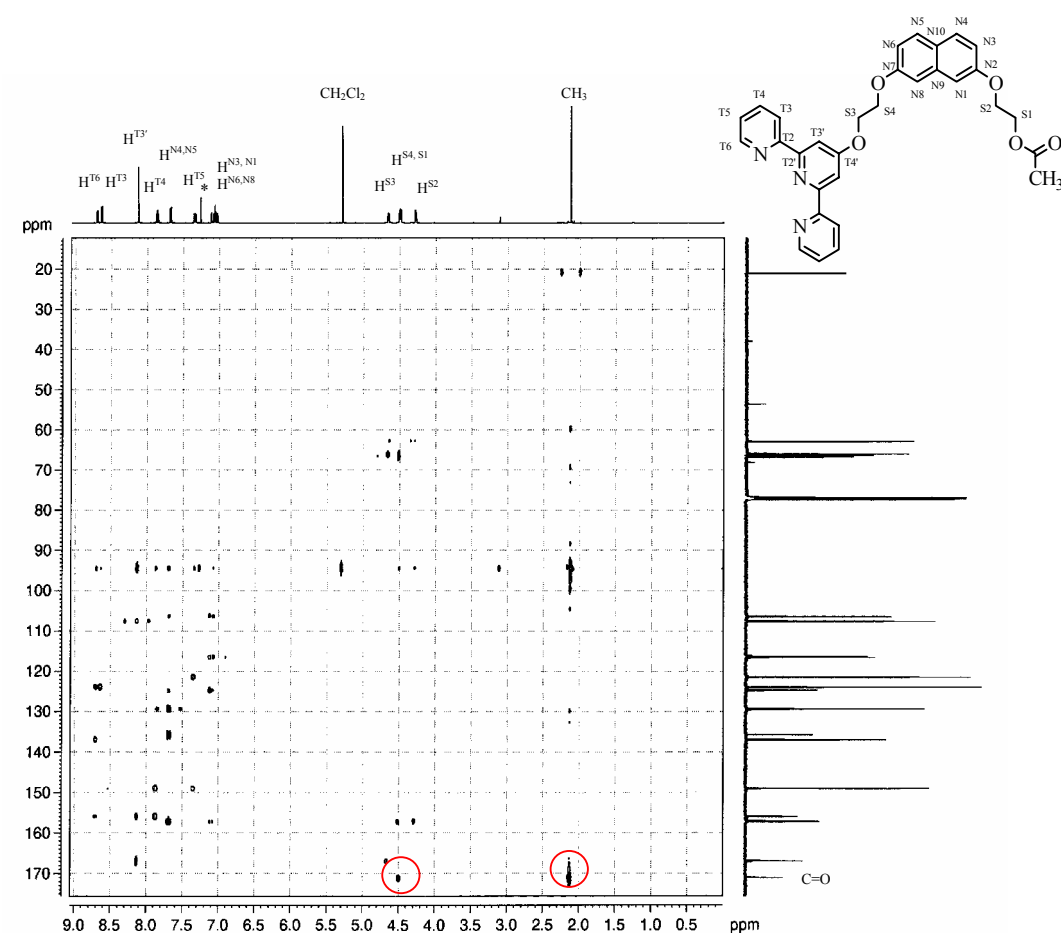
Figure 16. HMBC spectrum of the side product of the synthesis of L^{13} in CDCl$_3$ solution at room temperature. The signal marked * is the signal of CHCl$_3$.
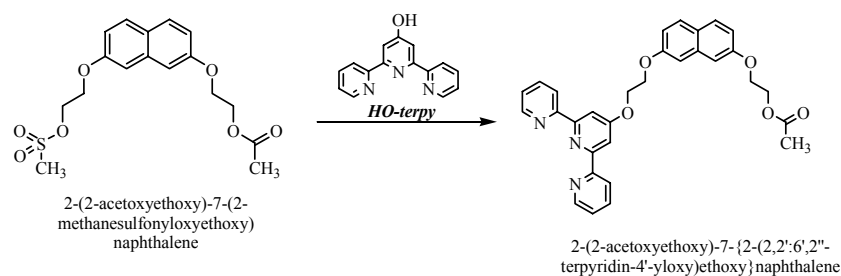
Scheme 10. Possible reaction for the formation of the side product.

5.7 Conclusion

In this chapter, homoditopic ligands L^{10}-L^{17}, which based upon a naphthalene unit bearing two 4′-substituted-2,2′:6′,2″-terpyridine-terminated bis(ethyleneoxy), were synthesised. All of these homoditopic 4′-substituted-2,2′:6′,2″-terpyridine ligands contain polyethyleneoxy chains which link to two different positions of the naphthalene unit and differ from one another in the length of the chains.

These ligands L^{10}-L^{17} have been synthesised and characterised with ^{1}H and ^{13}C NMR spectroscopy, mass spectrometry (FAB), IR spectroscopy and elemental analysis. The solid-state structure of ligand L^{12} and 2,7-di(2-hydroxyethoxy)naphthalene, which is a precursor for the synthesis of L^{13}, were determined by X-ray crystallography.

5.8   Experimental

❖ 2,6-Bis(2,2′:6′,2″-terpyridin-4′-yloxymethyl)naphthalene (***L^10***)

❖ 2,6-[Bis(2,2′:6′,2″-terpyridin-4′-yl)-1,4-dioxapentyl]naphthalene (***L^11***)

❖ 2,6-[Bis(2,2′:6′,2″-terpyridin-4′-yl)-1,4,7-trioxaoctyl]naphthalene (***L^12***)

❖ 2,7-[Bis(2,2′:6′,2″-terpyridin-4′-yl)-1,4-dioxabutyl]naphthalene (***L^13***)

❖ 2,7-Di[2-(2-hydroxyethoxy)ethoxy]naphthalene[36]

❖ 2,7-[Bis(2,2′:6′,2″-terpyridin-4′-yl)-1,4,7-trioxaheptyl]naphthalene (***L^14***)

❖ 2,7-Di{2-[2-(2-hydroxyethoxy)ethoxy]ethoxy}naphthalene

❖ 2,7-[Bis(2,2′:6′,2″-terpyridin-4′-yl)-1,4,7,10-tetraoxadecayl]naphthalene (***L^15***)

❖ 2,3-Di(ethoxycarbonylmethoxy)naphthalene

❖ 2,3-Di(2-hydroxyethoxy)naphthalene

❖ 2,3-[Bis(2,2′:6′,2″-terpyridin-4′-yl)-1,4-dioxabutyl]naphthalene (***L^16***)

❖ 2,3-Di[2-(2-hydroexyethoxy)ethoxy]naphthalene[37]

❖ 2,3-[Bis(2,2′:6′,2″-terpyridin-4′-yl)-1,4,7-trioxaheptyl]naphthalene (***L^17***)

4′-Hydroxy-2,2′:6′,2″-terpyridine (***HO-terpy***)[6], 4′-chloro-2,2′:6′,2″-terpyridine (***Cl-terpy***)[6], 2,6-bis(bromomethyl)naphthalene[38] and 2,7-bis(2-methanesulfonatoethoxy)naphthalene[39] were prepared as previously reported in the literature. ***L^1*** and ***L^2*** were prepared as in Chapter 2.

❖ 2,6-Bis(2,2′:6′,2″-terpyridin-4′-yloxymethyl)naphthalene (***L^10***)

2,6-Bis(2,2':6',2"-terpyridin-4'-yloxymethyl)naphthalene (***L^10***)

Molecular formula: $C_{42}H_{30}N_6O_2$
Molecular weight: 650.73
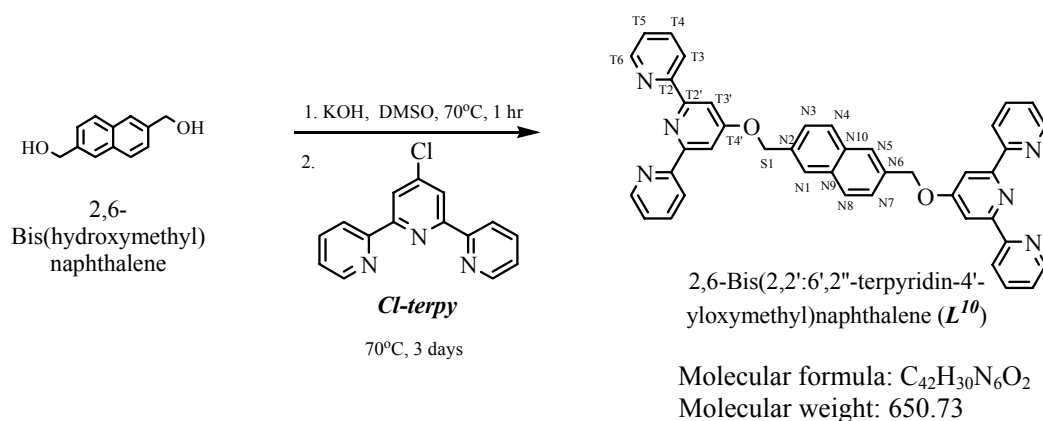
2,6-Bis(hydroxymethyl)naphthalene (0.50 g, 2.7 mmol) and finely powdered potassium hydroxide (1.8 g, 32 mmol) were stirred in 10 mL DMSO at 70ºC under nitrogen for 1 hour. The reaction mixture was kept stirring at 70ºC and under nitrogen throughout the reaction. 4′-Chloro-2,2′:6′,2″-terpyridine (***Cl-terpy***) (2.8 g, 10 mmol) in 5 mL DMSO was added to the suspension and the mixture was stirred for 3 days at 70ºC. The reaction mixture was cooled to room temperature and treated with water (300 mL). A yellow precipitate was obtained and was washed with plenty of water and dried. After column chromatography (Al$_2$O$_3$, CH$_2$Cl$_2$: hexane 2:1, then CH$_2$Cl$_2$/ 1% CH$_3$OH) and work up, a yellow powder of 2,6-bis(2,2′:6′,2″-terpyridin-4′-yloxymethyl)naphthalene (***L^{10}***) (0.5 g, 0.8 mmol, 30%) was obtained.

^{1}H NMR (400 MHz, CDCl$_3$): δ_H 5.51 (s, 4H, H^{S1}), 7.35 (ddd, *J* 1.0, 4.8, 7.3 Hz, 4H, H^{T5}), 7.62 (dd, *J* 1.3, 8.3 Hz, 2H, H$^{N3,\,N7}$), 7.87 (td, *J* 1.7, 7.7 Hz, 4H, H^{T4}), 7.92 (d, *J* 8.1 Hz, 2H, H$^{N4,\,N8}$), 7.99 (s, 2H, H$^{N1,\,N5}$), 8.19 (s, 4H, H$^{T3′}$), 8.64 (d, *J* 8.1 Hz, 4H, H^{T3}), 8.72 (dd, *J* 1.0, 4.0 Hz, 4H, H^{T6}).

^{13}C NMR (125 MHz, CDCl$_3$): δ_C 70.1 (C^{S1}), 107.8 (C$^{T3′}$), 121.5 (C^{T3}), 124.0 (C^{T5}), 125.8 (C$^{N3,\,N7}$), 126.4 (C$^{N1,\,N5}$), 128.7 (C$^{N4,\,N8}$), 133.1 (C$^{N9,\,N10}$), 134.1 (C$^{N2,\,N6}$), 137.0 (C^{T4}), 149.2 (C^{T6}), 156.2 (C^{T2}), 157.4 (C$^{T2′}$), 167.1 (C$^{T4′}$).

MS (FAB): *m/z* = 651 [M]$^+$ (29.5%), 402 [M-***O-terpy***]$^+$ (20.1%), 250 [***HO-terpy***]$^+$ (45.7%), 89 (46.7%), 77 (83.0%), 63 (55.4%), 51 (85.9%), 39 (100%).

IR(solid, cm^{-1}): 3055w, 3001w, 2924w, 2854w, 1734w, 1690w, 1605w, 1558s, 1512w, 1466m, 1443w, 1404s, 1350s, 1250w, 1196s, 1119w, 1095w, 1041m, 987w, 941m, 864s, 818w, 787s, 741m, 725m.

Elemental Analysis: Found: C, 76.31; H, 4.68; N, 12.22. Calc. for C$_{42}$H$_{30}$N$_6$O$_2$·¾CH$_3$OH: C, 76.09; H, 4.94; N, 12.46%.

Melting point: decomposes at around 230ºC.

❖ 2,6-[Bis(2,2′:6′,2″-terpyridin-4′-yl)-1,4-dioxapentyl]naphthalene (**L**^{11})

4'-(2-Hydroxyethoxy)-
2,2':6',2"-terpyridine
(**L**^{1})

1. NaH, THF, 80ºC, 1 hr
2.

in THF, 80ºC, 2 days

2,6-[Bis(2,2':6',2"-terpyridin-4'-yl)-1,4-
dioxapentyl]naphthalene (**L**^{11})
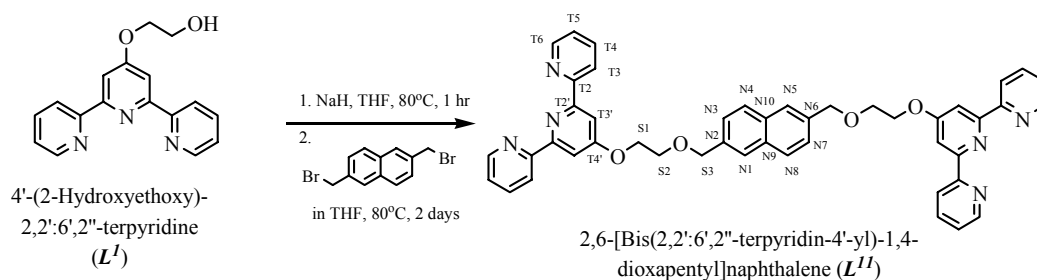
Molecular formula: $C_{46}H_{38}N_6O_4$

Molecular weight: 738.83

4′-(2-Hydroxyethoxy)-2,2′:6′,2″-terpyridine (**L**^{1}) (0.50 g, 1.7 mmol) and NaH (60% suspended in oil) (0.10 g, 2.5 mmol) were added to anhydrous THF (60 mL). The reaction mixture was stirred at 80ºC under nitrogen for 1 hour. Then, 2,6-bis(bromomethyl)naphthalene (0.22 g, 0.70 mmol) in 10 mL anhydrous THF was added dropwise to the suspension and the mixture was stirred for 2 days at 80ºC under nitrogen. The reaction was quenched with CH_3OH and water. The solvent was removed under reduced pressure. The solution was washed with CH_2Cl_2 (75 mL) twice. The organic layer was dried (MgSO$_4$), filtered and evaporated to dryness. The product **L**^{11} was obtained as a white powder (0.3 g, 0.4 mmol, 57%) after column chromatography (Al$_2$O$_3$, CH$_2$Cl$_2$/ 1% CH$_3$OH) and work up.

^{1}H NMR (500 MHz, CDCl$_3$): δ$_H$ 3.95 (t, *J* 4.7 Hz, 4H, H^{S2}), 4.45 (t, *J* 4.7 Hz, 4H, H^{S1}), 4.82 (s, 4H, H^{S3}), 7.32 (ddd, *J* 1.1, 4.8, 7.4 Hz, 4H, H^{T5}), 7.49 (dd, *J* 1.3, 8.3 Hz, 2H, H$^{N3, N7}$), 7.81 (m, 4H, H$^{N1, N5}$ and H$^{N4, N8}$), 7.84 (td, *J* 1.8, 7.7 Hz, 4H, H^{T4}), 8.07 (s, 4H, H$^{T3′}$), 8.61 (d, *J* 7.9 Hz, 4H, H^{T3}), 8.68 (m, 4H, H^{T6}).

^{13}C NMR (125 MHz, CDCl$_3$): δ$_C$ 67.8 (C^{S1}), 68.3 (C^{S2}), 73.5 (C^{S3}), 107.5 (C$^{T3′}$), 121.3 (C^{T3}), 123.8 (C^{T5}), 126.0 (C$^{N3, N7}$), 126.3 (C$^{N1, N5}$), 128.3 (C$^{N4, N8}$), 132.9 (C$^{N9, N10}$), 135.5 (C$^{N2, N6}$), 136.8 (C^{T4}), 149.1 (C^{T6}), 156.1 (C^{T2}), 157.1 (C$^{T2′}$), 167.0 (C$^{T4′}$).

ES (FAB): *m/z* = 739 [M]$^+$ (50.4%), 462 [M-**TerpyOCH$_2$CH$_2$**]$^+$ (23.7%), 277 [**Terpy-OCH$_2$CH$_2$**]$^+$ (24.6%), 250 [**HO-Terpy**]$^+$ (100%), 221 (56.6%).

IR (solid, cm^{-1}): 3097w, 3063w, 3045w, 3016w, 2962w, 29392, 2914w, 2870w, 2243w, 2189w, 1796w, 1793w, 1602w, 1583m, 1560s, 1468m, 1441m, 1404m, 1371m, 1346s, 1286w, 1275w, 1254m, 1238w, 1202s, 1169w, 1122m, 1095s, 1061m, 1043w, 1011m, 989m, 960m, 889m, 879m, 866m, 825s, 791m, 738s, 729m.

Elemental Analysis: Found: C, 73.35; H, 5.26; N, 11.00. Calc. for $C_{46}H_{38}N_6O_4 \cdot CH_3OH$: C, 73.23; H, 5.50; N, 10.90%.

Melting point: 181.3ºC-183.9ºC.

❖ 2,6-[Bis(2,2′:6′,2″-terpyridin-4′-yl)-1,4,7-trioxaoctyl]naphthalene (L^{12})

4′-[2-(2-Hydroxyethoxy)ethoxy]-
2,2′:6′,2″-terpyridine (L^2)

1. NaH, THF, 80ºC

2. (Br...Br) in THF, 80ºC, 4 days

2,6-[Bis(2,2′:6′,2″-terpyridin-4′-yl)-1,4,7-
trioxaoctyl]naphthalene (L^{12})
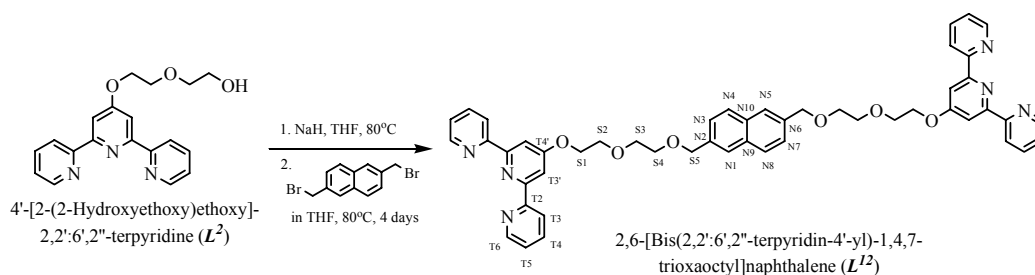
Molecular formula: $C_{50}H_{46}N_6O_6$
Molecular weight: 826.9

4′-[2-(2-Hydroxyethoxy)ethoxy]-2,2′:6′,2″-terpyridine (L^2) (0.7 g, 2 mmol) and NaH (60% suspended in oil) (0.12 g, 3.0 mmol) were added to anhydrous THF (50 mL). The reaction mixture was stirred at 80ºC under nitrogen for 1 hour. 2,6-Bisbromomethylnaphthalene (0.25 g, 0.80 mmol) in 30 mL dry THF was added dropwise to the suspension and the mixture was stirred for 4 days at 80ºC under nitrogen. The reaction was quenched with CH_3OH and water. The solvent was removed under reduced pressure. The yellow crude product was extracted with CH_2Cl_2 (50 mL) twice. The organic layer was dried ($MgSO_4$), filtered and evaporated to dryness. The product L^{12} was obtained as yellow oil (0.10 g, 0.12 mmol, 15%) after column chromatography (Al_2O_3, CH_2Cl_2/ 1% CH_3OH) and work up.

^{1}H NMR (500 MHz, $CDCl_3$): δ_H 3.70 (m, 4H, H^{S4}), 3.80 (m, 4H, H^{S3}), 3.95 (t, *J* 4.7 Hz, 4H, H^{S2}), 4.41 (t, *J* 4.7 Hz, 4H, H^{S1}), 4.72 (s, 4H, H^{S5}), 7.32 (dd, *J* 4.9, 6.5 Hz, 4H, H^{T5}), 7.44 (d, *J* 8.2 Hz, 2H, $H^{N3, N7}$), 7.74 (s, 2H, $H^{N1, N5}$), 7.77 (d, *J* 8.4 Hz, 2H, $H^{N4, N8}$), 7.84 (td, *J* 1.6, 7.7 Hz, 4H, H^{T4}), 8.05 (s, 4H, $H^{T3'}$), 8.60 (d, *J* 7.9 Hz, 4H, H^{T3}), 8.67 (d, *J* 4.1 Hz, 4H, H^{T6}).

^{13}C NMR (125 MHz, $CDCl_3$): δ_C 67.8 (C^{S1}), 69.5 (C^{S2} and C^{S4}), 71.1 (C^{S3}), 73.4 (C^{S5}), 107.5 ($C^{T3'}$), 121.3 (C^{T3}), 123.8 (C^{T5}), 126.0 ($C^{N3, N7}$), 126.3 ($C^{N1, N5}$), 128.2 ($C^{N4, N8}$), 132.8 ($C^{N9, N10}$), 135.7 ($C^{N2, N6}$), 136.8 (C^{T4}), 149.1 (C^{T6}), 156.1 (C^{T2}), 157.1 ($C^{T2'}$), 167.0 ($C^{T4'}$).

MS (FAB): *m/z* = 827 [**M**]$^+$ (23.6%), 262 [***Terpy-OCH$_2$***]$^+$ (31.2%), 250 [***HO-Terpy***]$^+$ (100%), 221 (27.8%), 136 (40.2%), 89 (42.1%), 77 (58.4%), 65 (25.5%), 57 (21.1%), 51 (34.4%), 41 (29.5%), 39 (45.4%).

IR (solid, cm^{-1}): 3057w, 2866w, 2860w, 1717w, 1600w, 1581m, 1558s, 1469m, 1441m, 1405m, 1347m, 1278w, 1252w, 1202m, 1125w, 1090m, 1055m, 1038m, 990m, 966m, 867m, 819w, 791s, 743m, 733m.

Elemental Analysis: Found: C, 72.22; H, 5.89; N, 10.20. Calc. for $C_{50}H_{46}N_6O_6$: C, 72.62; H, 5.62; N, 10.17%.

❖ 2,7-[Bis(2,2′:6′,2″-terpyridin-4′-yl)-1,4-dioxabutyl]naphthalene (***L^{13}***)

2,7-[Bis(2,2':6',2"-terpyridin-4'-yl)-1,4-dioxabutyl]naphthalene (***L^{13}***)
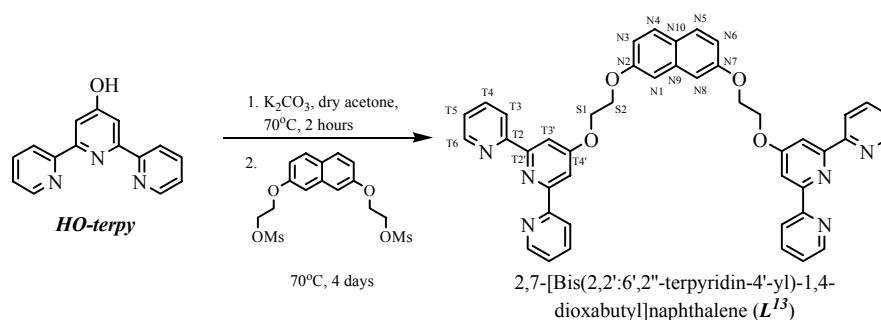
Molecular formula: $C_{44}H_{34}N_6O_4$

Molecular weight: 710.78

4′-Hydroxy-2,2′:6′,2″-terpyridine (***HO-Terpy***) (3.0 g, 12 mmol) was stirred with dry K$_2$CO$_3$ (16.7 g, 121 mmol) in 120 mL dry acetone for 2 hours at 70ºC under nitrogen. The reaction mixture was kept at 70ºC under nitrogen throughout the reaction. 2,7-Bis(2-methanesulfonatoethoxy)naphthalene (0.69 g, 1.7 mmol) was added to the reaction mixture. The reaction was completed after 4 days. The reaction mixture was then filtered and the solvent was removed. The crude product was extracted with CH$_2$Cl$_2$ (200 mL) and water (200 mL). The product was purified by column chromatography (Al$_2$O$_3$, CH$_2$Cl$_2$/ 0.5% CH$_3$OH). The second fraction was the product 2,7-[bis(2,2′:6′,2″-terpyridin-4′-yl)-1,4-dioxabutyl]naphthalene (***L^{13}***) as a white powder (0.7 g, 0.98 mmol, 58%).

^{1}H NMR (500 MHz, CDCl$_3$) δ_H 4.52 (m, 4H, H^{S2}), 4.67 (m, 4H, H^{S1}), 7.07 (dd, *J* 2.5, 8.9 Hz, 2H, H$^{N3, N6}$), 7.15 (d, *J* 2.5 Hz, 2H H$^{N1, N8}$), 7.33 (ddd, *J* 1.2, 4.8, 7.5 Hz, 4H, H^{T5}), 7.67 (d, *J* 9.0 Hz, 2H, H$^{N4, N5}$), 7.85 (td, *J* 1.8, 7.7 Hz, 4H, H^{T4}), 8.14 (s, 4H, H$^{T3'}$), 8.63 (dt, *J* 1.0, 8.0 Hz, 4H, H^{T3}), 8.69 (ddd, *J* 0.9, 1.8, 4.8 Hz, 4H, H^{T6}).

^{13}C NMR (125 MHz, CDCl$_3$): δ$_C$ 66.4 (C^{S2}), 66.7 (C^{S1}), 106.8 (C$^{N1,\,N8}$), 107.7 (C$^{T3'}$), 116.5 (C$^{N3,\,N6}$), 121.4 (C^{T3}), 123.8 (C^{T5}), 124.9 (C^{N10}), 129.3 (C$^{N4,\,N5}$), 135.8 (C^{N9}), 136.8 (C^{T4}), 148.9 (C^{T6}), 156.0 (C^{T2}), 157.2 (C$^{T2'}$ and C$^{N2,\,N7}$), 167.0 (C$^{T4'}$).

MS (FAB): *m/z* = 711 [M]$^+$ (51.7%), 250 [***HO-Terpy***]$^+$ (100%), 221 (46.9%), 57 (56.7%), 43 (59.5%).

IR (solid, cm^{-1}): 3680w, 3252w, 3061w, 2881w, 2311w, 1630w, 1597w, 1580m, 1560s, 1514m, 1468m, 1447w, 1439w, 1406s, 1387m, 1354m, 1329w, 1259m, 1229m, 1202s, 1155w, 1136w, 1068m, 1035m, 991m, 974w, 926w, 885w, 868m, 831s, 791s, 741s, 731s.

Elemental Analysis: Found: C, 73.42; H, 4.96; N, 11.43. Calc. for C$_{44}$H$_{34}$N$_6$O$_4$·½CH$_3$OH: C, 73.53; H, 5.00; N, 11.57%.

Melting point: 179.7ºC-181.4ºC.

Side product (fraction 1):
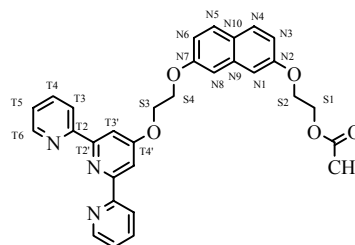
Molecular formula: C$_{31}$H$_{27}$N$_3$O$_5$

Molecular weight: 521.56

^{1}H NMR (500 MHz, CDCl$_3$) δ$_H$ 2.12 (s, 3H, H^{CH3}), 4.28 (m, 2H, H^{S2}), 4.49 (m, 4H, H^{S1} and H^{S4}), 4.66 (m, 2H, H^{S3}), 7.03 (dd, *J* 2.5, 8.8 Hz, 1H, H^{N3}), 7.07 (m, 2H, H^{N1} and H^{N6}), 7.11 (d, *J* 2.5 Hz, 1H H^{N8}), 7.34 (ddd, *J* 1.2, 4.8, 7.3 Hz, 2H, H^{T5}), 7.67 (d, *J* 8.8 Hz, 2H, H^{N4} and H^{N5}), 7.86 (td, *J* 1.8, 7.7 Hz, 2H, H^{T4}), 8.12 (s, 2H, H$^{T3'}$), 8.63 (dt, *J* 1.0, 8.0 Hz, 2H, H^{T3}), 8.69 (ddd, *J* 0.9, 1.8, 4.8 Hz, 2H, H^{T6}).

^{13}C NMR (125 MHz, CDCl$_3$): δ$_C$ 21.0 (C^{CH3}), 62.9 (C^{S1}), 65.9 (C^{S2}), 66.2 (C^{S4}), 66.7 (C^{S3}), 106.3 (C^{N1}), 106.4 (C^{N8}), 107.6 (C$^{T3'}$), 116.4 (C^{N3}), 116.6 (C^{N6}), 121.4 (C^{T3}), 123.9 (C^{T5}), 124.7 (C^{N10}), 129.3 (C^{N5} and C^{N4}), 135.7 (C^{N9}), 136.9 (C^{T4}), 149.0 (C^{T6}), 155.9 (C^{T2}), 157.1 (C^{N2} and C$^{T2'}$), 157.2 (C^{N7}), 166.9 (C$^{T4'}$), 171.1 (C^{CO}).

ES (FAB): *m/z* = 522 [M]$^+$ (39.6%), 250 [***HO-Terpy***]$^+$ (20.6%), 87 [CH$_3$CO$_2$CH$_2$CH$_2$]$^+$ (100.0%), 57 (22.3%), 43 [CH$_3$CO]$^+$ (55.3%).

IR (solid, cm^{-1}): 3607w, 3371br, 3059w, 2935w, 2881w, 1736s, 11628m, 1582m, 1562m, 1516m, 1470m, 1439m, 1389m, 1354m, 1300w, 1250m, 1204s, 1173m, 1142w, 1119w, 1092w, 1065m, 1041s, 995m, 964m, 941w, 918w, 872w, 841s, 791s, 729m.

Elemental Analysis: Found: C, 69.90; H, 5.48; N, 6.98. Calc. for C$_{31}$H$_{27}$N$_3$O$_5$·CH$_3$OH: C, 69.43; H, 5.64; N, 7.59%.

Melting point: 122.7ºC-124.6ºC.

❖ 2,7-Di[2-(2-hydroexyethoxy)ethoxy]naphthalene[36]
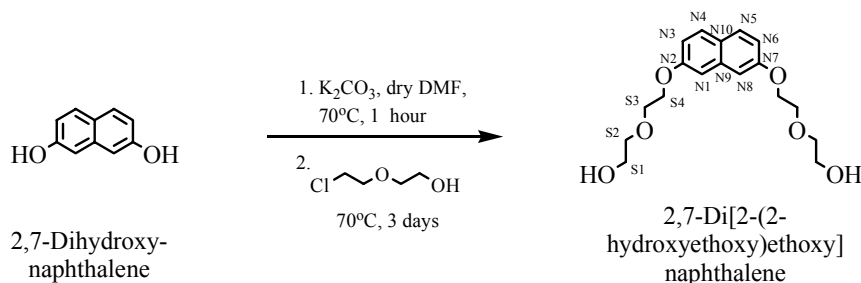
Molecular formula: $C_{18}H_{24}O_6$

Molecular weight: 336.38

2,7-Dihydroxynaphthalene (1.0 g, 6.2 mmol), K_2CO_3 (5.18 g, 37.5 mmol) were stirred in 60 mL dry DMF for 1 hour at 70ºC under nitrogen. The reaction mixture was kept at 70ºC under nitrogen throughout the reaction. Then, 2-(2-chloroethoxy)ethanol (2.3 g, 18 mmol) was added dropwise to the reaction mixture. After 1 day, 1 mL of 2-(2-chloroethoxy)ethanol was added and the reaction mixture was kept at 70ºC for 2 days. The reaction mixture was cooled to room temperature. The solvent was removed in vacuo and the residue partitioned between CH_2Cl_2 and water (200 mL). The organic layer was separated and dried ($MgSO_4$). The crude product was filtered and evaporated. The pure product was obtained after column chromatography (Al_2O_3, CH_2Cl_2/ 5% CH_3OH) and was isolated as a pale green powder (0.8 g, 2.4 mmol, 39%).

^{1}H NMR (500 MHz, CDCl$_3$) δ_H 2.36 (br, 2H, H^{OH}), 3.69 (m, 4H, H^{S2}), 3.78 (m, 4H, H^{S1}), 3.91 (m, 4H, H^{S3}), 4.23 (m, 4H, H^{S4}), 7.02 (m, 4H, H$^{N3, N6}$ and H$^{N1, N8}$), 7.65 (m, 2H, H$^{N4, N5}$).

^{13}C NMR (125 MHz, CDCl$_3$): δ_C 61.8 (C^{S1}), 67.4 (C^{S4}), 69.7 (C^{S3}), 72.6 (C^{S2}), 106.3 (C$^{N1, N8}$), 116.4 (C$^{N3, N6}$), 124.6 (C^{N10}), 129.2 (C$^{N4, N5}$), 135.7 (C^{N9}), 157.2 (C$^{N2, N7}$).

MS (EI): m/z = 336 [M]$^+$ (64.2%), 248 [M-(CH$_2$CH$_2$O)$_2$]$^+$ (27.6%), 160 [HO-Nap-OH]$^+$ (89.7%), 45 (100%).

IR (solid, cm^{-1}): 3398br, 3312br, 2935w, 2980m, 1896w, 1798w, 1745m, 1742m, 1717w, 1693w, 1630m, 1697w, 1560w, 1516m, 1487w, 1460w, 1437w, 1387m, 1339w, 1312w, 1252s, 1213s, 1177m, 1122s, 1090m, 1057m, 1030m, 1003m, 978w, 953w, 899w, 852m, 833m, 820m, 783w, 710w.

Elemental Analysis: Found: C, 63.73; H, 7.12; O, 29.19. Calc. for $C_{18}H_{24}O_6 \cdot \frac{1}{4}H_2O$: C, 63.42; H, 7.26; N, 29.34%.

Melting point: 66.5ºC-67.3ºC.

❖ 2,7-[Bis(2,2′:6′,2″-terpyridin-4′-yl)-1,4,7-trioxaheptyl]naphthalene (***L¹⁴***)

2,7-Di[2-(2-hydroxyethoxy)ethoxy] naphthalene

Cl-terpy

1. KOH, DMSO, 70ºC, 1 hr

2.

70ºC, 3 days

2,7-[Bis(2,2′:6′,2″-terpyridin-4′-yl)-1,4,7-trioxaheptyl]naphthalene (***L¹⁴***)
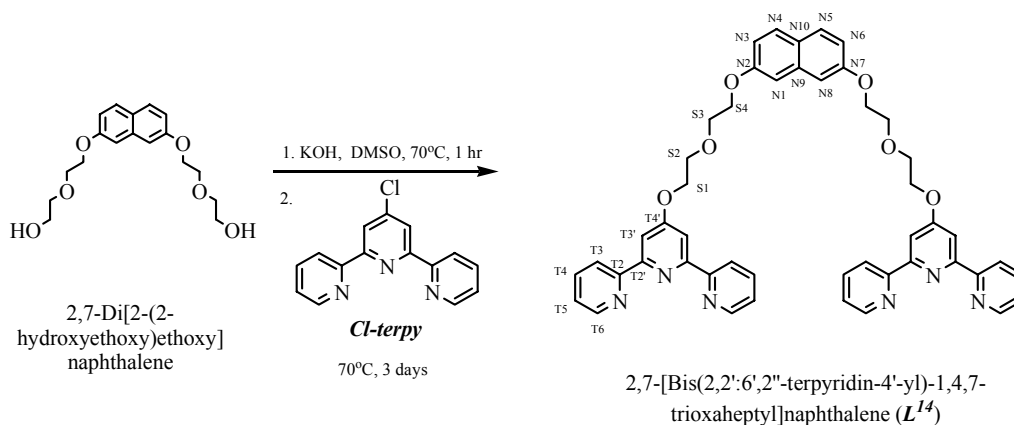
Molecular formula: $C_{48}H_{42}N_6O_6$

Molecular weight: 798.88

2,7-Di[2-(2-hydroxyethoxy)ethoxy]naphthalene (400 mg, 1.19 mmol) was added to a suspension of finely powdered potassium hydroxide (800 mg, 14.3 mmol) in 10 mL dry DMSO and the mixture was stirred for 1 hour at 70ºC under nitrogen. The reaction mixture was kept at 70ºC under nitrogen throughout the reaction. After this period, 4′-chloro-2,2′:6′,2″-terpyridine (***Cl-terpy***) (1.3 g, 4.9 mmol) was added and the reaction mixture was heated to 70ºC for 3 days. The reaction mixture was cooled to room temperature and treated with water (500 mL) to give a white precipitate, which was washed with plenty of water and dried to give white powder of 2,7-[bis(2,2′:6′,2″-terpyridin-4′-yl)-1,4,7-trioxaheptyl]naphthalene (***L¹⁴***) (0.7 g, 0.88 mmol, 74%).

¹H NMR (500 MHz, CDCl₃) δ_H 4.02 (m, 8H, H^{S3} and H^{S2}), 4.25 (t, *J* 4.8 Hz, 4H, H^{S4}), 4.44 (t, *J* 4.7 Hz, 4H, H^{S1}), 7.02 (m, 4H, H$^{N3, N6}$ and H$^{N1, N8}$), 7.31 (ddd, *J* 1.2, 4.8, 7.5 Hz, 4H, H^{T5}), 7.60 (d, *J* 8.7 Hz, 2H, H$^{N4, N5}$), 7.84 (td, *J* 1.8, 7.7 Hz, 4H, H^{T4}), 8.05 (s, 4H, H$^{T3′}$), 8.60 (dt, *J* 1.0, 8.0 Hz, 4H, H^{T3}), 8.67 (ddd, *J* 0.9, 1.8, 4.8 Hz, 4H, H^{T6}).

¹³C NMR (125 MHz, CDCl₃): δ_C 67.6 (C^{S4}), 68.0 (C^{S1}), 69.8 (C^{S2}), 70.2 (C^{S3}), 106.4 (C$^{N1, N8}$), 107.6 (C$^{T3′}$), 116.6 (C$^{N3, N6}$), 121.5 (C^{T3}), 124.0 (C^{T5}), 124.6 (C^{N10}), 129.2 (C$^{N4, N5}$), 135.9 (C^{N9}), 136.9 (C^{T4}), 149.2 (C^{T6}), 156.2 (C^{T2}), 157.3 (C$^{T2′}$), 157.4 (C$^{N2, N7}$), 167.1 (C$^{T4′}$).

MS (FAB): *m/z* = 799 [M]$^+$ (30.5%), 262 [M-***TerpyOCH$_2$***]$^+$ (20.9%), 250 [***HO-Terpy***]$^+$ (100.0%), 89 [OCH$_2$CH$_2$OCH$_2$CH$_2$]$^+$ (21.4%), 78 (26.4%), 77 (25.9%), 51 (28.9%).

IR (solid, cm^{-1}): 3055w, 2920w, 2874w, 1628m, 1582s, 1560s, 1516m, 1468m, 1441m, 1404s, 1350s, 1254m, 1202s, 1128s, 1090m, 1057s, 991s, 962m, 868m, 835m, 793s, 743s, 733s.

Elemental Analysis: Found: C, 70.06; H, 5.24; N, 10.00. Calc. for C$_{48}$H$_{42}$N$_6$O$_6$·H$_2$O: C, 70.57; H, 5.44; N, 10.29%.

Melting point: 116.4ºC-117.8ºC.

❖ 2,7-Di{2-[2-(2-hydroxyethoxy)ethoxy]ethoxy}naphthalene

2,7-Di{2-[2-(2-
hydroxyethoxy)ethoxy]ethoxy}
naphthalene

Molecular formula: C$_{22}$H$_{32}$O$_8$

Molecular weight: 424.48
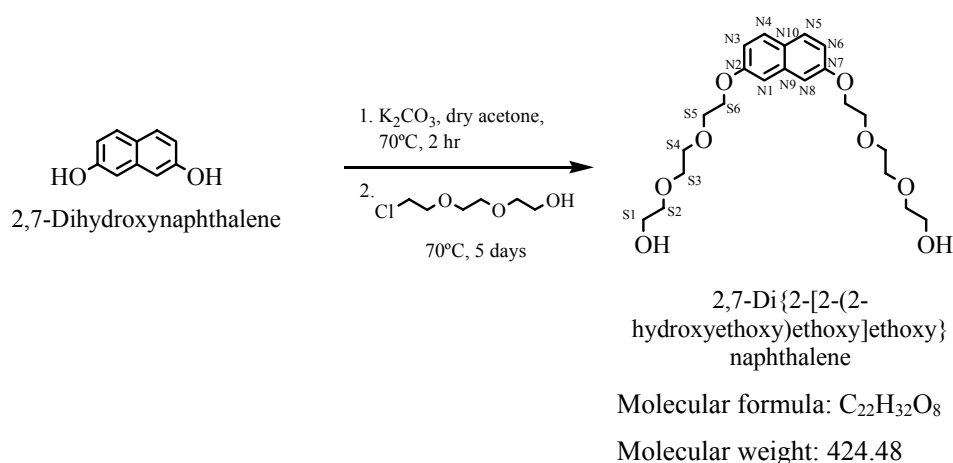
2,7-Dihydroxynaphthalene (1.6 g, 0.010 mol), K$_2$CO$_3$ (12 g, 0.090 mol) were stirred in 150 mL dry acetone for 2 hour at 70ºC under nitrogen. The reaction mixture was kept at 70ºC under nitrogen throughout the reaction. Then, 2-[2-(2-chloroethoxy)ethoxy]ethanol (5.06 g, 0.0300 mol) was added dropwise to the reaction mixture. After 3 day, 1.45 mL of 2-[2-(2-chloroethoxy)ethoxy]ethanol was added and the reaction mixture was kept at 70ºC for 2 days. The reaction mixture was cooled to room temperature. The solvent was removed in vacuo and the residue partitioned between CH$_2$Cl$_2$ and water (250 mL). The organic layer was separated and dried (MgSO$_4$). The product was obtained after filtration and drying to give a black oily solution (3.5 g, 8.2 mmol, 82%).

^{1}H NMR (500 MHz, CDCl$_3$) δ_H 2.76 (br, 2H, H^{OH}), 3.60 (m, 4H, H^{S2}), 3.71 (m, 12H, H^{S3}, H^{S1} and H^{S4}), 3.89 (m, 4H, H^{S5}), 4.22 (m, 4H, H^{S6}), 7.01 (m, 4H, H$^{N3, N6}$ and H$^{N1, N8}$), 7.62 (d, *J* 8.8 Hz, 2H, H$^{N4, N5}$).

^{13}C NMR (125 MHz, CDCl$_3$): δ$_C$ 61.8 (C^{S1}), 67.4 (C^{S6}), 69.8 (C^{S5}), 70.4 (C^{S3}), 70.9 (C^{S4}), 72.6 (C^{S2}), 106.3 (C$^{N1, N8}$), 116.5 (C$^{N3, N6}$), 124.6 (C^{N10}), 129.2 (C$^{N4, N5}$), 135.8 (C^{N9}), 157.3 (C$^{N2, N7}$).

MS (FAB): *m/z* = 425 [M]$^+$ (22.7%), 45 (100%).

IR (solid, cm^{-1}): 3418br, 2916m, 2870m, 1628s, 1512m, 1458m, 1358w, 1258m, 1211s, 1119s, 1065s, 957w, 887w, 833w.

Elemental Analysis: Found: C, 61.46; H, 7.57. Calc. for C$_{22}$H$_{32}$O$_8$·⅓H$_2$O: C, 61.37; H, 7.66%.

❖ 2,7-[Bis(2,2′:6′,2″-terpyridin-4′-yl)-1,4,7,10-tetraoxadecayl]naphthalene (**L^{15}**)

2,7-Di{2-[2-(2-hydroxyethoxy)ethoxy]ethoxy} naphthalene

Cl-terpy

70°C, 5 days

1. KOH, DMSO, 70°C, 1 hr
2.

2,7-[Bis(2,2′:6′,2″-terpyridin-4′-yl)-1,4,7,10-tetraoxadecayl]naphthalene (**L^{15}**)
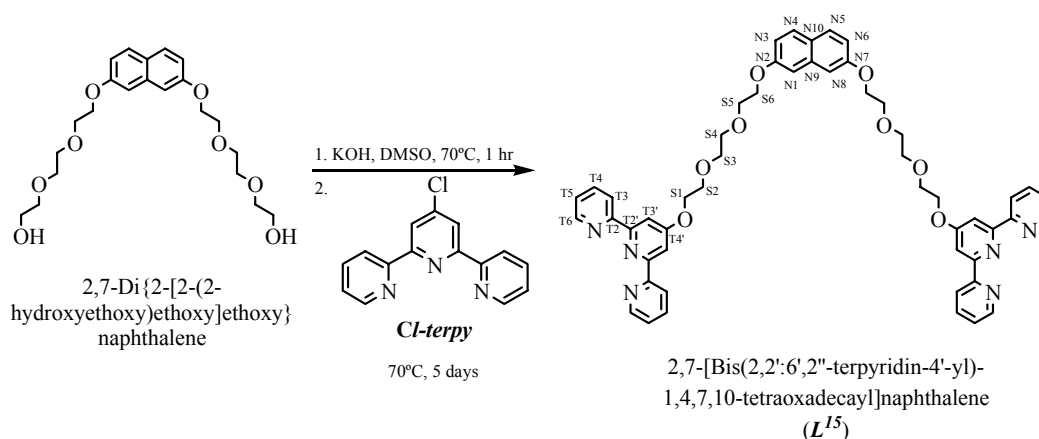
Molecular formula: C$_{52}$H$_{50}$N$_6$O$_8$

Molecular weight: 886.99

2,7-Di{2-[2-(2-hydroxyethoxy)ethoxy]ethoxy}naphthalene (0.70 g, 1.6 mmol) was added to a suspension of finely powdered potassium hydroxide (1.1 g, 20 mmol) in 15 mL dry DMSO and the mixture was stirred for 1 hour at 70°C under nitrogen. The reaction mixture was kept at 70°C under nitrogen throughout the reaction. After this period, 4′-chloro-2,2′:6′,2″-terpyridine (**Cl-terpy**) (1.3 g, 4.9 mmol) was added and the reaction mixture was heated to 70°C for 5 days. The reaction mixture was cooled to room temperature and treated with water (500 mL) to give a white precipitate, which was washed with plenty of water and dried. The crude product was purified from column chromatography (Al$_2$O$_3$, CH$_2$Cl$_2$/ 0.5% CH$_3$OH) to give 2,7-[bis(2,2′:6′,2″-terpyridin-4′-yl)-1,4,7,10-tetraoxadecayl]naphthalene (**L^{15}**) (0.20 g, 0.23 mmol, 14%) as an oily liquid.

^{1}H NMR (500 MHz, CDCl$_3$) δ$_H$ 3.78 (m, 8H, H^{S4} and H^{S3}), 3.91 (t, *J* 4.8 Hz, 4H, H^{S5}), 3.93 (t, *J* 4.7 Hz, 4H, H^{S2}), 4.19 (t, *J* 4.9 Hz, 4H, H^{S6}), 4.39 (t, *J* 4.7 Hz, 4H, H^{S1}), 6.98 (m,

4H, H$^{N3, N6}$ and H$^{N1, N8}$), 7.31 (ddd, *J* 1.2, 4.8, 7.5 Hz, 4H, H^{T5}), 7.58 (d, *J* 9.6 Hz, 2H, H^{N4,} ^{N5}), 7.83 (td, *J* 1.8, 7.7 Hz, 4H, H^{T4}), 8.04 (s, 4H, H$^{T3'}$), 8.59 (dt, *J* 1.0, 7.9 Hz, 4H, H^{T3}), 8.66 (ddd, *J* 0.9, 1.8, 4.8 Hz, 4H, H^{T6}).

^{13}C NMR (125 MHz, CDCl$_3$): δ$_C$ 67.4 (C^{S6}), 67.9 (C^{S1}), 69.6 (C^{S2}), 69.9 (C^{S5}), 71.0 (C^{S4}), 71.2 (C^{S3}), 106.3 (C$^{N1, N8}$), 107.6 (C$^{T3'}$), 116.5 (C$^{N3, N6}$), 121.5 (C^{T3}), 124.0 (C^{T5}), 124.5 (C^{N10}), 129.1 (C$^{N4, N5}$), 135.8 (C^{N9}), 137.0 (C^{T4}), 149.0 (C^{T6}), 156.0 (C^{T2}), 157.1 (C$^{T2'}$), 157.4 (C$^{N2, N7}$), 167.1 (C$^{T4'}$).

MS (FAB): *m/z* = 887 [**M**]$^+$ (18.2%), 262 [***CH$_2$O-terpy***]$^+$ (11.4%), 250 [***HO-terpy***]$^+$, 221 [***terpy***]$^+$ (21.4%), 97 (11.4%), 83 (17.0%), 71 (21.6%), 57 (47.7%), 43 (19.0%).

IR (solid, cm^{-1}): 3055w, 2870w, 1628m, 1582s, 1558s, 1512m, 1466m, 1443s, 1404s, 1350m, 1257m, 1204s, 1126s, 1056s, 995w, 964w, 872w, 833w, 795m, 733m, 702w.

Elemental Analysis: Found: C, 69.15; H, 5.61; N, 9.28. Calc. for C$_{52}$H$_{50}$N$_6$O$_8$·⅔H$_2$O: C, 69.47; H, 5.77; N, 9.35%.

❖ 2,3-Di(ethoxycarbonylmethoxy)naphthalene

2,3-Dihydroxynaphthalene

2,3-Di(ethoxycarbonylmethoxy) naphthalene

Molecular formula: C$_{18}$H$_{20}$O$_6$

Molecular weight: 332.35
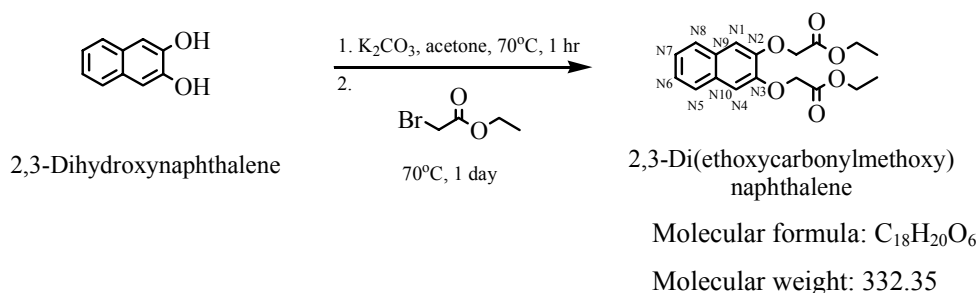
2,3-Dihydroxynaphthalene (5 g, 0.03 mol) was stirred with dry K$_2$CO$_3$ (43.1 g, 0.312 mol) in 125 mL dry acetone for 1 hour at 70ºC and ethyl bromoacetate (11.5 g, 68.9 mmol) was added to the reaction mixture. The reaction mixture was refluxed for 1 day. The mixture was allowed to cool, filtered and then concentrated to give the crude product. A white fine powder (5.7 g, 0.017 mol, 57%) was obtained after recrystallisation with hexane.

^{1}H NMR (400 MHz, CDCl$_3$) δ$_H$ 1.30 (t, *J* 7.1 Hz, 6H, H^{CH3}), 4.29 (q, *J* 7.1 Hz, 4H, H^{OCH2CH3}), 4.81 (s, 4H, H$^{OCH2C=O}$), 7.11 (s, 2H, H$^{N1, N4}$), 7.35 (m, 2H, H$^{N6, N7}$), 7.66 (m, 2H, H$^{N5, N8}$).

^{13}C NMR (100 MHz, CDCl$_3$): δ$_C$ 14.6 (C^{CH3}), 61.8 (C^{OCH2CH3}), 66.7 (C$^{OCH2C=O}$), 110.1 (C$^{N1, N4}$), 125.2 (C$^{N6, N7}$), 126.9 (C$^{N5, N8}$), 129.9 (C$^{N9, N10}$), 148.3 (C$^{N2, N3}$), 169.1 (C$^{C=O}$).

MS (EI): *m/z* = 332 [M]$^+$ (100%), 171 (31.7%), 59 (46.0%).

IR (solid, cm⁻¹): 2986w, 2908w, 1751m, 1720m, 1628w, 1597w, 1512m, 1481m, 1427m, 1404m, 1373m, 1288m, 1258m, 1211m, 1165s, 1111m, 1080m, 1018s, 949w, 918w, 856s, 748s.

Elemental Analysis: Found: C, 64.56; H, 5.95; O, 29.53. Calc. for $C_{18}H_{20}O_6 \cdot \frac{1}{5}H_2O$: C, 64.35; H, 6.13; O, 10.53%.

Melting point: 62.8ºC-63.7ºC.

❖ 2,3-Di(2-hydroxyethoxy)naphthalene

2,3-Di(ethoxycarbonylmethoxy)
naphthalene

2,3-Di(2-hydroxyethoxy)
naphthalene

Molecular formula: $C_{14}H_{16}O_4$

Molecular weight: 248.27
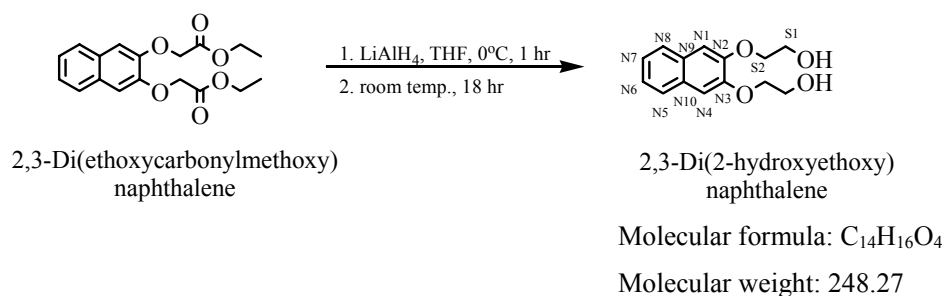
A solution of lithium aluminum hydride (0.4 g, 0.01 mol) in THF (40 mL) was cooled to 0ºC and a solution of 2,3-di(ethoxycarbonylmethoxy)naphthalene (2.3 g, 6.9 mmol) in THF (20 mL) was added. The resulting mixture was stirred for 1 hr and then allowed to warm to room temperature and stirred overnight. The reaction was quenched with aqueous NaOH solution. The white foam was filtered. The organic solvent was removed. A white solid (1.4 g, 5.6 mmol, 81%) was filtered from the aqueous phase NaOH.

¹H NMR (500 MHz, CDCl₃) δ_H 3.29 (br, 2H, OH), 4.03 (t, *J* 4.2 Hz, 4H, H^{S1}), 4.23 (t, *J* 4.4 Hz, 4H, H^{S2}), 7.22 (s, 2H, H^{N1, N4}), 7.36 (m, 2H, H^{N6, N7}), 7.68 (m, 2H, H^{N5, N8}).

¹³C NMR (125 MHz, CDCl₃): δ_C 61.3 (C^{S1}), 71.6 (C^{S2}), 110.3 (C^{N1, N4}), 124.8 (C^{N6, N7}), 126.6 (C^{N5, N8}), 129.8 (C^{N9, N10}), 149.0 (C^{N2, N3}).

MS (EI): *m/z* = 248.1 [M]⁺ (41.8%), 160.1 [HO-Nap-OH]⁺ (100.0%).

IR (solid, cm⁻¹): 3221br, 2947w, 2862w, 2772w, 2667w, 1624w, 1601w, 1510w, 1481w, 1450w, 1404w, 1375w, 1340w, 1256s, 1171s, 1117m, 1084w, 1034m, 928m,905m, 851m, 789s.

Elemental Analysis: Found: C, 63.10; H, 6.80; O, 30.26. Calc. for $C_{14}H_{16}O_4 \cdot H_2O$: C, 63.14; H, 6.83; N, 30.04%.

Melting point: 141.3ºC-142.8ºC.

❖ 2,3-[Bis(2,2′:6′,2″-terpyridin-4′-yl)-1,4-dioxabutyl]naphthalene (**L^16^**)

2,3-Di(2-hydroxyethoxy)naphthalene

Cl-terpy

70ºC, 3 days

2,3-[Bis(2,2′:6′,2″-terpyridin-4′-yl)-1,4-dioxabutyl]naphthalene (**L^16^**)

Molecular formula: $C_{44}H_{34}N_6O_4$

Molecular weight: 710.78
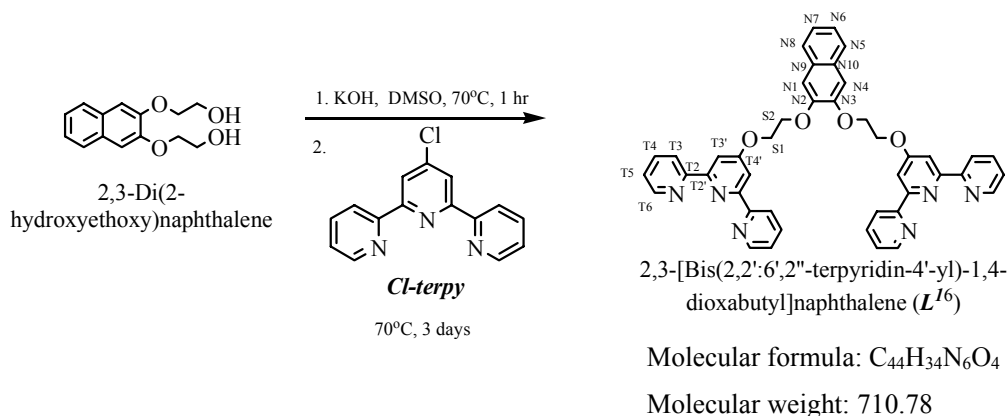
2,3-Di(2-hydroxyethoxy)naphthalene (0.5 g, 2 mmol) was added to a suspension of finely powdered potassium hydroxide (1.4 g, 25 mmol) in 20 mL dry DMSO and the mixture was stirred for 1 hour at 70ºC under nitrogen. The reaction mixture was kept at 70ºC under nitrogen throughout the reaction. After this period, 4′-chloro-2,2′:6′,2″-terpyridine (**Cl-terpy**) (2.2 g, 8.1 mmol) was added and the reaction mixture was heated to 70ºC for 3 days. The reaction mixture was cooled to room temperature and treated with water (500 mL) to give a white precipitate, which was washed with plenty of water and dried to give 2,3-[bis(2,2′:6′,2″-terpyridin-4′-yl)-1,4-dioxabutyl]naphthalene (**L^16^**) (0.52 g, 0.73 mmol, 37%).

^{1}H NMR (500 MHz, CDCl$_3$) δ_H 4.56 (t, *J* 4.8 Hz, 4H, H^{S2}), 4.70 (t, *J* 4.6 Hz, 4H, H^{S1}), 7.28 (s, 2H, H$^{N1, N4}$), 7.30 (dd, *J* 5.1, 7.0 Hz, 4H, H^{T5}), 7.35 (m, 2H, H$^{N6, N7}$), 7.70 (m, 2H, H$^{N5, N8}$), 7.83 (t, *J* 7.5 Hz, 4H, H^{T4}), 8.06 (s, 4H, H$^{T3'}$), 8.57 (d, *J* 8.0 Hz, 4H, H^{T3}), 8.64 (d, *J* 4.0 Hz, 4H, H^{T6}).

^{13}C NMR (125 MHz, CDCl$_3$): δ_C 67.0 (C^{S1}), 67.6 (C^{S2}), 108.1 (C$^{T3'}$), 110.1 (C$^{N1, N4}$), 121.8 (C^{T3}), 124.2 (C^{T5}), 124.7 (C$^{N6, N7}$), 126.6 (C$^{N5, N8}$), 129.7 (C$^{N9, N10}$), 137.5 (C^{T4}), 148.7 (C^{T6}), 149.1 (C$^{N2, N3}$), 155.3 (C^{T2}), 156.5 (C$^{T2'}$), 167.2 (C$^{T4'}$).

MS (FAB): *m/z* = 711 [M]$^+$ (10.3%), 250 [**HO-Terpy**]$^+$ (14.1%), 107 (16.6%), 89 (81.8%), 77 (100%), 63 (62.9%), 51 (87.8%), 39 (90.2%).

IR (solid, cm^{-1}): 1582s, 1558s, 1512w, 1474w, 1443m, 1404m, 1350m, 1250s, 1196m, 1165w, 1119w, 1065m, 995w, 972w, 933w, 879w, 849w, 795s, 733m.

Elemental Analysis: Found: C, 72.02; H, 5.00; N, 11.34. Calc. for $C_{44}H_{34}N_6O_4 \cdot \frac{1}{2}(CH_3)_2SO$: C, 72.08; H, 4.98; N, 11.21%.

Melting point: 216.3ºC-217.6ºC.

❖ 2,3-Di[2-(2-hydroexyethoxy)ethoxy]naphthalene[37]

2,3-Dihydroxynaphthalene

1. K_2CO_3, dry acetone, 70ºC, 1 hour

2. Cl⌒⌒O⌒⌒OH
70ºC, 3 days

2,3-Di[2-(2-hydroxyethoxy)ethoxy]naphthalene
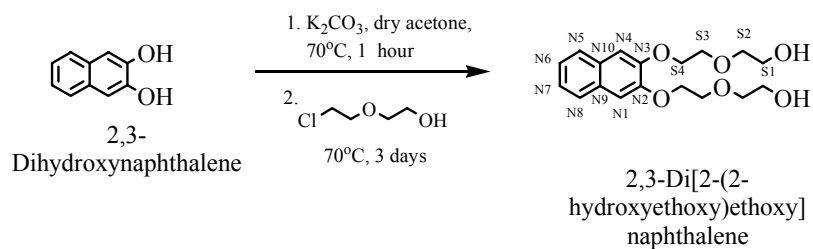
Molecular formula: $C_{18}H_{24}O_6$

Molecular weight: 336.38

2,3-Dihydroxynaphthalene (2.00 g, 12.5 mmol) and K_2CO_3 (12 g, 87 mmol) were stirred in 120 mL dry acetone for 1 hour at 70ºC under nitrogen. The reaction mixture was kept at 70ºC under nitrogen throughout the reaction. Then, 2-(2-chloroethoxy)ethanol (2.33 g, 18.7 mmol) was added dropwise to the reaction mixture. After 1 day, 1 mL of 2-(2-chloroethoxy)ethanol was added and the reaction mixture was kept at 70ºC for 2 days. The reaction mixture was cooled to room temperature. The solution was filtered to remove K_2CO_3 and the residue was washed with CH_2Cl_2. The solvent was removed in vacuo and the residue partitioned between CH_2Cl_2 and water (200 mL). The organic layer was separated and dried ($MgSO_4$). The product was filtered and evaporated to give a green powder (1.6 g, 4.8 mmol, 38%).

^1H NMR (400 MHz, $CDCl_3$) δ_H 3.26 (br, 2H, H^{OH}), 3.71 (m, 4H, H^{S2}), 3.78 (m, 4H, H^{S1}), 3.99 (t, J 4.4 Hz, 4H, H^{S3}), 4.27 (t, J 4.4 Hz, 4H, H^{S4}), 7.12 (s, 2H, $H^{N1, N4}$), 7.34 (m, 2H, $H^{N6, N7}$,), 7.66 (m, 2H, $H^{N8, N5}$).

^{13}C NMR (100 MHz, $CDCl_3$): δ_C 62.1 (C^{S1}), 68.6 (C^{S4}), 69.5 (C^{S3}), 73.3 (C^{S2}), 108.2 ($C^{N1, N4}$), 124.8 ($C^{N6, N7}$), 126.8 ($C^{N5, N8}$), 129.6 ($C^{N9, N10}$), 148.9 ($C^{N2, N3}$).

MS (FAB): m/z = 337 $[M]^+$ (30.3%), 89 $[OCH_2CH_2OCH_2CH_2]^+$ (19.1%), 45 (100%).

IR (solid, cm^{-1}): 3281br, 3055w, 2939w, 2897w, 2870w, 2162w, 1965w, 1701w, 1626w, 1597m, 1581w, 1508m, 1483m, 1460m, 1450m, 1418w, 1400w, 1391w, 1350m, 1337w, 1313w, 1250s, 1194w, 1171m, 1161m, 1132s, 1105s, 1086w, 1072m, 1055w, 1047m, 1020w, 989w, 953m, 941m, 930m, 901s, 883w, 874w, 851s, 750s.

Elemental Analysis: Found: C, 64.16; H, 7.21; O, 28.51. Calc. for $C_{18}H_{24}O_6$: C, 64.27; H, 7.21; N, 28.54%.

Melting point: 55.4ºC-57.3ºC.

❖ 2,3-[Bis(2,2′:6′,2″-terpyridin-4′-yl)-1,4,7-trioxaheptyl]naphthalene (**L^17**)

2,3-Di[2-(2-hydroxyethoxy)ethoxy]naphthalene

Cl-terpy

70°C, 3 days

2,3-[Bis(2,2′:6′,2″-terpyridin-4′-yl)-1,4,7-trioxaheptyl]naphthalene (**L^17**)
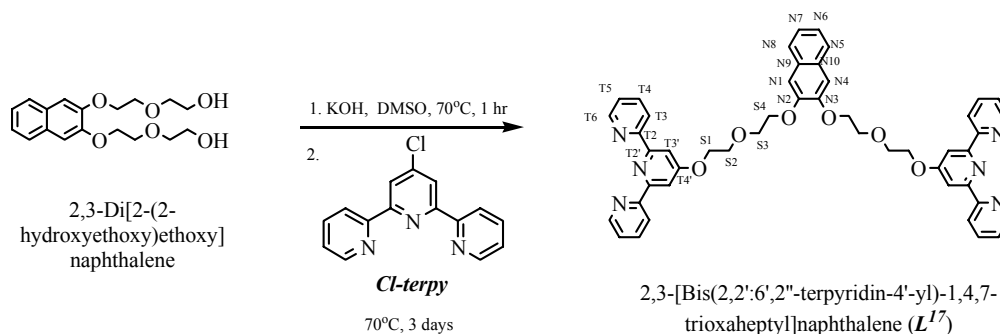
Molecular formula: $C_{48}H_{42}N_6O_6$

Molecular weight: 798.88

2,3-Di[2-(2-hydroxyethoxy)ethoxy]naphthalene (0.81 g, 2.4 mmol) was added to a suspension of finely powdered potassium hydroxide (1.6 g, 29 mmol) in 20 mL dry DMSO and the mixture was stirred for 1 hour at 70°C under nitrogen. The reaction mixture was kept at 70°C under nitrogen throughout the reaction. After this period, 4′-chloro-2,2′:6′,2″-terpyridine (**Cl-terpy**) (2.5 g, 9.3 mmol) was added and the reaction mixture was heated to 70°C for 3 days. The reaction mixture was cooled to room temperature and treated with water (500 mL) to give a white precipitate, which was washed with plenty of water and dried to give 2,3-[bis(2,2′:6′,2″-terpyridin-4′-yl)-1,4,7-trioxaheptyl]naphthalene (**L^17**) (1.6 g, 2.0 mmol, 83%).

¹H NMR (500 MHz, CDCl₃) δ_H 4.04 (m, 8H, H^S3 and H^S2), 4.29 (t, *J* 4.9 Hz, 4H, H^S4), 4.39 (t, *J* 4.7 Hz, 4H, H^S1), 7.14 (s, 2H, H^N1, N4), 7.28 (m, 6H, H^T5 and H^N6, N7), 7.63 (m, 2H, H^N5, N8), 7.80 (td, *J* 1.8, 7.7 Hz, 4H, H^T4), 8.02 (s, 4H, H^T3′), 8.56 (dt, *J* 1.0, 8.0 Hz, 4H, H^T3), 8.64 (ddd, *J* 0.9, 1.8, 4.8 Hz, 4H, H^T6).

¹³C NMR (125 MHz, CDCl₃): δ_C 68.0 (C^S1), 68.7 (C^S4), 69.9 (C^S2), 70.0 (C^S3), 107.6 (C^T3′), 108.7 (C^N1, N4), 121.4 (C^T3), 123.9 (C^T5), 124.3 (C^N6, N7), 126.5 (C^N5, N8), 129.5 (C^N9, N10), 136.8 (C^T4), 149.10 (C^N2, N3), 149.13 (C^T6), 156.1 (C^T2), 157.2 (C^T2′), 167.1 (C^T4′).

MS (FAB): *m/z* = 799 [**M**]⁺ (43.3%), 262 [**TerpyOCH₂**]⁺ (30.3%), 250 [**HO-Terpy**]⁺ (100.0%), 221 (20.5%).

IR (solid, cm⁻¹): 3055w, 3016w, 2939w, 2878w, 1582s, 1558s, 1466w, 1443m, 1404m, 1366w, 1335w, 1257s, 1180m, 1134m, 1088w, 1041m, 987w, 933w, 872m, 849m, 787s, 741s.

Elemental Analysis: Found: C, 71.64; H, 5.35; N, 10.49. Calc. for $C_{48}H_{42}N_6O_6 \cdot \frac{1}{4}H_2O$: C, 71.76; H, 5.34; N, 10.46%.

Melting point: 130.4ºC-131.5ºC.

5.9   References

1.   F. Kröhnke, *Synthesis*, 1976, 1.

2.   A. M. W. Cargill Thompson, *Coord. Chem. Rev.*, 1997, **160**, 1.

3.   S. Encinas, L. Flamigni, F. Barigelletti, E. C. Constable, C. E. Housecroft, E. R. Schofield, E. Figgemeier, D. Fenske, M. Neuburger, J. G. Vos, and M. Zehnder, *Chem. Eur. J.*, 2002, **8**, 137.

4.   E. C. Constable, A. J. Edwards, M. D. Marcos, P. R. Raithby, R. Martínez-Máñez, and M. J. L. Tendero, *Inorg. Chim. Acta*, 1994, **224**, 11.

5.   J.-P. Collin, P. Lainé, J.-P. Launay, J.-P. Sauvage, and A. Sour, *J. Chem. Soc., Chem. Commun.*, 1993, 434.

6.   E. C. Constable, and M. D. Ward, *J. Chem. Soc., Dalton Trans.*, 1990, 1405.

7.   E. C. Constable, and A. M. W. Cargill Thompson, *J. Chem. Soc., Dalton Trans.*, 1992, 3467.

8.   E. C. Constable, A. M. W. Cargill Thompson, and S. Greulich, *J. Chem. Soc., Chem. Commun.*, 1993, 1444.

9.   C. Ringenbach, A. De Nicola, and R. Ziessel, *J. Org. Chem.,* 2003, **68**, 4708.

10.   E. C. Constable, A. M. W. Cargill Thompson, P. Harveson, L. Macko, and M. Zehnder, *Chem. Eur. J.*, 1995, **1**, 360.

11   B. Whittle, S. R. Batten, J. C. Jeffery, L. H. Rees, and M. D. Ward, *J. Chem. Soc., Dalton Trans.*, 1996, 4249.

12.   D. Armspach, E. C. Constable, F. Diederich, C. E. Housecroft, and J.-F. Nierengarten, *Chem. Commun.*, 1996, 2009.

13.   D. Armspach, E. C. Constable, F. Diederich, C. E. Housecroft, and J.-F. Nierengarten, *Chem. Eur. J.*, 1998, **4**, 723.

14.   D. Armspach, E. C. Constable, C. E. Housecroft, M. Neuburger, and M. Zehnder, *J. Organomet. Chem.*, 1998, **550**, 193.

15.   G. R. Newkome, F. Cardullo, E. C. Constable, C. N. Moorefield, and A. M. W. Cargill Thompson, *J. Chem. Soc., Chem. Commun.*, 1993, 925.

16.   P. R. Andres, R. Lunkwitz, G. R. Pabst, K. Böhn, D. Wouters, S. Schmatloch, and U. S. Schubert, *Eur. J. Org. Chem.*, 2003, 3769.

17.   L. Zapata, K. Bathany, J.-M. Schmitter, and S. Moreau, *Eur. J. Org. Chem.*, 2003, 1022.

18.   C. Kim, and H. Kim, *J. Organomet. Chem.*, 2003, **673**, 77.

19.   B. G. G. Lohmeijer, and U. S. Schubert, *Angew. Chem. Int. Ed.*, 2002, **41**, 3825.

20. Y. Molard, and H. Parrot-Lopez, *Tetrahedron Lett.*, 2002, **43**, 6355.

21. O. Inhoff, J. M. Richards, J. W. Brîet, G. Lowe, and R. L. Krauth-Siegel, *J. Med. Chem.*, 2002, **45**, 4524.

22. U. S. Schubert, C. Eschbaumer, O. Hien, and P. R. Andres, *Tetrahedron Lett.*, 2001, **42**, 4705.

23. T. Mutai, J.-D. Cheon, S. Arita, and K. Araki, *J. Chem. Soc., Perkin Trans. 2*, 2001, 1045.

24. G. R. Newkome, E. He, L. A. Godínez, and G. R. Gregory, *J. Am. Chem. Soc.*, 2000, **122**, 9993.

25. G. R. Newkome, E. He, L. A. Godínez, and G. R. Baker, *Chem. Commun.*, 1999, 27.

26. G. Lowe, A. S. Droz, T. Vilaivan, G. W. Weaver, L. Tweedale, J. M. Pratt, P. Rock, V. Yardley, and S. L. Croft, *J. Med. Chem.*, 1999, **42**, 999.

27. G. Lowe, A.-S. Droz, J. J. Park, and G. W. Weaver, *Bioorg. Chem.*, 1999, **27**, 477.

28. V. Marvaud, and D. Astruc, *Chem. Commun.*, 1997, 773.

29. C. B. Smith, E. C. Constable, C. E. Housecroft, and B. M. Kariuki, *Chem. Commun.*, 2002, 2068.

30. E. C. Constable, C. E. Housecroft, M. Cattalini, and D. Phillips, *New J. Chem.*, 1998, 193.

31. J.-S. Yang, C.-S. Lin, C.-Y. Hwang, *Org. Lett.*, 2001, **3**, 889.

32. E. C. Constable, A. M. W. Cargill Thompson, D. A. Tocher, and M. A. M. Daniels, *New J. Chem.*, 1992, **16**, 855.

33. E. C. Constable, J. Lewis, M. C. Liptrot, and P. R. Raithby, *Inorg. Chim. Acta*, 1990, **178**, 47.

34. R.-A. Fallahpour, M. Neuburger, and M. Zehnder, *Polyhedron*, 1999, **18**, 2445.

35. T. Steiner, *Angew. Chem. Int. Ed.*, 2002, **41**, 48.

36. M. Asakawa, P. R. Ashton, S. E. Boyd, C. L. Brown, R. E. Gillard, O. Kocian, F. M. Raymo, J. F. Stoddart, M. S. Tolley, A. J. P. White, and D. J. Williams, *J. Org. Chem.*, 1997, **62**, 26.

37. A. M. Bond, K. P. Ghiggino, C. F. Hogan, J. A. Hutchison, S. J. Langford, E. Lygris, and M. N. Paddon-Row, *Aust. J. Chem.*, 2001, **54**, 735.

38. J. C. Rosa, D. Galanakis, C. R. Ganellin, and P. M. Dunn, *J. Med. Chem.*, 1996, **39**, 4247.

39. S. K. Armstrong, R. J. Cross, L. J. Farrugia, D. A. Nichols, and A. Perry, *Eur. J. Inorg. Chem.*, 2002, 141.

Chapter 6

Synthesis of Linear Homodinuclear Ruthenium(II) Complexes from Homoditopic 4′-Substituted-2,2′:6′,2″-Terpyridine Ligands

In Chapter 3, we mentioned the interesting properties of the complexes of 2,2′-bipyridine and 2,2′:6′,2″-terpyridine derivatives. Not only the photochemical and photophysical properties of the mononuclear complexes, but also those of the dinuclear complexes formed from rigid bridging bis(terpyridine) ligands (**Figure 1a**) have been investigated.[1-9]. The spacers have two main roles: (1) to control the supramolecular structure, especially the intercomponent distances and angles, and (2) to control the electronic communication between components through through-bond energy or electron transfer.
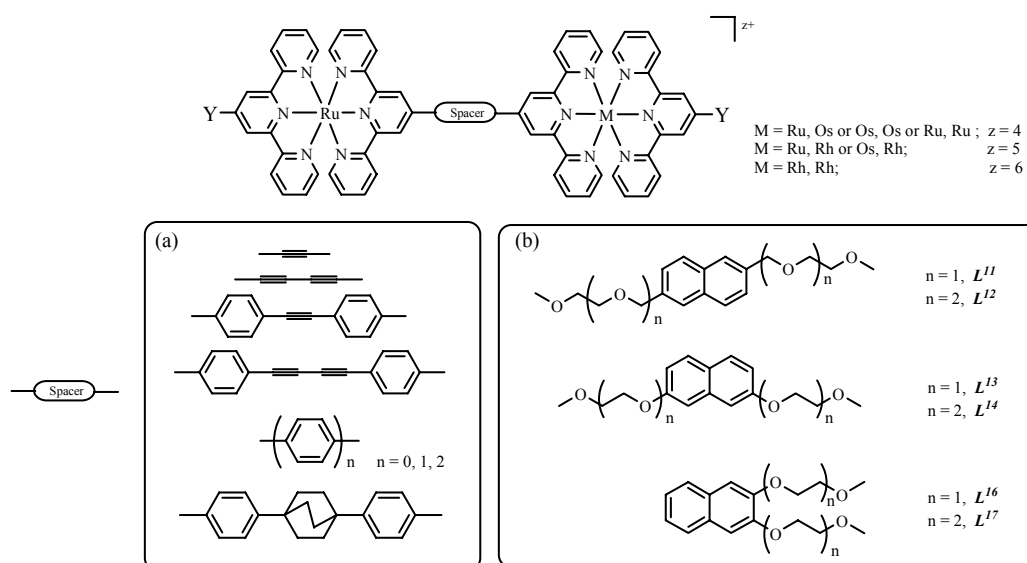
Figure 1. Diagram showing dinuclear complexes with different spacers (a) complexes from the literature, and (b) complexes described in this chapter.

In this chapter, some linear homodinuclear Ru(II) complexes, which incorporate ligands in which a naphthalene bis(ethyleneoxy) unit bridges the 4′-position of two 2,2′:6′,2″-terpyridine domains, are discussed (**Figure 1b**). Only the structural characterisations are discussed in this chapter. There are two reasons for this. (1) In most of the cases found in the literature, rigid spacers containing ethynyl groups and

aromatic rings are more common than flexible spacers. The naphthalene bis(ethyleneoxy) spacer of ligands L^{11}-L^{14}, L^{16}-L^{17} does not have the appropriate characteristics to allow good electronic communication between two metal centres. (2) According to the literature, heterodinuclear complexes, such as Ru-Os or Ru-Rh systems, are more favoured for the energy-transfer than homodinuclear Ru-Ru complexes. No investigations of the electrochemical properties of the homodinuclear Ru(II) complexes described in this chapter were attempted.

6.1   Synthesis

The adduct [Ru(L^a)Cl$_3$] (where L^a = *terpy* or L^4) were readily prepared as brown solids by directly heating RuCl$_3$·3H$_2$O with L^a in CH$_3$OH for 3 hours. The reaction of 1 equivalent of L^b (L^{11}-L^{14}, L^{16}-L^{17}) and 2 equivalents of [Ru(L^a)Cl$_3$] (where L^a = *terpy* or L^4) with a few drops of *N*-ethylmorpholine (NEM) in boiling CH$_3$OH for 3 hours gave red solutions, which after chromatographic workup, gave the linear homodinuclear complexes [(L^a)Ru(L^b)Ru(L^a)][PF$_6$]$_4$.[10-14] The yield of the [(L^a)Ru(L^b)Ru(L^a)][PF$_6$]$_4$ complexes (where L^b = L^{11}-L^{14}, L^{16}-L^{17} and L^a = *terpy* or L^4) ranged from 10-66% (**Scheme 1**).
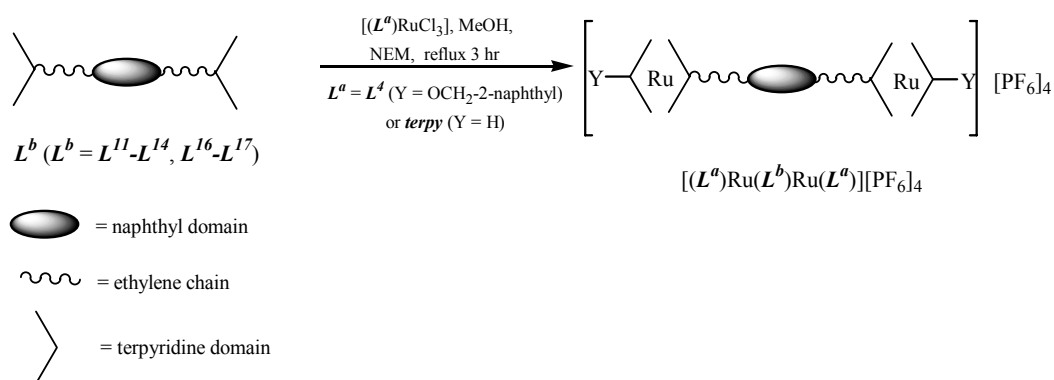
Scheme 1.   The general syntheses of linear homodinuclear complexes [(L^a)Ru(L^b)Ru(L^a)][PF$_6$]$_4$ (where L^b = L^{11}-L^{14}, L^{16}-L^{17} and L^a = *terpy* or L^4).

6.2 ¹H NMR spectroscopic characterisation

All the complexes were characterised by ¹H NMR spectroscopy in CD₃CN solution. The ¹H NMR spectra of the homodinuclear complexes $[(L^a)Ru(L^b)Ru(L^a)][PF_6]_4$ exhibit resonances which are assigned to two different terpyridine groups. One set results from the terpyridine system of ligand L^a (L^a = *terpy* or L^4) and the other one is due to the terpyridine system of ligand L^b (L^b = L^{11}-L^{14}, L^{16}-L^{17}). Assignments have been made using COSY and NOESY or ROESY experiments and by comparison with the spectra of symmetrical $[Ru(L^a)_2][PF_6]_2$ complexes. The terpyridine proton signals are similar in all the complexes, except in the case of $[(L^4)Ru(L^{13})Ru(L^4)][PF_6]_4$, where L^a is L^4 instead of *terpy*, and $[(terpy)Ru(L^{16})Ru(terpy)][PF_6]_4$, where the two metal centres are very close (**Table 1**).

$[(terpy)Ru(L^{11})Ru(terpy)][PF_6]_4$

$[(terpy)Ru(L^{12})Ru(terpy)][PF_6]_4$

$[(L^4)Ru(L^{13})Ru(L^4)][PF_6]_4$

$[(terpy)Ru(L^{14})Ru(terpy)][PF_6]_4$

$[(terpy)Ru(L^{16})Ru(terpy)][PF_6]_4$

$[(terpy)Ru(L^{17})Ru(terpy)][PF_6]_4$
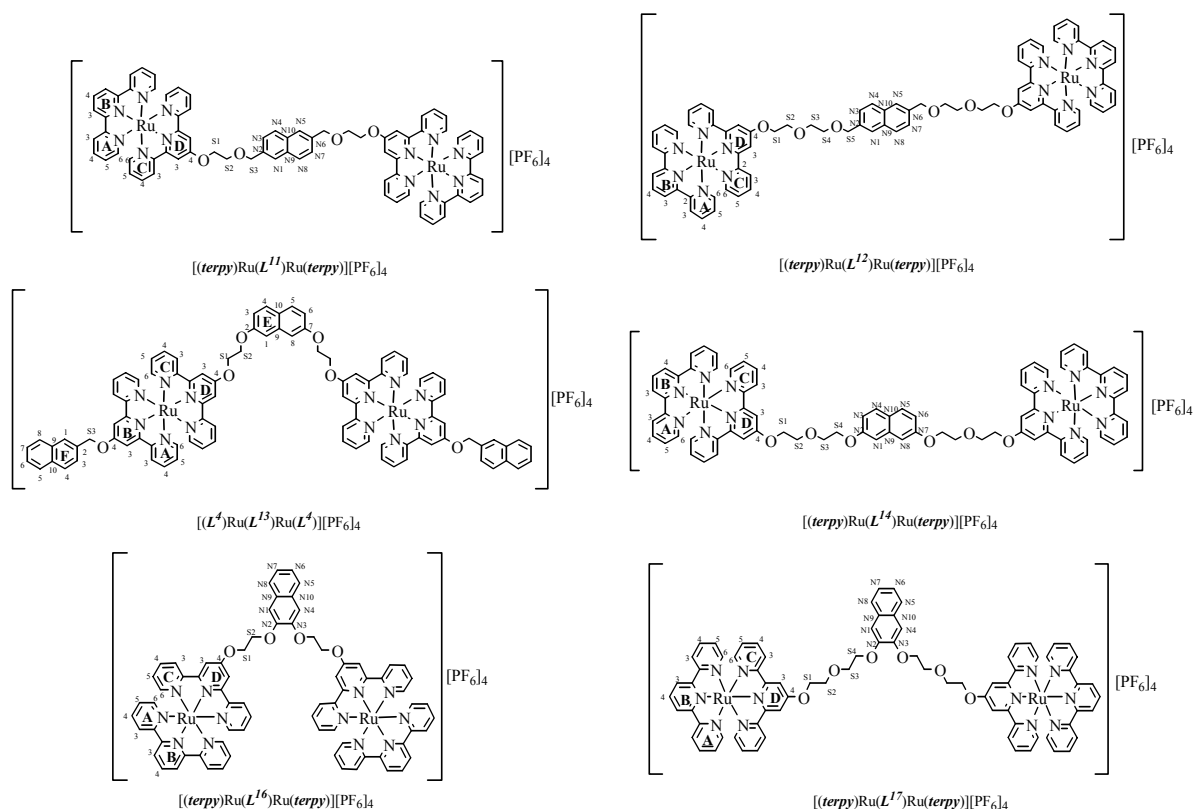
Scheme 2. The structures and the atom labelling scheme of the six homodinuclear linear complexes $[(L^a)Ru(L^b)Ru(L^a)][PF_6]_4$ (where L^b = L^{11}-L^{14}, L^{16}-L^{17} and L^a = *terpy* or L^4).

| | Proton resonance (δ) | | | | | | | | | | |
| | $L^b = L^{11}\text{-}L^{14}, L^{16}\text{-}L^{17}$ | | | | | $L^a = \textbf{\textit{terpy}}$ or L^4 | | | | | |
	H^{C5}	H^{C6}	H^{C4}	H^{C3}	H^{D3}	H^{A5}	H^{A6}	H^{A4}	H^{A3}	H^{B3}	H^{B4}
[Ru(***terpy***)$_2$][PF$_6$]$_2$[15]						7.15	7.33	7.91	8.48	8.74	8.40
[Ru(L^4)$_2$][PF$_6$]$_2$						7.16 (ddd) J 1.4, 5.7, 7.5 Hz	7.39 (ddd) J 0.6, 1.4, 5.6 Hz	7.90 (td) J 1.5, 7.9 Hz	8.47 (dt) J 0.9, 8.1 Hz	8.45 (s)	
[(***terpy***)Ru(L^{11})Ru(***terpy***)][PF$_6$]$_4$	7.11 (ddd) J 1.3, 5.6, 7.6 Hz	7.29 (ddd) J 0.7, 1.4, 5.6 Hz	7.86 (m)	8.42 (ddd) J 0.8, 1.2, 8.1 Hz	8.36 (s)	7.14 (ddd) J 1.4, 5.6, 7.6 Hz	7.40 (ddd) J 0.7, 1.4, 5.6 Hz	7.90 (m)	8.47 (ddd) J 0.8, 1.2, 8.1 Hz	8.72 (d) J 8.2 Hz	8.36 (t) J 8.1 Hz
[(***terpy***)Ru(L^{12})Ru(***terpy***)][PF$_6$]$_4$	7.10 (m)	7.28 (d) J 5.4 Hz	7.85 (td) J 1.6, 7.8 Hz	8.43 (d) J 8.4 Hz	8.33 (s)	7.15 (m)	7.40 (d) J 6.0 Hz	7.90 (td) J 1.2, 7.8 Hz	8.47 (d) J 8.4 Hz	8.72 (d) J 8.4 Hz	8.37 (t) J 8.1 Hz
[(L^4)Ru(L^{13})Ru(L^4)][PF$_6$]$_4$	7.16 (m)	7.42 (m)	7.90 (m)	8.49 (d) J 7.7 Hz	8.40 (s)	7.16 (m)	7.42 (m)	7.90 (m)	8.49 (d) J 7.7 Hz	8.47 (s)	
[(***terpy***)Ru(L^{14})Ru(***terpy***)][PF$_6$]$_4$	7.08 (ddd) J 1.3, 5.6, 7.6 Hz	7.27 (ddd) J 0.6, 1.4, 5.6 Hz	7.83 (td) J 1.4, 7.9 Hz	8.40 (ddd) J 0.7, 1.1, 8.1 Hz	8.33 (s)	7.16 (ddd) J 1.3, 5.7, 7.6 Hz	7.41 (ddd) J 0.7, 1.4, 5.6 Hz	7.90 (td) J 1.4, 7.9 Hz	8.47 (ddd) J 0.8, 1.1, 8.1 Hz	8.72 (d) J 8.2 Hz	8.36 (t) J 8.2 Hz
[(***terpy***)Ru(L^{16})Ru(***terpy***)][PF$_6$]$_4$	6.94 or 7.08 (ddd) J 1.3, 5.7, 7.5 Hz	7.28 or 7.39 (ddd) J 0.6 (0.7), 1.4, 5.6 Hz	7.75 (m)	8.43 (m)	8.41 (s)	7.08 or 6.94 (ddd) J 1.3, 5.7, 7.5 Hz	7.39 or 7.28 (ddd) J 0.7 (0.6), 1.4, 5.6 Hz	7.75 (m)	8.43 (m)	8.71 (d) J 8.2 Hz	8.36 (t) J 8.1 Hz
[(***terpy***)Ru(L^{17})Ru(***terpy***)][PF$_6$]$_4$	7.08 (ddd) J 1.3, 5.6, 7.6 Hz	7.27 (ddd) J 0.6, 1.4, 5.6 Hz	7.82 (td) J 1.5, 7.5 Hz	8.39 (ddd) J 0.7, 1.1, 8.1 Hz	8.32 (s)	7.15 (ddd) J 1.3, 5.6, 7.6 Hz	7.41 (ddd) J 0.7, 1.4, 5.6 Hz	7.89 (td) J 1.5, 7.9 Hz	8.47 (ddd) J 0.7, 1.2, 8.2 Hz	8.72 (d) J 8.2 Hz	8.36 (t) J 8.2 Hz
J	J_{C34} 8.1 Hz; J_{C45} 7.6 Hz; J_{C46} 1.4 Hz; J_{C53} 1.2 Hz; J_{C56} 5.6 Hz; J_{C63} 0.7 Hz					J_{A34} 8.1 Hz; J_{A45} 7.6 Hz; J_{A46} 1.4 Hz; J_{A53} 1.3 Hz; J_{A56} 5.6 Hz; J_{A63} 0.7 Hz; J_{B34} 8.2 Hz					

(to be continued)

	Proton resonance (δ)										
	H^{S1}	H^{S2}	H^{S3}	H^{S4}	H^{S5}	$H^{N3, N7}$	$H^{N4, N8}$	$H^{N1, N5}$			
[(**terpy**)Ru(**L**^{11})Ru(**terpy**)][PF$_6$]$_4$	4.75 (m)	4.13 (m)	4.86 (s)			7.56 (dd) J 1.4, 8.5 Hz	7.86 (m)	7.92 (s)			
[(**terpy**)Ru(**L**^{12})Ru(**terpy**)][PF$_6$]$_4$	4.69 (m)	4.07 (t) J 4.2 Hz	3.84 (m)	3.75 (m)	4.69 (m)	7.47 (dd) J 1.2, 7.2 Hz	7.81 (d) J 7.8 Hz	7.79 (s)			
	H^{S1}	H^{S2}	H^{S3}	$H^{E3, E6}$	$H^{E1, E8}$	$H^{E4, E5}$	$H^{F6, F7}$	H^{F3}	$H^{F5, F8}$	H^{F4}	H^{F1}
[Ru(**L**^{4})$_2$][PF$_6$]$_2$	5.79 (s)						7.62 (m)	7.79 (dd) J 1.8, 8.4 Hz	8.00 (m) and 8.03 (m)	8.08 (d) J 8.5 Hz	8.20 (s)
[(**L**^{4})Ru(**L**^{13})Ru(**L**^{4})][PF$_6$]$_4$	4.97 (m)	4.71 (m)	5.79 (s)	7.16 (m)	7.42 (m)	7.83 (d) J 9.0 Hz	7.61 (m)	7.79 (dd) J 1.7, 8.4 Hz	7.98 (m)	8.07 (d) J 8.5 Hz	8.20 (s)
	H^{S1}	H^{S2}	H^{S3}	H^{S4}		$H^{N3, N6}$	$H^{N1, N8}$	$H^{N4, N5}$			
[(**terpy**)Ru(**L**^{14})Ru(**terpy**)][PF$_6$]$_4$	4.71 (m)	4.15 (m)	4.04 (m)	4.28 (m)		6.97 (dd) J 2.5, 8.9 Hz	7.14 (d) J 2.7 Hz	7.58 (d) J 9.0 Hz			
	H^{S1}	H^{S2}	H^{S3}	H^{S4}		$H^{N7, N6}$	$H^{N1, N4}$	$H^{N8, N5}$			
[(**terpy**)Ru(**L**^{16})Ru(**terpy**)][PF$_6$]$_4$	5.01 (m)	4.83 (m)				7.43 (m)	7.58 (s)	7.86 (m)			
[(**terpy**)Ru(**L**^{17})Ru(**terpy**)][PF$_6$]$_4$	4.74 (m)	4.21 (m)	4.12 (m)	4.40 (m)		7.24 (m)	7.33 (s)	7.63 (m)			

Table 1. ^{1}H NMR spectroscopic data for the proton signals of the six [(**L**^{a})Ru(**L**^{b})Ru(**L**^{a})][PF$_6$]$_4$ (where **L**^{b} = **L**^{11}-**L**^{14}, **L**^{16}-**L**^{17} and **L**^{a} = **terpy** or **L**^{4}) complexes in CD$_3$CN solution at room temperature (except [(**terpy**)Ru(**L**^{12})Ru(**terpy**)][PF$_6$]$_4$ was measured at 600 MHz; all the rest were measured at 500 MHz). The structures and the labeling scheme are shown in **Scheme 2** on p.225.
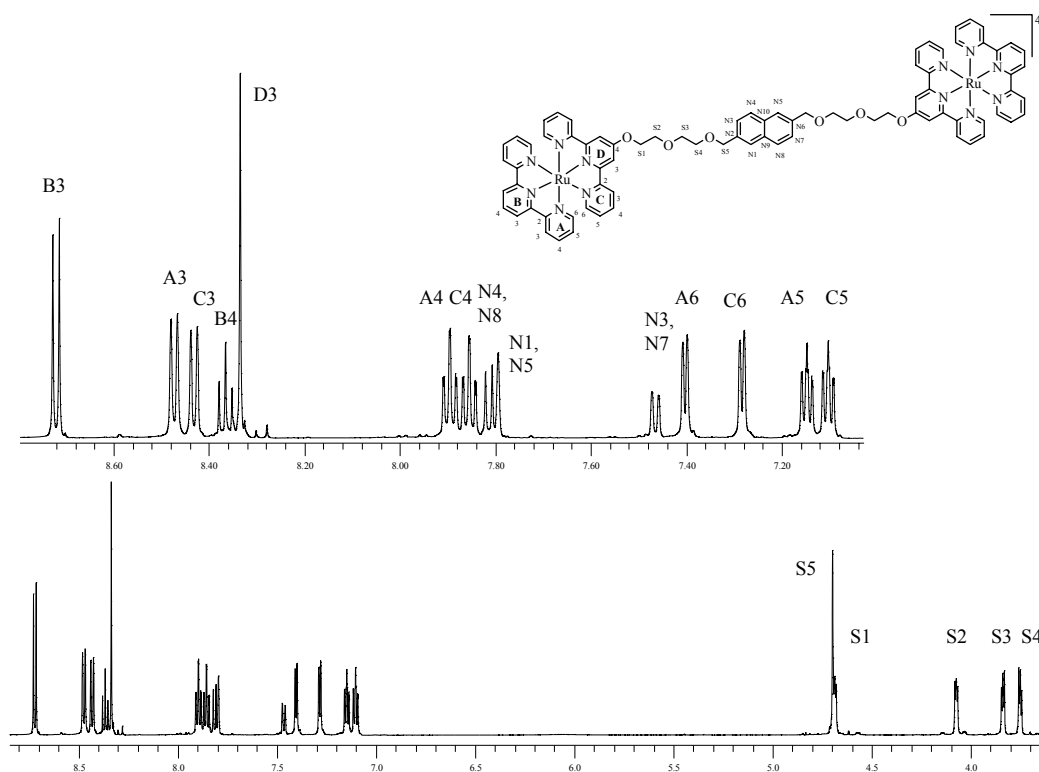
Figure 2. The ^{1}H NMR spectrum (600 MHz) of [(*terpy*)Ru(L^{12})Ru(*terpy*)][PF$_6$]$_4$ in CD$_3$CN solution at room temperature.

The ^{1}H NMR spectrum of [(*terpy*)Ru(L^{12})Ru(*terpy*)][PF$_6$]$_4$ in CD$_3$CN solution has only nineteen proton resonances due to the symmetry of this complex (**Figure 2**). The absolute assignment of the two terpyridine systems (A, B and C, D rings) was made by using COSY and ROESY techniques. The doublet at δ 8.43, which exhibits a ROESY cross peak to the singlet signal for H^{D3} at δ 8.33, is assigned to H^{C3} (**Figure 3**). Once the H^{C3} signal was assigned, the rest of the signals belonging to the C ring were assigned from a COSY spectrum (**Figure 4**). The triplet for H^{B4} at δ 8.37 gives a COSY cross peak to the signal at δ 8.72, and this is then assigned to H^{B3} (**Figure 4**). The signal for H^{B3} exhibits a ROESY cross peak to the doublet signal at δ 8.47, and this is assigned to H^{A3} (**Figure 3**). Similarly, the rest of the A ring signals were assigned from a COSY spectrum (**Figure 4**). The assignment for the ethyleneoxy proton signals in the ^{1}H NMR spectrum was made using the ROESY method. The signals for H^{D3} and H$^{N1, N5}$ showed strong ROESY cross peaks to H^{S1} and H^{S5} respectively. The signal for H^{S5} exhibits a ROESY cross peak to δ 3.75, and this signal is assigned to H^{S4}. Therefore, H^{S2} and H^{S3} were assigned by a COSY spectrum since there were COSY cross peaks to H^{S1} and H^{S4} respectively.
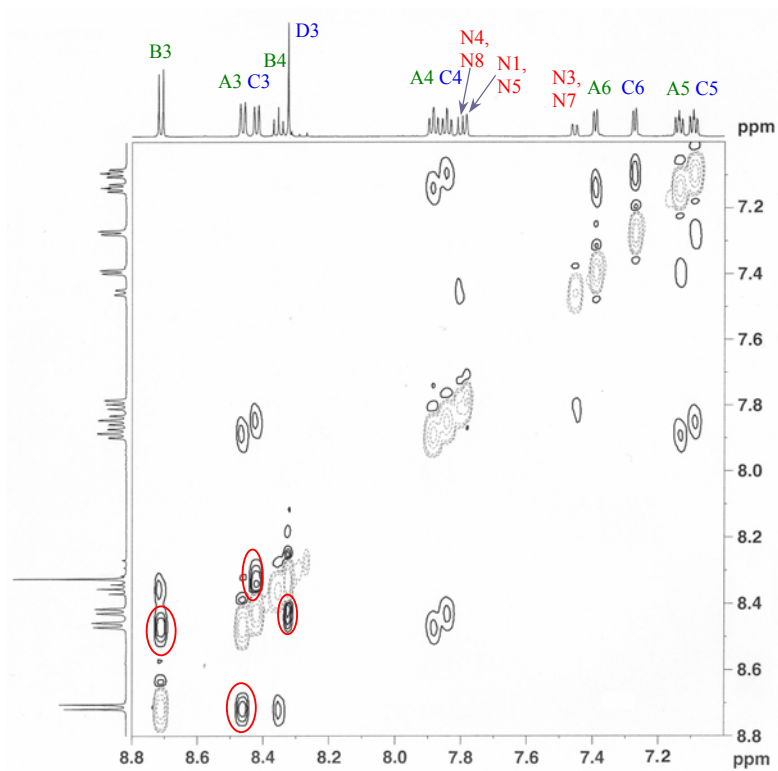
Figure 3. ROESY spectrum (600 MHz) of [(*terpy*)Ru(*L^12*)Ru(*terpy*)][PF$_6$]$_4$ in CD$_3$CN solution at room temperature.
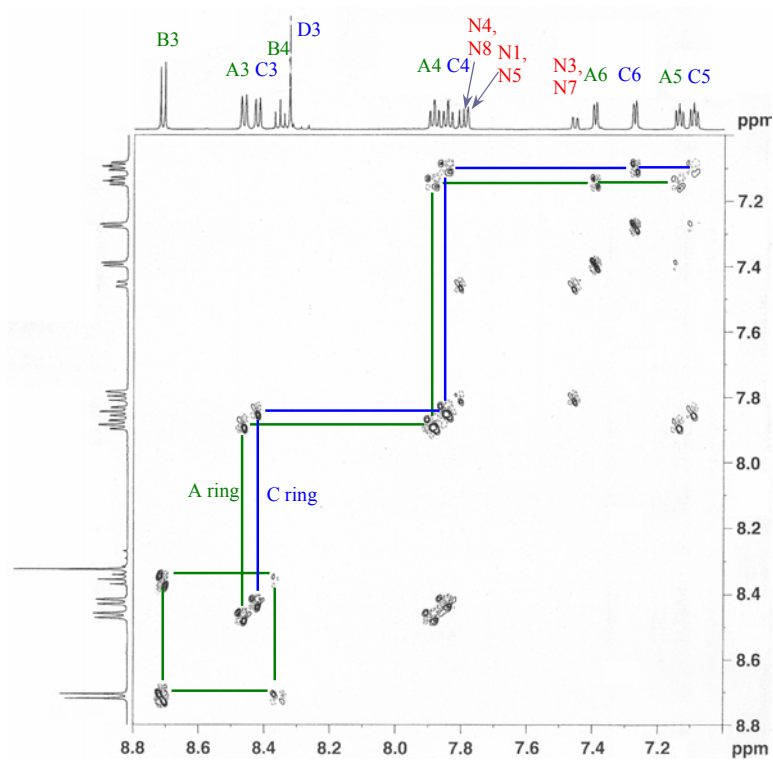
Figure 4. COSY spectrum (600 MHz) of [(*terpy*)Ru(*L^12*)Ru(*terpy*)][PF$_6$]$_4$ in CD$_3$CN solution at room temperature.
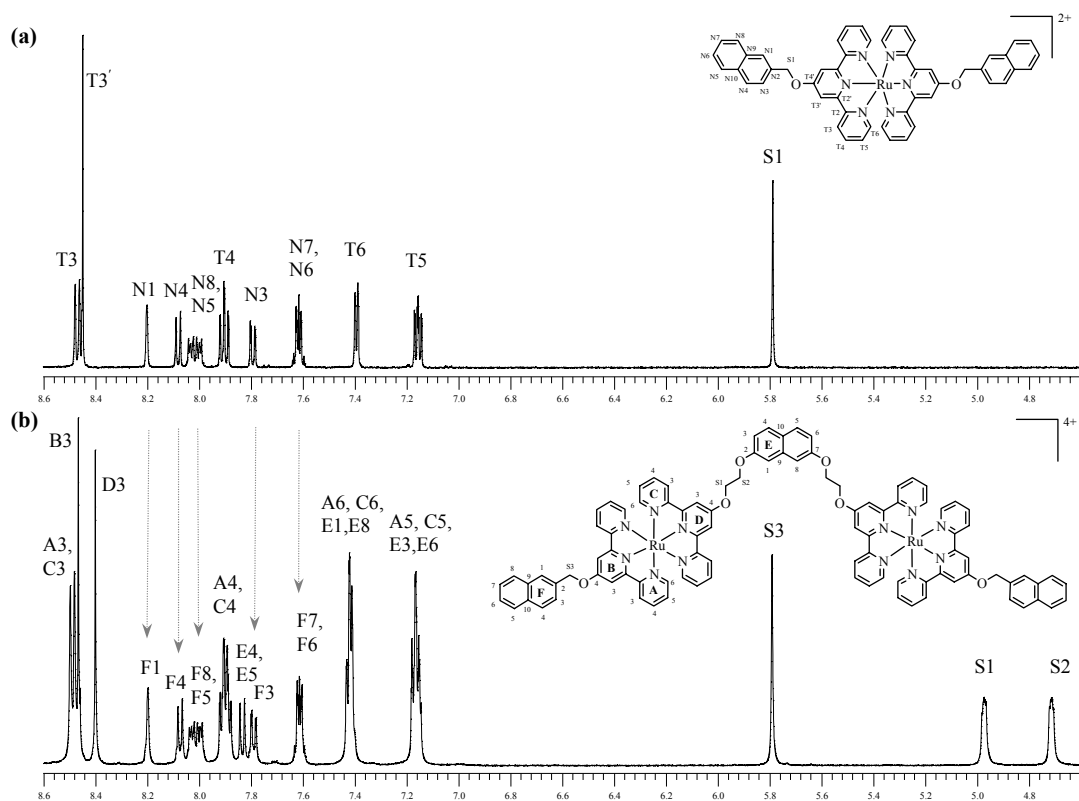
Figure 5. The ^{1}H NMR spectrum (500 MHz) of (a) [Ru(L^4)$_2$][PF$_6$]$_2$ and (b) [(L^4)Ru(L^{13})Ru(L^4)][PF$_6$]$_4$ in CD$_3$CN solution at room temperature.

The ^{1}H NMR spectrum of [(L^4)Ru(L^{13})Ru(L^4)][PF$_6$]$_4$ was assigned by using COSY and NOESY techniques and also by making a comparison with the spectrum of the corresponding mononuclear [Ru(L^4)$_2$][PF$_6$]$_2$ complex. The substituents on the two 4′-positions of the 2,2′:6′,2″-terpyridine rings are similar; therefore, all the terpyridine proton signals of the two systems overlap (**Figure 5**).
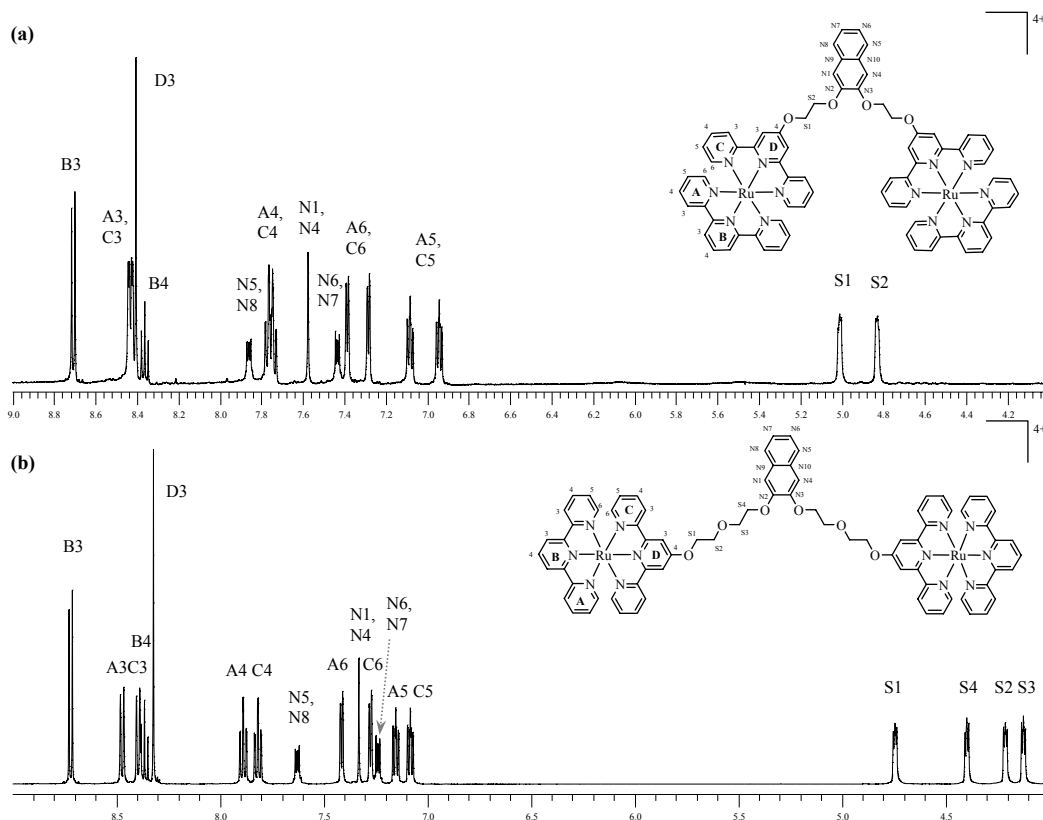
Figure 6. The ^{1}H NMR spectrum (500 MHz) of (a) [(*terpy*)Ru(***L***^{16})Ru(*terpy*)][PF$_6$]$_4$ and (b) [(*terpy*)Ru(***L***^{17})Ru(*terpy*)][PF$_6$]$_4$ in CD$_3$CN solution at room temperature.

The ^{1}H NMR spectrum of [(*terpy*)Ru(***L***^{17})Ru(*terpy*)][PF$_6$]$_4$ in CD$_3$CN solution exhibits eighteen proton signals (**Figure 6b**). The proton signals of the two terpyridine systems were assigned as previously described from the NOESY and COSY spectra. The triplet for H^{B4} at δ 8.36 gives a COSY cross peak to the signal at δ 8.72, and this is then assigned to H^{B3} (**Figure 7**). The signal for H^{B3} exhibits an NOE signal to H^{A3} at δ 8.47 (**Figure 8**). Therefore, the rest of the A ring signals were assigned from the COSY spectrum (**Figure 7**). The singlet signal for H^{D3} at δ 8.32 exhibits NOE signals to δ 8.39 and δ 4.74 (**Figure 8**). The signal at δ 8.39 is assigned to H^{C3} and the signal at δ 4.74 is then assigned to H^{S1}. Similarly, the rest of the C ring signals were assigned from the COSY spectrum (**Figure 7**). The rest of the signals for the ethyleneoxy chain are fully assigned by COSY and NOESY spectra. The signal for H^{S4} at δ 4.40 exhibits an NOE signal to a singlet for H$^{N1, N4}$ at δ 7.33 (**Figure 8**). Then, the multiplet signal at δ 7.63, which exhibits an NOE signal to H$^{N1, N4}$, is assigned to H$^{N5, N8}$ (**Figure 8**). The signal for H$^{N5, N8}$ gives a COSY cross peak to the multiplet signal at δ 7.24, and this is then assigned to H$^{N6, N7}$ (**Figure 7**).
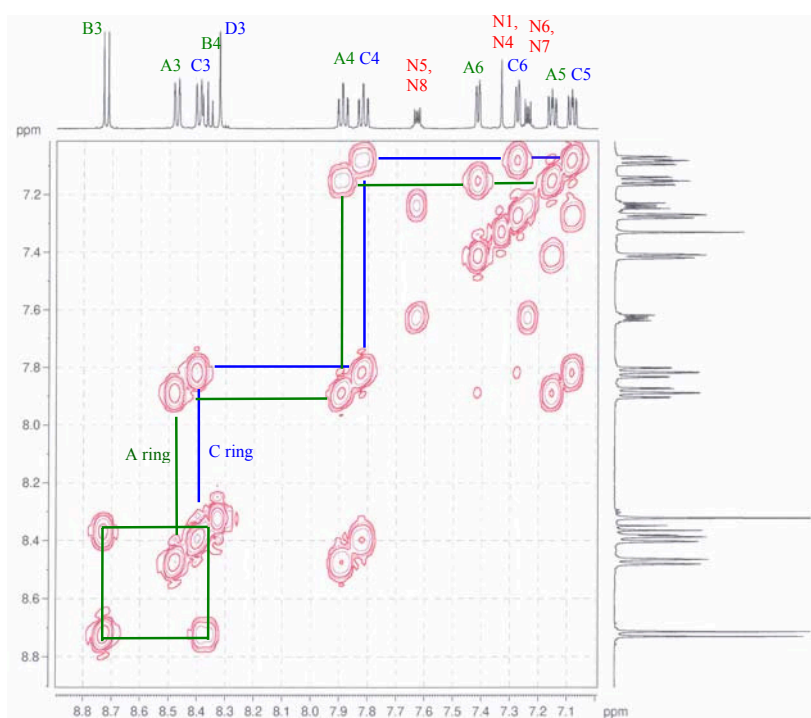
Figure 7. COSY spectrum (500 MHz) of [(***terpy***)Ru(***L^17***)Ru(***terpy***)][PF$_6$]$_4$ in CD$_3$CN solution at room temperature.
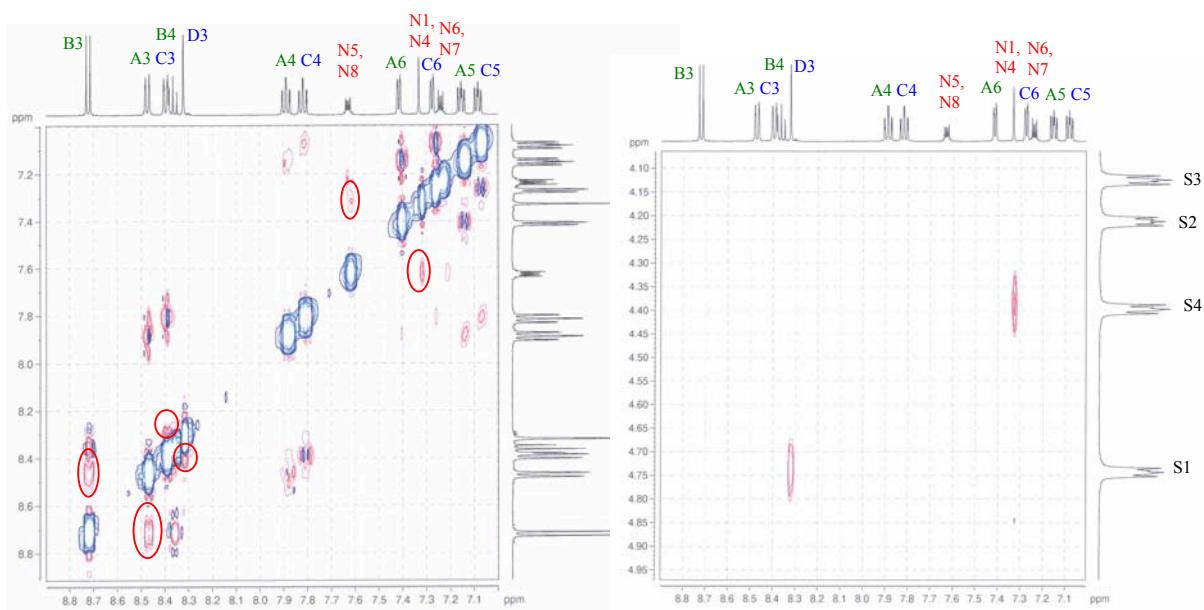
Figure 8. NOESY spectrum (500 MHz) of [(***terpy***)Ru(***L^17***)Ru(***terpy***)][PF$_6$]$_4$ in CD$_3$CN solution at room temperature.

The ^{1}H NMR spectra of [(***terpy***)Ru(***L^16***)Ru(***terpy***)][PF$_6$]$_4$ in CD$_3$CN solution were assigned according to the spectrum for[(***terpy***)Ru(***L^17***)Ru(***terpy***)][PF$_6$]$_4$. There are no

significant differences in the chemical shift of the terpyridine signals (**Table 1** and **Figure 6**). However, the proton signals for the naphthyl ring shifted 0.2 ppm (**Figure 6**).

6.3   Mass spectrometric characterisation

Electrospray ionisation mass spectrometry (ES-MS) was used to characterise the new complexes. The mass spectrum shows peaks for ions with particular mass to charge ratios (*m/z*). Each signal arises from a unique combination of the isotopes of the elements in the complexes. The difference between the *m/z* values for each of the signals within the peak envelope is the reciprocal of the charge on the fragment from which the signal originates; e.g. if $z = 4$, the separation between peaks in an envelope is 0.25 mass units. Normally, ES-MS is a relatively soft ionisation method and, $[M-PF_6]^+$, $[M-2PF_6]^{2+}$, $[M-3PF_6]^{3+}$ and $[M-4PF_6]^{4+}$ peaks are found as the major peaks for homodinuclear Ru(II) complexes. However, if the voltage used to ionise the samples is relatively high, some other fragments are observed in the spectra (**Table 2**).

	m/z				
	$[M-PF_6]^+$	$[M-2PF_6]^{2+}$	$[M-3PF_6]^{3+}$	$[M-4PF_6]^{4+}$	Others
$[(\textit{terpy})Ru(\textbf{\textit{L}}^{11})Ru(\textit{terpy})][PF_6]_4$				351.8	
$[(\textit{terpy})Ru(\textbf{\textit{L}}^{12})Ru(\textit{terpy})][PF_6]_4$		891.8	546.4	374.1	
$[(\textbf{\textit{L}}^{4})Ru(\textbf{\textit{L}}^{13})Ru(\textbf{\textit{L}}^{4})][PF_6]_4$					706.0, 598.6
$[(\textit{terpy})Ru(\textbf{\textit{L}}^{14})Ru(\textit{terpy})][PF_6]_4$		879.2	537.5	367.4	
$[(\textit{terpy})Ru(\textbf{\textit{L}}^{16})Ru(\textit{terpy})][PF_6]_4$			508.4	344.8	
$[(\textit{terpy})Ru(\textbf{\textit{L}}^{17})Ru(\textit{terpy})][PF_6]_4$				367.2	

Table 2. The ES-MS data of the six homodinuclear Ru(II) complexes.

In the ES-MS spectrum of $[(\textit{terpy})Ru(\textbf{\textit{L}}^{14})Ru(\textit{terpy})][PF_6]_4$, which is shown in **Figure 9**, a peak at *m/z* 367.4 assigned to $[M-4PF_6]^{4+}$ was the major signal. The other two minor signals at *m/z* 879.2 and 537.5 correspond to $[M-2PF_6]^{2+}$ and $[M-3PF_6]^{3+}$ respectively.
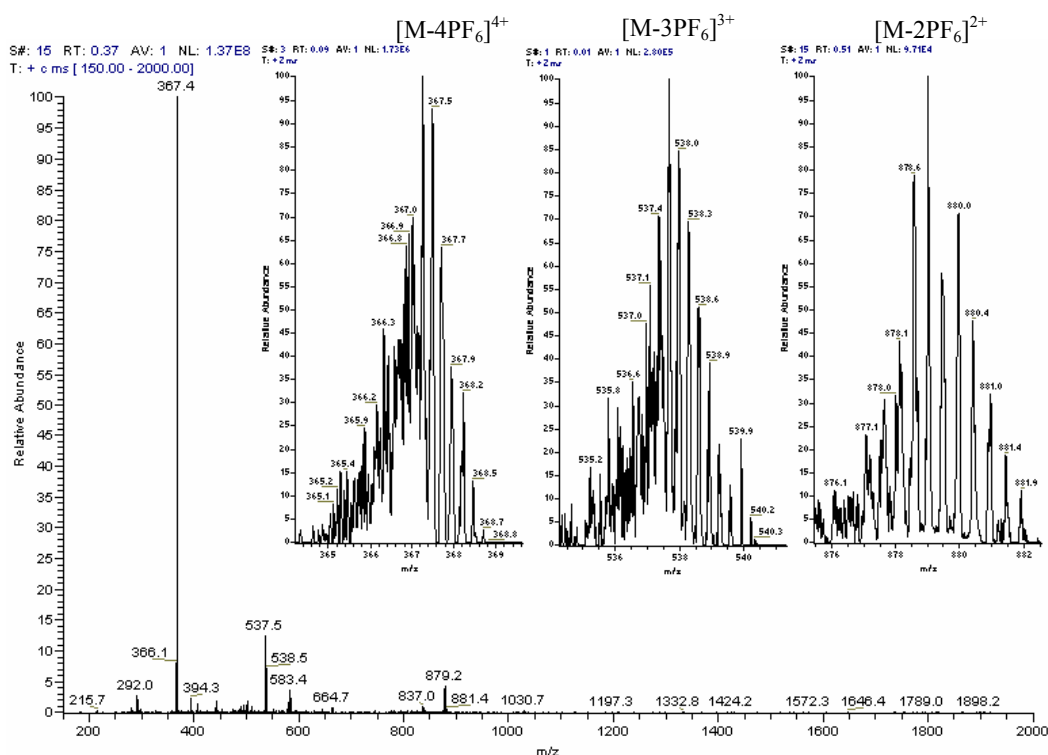
Figure 9. The ES-MS spectrum of [(***terpy***)Ru(***L***^{14})Ru(***terpy***)][PF$_6$]$_4$.

6.4   Absorption spectroscopic characterisation

The electronic spectra of the dinuclear Ru(II) complexes were recorded in HPLC grade acetonitrile solution. The absorption spectra of these complexes are similar to the sum of the spectra of [Ru(***terpy***)$_2$]$^{2+}$ and those of the substituents. The absorption data for these six homodinuclear complexes are summarised in **Table 3**. The very intense bands in the UV region are assigned to the ligand-centred π*←π transitions. The Ru(II) complexes exhibit a low energy metal-to-ligand charge transfer (MLCT) transition with λ$_{max}$ between 475 to 483 nm. The absorption coefficients of these dinuclear complexes are nearly double those observed for the mononuclear complexes.[12-14]

	λ_{max}, nm (ε / 10^3 M^{-1}cm^{-1})	
	LC	LMCT
[(*terpy*)Ru(***L***^{11})Ru(*terpy*)][PF$_6$]$_4$	226 (182), 238 (98.4), 267 (111), 303 (132)	475 (36.5)
[(*terpy*)Ru(***L***^{12})Ru(*terpy*)][PF$_6$]$_4$	229 (141), 241 (76.6), 269 (84.7), 305 (107)	480 (28.5)
[(***L***^{4})Ru(***L***^{13})Ru(***L***^{4})][PF$_6$]$_4$	221 (218), 233 (130), 267 (108), 301 (95.7)	483 (27.8)
[(*terpy*)Ru(***L***^{14})Ru(*terpy*)][PF$_6$]$_4$	234 (158), 269 (103), 305 (128)	481 (34.5)
[(*terpy*)Ru(***L***^{16})Ru(*terpy*)][PF$_6$]$_4$	229 (126), 267 (89.1), 303 (105)	477 (28.9)
[(*terpy*)Ru(***L***^{17})Ru(*terpy*)][PF$_6$]$_4$	230 (135), 267 (92.9), 303 (115)	476 (31.5)

Table 3. Electronic spectroscopic data for the complexes in acetonitrile solution.

6.5   Conclusion

All six new homodinuclear Ru(II) complexes [(***L***^{a})Ru(***L***^{b})Ru(***L***^{a})][PF$_6$]$_4$ (where ***L***^{b} = ***L***^{11}-***L***^{14}, ***L***^{16}-***L***^{17} and ***L***^{a} = ***terpy*** or ***L***^{4}), which incorporate ligands in which a naphthalene unit bridges the 4′-positions of two 2,2′:6′,2″-terpyridine domains, have been synthesised and characterised with ^{1}H NMR spectroscopy, ES-MS spectrometry, UV/VIS spectroscopy and elemental analysis.

6.6   Experimental

❖ [(**terpy**)Ru(**L^{11}**)Ru(**terpy**)][PF$_6$]$_4$

❖ [(**terpy**)Ru(**L^{12}**)Ru(**terpy**)][PF$_6$]$_4$

❖ [(**L^4**)Ru(**L^{13}**)Ru(**L^4**)][PF$_6$]$_4$

❖ [(**terpy**)Ru(**L^{14}**)Ru(**terpy**)][PF$_6$]$_4$

❖ [(**terpy**)Ru(**L^{16}**)Ru(**terpy**)][PF$_6$]$_4$

❖ [(**terpy**)Ru(**L^{17}**)Ru(**terpy**)][PF$_6$]$_4$

where   **L^{11}**   2,6-[Bis(2,2′:6′,2″-terpyridin-4′-yl)-1,4-dioxapentyl]naphthalene

L^{12}   2,6-[Bis(2,2′:6′,2″-terpyridin-4′-yl)-1,4,7-trioxaoctyl]naphthalene

L^{13}   2,7-[Bis(2,2′:6′,2″-terpyridin-4′-yl)-1,4-dioxabutyl]naphthalene

L^{14}   2,7-[Bis(2,2′:6′,2″-terpyridin-4′-yl)-1,4,7-trioxaheptyl]naphthalene

L^{16}   2,3-[Bis(2,2′:6′,2″-terpyridin-4′-yl)-1,4-dioxabutyl]naphthalene

L^{17}   2,3-[Bis(2,2′:6′,2″-terpyridin-4′-yl)-1,4,7-trioxaheptyl]naphthalene

L^4   4′-(Naphthalen-2-ylmethoxy)-2,2′:6′,2″-terpyridine

terpy   2,2′:6′,2″-terpyridine

General synthesis of linear homodinuclear ruthenium(II) metal complexes[10-14]

L^b (**L^b** = **L^{11}-L^{14}**, **L^{16}-L^{17}**)

⬬ = naphthyl domain

〰 = ethylene chain

⟩ = terpyridine domain

[(**L^a**)Ru(**L^b**)Ru(**L^a**)][PF$_6$]$_4$
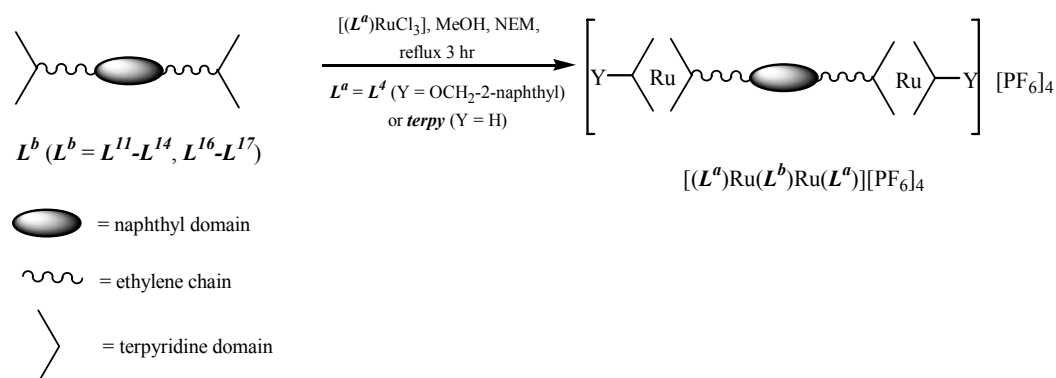
1 equivalent of **L^b** (**L^{11}-L^{14}**, **L^{16}-L^{17}**), 2 equivalents of [Ru(**L^a**)Cl$_3$] (where **L^a** = **terpy** or **L^4**) and a few drops of *N*-ethylmorpholine (NEM) were heated to reflux for 3 hours in CH$_3$OH. The deep red reaction mixture was cooled, and excess aqueous NH$_4$PF$_6$ were added to precipitate the crude product. The crude product was collected by filtration. The red product was obtained after column chromatography or preparative TLC (SiO$_2$, CH$_3$CN: saturated aqueous KNO$_3$: water 14:2:1).

❖ [(***terpy***)Ru(***L^11***)Ru(***terpy***)][PF₆]₄

Molecular formula: $C_{76}H_{60}N_{12}O_4Ru_2P_4F_{24}$

Molecular weigtht: 1987.36

L^11 (0.05 g, 0.07 mmol) and [Ru(***terpy***)Cl₃] (60 mg, 0.14 mmol) were used. After column chromatography (SiO₂, CH₃CN: saturated aqueous KNO₃: water 14:2:1), a red powder of [(***terpy***)Ru(***L^11***)Ru(***terpy***)][PF₆]₄ (14.1 mg, 10.1%) was obtained.

¹H NMR (500 MHz, CD₃CN): δ_H 4.13 (m, 4H, H^{S2}), 4.75 (m, 4H, H^{S1}), 4.86 (s, 4H, H^{S3}), 7.11 (ddd, *J* 1.3, 5.6, 7.6 Hz, 4H, H^{C5}), 7.14 (ddd, *J* 1.4, 5.6, 7.6 Hz, 4H, H^{A5}), 7.29 (ddd, *J* 0.7, 1.4, 5.6 Hz, 4H, H^{C6}), 7.40 (ddd, *J* 0.7, 1.4, 5.6 Hz, 4H, H^{A6}), 7.56 (dd, *J* 1.4, 8.5 Hz, 2H, H$^{N3, N7}$), 7.86 (m, 6H, H$^{N4, N8}$ and H^{C4}), 7.90 (m, 4H, H^{A4}), 7.92 (s, 2H, H$^{N1, N5}$), 8.36 (s, 4H, H^{D3}), 8.36 (t, *J* 8.1 Hz, 2H, H^{B4}), 8.42 (ddd, *J* 0.8, 1.2, 8.1 Hz, 4H, H^{C3}), 8.47 (ddd, *J* 0.8, 1.2, 8.1 Hz, 4H, H^{A3}), 8.72 (d, *J* 8.2 Hz, 4H, H^{B3}).

MS (ES): *m/z* = 351.8 [M-4PF₆]⁴⁺.

UV/VIS (CH₃CN): λ*max*/ nm (ε*max*, M⁻¹cm⁻¹) 226 (182 x 10³), 238 (98.4 x 10³), 267 (111 x 10³), 303 (132 x 10³), 475 (36.5 x 10³).

Elemental Analysis: Found: C, 44.69; H, 3.07; N, 8.42. Calc. for $C_{76}H_{60}N_{12}O_4P_4F_{24}Ru_2 \cdot 3H_2O$: C, 44.71; H, 3.27; N, 8.24%.

❖ [(***terpy***)Ru(***L^12***)Ru(***terpy***)][PF₆]₄

Molecular formula: $C_{80}H_{68}N_{12}O_6Ru_2P_4F_{24}$

Molecular weight: 2075.47

L^{12} (0.13 g, 0.16 mmol) and [Ru(**terpy**)Cl$_3$] (0.14 g, 0.32 mmol) were used. After preparative TLC (SiO$_2$, CH$_3$CN: saturate aqueous KNO$_3$: water 14:2:1), a red powder of [(**terpy**)Ru(**L^{12}**)Ru(**terpy**)][PF$_6$]$_4$ (89.8 mg, 27.0%) was obtained.

^{1}H NMR (600 MHz, CD$_3$CN): δ$_H$ 3.75 (m, 4H, H^{S4}), 3.84 (m, 4H, H^{S3}), 4.07 (t, *J* 4.2 Hz, 4H, H^{S2}), 4.69 (m, 8H, H^{S1} and H^{S5}), 7.10 (m, 4H, H^{C5}), 7.15 (m, 4H, H^{A5}), 7.28 (d, *J* 5.4 Hz, 4H, H^{C6}), 7.40 (d, *J* 6.0 Hz, 4H, H^{A6}), 7.47 (dd, *J* 1.2, 7.2 Hz, 2H, H$^{N3,\,N7}$), 7.79 (s, 2H, H$^{N1,\,N5}$), 7.81 (d, *J* 7.8 Hz, 2H, H$^{N4,\,N8}$), 7.85 (td, *J* 1.6, 7.8 Hz, 4H, H^{C4}), 7.90 (td, *J* 1.2, 7.8 Hz, 4H, H^{A4}), 8.33 (s, 4H, H^{D3}), 8.37 (t, *J* 8.1 Hz, 2H, H^{B4}), 8.43 (d, *J* 8.4 Hz, 4H, H^{C3}), 8.47 (d, *J* 8.4 Hz, 4H, H^{A3}), 8.72 (d, *J* 8.4 Hz, 4H, H^{B3}).

MS (ES): *m/z* = 891.8 [M-2PF$_6$]$^{2+}$, 546.4 [M-3PF$_6$]$^{3+}$, 374.1 [M-4PF$_6$]$^{4+}$.

UV/VIS (CH$_3$CN): λ$_{max}$/ nm (ε$_{max}$, M^{-1}cm^{-1}) 229 (141 x 10^3), 241 (76.6 x 10^3), 269 (84.7 x 10^3), 305 (107 x 10^3), 480 (28.5 x 10^3).

Elemental Analysis: Found: C, 45.05; H, 3.38; N, 7.89. Calc. for C$_{80}$H$_{68}$N$_{12}$O$_6$P$_4$F$_{24}$Ru$_2$·2H$_2$O: C, 45.50; H, 3.44; N, 7.96%.

❖ [(**L^4**)Ru(**L^{13}**)Ru(**L^4**)][PF$_6$]$_4$
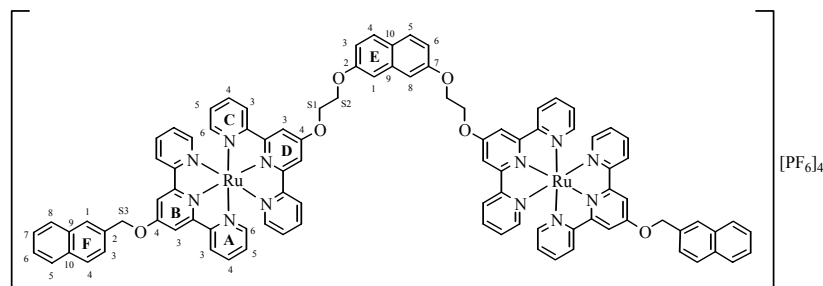
Molecular formula: C$_{96}$H$_{72}$N$_{12}$O$_6$Ru$_2$P$_4$F$_{24}$
Molecular weight: 2271.67

L^{13} (0.071 g, 0.10 mmol) and [Ru(**L^4**)Cl$_3$] (0.12 g, 0.20 mmol) were used. After column chromatography (SiO$_2$, CH$_3$CN: saturate aqueous KNO$_3$: water 14:2:1), a red powder of [(**L^4**)Ru(**L^{13}**)Ru(**L^4**)][PF$_6$]$_4$ (75.3 mg, 33.1%) was obtained.

^{1}H NMR (500 MHz, CD$_3$CN): δ$_H$ 4.71 (m, 4H, H^{S2}), 4.97 (m, 4H, H^{S1}), 5.79 (s, 4H, H^{S3}), 7.16 (m, 10H, H^{A5}, H^{C5} and H$^{E3,\,E6}$), 7.42 (m, 10H, H^{A6}, H^{C6} and H$^{E1,\,E8}$), 7.61 (m, 4H, H^{F6} and H^{F7}), 7.79 (dd, *J* 1.7, 8.4 Hz, 2H, H^{F3}), 7.83 (d, *J* 9.0 Hz, 2H, H$^{E4,\,E5}$), 7.90 (m, 8H, H^{A4} and H^{C4}), 7.98 (m, 4H, H^{F5} and H^{F8}), 8.07 (d, *J* 8.5 Hz, 2H, H^{F4}), 8.20 (s, 2H, H^{F1}), 8.40 (s, 4H, H^{D3}), 8.47 (s, 4H, H^{B3}), 8.49 (d, *J* 7.7 Hz, 8H, H^{A3} and H^{C3}).

MS (ES): m/z = 706.0 [(**O-Terpy**)Ru(**L^{13}**)Ru(**Terpy-O**)]$^{2+}$, 598.6 [Ru(**O-terpy**)(**HO-terpy**)]$^{+}$.

UV/VIS (CH$_3$CN): λ_{max}/ nm (ε_{max}, M^{-1}cm^{-1}) 221 (218 x 10^3), 233 (130 x 10^3), 267 (108 x 10^3), 301 (95.7 x 10^3), 483 (27.8 x 10^3).

Elemental Analysis: Found: C, 50.33; H, 3.60; N, 7.17. Calc. for C$_{96}$H$_{72}$N$_{12}$O$_6$P$_4$F$_{24}$Ru$_2$: C, 50.76; H, 3.19; N, 7.40%.

❖ [(**terpy**)Ru(**L^{14}**)Ru(**terpy**)][PF$_6$]$_4$
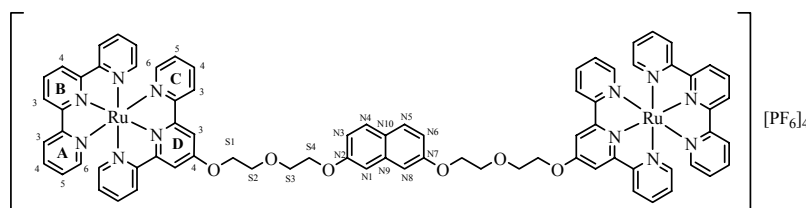
Molecular formula: C$_{78}$H$_{64}$N$_{12}$O$_6$Ru$_2$P$_4$F$_{24}$
Molecular weight: 2047.42

L^{14} (0.08 g, 0.1 mmol) and [Ru(**terpy**)Cl$_3$] (0.09 g, 0.2 mmol) were used. After column chromatography (SiO$_2$, CH$_3$CN: saturate aqueous KNO$_3$: water 14:2:1), a red powder of [(**terpy**)Ru(**L^{14}**)Ru(**terpy**)][PF$_6$]$_4$ (69.0 mg, 33.7%) was obtained.

^{1}H NMR (500 MHz, CD$_3$CN): δ_H 4.04 (m, 4H, H^{S3}), 4.15 (m, 4H, H^{S2}), 4.28 (m, 4H, H^{S4}), 4.71 (m, 4H, H^{S1}), 6.97 (dd, J 2.5, 8.9 Hz, 2H, H$^{N3, N6}$), 7.08 (ddd, J 1.3, 5.6, 7.6 Hz, 4H, H^{C5}), 7.14 (d, J 2.7 Hz, 2H, H$^{N1, N8}$), 7.16 (ddd, J 1.3, 5.7, 7.6 Hz, 4H, H^{A5}), 7.27 (ddd, J 0.6, 1.4, 5.6 Hz, 4H, H^{C6}), 7.41 (ddd, J 0.7, 1.4, 5.6 Hz, 4H, H^{A6}), 7.58 (d, J 9.0 Hz, 2H, H$^{N4, N5}$), 7.83 (td, J 1.4, 7.9 Hz, 4H, H^{C4}), 7.90 (td, J 1.4, 7.9 Hz, 4H, H^{A4}), 8.33 (s, 4H, H^{D3}), 8.36 (t, J 8.2 Hz, 2H, H^{B4}), 8.40 (ddd, J 0.7, 1.1, 8.1 Hz, 4H, H^{C3}), 8.47 (ddd, J 0.8, 1.1, 8.1 Hz, 4H, H^{A3}), 8.72 (d, J 8.2 Hz, 4H, H^{B3}).

MS (ES): m/z = 879.2 [M-2PF$_6$]$^{2+}$, 537.5 [M-3PF$_6$]$^{3+}$, 367.4 [M-4PF$_6$]$^{4+}$.

UV/VIS (CH$_3$CN): λ_{max}/ nm (ε_{max}, M^{-1}cm^{-1}) 234 (158 x 10^3), 269 (103 x 10^3), 305 (128 x 10^3), 481 (34.5 x 10^3).

Elemental Analysis: Found: C, 44.99; H, 3.25; N, 8.03. Calc. for C$_{78}$H$_{64}$N$_{12}$O$_6$P$_4$F$_{24}$Ru$_2$·H$_2$O: C, 45.35; H, 3.23; N, 8.14%.

❖ [(***terpy***)Ru(***L***^{16})Ru(***terpy***)][PF$_6$]$_4$
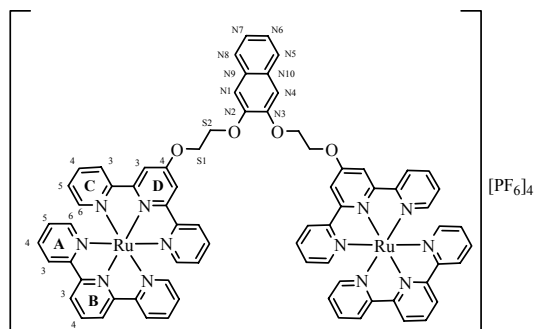
Molecular formula: C$_{74}$H$_{56}$N$_{12}$O$_4$Ru$_2$P$_4$F$_{24}$

Molecular weight: 1959.31

L^{16} (0.04 g, 0.06 mmol) and [Ru(***terpy***)Cl$_3$] (50 mg, 0.12 mmol) were used. A red powder of [(***terpy***)Ru(***L***^{16})Ru(***terpy***)][PF$_6$]$_4$ (25.2 mg, 21.4%) was obtained.

^{1}H NMR (500 MHz, CD$_3$CN): δ$_H$ 4.83 (m, 4H, H^{S2}), 5.01 (m, 4H, H^{S1}), 6.94 (ddd, *J* 1.3, 5.7, 7.5 Hz, 4H, H$^{C5/A5}$), 7.08 (ddd, *J* 1.3, 5.7, 7.5 Hz, 4H, H$^{A5/C5}$), 7.28 (ddd, *J* 0.6, 1.4, 5.6 Hz, 4H, H$^{A6/C6}$), 7.39 (ddd, *J* 0.7, 1.4, 5.6 Hz, 4H, H$^{A6/C6}$), 7.43 (m, 2H, H$^{N7, N6}$), 7.58 (s, 2H, H$^{N1, N4}$), 7.75 (m, 8H, H^{A4} and H^{C4}), 7.86 (m, *2*H, H$^{N8, N5}$), 8.36 (t, *J* 8.1 Hz, 2H, H^{B4}), 8.41 (s, 4H, H^{D3}), 8.43 (m, 8H, H^{A3} and H^{C3}), 8.71 (d, *J* 8.2 Hz, 4H, H^{B3}).

MS (ES): *m/z* = 508.4 [M-3PF$_6$]$^{3+}$, 344.8 [M-4PF$_6$]$^{4+}$.

UV/VIS (CH$_3$CN): λ$_{max}$/ nm (ε$_{max}$, M^{-1}cm^{-1}) 229 (126 x 10^3), 267 (89.1 x 10^3), 303 (105 x 10^3), 477 (28.9 x 10^3).

Elemental Analysis: Found: C, 43.58; H, 3.06; N, 8.06. Calc. for C$_{74}$H$_{56}$N$_{12}$O$_4$P$_4$F$_{24}$Ru$_2$·4H$_2$O: C, 43.75; H, 3.18; N, 8.28%.

❖ [(*terpy*)Ru(*L^17*)Ru(*terpy*)][PF$_6$]$_4$
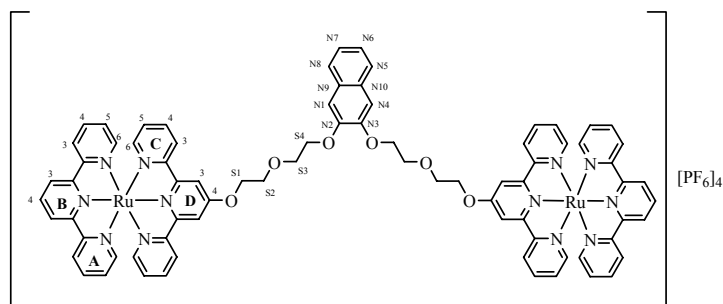
Molecular formula: C$_{78}$H$_{64}$N$_{12}$O$_6$Ru$_2$P$_4$F$_{24}$

Molecular weight: 2047.42

L^17 (0.05 g, 0.06 mmol) and [Ru(*terpy*)Cl$_3$] (50 mg, 0.12 mmol) were used. After column chromatography (SiO$_2$, CH$_3$CN: saturate aqueous KNO$_3$: water 14:2:1), a red powder of [(*terpy*)Ru(*L^17*)Ru(*terpy*)][PF$_6$]$_4$ (81.2 mg, 66.1%) was obtained.

^{1}H NMR (500 MHz, CD$_3$CN): δ_H 4.12 (m, 4H, H^{S3}), 4.21 (m, 4H, H^{S2}), 4.40 (m, 4H, H^{S4}), 4.74 (m, 4H, H^{S1}), 7.08 (ddd, *J* 1.3, 5.6, 7.6 Hz, 4H, H^{C5}), 7.15 (ddd, *J* 1.3, 5.6, 7.6 Hz, 4H, H^{A5}), 7.24 (m, 2H, H$^{N6, N7}$), 7.27 (ddd, *J* 0.6, 1.4, 5.6 Hz, 4H, H^{C6}), 7.33 (s, 2H, H$^{N1, N4}$), 7.41 (ddd, *J* 0.7, 1.4, 5.6 Hz, 4H, H^{A6}), 7.63 (m, 2H, H$^{N5, N8}$), 7.82 (td, *J* 1.5, 7.5 Hz, 4H, H^{C4}), 7.89 (td, *J* 1.5, 7.9 Hz, 4H, H^{A4}), 8.32 (s, 4H, H^{D3}), 8.36 (t, *J* 8.2 Hz, 2H, H^{B4}), 8.39 (ddd, *J* 0.7, 1.1, 8.1 Hz, 4H, H^{C3}), 8.47 (ddd, *J* 0.7, 1.2, 8.2 Hz, 4H, H^{A3}), 8.72 (d, *J* 8.2 Hz, 4H, H^{B3}).

MS (ES): *m/z* = 367.2 [M-4PF$_6$]$^{4+}$.

UV/VIS (CH$_3$CN): λ_{max}/ nm (ε_{max}, M^{-1}cm^{-1}) 230 (135 x 10^3), 267 (92.9 x 10^3), 303 (115 x 10^3), 476 (31.5 x 10^3).

Elemental Analysis: Found: C, 44.60; H, 3.45; N, 8.11. Calc. for C$_{78}$H$_{64}$N$_{12}$O$_6$P$_4$F$_{24}$Ru$_2$·2H$_2$O: C, 44.96; H, 3.30; N, 8.07%.

6.7   References

1.   J.-P. Sauvage, J.-P. Collin, J.-C. Chambron, S. Guillerez, C. Coudret, V. Balzani, F. Barigelletti, L. De Cola, and L. Flamigni, *Chem. Rev.*, 1994, **94**, 993.

2.   J.-P. Collin, P. Gaviña, V. Heitz, and J.-P. Sauvage, *Eur. J. Inorg. Chem.*, 1998, 1.

3.   U. S. Schubert, and C. Eschbaumer, *Angew. Chem. Int. Ed.*, 2002, **41**, 2892.

4.   V. Grosshenny, and R. Ziessel, *J. Organomet. Chem.*, 1993, **453**, C19.

5.   V. Grosshenny, A. Harriman, J.-P. Gisselbrecht, and R. Ziessel, *J. Am. Chem. Soc.*, 1996, **118**, 10315.

6.   M. Hissler, A. El-ghayoury, A. Harriman, and R. Ziessel, *Angew. Chem. Int. Ed.*, 1998, **37**, 1717.

7.   F. Barigelletti, L. Flamigni, V. Balzani, J.-P. Collin, J.-P. Sauvage, A. Sour, E. C. Constable, and A. M. W. Cargill Thompson, *J. Chem. Soc., Chem. Commun.*, 1993, 942.

8.   F. Barigelletti, L. Flamigni, V. Balzani, J.-P. Collin, J.-P. Sauvage, A. Sour, E. C. Constable, and A. M. W. Cargill Thompson, *J. Am. Chem. Soc.*, 1994, **116**, 7692.

9.   F. Barigelletti, L. Flamigni, J.-P. Collin, and J.-P. Sauvage, *Chem. Commun.*, 1997, 333.

10.   B. Whittle, S. R. Batten, J. C. Jeffery, L. H. Rees, and M. D. Ward, *J. Chem. Soc., Dalton Trans.*, 1996, 4249.

11.   S. Encinas, L. Flamigni, F. Barigelletti, E. C. Constable, C. E. Housecroft, E. R. Schofield, E. Figgemeier, D. Fenske, M. Neuburger, J. G. Vos, and M. Zehnder, *Chem. Eur. J.*, 2002, **8**, 137.

12.   E. C. Constable, and M. D. Ward, *J. Chem. Soc., Dalton Trans.*, 1990, 1405.

13.   E. C. Constable, and A. M. W. Cargill Thompson, *J. Chem. Soc., Dalton Trans.*, 1992, 3467.

14.   E. C. Constable, A. M. W. Cargill Thompson, P. Harveson, L. Macko, and M. Zehnder, *Chem. Eur. J.*, 1995, **1**, 360.

15.   E. C. Constable, and A. M. W. Cargill Thompson, *J. Chem. Soc., Dalton Trans.*, 1995, 1615.

Chapter 7

Synthesis of Metallomacrocyclic Ruthenium(II) and Iron(II) Complexes from Homoditopic 4′-Substituted-2,2′:6′,2″-Terpyridine Ligands

Multitopic bipyridine, terpyridine or derivative ligands are used for metal-directed self-assembly of supramolecular systems[1,2], such as rods[3-7], helices[8-20], knots[21], catenates[21-24], rotaxanes[25], boxes[26-36], grids[37-42], racks[43], ladders[44], cylinders[45], cages[46-48], and dendrimers[49-50]. Most of these metallosupramolecules are formed spontaneously by the reaction of labile metal ions with multidentate ligands. The principle of their formation depends mainly on (1) the number and orientation of the coordination sites of the ligand and (2) the coordination number and geometry of the metal ion.[1,51] For example, 2,2′:6′,2″:6″,2‴-quaterpyridine (*qterpy*), which contains two bidentate 2,2′-bipyridine metal binding domains, react with metal ions that favour a tetrahedral coordination geometry [like copper(I) or silver(I)] and result in a dinuclear double helicate (**Scheme 1**).[8,52]

<div align="center">

2,2′:6′,2″:6″,2‴-quaterpyridine
(*qterpy*)

$[M(\textit{qterpy})]_2^{2+}$
M = Cu(I) or Ag(I)

</div>
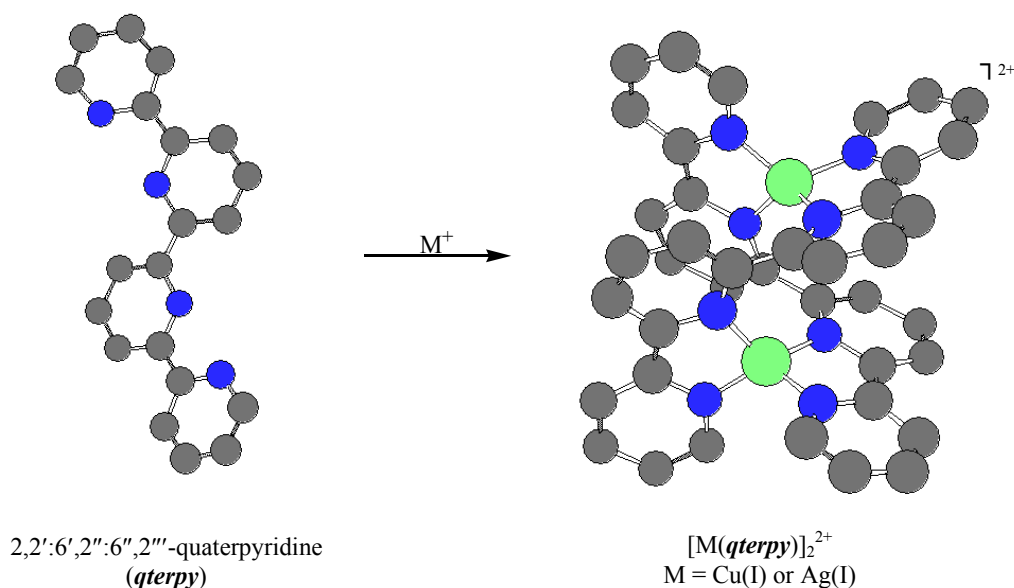
Scheme 1. The double helicate formed by two tetrahedral metal ions and two 2,2′:6′,2″:6″,2‴-quaterpyridine (*qterpy*) ligands (Chem3D Pro7.0).

In this chapter, we show that the ligands L^{11}-L^{17}, which have two tridentate binding sites, react with octahedral coordinated metal ions and give a range of [$n+n$] metallomacrocycles. The size of the metallomacrocycles depends on the rigidity and length of the spacer group between the metal binding sites (**Scheme 2**).

L^{11}	n = 1
L^{12}	n = 2
L^{13}	n = 1
L^{14}	n = 2
L^{15}	n = 3
L^{16}	n = 1
L^{17}	n = 2
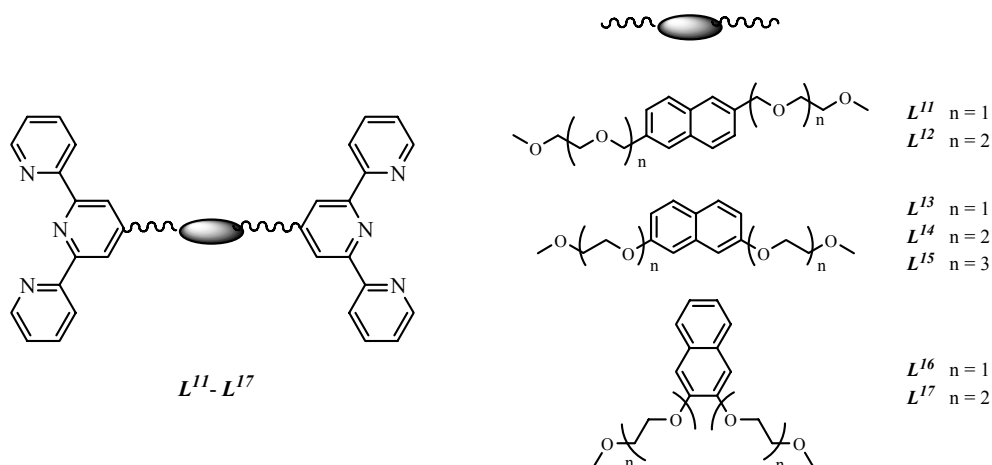
L^{11}-L^{17}

Scheme 2. The homoditopic ligands (L^{11}-L^{17}) used for the synthesis of the [$n+n$] metallomacrocycles.

7.1 Synthesis

(a) General synthesis of macrocyclic ruthenium(II) metal complexes

The self-assembled macrocyclic homoleptic Ru(II) complexes were prepared by reaction of the free bis(terpyridine) ligands L (L^{11}, L^{13}-L^{14}, L^{16}-L^{17}) with one equivalent of the adduct [Cl$_3$RuLRuCl$_3$] and a few drops of *N*-ethylmorpholine (NEM) in CH$_3$OH heated for a few hours at reflux.[36] The same ligand L is used in both components to yield homoleptic complexes. The TLC analysis (on silica) of the red solutions with A sol indicated that more than one ruthenium complexes were present and precipitation with NH$_4$PF$_6$ gave [{Ru(L)}$_n$][PF$_6$]$_{2n}$ as red powders. The yields of the major [{Ru(L)}$_n$][PF$_6$]$_{2n}$ (L = L^{11}, L^{13}-L^{14}, L^{16}-L^{17}, n = 2 or 3) complexes are low (ranging from 1-26% yield) after chromatographic workup (**Scheme 3**). There was no attempt to analyse the material (assumed to be polymeric) that remained on the baseline of the TLC plate.
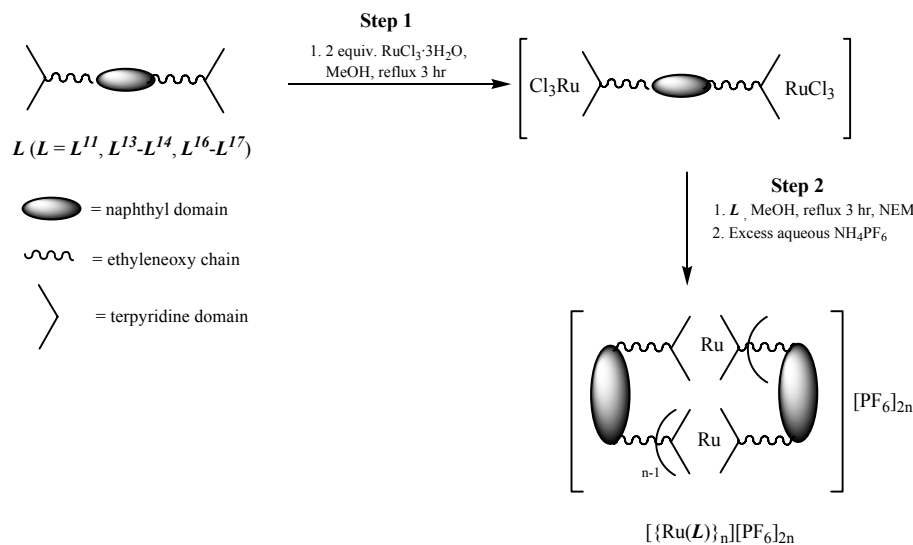
Scheme 3. The general synthesis of the metallomacrocyclic $[\{Ru(L)\}_n][PF_6]_{2n}$ complexes (where $L = L^{11}$, L^{13}-L^{14}, L^{16}-L^{17}). Only homoleptic complexes were made.

(b) General synthesis of macrocyclic iron(II) metal complexes

Reaction of L (L^{11}-L^{17}) with $FeCl_2 \cdot 4H_2O$ (1:1) in CH_3OH at room temperature gave purple solutions.[33-35] The TLC analysis (on silica) of the purple solutions with A sol indicated that more than one iron complexes were present and precipitation with NH_4PF_6 gave $[\{Fe(L)\}_n][PF_6]_{2n}$ as purple powders. After chromatographic workup, $[\{Fe(L)\}_n][PF_6]_{2n}$ (n = 1, 2 or 3) complexes were separated (**Scheme 4**). The yield of the major $[\{Fe(L)\}_n][PF_6]_{2n}$ (where $L = L^{11}$-L^{17}, n = 1, 2 or 3) complexes ranged from 1-47%. There was no attempt to analyse the material (assumed to be polymeric) that remained on the baseline of the TLC plate.
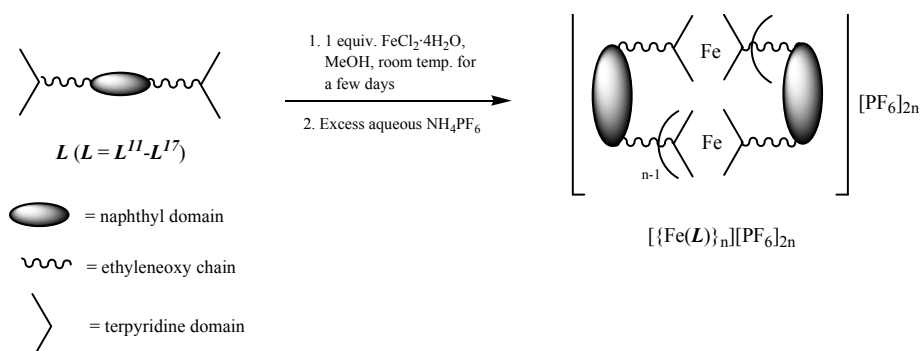
Scheme 4. The general synthesis of the metallomacrocyclic $[\{Fe(L)\}_n][PF_6]_{2n}$ complexes (where $L = L^{11}$-L^{17}).

7.2 ^{1}H NMR spectroscopic and electrospray ionisation mass spectrometric characterisation

Tables of the ^{1}H NMR spectroscopic data of the metallomacrocyclic [{Ru(L)}$_n$][PF$_6$]$_{2n}$ (L = L^{11}, L^{13}-L^{14}, L^{16}-L^{17}) complexes and [{Fe(L)}$_n$][PF$_6$]$_{2n}$ (L = L^{11}-L^{17}) complexes are shown in **Appendix VI**. All the ^{1}H NMR spectra of the metallomacrocycles are consistent with symmetrical complexes and, as usual, they exhibit five terpyridine signals, with the exception of the ^{1}H NMR spectrum of [{Fe(L^{14})}][PF$_6$]$_2$. Assignments have been made from COSY and NOESY experiments. However, the nuclearity of the metallomacrocycles cannot be elucidated by ^{1}H NMR technique. It can be determined by ES-MS. The isotopic patterns of the metallomacrocycles with different nuclearities are diagnostic (i.e. the isotopic pattern of a parent ion of a [2+2] metallomacrocycle is different from that of a [3+3] metallomacrocycle). The ES-MS spectra of all the metallomacrocycles are shown in **Appendix VI**.

(a) Macrocyclic ruthenium(II) metal complexes

❖ [{Ru(L^{11})}$_2$][PF$_6$]$_4$

When L^{11} was treated with [Cl$_3$RuL^{11}RuCl$_3$], a range of [{Ru(L^{11})}$_n$][PF$_6$]$_{2n}$ complexes was formed. The ES-MS spectrum of the major metallomacrocycle [{Ru(L^{11})}$_n$]$^{2n+}$, which was obtained after chromatography, in CH$_3$CN solution showed a major peak at *m/z* 420.1, with 0.25 mass units for the separation between peaks in an envelope, corresponding to [{Ru(L^{11})}$_2$]$^{4+}$. This was assigned to a [2+2] [{Ru(L^{11})}$_2$][PF$_6$]$_4$ species. The ^{1}H NMR spectrum of the metallomacrocyclic [{Ru(L^{11})}$_2$][PF$_6$]$_4$ complex shows that this coordinated complex is symmetrical with three aliphatic and eight aromatic proton resonances present (**Figure 1b**). The five terpyridine proton signals were assigned by comparison with signals in the spectrum of the mononuclear [Ru(L^5)$_2$]$^{2+}$ complex (**Figure 1a**) discussed in Chapter 3. There are around 0.1 ppm differences for the terpyridine proton signals between the mononuclear [Ru(L^5)$_2$]$^{2+}$ complex and the metallomacrocyclic [{Ru(L^{11})}$_2$]$^{4+}$ complex (**Figure 1**).
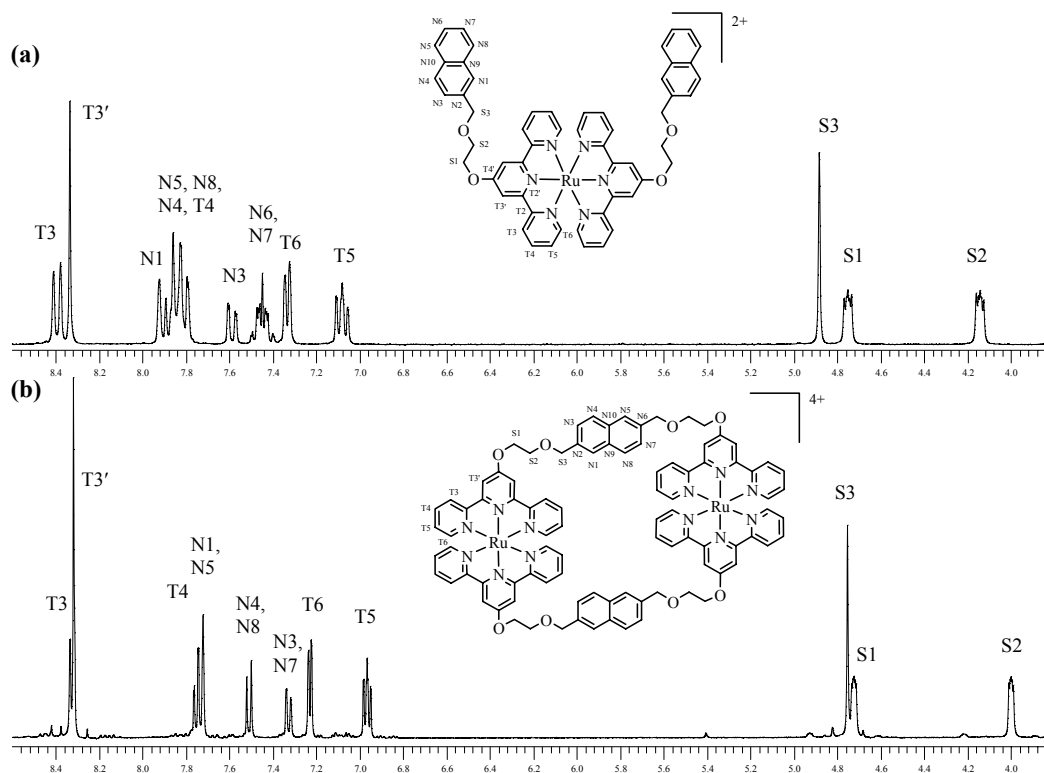
Figure 1. ^{1}H NMR spectra of (a) mononuclear [Ru(L^5)$_2$][PF$_6$]$_2$ (250 MHz) and (b) metallomacrocyclic [{Ru(L^{11})}$_2$][PF$_6$]$_4$ (400 MHz) in CD$_3$CN solution at room temperature.

❖ [{Ru(L^{13})}$_2$][PF$_6$]$_4$ and [{Ru(L^{13})}$_3$][PF$_6$]$_6$

When L^{13} was treated with [Cl$_3$RuL^{13}RuCl$_3$], a range of [{Ru(L^{13})}$_n$][PF$_6$]$_{2n}$ complexes was formed. From the TLC analysis of the crude product [{Ru(L^{13})}$_n$][PF$_6$]$_{2n}$, there were two very close red bands (R$_f$ values are 0.50 and 0.48 in A sol) plus a large amount of presumably polymeric material which remained on the baseline of the TLC plate. Preparative TLC was used to separate the two bands. ES-MS analysis of each band in CH$_3$CN solution provides strong evidence for the metallomacrocycles formation. The spectrum of the product with the R$_f$ value 0.50 contained a doubly charged ion at *m/z* 957.1 {[{Ru(L^{13})}$_2$][PF$_6$]$_2$}$^{2+}$, a triply charged ion at *m/z* 589.7 {[{Ru(L^{13})$_2$][PF$_6$]}$^{3+}$, and a quadruply charged ion at *m/z* 406.4 {[{Ru(L^{13})}$_2$]}$^{4+}$. The other spectrum of the product with the R$_f$ value 0.48 contained a triply charged ion at *m/z* 957.0 {[{Ru(L^{13})}$_3$][PF$_6$]$_3$}$^{3+}$, a quadruply charged ion at

m/z 681.2 $\{[\{Ru(\boldsymbol{L^{13}})\}_3][PF_6]_2\}^{4+}$, and a quintuply charged ion at *m/z* 515.8$\{[\{Ru(\boldsymbol{L^{13}})\}_3][PF_6]\}^{5+}$. As mentioned before, the isotopic pattern of a peak depends on the number of metal atoms and ligand molecules present. Therefore, the $[\{Ru(\boldsymbol{L^{13}})\}_2][PF_6]_4$ and $[\{Ru(\boldsymbol{L^{13}})\}_3][PF_6]_6$ can be distinguished by ES-MS. Peaks in the ES-MS of the metallomacrocyclic $[\{Ru(\boldsymbol{L^{13}})\}_2][PF_6]_4$ complex (higher R_f value) show an isotopic pattern which matches that of the calculated one (**Figure 2**).

$[\{Ru(\boldsymbol{L^{13}})\}_2][PF_6]_4$ $[\{Ru(\boldsymbol{L^{13}})\}_3][PF_6]_6$
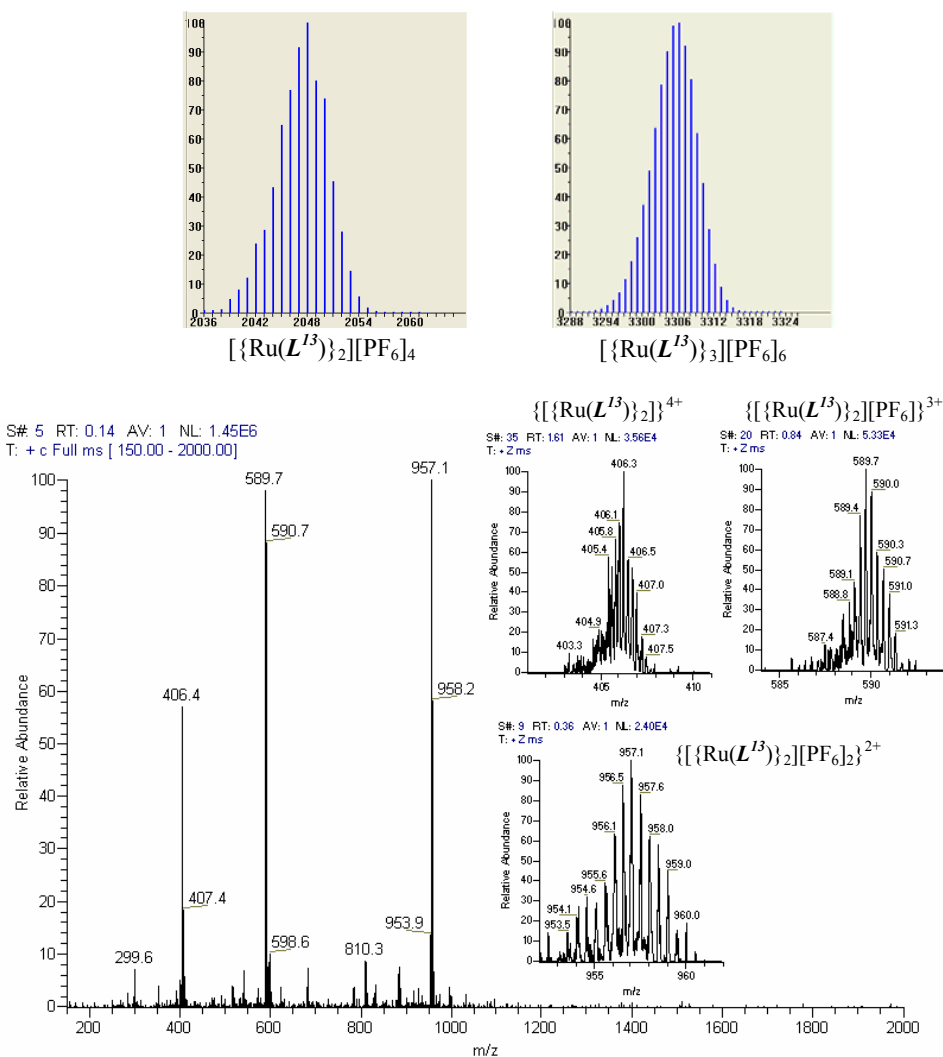
Figure 2. The ES-MS of the metallomacrocyclic $[\{Ru(\boldsymbol{L^{13}})\}_2][PF_6]_4$ complex.

The ^{1}H NMR spectra of $[\{Ru(\boldsymbol{L^{13}})\}_2][PF_6]_4$ (R_f value 0.50) and $[\{Ru(\boldsymbol{L^{13}})\}_3][PF_6]_6$ (R_f value 0.48) in CD$_3$CN solution were assigned as before. The data show each fraction contains one major component mixed with a minor amount of the second component. The spectra of the two species are highly symmetrical and the chemical shift

differences are evident in the aromatic and also aliphatic regions of both species (**Figure 3**). There are significant differences in the chemical shifts for H^{S2}, $H^{N1, N8}$, H^{T3} and $H^{T3'}$ between the two species.
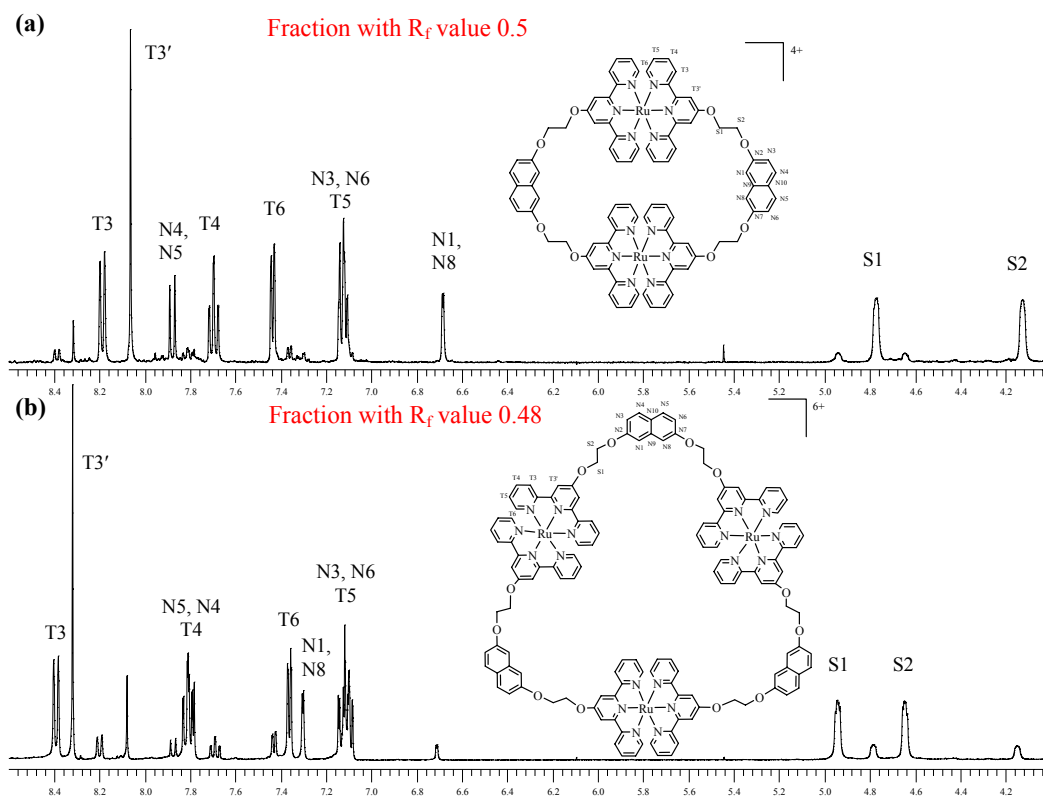
Figure 3. ^1H NMR spectra (400 MHz) of (a) the fraction at R_f value 0.50, which contains mainly dinuclear $[\{Ru(\boldsymbol{L^{13}})\}_2][PF_6]_4$ and (b) the fraction at R_f value 0.48, which contains mainly trinuclear $[\{Ru(\boldsymbol{L^{13}})\}_3][PF_6]_6$ in CD_3CN solution at room temperature.

❖ $[\{Ru(\boldsymbol{L^{14}})\}_2][PF_6]_4$

When $\boldsymbol{L^{14}}$ was treated with $[Cl_3Ru\boldsymbol{L^{14}}RuCl_3]$, a range of $[\{Ru(\boldsymbol{L^{14}})\}_n][PF_6]_{2n}$ complexes was formed. The ES-MS spectrum of the metallomacrocycles $[\{Ru(\boldsymbol{L^{14}})\}_n][PF_6]_{2n}$ in CH_3CN solution, which were obtained after chromatographic workup, showed a major peak at *m/z* 648.8 with 0.33 mass units for the separation between peaks in an envelope (corresponding to $\{[\{Ru(\boldsymbol{L^{14}})\}_2][PF_6]\}^{3+}$), and also peaks at *m/z* 1045.2 for a doubly charged ion $\{[\{Ru(\boldsymbol{L^{14}})\}_2][PF_6]_2\}^{2+}$ and at *m/z* 450.7 for a quadruply charged ion $\{[\{Ru(\boldsymbol{L^{14}})\}_2]\}^{4+}$. This was assigned to a [2+2]

$[\{Ru(\boldsymbol{L^{14}})\}_2][PF_6]_4$ species. The ^{1}H NMR spectrum of this metallomacrocyclic $[\{Ru(\boldsymbol{L^{14}})\}_2][PF_6]_4$ complex showed that this coordinated complex was symmetrical with four aliphatic and eight aromatic proton resonances present. The five terpyridine proton signals were assigned as before. The signal for $H^{T3'}$ showed a cross peak to the signal for H^{S1}. Therefore, the assignments of the ethyleneoxy spacer resonances in the ^{1}H NMR spectrum were made by using COSY and NOESY. Also, the signal for H^{S4} showed a cross peak to the signal for $H^{N1, N8}$.

❖ $[\{Ru(\boldsymbol{L^{16}})\}_2][PF_6]_4$

When $\boldsymbol{L^{16}}$ was treated with $[Cl_3Ru\boldsymbol{L^{16}}RuCl_3]$, a range of $[\{Ru(\boldsymbol{L^{16}})\}_n][PF_6]_{2n}$ complexes was formed. The ES-MS of a CH_3CN solution of $[\{Ru(\boldsymbol{L^{16}})\}_n][PF_6]_{2n}$, which was obtained after chromatographic work up, exhibited peaks that could be assigned to a [2+2] $[\{Ru(\boldsymbol{L^{16}})\}_2][PF_6]_4$ species (*m/z* 957.0 for a doubly charged ion $\{[\{Ru(\boldsymbol{L^{16}})\}_2][PF_6]_2\}^{2+}$, *m/z* 589.3 for a triply charged ion $\{[\{Ru(\boldsymbol{L^{16}})\}_2][PF_6]\}^{3+}$ and *m/z* 406.2 for a quadruply charged ion $\{[\{Ru(\boldsymbol{L^{16}})\}_2]\}^{4+}$). The ^{1}H NMR spectrum of the metallomacrocyclic $[\{Ru(\boldsymbol{L^{16}})\}_2][PF_6]_4$ complex is shown in **Figure 4a**. The assignments of the ^{1}H NMR spectrum were made by COSY and NOESY techniques. The five terpyridine proton signals were assigned as before. The signals for $H^{T3'}$ and $H^{N1, N4}$ showed cross peaks to H^{S1} and H^{S2} respectively. This allowed the assignment of the ethyleneoxy spacer resonances.
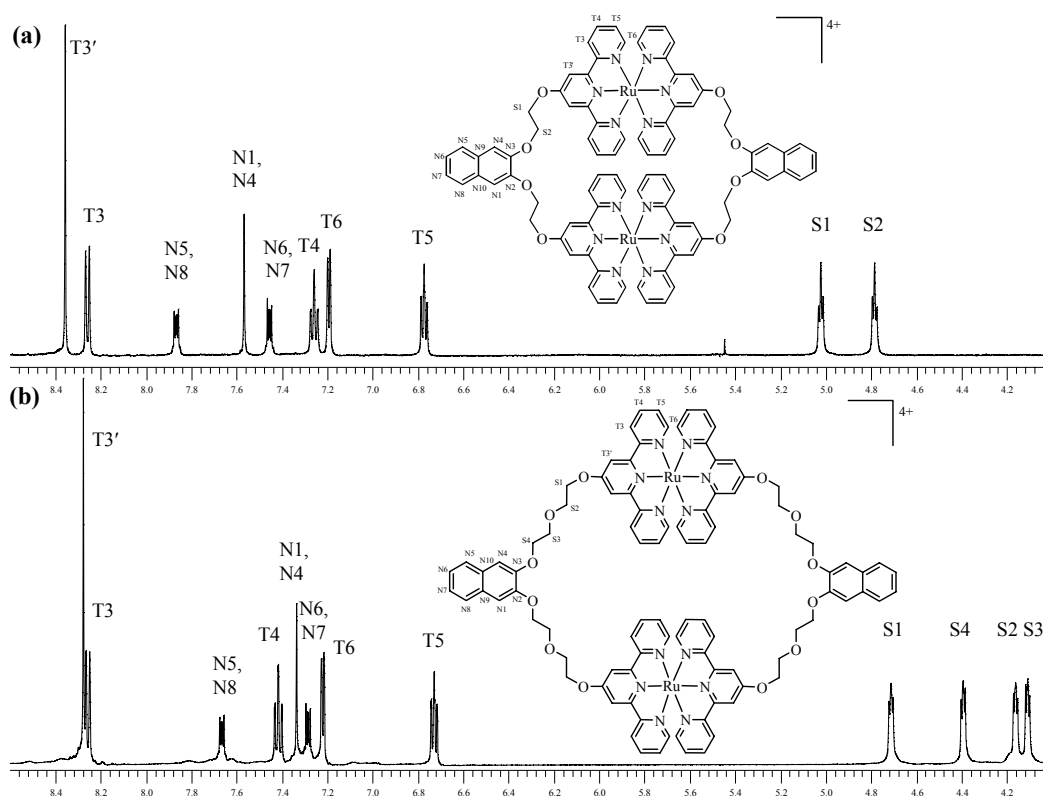
Figure 4. ^{1}H NMR spectra (500 MHz) of (a) dinuclear $[\{Ru(\textbf{\textit{L}}^{\textbf{\textit{16}}})\}_2][PF_6]_4$ and (b) dinuclear $[\{Ru(\textbf{\textit{L}}^{\textbf{\textit{17}}})\}_2][PF_6]_4$ in CD_3CN solution at room temperature.

❖ $[\{Ru(\textbf{\textit{L}}^{\textbf{\textit{17}}})\}_2][PF_6]_4$

When $\textbf{\textit{L}}^{\textbf{\textit{17}}}$ was treated with $[Cl_3Ru\textbf{\textit{L}}^{\textbf{\textit{17}}}RuCl_3]$, a range of $[\{Ru(\textbf{\textit{L}}^{\textbf{\textit{17}}})\}_n][PF_6]_{2n}$ complexes was formed. The ES-MS of a CH_3CN solution of $[\{Ru(\textbf{\textit{L}}^{\textbf{\textit{17}}})\}_n][PF_6]_{2n}$, which was obtained after chromatography, exhibited a peak that could be assigned to a [2+2] $[\{Ru(\textbf{\textit{L}}^{\textbf{\textit{17}}})\}_2][PF_6]_4$ species (*m/z* 449.9 for a quadruply charged ion $\{[\{Ru(\textbf{\textit{L}}^{\textbf{\textit{17}}})\}_2]\}^{4+}$). The ^{1}H NMR spectrum of the metallomacrocyclic $[\{Ru(\textbf{\textit{L}}^{\textbf{\textit{17}}})\}_2][PF_6]_4$ complex is shown in **Figure 4b**. The assignments of the ^{1}H NMR spectrum were made by COSY and NOESY techniques. The five terpyridine proton signals were assigned as before. The signal for $H^{T3'}$ at δ 8.28 shows an NOE signal to the signal at δ 4.71, and this is assigned to H^{S1} (**Figure 5**). The signal for H^{S1} gives a COSY cross peak to the signal for H^{S2} at δ 4.16 (**Figure 6**). And, the signal for H^{S2} exhibits an NOE cross peak to the signal for H^{S3} at δ 4.11 (**Figure 5**). The signal for

H^{S3} gives a COSY cross peak to the signal at δ 4.39, and this is assigned to H^{S4} (**Figure 6**). The signal for H^{S4} exhibits a strong NOE cross peak to $H^{N1, N4}$ at δ 7.34 (**Figure 5**). The signal for $H^{N1, N4}$ exhibits an NOE signal to $H^{N5, N8}$ at δ 7.67. The signal for $H^{N5, N8}$ gives a COSY cross peak to the signal at δ 7.29, and this is assigned to $H^{N6, N7}$.
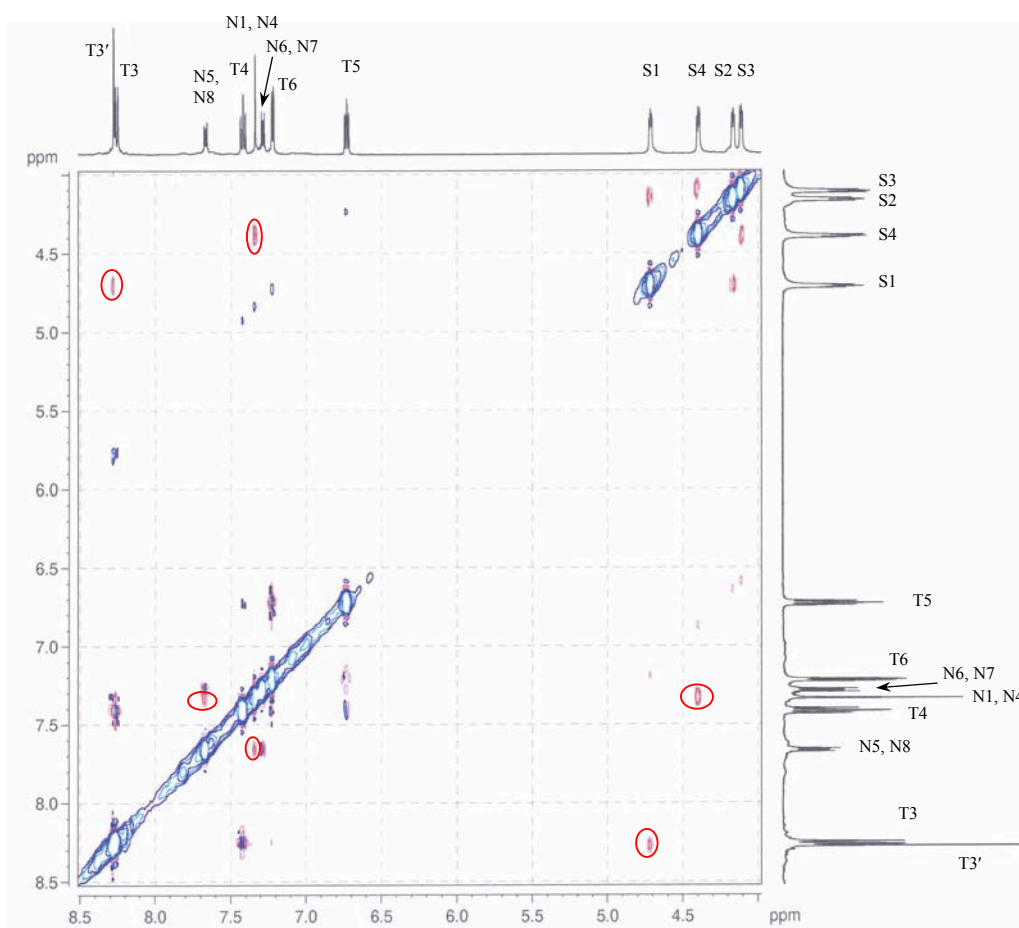
Figure 5. NOESY spectrum (500 MHz) of dinuclear $[\{Ru(\boldsymbol{L^{17}})\}_2][PF_6]_4$ in CD$_3$CN solution at room temperature.
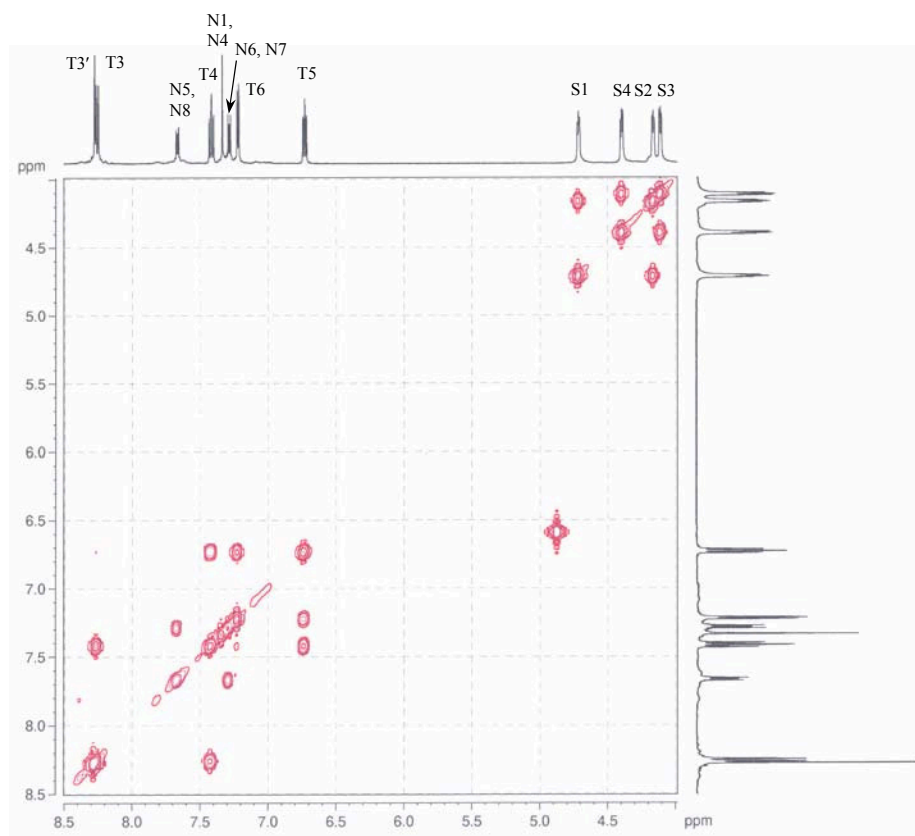
Figure 6. COSY spectrum (500 MHz) of dinuclear $[\{Ru(L^{17})\}_2][PF_6]_4$ in CD_3CN solution at room temperature.

(b) Macrocyclic iron(II) metal complexes

❖ $[\{Fe(L^{11})\}_2][PF_6]_4$

When ligand L^{11} was treated with $FeCl_2 \cdot 4H_2O$, a range of $[\{Fe(L^{11})\}_n][PF_6]_{2n}$ complexes was formed. The ES-MS of a CH_3CN solution of the major product $[\{Fe(L^{11})\}_n][PF_6]_{2n}$ obtained after chromatography exhibits peaks that could be assigned to a [2+2] $[\{Fe(L^{11})\}_2][PF_6]_4$ species (*m/z* 578.2 for a triply charged ion $\{[\{Fe(L^{11})\}_2][PF_6]\}^{3+}$ and *m/z* 397.5 for a quadruply charged ion $\{[\{Fe(L^{11})\}_2]\}^{4+}$) (**Figure 7**). The isotope patterns match those of the simulated spectra. The ^{1}H NMR spectrum of the metallomacrocyclic $[\{Fe(L^{11})\}_2][PF_6]_4$ complex is shown in **Figure 8**. The assignments of the ^{1}H NMR spectrum were made by COSY and NOESY techniques. The five terpyridine proton signals were assigned as before. The signals

for $H^{T3'}$ and $H^{N1, N5}$ showed cross peaks to the signals for H^{S1} and H^{S3} respectively. This allowed the assignment of the ethyleneoxy resonances.
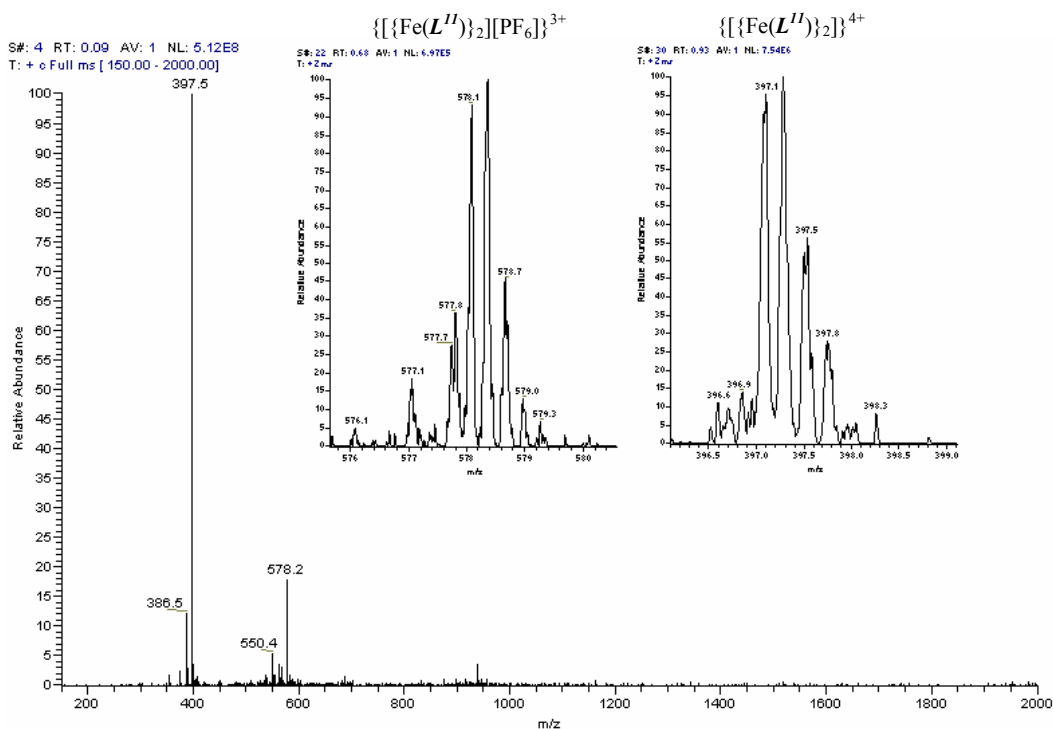
Figure 7. The ES-MS spectrum of $[\{Fe(\mathbf{\textit{L}^{II}})\}_2][PF_6]_4$.
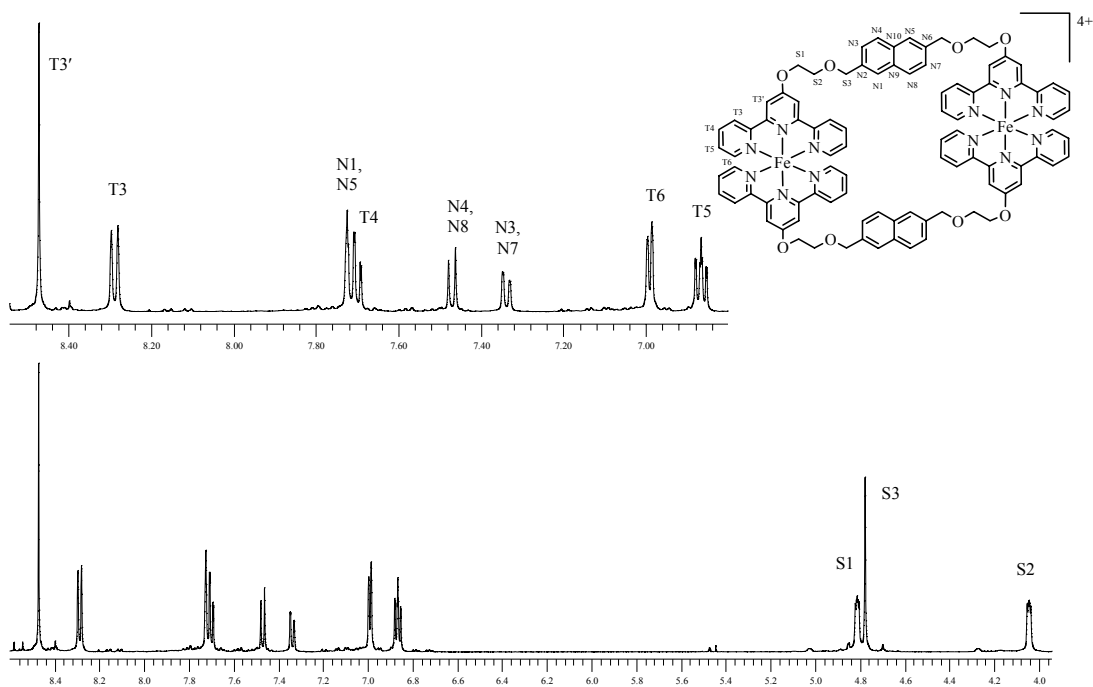
Figure 8. ^{1}H NMR spectrum (500 MHz) of the metallomacrocyclic $[\{Fe(\mathbf{\textit{L}^{II}})\}_2][PF_6]_4$ complex in CD$_3$CN solution at room temperature.
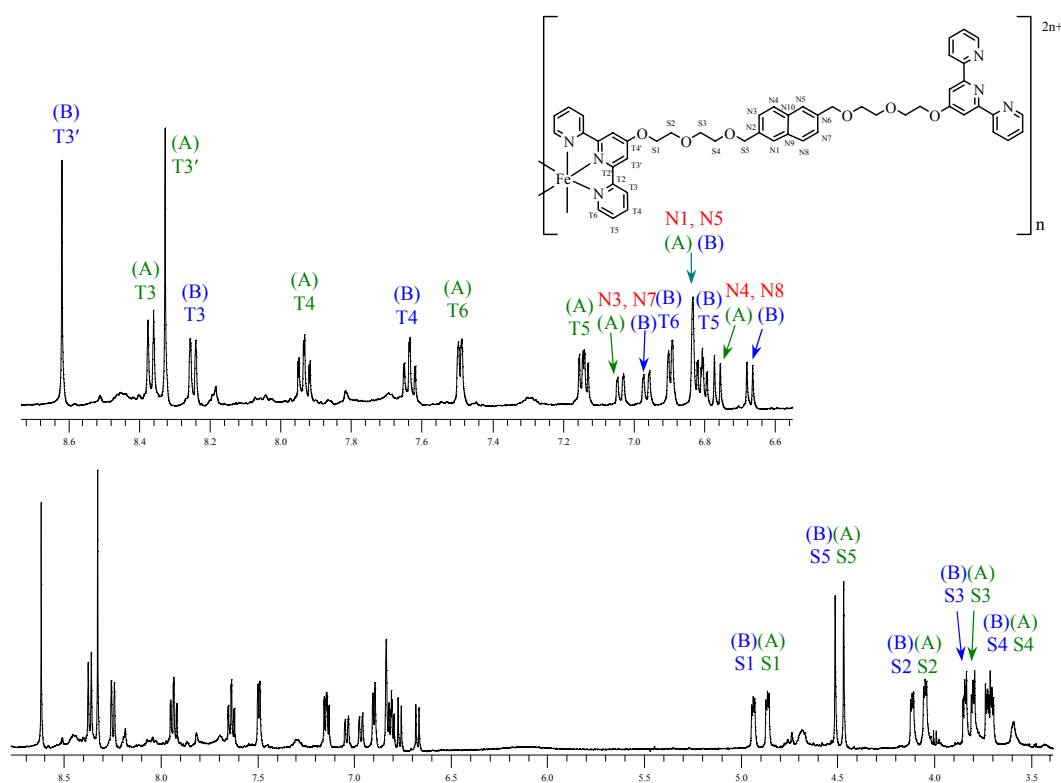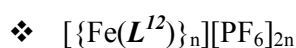
❖ $[\{Fe(\boldsymbol{L^{12}})\}_n][PF_6]_{2n}$

Figure 9. The ^1H NMR spectrum (500 MHz) of the major band of metallomacrocycles $[\{Fe(\boldsymbol{L^{12}})\}_n][PF_6]_{2n}$, which contained two compounds (A and B), in CD_3CN solution at room temperature.

When ligand $\boldsymbol{L^{12}}$ was treated with $FeCl_2 \cdot 4H_2O$, a range of $[\{Fe(\boldsymbol{L^{12}})\}_n][PF_6]_{2n}$ species was formed. The major band of metallomacrocycles $[\{Fe(\boldsymbol{L^{12}})\}_n][PF_6]_{2n}$ was obtained after preparative TLC chromatography. ES-MS analysis of this fraction in CH_3CN solution provided evidence for the metallomacrocycle formation. The spectrum contained a singly charged ion at *m/z* 1027.2 $\{[\{Fe(\boldsymbol{L^{12}})\}][PF_6]\}^+$, a singly charged ion at *m/z* 901.6 $\{[\{Fe(\boldsymbol{L^{12}})\}]F\}^+$, and a doubly charged ion at *m/z* 441.7 $\{[\{Fe(\boldsymbol{L^{12}})\}]\}^{2+}$. This indicated a [1+1] metallomacrocycle was formed. However, the ^1H NMR spectrum of this major fraction in CD_3CN solution shows that there are two sets of proton signals. The ratio of the two sets of signals varied from ≈ 1:1 to ≈ 1.5:1 when the reaction was repeated. Each sub-spectrum is consistent with a symmetrical product (**Figure 9**). This was proved by a range of NMR techniques, such as COSY, NOESY, HMQC, HMBC and NOE difference experiment at high temperature, that this fraction of the product contained two major compounds (A and B). This major

fraction remained as one band on the TLC plate in a variety of solvent systems, and the two compounds could not be separated. It was not possible to unambiguously assign compositions to the products A and B. Possibly, they are two different [*n+n*] metallomacrocycles although the ES-MS showed it is a [1+1] metallomacrocycle. In the case below, although the ES-MS of the fraction showed only peaks belonged to a [2+2] [Fe{(**L**^{13})}$_2$][PF$_6$]$_4$ metallomacrocycle, the fraction actually contained both [Fe{(**L**^{13})}$_2$][PF$_6$]$_4$ and [{Fe(**L**^{13})}$_3$][PF$_6$]$_6$.

❖ [Fe{(**L**^{13})}$_2$][PF$_6$]$_4$ and [{Fe(**L**^{13})}$_3$][PF$_6$]$_6$
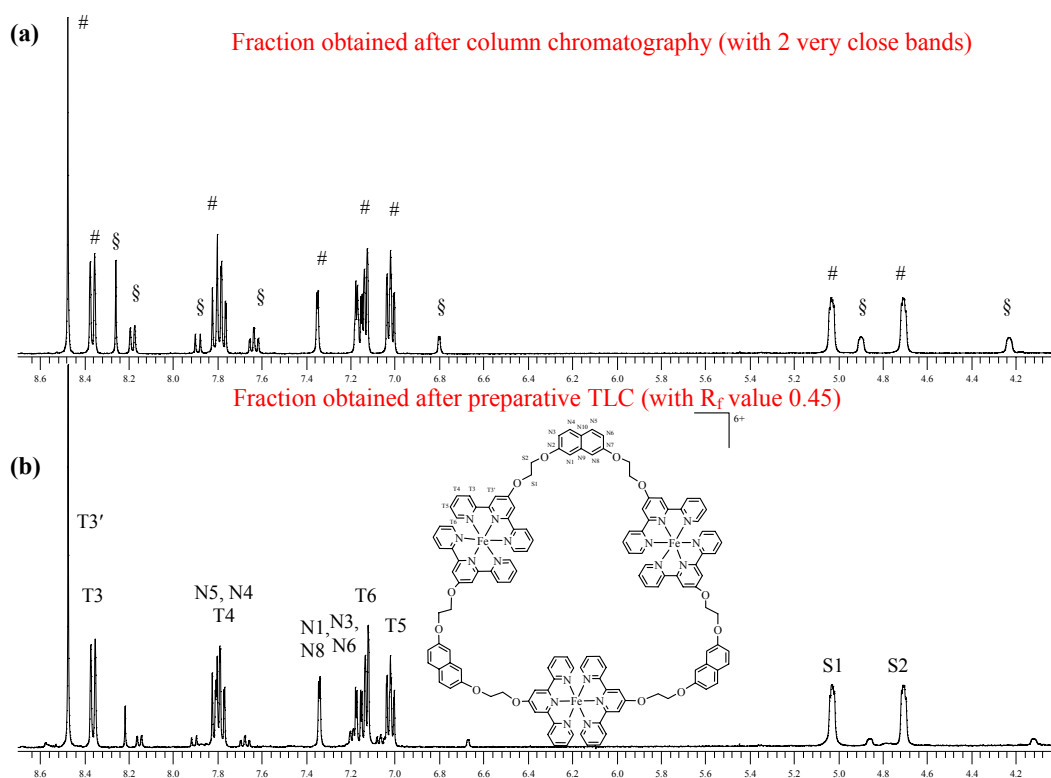
Figure 10. ^{1}H NMR spectra (400 MHz) of (a) the fraction obtained after column chromatography [{Fe(**L**^{13})}$_n$][PF$_6$]$_{2n}$ (n = 2 and 3) [$^#$ and § indicated two sets of signals] and (b) the fraction with R$_f$ value 0.45, which contains mainly trinuclear [{Fe(**L**^{13})}$_3$][PF$_6$]$_6$ obtained after preparative TLC in CD$_3$CN solution at room temperature.

When ligand **L**^{13} was treated with FeCl$_2$·4H$_2$O, a range of [{Fe(**L**^{13})}$_n$][PF$_6$]$_{2n}$ complexes was formed. There were two very close bands of metallomacrocycles

$[\{Fe(\boldsymbol{L^{13}})\}_n][PF_6]_{2n}$ (R_f value are 0.47 and 0.45 in A sol) and also a large amount of presumably polymeric material which remained on the baseline of the TLC plate. Firstly, an attempt to separate the two close bands of the metallomacrocycles by column chromatography failed. The ^{1}H NMR spectrum shows two sets of proton resonances (**Figure 10a**). However, the ES-MS analysis indicated it is only a [2+2] metallomacrocycle.

Secondly, the two close bands were separated by preparative TLC. The two fractions were assigned to [2+2] and [3+3] metallomacrocycles from ES-MS analysis. The spectrum of higher R_f product contained a doubly charged ion at m/z 911.6 $\{[\{Fe(\boldsymbol{L^{13}})\}_2][PF_6]_2\}^{2+}$, a triply charged ion at m/z 559.6 $\{[\{Fe(\boldsymbol{L^{13}})\}_2][PF_6]\}^{3+}$, and a quadruply charged ion at m/z 383.5 $\{[\{Fe(\boldsymbol{L^{13}})\}_2]\}^{4+}$. This fraction can be assigned to a [2+2] metallomacrocycle. The mass spectrum of the other product with the R_f value 0.45 contained a doubly charged ion at m/z 1440.3 $\{[\{Fe(\boldsymbol{L^{13}})\}_3][PF_6]_4\}^{2+}$, a triply charged ion at m/z 911.4 $\{[\{Fe(\boldsymbol{L^{13}})\}_3][PF_6]_3\}^{3+}$, a quadruply charged ion at m/z 647.5 $\{[\{Fe(\boldsymbol{L^{13}})\}_3][PF_6]_2\}^{4+}$, a quintuply charged ion at m/z 489.1 $\{[\{Fe(\boldsymbol{L^{13}})\}_3][PF_6]\}^{5+}$ and a sextuply charged ion at m/z 383.6 $\{[\{Fe(\boldsymbol{L^{13}})\}_3]\}^{6+}$. This indicated that this fraction is a [3+3] metallomacrocycle. The ^{1}H NMR spectrum of the higher R_f value fraction could not be measured due to an insufficient amount of product. The ^{1}H NMR spectrum of the fraction with R_f value 0.45 (i.e. the [3+3] metallomacrocycle) in CD$_3$CN solution is highly symmetrical but the spectrum showed the presence of a small amount of [2+2] metallomacrocycle (**Figure 10b**). There is significant shifting for the proton signals, especially the signals at δ 6.80 and δ 4.23 of the [2+2] metallomacrocycle in the spectrum of the fraction after column (**Figure 10a**) compare with those signals in the spectrum of the fraction after preparative TLC (**Figure 10b**). It seems these two proton signals of the [2+2] metallomacrocycle are concentration dependent.

❖ $[\{Fe(\boldsymbol{L^{14}})\}][PF_6]_2$

The ES-MS of a CH$_3$CN solution of the major product obtained from the reaction of $\boldsymbol{L^{14}}$ with FeCl$_2$·4H$_2$O only exhibited peaks that could be assigned to a [1+1] $[\{Fe(\boldsymbol{L^{14}})\}][PF_6]_2$ species. The spectrum contained singly charged ions at m/z 999.0

and 873.5, which were ${[\{Fe(\pmb{L^{14}})\}][PF_6]\}}^+$ and ${[\{Fe(\pmb{L^{14}})\}]F\}}^+$ respectively, and a doubly charged ion at *m/z* 427.1 assigned to $\{Fe(\pmb{L^{14}})\}^{2+}$. The ^{1}H NMR spectrum of a CD$_3$CN solution of $[\{Fe(\pmb{L^{14}})\}][PF_6]_2$ shows unusual features (**Figure 11**). The absolute assignments of the signals were made by using COSY, NOESY, HMQC and HMBC techniques. The spectrum shows two sets of signals assigned to coordinated terminal rings of the terpyridine ring, two H$^{T3'}$ signals from the terpyridine central ring (which are doublets with 2.2 Hz coupling constant) and two sets of signals for the ethyleneoxy group of the spacer, in each case in a 1:1 ratio. However, the naphthalene unit only gave rise to three signals with the resonances assigned to H$^{N1,\ N8}$ being unusually highly shielded.
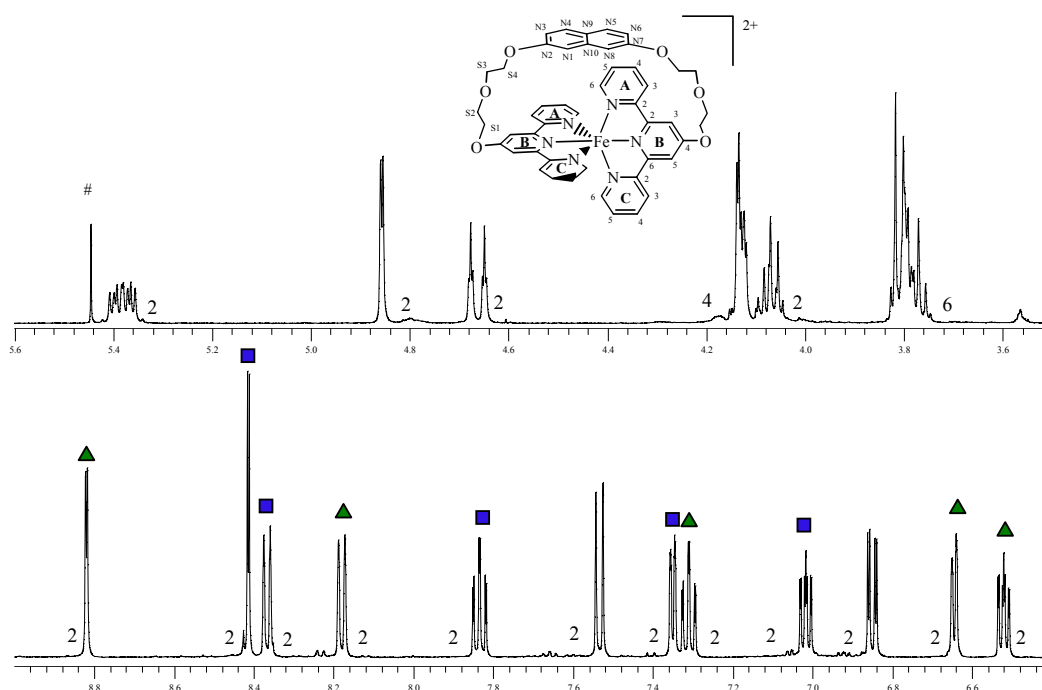
Figure 11. The ^{1}H NMR spectrum (500 MHz) of $[\{Fe(\pmb{L^{14}})\}][PF_6]_2$ in CD$_3$CN solution at room temperature. ($^\#$ is the signal of impurity CH$_2$Cl$_2$, the number next to the signal is the relative integral, and the ▲ and ■ indicated two sets of terpyridine proton signals).
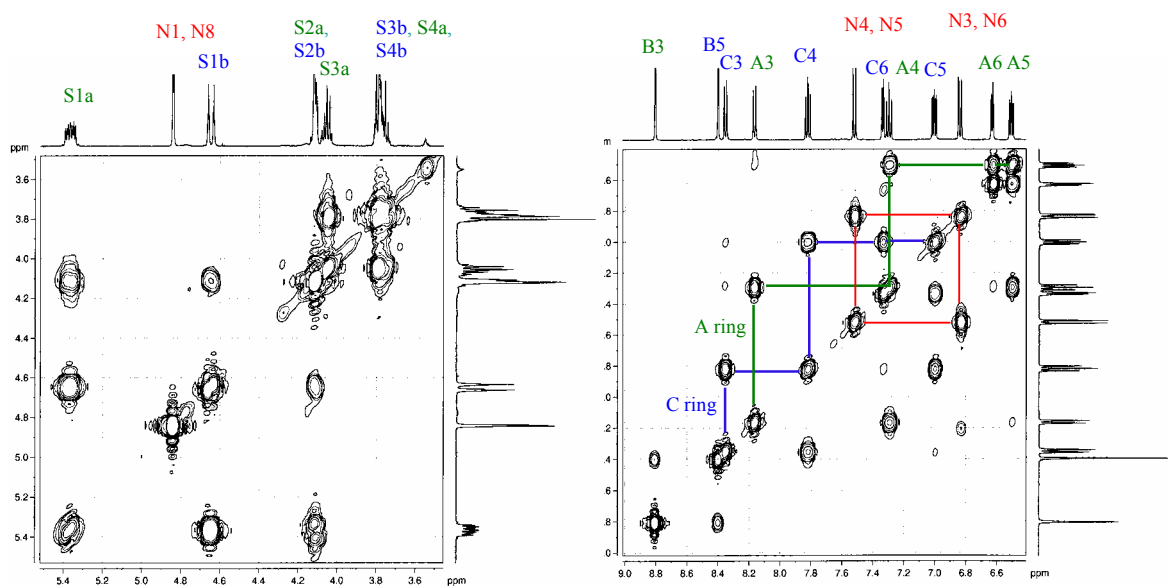
Figure 12. COSY spectra (500 MHz) of [{Fe(L^{14})}][PF$_6$]$_2$ in CD$_3$CN solution at room temperature.
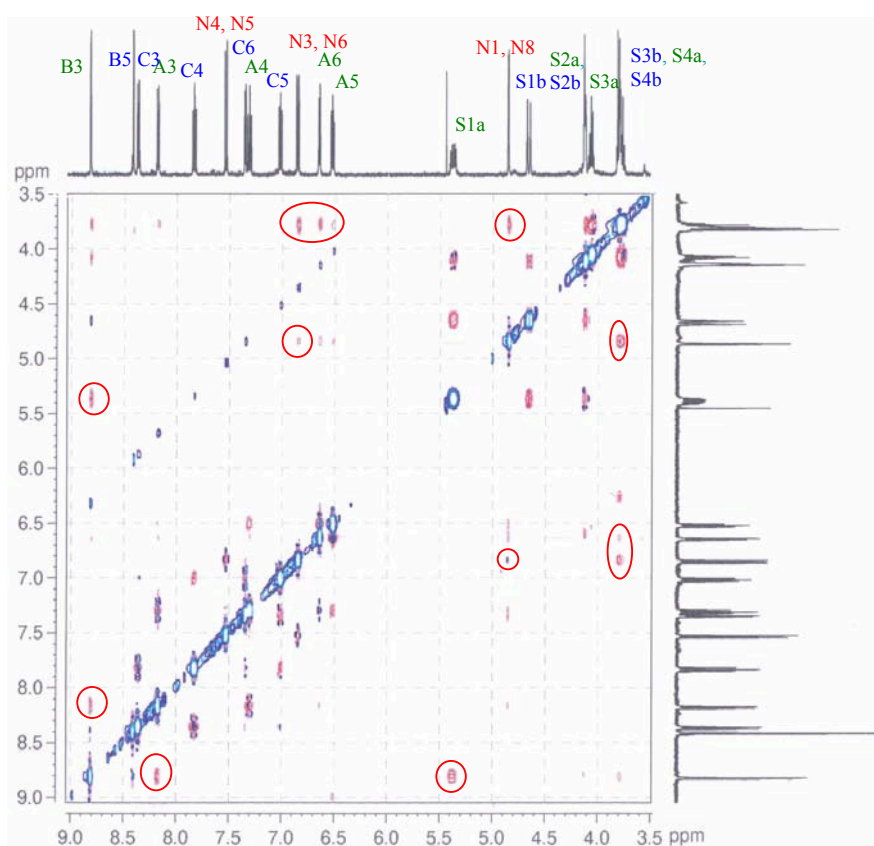
Figure 13. NOESY spectrum (500 MHz) of [{Fe(L^{14})}][PF$_6$]$_2$ in CD$_3$CN solution at room temperature.

259

There are two sets of terpyridine proton signals (A and C ring) (**Figure 11**). The H^{B3} signal and H^{B5} signal exhibit NOE signals to H^{A3} and H^{C3} respectively (**Figure 13**). Therefore, the proton signals for A and C ring are assigned (**Figure 12**). There is a pair of cross peaks between a doublet of doublets (*J* 2.5, 8.9 Hz) at δ 6.85 and a doublet (*J* 9.0 Hz) at δ 7.53 (**Figure 12**). Therefore, the doublet of doublets at δ 6.85 and the doublet at δ 7.53 are assigned to $H^{N3, N6}$ and $H^{N4, N5}$ respectively. Also, the signal for $H^{N3, N6}$ at δ 6.85 exhibits an NOE signal to a doublet (*J* 2.4 Hz) for $H^{N1, N8}$ at δ 4.86 (**Figure 13**). The signal for $H^{N1, N8}$ exhibits an NOE signal to the signal at δ 3.79 (with 3 times the relative integral of the signal for $H^{N1, N8}$), and this signal is assigned to H^{S4}. The signal for H^{S4} gives a COSY cross peak to the signal at δ 4.07 and this is assigned to H^{S3} (with a relative integral equal to that of the signal for $H^{N1, N8}$). The signal for H^{S3} exhibits an NOE signal to the signal for H^{S2} at δ 4.13. The signal for H^{S2} at δ 4.13 also exhibits an NOE signal to the signal at δ 3.79 (which 2/3 relative integral belongs to H^{S4}), and therefore this is assigned to another diastereotopic pair of the H^{S3}. The signal for H^{S2} gives COSY cross peaks to the signals for H^{S1} at δ 4.66 and δ 5.38. The CH$_2$ protons appear as eight, partially overlapping resonances in the ^{1}H NMR spectrum but there are only four ^{13}C NMR signals. The pairwise relationship of the eight CH$_2$ protons resonances to four carbon resonances was made from a ^{1}H-^{13}C correlation spectrum (**Figure 14**).
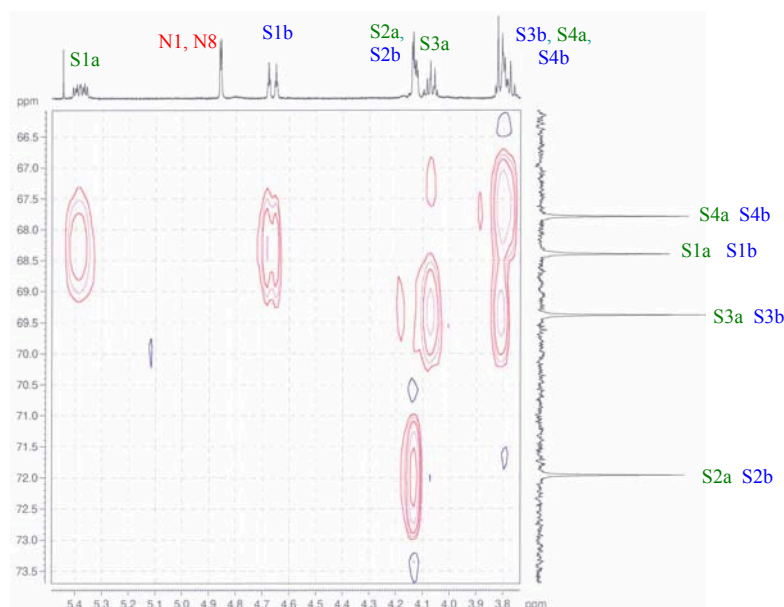
Figure 14. HMQC spectrum (500 MHz) of [{Fe(***L***^{14})}][PF$_6$]$_2$ in CD$_3$CN solution at room temperature.

The ^{1}H NMR spectroscopic data suggested that the naphthalene and the ethyleneoxy spacer are trapped between two terminal pyridine rings (A ring) of the terpyridine domains. That is due to the fact that the spacer is not long enough to allow it to rotate around the complex. Therefore, one terminal pyridine ring (A ring) of the terpyridine is different from the other terminal pyridine ring (C ring). This explained why there are two sets of terpyridine protons signals and two sets of diastereotopic CH$_2$ protons. From a modelled structure and the single crystal structure of [{Fe(L^{14})}][PF$_6$]$_2$ (see **Section 7.4**), H$^{N1, N8}$ points towards the [Fe(*terpy*)$_2$]$^{2+}$ unit and lies in the shielding, anisotropic region above a pyridine ring. This explains the high field shift of the proton signal for H$^{N1, N8}$ at δ 4.86 (**Figure 11**).

❖ [{Fe(L^{15})}][PF$_6$]$_2$

Reaction of a longer chain ligand L^{15} with FeCl$_2$·4H$_2$O resulted in the formation of a [1+1] metallomacrocycle as the major product. The ES-MS of this product in CH$_3$CN solution exhibited peaks that could be assigned to a [1+1] [{Fe(L^{15})}][PF$_6$]$_2$ species. The spectrum contained singly charged ions at *m/z* 1086.9, 961.3 and 553.3, which were assigned to {[{Fe(L^{15})}][PF$_6$]}$^+$, {[{Fe(L^{15})}]F}$^+$ and {[Fe(*HO-Terpy*)(*O-Terpy*)]}$^+$ respectively, and doubly charged ions at *m/z* 471.3 and 277.4, which was {[{Fe(L^{15})}]}$^{2+}$ and {[Fe(*O-Terpy*)$_2$]}$^{2+}$ respectively. The ^{1}H NMR spectrum of [{Fe(L^{15})}][PF$_6$]$_2$ in CD$_3$CN solution has a symmetrical appearance (**Figure 15**). The absolute assignments of the signals were made by using COSY and NOESY techniques. There are only six proton signals in the aromatic region but seven proton signals in the aliphatic region. As was seen for the [{Fe(L^{14})}][PF$_6$]$_2$ complex, the H$^{N1, N8}$ signal (δ 5.44) of [{Fe(L^{15})}][PF$_6$]$_2$ is shifted to the high field.
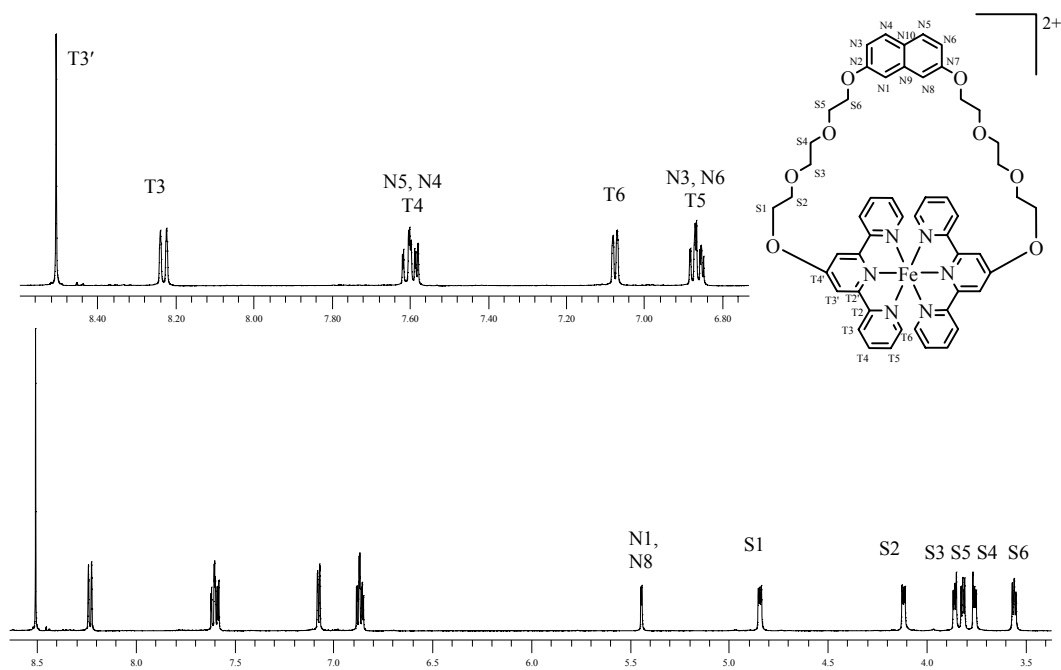
Figure 15. The ^{1}H NMR spectrum (500 MHz) of [{Fe(L^{15})}][PF$_6$]$_2$ in CD$_3$CN solution at room temperature.

A low temperature proton NMR experiment on the [{Fe(L^{15})}][PF$_6$]$_2$ in CD$_2$Cl$_2$ solution was made to investigate possible locking of the naphthalene ring as in the [{Fe(L^{14})}][PF$_6$]$_2$. However, there is no evidence for splitting into two sets of signals as in [{Fe(L^{14})}][PF$_6$]$_2$, even when the temperature was lowered to 180K. However, the signals for H$^{N1, N8}$, H^{T3} and H^{T4} started to coalesce at around 190K but those for H$^{N4, N6}$ and H^{T6} remained relatively sharp (**Figure 16**). This gives some information about the movement for the naphthalene ring. It seems that when the naphthalene ring is rotating around the [Fe(*terpy*)$_2$]$^{2+}$ unit, the H$^{N1, N8}$ protons remain close to the H^{T3} and H^{T4} protons.
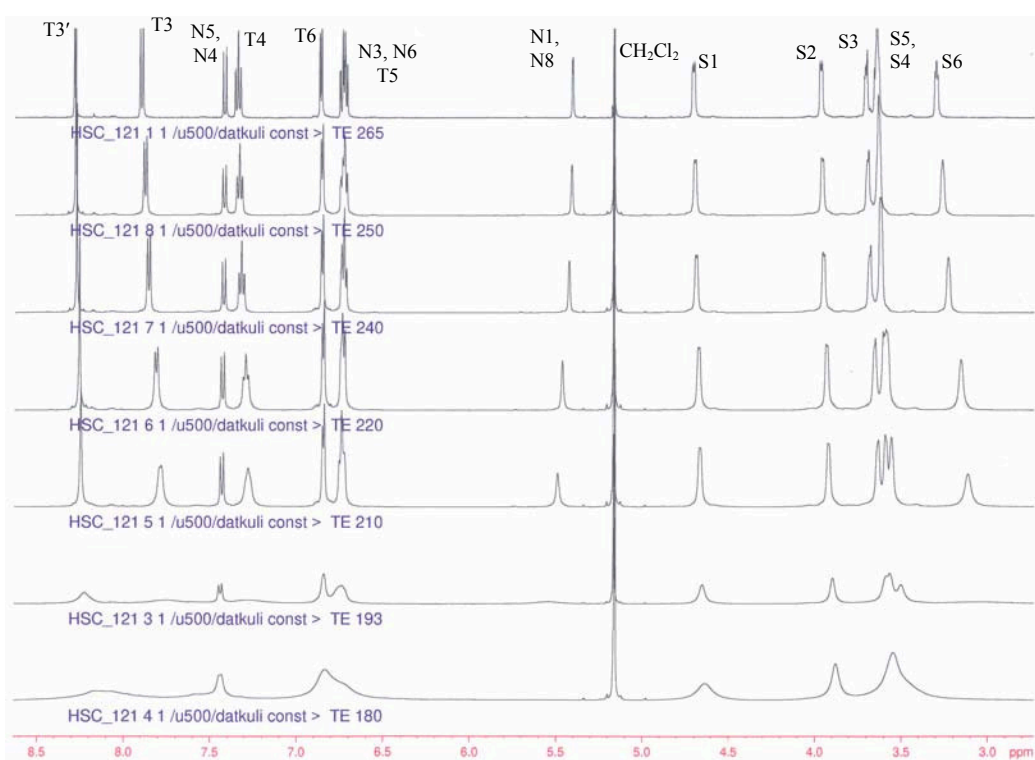
Figure 16. The ^{1}H NMR spectrum (500 MHz) of $[\{Fe(\boldsymbol{L^{15}})\}][PF_6]_2$ in CD_2Cl_2 solution at different temperatures (TE = temperature in K).

❖ $[\{Fe(\boldsymbol{L^{16}})\}_3][PF_6]_6$

When $\boldsymbol{L^{16}}$ was treated with $FeCl_2·4H_2O$, a range of $[\{Fe(\boldsymbol{L^{16}})\}_n][PF_6]_{2n}$ complexes was formed. The TLC analysis of the reaction mixture indicated there was one major component, and small amounts of other component close to the major component plus some polymeric material on the TLC plate. The ES-MS spectrum of the major component was consistent with the formation of a [3+3] metallomacrocycle. The spectrum contained a triply charged ion at *m/z* 911.4 $\{[\{Fe(\boldsymbol{L^{16}})\}_3][PF_6]_3\}^{3+}$, a quadruply charged ion at *m/z* 647.5 $\{[\{Fe(\boldsymbol{L^{16}})\}_3][PF_6]_2\}^{4+}$, a quintuply charged ion at *m/z* 489.0 $\{[\{Fe(\boldsymbol{L^{16}})\}_3][PF_6]\}^{5+}$ and a sextuply charged ion at *m/z* 383.4 $\{[\{Fe(\boldsymbol{L^{16}})\}_3]\}^{6+}$. The ^{1}H NMR spectrum showed eight aromatic and two aliphatic proton resonances.

❖ $[\{Fe(\boldsymbol{L^{17}})\}_2][PF_6]_4$

When $\boldsymbol{L^{17}}$ was treated with $FeCl \cdot 4H_2O$, a range of $[\{Fe(\boldsymbol{L^{17}})\}_n][PF_6]_{2n}$ complexes was formed. The ES-MS analysis suggested that the major product separated from the reaction mixture was $[\{Fe(\boldsymbol{L^{17}})\}_2][PF_6]_4$. The ES-MS spectrum exhibited peaks at *m/z* 617.9 $\{[\{Fe(\boldsymbol{L^{17}})\}_2][PF_6]\}^{3+}$ and at *m/z* 427.1 $\{[\{Fe(\boldsymbol{L^{17}})\}_2]\}^{4+}$. The compound had the expected spectroscopic properties with eight aromatic and four aliphatic proton resonances (**Figure 17**). The assignments were made by COSY and NOESY techniques. The signal for $H^{T3'}$ and $H^{N1, N4}$ showed strong cross peak to H^{S1} and, H^{S4} and also $H^{N5, N8}$, respectively.
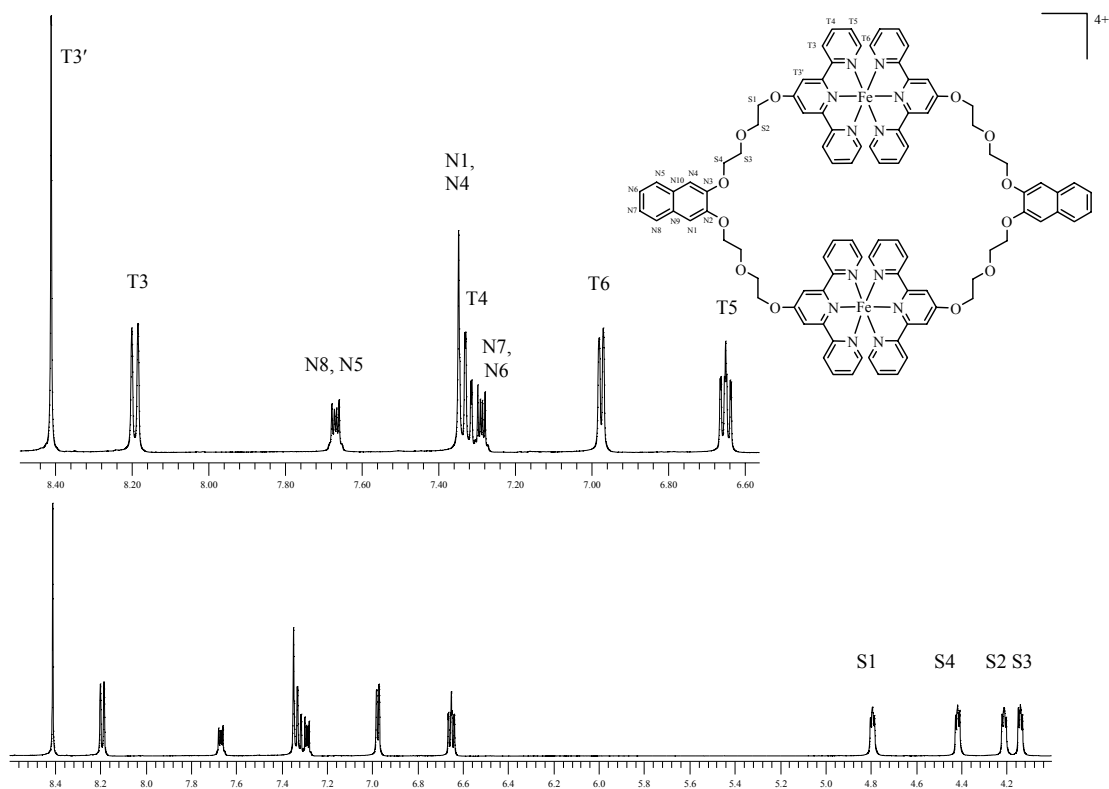
Figure 17. The ^1H NMR spectrum (500 MHz) of $[\{Fe(\boldsymbol{L^{17}})\}_2][PF_6]_4$ in CD_3CN solution at room temperature.

7.3   Absorption spectroscopic characterisation

The electronic spectra of the macrocyclic Ru(II) and Fe(II) complexes were recorded in HPLC grade acetonitrile solution. The absorption spectra of these complexes are similar to the sum of the spectra of $[M(terpy)_2]^{2+}$, where M is Fe (II) or Ru(II), and those of the substituents. The absorption data for these macrocyclic homonuclear complexes are summarised in **Table 1**. The very intense bands in the UV region are assigned to the ligand-centred $\pi^* \leftarrow \pi$ transitions. The Ru(II) complexes exhibit a low energy metal-to-ligand charge transfer (MLCT) transition with λ_{max} between 484 to 486 nm while the Fe(II) complexes exhibit a low energy metal-to-ligand charge transfer (MLCT) transition with λ_{max} between 552 to 560 nm.

	λ_{max}, nm (ε / 10^3, $M^{-1}cm^{-1}$)	
	LC	LMCT
$[\{Ru(L^{11})\}_2][PF_6]_4$	226 (266), 239 (120), 265 (123), 302 (132)	484 (39.0)
$[\{Ru(L^{13})\}_2][PF_6]_4$	-	-
$[\{Ru(L^{13})\}_3][PF_6]_6$	-	-
$[\{Ru(L^{14})\}_2][PF_6]_4$	235 (272), 267 (138), 304 (155)	486 (41.4)
$[\{Ru(L^{16})\}_2][PF_6]_4$	230 (179), 264 (113), 303 (112)	485 (35.0)
$[\{Ru(L^{17})\}_2][PF_6]_4$	231 (224), 264 (120), 302 (126)	484 (35.7)
$[\{Fe(L^{11})\}_2][PF_6]_4$	226 (145), 241 (64.8), 270 (64.3), 314 (38.2)	552 (12.2)
$[\{Fe(L^{12})\}_n][PF_6]_{2n}$	-	-
$[\{Fe(L^{13})\}_2][PF_6]_4$	-	-
$[\{Fe(L^{13})\}_3][PF_6]_6$	-	-
$[\{Fe(L^{14})\}][PF_6]_2$	233 (80.0), 269 (40.7), 314 (31.3),	555 (9.30)
$[\{Fe(L^{15})\}][PF_6]_2$	232 (170), 269 (87.4), 313 (68.9)	554 (20.3)
$[\{Fe(L^{16})\}_3][PF_6]_6$	230 (143), 270 (103), 315 (84.2)	560 (40.4)
$[\{Fe(L^{17})\}_2][PF_6]_4$	231 (111), 269 (57.9), 314 (40.7)	553 (12.0)

Table 1. Electronic spectroscopic data for the complexes in acetonitrile solution.

7.4 Crystal structures of $[\{Ru(L^{11})\}_2][PF_6]_4 \cdot \frac{4}{5}(C_2H_5)_2O \cdot 2CH_3CN$, $[\{Fe(L^{14})\}][PF_6]_2 \cdot (C_2H_5)_2O \cdot \frac{1}{2}CH_3CN$ and $[\{Fe(L^{15})\}][PF_6]_2 \cdot CH_3CN$

(a) Crystal structure of $[\{Ru(L^{11})\}_2][PF_6]_4 \cdot \frac{4}{5}(C_2H_5)_2O \cdot 2CH_3CN$

Crystals of $[\{Ru(L^{11})\}_2][PF_6]_4 \cdot \frac{4}{5}(C_2H_5)_2O \cdot 2CH_3CN$ were obtained by slow diffusion of diethyl ether vapour into an acetonitrile solution of $[\{Ru(L^{11})\}_2][PF_6]_4$. The crystals were of X-ray quality and the molecular structure of $[\{Ru(L^{11})\}_2][PF_6]_4 \cdot \frac{4}{5}$ $(C_2H_5)_2O \cdot 2CH_3CN$ was determined. The structure of the $[\{Ru(L^{11})\}_2]^{4+}$ cation is presented in **Figure 18**. Crystallographic data are given in **Appendix V** and selected bond lengths and angles are given in **Table 2**.
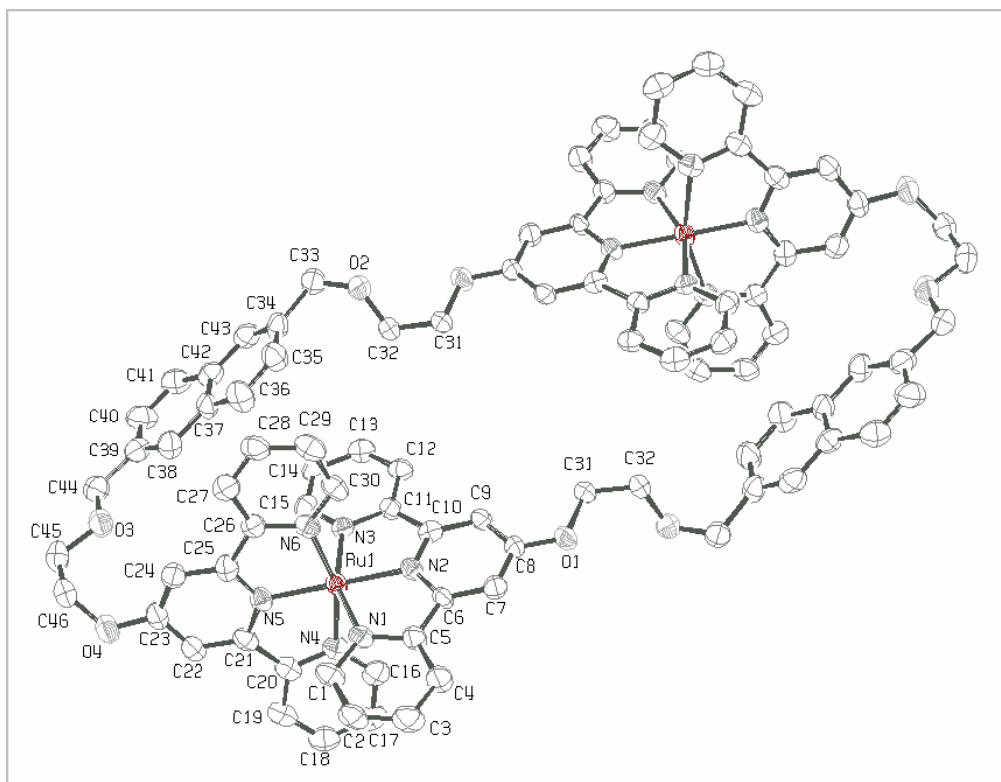
Figure 18. An ORTEP representation (50% probability ellipsoids) of the $[\{Ru(L^{11})\}_2]^{4+}$ cation in $[\{Ru(L^{11})\}_2][PF_6]_4 \cdot \frac{4}{5}(C_2H_5)_2O \cdot 2CH_3CN$. Hydrogen atoms are omitted for clarity.

As expected, the tridentate domains of the ligands exhibit the *cisoid* conformation about the interannular C-C bonds, which is necessary for the adoption of the chelating mode. The coordination sphere of the Ru(II) centre is similar to those in other complexes containing tridentate 2,2′:6′,2″-terpyridine ligands.[53-55] The three pyridine rings in each domain are close to being coplanar and the torsion angles N1-C5-C6-N2, N2-C10-C11-N3, N4-C20-C21-N5 and N5-C25-C26-N6 are -5.20˚, -0.17˚, -6.71˚ and 1.45˚ respectively. The angle between the planes containing atoms N1, N2, N3 and N4, N5, N6 is 83.3˚.[54-55]

Ru1-N1	2.072(4)	N1-C1	1.353(6)	C5-C6	1.460(6)
Ru1-N2	1.986(4)	N1-C5	1.370(7)	C10-C11	1.474(7)
Ru1-N3	2.085(4)	N2-C6	1.349(6)	C20-C21	1.484(8)
Ru1-N4	2.080(4)	N2-C10	1.345(6)	C25-C26	1.497(7)
Ru1-N5	1.983(4)	N3-C11	1.372(6)		
Ru1-N6	2.069(4)	N3-C15	1.340(6)	C8-O1	1.350(6)
		N4-C16	1.353(7)	C31-O1	1.433(6)
		N4-C20	1.349(7)	C23-O4	1.352(6)
		N5-C21	1.339(7)	C46-O4	1.457(8)
		N5-C25	1.337(7)		
		N6-C26	1.365(7)		
		N6-C30	1.353(7)		
N1-Ru1-N2	79.3(2)	N4-Ru1-N5	78.9(2)	C7-C8-O1	115.0(4)
N1-Ru1-N3	158.0(2)	N4-Ru1-N6	157.7(2)	C9-C8-O1	124.8(4)
N2-Ru1-N3	78.7(2)	N5-Ru1-N6	78.9(2)	C8-O1-C31	117.6(4)
N1-Ru1-N4	84.4(2)	N3-Ru1-N6	86.9(2)	C24-C23-O4	126.0(6)
N2-Ru1-N4	100.6(2)	N1-Ru1-N5	101.0(2)	C22-C23-O4	113.7(5)
N3-Ru1-N4	99.4(2)	N1-Ru1-N6	97.8(2)	C23-O4-C46	120.4(5)
N3-Ru1-N5	101.0(2)	N2-Ru1-N6	101.6(2)		
		N2-Ru1-N5	179.3(2)		

Table 2. Selected bond lengths (Å) and angles (˚) of the $[\{Ru(\textbf{\textit{L}}^{II})\}_2]^{4+}$ cation in $[\{Ru(\textbf{\textit{L}}^{II})\}_2][PF_6]_4 \cdot \frac{4}{5}(C_2H_5)_2O \cdot 2CH_3CN$.

All the bond lengths of the interannular C-C bonds and N-C bonds are comparable to the corresponding bond lengths of other Ru(II) complexes containing tridentate 2,2′:6′,2″-terpyridine ligands.[54-55] The Ru-N contacts to the central ring of the 4′-substituted-2,2′:6′,2″-terpyridine ligand (Ru1-N2, Ru1-N5) are shorter than those to the terminal rings (Ru1-N1, Ru1-N3, Ru1-N4 and Ru1-N6), which are within the reported range of Ru(II) complexes with 2,2′:6′,2″-terpyridine ligands.[54-55] The torsion angles C9-C8-O1-C31 and C24-C23-O4-C46 are 10.97˚ and 13.47˚ respectively. The

bond lengths O1-C8 and O4-C23 are 1.350(6) Å and 1.352(6) Å respectively which are similar to the corresponding distances in the [Ru(***poterpy***)$_2$]$^{2+}$ cation in the solid-state structure of [Ru(***poterpy***)$_2$][PF$_6$]$_2$·(CH$_3$)$_2$CO (***poterpy*** = 4′-(2-propynyl-1-oxy)-2,2′:6′,2″-terpyridine)[55]. The bond angles C7-C8-O1, C9-C8-O1, C22-C23-O4 and C24-C23-O4 are within the range reported in the [Ru(***poterpy***)$_2$]$^{2+}$ cation[55]. Also the bond angles C8-O1-C31 and C23-O4-C46 are 117.6(4)° and 120.4(5)° respectively which are within the experimental error for the corresponding angles in ([Ru(***poterpy***)$_2$]$^{2+}$ cation (117.5(3)° and 118.1(3)°)[55].

There are no π-π interactions between the molecules. Also, there are no solvent molecules or anions in the cavity of this [2+2] metallomacrocycle. The Ru-Ru distance is 13.1 Å.

*(b) Crystal structure of [{Fe(**L^{14}**)}][PF$_6$]$_2$·(C$_2$H$_5$)$_2$O·½CH$_3$CN*

Crystals of [{Fe(**L^{14}**)}][PF$_6$]$_2$·(C$_2$H$_5$)$_2$O·½CH$_3$CN were obtained by slow diffusion of diethyl ether vapour into an acetonitrile solution of [{Fe(**L^{14}**)}][PF$_6$]$_2$. The crystals were of X-ray quality and the molecular structure of [{Fe(**L^{14}**)}][PF$_6$]$_2$·(C$_2$H$_5$)$_2$O·½CH$_3$CN was determined. The structure of the [{Fe(**L^{14}**)}]$^{2+}$ cation is presented in **Figure 19**. Crystallographic data are given in **Appendix V** and selected bond lengths and angles are given in **Table 3**.

As expected, the tridentate domains of the ligand exhibit the *cisoid* conformation about the interannular C-C bonds, which is necessary for the adoption of the chelating mode. The coordination sphere of the Fe(II) centre is similar to those in other complexes containing tridentate 2,2′:6′,2″-terpyridine ligands. The three pyridine rings in each domain are close to being coplanar and the torsion angles N1-C5-C6-N2, N2-C10-C11-N3, N4-C38-C39-N5 and N5-C43-C44-N6 are 2.32°, -0.24°, 1.45° and -0.51° respectively. The angle between the planes containing atoms N1, N2, N3 and N4, N5, N6 is 88.7°.[56-60]
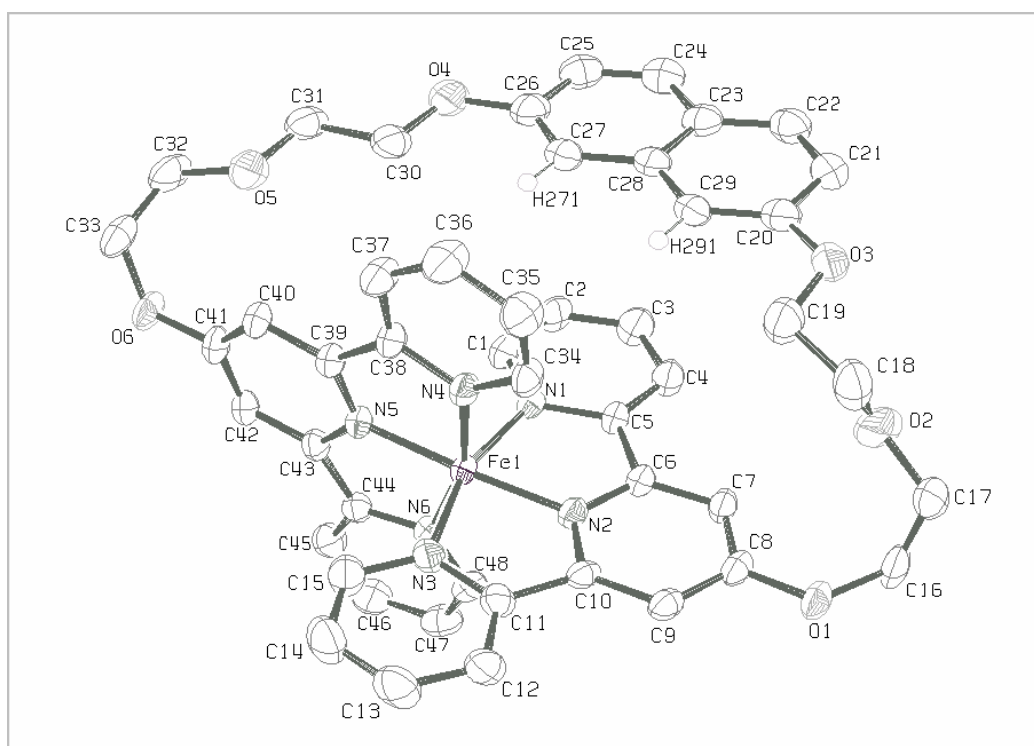
Figure 19. An ORTEP representation (50% probability ellipsoids) of the $[\{Fe(\boldsymbol{L^{14}})\}]^{2+}$ cation in $[\{Fe(\boldsymbol{L^{14}})\}][PF_6]_2 \cdot (C_2H_5)_2O \cdot \frac{1}{2}CH_3CN$. Hydrogen atoms are omitted for clarity except atoms H271 and H291.

All the bond lengths of the interannular C-C bonds and N-C bonds are comparable to the corresponding bond lengths of other Fe(II) complexes containing tridentate 2,2′:6′,2″-terpyridine ligands.[56-57,59-60] The Fe-N contacts to the central ring of the 4′-substituted-2,2′:6′,2″-terpyridine ligand (Fe1-N2 and Fe1-N5) are shorter than those to the terminal rings (Fe1-N1, Fe1-N3, Fe1-N4 and Fe1-N6), which are within the reported range of Fe(II) complexes with 2,2′:6′,2″-terpyridine ligands.[56-60] The torsion angles C7-C8-O1-C16, C40-C41-O6-C33, C19-O3-C20-C29 and C30-O4-C26-C27 are 4.50˚, 10.61˚, 10.80˚ and -7.01˚ respectively. The bond lengths O1-C8 and O6-C41 are 1.346(4) Å and 1.344(4) Å respectively which are similar to the corresponding distances in (5,5′-bis(3-(10-(2,6-bis(pyrid-2-yl)pyrid-4-yl)-1,4,7,10-tetraoxadecyl)phenyl)-2,2′-bipyridyl)-iron(II) bis(hexafluorophosphate) acetone solvate[60]. The bond angles C7-C8-O1, C9-C8-O1, C40-C41-O6 and C42-C41-O6 are within the range reported in the [Ru(***poterpy***)$_2$]$^{2+}$ cation in the solid-state structure of [Ru(***poterpy***)$_2$][PF$_6$]$_2 \cdot$(CH$_3$)$_2$CO[55]. The bond angles C8-O1-C16 and C41-O6-C33 are 121.8(3)˚ and 120.5(3)˚ respectively which, are bigger than the corresponding angles

in ([Ru(***poterpy***)₂]²⁺ cation (117.5(3)° and 118.1(3)°)[55] and in (5,5′-bis(3-(10-(2,6-bis(pyrid-2-yl)pyrid-4-yl)-1,4,7,10-tetraoxadecyl)phenyl)-2,2′-bipyridyl)-iron(II) bis(hexafluorophosphate) acetone solvate (115.55° and 113.22°)[60].

Fe1-N1	1.962(3)	N1-C1	1.343(5)	C5-C6	1.471(5)
Fe1-N2	1.876(3)	N1-C5	1.371(4)	C10-C11	1.463(5)
Fe1-N3	1.970(3)	N2-C6	1.334(4)	C38-C39	1.471(5)
Fe1-N4	1.970(3)	N2-C10	1.346(4)	C43-C44	1.465(5)
Fe1-N5	1.874(3)	N3-C11	1.365(5)		
Fe1-N6	1.961(3)	N3-C15	1.330(5)	C8-O1	1.346(4)
		N4-C34	1.344(5)	C16-O1	1.428(5)
		N4-C38	1.370(4)	C19-O3	1.422(6)
		N5-C39	1.345(5)	C20-O3	1.366(5)
		N5-C43	1.350(4)	C30-O4	1.420(6)
		N6-C44	1.370(4)	C26-O4	1.361(5)
		N6-C48	1.337(5)	C41-O6	1.344(4)
				C33-O6	1.447(5)
N1-Fe1-N2	80.9(1)	N4-Fe1-N5	80.9(1)	C7-C8-O1	125.4(3)
N1-Fe1-N3	161.9(1)	N4-Fe1-N6	161.9(1)	C9-C8-O1	114.7(3)
N2-Fe1-N3	81.0(1)	N5-Fe1-N6	81.0(1)	C8-O1-C16	121.8(3)
N1-Fe1-N4	92.8(1)	N3-Fe1-N6	92.7(1)	C21-C20-O3	114.1(4)
N2-Fe1-N4	96.7(1)	N1-Fe1-N5	97.5(1)	C29-C20-O3	125.0(4)
N3-Fe1-N4	90.2(1)	N1-Fe1-N6	89.9(1)	C25-C26-O4	114.4(4)
N3-Fe1-N5	100.6(1)	N2-Fe1-N6	101.4(1)	C27-C26-O4	125.0(4)
		N2-Fe1-N5	177.1(1)	C40-C41-O6	124.3(3)
				C42-C41-O6	115.6(3)
				C41-O6-C33	120.5(3)

Table 3. Selected bond lengths (Å) and angles (°) of the [{Fe(***L¹⁴***)}]²⁺ cation in [{Fe(***L¹⁴***)}][PF₆]₂·(C₂H₅)₂O·½CH₃CN.

The ehtyleneoxy chains and naphthalene unit lie snuggly in the cleft between two terminal pyridine rings (A ring) of the terpyridine as predicted from the ¹H NMR spectroscopic data. There are π-π interactions between the naphthalene and the terminal pyridine rings with an interplanar separation of 3.6 Å and a least squares interplane angle of 5.9°. The atoms H271 and H291 lie directly above the other non-stacked pyridine terminal ring. The distance between the plane of N4 ring to C27 atom of the napthyl ring is 4.603 Å.

(c) Crystal structure of [{Fe(L^{15})}][PF$_6$]$_2$·CH$_3$CN

Crystals of [{Fe(L^{15})}][PF$_6$]$_2$·CH$_3$CN were obtained by slow diffusion of diethyl ether vapour into an acetonitrile solution of [{Fe(L^{15})}][PF$_6$]$_2$. The crystals were of X-ray quality and the molecular structure of [{Fe(L^{15})}][PF$_6$]$_2$·CH$_3$CN was determined. The structure of the [{Fe(L^{15})}]$^{2+}$ cation is presented in **Figure 20**. Crystallographic data are given in **Appendix V** and selected bond lengths and angles are given in **Table 4**. The crystal structure of this [{Fe(L^{15})}]$^{2+}$ cation is very similar to that of the [{Fe(L^{14})}]$^{2+}$ cation previously described.
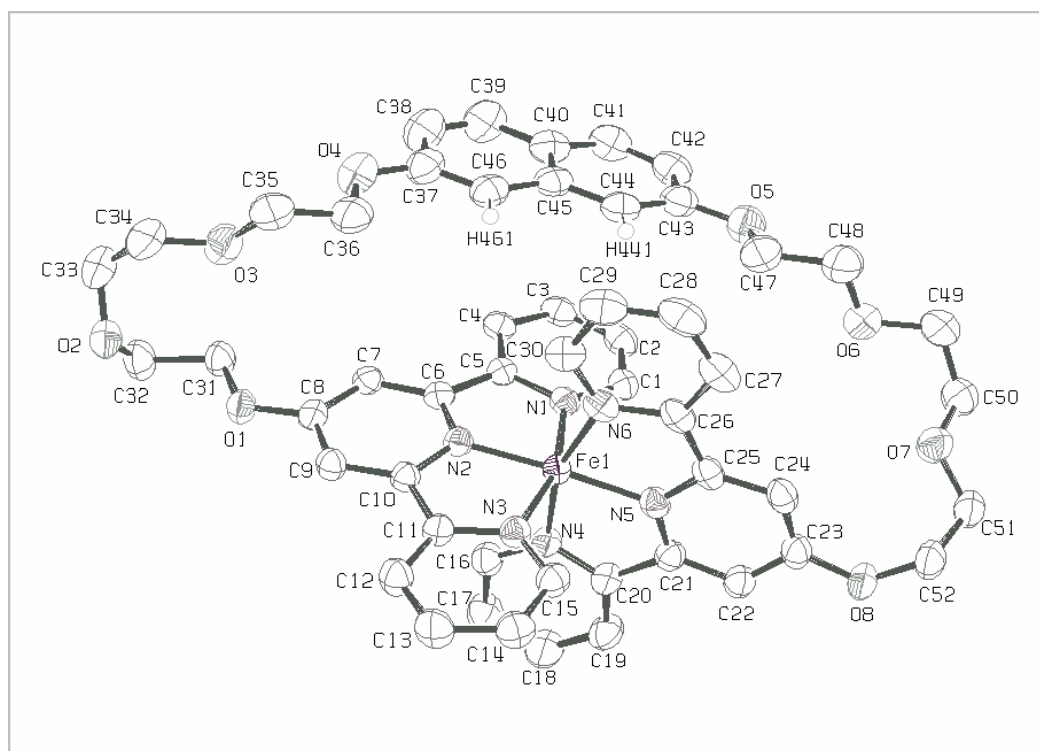
Figure 20. An ORTEP representation (50% probability ellipsoids) of the [{Fe(L^{15})}]$^{2+}$ cation in [{Fe(L^{15})}][PF$_6$]$_2$·CH$_3$CN. Hydrogen atoms are omitted for clarity except atoms H441 and H461.

As expected, the tridentate domains of the ligand exhibit the *cisoid* conformation about the interannular C-C bonds, which is necessary for the adoption of the chelating mode. The coordination sphere of the Fe(II) centre is similar to those in other complexes containing tridentate 2,2′:6′,2″-terpyridine ligands. The three pyridine rings in each domain are close to being coplanar and the torsion angles N1-C5-C6-N2, N2-C10-C11-N3, N4-C20-C21-N5 and N5-C25-C26-N6 are 3.09˚, -0.88˚, 2.73˚ and -

0.44˚ respectively. The angle between the planes containing atoms N1, N2, N3 and N4, N5, N6 is 88.7˚.[56-60]

Fe1-N1	1.979(2)	N1-C1	1.349(3)	C5-C6	1.472(4)
Fe1-N2	1.881(2)	N1-C5	1.364(3)	C10-C11	1.466(4)
Fe1-N3	1.971(2)	N2-C6	1.352(3)	C20-C21	1.466(4)
Fe1-N4	1.980(2)	N2-C10	1.358(3)	C25-C26	1.461(4)
Fe1-N5	1.898(2)	N3-C11	1.366(3)		
Fe1-N6	1.968(2)	N3-C15	1.346(3)	C8-O1	1.343(3)
		N4-C16	1.349(4)	C31-O1	1.447(3)
		N4-C20	1.358(4)	C36-O4	1.429(4)
		N5-C21	1.346(4)	C37-O4	1.368(4)
		N5-C25	1.343(4)	C47-O5	1.430(4)
		N6-C26	1.377(4)	C43-O5	1.367(4)
		N6-C30	1.337(4)	C23-O8	1.352(4)
				C52-O8	1.437(4)
N1-Fe1-N2	80.70(9)	N4-Fe1-N5	80.7(1)	C7-C8-O1	125.0(2)
N1-Fe1-N3	161.85(9)	N4-Fe1-N6	161.2(1)	C9-C8-O1	115.1(2)
N2-Fe1-N3	81.15(9)	N5-Fe1-N6	80.5(1)	C8-O1-C31	118.5(2)
N1-Fe1-N4	92.55(9)	N3-Fe1-N6	92.94(9)	C38-C37-O4	114.3(3)
N2-Fe1-N4	95.45(9)	N1-Fe1-N5	99.98(9)	C46-C37-O4	125.3(3)
N3-Fe1-N4	88.97(9)	N1-Fe1-N6	91.41(9)	C42-C43-O5	114.5(3)
N3-Fe1-N5	98.12(9)	N2-Fe1-N6	103.3(1)	C44-C43-O5	124.8(3)
		N2-Fe1-N5	176.1(1)	C24-C23-O8	126.8(3)
				C22-C23-O8	112.8(3)
				C23-O8-C52	122.2(3)

Table 4. Selected bond lengths (Å) and angles (˚) of the $[\{Fe(L^{15})\}]^{2+}$ cation in $[\{Fe(L^{15})\}][PF_6]_2 \cdot CH_3CN$.

All the bond lengths of the interannular C-C bonds and N-C bonds are comparable to the corresponding bond lengths of other Fe(II) complexes containing tridentate 2,2′:6′,2″-terpyridine ligands.[56-57,59-60] The Fe-N contacts to the central ring of the 4′-substituted-2,2′:6′,2″-terpyridine ligand (Fe1-N2 and Fe1-N5) are shorter than those to the terminal rings (Fe1-N1, Fe1-N3, Fe1-N4 and Fe1-N6), which are within the reported range of Fe(II) complexes with 2,2′:6′,2″-terpyridine ligands.[56-60] The torsion angles C7-C8-O1-C31, C24-C23-O8-C52, C36-O4-C37-C46 and C47-O5-C43-C44 are -0.54˚, 2.40˚, -4.01˚ and -6.69˚ respectively. The bond lengths O1-C8 and O8-C23 are 1.343(3) Å and 1.352(4) Å respectively which are similar to the corresponding distances in (5,5′-bis(3-(10-(2,6-bis(pyrid-2-yl)pyrid-4-yl)-1,4,7,10-

tetraoxadecyl)phenyl)-2,2′-bipyridyl)-iron(II)   bis(hexafluorophosphate)   acetone solvate[60]. The bond angles C7-C8-O1, C9-C8-O1, C24-C23-O8 and C22-C23-O8 are within the range reported in the [Ru(***poterpy***)$_2$]$^{2+}$ cation in the solid-state structure of [Ru(***poterpy***)$_2$][PF$_6$]$_2$·(CH$_3$)$_2$CO[55]. The bond angles C8-O1-C31 and C23-O8-C52 are 118.5(2)° and 122.2(3)° respectively which, are bigger than the corresponding angles in ([Ru(***poterpy***)$_2$]$^{2+}$ cation (117.5(3)° and 118.1(3)°)[55] and in (5,5′-bis(3-(10-(2,6-bis(pyrid-2-yl)pyrid-4-yl)-1,4,7,10-tetraoxadecyl)phenyl)-2,2′-bipyridyl)-iron(II) bis(hexafluorophosphate) acetone solvate (115.55° and 113.22°)[60].

The ethyleneoxy chains and naphthalene unit lie snuggly in the cleft between two terminal pyridine rings of the terpyridine. There are π-π interactions between the naphthalene and the terminal pyridine rings with an interplanar separation of 3.6 Å. The closest distance between the C3 atom of N1 ring to C44 atom of the naphthyl ring is 3.526 Å. The atoms H441 and H461 lie directly above the other non-stacked pyridine terminal ring.

7.5 Stereochemical properties of the chiral complex [{Fe(L^{14})}][PF$_6$]$_2$

Chiral products are not only involved in chemical reactions, but also produced in the supramolecular self-assembly systems. Reaction of the octahedral metal ions, Co(II), Fe(II) or Ru(II), and 2,2′-bipyridine (***bipy***) or 1,10-phenanthroline (***phen***) with a variety of substituents give Δ- and Λ-[M(***X-bipy***)$_3$]$^{2+}$ or [M(***X-phen***)$_3$]$^{2+}$ (M = Co, Fe or Ru) complexes (**Figure 21**).[61] Reaction of achiral di-bidentate ligands (***L***) with octahedral metal ion resulted in *plus* (*P*) and *minus* (*M*) trihelical enantiomers (**Figure 22**).[62-63] von Zelewsky has reported a reaction of achiral di-tridentate ligand 2,5-bis([2,2′]bipyridin-6-yl)-pyrazine with octahedral metal ions which resulted in grid-like complexes or chiral molecular squares (**Figure 23**).[64]
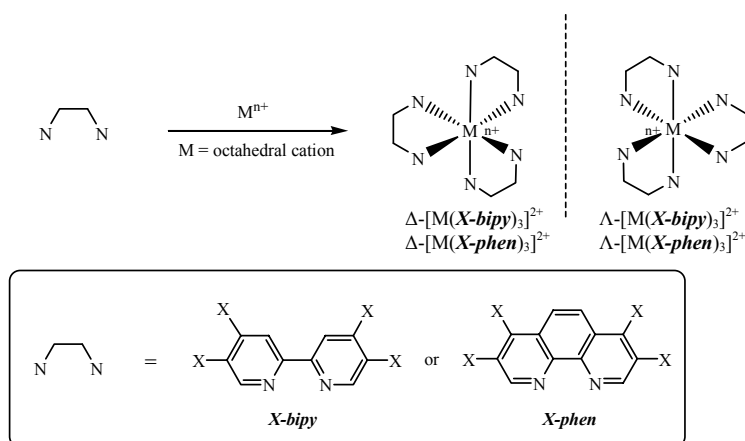
Figure 21. The Δ and Λ enantiomers formed from the reaction of an octahedral cation with three bidentate ligands.
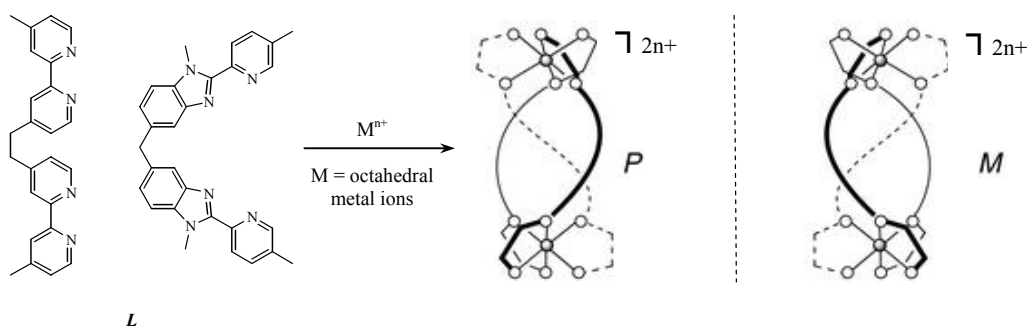
Figure 22. The *P* and *M* trihelical enantiomers formed from the reaction of an octahedral cation with three bis-bidentate ligands.
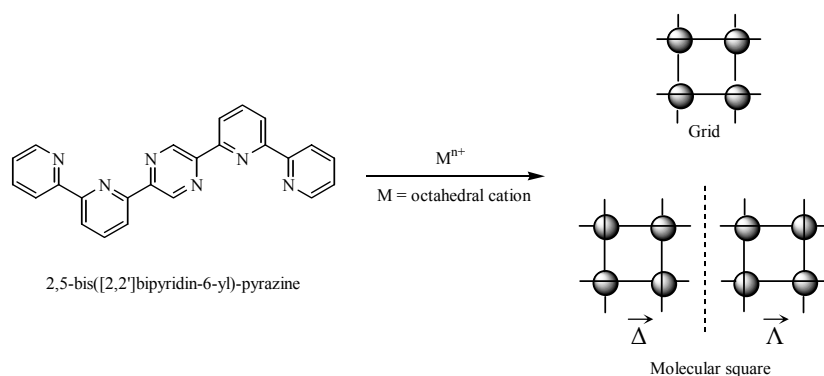
Figure 23. The grid and two enantiomers of the molecular square formed from the reaction of an octahedral cation with four di-trientate ligands.

A few pairs of enantiomeric complexes have been successfully separated by ion-pair chromatography[63,65-66] or selective crystallisation[67-68] with an enantiopure anion. In the last decades, NMR spectroscopy has been used to measure the enantiomeric purity

of the chiral species.[69] This method requires addition of a chiral auxiliary that converts the mixture of enantiomers into a mixture of diastereoisomeric ion pairs. As long as the analogous proton signals of the two diastereoisomeric complexes are well separated, the enantiomeric purity can be determined by direct measurement of the integral of the two analogous proton signals.

Chiral lanthanide shift reagents have been used for analyses the enantiomeric purity of the chiral species by using NMR spectroscopy. However, the lack of interactions with chiral cations, line broadening and distorted baselines limit their efficiency.[70] Recently, a series of hexacoordinated phosphate anions, such as TRISPHAT, BINPHAT, HYPHAT and TARPHAT have been reported by Lacour and applied as NMR chiral shift agents (**Figure 24**).[71-73] These anions can also be used as resolving agents and asymmetry-inducers.
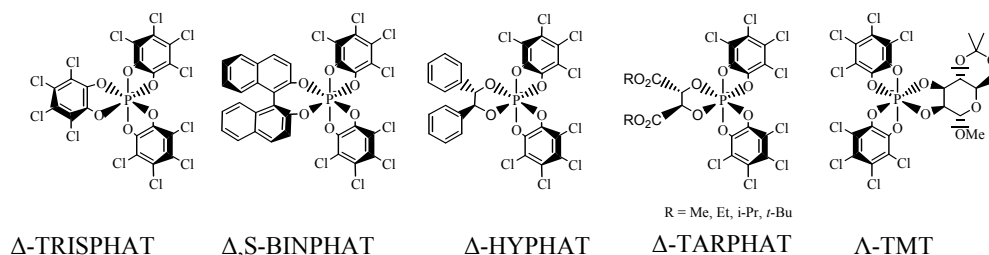
Figure 24. A series of hexacoordinated phosphate anions.

There is report on the resolution of the chiral cations, [Ru(*bipy*)$_3$]$^{2+}$ and [Ru(*Me$_2$-bipy*)$_3$]$^{2+}$, with enantiopure TRISPHAT by thin layer chromatography over silica gel (eluent CH_2Cl_2).[74] This method was also extended to the separation of Δ and Λ enantiomers of a mononulear iron(II) tris(diimine) complex.[75] There is also a report of the resolution of racemic ruthenium(II) tris(diimine) derivatives with enantiopure TRISPHAT by extraction since one of the diastereoisomeric pairs is more soluble in $CHCl_3$ than in water (**Figure 25**).[76] The diastereoisomeric ratio (d.r.) can be up to 49:1. By using the same protocol for a diiron(II) triple helicate, *P* and *M* enantiomers of this helicate can be separated.[77]
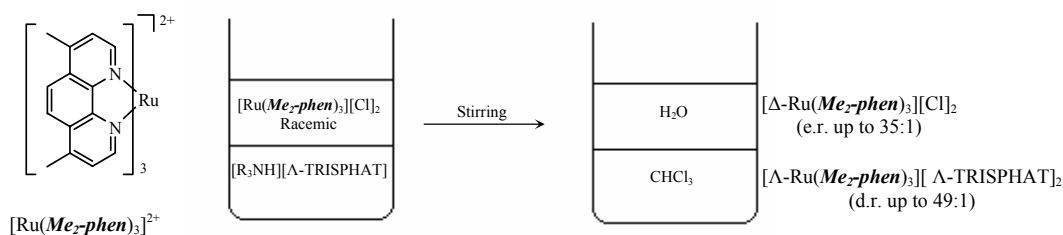
Figure 25. Stereoselective extraction of racemic [Ru(*Me₂-phen*)₃][Cl]₂ complexes by [R₃NH][Λ-TRISPHAT].

It is possible to use these hexacoordinated phosphate anions to afford selectively intermolecular diastereoselective interactions and then control the stereoselectivity between the two pair of diastereoisomeric pairs (Pfeiffer effect).[78] Iron(II) tris(diimine) complexes[79-81] and dicobalt(II) helicates[82] were studied with TRISPHAT anions in different solvent polarities. The NMR signals of the chiral cations were split by the presence of the anions and the diastereoisomeric ratio (d.r.) can be up to 50:1.

The homoditopic achiral ligand L^{14} reacted with octahedral iron(II) metal ions and resulted in a [1+1] mononuclear iron(II) complex. Since the naphthalene ring and the ethyleneoxy spacer chains are locked in between two terminal rings of terpyridine and cannot rotate freely around the molecule, the complex becomes chiral. This was confirmed by the solid-state structure and the unusual proton NMR spectrum (see **Section 7.4(b)** and **7.2**). As the complex is chiral, we did some preliminary studies of its stereochemical properties by using hexacoordinated phosphate NMR chiral shift agents. The following results were done by Dr. R. Frantz and Professor J. Lacour at the University of Geneva.

Firstly, the hexacoordinated phosphate anions [Bu₄N][Δ-TRISPHAT] or [Me₂NH₂][Λ-TMT] were added to the racemic [{Fe(L^{14})}][PF₆]₂ in CH₂Cl₂/acetone. The desired complexes [{Fe(L^{14})}][Δ-TRISPHAT]₂ or [{Fe(L^{14})}][Λ-TMT]₂ were isolated on a small preparative chromatography plate. There is an NMR enantiodifferentiation in both cases. Some of the proton signals indicated the splitting of the signals in roughly 1:1 ratio for the diastereoisomeric pairs (**Figure 26**).

NMR (^{1}H, 500 MHz, CD$_2$Cl$_2$)
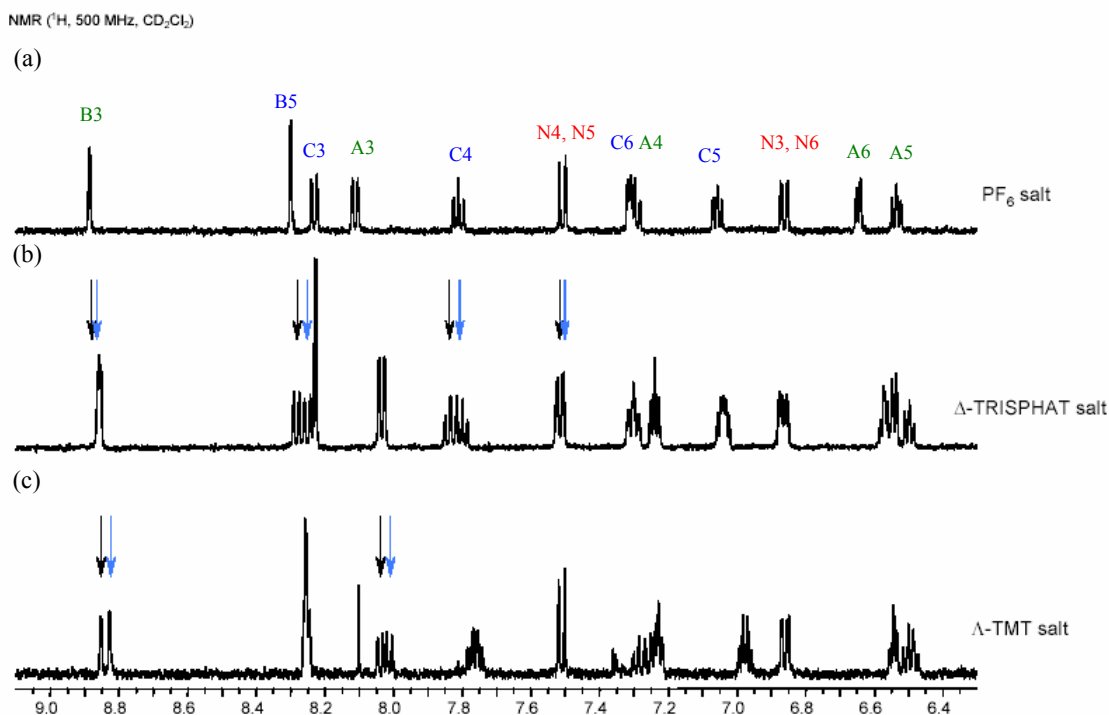
Figure 26. The ^{1}H NMR spectra (500 MHz, δ 6.3-9) of the chiral cation [{Fe($\boldsymbol{L^{14}}$)}]$^{2+}$
(a) in PF$_6$ salt, (b) in [Δ-TRISPHAT] salt and (c) [Λ-TMT] salt in CD$_2$Cl$_2$
at room temperature.
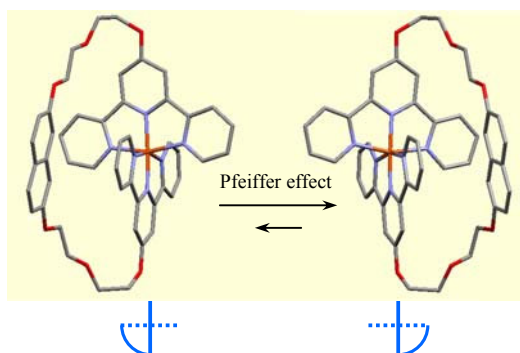
Figure 27. Diagram representing the Pfeiffer effect on [{Fe($\boldsymbol{L^{14}}$)}][Δ,S-BINPHAT].

Secondly, increasing amounts of hexacoordinated phosphate anions [Bu$_4$N][Δ,S-BINPHAT] were added to racemic [{Fe($\boldsymbol{L^{14}}$)}][PF$_6$]$_2$ in CD$_2$Cl$_2$. Not only enantiodifferentiation of the enantiomers of the cation was observed, but also an asymmetric induction (where the splitting of the signals was not 1:1 any more) resulted. This is because one of the diastereoisomeric pair becomes predominant (i.e. Pfeiffer effect) (**Figure 27**). The diastereoselectivity (*de*) is up to 45% (±2%) when 10 equivalents of [Bu$_4$N][Δ,S-BINPHAT] were added. The Pfeiffer effect was

maximised upon the decreasing the solvent polarity (decease the % of DMSO in CDCl$_3$).

When the solvent polarity decreased, one of the diastereoisomeric pairs has better interactions between the cation and [Δ,S-BINPHAT] anion than the other pair. The diastereoselectivity (*de*) is up to 60% (±2%) when the sample was measured with 2% DMSO in CDCl$_3$ (**Figure 28**). In 1% DMSO/CHCl$_3$, the complex exhibits a Cotton effect in the circular dichroism (CD) spectrum with the value $\Delta_{\varepsilon618}$ = 1.1 dm^{3}mol^{-1}cm^{-1} and $\Delta_{\varepsilon559}$ = -1.2 dm^{3}mol^{-1}cm^{-1} for the MLCT band. Since there are no CD spectra of other similar compounds to which we can compare our results, a time-dependent density functional theory (TDDFT) calculation for the CD spectrum of [{Fe(*L^{14}*)}][PF$_6$]$_2$ is currently being undertaken.
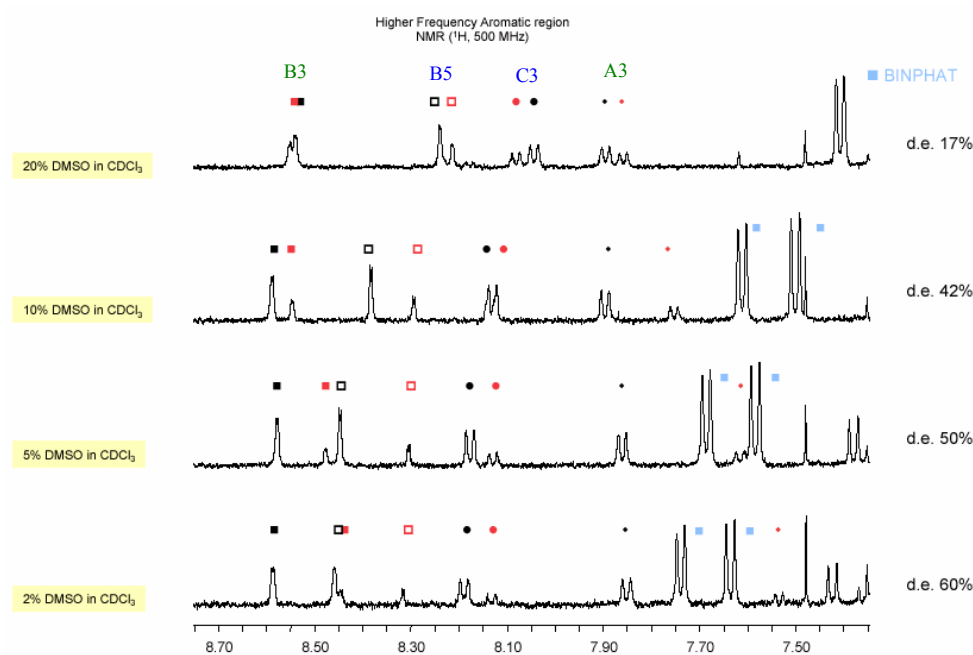
Figure 28. The ^{1}H NMR spectra (500 MHz, δ 7.3-8.7) of [{Fe(*L^{14}*)}][Δ,S-BINPHAT] in decreasing amount of DMSO in CDCl$_3$ at room temperature. The signals with black and red are the two diastereoisomeric pairs.

7.6 Conclusion

Mono-, di- and tri-nuclear metallomacrocyclic Ru(II) and Fe(II) complexes $[\{M(L)\}_n][PF_6]_{2n}$, where M = Ru(II) or Fe(II), $L = L^{11}$-L^{17} and n = 1, 2 or 3, have been synthesised and characterised with ^1H NMR spectroscopy, ES-MS spectrometry, UV/VIS spectroscopy and elemental analysis. Three representative crystal structures have been determined. The formation of different nuclearity metallomacrocycles depends on the rigidity and length of the spacer group between the metal binding sites. ^1H NMR spectroscopy can give the information about the purity of the metallomacrocycles while ES-MS spectrometry can confirm the size of the metallomacrocycles. The solid state structures of $[\{Ru(L^{11})\}_2][PF_6]_4$, $[\{Fe(L^{14})\}][PF_6]_2$ and $[\{Fe(L^{15})\}][PF_6]_2$ proved that the size of the metallomacrocycles can be correctly assigned using these two techniques.

7.7   Experimental

❖ [{Ru(L^{11})}$_2$][PF$_6$]$_4$ ❖ [{Fe(L^{11})}$_2$][PF$_6$]$_4$

                                                ❖ [{Fe(L^{12})}$_n$][PF$_6$]$_{2n}$

❖ [{Ru(L^{13})}$_n$][PF$_6$]$_{2n}$ (n = 2 or 3)   ❖ [{Fe(L^{13})}$_n$][PF$_6$]$_{2n}$ (n = 2 or 3)

❖ [{Ru(L^{14})}$_2$][PF$_6$]$_4$ ❖ [{Fe(L^{14})}][PF$_6$]$_2$

                                                ❖ [{Fe(L^{15})}][PF$_6$]$_2$

❖ [{Ru(L^{16})}$_2$][PF$_6$]$_4$ ❖ [{Fe(L^{16})}$_3$][PF$_6$]$_6$

❖ [{Ru(L^{17})}$_2$][PF$_6$]$_4$ ❖ [{Fe(L^{17})}$_2$][PF$_6$]$_4$

where L^{11} 2,6-[Bis(2,2′:6′,2″-terpyridin-4′-yl)-1,4-dioxapentyl]naphthalene

        L^{12} 2,6-[Bis(2,2′:6′,2″-terpyridin-4′-yl)-1,4,7-trioxaoctyl]naphthalene

        L^{13} 2,7-[Bis(2,2′:6′,2″-terpyridin-4′-yl)-1,4-dioxabutyl]naphthalene

        L^{14} 2,7-[Bis(2,2′:6′,2″-terpyridin-4′-yl)-1,4,7-trioxaheptyl]naphthalene

        L^{15} 2,7-[Bis(2,2′:6′,2″-terpyridin-4′-yl)-1,4,7,10-tetraoxadecayl]naphthalene

        L^{16} 2,3-[Bis(2,2′:6′,2″-terpyridin-4′-yl)-1,4-dioxabutyl]naphthalene

        L^{17} 2,3-[Bis(2,2′:6′,2″-terpyridin-4′-yl)-1,4,7-trioxaheptyl]naphthalene

(a) General synthesis of macrocyclic ruthenium(II) metal complexes[36]
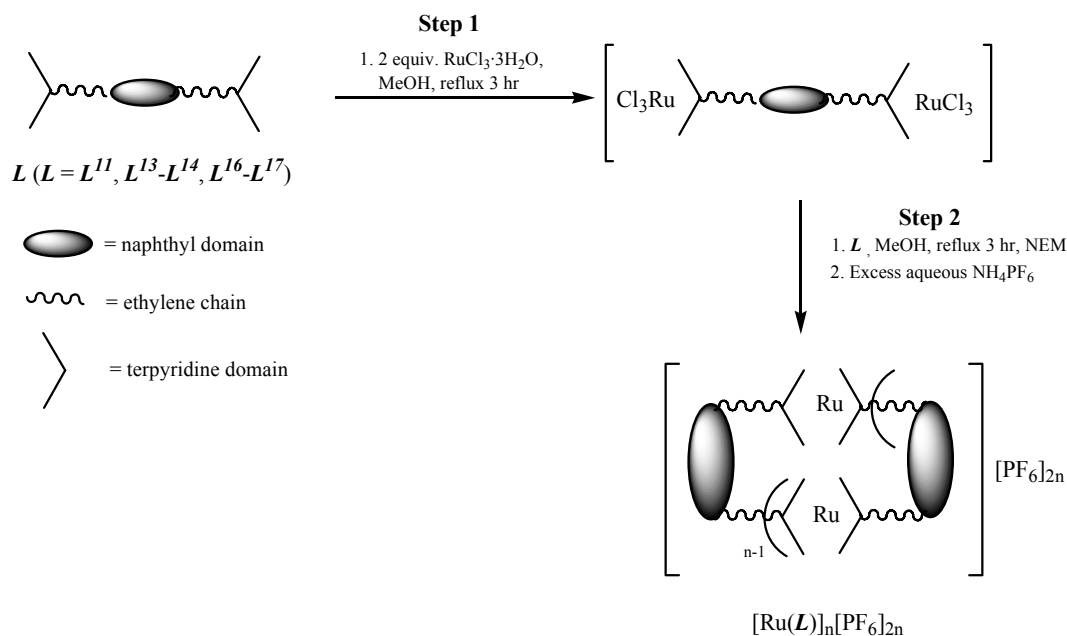
Step 1

1 equivalent of **L** (**L^{11}**, **L^{13}**-**L^{14}**, **L^{16}**-**L^{17}**) and 2 equivalents of RuCl$_3$·3H$_2$O were heated to reflux for 3 hours in CH$_3$OH. The brownish red precipitate [Cl$_3$Ru**L**RuCl$_3$] was filtered,

collected and washed well with water. The crude product was used for the second step without purification.

Step 2

1 equivalent of L (L^{11}, L^{13}-L^{14}, L^{16}-L^{17}), 1 equivalent of [Cl$_3$RuLRuCl$_3$] (where $L = L^{11}$, L^{13}-L^{14}, L^{16}-L^{17}) and a few drops of *N*-ethylmorpholine (NEM) were heated to reflux for 3 hours in CH$_3$OH. The deep red reaction mixture was cooled, and excess aqueous NH$_4$PF$_6$ were added to precipitate the crude product. The crude product was collected by filtration and redissolved in CH$_3$CN. The solvent was removed again and a red powder was obtained. The major red product was obtained after column chromatography or preparative TLC (SiO$_2$, CH$_3$CN: saturated aqueous KNO$_3$: water 14:2:1).

❖ [{Ru(L^{11})}$_2$][PF$_6$]$_4$

L^{11} (0.06 g, 0.08 mmol) and 2 equivalents of RuCl$_3$·3H$_2$O (43 mg, 0.16 mmol) were refluxed in 10 mL CH$_3$OH. The crude product [Cl$_3$RuL^{11}RuCl$_3$] (0.08 g, 0.07 mmol) was used for the second step without purification.

[Cl$_3$RuL^{11}RuCl$_3$] (0.08 g, 0.07 mmol) and L^{11} (0.05 g, 0.07 mmol) were used for the second step. After preparative TLC (SiO$_2$, CH$_3$CN: saturated aqueous KNO$_3$: water 14:2:1), a red powder of [{Ru(L^{11})}$_2$][PF$_6$]$_4$ (40 mg, 0.018 mmol, 26% yield in this step) were obtained as the major product.
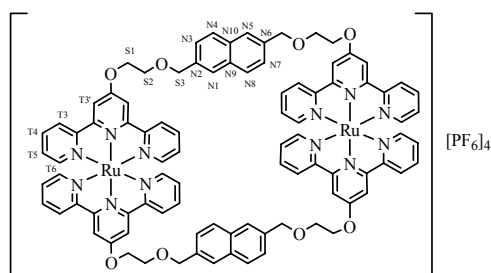
Molecular formula: C$_{92}$H$_{76}$N$_{12}$O$_8$Ru$_2$P$_4$F$_{24}$
Molecular weight: 2259.66

^{1}H NMR (400 MHz, CD$_3$CN): δ_H 4.00 (m, 8H, H^{S2}), 4.72 (m, 8H, H^{S1}), 4.75 (s, 8H, H^{S3}), 6.97 (m, 8H, H^{T5}), 7.23 (d, *J* 5.6 Hz, 8H, H^{T6}), 7.33 (dd, *J* 1.0, 8.6 Hz, 4H, H$^{N3, N7}$), 7.51 (d, *J* 8.1 Hz, 4H, H$^{N4, N8}$), 7.74 (m, 12H, H^{T4} and H$^{N1, N5}$), 8.32 (s, 8H, H$^{T3'}$), 8.33 (m, 8H, H^{T3}).

MS (ES): *m/z* = 420.1 [M-4PF$_6$]$^{4+}$.

UV/VIS (CH$_3$CN): λ_{max}/ nm (ε_{max}, M^{-1}cm^{-3}) 226 (266 x 10^3), 239 (120 x 10^3), 265 (123 x 10^3), 302 (132 x 10^3), 484 (39.0 x 10^3).

Elemental analysis: Found: C, 45.59; H, 3.45; N, 7.34. Calc. for $C_{92}H_{76}N_{12}O_8P_4F_{24}Ru_2 \cdot 9H_2O$: C, 45.62; H, 3.92; N, 6.94%.

❖ $[\{Ru(\boldsymbol{L^{13}})\}_n][PF_6]_{2n}$
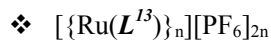
$\boldsymbol{L^{13}}$ (71 mg, 0.10 mmol) and 2 equivalents of $RuCl_3 \cdot 3H_2O$ (53 mg, 0.20 mmol) were refluxed in 10 mL CH_3OH. The crude product $[Cl_3Ru\boldsymbol{L^{13}}RuCl_3]$ (112 mg, 0.100 mmol) was used for the second step without purification.

$[Cl_3Ru\boldsymbol{L^{13}}RuCl_3]$ (112 mg, 0.100 mmol) and $\boldsymbol{L^{13}}$ (71 mg, 0.10 mmol) were used for the second step. After preparative TLC (SiO_2, CH_3CN: saturated aqueous KNO_3: water 14:2:1), there are two fractions, which are very close together on the TLC plate. A red powder of $[\{Ru(\boldsymbol{L^{13}})\}_2][PF_6]_4$ (8.8 mg, 0.0040 mmol, 4.0% yield in this step) and $[\{Ru(\boldsymbol{L^{13}})\}_3][PF_6]_6$ (6.1 mg, 0.0018 mmol, 1.8% yield in this step) were obtained. However, both fractions are not pure and they have small amount of the other fraction.

Fraction 1 $R_f = 0.5$: (with around 10% Fraction 2)
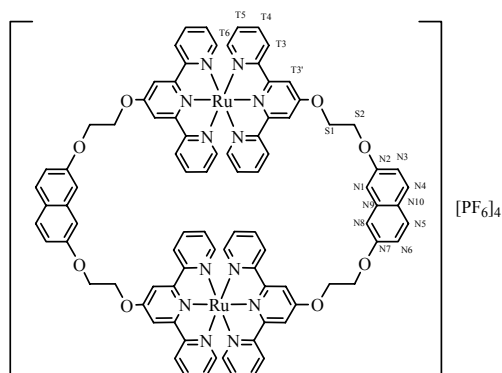
Molecular formula: $C_{88}H_{68}N_{12}O_8Ru_2P_4F_{24}$
Molecular weight: 2203.55

^1H NMR (400 MHz, CD_3CN): δ_H 4.13 (s, 8H, H^{S2}), 4.77 (s, 8H, H^{S1}), 6.68 (d, J 2.0 Hz, 4H, $H^{N1, N8}$), 7.12 (m, 12H, H^{T5} and $H^{N3, N6}$), 7.44 (d, J 5.2 Hz, 8H, H^{T6}), 7.70 (td, J 1.2, 7.8 Hz, 8H, H^{T4}), 7.88 (d, J 9.2 Hz, 4H, $H^{N4, N5}$), 8.06 (s, 8H, $H^{T3'}$), 8.19 (d, J 8.0 Hz, 8H, H^{T3}).

MS (ES): m/z = 957.1 $[M-2PF_6]^{2+}$, 589.7 $[M-3PF_6]^{3+}$, 406.4 $[M-4PF_6]^{4+}$.

Fraction 2 R$_f$ = 0.48: (with around 20% Fraction 1)
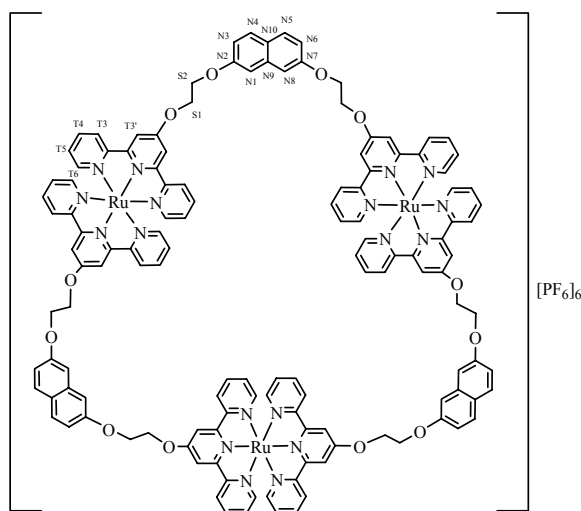
Molecular formula:
C$_{132}$H$_{102}$N$_{18}$O$_{12}$Ru$_3$P$_6$F$_{36}$
Molecular weight: 3305.33

^{1}H NMR (400 MHz, CD$_3$CN): δ$_H$ 4.65 (m, 12H, H^{S2}), 4.94 (m, 12H, H^{S1}), 7.12 (m, 18H, H^{T5} and H$^{N3, N6}$), 7.30 (d, *J* 2.4 Hz, 6H, H$^{N1, N8}$), 7.36 (d, *J* 5.6 Hz, 12H, H^{T6}), 7.81 (m, 18H, H^{T4} and H$^{N4, N5}$), 8.32 (s, 12H, H$^{T3'}$), 8.39 (d, *J* 8.0 Hz, 12H, H^{T3}).

MS (ES): *m/z* = 957.0 [M-3PF$_6$]$^{3+}$, 681.2 [M-4PF$_6$]$^{4+}$, 515.8 [M-5PF$_6$]$^{5+}$.

❖ [{Ru(*L^{14}*)}$_2$][PF$_6$]$_4$

L^{14} (60 mg, 0.075 mmol) and 2 equivalents of RuCl$_3$·3H$_2$O (39 mg, 0.15 mmol) were refluxed in 10 mL CH$_3$OH. The crude product [Cl$_3$Ru*L^{14}*RuCl$_3$] (90 mg, 0.074 mmol) was used for the second step without purification.

[Cl$_3$Ru*L^{14}*RuCl$_3$] (90 mg, 0.074 mmol) and *L^{14}* (59 mg, 0.074 mmol) were used for the second step. After column chromatography (SiO$_2$, CH$_3$CN: saturated aqueous KNO$_3$: water 14:2:1), a red powder of [{Ru(*L^{14}*)}$_2$][PF$_6$]$_4$ (21.3 mg, 0.00895 mmol, 12.1% yield in this step) was obtained as the major product.
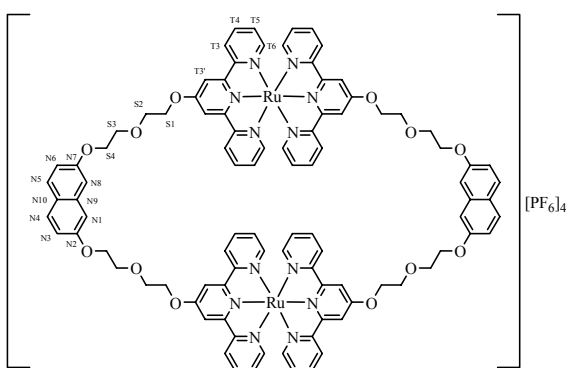
Molecular formula:
C$_{96}$H$_{84}$N$_{12}$O$_{12}$Ru$_2$P$_4$F$_{24}$
Molecular weight: 2379.76

^{1}H NMR (500 MHz, CD$_3$CN): δ_H 3.98 (m, 8H, H^{S3}), 4.06 (m, 8H, H^{S4}), 4.12 (m, 8H, H^{S2}), 4.72 (m, 8H, H^{S1}), 6.69 (d, *J* 2.4 Hz, 4H, H$^{N1, N8}$), 6.85 (dd, *J* 2.5, 8.9 Hz, 4H, H$^{N3, N6}$), 7.00 (ddd, *J* 1.3, 5.7, 7.5 Hz, 8H, H^{T5}), 7.29 (ddd, *J* 0.7, 1.5, 5.6 Hz, 8H, H^{T6}), 7.39 (d, *J* 9.0 Hz, 4H, H$^{N4, N5}$), 7.69 (td, *J* 1.5, 7.9 Hz, 8H, H^{T4}), 8.27 (m, 8H, H^{T3}), 8.28 (s, 8H, H$^{T3'}$).

MS (ES): *m/z* = 1045.2 [M-2PF$_6$]$^{2+}$, 648.8 [M-3PF$_6$]$^{3+}$, 450.7 [M-4PF$_6$]$^{4+}$.

UV/VIS (CH$_3$CN): λ_{max}/ nm (ε_{max}, M^{-1}cm^{-3}) 235 (272 x 10^3), 267 (138 x 10^3), 304 (155 x 10^3), 486 (41.4 x 10^3).

Elemental analysis: Found: C, 47.62; H, 3.73; N, 6.88. Calc. for C$_{96}$H$_{84}$N$_{12}$O$_{12}$P$_4$F$_{24}$Ru$_2$·H$_2$O: C, 48.08; H, 3.62; N, 7.01%.

❖ [{Ru(*L^{16}*)}$_2$][PF$_6$]$_4$

L^{16} (92 mg, 0.13 mmol) and 2 equivalents of RuCl$_3$·3H$_2$O (68 mg, 0.26 mmol) were refluxed in 25 mL CH$_3$OH. The crude product [Cl$_3$Ru*L^{16}*RuCl$_3$] (124 mg, 0.110 mmol) was used for the second step without purification.

[Cl$_3$Ru*L^{16}*RuCl$_3$] (124 mg, 0.110 mmol) and *L^{16}* (75 mg, 0.11 mmol) were used for the second step. After preparative TLC (SiO$_2$, CH$_3$CN: saturated aqueous KNO$_3$: water 14:2:1), a red powder of [{Ru(*L^{16}*)}$_2$][PF$_6$]$_4$ (2.6 mg, 0.0012 mmol, 1.1% yield in this step) was obtained as the major product. The red product remained on the silica of the TLC plate even when washed with A sol. Therefore, the yield was low.

Molecular formula: C$_{88}$H$_{68}$N$_{12}$O$_8$Ru$_2$P$_4$F$_{24}$

Molecular weight: 2203.55
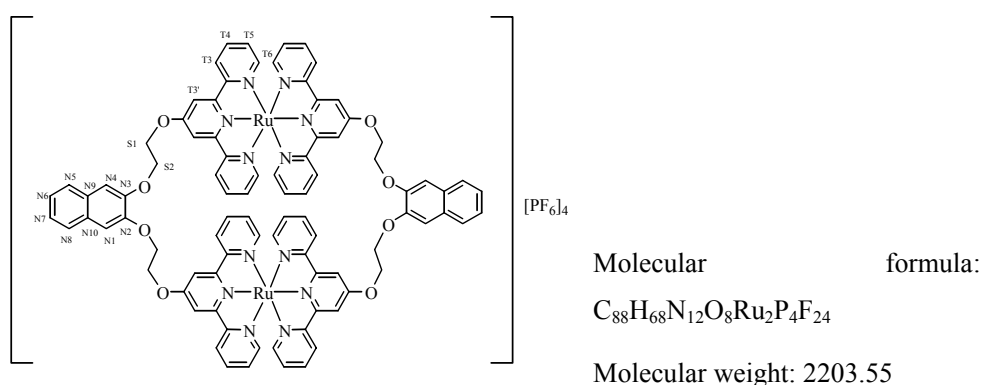
^{1}H NMR (500 MHz, CD$_3$CN): δ_H 4.79 (t, *J* 5.0 Hz, 8H, H^{S2}), 5.02 (t, *J* 5.1 Hz, 8H, H^{S1}), 6.77 (m, 8H, H^{T5}), 7.19 (dd, *J* 0.7, 5.6 Hz, 8H, H^{T6}), 7.26 (m, 8H, H^{T4}), 7.46 (m, 4H, H$^{N6, N7}$), 7.57 (s, 4H, H$^{N1, N4}$), 7.87 (m, 4H, H$^{N5, N8}$), 8.26 (d, *J* 7.9 Hz, 8H, H^{T3}), 8.36 (s, 8H, H$^{T3'}$).

MS (ES): m/z = 957.0 [M-2PF$_6$]$^{2+}$, 589.3 [M-3PF$_6$]$^{3+}$, 406.2 [M-4PF$_6$]$^{4+}$.

UV/VIS (CH$_3$CN): λ_{max}/ nm (ε_{max}, M^{-1}cm^{-3}) 230 (179 x 10^3), 264 (113 x 10^3), 303 (112 x 10^3), 485 (35.0 x 10^3).

❖ [{Ru($\boldsymbol{L^{17}}$)}$_2$][PF$_6$]$_4$

$\boldsymbol{L^{17}}$ (60 mg, 0.075 mmol) and 2 equivalents of RuCl$_3$·3H$_2$O (39 mg, 0.15 mmol) were refluxed in 10 mL CH$_3$OH. The crude product [Cl$_3$Ru$\boldsymbol{L^{17}}$RuCl$_3$] (79 mg, 0.065 mmol) was used for the second step without purification.

[Cl$_3$Ru$\boldsymbol{L^{17}}$RuCl$_3$] (79 mg, 0.065 mmol) and $\boldsymbol{L^{17}}$ (52 mg, 0.065 mmol) were used for the second step. After column chromatography (SiO$_2$, CH$_3$CN: saturated aqueous KNO$_3$: water 14:2:1), a red powder of [{Ru($\boldsymbol{L^{17}}$)}$_2$][PF$_6$]$_4$ (18.2 mg, 0.00765 mmol, 11.8%) was obtained as the major product.
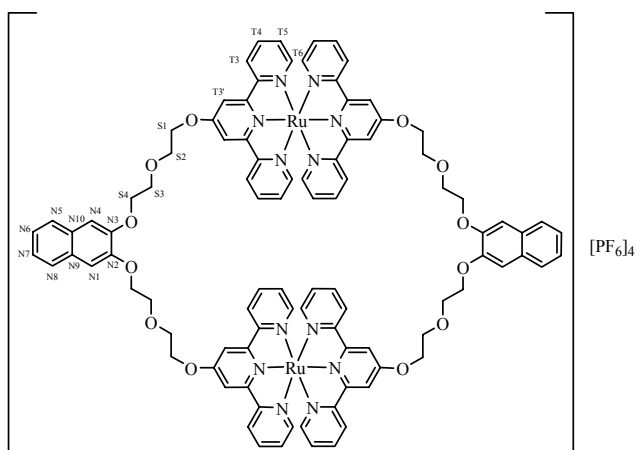
Molecular formula:
C$_{96}$H$_{84}$N$_{12}$O$_{12}$Ru$_2$P$_4$F$_{24}$
Molecular weight: 2379.76

^{1}H NMR (500 MHz, CD$_3$CN): δ_H 4.11 (m, 8H, H^{S3}), 4.16 (m, 8H, H^{S2}), 4.39 (m, 8H, H^{S4}), 4.71 (t, J 4.5 Hz, 8H, H^{S1}), 6.73 (ddd, J 1.3, 5.6, 7.5 Hz, 8H, H^{T5}), 7.22 (ddd, J 0.6, 1.4, 5.6 Hz, 8H, H^{T6}), 7.29 (m, 4H, H$^{N6, N7}$), 7.34 (s, 4H, H$^{N1, N4}$), 7.42 (td, J 1.4, 7.8 Hz, 8H, H^{T4}), 7.67 (m, 4H, H$^{N5, N8}$), 8.26 (d, J 7.8 Hz, 8H, H^{T3}), 8.28 (s, 8H, H$^{T3'}$).

MS (ES): m/z = 449.9 [M-4PF$_6$]$^{4+}$.

UV/VIS (CH$_3$CN): λ_{max}/ nm (ε_{max}, M^{-1}cm^{-3}) 231 (224 x 10^3), 264 (120 x 10^3), 302 (126 x 10^3), 484 (35.7 x 10^3).

Elemental analysis: Found: C, 46.97; H, 3.67; N, 7.18. Calc. for C$_{96}$H$_{84}$N$_{12}$O$_{12}$P$_4$F$_{24}$Ru$_2$·3H$_2$O: C, 47.37; H, 3.73; N, 6.90%.

(b) General synthesis of macrocyclic iron(II) metal complexes[33-35]
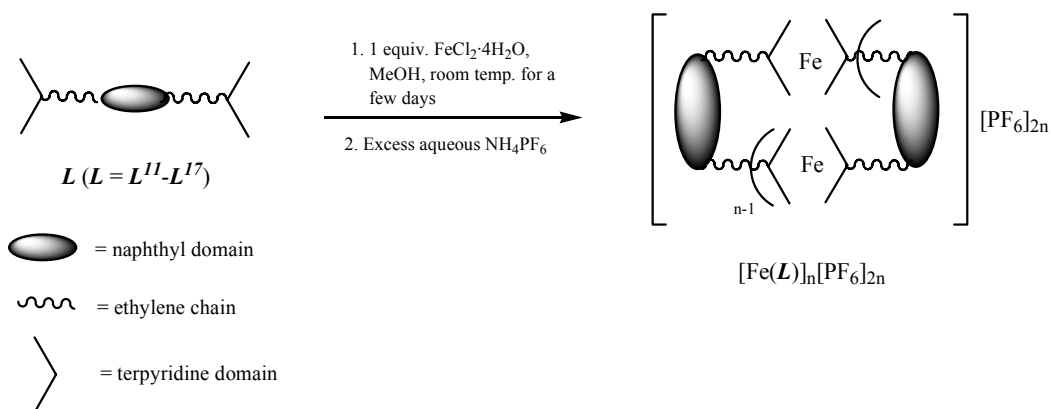
1 equivalent of $FeCl_2 \cdot 4H_2O$ in CH_3OH was added to 1 equivalent of **L** (**L[11]-L[17]**) in CH_3OH dropwise and the mixture were stirred for a few days. The deep purple reaction mixture was filtered and concentrated. Excess aqueous NH_4PF_6 were added to precipitate the crude product. The crude product was collected by filtration and redissolved in CH_3CN. The solvent was removed and a purple powder was obtained. The major product was obtained after column chromatography or preparative TLC (SiO_2, CH_3CN: saturated aqueous KNO_3: water 14:2:1).

❖ [{Fe(**L[11]**)}₂][PF₆]₄

$FeCl_2 \cdot 4H_2O$ (40 mg, 0.20 mmol) in 20 mL CH_3OH was added to **L[11]** (0.15 g, 0.20 mmol) in 750 mL CH_3OH dropwise and the mixture were stirred for 4 days. After preparative TLC (SiO_2, CH_3CN: saturated aqueous KNO_3: water 14:2:1), a purple powder of [{Fe(**L[11]**)}₂][PF₆]₄ (62.4 mg, 0.0288 mmol, 28.8%) was obtained as the major product.

Molecular formula: $C_{92}H_{76}N_{12}O_8Fe_2P_4F_{24}$

Molecular weight: 2169.21
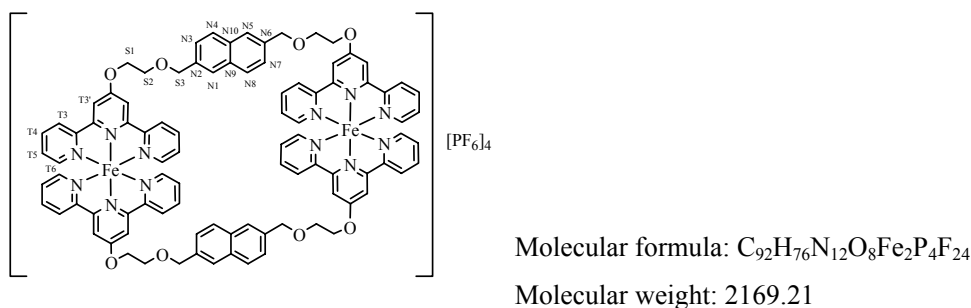
^{1}H NMR (500 MHz, CD_3CN): δ_H 4.05 (m, 8H, H^{S2}), 4.78 (s, 8H, H^{S3}), 4.81 (m, 8H, H^{S1}), 6.87 (ddd, J 1.3, 5.7, 7.4 Hz, 8H, H^{T5}), 6.99 (ddd, J 0.7, 1.4, 5.6 Hz, 8H, H^{T6}), 7.34 (dd, J

1.3, 8.4 Hz, 4H, H$^{N3, N7}$), 7.47 (d, *J* 8.3 Hz, 4H, H$^{N4, N8}$), 7.71 (m, 8H, H^{T4}), 7.72 (s, 4H, H$^{N1, N5}$), 8.29 (dt, *J* 0.9, 8.0 Hz, 8H, H^{T3}), 8.47 (s, 8H, H$^{T3'}$).

MS (ES): *m/z* = 578.2 [M-3PF$_6$]$^{3+}$, 397.5 [M-4PF$_6$]$^{4+}$.

UV/VIS (CH$_3$CN): λ_{max}/ nm (ε_{max}, M^{-1}cm^{-3}) 226 (145 x 10^3), 241 (64.8 x 10^3), 270 (64.3 x 10^3), 314 (38.2 x 10^3), 552 (12.2 x 10^3).

Elemental analysis: Found: C, 47.89; H, 3.63; N, 7.47. Calc. for C$_{92}$H$_{76}$N$_{12}$O$_8$P$_4$F$_{24}$Fe$_2$·7H$_2$O: C, 48.14; H, 3.96; N, 7.32%.

❖ [{Fe(***L***^{12})}$_n$][PF$_6$]$_{2n}$

FeCl$_2$·4H$_2$O (26 mg, 0.13 mmol) in 20 mL CH$_3$OH was added to ***L***^{12} (0.11 g, 0.13 mmol) in 750 mL CH$_3$OH dropwise and the mixture were stirred for 4 days. After preparative TLC (SiO$_2$, CH$_3$CN: saturated aqueous KNO$_3$: water 14:2:1), a purple powder of [{Fe(***L***^{12})}$_n$][PF$_6$]$_{2n}$ were obtained. However, from the proved of the NMR experiment, this fraction contains two components (A and B) although the ES-MS suggests it is [{Fe(***L***^{12})}][PF$_6$]$_2$.

[{Fe(***L***^{12})}$_n$][PF$_6$]$_{2n}$ (A:B = 1.09: 1)

^{1}H NMR (500 MHz, CD$_3$CN): δ$_H$ 3.70 (m, 4H, H$^{(A)S4}$), 3.73 (m, 4H, H$^{(B)S4}$), 3.80 (m, 4H, H$^{(A)S3}$), 3.84 (m, 4H, H$^{(B)S3}$), 4.05 (m, 4H, H$^{(A)S2}$), 4.11 (m, 4H, H$^{(B)S2}$), 4.47 (s, 4H, H$^{(A)S5}$), 4.51 (s, 4H, H$^{(B)S5}$), 4.86 (m, 4H, H$^{(A)S1}$), 4.94 (m, 4H, H$^{(B)S1}$), 6.67 (d, *J* 8.3 Hz, 2H, H$^{(B)N4, N8}$), 6.76 (d, *J* 8.2 Hz, 2H, H$^{(A)N4, N8}$), 6.81 (ddd, *J* 1.3, 5.7, 7.5 Hz, 4H, H$^{(B)T5}$), 6.83 (s, 4H, H$^{(A,B)N1, N5}$), 6.90 (ddd, *J* 0.7, 1.4, 5.6 Hz, 4H, H$^{(B)T6}$), 6.96 (dd, *J* 1.5, 8.4 Hz, 2H, H$^{(A)N3, N7}$), 7.04 (dd, *J* 1.3, 8.4 Hz, 2H, H$^{(B)N3, N7}$), 7.14 (ddd, *J* 1.0, 5.1, 7.6 Hz, 4H, H$^{(A)T5}$), 7.49 (ddd, *J* 0.9, 1.6, 5.1 Hz, 4H, H$^{(A)T6}$), 7.63 (ddd, *J* 1.5, 7.6, 8.0 Hz, 4H, H$^{(B)T4}$), 7.93 (ddd, *J* 1.7, 7.6, 8.0 Hz, 4H, H$^{(A)T4}$), 8.25 (ddd, *J* 0.8, 1.3, 8.0 Hz, 4H, H$^{(B)T3}$), 8.33 (s, 4H, H$^{(A)T3'}$), 8.37 (dt, *J* 1.0, 8.1 Hz, 4H, H$^{(A)T3}$), 8.62 (s, 4H, H$^{(B)T3'}$).

MS (ES): *m/z* = 1027.2 [M-PF$_6$]$^+$, 901.6 [M-PF$_6$-PF$_5$]$^+$, 441.7 [M-2PF$_6$]$^{2+}$.

❖ [{Fe($\boldsymbol{L^{13}}$)}$_n$][PF$_6$]$_{2n}$

FeCl$_2$·4H$_2$O (20 mg, 0.10 mmol) in 20 mL CH$_3$OH was added to $\boldsymbol{L^{13}}$ (71 mg, 0.10 mmol) in 750 mL CH$_3$OH dropwise and the mixture were stirred for 5 days. After preparative TLC (SiO$_2$, CH$_3$CN: saturated aqueous KNO$_3$: water 14:2:1), a purple powder of [{Fe($\boldsymbol{L^{13}}$)}$_2$][PF$_6$]$_4$ (1 mg, 0.0005 mmol, 1%) and [{Fe($\boldsymbol{L^{13}}$)}$_3$][PF$_6$]$_6$ (5 mg, 0.002 mmol, 6%) were obtained. However, both fractions were not pure and contained a small amount of the other fractions.

<u>Fraction 1: [{Fe($\boldsymbol{L^{13}}$)}$_2$][PF$_6$]$_4$ (R$_f$ value = 0.47)</u>
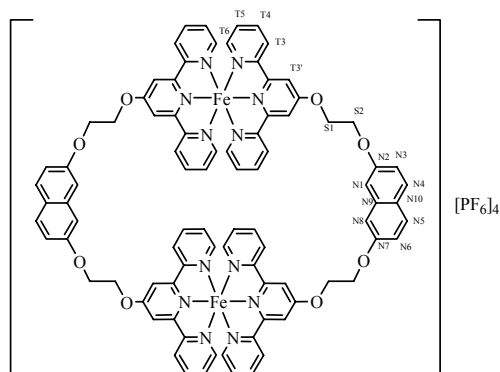
Molecular formula: C$_{88}$H$_{68}$N$_{12}$O$_8$Fe$_2$P$_4$F$_{24}$
Molecular weight: 2113.10

^{1}H NMR: the amount of material was too small for NMR investigation.

MS (ES): m/z = 911.6 [M-2PF$_6$]$^{2+}$, 828.3 [Fe+$\boldsymbol{L}$+NO$_3$]$^+$, 785.5 [Fe+$\boldsymbol{L}$+F]$^+$, 559.6 [M-3PF$_6$]$^{3+}$, 383.5 [M-4PF$_6$]$^{4+}$.

<u>Fraction 2: [{Fe($\boldsymbol{L^{13}}$)}$_3$][PF$_6$]$_6$ (R$_f$ value = 0.45)</u>
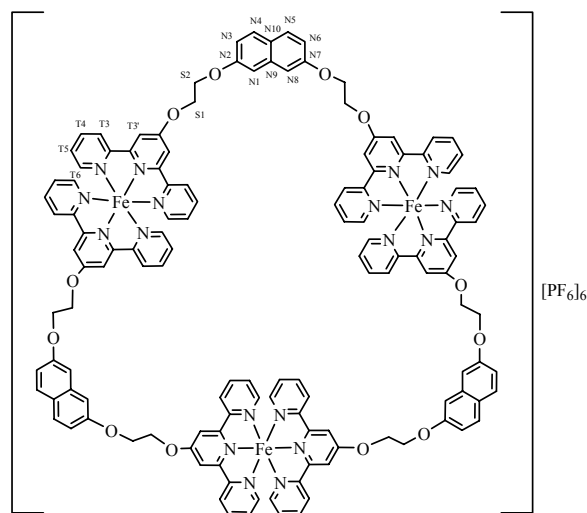
Molecular formula:
C$_{132}$H$_{102}$N$_{18}$O$_{12}$Fe$_3$P$_6$F$_{36}$
Molecular weight: 3169.66

^{1}H NMR (400 MHz, CD$_3$CN): δ$_H$ 4.71 (m, 12H, H^{S2}), 5.03 (m, 12H, H^{S1}), 7.02 (m, 12H, H^{T5}), 7.13 (d, J 4.8 Hz, 12H, H^{T6}), 7.16 (dd, J 2.6, 9.0 Hz, 6H, H$^{N3, N6}$), 7.34 (d, J 2.0 Hz,

6H, $H^{N1, N8}$), 7.80 (m, 18H, H^{T4} and $H^{N4, N5}$), 8.36 (d, *J* 8.4 Hz, 12H, H^{T3}), 8.47 (s, 12H, $H^{T3'}$).

MS (ES): *m/z* = 1440.3 [M-2PF$_6$]$^{2+}$, 911.4 [M-3PF$_6$]$^{3+}$, 647.5 [M-4PF$_6$]$^{4+}$, 489.1 [M-5PF$_6$]$^{5+}$, 383.6 [M-6PF$_6$]$^{6+}$.

❖ [{Fe(***L***^{14})}][PF$_6$]$_2$

FeCl$_2$·4H$_2$O (19 mg, 0.09 mmol) in 20 mL CH$_3$OH was added to ***L***^{14} (75 mg, 0.09 mmol) in 750 mL CH$_3$OH dropwise and the mixture were stirred for 2 days. After column chromatography (SiO$_2$, CH$_3$CN: saturated aqueous KNO$_3$: water 14:2:1), a purple powder of [{Fe(***L***^{14})}][PF$_6$]$_2$ (40.4 mg, 0.0353 mmol, 39.2%) was obtained as the major product.

Molecular formula: C$_{48}$H$_{42}$N$_6$O$_6$FeP$_2$F$_{12}$
Molecular weight: 1144.65

^{1}H NMR (500 MHz, CD$_3$CN): δ_H 3.79 (m, 6H, H^{S4a}, H^{S4b} and H^{S3b}), 4.07 (m, 2H, H^{S3a}), 4.13 (m, 4H, H^{S2a} and H^{S2b}), 4.66 (dt, *J* 2.0, 13.9 Hz, 2H, H^{S1b}), 4.86 (d, *J* 2.4 Hz 2H, $H^{N1, N8}$), 5.38 (m, 2H, H^{S1a}), 6.52 (ddd, *J* 1.3, 5.7, 7.5 Hz, 2H, H^{A5}), 6.65 (ddd, *J* 0.7, 1.4, 5.6 Hz, 2H, H^{A6}), 6.85 (dd, *J* 2.5, 8.9 Hz, 2H, $H^{N3, N6}$), 7.02 (ddd, *J* 1.3, 5.6, 7.5 Hz, 2H, H^{C5}), 7.31 (td, *J* 1.5, 7.8 Hz, 2H, H^{A4}), 7.35 (ddd, *J* 0.7, 1.4, 5.6 Hz, 2H, H^{C6}), 7.53 (d, *J* 9.0 Hz, 2H, $H^{N4, N5}$), 7.84 (td, *J* 1.5, 7.8 Hz, 2H, H^{C4}), 8.18 (d, *J* 7.8 Hz, 2H, H^{A3}), 8.37 (dt, *J* 1.0, 8.0 Hz, 2H, H^{C3}), 8.41 (d, *J* 2.2 Hz, 2H, H^{B5}), 8.82 (d, *J* 2.2 Hz, 2H, H^{B3}).

MS (ES): *m/z* = 999.0 [M-PF$_6$]$^+$, 873.5 [M-PF$_6$-PF$_5$]$^+$.

UV/VIS (CH$_3$CN): λ_{max}/ nm (ε_{max}, M^{-1}cm^{-3}) 233 (80.0 x 10^3), 269 (40.7 x 10^3), 314 (31.3 x 10^3), 555 (9.30 x 10^3).

Elemental analysis: Found: C, 50.10; H, 3.71; N, 7.51. Calc. for C$_{48}$H$_{42}$N$_6$O$_6$P$_2$F$_{12}$Fe: C, 50.36; H, 3.71; N, 7.34%.

❖ [{Fe(L^{15})}][PF$_6$]$_2$

FeCl$_2$·4H$_2$O (32 mg, 0.16 mmol) in 20 mL CH$_3$OH was added to L^{15} (0.14 g, 0.16 mmol) in 750 mL CH$_3$OH dropwise and the mixture were stirred for 3 days. After column chromatography (SiO$_2$, CH$_3$CN: saturated aqueous KNO$_3$: water 14:2:1), a purple powder of [{Fe(L^{15})}][PF$_6$]$_2$ (93.6 mg, 0.0759 mmol, 47.4%) was obtained as the major product.
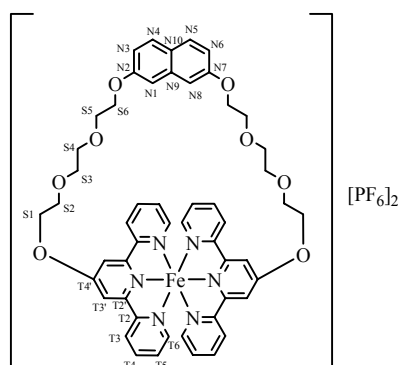
Molecular formula: C$_{52}$H$_{50}$N$_6$O$_8$FeP$_2$F$_{12}$
Molecular weight: 1232.76

^{1}H NMR (500 MHz, CD$_3$CN): δ$_H$ 3.56 (t, *J* 4.7 Hz, 4H, H^{S6}), 3.76 (m, 4H, H^{S4}), 3.82 (m, 4H, H^{S5}), 3.86 (m, 4H, H^{S3}), 4.12 (m, 4H, H^{S2}), 4.84 (m, 4H, H^{S1}), 5.44 (d, *J* 2.4 Hz, 2H, H$^{N1, N8}$), 6.87 (m, 6H, H^{T5} and H$^{N3, N6}$), 7.07 (ddd, *J* 0.7, 1.3, 5.6 Hz, 4H, H^{T6}), 7.59 (d, *J* 9.0 Hz, 4H, H$^{N4, N5}$), 7.60 (td, *J* 1.5, 7.8 Hz, 4H, H^{T4}), 8.23 (dt, *J* 0.9, 7.8 Hz, 4H, H^{T3}), 8.51 (s, 4H, H$^{T3'}$).

MS (ES): *m/z* = 1086.9 [M-PF$_6$]$^+$, 961.3 [M-PF$_6$-PF$_5$]$^+$, 553.3 [Fe+**HO-Terpy**+**O-Terpy**]$^+$, 471.3 [M-2PF$_6$]$^{2+}$, 227.4 [Fe+**O-Terpy**+**O-Terpy**]$^{2+}$.

UV/VIS (CH$_3$CN): λ$_{max}$/ nm (ε$_{max}$, M^{-1}cm^{-3}) 232 (170 x 10^3), 269 (87.4 x 10^3), 313 (68.9 x 10^3), 554 (20.3 x 10^3).

Elemental analysis: Found: C, 51.47; H, 4.24; N, 6.47. Calc. for C$_{52}$H$_{50}$N$_6$O$_8$P$_2$F$_{12}$Fe: C, 50.66; H, 4.09; N, 6.82%.

❖ [{Fe(L^{16})}$_3$][PF$_6$]$_6$

FeCl$_2$·4H$_2$O (40 mg, 0.20 mmol) in 20 mL CH$_3$OH was added to L^{16} (0.14 g, 0.20 mmol) in 750 mL CH$_3$OH dropwise and the mixture was stirred for 4 days. After column chromatography (SiO$_2$, CH$_3$CN: saturated aqueous KNO$_3$: water 14:2:1), a purple powder of [{Fe(L^{16})}$_3$][PF$_6$]$_6$ (80.9 mg, 0.0255 mmol, 38.3%) was obtained as the major product.

Molecular formula:
$C_{132}H_{102}N_{18}O_{12}Fe_3P_6F_{36}$
Molecular weight: 3169.66
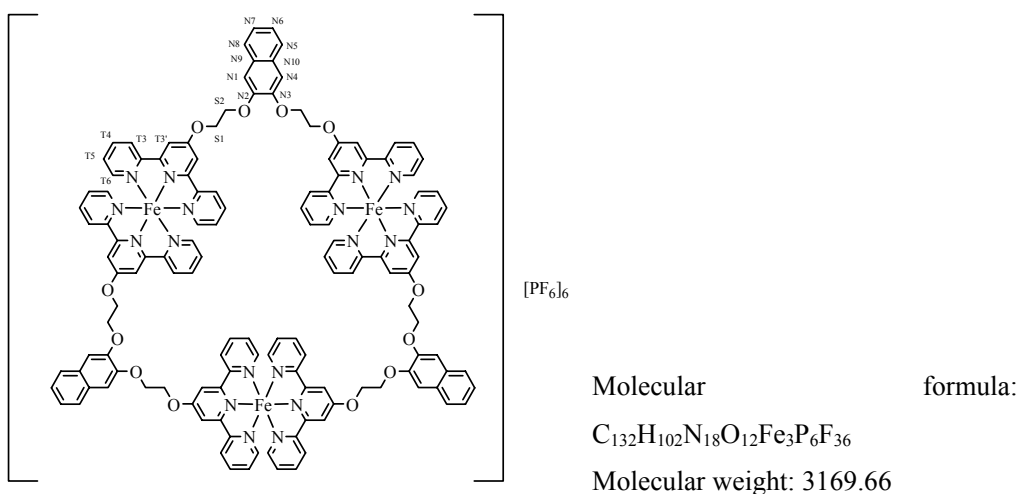
^{1}H NMR (250 MHz, CD$_3$CN): δ_H 4.84 (br, 12H, H^{S2}), 5.06 (br, 12H, H^{S1}), 6.87 (t, J 6.5 Hz, 12H, H^{T5}), 7.12 (d, J 5.8 Hz, 12H, H^{T6}), 7.46 (m, 6H, H$^{N6, N7}$), 7.59 (s, 6H, H$^{N1, N4}$), 7.60 (m, 12H, H^{T4}), 7.88 (m, 6H, H$^{N5, N8}$), 8.35 (d, J 8.0 Hz, 12H, H^{T3}), 8.54 (s, 12H, H$^{T3'}$).

MS (ES): m/z = 911.4 [M-3PF$_6$]$^{3+}$, 647.5 [M-4PF$_6$]$^{4+}$, 489.0 [M-5PF$_6$]$^{5+}$, 383.4 [M-6PF$_6$]$^{6+}$.

UV/VIS (CH$_3$CN): λ_{max}/ nm (ε_{max}, M^{-1}cm^{-3}) 230 (143 x 10^3), 270 (103 x 10^3), 315 (84.2 x 10^3), 560 (40.4 x 10^3).

Elemental analysis: Found: C, 43.79; H, 3.41; N, 6.87. Calc. for $C_{132}H_{102}N_{18}O_{12}P_6F_{36}Fe \cdot 23H_2O$: C, 44.23; H, 4.17; N, 7.04%.

❖ [{Fe($\boldsymbol{L^{17}}$)}$_2$][PF$_6$]$_4$

FeCl$_2$·4H$_2$O (40 mg, 0.20 mmol) in 20 mL CH$_3$OH was added to $\boldsymbol{L^{17}}$ (0.16 g, 0.20 mmol) in 750 mL CH$_3$OH dropwise and the mixture were stirred for 4 days. After column chromatography (SiO$_2$, CH$_3$CN: saturated aqueous KNO$_3$: water 14:2:1), a purple powder of [{Fe($\boldsymbol{L^{17}}$)}$_2$][PF$_6$]$_4$ (75 mg, 0.033 mmol, 33%) was obtained as the major product.
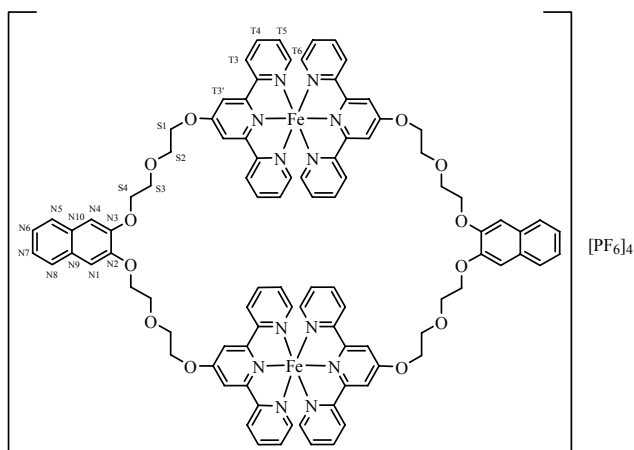
Molecular formula:

$C_{96}H_{84}N_{12}O_{12}Fe_2P_4F_{24}$

Molecular weight: 2289.31

^{1}H NMR (500 MHz, CD$_3$CN): δ_H 4.14 (m, 8H, H^{S3}), 4.21 (m, 8H, H^{S2}), 4.42 (m, 8H, H^{S4}), 4.79 (m, 8H, H^{S1}), 6.65 (m, 8H, H^{T5}), 6.98 (dd, *J* 0.6, 5.6 Hz, 8H, H^{T6}), 7.29 (m, 4H, H$^{N6, N7}$), 7.33 (m, 8H, H^{T4}), 7.35 (s, 4H, H$^{N1, N4}$), 7.67 (m, 4H, H$^{N5, N8}$), 8.19 (d, *J* 8.0 Hz, 8H, H^{T3}), 8.41 (s, 8H, H$^{T3'}$).

MS (ES): *m/z* = 617.9 [M-3PF$_6$]$^{3+}$, 427.1 [M-4PF$_6$]$^{4+}$.

UV/VIS (CH$_3$CN): λ_{max}/ nm (ε_{max}, M^{-1}cm^{-3}) 231 (111 x 10^3), 269 (57.9 x 10^3), 314 (40.7 x 10^3), 553 (12.0 x 10^3).

Elemental analysis: Found: C, 41.55; H, 3.42; N, 6.14. Calc. for C$_{96}$H$_{84}$N$_{12}$O$_{12}$P$_4$F$_{24}$Fe$_2$·2KPF$_6$·6H$_2$O: C, 41.69; H, 3.51; N, 6.08%.

7.8   References

1.   G. F. Swiegers, and T. J. Malefetse, *Chem. Rev.*, 2000, **100**, 3483.

2.   C. Kaes, A. Katz, and M. W. Hosseini, *Chem. Rev.*, 2000, **100**, 3553.

3.   V. Grosshenny, and R. Ziessel, *J. Organomet. Chem.*, 1993, **453**, C19.

4.   F. Barigelletti, L. Flamigni, V. Balzani, J.-P. Collin, J.-P. Sauvage, A. Sour, E. C. Constable, and A. M. W. Cargill Thompson, *J. Am. Chem. Soc.*, 1994, **116**, 7692.

5.   E. C. Constable, and A. M. W. Cargill Thompson, *J. Chem. Soc., Dalton Trans.*, 1995, 1615.

6.   M. Hissler, A. El-ghayoury, A. Harriman, and R. Ziessel, *Angew. Chem. Int. Ed.*, 1998, **37**, 1717.

7.   S. Encinas, L. Flamigni, F. Barigelletti, E. C. Constable, C. E. Housecroft, E. R. Schofield, E. Figgemeier, D. Fenske, M. Neuburger, J. G. Vos, and M. Zehnder, *Chem. Eur. J.*, 2002, **8**, 137.

8.   E. C. Constable, *Tetrahedron*, 1992, **48**, 10013.

9.   C. Piguet, G. Bernardinelli, and G. Hopfgarten, *Chem. Rev.*, 1997, **97**, 2005.

10.   M. Albrecht, *Chem Rev.*, 2001, **101**, 3457.

11.   E. C. Constable, M. D. Ward, and D. A. Tocher, *J. Am. Chem. Soc.,* 1990, **112**, 1256.

12.   M.-T. Youinou, R. Ziessel, and J.-M. Lehn, *Inorg. Chem.*, 1991, **30**, 2144.

13.   E. C. Constable, and J. V. Walker, *J. Chem. Soc., Chem. Commun.*, 1992, 884.

14.   G. Baum, E. C. Constable, D. Fenske, and T. Kulke, *J. Chem. Soc., Chem. Commun.*, 1997, 2043.

15.   O. Mamula, A. von Zelewsky, and G. Bernardinelli, *Angew. Chem. Int. Ed.*, 1998, **37**, 290.

16.   G. Baum, E. C. Constable, D. Fenske, C. E. Housecroft, and T. Kulke, *Chem. Eur. J.*, 1999, **5**, 1862.

17.   G. Baum, E. C. Constable, D. Fenske, C. E. Housecroft, T. Kulke, M. Neuburger, and M. Zehnder, *J. Chem. Soc., Dalton Trans.*, 2000, 945.

18.   R. L. Paul, S. M. Couchman, J. C. Jeffery, J. A. McCleverty, Z. R. Reeves, and M. D. Ward, *J. Chem. Soc., Dalton Trans.*, 2000, 845.

19.   A. Lützen, M. Hapke, J. Griep-Raming, D. Haase, and W. Saak, *Angew. Chem. Int. Ed.*, 2002, **41**, 2086.

20.   E. C. Constable, I. A. Hougen, C. E. Housecroft, M. Neuburger, S. Schaffner, and L. A. Whall, *Inorg. Chem. Commun.*, 2004, **7**, 1128.

21. J.-P. Sauvage, *Acc. Chem. Res.*, 1990, **23**, 319.

22. C. Dietrich-Buchecker, and J.-P. Sauvage, *Tetrahedron*, 1990, **46**, 503.

23. B. Mohr, M. Weck, J.-P. Sauvage, and R. H. Grubbs, *Angew. Chem. Int. Ed.*, 1997, **36**, 1308.

24. C. Dietrich-Buchecker, and J.-P. Sauvage, *Chem. Commun.*, 1999, 615.

25. F. Diederich, C. Dietrich-Buchecker, J.-F. Nierengarten, and J.-P. Sauvage, *J. Chem. Soc., Chem. Commun.*, 1995, 781.

26. P. J. Stang, *Chem. Eur. J.*, 1998, **4**, 19.

27. P. D. Beer, J. W. Wheeler, and C. P. Moore, *J. Chem. Soc., Dalton Trans.*, 1992, 2667.

28. A. Bilyk, and M. M. Harding, *J. Chem. Soc., Dalton Trans.*, 1994, 77.

29. A. Bilyk, M. M. Harding, P. Turner, and T. W. Hambley, *J. Chem. Soc., Dalton Trans.*, 1994, 2783.

30. A. Bilyk, M. M. Harding, P. Turner, and T. W. Hambley, *J. Chem. Soc., Dalton Trans.*, 1995, 2549.

31. M. A. Houghton, A. Bilyk, M. M. Harding, P. Turner, and T. W. Hambley, *J. Chem. Soc., Dalton Trans.*, 1997, 2725.

32. P. I. Anderberg, J. J. Turner, K. J. Evans, L. M. Hutchins, and M. M. Harding, *J. Chem. Soc., Dalton Trans.*, 2004, 1708.

33. E. C. Constable, and E. Schofield, *Chem. Commun.*, 1998, 403.

34. E. C. Constable, C. E. Housecroft, and C. B. Smith, *Inorg. Chem. Commun.*, 2003, **6**, 1011.

35. F. M. Romero, R. Ziessel, A. Dupont-Gervais, and A. V. Dorsselaer, *Chem. Commun.*, 1996, 551.

36. G. R. Newkome, T. J. Cho, C. N. Moorefield, R. Cush, P. S. Russo, L. A. Godínez, M. J. Saunders, and P. Mohapatra, *Chem. Eur. J.*, 2002, **8**, 2946.

37. P. N. W. Baxter, J.-M. Lehn, B. O. Kneisel, and D. Fenske, *Chem. Commun.*, 1997, 2231.

38. E. Breuning, M. Ruben, J.-M. Lehn, F. Renz, Y. Garcia, V. Ksenofontov, P. Gütlich, E. Wegelius, and K. Rissanen, *Angew. Chem. Int. Ed.*, 2000, **39**, 2504.

39. M. Ruben, E. Breuning, J.-P. Gisselbrecht, and J.-M. Lehn, *Angew. Chem. Int. Ed.*, 2000, **39**, 4139.

40. E. Breuning, U. Ziener, J.-M. Lehn, E. Wegelius, and K. Rissanen, *Eur. J. Inorg. Chem.*, 2001, 1515.

41. R. Ziessel, L. Charbonnière, M. Cesario, T. Prangé, and H. Nierengarten, *Angew. Chem. Int. Ed.*, 2002, **41**, 975.

42.　J. P. Plante, P. D. Jones, D. R. Powell, and T. E. Glass, *Chem. Commun.*, 2003, 336.

43.　P. N. W. Baxter, H. Sleiman, J.-M. Lehn, and K. Rissanen, *Angew. Chem. Int. Ed.*, 1997, **36**, 1294.

44.　P. N. W. Baxter, G. S. Hanan, and J.-M. Lehn, *Chem. Commun.*, 1996, 2019.

45.　P. N. W. Baxter, J.-M. Lehn, B. O. Kneisel, G. Baum, and D. Fenske, *Chem. Eur. J.*, 1999, **5**, 113.

46.　W.-Y. Sun, M. Yoshizawa, T. Kusukawa, and M. Fujita, *Curr. Opin. Chem. Bio.*, 2002, **6**, 757.

47.　M. Aoyagi, S. Tashiro, M. Tominaga, K. Biradha, and M. Fujita, *Chem. Commun.*, 2002, 2036.

48.　M. Yoshizawa, M. Nagao, K. Umemoto, K. Biradha, M. Fujita, S. Sakamoto, and K. Yamaguchi, *Chem. Commun.*, 2003, 1808.

49.　E. C. Constable, C. E. Housecroft, and I. Poleschak, *Inorg. Chem. Commun.*, 1999, **2**, 565.

50.　E. C. Constable, C. E. Housecroft, M. Neuburger, I. Poleschak, and M. Zehnder, *Polyhedron*, 2003, **22**, 93.

51.　E. C. Constable, *Metals and Ligands Reactivity*, VCH, Weinheim, 1995.

52.　E. C. Constable, S. M. Elder, M. J. Hannon, A. Martin, P. R. Raithby, and D. A. Tocher, *J. Chem. Soc., Dalton Trans.*, 1996, 2423.

53.　E. C. Constable, *Adv. Inorg. Chem. Radiochem.*, 1987, **30**, 69.

54.　E. C. Constable, A. M. W. Cargill Thompson, D. A. Tocher, and M. A. M. Daniels, *New J. Chem.*, 1992, **16**, 855.

55.　E. C. Constable, C. E. Housecroft, L. A. Johnston, D. Armspach, M. Neuburger, and M. Zehnder, *Polyhedron*, 2001, **20**, 483.

56.　A. T. Baker, and H. A. Goodwin, *Aust. J. Chem.*, 1985, **38**, 207.

57.　P. Lainé, A. Gourdon, and J.-P. Launay, *Inorg. Chem.*, 1995, **34**, 5156.

58.　E. C. Constable, J. E. Davies, D. Phillips, and P. R. Raithby, *Polyhedron*, 1998. **17**, 3989.

59.　E. C. Constable, C. E. Housecroft, M. Neuburger, D. Phillips, P. R. Raithby, E. Schofield, E. Sparr, D. A. Tocher, M. Zehnder, and Y. Zimmermann, *J. Chem. Soc., Dalton Trans.*, 2000, 2219.

60.　C. B. Smith, E. C. Constable, C. E. Housecroft, and B. M. Kariuki, *Chem. Commun.*, 2002, 2068.

61.　A. von Zelewsky, *Stereochemistry of Coordination Compounds*, Wiley, New York, 1996.

62.   B. R. Serr, K. A. Andersen, C. M. Elliott, and O. P. Anderson, *Inorg. Chem.*, 1988, **27**, 4499.

63.   L. J. Charbonniere, G. Bernardinelli, C. Piguet, A. M. Sargeson, and A. F. Williams, *J. Chem. Soc., Chem. Commun.*, 1994, 1419.

64.   T. Bark, A. von Zelewsky, D. Rappoport, M. Neuburger, S. Schaffner, J. Lacour, and J. Jodry, *Chem. Eur. J.*, 2004, **10**, 4839**.**

65.   B. Hasenknopf, and J.-M. Lehn, *Helv. Chim. Acta*, 1996, **79**, 1643.

66.   G. Rapenne , B. T. Patterson , J.-P. Sauvage, and F. R. Keene, *Chem. Commun.*, 1999, 1853.

67.   R. Krämer, J.-M. Lehn, A. De Cian, and J. Fischer, *Angew. Chem. Int. Ed.*, 1993, **32**, 703.

68.   C. Dietrich-Buchecker, G. Rapenne, J.-P. Sauvage, A. De Cian, and J. Fischer, *Chem. Eur. J.*, 1999, **5**, 1432.

69.   D. Parker, *Chem. Rev.*, 1991, **91**, 1441.

70.   G. Bruylants, C. Bresson, A. Boisdenghien, F. Pierard, A. K. Mesmaeker, J. Lacour and K. Bartik, *New. J. Chem.*, 2003, **27**, 748.

71.   J. Lacour, and V. Hebbe-Viton, *Chem. Soc. Rev.*, 2003, **32**, 373.

72.   J. Lacour, *Chimia*, 2003, **56**, 672.

73.   J. Lacour, C. Goujon-Ginglinger, F. Favarger, and S. Torche-Haldimann, *Chem. Commun.*, 1997, 2285.

74.   J. Lacour, S. Torche-Haldimann , J. J. Jodry, C. Goujon-Ginglinger, and F. Favarger, *Chem. Commun.*, 1998, 1733.

75.   D. Monchaud, J. J. Jodry, D. Pomeranc, V. Heitz, J-C. Chambron, J-P. Sauvage, and J. Lacour, *Angew. Chem. Int. Ed.*, 2002, **41**, 2317.

76.   J. Lacour, C. Goujon-Ginglinger, S. Torche-Haldimann, and J. J. Jodry, *Angew. Chem. Int. Ed.*, 2000, **39**, 3695.

77.   J, J, Jodry, and J. Lacour, *Chem. Eur. J.*, 2000, **6**, 4297.

78.   R. M. Yeh, M. Ziegler, D. W. Johnson, A. J. Terpin, and K. N. Raymond, *Inorg. Chem.*, 2001, **40**, 2216.

79.   J. Lacour, J. J. Jodry, C. Goujon-Ginglinger, and S. Torche-Haldimann, *Angew. Chem. Int. Ed.*, 1998, **37**, 2379.

80.   J. J. Jodry, R. Frantz, and J. Lacour, *Inorg. Chem.*, 2004, **43**, 3329.

81.   E. C. Constable, R. Frantz, C. E. Housecroft, J. Lacour, and A. Mahmood, *Inorg. Chem.*, 2004, **43**, 4817.

82.   J. Lacour, J. J. Jodry, and D. Monchaud, *Chem. Commun.*, 2001, 2302.

Appendices

Appendix I

(a) Single X-ray crystallographic data of L^2

Crystal data	
Formula	$C_{19}H_{19}N_3O_3$
Formula weight	337.38
Crystal system	Monoclinic
Space group	Cc (No. 9)
a, b, c [Å]	10.5509(3), 22.5202(7), 7.2890(2)
α, β, γ [°]	90, 109.0636(16), 90
V [Å^3]	1636.94(8)
Z	4
D(calc) [gcm^{-3}]	1.369
μ (MoK$_\alpha$) [mm^{-1}]	0.094
F(000)	712
Crystal size [mm]	0.04 x 0.21 x 0.32
Data Collection	
Temperature (K)	173
Radiation [Å]	MoK$_\alpha$, 0.71073
θ Min (Max) [°]	4.9 (31.9)
Total number of reflections	5652
Number of unique reflections	2835
R(int)	0.020
Observed data [I > 2.0 σ(I)]	1970
Refinement	
Number of reflections	1970
Number of parameters	227
R	0.0502
wR$_2$	0.0580
Goodness of fit (GOF)	1.06
Max. and av. Shift/Error	0.00, 0.00
Min. and max. residual electron Density [eÅ^{-3}]	-0.32, 0.67

The cif file is provided in the attached CD.

(b) Single X-ray crystallographic data of [HL^9]$^+$Cl$^-$·H$_2$O

Crystal data	
Formula	(C$_{25}$H$_{18}$N$_3$S$_1$)$^+$Cl$^-$·H$_2$O
Formula weight	445.97
Crystal system	Orthorhombic
Space group	Pca21 (No. 29)
a, b, c [Å]	41.930(7), 5.1238(11), 9.745(4)
α, β, γ [°]	90, 90, 90
V [Å^3]	2093.6(10)
Z	4
D(calc) [gcm^{-3}]	1.415
μ (MoK$_\alpha$) [mm^{-1}]	0.306
F(000)	928
Crystal size [mm]	0.10 x 0.10 x 0.40
Data Collection	
Temperature (K)	173
Radiation [Å]	MoK$_\alpha$, 0.71073
θ Min (Max) [°]	4.5 (32.0)
Total number of reflections	42258
Number of unique reflections	7178
R(int)	0.110
Observed data [I > 2.0 σ(I)]	3301
Refinement	
Number of reflections	3301
Number of parameters	352
R	0.0405
wR$_2$	0.0394
Goodness of fit (GOF)	1.03
Max. and av. Shift/Error	0.01, 0.00
Min. and max. residual electron Density [eÅ^{-3}]	-0.56, 0.58

The cif file is provided in the attached CD.

Appendix II

(a) Crystal structure of [Fe($\mathbf{L^4}$)$_2$][PF$_6$]$_2$·CH$_3$CN

Crystal data	
Formula	$C_{54}H_{41}F_{12}Fe_1N_7O_2P_2$
Formula weight	1165.74
Crystal system	Triclinic
Space group	P-1 (No. 2)
a, b, c [Å]	12.640(2), 13.617(3), 14.744(2)
α, β, γ [°]	85.194(13), 85.942(11), 76.607(13)
V [Å^3]	2456.6(8)
Z	2
D(calc) [gcm^{-3}]	1.576
μ (MoK$_\alpha$) [mm^{-1}]	0.470
F(000)	1188
Crystal size [mm]	0.20 x 0.21 x 0.41
Data Collection	
Temperature (K)	173
Radiation [Å]	MoK$_\alpha$, 0.71073
θ Min (Max) [°]	4.1 (32.5)
Total number of reflections	126877
Number of unique reflections	17732
R(int)	0.080
Observed data [I > 2.0 σ(I)]	11423
Refinement	
Number of reflections	11423
Number of parameters	703
R	0.0347
wR$_2$	0.0362
Goodness of fit (GOF)	1.08
Max. and av. Shift/Error	0.00, 0.00
Min. and max. residual electron Density [eÅ^{-3}]	-0.46, 0.51

The cif file is provided in the attached CD.

(b) Crystal structure of [Ru($\textbf{\textit{L}}^4$)$_2$][PF$_6$]$_2$·CH$_3$CN

Crystal data	
Formula	$C_{54}H_{41}F_{12}N_7O_2P_2Ru_1$
Formula weight	1210.96
Crystal system	Triclinic
Space group	P-1 (No. 2)
a, b, c [Å]	12.5716(7), 13.6977(16), 14.845(2)
α, β, γ [°]	85.459(11), 86.045(7), 76.722(7)
V [Å^3]	2476.8(5)
Z	2
D(calc) [gcm^{-3}]	1.624
μ (MoK$_\alpha$) [mm^{-1}]	0.479
F(000)	1224
Crystal size [mm]	0.20 x 0.27 x 0.35
Data Collection	
Temperature (K)	193
Radiation [Å]	MoK$_\alpha$, 0.71073
θ Min (Max) [°]	5.0 (30.0)
Total number of reflections	62842
Number of unique reflections	14311
R(int)	0.070
Observed data [I > 2.0 σ(I)]	9830
Refinement	
Number of reflections	9830
Number of parameters	703
R	0.0335
wR$_2$	0.0301
Goodness of fit (GOF)	1.10
Max. and av. Shift/Error	0.00, 0.00
Min. and max. residual electron Density [eÅ^{-3}]	-0.47, 0.48

The cif file is provided in the attached CD.

(c) Crystal structure of [Fe($\textbf{L}^5$)$_2$][PF$_6$]$_2$

Crystal data	
Formula	Fe$_1$C$_{56}$H$_{46}$N$_6$O$_4$P$_2$F$_{12}$
Formula weight	1212.79
Crystal system	Monoclinic
Space group	P21/n (No. 14)
a, b, c [Å]	16.897(3), 32.914(11), 18.693(11)
α, β, γ [°]	90, 85.16(2), 90
V [Å^3]	10359(7)
Z	8
D(calc) [gcm^{-3}]	1.555
μ (MoK$_\alpha$) [mm^{-1}]	0.452
F(000)	4960
Crystal size [mm]	0.10 x 0.22 x 0.27
Data Collection	
Temperature (K)	173
Radiation [Å]	MoK$_\alpha$, 0.71073
θ Min (Max) [°]	1.2 (24.0)
Total number of reflections	64205
Number of unique reflections	16197
R(int)	0.110
Observed data [I > 2.0 σ(I)]	8382
Refinement	
Number of reflections	8382
Number of parameters	1459
R	0.0800
wR$_2$	0.1149
Goodness of fit (GOF)	1.06
Max. and av. Shift/Error	0.00, 0.00
Min. and max. residual electron Density [eÅ^{-3}]	-0.73, 1.04

The cif file is provided in the attached CD.

(d) Crystal structure of [Ru(L^5)$_2$][PF$_6$]$_2$

Crystal data	
Formula	C$_{56}$H$_{46}$F$_{12}$N$_6$O$_4$P$_2$Ru$_1$
Formula weight	1258.01
Crystal system	Monoclinic
Space group	P21/n (No. 14)
a, b, c [Å]	16.8109(3), 33.2255(11), 18.7663(5)
α, β, γ [°]	90, 93.5640(15), 90
V [Å^3]	10461.7(5)
Z	8
D(calc) [gcm^{-3}]	1.597
μ (MoK$_\alpha$) [mm^{-1}]	0.459
F(000)	5104
Crystal size [mm]	0.17 x 0.30 x 0.33
Data Collection	
Temperature (K)	173
Radiation [Å]	MoK$_\alpha$, 0.71073
θ Min (Max) [°]	1.2 (27.5)
Total number of reflections	187884
Number of unique reflections	24040
R(int)	0.080
Observed data [I > 2.0 σ(I)]	14204
Refinement	
Number of reflections	14204
Number of parameters	1495
R	0.0657
wR$_2$	0.0272
Goodness of fit (GOF)	1.14
Max. and av. Shift/Error	0.00, 0.00
Min. and max. residual electron Density [eÅ^{-3}]	-0.89, 1.31

The cif file is provided in the attached CD.

Appendix III

(a) Crystal structure of [Co(L^4)$_2$][PF$_6$]$_2$

Crystal data	
Formula	$C_{52}H_{38}Co_1F_{12}N_6O_2P_2$
Formula weight	1127.77
Crystal system	Triclinic
Space group	P-1 (No. 2)
a, b, c [Å]	8.6442(11), 14.5481(11), 19.3199(11)
α, β, γ [°]	94.776(6), 100.481(7), 92.586(9)
V [Å^3]	2376.3(4)
Z	2
D(calc) [gcm^{-3}]	1.576
μ (MoK$_\alpha$) [mm^{-1}]	0.526
F(000)	1146
Crystal size [mm]	0.07 x 0.11 x 0.53
Data Collection	
Temperature (K)	193
Radiation [Å]	MoK$_\alpha$, 0.71073
θ Min (Max) [°]	3.0 (28.5)
Total number of reflections	90328
Number of unique reflections	12042
R(int)	0.070
Observed data [I > 2.0 σ(I)]	6690
Refinement	
Number of reflections	6690
Number of parameters	679
R	0.0540
wR$_2$	0.0673
Goodness of fit (GOF)	1.10
Max. and av. Shift/Error	0.00, 0.00
Min. and max. residual electron Density [eÅ^{-3}]	-0.64, 0.94

The cif file is provided in the attached CD.

(b) Crystal structure of [Co($\boldsymbol{L^8}$)$_2$][PF$_6$]$_2$·1¾CH$_3$CN

Crystal data	
Formula	C$_{63.50}$H$_{47.25}$Co$_1$F$_{12}$N$_{7.75}$O$_2$P$_2$
Formula weight	1299.73
Crystal system	Monoclinic
Space group	P21/c (No. 14)
a, b, c [Å]	14.3860(16), 16.9112(16), 23.923(2)
α, β, γ [°]	90, 91.326(8), 90
V [Å^3]	5819.5(10)
Z	4
D(calc) [gcm^{-3}]	1.484
μ (MoK$_\alpha$) [mm^{-1}]	0.442
F(000)	2654
Crystal size [mm]	0.08 x 0.10 x 0.27
Data Collection	
Temperature (K)	193
Radiation [Å]	MoK$_\alpha$, 0.71073
θ Min (Max) [°]	3.1 (27.5)
Total number of reflections	56031
Number of unique reflections	13258
R(int)	0.080
Observed data [I > 2.0 σ(I)]	7122
Refinement	
Number of reflections	7122
Number of parameters	803
R	0.0822
wR$_2$	0.0888
Goodness of fit (GOF)	1.02
Max. and av. Shift/Error	0.05, 0.00
Min. and max. residual electron Density [eÅ^{-3}]	-0.63, 0.67

The cif file is provided in the attached CD.

Appendix IV

(a) Crystal structure of L^{14}

Crystal data	
Formula	$C_{48}H_{42}N_6O_6$
Formula weight	798.90
Crystal system	Monoclinic
Space group	P21/c (No. 14)
a, b, c [Å]	24.985(3), 10.5259(6), 15.4926(19)
α, β, γ [°]	90, 104.514(9), 90
V [Å^3]	3944.4(7)
Z	4
D(calc) [gcm^{-3}]	1.345
μ (MoK$_\alpha$) [mm^{-1}]	0.090
F(000)	1680
Crystal size [mm]	0.08 x 0.10 x 0.24
Data Collection	
Temperature (K)	173
Radiation [Å]	MoK$_\alpha$, 0.71073
θ Min (Max) [°]	5.0 (26.2)
Total number of reflections	60269
Number of unique reflections	7914
R(int)	0.070
Observed data [I > 2.0 σ(I)]	4337
Refinement	
Number of reflections	4337
Number of parameters	541
R	0.0931
wR$_2$	0.0891
Goodness of fit (GOF)	0.85
Max. and av. Shift/Error	0.00, 0.00
Min. and max. residual electron Density [eÅ^{-3}]	-0.45, 0.49

The cif file is provided in the attached CD.

(b) Crystal structure of 2,7-di(2-hydroxyethoxy)naphthalene

Crystal data	
Formula	$C_{14}H_{16}O_4$
Formula weight	248.28
Crystal system	Monoclinic
Space group	C2/c (No. 15)
a, b, c [Å]	23.639(2), 11.4451(9), 9.1870(5)
α, β, γ [°]	90, 105.391(6), 90
V [Å^3]	2396.4(3)
Z	8
D(calc) [gcm^{-3}]	1.376
μ (MoK$_\alpha$) [mm^{-1}]	0.100
F(000)	1056
Crystal size [mm]	0.20 x 0.30 x 0.32
Data Collection	
Temperature (K)	173
Radiation [Å]	MoK$_\alpha$, 0.71073
θ Min (Max) [°]	4.2 (35.0)
Total number of reflections	86650
Number of unique reflections	5278
R(int)	0.090
Observed data [I > 2.0 σ(I)]	2690
Refinement	
Number of reflections	2690
Number of parameters	168
R	0.0415
wR$_2$	0.0451
Goodness of fit (GOF)	1.02
Max. and av. Shift/Error	0.01, 0.00
Min. and max. residual electron Density [eÅ^{-3}]	-0.37, 0.44

The cif file is provided in the attached CD.

Appendix V

(a) Crystal structure of [{Ru(L^{11})}$_2$][PF$_6$]$_4$·$^4/_5$(C$_2$H$_5$)$_2$O·2CH$_3$CN

Crystal data	
Formula	$C_{51.60}H_{48}F_{12}N_8O_{4.40}P_2Ru_1$
Formula weight	1241.59
Crystal system	Monoclinic
Space group	P21/c (No. 14)
a, b, c [Å]	14.9497(5), 11.6405(5), 30.8449(9)
α, β, γ [°]	90, 101.256(2), 90
V [Å^3]	5264.4(3)
Z	4
D(calc) [gcm^{-3}]	1.566
μ (MoK$_\alpha$) [mm^{-1}]	0.456
F(000)	2523
Crystal size [mm]	0.16 x 0.17 x 0.20
Data Collection	
Temperature (K)	123
Radiation [Å]	MoK$_\alpha$, 0.71073
θ Min (Max) [°]	3.2 (27.5)
Total number of reflections	65618
Number of unique reflections	12056
R(int)	0.120
Observed data [I > 2.0 σ(I)]	7487
Refinement	
Number of reflections	7487
Number of parameters	739
R	0.0784
wR$_2$	0.0823
Goodness of fit (GOF)	0.90
Max. and av. Shift/Error	0.03, 0.00
Min. and max. residual electron Density [eÅ^{-3}]	-0.73, 1.20

The cif file is provided in the attached CD.

*(b) Crystal structure of [{Fe(**L**^{14})}][PF$_6$]$_2$·(C$_2$H$_5$)$_2$O·½CH$_3$CN*

Crystal data	
Formula	[FeC$_{48}$H$_{42}$N$_6$O$_6$]·2PF$_6$·0.5(C$_4$H$_{10}$O)·CH$_3$CN
Formula weight	1222.78
Crystal system	Triclinic
Space group	P-1, (No. 2)
a, b, c [Å]	11.4241(11), 13.635(2), 18.271(2)
α, β, γ [°]	75.402(9), 87.442(9), 78.327(11)
V [Å^3]	2697.1(6)
Z	2
D(calc) [gcm^{-3}]	1.506
μ (MoK$_\alpha$) [mm^{-1}]	0.438
F(000)	1254
Crystal size [mm]	0.02 x 0.15 x 0.31
Data Collection	
Temperature (K)	173
Radiation [Å]	MoK$_\alpha$, 0.71073
θ Min (Max) [°]	4.1 (27.5)
Total number of reflections	67536
Number of unique reflections	12329
R(int)	0.120
Observed data [I > 2.0 σ(I)]	7800
Refinement	
Number of reflections	7800
Number of parameters	820
R	0.0610
wR$_2$	0.0665
Goodness of fit (GOF)	1.11
Max. and av. Shift/Error	0.01, 0.00
Min. and max. residual electron Density [eÅ^{-3}]	-0.81, 0.72

The cif file is provided in the attached CD.

(c) Crystal structure of [{Fe($\boldsymbol{L^{15}}$)}][PF$_6$]$_2$·CH$_3$CN

Crystal data	
Formula	[C$_{52}$H$_{50}$FeN$_6$O$_8$]·2PF$_6$·C$_2$H$_3$N
Formula weight	1273.83
Crystal system	Monoclinic
Space group	P2$_1$/c (No. 14)
a, b, c [Å]	18.2659(1), 14.8059(1), 20.5792(2)
α, β, γ [°]	90, 92.9257(5), 90
V [Å^3]	5558.25(7)
Z	4
D(calc) [gcm^{-3}]	1.522
μ (MoK$_\alpha$) [mm^{-1}]	0.430
F(000)	2616
Crystal size [mm]	0.12 x 0.27 x 0.30
Data Collection	
Temperature (K)	173
Radiation [Å]	MoK$_\alpha$, 0.71073
θ Min (Max) [°]	1.7 (28.7)
Total number of reflections	54042
Number of unique reflections	14324
R(int)	0.048
Observed data [I > 2.0 σ(I)]	8366
Refinement	
Number of reflections	8366
Number of parameters	811
R	0.0425
wR$_2$	0.0660
Goodness of fit (GOF)	1.12
Max. and av. Shift/Error	0.03, 0.00
Min. and max. residual electron Density [eÅ^{-3}]	-0.46, 0.59

The cif file is provided in the attached CD.

Appendix VI

(a)   Table of the ^{1}H NMR spectroscopic data for the terpyridine, ethyleneoxy spacer and the naphthyl signals of the metallomacrocyclic complexes $[\{Ru(\boldsymbol{L})\}_n][PF_6]_{2n}$ ($\boldsymbol{L} = \boldsymbol{L^{11}}$, $\boldsymbol{L^{13}}$-$\boldsymbol{L^{14}}$, $\boldsymbol{L^{14}}$-$\boldsymbol{L^{17}}$, n = 1, 2 or 3).

(b)   Table of the ^{1}H NMR spectroscopic data for the terpyridine signals of the metallomacrocyclic complexes $[\{Fe(\boldsymbol{L})\}_n][PF_6]_{2n}$ ($\boldsymbol{L} = \boldsymbol{L^{11}}$-$\boldsymbol{L^{17}}$, n = 1, 2 or 3).

(c)   Table of the ^{1}H NMR spectroscopic data for the ethyleneoxy spacer and the naphthyl signals of the metallomacrocyclic complexes $[\{Fe(\boldsymbol{L})\}_n][PF_6]_{2n}$ ($\boldsymbol{L} = \boldsymbol{L^{11}}$-$\boldsymbol{L^{17}}$, n = 1, 2 or 3).

(d)   The ES-MS spectra of the metallomacrocyclic complexes $[\{Ru(\boldsymbol{L})\}_n][PF_6]_{2n}$ ($\boldsymbol{L} = \boldsymbol{L^{11}}$, $\boldsymbol{L^{13}}$-$\boldsymbol{L^{14}}$, $\boldsymbol{L^{14}}$-$\boldsymbol{L^{17}}$, n = 1, 2 or 3) and $[\{Fe(\boldsymbol{L})\}_n][PF_6]_{2n}$ ($\boldsymbol{L} = \boldsymbol{L^{11}}$-$\boldsymbol{L^{17}}$, n = 1, 2 or 3).

	Proton resonance (δ)											
	H^T5	H^T6	H^T4	H^T3′	H^T3	H^S1	H^S2	H^S3	H^S4	H^N3, N7	H^N4, N8	H^N1, N5
[{Ru(L^{11})}$_2$][PF$_6$]$_4$ (400)	6.97 (m)	7.23 (d) J 5.6 Hz	7.74 (m)	8.32 (s)	8.33 (m)	4.72 (m)	4.00 (m)	4.75 (s)		7.33 (dd) J 1.0, 8.6 Hz	7.51 (d) J 8.1 Hz	7.74 (m)
										H^N1, N8	H^N3, N6	H^N4, N5
[{Ru(L^{13})}$_2$][PF$_6$]$_4$ (400)	7.12 (m)	7.44 (d) J 5.2 Hz	7.70 (td) J 1.2, 7.8 Hz	8.06 (s)	8.19 (d) J 8.0 Hz	4.77 (m)	4.13 (m)			6.68 (d) J 2.0 Hz	7.12 (m)	7.88(d) J 9.2 Hz
[{Ru(L^{13})}$_3$][PF$_6$]$_6$ (400)	7.12 (m)	7.36 (d) J 5.6 Hz	7.81 (m)	8.32 (s)	8.39 (d) J 8.0 Hz	4.94 (m)	4.65 (m)			7.30 (d) J 2.4 Hz	7.12 (m)	7.81 (m)
[{Ru(L^{14})}$_2$][PF$_6$]$_4$ (500)	7.00 (ddd) J 1.3, 5.7, 7.5 Hz	7.29 (ddd) J 0.7, 1.5, 5.6 Hz	7.69 (td) J 1.5, 7.9 Hz	8.28 (s)	8.27 (m)	4.72 (m)	4.12 (m)	3.98 (m)	4.06 (m)	6.69 (d) J 2.4 Hz	6.85 (dd) J 2.5, 8.9 Hz	7.39 (d) J 9.0 Hz
										H^N7, N6	H^N1, N4	H^N8, N5
[{Ru(L^{16})}$_2$][PF$_6$]$_4$ (500)	6.77 (m)	7.19 (dd) J 0.7, 5.6 Hz	7.26 (m)	8.36 (s)	8.26 (d) J 7.9 Hz	5.02 (t) J 5.1 Hz	4.79 (t) J 5.0 Hz			7.46 (m)	7.57 (s)	7.87 (m)
[{Ru(L^{17})}$_2$][PF$_6$]$_4$ (500)	6.73 (ddd) J 1.3, 5.6, 7.5 Hz	7.22 (ddd) J 0.6, 1.4, 5.6 Hz	7.42 (td) J 1.4, 7.8 Hz	8.28 (s)	8.26 (d) J 7.8 Hz	4.71 (t) J 4.5 Hz	4.16 (m)	4.11 (m)	4.39 (m)	7.29 (m)	7.34 (s)	7.67 (m)
J	J_{34} 7.9 Hz; J_{45} 7.7 Hz; J_{46} 1.4 Hz; J_{53} 1.3 Hz; J_{56} 5.6 Hz; J_{63} 0.7 Hz											

Table (a). The ^{1}H NMR spectroscopic data for the terpyridine, ethyleneoxy spacer and the naphthyl signals of the metallomacrocyclic complexes [{Ru(L)}$_n$][PF$_6$]$_{2n}$ ($L = L^{11}$, L^{13}-L^{14}, L^{14}-L^{17}, n = 1, 2 or 3).

	Proton resonance (δ)				
	H^{T5}	H^{T6}	H^{T4}	H^{T3}	$H^{T3'}$
$[\{Fe(\boldsymbol{L^{11}})\}_2][PF_6]_4$ (500)	6.87 (ddd) J 1.3, 5.7, 7.4 Hz	6.99 (ddd) J 0.7, 1.4, 5.6 Hz	7.71 (m)	8.29 (dt) J 0.9, 8.0 Hz	8.47 (s)
$[\{Fe(\boldsymbol{L^{12}})\}_n][PF_6]_{2n}$ (A) (500)	7.14 (ddd) J 1.0, 5.1, 7.6 Hz	7.49 (ddd) J 0.9, 1.6, 5.1 Hz	7.93 (ddd) J 1.7, 7.6, 8.0 Hz	8.37 (dt) J 1.0, 8.1 Hz	8.33 (s)
$[\{Fe(\boldsymbol{L^{12}})\}_n][PF_6]_{2n}$ (B) (500)	6.81 (ddd) J 1.3, 5.7, 7.5 Hz	6.90 (ddd) J 0.7, 1.4, 5.6 Hz	7.63 (ddd) J 1.5, 7.6 8.0 Hz	8.25 (ddd) J 0.8, 1.3, 8.0 Hz	8.62 (s)
$[\{Fe(\boldsymbol{L^{13}})\}_2][PF_6]_4$ (400)					
$[\{Fe(\boldsymbol{L^{13}})\}_3][PF_6]_6$ (400)	7.02 (m)	7.13 (d) J 4.8 Hz	7.80 (m)	8.36 (d) J 8.4 Hz	8.47 (s)
$[\{Fe(\boldsymbol{L^{14}})\}][PF_6]_2$ (500)	6.52 (ddd) J 1.3, 5.7, 7.5 Hz and 7.02 (ddd) J 1.3, 5.6, 7.5 Hz	6.65 (ddd) J 0.7, 1.4, 5.6 Hz and 7.35 (ddd) J 0.7, 1.4, 5.6 Hz	7.31 (td) J 1.5, 7.8 Hz and 7.84 (td) J 1.5, 7.8 Hz	8.18 (d) J 7.8 Hz and 8.37 (dt) J 1.0, 8.0 Hz	8.41 (d) J 2.2 Hz and 8.82 J 2.2 Hz (d)
$[\{Fe(\boldsymbol{L^{15}})\}][PF_6]_2$ (500)	6.87 (m)	7.07 (ddd) J 0.7, 1.3, 5.6 Hz	7.60 (td) J 1.5, 7.8 Hz	8.23 (dt) J 0.9, 7.8 Hz	8.51 (s)
$[\{Fe(\boldsymbol{L^{16}})\}_2][PF_6]_4$ (250)	6.87 (t) J 6.5 Hz	7.12 (d) J 5.8 Hz	7.60 (m)	8.35 (d) J 8.0 Hz	8.54 (s)
$[\{Fe(\boldsymbol{L^{17}})\}_2][PF_6]_4$ (500)	6.65 (m)	6.98 (dd) J 0.6, 5.6 Hz	7.33 (m)	8.19 (d) J 8.0 Hz	8.41 (s)
J	J_{34} 7.9 Hz; J_{45} 7.7 Hz; J_{46} 1.4 Hz; J_{53} 1.3 Hz; J_{56} 5.6 Hz; J_{63} 0.7 Hz				

Table (b). The ^{1}H NMR spectroscopic data for the terpyridine signals of the metallomacrocyclic complexes $[\{Fe(\boldsymbol{L})\}_n][PF_6]_{2n}$ ($\boldsymbol{L} = \boldsymbol{L^{11}}$-$\boldsymbol{L^{17}}$, n = 1, 2 or 3).

|	Proton resonance (δ)								
	H^{S1}	H^{S2}	H^{S3}	H^{S4}	H^{S5}	H^{S6}	$H^{N3, N7}$	$H^{N4, N8}$	$H^{N1, N5}$
$[\{Fe(\boldsymbol{L^{11}})\}_2][PF_6]_4$ [(500)]	4.81 (m)	4.05 (m)	4.78 (s)				7.34 (dd) J 1.3, 8.4 Hz	7.47 (d) J 8.3 Hz	7.72 (s)
$[\{Fe(\boldsymbol{L^{12}})\}_n][PF_6]_{2n}$ (A) [(500)]	4.86 (m)	4.05 (m)	3.80 (m)	3.70 (m)	4.47 (s)		6.96 (dd) J 1.5, 8.4 Hz	6.76 (d) J 8.2 Hz	6.83 (s)
$[\{Fe(\boldsymbol{L^{12}})\}_n][PF_6]_{2n}$ (B) [(500)]	4.91 (m)	4.11 (m)	3.84 (m)	3.73 (m)	4.51 (s)		7.04 (dd) J 1.3, 8.4 Hz	6.67 (d) J 8.3 Hz	6.83 (s)
	H^{S1}	H^{S2}	H^{S3}	H^{S4}	H^{S5}	H^{S6}	$H^{N1, N8}$	$H^{N3, N6}$	$H^{N4, N5}$
$[\{Fe(\boldsymbol{L^{13}})\}_2][PF_6]_4$ [(400)]									
$[\{Fe(\boldsymbol{L^{13}})\}_3][PF_6]_6$ [(400)]	5.03 (m)	4.71 (m)					7.34 (d) J 2.0 Hz	7.16 (m)	7.80 (m)
$[\{Fe(\boldsymbol{L^{14}})\}][PF_6]_2$ [(500)]	4.66 (dt) J 2.0, 13.9 Hz and 5.38 (m)	4.13 (m)	3.79 and 4.07 (m)	3.79 (m)			4.86 (d) J 2.4 Hz	6.85 (dd) J 2.5, 8.9 Hz	7.53 (d) J 9.0 Hz
$[\{Fe(\boldsymbol{L^{15}})\}][PF_6]_2$ [(500)]	4.84 (m)	4.12 (m)	3.86 (m)	3.76 (m)	3.82 (m)	3.56 (t) J 4.7 Hz	5.44 (d) J 2.4 Hz	6.87 (m)	7.59 (d) J 9.0 Hz
	H^{S1}	H^{S2}	H^{S3}	H^{S4}			$H^{N7, N6}$	$H^{N1, N4}$	$H^{N8, N5}$
$[\{Fe(\boldsymbol{L^{16}})\}_2][PF_6]_4$ [(250)]	5.06 (br)	4.84 (br)					7.46 (m)	7.59 (s)	7.88 (m)
$[\{Fe(\boldsymbol{L^{17}})\}_2][PF_6]_4$ [(500)]	4.79 (m)	4.21 (m)	4.14 (m)	4.42 (m)			7.29 (m)	7.35 (s)	7.67 (m)

Table (c). The ^{1}H NMR spectroscopic data for the ethyleneoxy spacer and the naphthyl signals of the metallomacrocyclic complexes $[\{Fe(\boldsymbol{L})\}_n][PF_6]_{2n}$ ($\boldsymbol{L} = \boldsymbol{L^{11}}$-$\boldsymbol{L^{17}}$, n = 1, 2 or 3).

(d) The ES-MS spectra of the metallomacrocyclic complexes [{Ru(***L***)}$_n$][PF$_6$]$_{2n}$ (***L*** =
L^{11}, ***L***^{13}-***L***^{14}, ***L***^{14}-***L***^{17}, n = 1, 2 or 3) and [{Fe(***L***)}$_n$][PF$_6$]$_{2n}$ (***L*** = ***L***^{11}-***L***^{17}, n = 1, 2 or
3).

❖   The ES-MS spectrum of [{Ru(***L***^{11})}$_2$][PF$_6$]$_4$
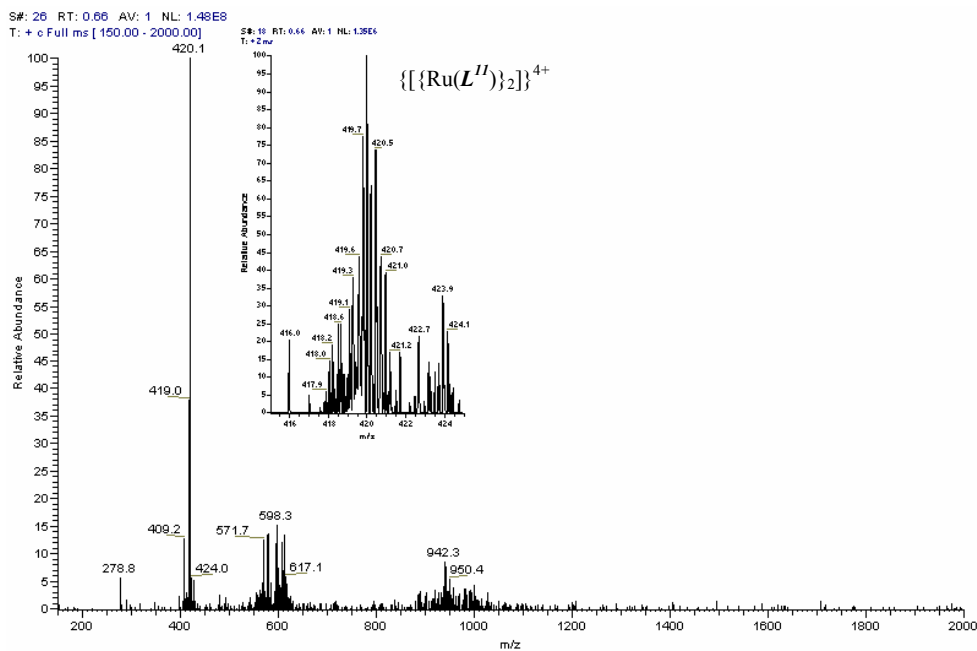
❖   The ES-MS spectrum of [{Ru(***L***^{13})}$_2$][PF$_6$]$_4$

315
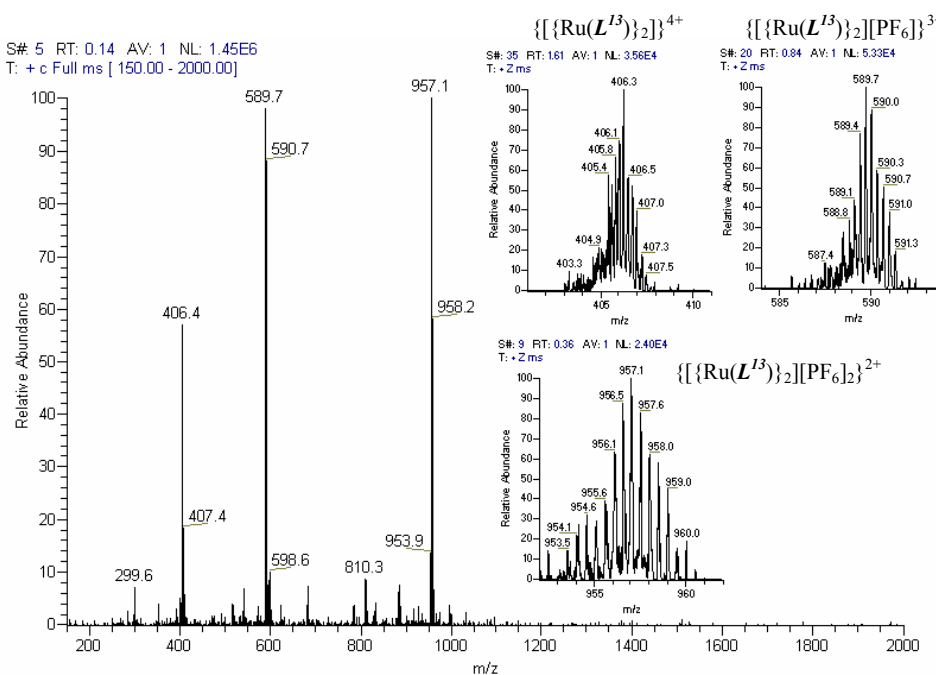
❖ The ES-MS spectrum of $[\{Ru(\boldsymbol{L^{13}})\}_3][PF_6]_6$
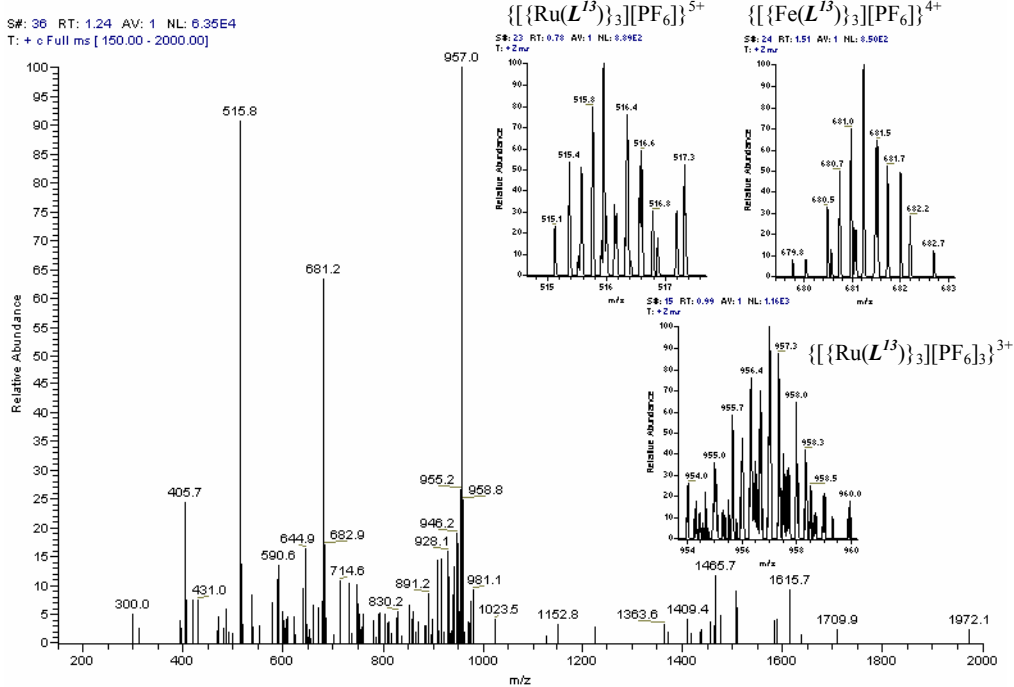
❖ The ES-MS spectrum of $[\{Ru(\boldsymbol{L^{14}})\}_2][PF_6]_4$
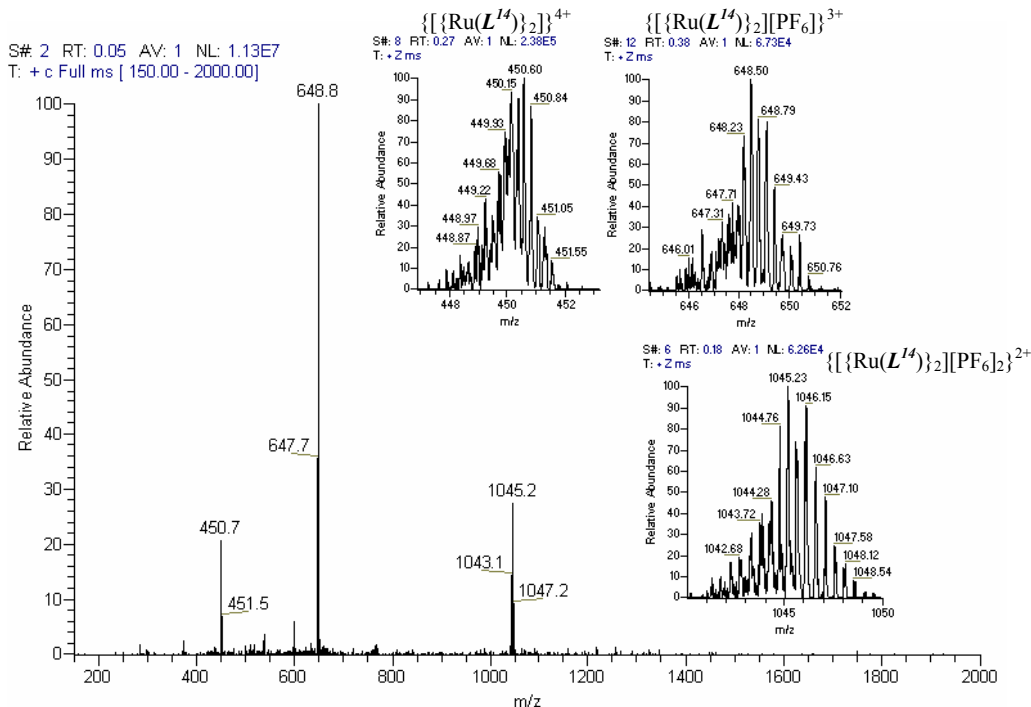
❖   The ES-MS spectrum of $[\{Ru(\boldsymbol{L^{16}})\}_2][PF_6]_4$

$\{[\{Ru(\boldsymbol{L^{16}})\}_2]\}^{4+}$ $\{[\{Ru(\boldsymbol{L^{16}})\}_2][PF_6]\}^{3+}$ $\{[\{Ru(\boldsymbol{L^{16}})\}_2][PF_6]_2\}^{2+}$
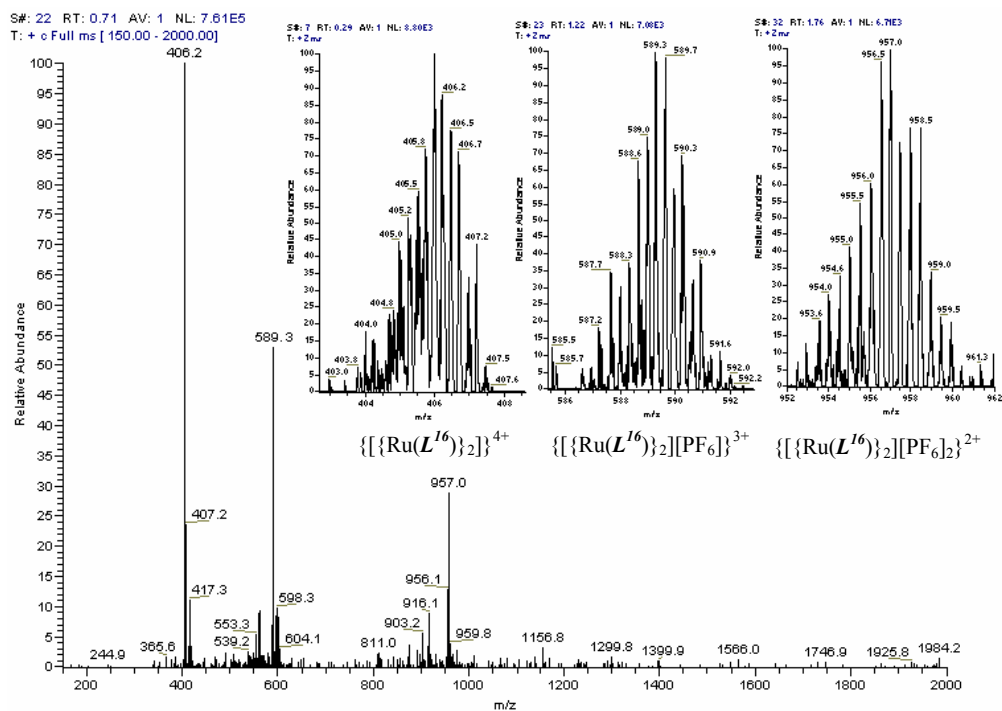
❖   The ES-MS spectrum of $[\{Ru(\boldsymbol{L^{17}})\}_2][PF_6]_4$
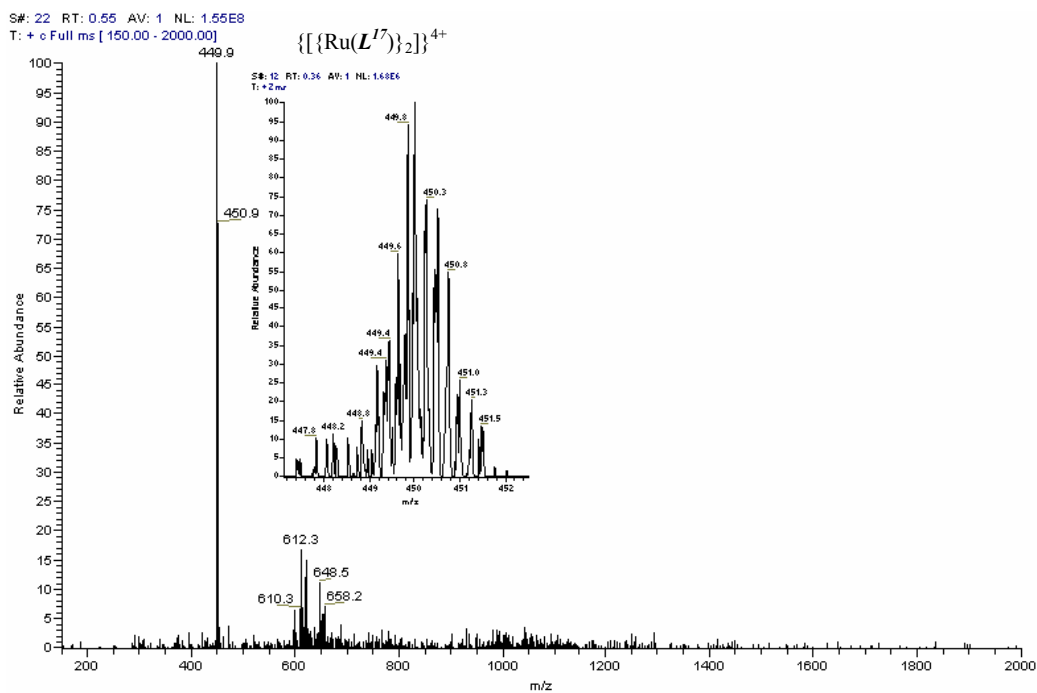
$\{[\{Ru(\boldsymbol{L^{17}})\}_2]\}^{4+}$

❖ The ES-MS spectrum of $[\{Fe(\boldsymbol{L^{11}})\}_2][PF_6]_4$

$\{[\{Fe(\boldsymbol{L^{11}})\}_2][PF_6]\}^{3+}$ $\{[\{Fe(\boldsymbol{L^{11}})\}_2]\}^{4+}$

❖ The ES-MS spectrum of $[\{Fe(\boldsymbol{L^{12}})\}_n][PF_6]_{2n}$

$\{[\{Fe(\boldsymbol{L^{12}})\}]\}^{2+}$ $\{[\{Fe(\boldsymbol{L^{12}})\}]F\}^+$

$\{[\{Fe(\boldsymbol{L^{12}})\}][PF_6]\}^+$
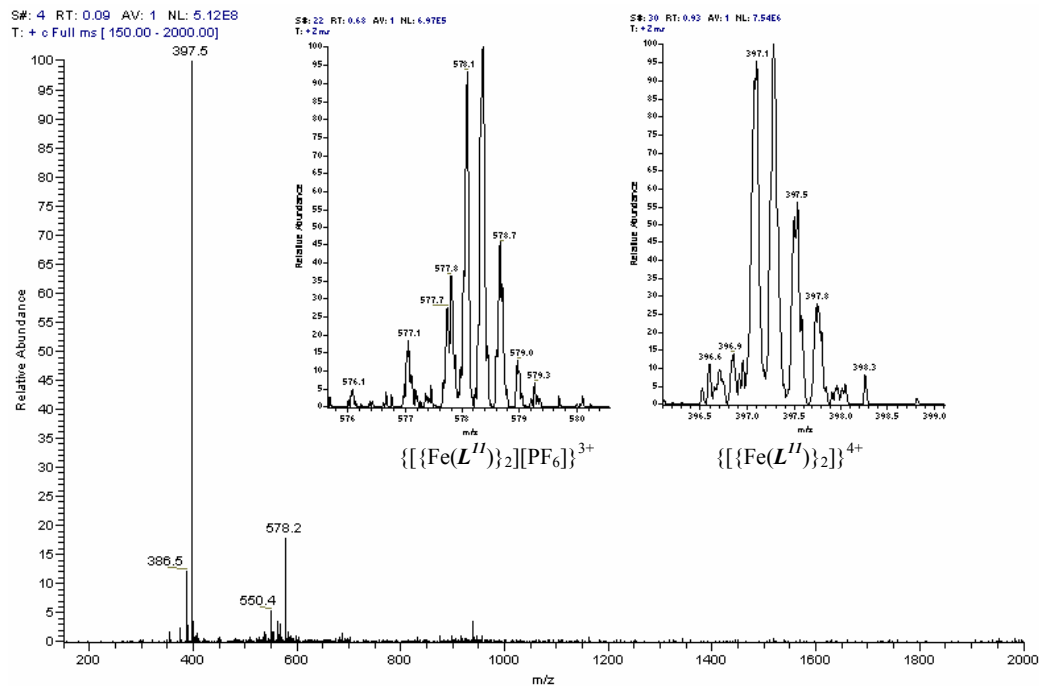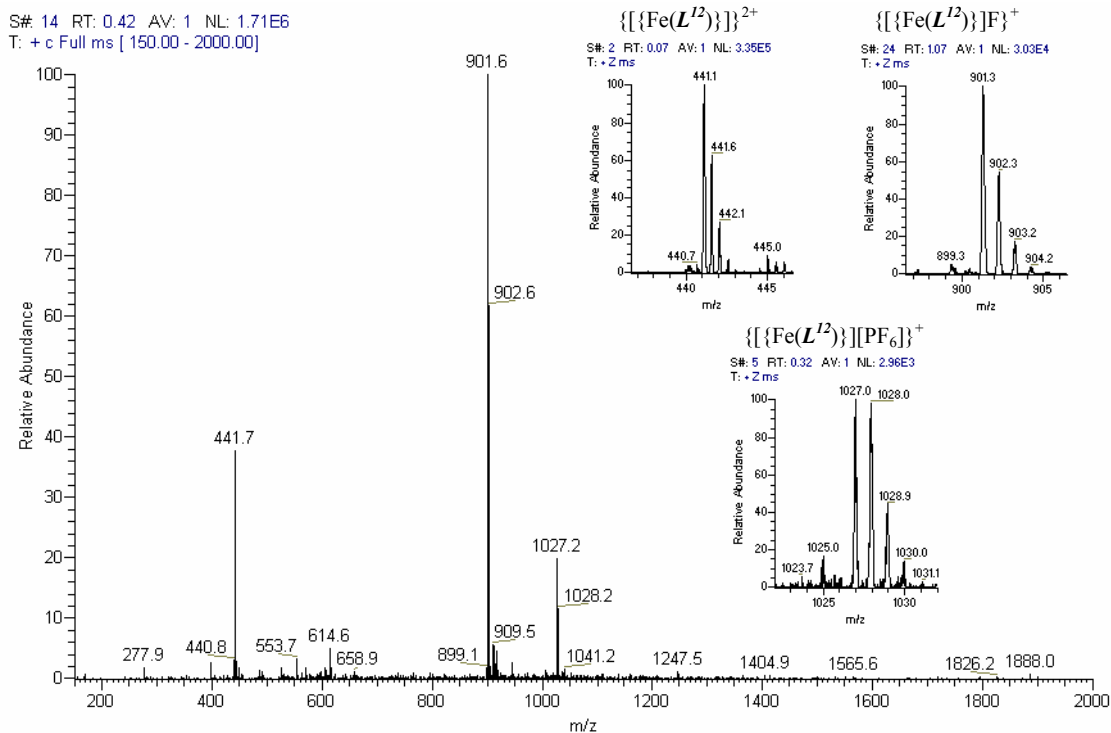
❖ The ES-MS spectrum of $[\{Fe(\boldsymbol{L^{13}})\}_2][PF_6]_4$
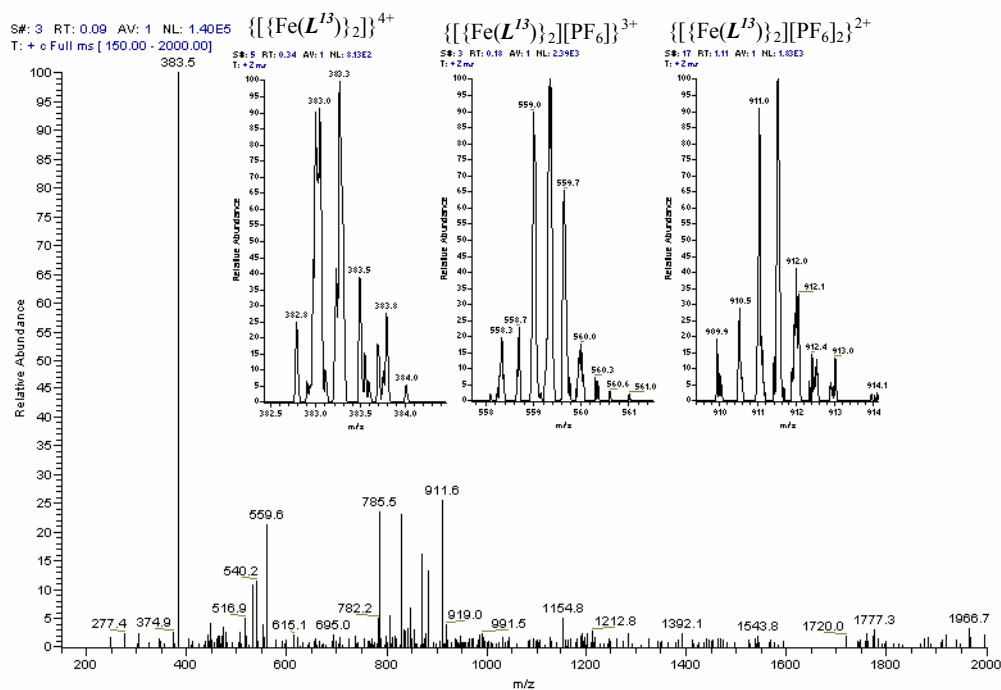
❖ The ES-MS spectrum of $[\{Fe(\boldsymbol{L^{13}})\}_3][PF_6]_6$
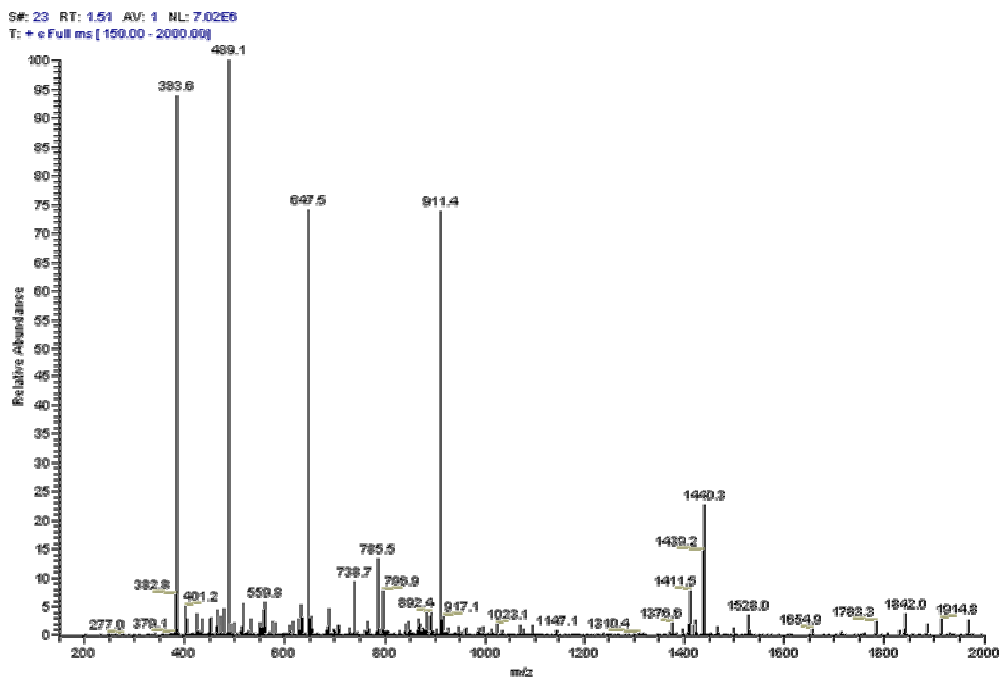
The insert spectra are shown in the next page.

The insert spectra of $[\{Fe(\boldsymbol{L^{13}})\}_3][PF_6]_6$:
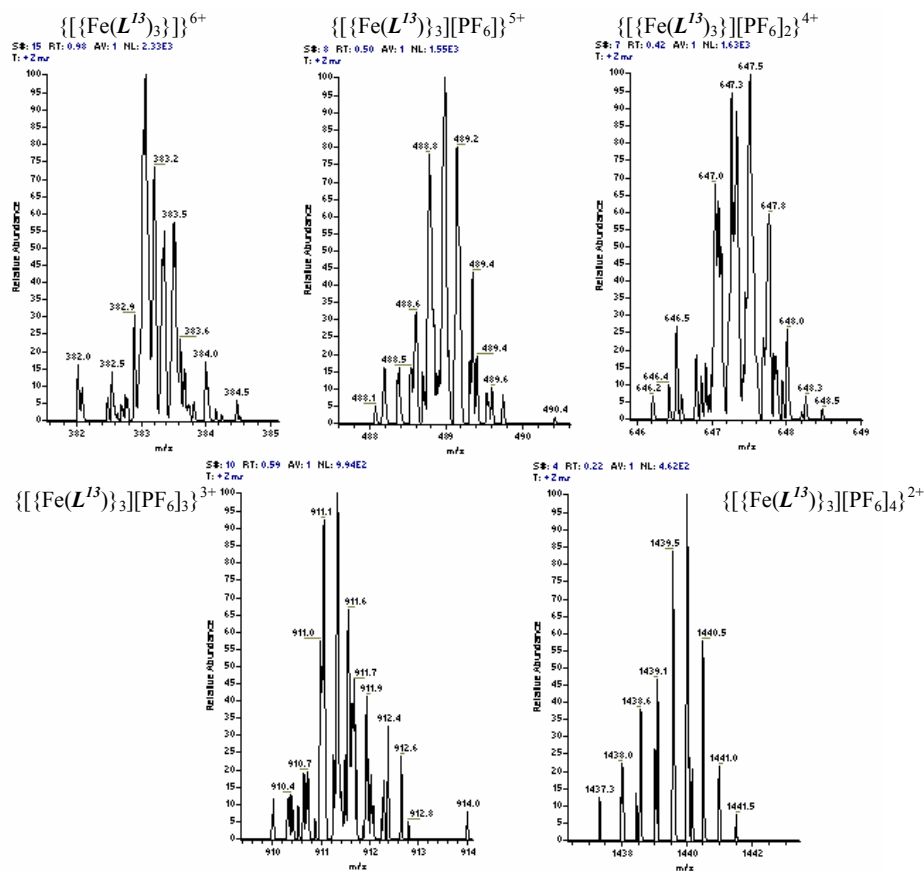
$\{[\{Fe(\boldsymbol{L^{13}})_3\}]\}^{6+}$

$\{[\{Fe(\boldsymbol{L^{13}})\}_3][PF_6]\}^{5+}$

$\{[\{Fe(\boldsymbol{L^{13}})_3\}][PF_6]_2\}^{4+}$

$\{[\{Fe(\boldsymbol{L^{13}})\}_3][PF_6]_3\}^{3+}$

$\{[\{Fe(\boldsymbol{L^{13}})\}_3][PF_6]_4\}^{2+}$

❖ The ES-MS spectrum of $[\{Fe(\boldsymbol{L^{14}})\}][PF_6]_2$

$\{[\{Fe(\boldsymbol{L^{14}})\}]F\}^+$

$\{[\{Fe(\boldsymbol{L^{14}})\}][PF_6]\}^+$
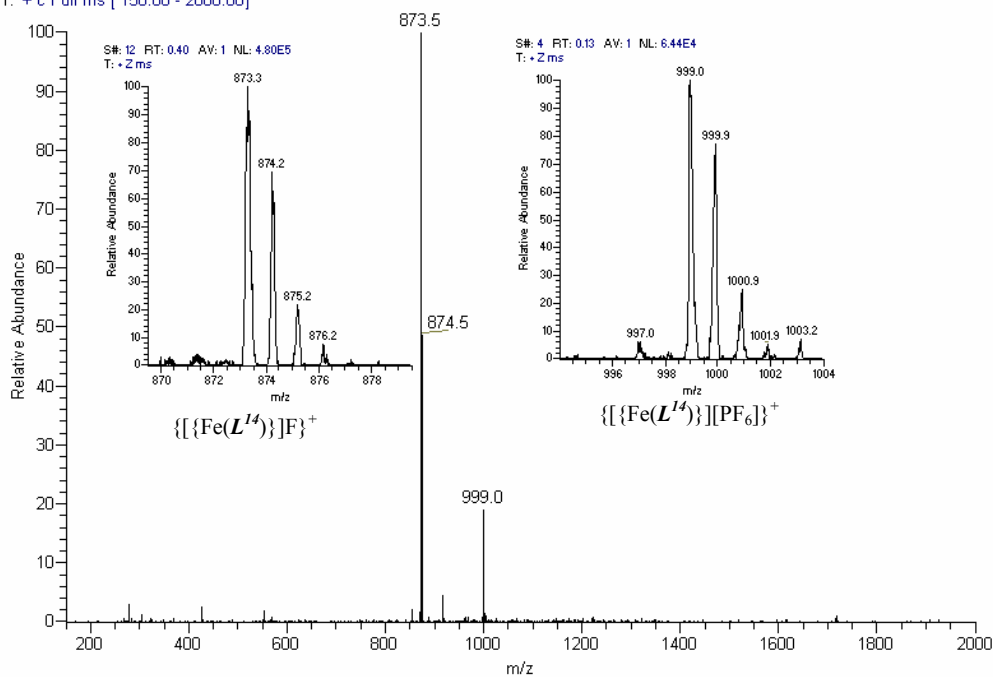
❖ The ES-MS spectrum of $[\{Fe(\boldsymbol{L^{15}})\}][PF_6]_2$

The insert spectra are shown below.

$\{[Fe(\boldsymbol{O\text{-}terpy})_2]\}^{2+}$

$\{[\{Fe(\boldsymbol{L^{15}})\}]\}^{2+}$

$\{[Fe(\boldsymbol{O\text{-}terpy})(\boldsymbol{HO\text{-}terpy})]\}^+$

$\{[\{Fe(\boldsymbol{L^{15}})\}]F\}^+$

$\{[\{Fe(\boldsymbol{L^{15}})\}][PF_6]\}^+$
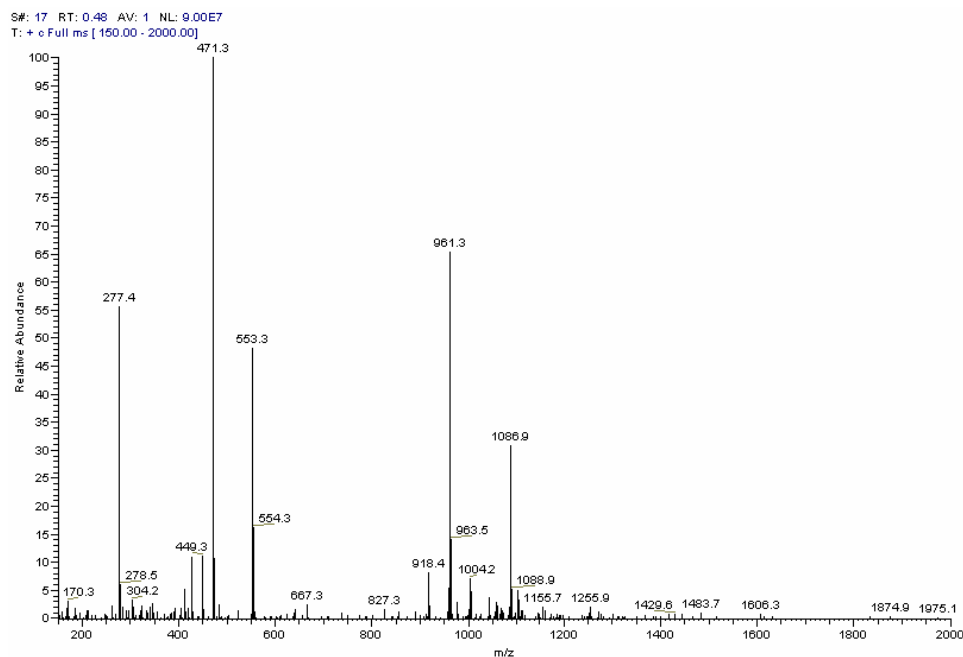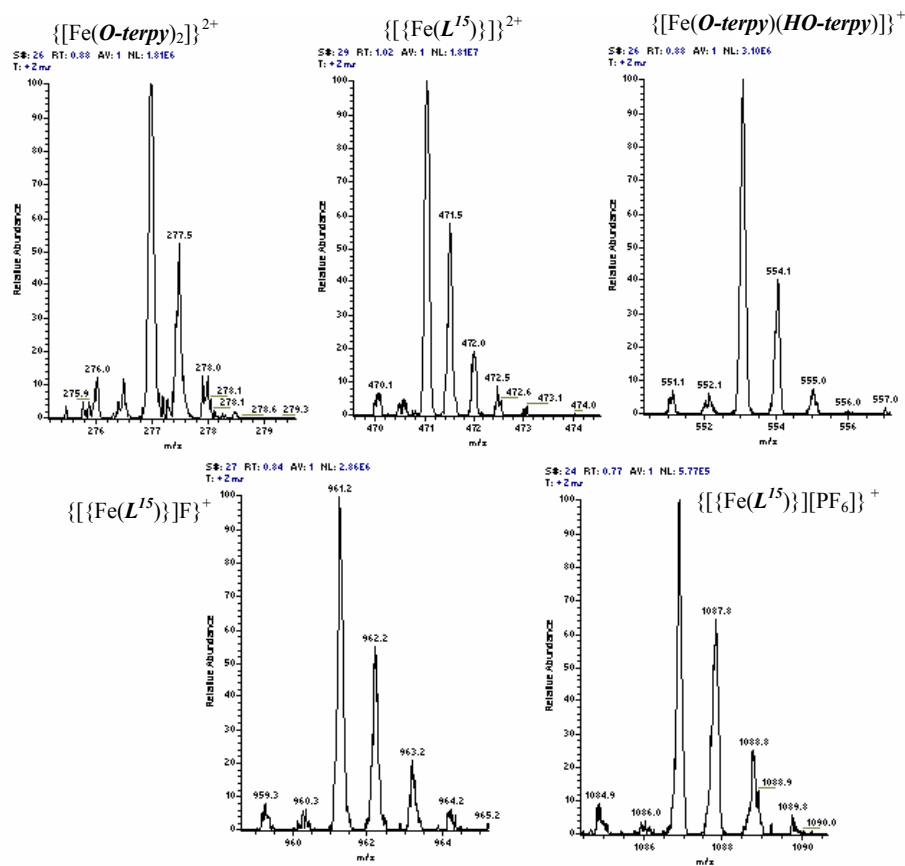
❖ The ES-MS spectrum of $[\{Fe(\boldsymbol{L^{16}})\}_3][PF_6]_6$

$\{[\{Fe(\boldsymbol{L^{16}})\}_3]\}^{6+}$ $\{[\{Fe(\boldsymbol{L^{16}})\}_3][PF_6]_2\}^{4+}$

$\{[\{Fe(\boldsymbol{L^{16}})\}_3][PF_6]\}^{5+}$ $\{[\{Fe(\boldsymbol{L^{16}})\}_3][PF_6]_3\}^{3+}$
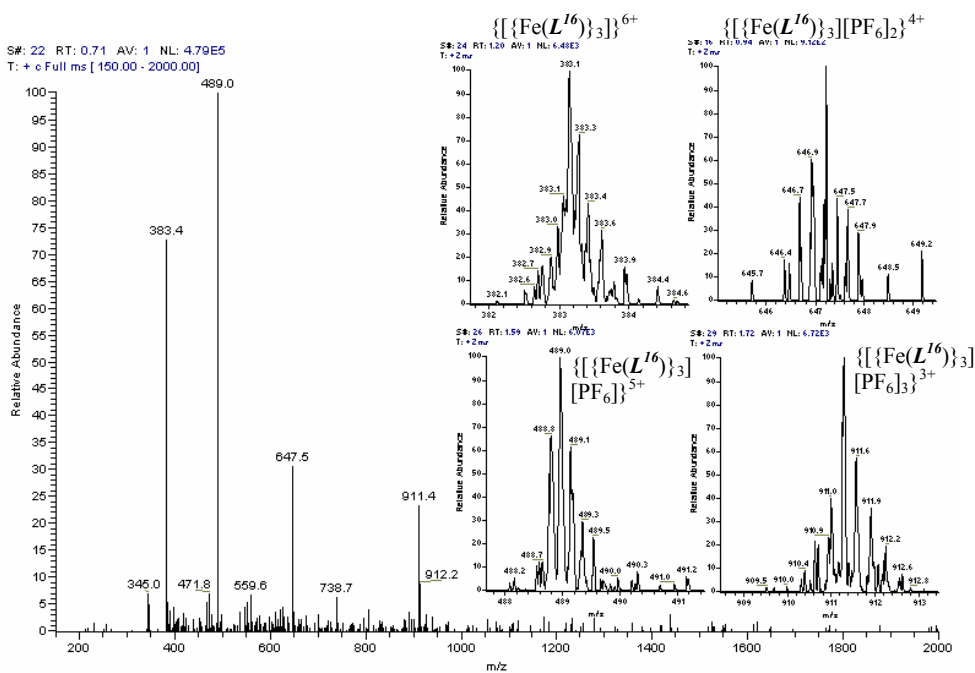
❖ The ES-MS spectrum of $[\{Fe(\boldsymbol{L^{17}})\}_2][PF_6]_4$

$\{[\{Fe(\boldsymbol{L^{17}})\}_2]\}^{4+}$ $\{[\{Fe(\boldsymbol{L^{17}})\}_2][PF_6]\}^{3+}$
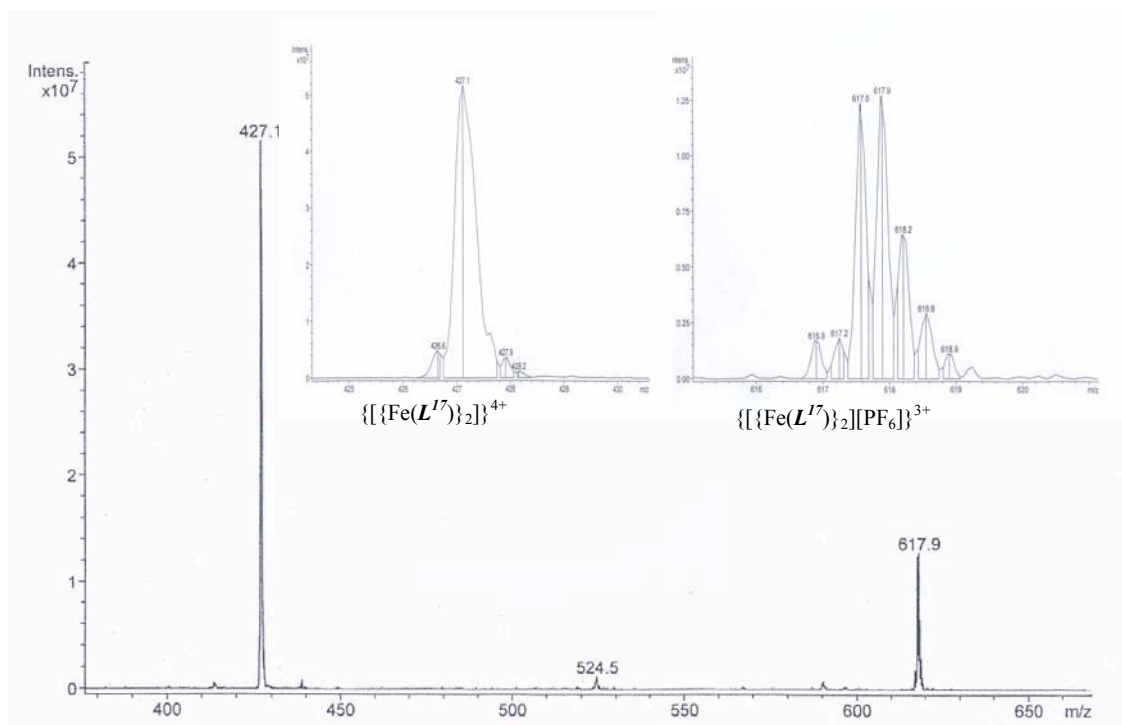
Hoi Shan <u>CHOW</u>

PERSONAL INFORMATION

Nationality: British (Overseas)

Place of Birth: Hong Kong

Date of Birth: 12 March 1979

Gender: Female

EDUCATION

2002- 2005	University of Basel	Switzerland

Ph.D. awarded January 2005 (magna cum laude, a score of 5.5 out of 6.0)

Project title: Metal Complexes of 4′-Substituted-2,2′:6′,2″-Terpyridines in Supramolecular Chemistry

Supervisors: Prof. E. C. Constable and Prof. C. E. Housecroft

2001- 2002	University of Birmingham	U.K.

Studied towards Ph.D. (transferred to University of Basel)

1998 - 2001	University of Kent at Canterbury	U.K.

B.Sc. Pharmaceutical Chemistry

1st class honours

PROFESSIONAL

2004 - current   Member of Swiss Chemical Society

2001 - current   Associate Member of Royal Society of Chemistry

EXPERIENCES

2002 – 2004   Two years as group operator of highfield NMR spectrometer at University of Basel.

2004 - 2004   Two years as group operator of electrospray mass spectrometer at University of Basel.

2004 -2004   Two years as editorial assistant to Prof. Catherine E. Housecroft for the journal Polyhedron.

PRESENTATIONS AT MEETINGS

1. Fall meeting 2004 of the Swiss Chemical Society,   Poster presentation.

   Zurich, Switzerland.

   7 October 2004

2. RSC Coordination Chemistry Discussion Group Meeting,   Poster and oral

   Leicester, UK.   presentation.

   12-14 July 2004

LIST OF PUBLICATIONS

1. When electron exchange is chemical exchange-assignment of ^{1}H NMR spectra of paramagnetic cobalt(II)-2,2′:6′,2″-terpyridine complexes.

   Hoi Shan Chow, Edwin C. Constable, Catherine E. Housecroft, Klaus J. Kulicke, and Yaqui Tao, *Dalton Trans.*, 2005, 236.

2. Metal-directed assembly of a conformationally restricted metallomacrocycle.

   Hoi Shan Chow, Edwin C. Constable, Catherine E. Housecroft, and Markus Neuburger, *Dalton Trans.*, 2003, 4568.

REFERENCES

Prof. E. C. Constable	Prof. C. E. Housecroft
Department of Chemistry	Department of Chemistry
University of Basel	University of Basel
Spitalstrasse 51	Spitalstrasse 51
4056 Basel	4056 Basel
Switzerland	Switzerland
Email: Edwin.constable@unibas.ch	Email: Catherine.housecroft@unibas.ch
Fax: +41 61 267 1015	Fax: +41 61 267 1018
Phone: +41 61 267 1001 / (1022)	Phone: +41 61 267 1008